

**METAL CHELATES OF 1,3-DIKETONES
STRUCTURALLY RELATED TO
CURCUMINOIDS**



**THESIS SUBMITTED TO THE UNIVERSITY OF CALICUT IN
PARTIAL FULFILLMENT OF THE REQUIREMENTS FOR THE
AWARD OF THE DEGREE OF DOCTOR OF PHILOSOPHY IN
CHEMISTRY**

BY

DEEPTHI. T.V

POST GRADUATE AND RESEARCH

DEPARTMENT OF CHEMISTRY

(UNIVERSITY OF CALICUT)

SREE NEELAKANTA GOVERNMENT SANSKRIT COLLEGE

PATTAMBI – 679306

MAY – 2017

**METAL CHELATES OF 1,3-DIKETONES
STRUCTURALLY RELATED TO
CURCUMINOIDS**



**THESIS SUBMITTED TO THE UNIVERSITY OF CALICUT IN
PARTIAL FULFILLMENT OF THE REQUIREMENTS FOR THE
AWARD OF THE DEGREE OF DOCTOR OF PHILOSOPHY IN
CHEMISTRY**

BY

DEEPTHI. T.V

**POST GRADUATE AND RESEARCH
DEPARTMENT OF CHEMISTRY
(UNIVERSITY OF CALICUT)**

SREE NEELAKANTA GOVERNMENT SANSKRIT COLLEGE

PATTAMBI – 679306

MAY – 2017

POST GRADUATE AND RESEARCH
DEPARTMENT OF CHEMISTRY
SREE NEELAKANTA GOVERNMENT
SANSKRIT COLLEGE, PATTAMBI



CERTIFICATE

This is to certify that the thesis entitled “**Metal chelates of 1,3-diketones structurally related to curcuminoids**” bound herewith is a bonafide work done by Miss. Deepthi.T.V under my supervision in the Department of Chemistry, S.N.G.S. College, Pattambi in partial fulfillment of the requirement for the award of degree of **Doctor of Philosophy** in chemistry of the University of Calicut, and that the work has not been included in any other thesis submitted previously for the award of any other degree.

Place: Pattambi
Date: 03.05.2017

Dr.P.Venugopalan
Supervising Teacher
Department of Chemistry
S.N.G.S. College, Pattambi

DECLARATION

I hereby declare that the work presented in the thesis “**Metal chelates of 1,3-diketones structurally related to curcuminoids**” is an authentic record of the original work done by me under the guidance of Dr.P.Venugopalan, Assistant Professor and Head, Department of Chemistry S.N.G.S. College, Pattambi in partial fulfillment of the requirement for the award of degree of Doctor of Philosophy in chemistry of the University of Calicut, and further that no part of thereof has been included in any other thesis submitted previously for the award of any other degree of this university.

Place: Pattambi
Date: 03.05.2017

Deepthi. T.V

ACKNOWLEDGEMENTS

I would like to express my deep sense of gratitude, indebtedness and sincere thanks to Dr.P.Venugopalan, Head of the Department and Supervising Teacher, Post Graduate and Research Department of Chemistry, SreeNeelakanta Government Sanskrit College Pattambi, for his valuable guidance, precious suggestions and constant encouragement during the course of this investigation.

I wish to express my sincere thanks to Prof. P.N. Anithakumari, Principal, Sree Neelakanta Government Sanskrit College Pattambi for providing necessary facilities.

I would like to express profound gratitude and sincere thanks to Dr. Ramadasankuttan, Director, Amala Cancer Research Centre, Thrissur for sharing expertise, valuable directions and encouragement extended to me during the biological studies.

I express my sincere thanks to Dr. Resmi.M.R., Assistant Professor, Dr. Binitha.N.N, Assistant Professor, Dr.T.P.Manoj, Assistant Professor, Department of Chemistry, S.N.G.S. College Pattambi and all other faculty members in the department for their valuable suggestions and generous help throughout the course of this work.

I would also like to express my gratitude to Mr. N. Surendranath, Lab assistant, S.N.G.S. College Pattambi and all other staff for their cooperation and help during the entire period.

I express my gratitude to Mrs. Shaniba.C.P and Mr. Mohammed Akbar. P., research scholars, Department of Chemistry, S.N.G.S. College Pattambi who have been extremely sincere to me and have provided me all

sorts of help whenever needed. I would also like to acknowledge my thanks to Mrs.Sudha.K.C, Mrs. Divya. P.N, Mr. Vinu.V.V, Ms. Rajeena.U, Mrs.Sowmya.B., Mrs. Sreeja. K, Dr. Silija.P.P and Ms. Vijayasree Haridas for their love, support and cooperation.

I would like to express my sincere thanks to Mrs. Preetha, Ms. Liji, Mr.Liju, Mrs.Binitha, Mrs. Sumitha and all other members in the Biochemistry Lab, Amala Cancer Research Centre, Thrissur for their help. I would also express my thanks to Mrs.Divya.T, Research scholar, Department of Chemistry, University of Calicut, for her support and all sorts of help she rendered.

I extend my gratitude to SAIF IIT Madras, SAIF IIT Bombay, STIC CUSAT, Cochin and CDRI Lucknow for spectral analysis.

I would like to express my sincere thanks to Dr. Jim D. Atwood, Professor of Chemistry at the State University of New York and Editor, Journal of Coordination Chemistry and Dr. Jeremy M. Smith, Professor of Chemistry at New Mexico State University and Editor, Inorganica Chimica Acta for kindly accepting our manuscripts.

I extend my gratitude to Higher Education Department, Government of Kerala for providing research fellowship.

I would like to express my hearty thanks to my father, mother, sister, brother in law and aunty for their great support, endurance, prayer and encouragement during every stage of this work.

Above all I am greatly thankful to God almighty for giving me courage to move on.

Deepthi.T.V.

PREFACE

Curcumin, the active ingredient of turmeric, is well known for its efficacy against a large number of diseases including ulcers, parasitic infections, various skin diseases, different types of cancer, psoriasis, arthritis and rheumatism, sinusitis, jaundice and other liver ailments. Unfortunately, its clinical application is restricted by its the poor solubility in water, low absorption and bioavailability. Structural modifications including metal chelation improved its potential as a drug in several studies. In the present investigation a series of structurally modified derivatives of curcumin and their metal complexes were synthesised and characterized by electronic, IR, ^1H NMR, ^{13}C NMR and mass spectral studies. All the ligands were found to be existing in their enolic form and Ni(II), Cu(II) and Zn(II) complexes of these ligands have 1:2 metal-ligand stoichiometry.

In view of reported dominant biological activities of curcumin, its synthetic analogues and metal complexes, some of the possible biological activities are also studied with the ligands and their metal complexes. The antioxidant activity of ligands and their metal complexes were studied by DPPH radical scavenging, super oxide radical scavenging, hydroxyl radical scavenging and lipid peroxidation inhibitory methods. The DNA binding properties of ligand and metal complexes were studied by absorption titrations, fluorescence quenching experiments and by viscosity measurements with calf thymus DNA. The *in vitro* and *in vivo* antitumor studies of free ligands and their copper(II) chelates against Daltons lymphoma ascites cell lines are also included in this study.

The thesis is presented in five sections. In the first section, a general **introduction** about metal ions in biological systems and medicinal applications of metal complexes are briefly discussed. Curcumin and its potential therapeutic applications are highlighted. Difficulties with the use of curcumin in its therapeutic applications and possible remedies are mentioned. Importance of structural modifications and metal chelation to enhance the biological activities

of curcumin are also included. This section ends with a brief outline of the present investigation.

In the **review of literature**, the chemistry of curcumin and various biological applications of curcumin are detailed. Structural modifications of curcumin, biological activities/applications of metal complexes of curcumin and its synthetic analogues are also presented. An account of materials, instruments used and methods adopted in this study are included in section **III**.

Results and discussion is divided into two parts. In **Part A**, the synthesis and characterization of ligands and their metal complexes are presented in detail with supporting spectral data. It is grouped into five chapters based on the nature of ligands involved. Results obtained from studies on antioxidant activities, DNA binding properties and antitumor activities are separately presented as three chapters under **Part B** of the thesis. The ligands are found to be potent antioxidants against DPPH, super oxide, hydroxyl and lipid peroxy free radicals. The presence of phenolic group in the aryl rings enhanced antioxidant properties, but it is not essential. In all cases metal complexation reduced the activity.

Studies on DNA binding properties of ligand and metal complexes revealed strong to moderate interaction with CT DNA. Interaction of copper(II) complexes were found to be higher than that of free ligands in all methods. The observed intrinsic binding constants suggest that the binding involves intercalative mode through non covalent interactions and produced conformational changes in the structure of DNA. It is further supported by viscosity measurements and by fluorescence quenching measurements with ET bound DNA.

All the compounds were found to be cytotoxic towards Daltons lymphoma ascites cells in both *in vitro* and *in vivo* studies. It was found that copper chelates are remarkably active compared with free curcumin analogues.

Major conclusions derived from the study are presented in section V. References are listed at the end of thesis in serial order.

List of publications:

1. T.V. Deepthi and P. Venugopalan
Synthesis, DNA-binding, and cytotoxic studies on three copper(II) complexes of unsymmetrical synthetic analogues of curcumin, *Journal of Coordination Chemistry*, 2016, **69(22)**, 3403-3416.
2. T.V. Deepthi and P. Venugopalan
Synthesis, characterization and biological studies on Ni(II) and Cu(II) complexes of two novel α,β -unsaturated 1,3-diketones related to curcuminoids.
Inorganica Chimica Acta, 2016, **450**, 243-250.
3. T.V. Deepthi and P. Venugopalan
Synthesis, DNA binding and Cytotoxic studies on copper(II) and nickel(II) complexes of two unsymmetrical conjugated 1,3-diketones related to curcuminoids (communicated to Journal of Pure and Applied Chemical Sciences)
4. P. Venugopalan and T.V. Deepthi
Metal Chelates of Congugated 1, 3-Diketones that are Structurally Related to Curcuminoids (to be communicated)
5. P. Venugopalan and T. V. Deepthi
Synthesis, Characterization and Antitumor activities of copper(II) and nickel(II) complexes of two curcumin based ligands (to be communicated)

6. T.V. Deepthi and P. Venugopalan
Synthesis, characterization, DNA binding and cytotoxic studies on Copper(II) and Nickel(II) complexes of three conjugated 1,3-diketones related to curcuminoids (to be communicated)

Conference Papers

1. T.V. Deepthi and P. Venugopalan
Synthesis, characterization and biological studies on copper(II) and nickel(II) complexes of curcumin based ligands, UGC Sponsored Two days National Seminar on “EMERGING TRENDS IN CHEMICAL RESEARCH”, Research and Post Graduate Department of Chemistry, Christ College (Autonomus), Irinjalakuda.

Important abbreviations used in this thesis are:

Ar	aryl group
BM	Bohr Magneton
CMC	Carboxy methyl cellulose
CT-DNA	Calf ThymasDNA
DLA	Dalton's lymphoma ascites
DMSO	Dimethyl sulphoxide
DPPH	1, 1-Diphenyl-2-picrylhydrazyl
EB	Ethidium bromide
EC50	Half maximal effective concentration
EDTA	Ethylene diammine tetra acetic acid
Hz	Hertz
ILS	Increase in life span
J	Coupling constant
M	Central metal ion in a metal complex
MDA	Malondialdehyde
μ_{eff}	Effective magnetic moment in Bohr magnetons
MP	Melting point
NBT	Nitro Blue tetrazolium chloride
ppm	parts per million
TBA	Thiobarbituric acid
TBARS	Thiobarbituricacid-reactive-substances
Tris buffer	Tris(hydroxymethyl) aminomethane
W	Watt



E-mail : amalacancerresearch@gmail.com

Phone: 0487 2307968

Institutional Animal Ethical Committee

(Reg. No. 149/1999/CPCSEA)

Amala Cancer Research Centre

RESEARCH DIRECTOR &
CHAIRMAN, IAEC

: DR. RAMADASAN KUTTAN, Ph.D.

AMALANAGAR - 680 555, THRISSUR
KERALA, INDIA

Ref :

Date:
20.2.2016

CERTIFICATE

This is to certify that the Ph.D. Thesis of Deepthi, T.V. entitled "Metal chelates 1,3-diketones structurally related to curcuminoids" approved (No.ACRC/IAEC/16-01(1)) by the Institutional Animal Ethics Committee under the direction of Dr. Ramadasan Kuttan.

Dr. Jose Padikkala, Ph.D.

Secretary, IAEC

SECRETARY
Institutional Animal Ethical Committee
Reg.No. 149/1999/CPCSEA
Amala Cancer Research Centre

Sl. No.	Contents	Page No.
I	INTRODUCTION	
	Metal ions in biological systems	1
	Curcuminoids and curcumin	9
	Importance of present investigation	14
	Description of research problem	16
II	REVIEW OF LITERATURE	
	Turmeric	19
	Composition of Turmeric oil	19
	Isolation of curcumin	21
	Structural characteristics of curcumin	23
	Synthesis of curcumin	24
	Reactivity of curcumin	26
	Biological activities of curcumin	35
	Synthetic analogues of curcumin	47
	Biological activities of metal complexes of curcumin and its synthetic analogues	52
III	MATERIALS, METHODS AND INSTRUMENTS	
	Materials	65
	Instruments	66
	Methods	67
IV-A	RESULTS AND DISCUSSION	
	PART A	
	SYNTHESIS AND CHARACTERISATION	
	Chapter 1 Ligands with ortho substituted phenyl rings	
	Synthesis of ligands	73
	Synthesis of Cu ^{II} , Ni ^{II} and Zn ^{II} complexes	74
	Results and discussion	75
	Characterisation of ligands	77
	Characterization of metal complexes	103

Chapter 2 Ligands with para substituted phenyl rings

Synthesis of ligands	133
Synthesis of Cu ^{II} , Ni ^{II} and Zn ^{II} complexes	133
Results and discussion	134
Characterisation of ligands	134
Characterization of metal complexes	156

Chapter 3 Ligands with 3,4-disubstituted phenyl rings

Synthesis of ligands	179
Synthesis of Cu ^{II} , Ni ^{II} and Zn ^{II} complexes	179
Results and discussion	179
Characterisation of ligands	180
Characterization of metal complexes	194

Chapter 4 Ligands with heterocyclic aryl rings

Synthesis of ligands	213
Synthesis of Cu ^{II} , Ni ^{II} and Zn ^{II} complexes	213
Results and discussion	214
Characterisation of ligands	214
Characterization of metal complexes	226

Chapter 5 Ligands with naphthyl rings

Synthesis of ligands	238
Synthesis of Cu ^{II} , Ni ^{II} and Zn ^{II} complexes	238
Results and discussion	239
Characterisation of ligands	239
Characterization of metal complexes	250

	RESULTS AND DISCUSSION	
IV-B	PART B	
	BIOLOGICAL STUDIES	
	Chapter 6 Studies on Antioxidant Activity	
	DPPH scavenging method	268
	Lipid peroxidation method	270
	Superoxide scavenging method	272
	Hydroxy radical method	273
	Comparison of antioxidant activities	274
	Chapter 7 Studies on DNA Binding Properties	
	UV spectrometric method	282
	Viscosity method	295
	Fluorescence quenching method	299
	Chapter 8 Studies on Antitumor Activities	
	<i>In vitro</i> studies	303
	<i>In vivo</i> studies	311
V	CONCLUSIONS	319
VI	REFERENCES	322
VII	PUBLICATIONS	338

INTRODUCTION

1. Metal ions in biological systems

Coordination compounds are widely present in the mineral, plant and animal world and are known to play important functions in diverse areas such as analytical chemistry, metallurgy, biological systems, industry and medicine. Naturally occurring coordination compounds are vital to living organisms. Perhaps, the most significant metal complex in our body is the hemoglobin. Erythrocytes are red due to the presence of hemoglobin, the conglomerate macromolecule responsible for oxygen transport. Hemoglobin contains iron-porphyrin complexes, its role as an oxygen carrier being related to the ability of the iron atoms to coordinate oxygen molecules reversibly^[1].

Hemoglobin is composed of four subunits, each consisting of a non-protein group heme surrounded by a coiled protein (globin). Each heme group contains an iron (Fe^{II}) ion surrounded by a heterocyclic ring. The iron center has six potential coordination sites, four of which are occupied by porphyrin nitrogens (N). The fifth coordination site (below the plane of the ring) covalently bonds with a histidine (His) residue from the F8 position of its respective globin chain. The sixth coordination site (above the plane of the ring) is where all the "action" occurs. This is the place oxygen and other small molecules transiently bind to the iron atom (**Figure 1**). Other biologically important coordination compounds include chlorophyll, a magnesium-porphyrin complex and vitamin B₁₂ or cyanocobalamin, a complex of cobalt(III) with a macrocyclic ligand known as corrin (**Figure 2**)^[2].

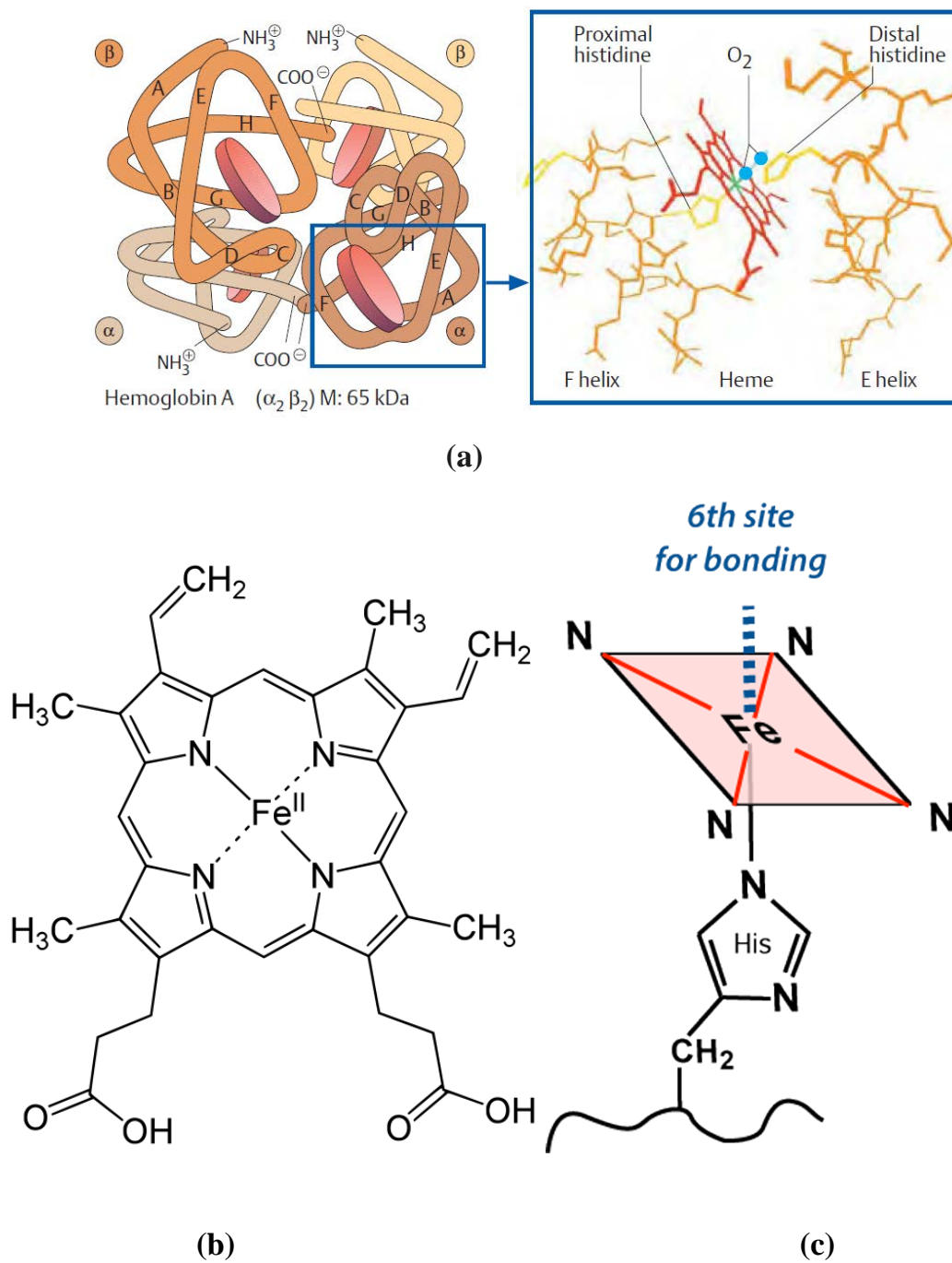
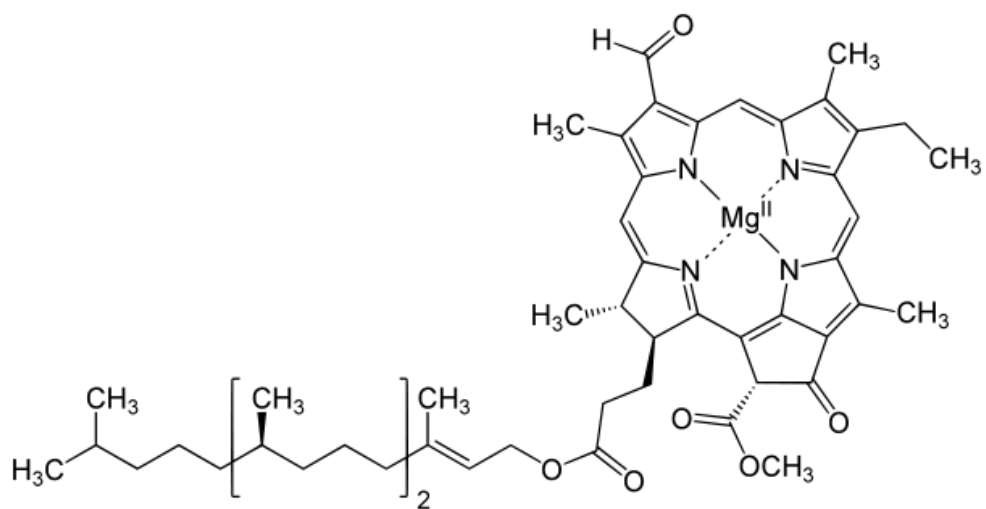
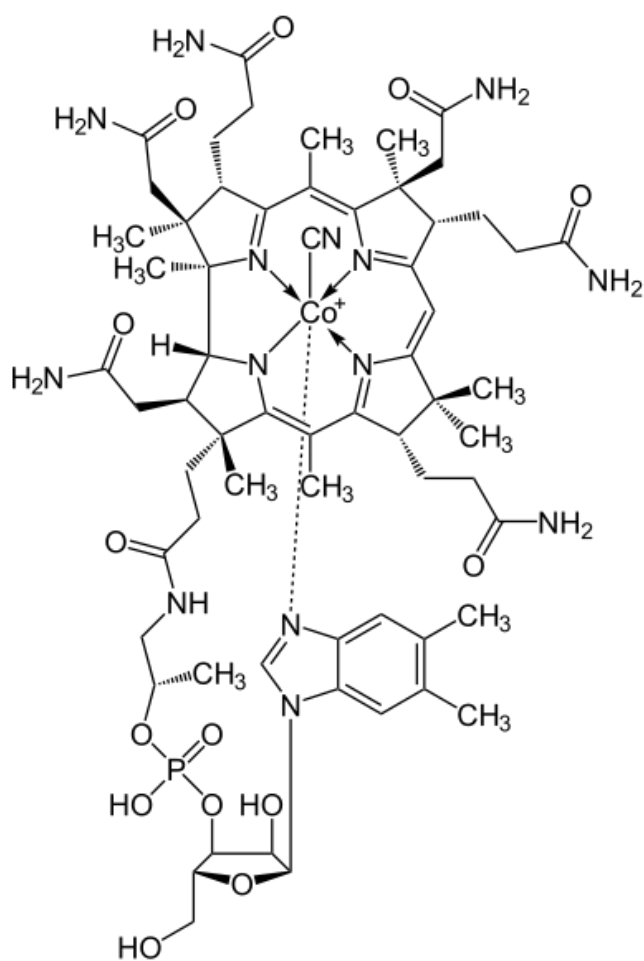


Figure 1. Structure of haemoglobin (a) A computer graphic of structure of hemoglobin , (b) heme, (c) coordinating site in hemoglobin



(a)



(b)

Figure 2. Chemical structure of chlorophyll (a) and cyanocobalamin(b)

With the application of new and sophisticated machines to study biological and biochemical systems, it is increasingly recognized that metal ions are involved in various cellular and sub-cellular functions. Today, it is known that metals are important ingredients in living cells, just as the organic molecules. For instance, the divalent magnesium and calcium ions play important regulatory roles in cells. The divalent cations Zn^{2+} , Ca^{2+} and Mg^{2+} prevent cytotoxicity and *in vivo* antagonize Cd-induced carcinogenesis. The transport of iron and other metal ions by the blood plasma is achieved through the formation of protein complexes^[3]. Lack of body iron is common in cancer patients and it is associated with complications in surgery and in animal experiments. Copper is recognized as an essential metalloelement and is primarily associated with copper-dependent cellular enzymes^[4].

In the fascinating field of 'metals in biology', by virtue of direct interactions with amino acid side-chains within polypeptide chains, metals play unique and critical roles in biology, promoting structures and chemistries that would not otherwise be available to proteins alone^[5]. Metal ions play essential roles in about one third of enzymes. Many enzymes that regulate biological processes are metal complexes (metalloenzymes); for example, carboxy peptidase, a hydrolytic enzyme important in digestion, contains a zinc ion coordinated to several amino acid residues of the protein. Another enzyme, catalase, which is an efficient catalyst for the decomposition of hydrogen peroxide, contains iron-porphyrin complexes. In both cases, the coordinated metal ions are probably the sites of catalytic activity. These ions can modify electron flow in a substrate or enzyme, thus effectively controlling an enzyme-catalyzed reaction. They can serve to bind and orient substrate with respect to functional groups in the active site, and they can provide a site for redox activity if the metal has several valence states^[6].

Metal ions are generally positively charged and act as electrophiles, seeking the possibility of accepting electron pairs with other atoms so that a bond or dipole-dipole interaction can be formed. They behave rather like hydrogen ions. However, metal ions often have positive charges greater than 1, and have a larger ionic volume so that they can accommodate many ligands around them at the same time. In addition, metal ion concentrations can be high at neutral pH values, while hydrogen ion concentrations are, by the definition of pH, low at these values ^[7].

Ligands are the atoms or group of atoms that are bonded to the metal ion, generally in an electrostatic manner. They are usually neutral or negatively charged and they donate electron density to the metal ion. The coordination number of a metal ion, that is, the number of ligand atoms bound to it, is viewed in terms of concentric spheres; the inner sphere containing those atoms in contact with the metal ion, the second sphere containing those in contact with the inner sphere ligand atoms. The number of atoms in these spheres will depend on the size of the metal ion and the sizes of the ligand atoms ^[8].

The charge distribution in the active site of an enzyme is designed to stabilize the transition state of the catalyzed reaction relative to that of the substrate. In enzyme-catalyzed reactions it is essential that the reactants be brought together with the correct spatial orientation, otherwise the chance of the reaction taking place is diminished and the reaction rate will be too low. The electrostatic environment in the active site is a major factor that serves to guide the substrate to the binding site in the correct orientation. Metal ions can assist in this process, often binding groups in a stereochemically rigid manner, thereby helping to control the action of the enzyme. Thus, an enzyme will bind its substrate in such a manner that immobilization and alignment, ready formation of the transition state of the reaction to be catalyzed, and then easy

release of the product will result; metal ions often help in accomplishing this process ^[9].

The enzyme provides an arrangement of side-chain functional groups having an appropriate sized hole with the preferred groups on enzyme side chains needed to bind the required metal ion. The optimal number of such binding groups is chosen for the particular metal ion, together with the appropriate hydrophobic or hydrophilic environment in the binding site ^[10]. Metal ions may be bound by main-chain amino and carbonyl groups, but specific binding is achieved by the amino acid side chains. No set of general rules exists that describes how a given metal ion will behave in an enzyme. Now that many crystal structures of proteins are being studied by X-ray diffraction, information on the binding of metal ions in the active sites of enzymes is available and should provide clues to the mechanism of action of the enzyme ^[11].

It is less well known than the fact that metal ions are required in biology is their role as pharmaceuticals. Two major drugs based on metals that have no known natural biological function, cisplatin (Pt) and auranofin (Au), are widely used for the treatment of genitourinary and head and neck tumours and of rheumatoid arthritis, respectively (**Figure 3**). In addition, compounds of radioactive metal ions such as ⁹⁹Tc and complexes of paramagnetic metals such as Gd(III) are now in wide spread use as imaging agents for the diagnosis of diseases ^[12].

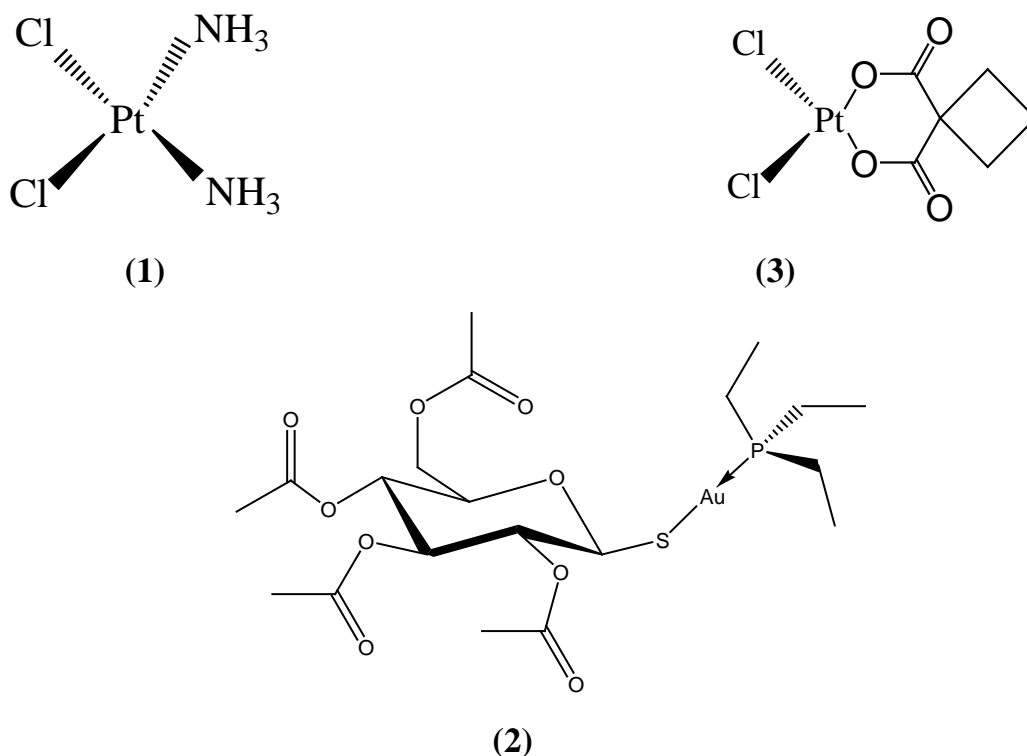


Figure 3. Chemical structure of cisplatin (1), auranofin (2) and carboplatin (3)

Cisplatin (1,) is perhaps the best known example of a small molecule metal-containing drug. Its use and effectiveness in cancer chemotherapy since the entry into the clinic in the late 1970s has been thoroughly documented. Cisplatin is cited for treatment of germ-cell cancers, gestational trophoblastic tumours, epithelial ovarian cancer, and small cell lung cancer as well as for palliation of bladder, cervical, nasopharyngeal, esophageal, and head and neck cancers. Despite this success, there is still a limited range of tumours sensitive to cisplatin intervention—some cancers are inherently resistant. The side effects of cisplatin treatment are severe and include the dose-limiting nephrotoxicity, neurotoxicity, ototoxicity, and emetogenesis ^[13].

The “second-generation” compounds based on the cisplatin structure were developed in attempts to reduce toxicity and/or expand the range of

useful anticancer activity. Carboplatin ((**3**), **Figure 3**) entered the clinic in 1998, principally in response to the necessity to reduce the toxic side effects of the parent drug. Despite this lower toxicity, carboplatin is essentially active in the same set of tumours as cisplatin and a broader spectrum of activity is not indicated. For some tumours, cisplatin appears to be therapeutically more effective than carboplatin (germ cell tumours, head and neck, and bladder) whereas for lung cancer and ovarian cancer effectiveness is comparable^[14].

Since the advent of cisplatin in the clinic, the consistent goals for drug development have been improvement of toxicity profile, circumvention of resistance, and expansion of the tumors sensitive to treatment by cisplatin. To achieve these goals, modified versions of cisplatin and a large number of non-platinum complexes are explored for their cytotoxicity. In the past few years, for easy accessibility and less toxicity, complexes based on earlier transition metals, particularly Cu, have also attracted considerable interest^[15].

Copper complexes have been shown to possess a broader spectrum of activity and a lower toxicity than platinum drugs and are suggested to be able to overcome inherited and/or acquired resistance to cisplatin^[16]. These features are consistent with the hypothesis that copper complexes possess mechanism(s) of action different from platinum drugs that covalently bind to DNA. However, little information is available on the molecular basis for the mode of action of copper complexes. At present, most investigations still focus on the ability of these complexes or fragments thereof, to interact with DNA. However, other cellular constituents such as topoisomerases or the proteasome multiprotein complex are emerging as new putative targets^[17]. Since 1969, copper has been found to possess high DNA binding affinity. Analogously to what has been widely illustrated for cisplatin,^[18] This binding was dependent on copper complex size, electron affinity, and geometry of the formed adduct, inducing an irreversible modification of the DNA conformational structure. According to these observations, a high number of

copper complexes has been and is still being tested as DNA-targeting agents [19].

Metal complexes have tremendous potential use as anticancer agents, due to their wide and diverse structural types, varied ligand bonding modes and a large number of metal complexes have been tested as anti-cancer drugs in an effort to find compounds with higher selectivity and lesser side effects than those commercially available. Due to unique magneto-structural correlations resulting from the interaction with macromolecules present in living cells, metal complexes exert a range of biological activities having therapeutic values and many of them successfully cleared clinical trials. The term metallodrug is used to describe such compounds and a number of them are already in use to treat many diseases including different types of cancer [20].

2. Curcuminoids and curcumin

The term curcuminoids represent a group of structurally related compounds present in the roots and shoots of herbaceous plant *Curcuma Longa L* (turmeric) and several other related *Curcuma* species of the family *Zingiberaceae*. Turmeric has traditionally been used for medical purposes for many centuries in countries such as India and China for treatment of ulcers, parasitic infections, various skin diseases, psoriasis, arthritis and rheumatism, sinusitis, jaundice and other liver ailments. It has been recognized that most of the therapeutic applications of turmeric is due to curcuminoids, the colouring matter of turmeric, comprising a mixture of curcumin(I), demethoxy curcumin(II) and bis(demethoxy)curcumin(III), the major component being curcumin (**Figure 4**) [21].

Chemically they can be defined as 1,7- diarylheptanoids having a substituted unsaturated β -diketo moiety in a seven carbon chain with two aryl groups at both ends. There are several reports on the separation of the three curcumoinoids from the crude extract using different chromatographic

techniques. They can easily and effectively be separated by column chromatography using different mobile phases including chloroform, acetone, diethyl ether, benzene, etc. Curcumin I is the major component and eluted first from the column followed by curcumin II and curcumin III. Recently, an improved separation of the three curcuminoids was realized using a combination of normal phase column chromatography and phosphate-impregnated preparative-thin layer chromatography^[22].

A combination of normal phase column chromatography and phosphate-impregnated preparative-thin layer chromatography technique has been reported as an efficient tool to separate the three curcuminoids^[23].

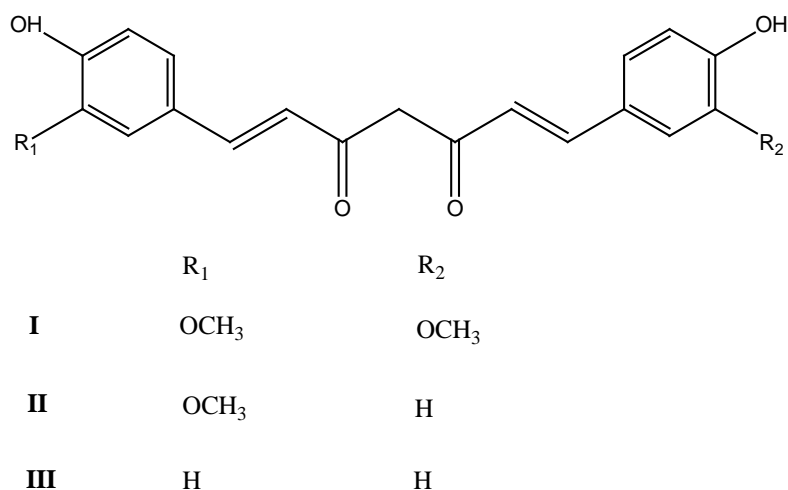


Figure 4. Structure of curcuminoids

Subsequent to the first seminal paper published in “Nature” in 1949, numerous preclinical studies have provided a solid basis for examining efficiency of curcumin against human diseases^[24]. More than 15,000 articles published within the past two decades have discussed the molecular basis for the antioxidant, anti-inflammatory, antibacterial, antiviral, antifungal, and anticancer activities assigned to curcumin. Clinical trials conducted on this molecule, have shed light on the role of curcumin in various chronic conditions, including autoimmune, cardiovascular, neurological, and

psychological diseases, as well as diabetes and cancer. Common to all of these clinical studies have been the safety, tolerability, and non-toxicity even at high doses. The underlying mechanism for clinical efficiency of curcumin seems to be modulation of numerous signaling molecules. However, because of the complex nature of the diseases, the underlying mechanism in many cases remains unclear^[25].

Literature is extensive on the antitumor activity of curcumin and its structural analogues. In a large number of studies, it was found that these compounds are toxic to cancerous cells and cytoprotective to healthy cells. Various animal models or human studies proved that curcumin is extremely safe even at very high doses. For example, different clinical trials indicated that curcumin, when taken as high as 12 g per day, is well tolerated^[26,27]. Similarly, the efficiency of curcumin in various diseases including cancer has been well established. The pharmacological safety and efficacy of curcumin makes it a potential compound for treatment and prevention of a wide variety of human diseases^[28].

Numerous published articles, audio recordings, and videos on this subject are available to the public. Some links to videos about the use and health benefits of turmeric and curcumin are summarised in **Table 1**.

Table 1. Online video describing the use and health benefits of curcumin

Topic	Links
Curcumin benefits—all you should know about curcumin benefits	http://www.youtube.com/watch?v=PmunAxElzoc
Anti-cancer and other health properties of curcumin	http://www.youtube.com/watch?v=ArzTQsG1yVw
Curcumin for cancer prevention	http://www.youtube.com/watch?v=9iGWifv6ldo
Turmeric curcumin—natural cancer-fighting spice reduces tumors	http://www.youtube.com/watch?v=oP7S5VDHtFY
Truly essential curcumin cures cancer in 1 year	http://www.youtube.com/watch?v=YgG0o9EGkmo
Turmeric curcumin—cancer cure and more!	http://www.youtube.com/watch?v=cKzOyLxpSS4
Curcumin kills cancer cells	http://www.youtube.com/watch?v=pAzwGKC_Cls
Why is curcumin a suitable anti-cancer agent?	http://www.youtube.com/watch?v=NJI4WsJst5g
Curcumin for colon cancer	http://www.youtube.com/watch?v=eIQFAv6hNRo
Turmeric: naturally reverse cancer, arthritis and inflammation	http://www.youtube.com/watch?v=YS-nyqBJeGc&list=PL4E92A08A28D8A361
Brain injury recovery, curcumin, minority health	http://www.youtube.com/watch?v=kTH4jBYOudA
Benefits of curcumin capsules	http://www.youtube.com/watch?v=y5mhTUKv8rU
Curcumin in prevention of cancer	http://www.youtube.com/watch?v=xmxlyZY9eRo
Curcumin (turmeric) is a potent anti inflammatory	http://www.youtube.com/watch?v=8PN7X3RsVRs
Using turmeric to prevent and cure cancer	http://www.youtube.com/watch?v=FXIIreujNyo
Curcumin may help prevent type 2 diabetes	http://www.youtube.com/watch?v=KnAW-aQZk6U
Curcumin–tumeric benefits–uses and curcumin capsules	http://www.youtube.com/watch?v=SoeAvQTL5Ek

Most of the drugs used in chemotherapy are potential poisons at higher doses than prescribed by a physician and most of them have one or other severe side effects. Public awareness about these aspects of chemotherapy increasingly necessitating the search for drugs having natural origin and physiologically active biomolecules are thoroughly investigated by modern techniques to explore their possible applications in the diagnosis and treatment of various diseases. In this context, curcumin has a unique record that more than 15,000 publications have appeared from 1990s to date claiming different beneficial biological effects. The pace of curcumin research is growing rapidly in diverse fields ^[29].

While the majority of researchers have been pursuing the biological aspects, a few others were interested in understanding the important chemistry of curcumin behind its unique biological activity. Curcumin research has become one of the most favourite subjects in different branches of chemistry. In organic chemistry the extraction and synthesis of curcumin and new synthetic derivatives was the main focus of research. Inorganic chemists have used its metal chelating abilities through the β -diketo group to form new structural entities with modified biochemical activities. Physical chemists have focused on the highly sensitive spectroscopic properties of curcumin to study its interactions with micro heterogeneous systems and biomolecules. Analytical chemists have been employing curcumin's unique absorption spectroscopic properties to identify and quantitatively estimate trace elements like for e.g., estimation of boron, as a red coloured product. Other chemistry studies that are useful in understanding the biological activity of curcumin are its chemical reactivity with reactive oxygen species (ROS), addition reactions, degradation and formation of nanoconjugates and formulations ^[30,-32].

3. Importance of present investigation

The pharmacological safety and efficacy of curcumin makes it a potential compound for treatment and prevention of a wide variety of human diseases. Unfortunately, its clinical application is restricted by its poor solubility in water, light sensitivity, low absorption and bioavailability. The reasons for reduced bioavailability of any agent within the body are low intrinsic activity, poor absorption, high rate of metabolism, inactivity of metabolic products and/or rapid elimination and clearance from the body^[33]. Studies over the past three decades related to absorption, distribution, metabolism and excretion of curcumin have revealed poor absorption and rapid metabolism of curcumin that severely curtails its bioavailability. Problems of curcumin bioavailability such as low serum levels, limited tissue distribution, apparent rapid metabolism and short half-life are to be modified to enhance its bioavailability and potential as a drug^[34].

Adjuvants, which can block metabolic pathways of curcumin, are one of the major means that are being used to improve its bioavailability. Nanoparticles, liposomes, micelles, use of absorption factors (e.g. piperidine/piperine), the encapsulation of curcumin in the cavities of cyclodextrins, and phospholipid complexes are other promising novel formulations, which appear to provide longer circulation, better permeability, and resistance to metabolic processes^[35].

The chemical structure of curcumin plays a pivotal role in its biological activity. It has three important functionalities: an aromatic o-methoxy phenolic group, α , β -unsaturated β -diketo moiety and a seven carbon linker. Research in the last two decades has provided evidence for the role of these different functional groups in its crucial biological activities. The o-methoxy phenol group and methylenic hydrogen are responsible for the antioxidant activity of curcumin, and curcumin donates an electron/ hydrogen atom to reactive

oxygen species. Curcumin interacts with a number of biomolecules through non-covalent and covalent binding. The hydrogen bonding and hydrophobicity of curcumin, arising from the aromatic and tautomeric structures along with the flexibility of the linker group are responsible for the non-covalent interactions^[36].

The β -diketo group forms chelates with transition metals, thereby reducing the metal induced toxicity and some of the metal complexes exhibit improved antitumor activity. In order to enhance the biological properties and antitumor activity of curcumin, a large number of curcumin derivatives and analogues have been designed and synthesized through structural modifications such as variation of the aromatic rings and their substituents or replacing the heptadione bridge chain of curcumin and other linkers. Numerous studies dealing with the enhanced biological activity of curcumin derivatives and/or analogues can be found in the literature^[37, 38].

Another strategy to improve the biological activity of curcumin was to chelate it with metals. The presence of enolisable β -diketo group in a curcumin molecule makes it an excellent ligand for metal chelation. Several metal chelates of curcumin are reported to possess biological activity over that of free curcumin^[39]. The past 10 years have witnessed a dramatic increase in studies directed to the synthesis, characterization and biological investigation of metal curcumin complexes. Highly promising results with metal curcumin complexes have also been reported in the fields of antiarthritic/antirheumatic activity, antimicrobial/antifungal activity, anti-viral/anti-HIV activity and biological imaging/radio imaging^[40]. Copper complexes of curcumin and its derivatives were found to be better antitumor agents than were the parent compounds^[41].

Clinical trials are ongoing to test the efficacy of curcumin against a large number of diseases. Intense research is also being undertaken to modify

the structure of curcumin so as to increase the bioavailability and potency while maintaining the relative non-toxic nature of this natural product. Synthesis of compounds structurally related to curcumin by new methods or by reported methods with varying structural features not encountered in natural sources is an active area of research and such studies developed a large number of products with greater beneficial properties than curcumin. Recently there is a surge of activity on preparation and characterization of curcumin-metal complexes due to the strong affinity of β -diketo moiety as an efficient metal chelator. Although it is confirmed that curcumin reduces metal toxicity in living systems through complexation, the actual role of these metal complexes in curcumin biology appears to be complex and unclear. Detailed research is warranted on structure-activity evaluation of the curcumin-metal-complexes in solution^[42,43].

4. Description of research problem

We are interested in the development of novel curcumin analogues with improved biological profiles. In our studies, the seven carbon linker in the structure of curcumin molecule is modified by incorporating a cyclopentane ring to the enolizable β -diketone moiety. The reported synthesis of curcumin involves a condensation reaction with appropriate aromatic aldehyde and acetylacetone in its boron chelate form to avoid side reactions at the active methylene group^[44]. Most of these methods are time consuming and tedious. In the present investigation, we used conventional reaction under microwave to synthesise these compounds.

Numerous microwave-assisted aldol condensations have been reported but the use of microwave energy in carrying out boron-assisted regioselective aldol condensation was less found in literature. Owing to the simplicity, rapidity, turnover and environment friendliness, use of microwave in organic synthesis has become very popular. Since the reported procedure for synthesis

of analogues of curcumin involved heating conditions, it appeared logical to attempt their synthesis under microwave irradiation conditions. Moderate to excellent yields of the desired compounds were obtained when the reaction mixture was irradiated with microwaves for 3 minutes. It should be noted that the reactions were carried out in a conventional microwave oven and these reactions were qualitatively reproducible.

In the present investigation, the basic curcumin ligand system is modified and a series of unsymmetrical curcumin analogues were synthesized. The modification of the curcumin skeleton included both incorporation of a cyclopentane ring to the enolizable β -diketone moiety which is common to all ligands and a deviation in the nature and position of phenyl substituent, as well as replacing phenyl ring with hetero aryl and naphthyl / substituted naphthyl rings. Copper (II), nickel(II) and zinc(II) complexes of all these ligands were also synthesised. The ligands and their metal complexes were characterized by various physico-chemical methods including electronic, IR, ^1H NMR, ^{13}C NMR and mass spectral studies. The ligands were found to be existing in their enolic form and the metal complexes have 1:2 metal ligand stoichiometry.

In view of reported biological activities of curcumin, the possible antioxidant, antitumor and DNA binding properties of both free ligands and their complexes were carried out by standard methods. The results obtained were compared with curcumin reported in the literature. The antioxidant activity of ligands and their metal complexes were studied by measuring DPPH radical scavenging, super oxide radical scavenging, lipid peroxidation inhibitory and hydroxyl radical scavenging activities.

The DNA binding properties with calf thymus (CT) DNA were studied by recording the absorption spectra of the compounds in the absence and presence of CT-DNA, fluorescent quenching studies with ET (Ethidium bromide)-bound CT DNA and by viscosity methods. *In vitro* cytotoxicity studies were carried out using Dalton's lymphoma ascites (DLA) cell lines.

For evaluating *in vivo* cytotoxicity, DLA was maintained as ascites tumours in female Swiss albino mice. The effect of compounds on DLA cell induced solid tumour model was also carried out.

REVIEW OF LITERATURE

1. Turmeric

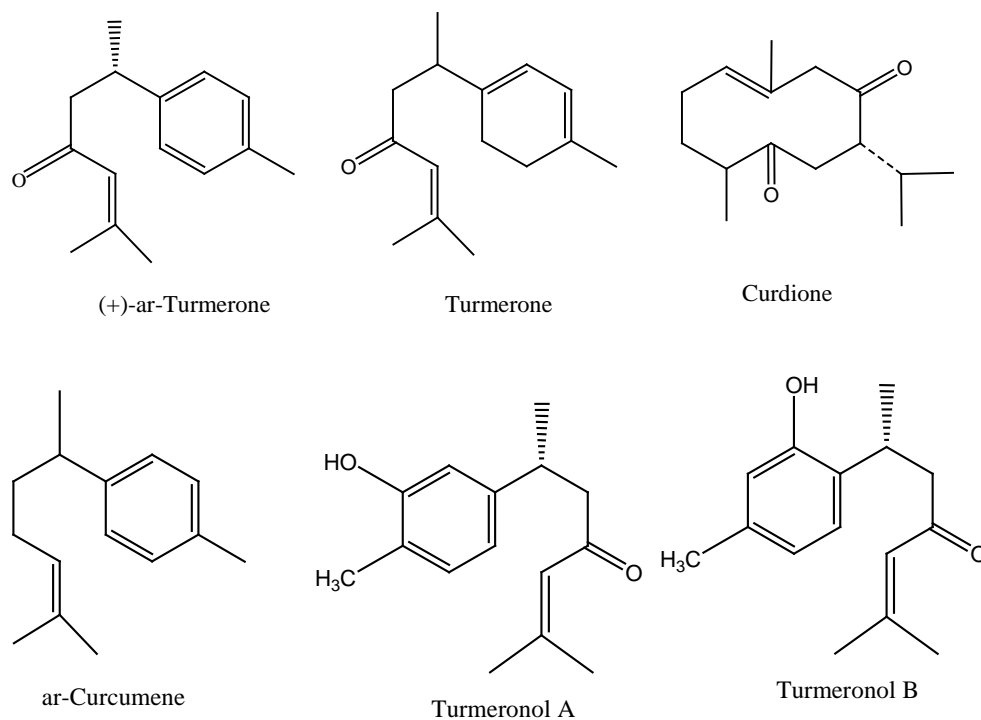
Turmeric (*Curcuma longa L*) is a dietary spice, frequently used in Asian cooking. Turmeric is of special importance to humans with the discovery that its rhizome powder, when added to various food preparations, preserves their freshness and imparts a characteristic flavour and colour^[45]. It is used as a household remedy for various skin infections and dietary problems since ancient times. In *Ayurveda*, turmeric has been used internally as a stomachic, tonic and blood purifier and externally in the prevention and treatment of skin diseases. Traditional Indian medicinal systems claim the use of its rhizome against biliary disorders, anorexia, coryza, cough, diabetic wounds, hepatic disorder, rheumatism and sinusitis^[46]. Modern interest in turmeric began in 1970's when researchers found evidence suggesting that the herb may possess anti-inflammatory properties and anticancer properties. Products isolated from turmeric showed a strong antioxidant action when tested on the model systems like oxidation of linoleic acid and in vitro peroxidation of brain lipids. A large number of reports and several reviews have appeared on the chemistry, processing and technology of turmeric^[47-49].

2. Composition of turmeric oil

The aroma of turmeric is due to its volatile oil, while the phenolic compounds and its analogues account for its bright yellow colour. Due to its lower commercial importance, the chemistry of turmeric oil has not received much attention earlier. Kelkar and Sanjeev Rao reported that steam distilled volatile oil is predominantly a mixture of sesquiterpene ketones and alcohols^[50]. Malingre reported p-cymene, β -sesquiphellandrene, turmerone, ar-turmerone and sesquiterpene alcohols from *Curcuma longa*^[45]. Chen, Yu and Fangy compared composition of the volatile oils of rhizome and tuber of *Curcuma longa* of Chinese origin. Turmerone (24%), ar-turmerone (8.4%) and

curdione (11.58%) are found to be the major compounds in both the oils. However, ar-curcumene was found in rhizome oil to the extent of 12.2%, but it was not reported in tuber oil^[45].

Kiso, Suzuki, Oshima, and Hikino isolated a new oxygenated sesquiterpene, curlone, from aqueous ethanolic extract of *Curcuma longa* rhizomes^[51]. There was considerable quantitative variation in the main components depending upon the cultivars from which the oil was produced. Cooray, Jansz, Ranatunga, and Wimalasena examined the effect of maturity on the major components of the rhizome oil produced from a single turmeric cultivar grown in Sri Lanka, and it was reported that ar-turmerone (24.7–48.9%) and turmerone (20–39%) are the major compounds^[52]. Imai, Morikiyo, Furihata, Hayakawa, and Seto reported the two new sesquiterpene keto-alcohols viz. turmeronol A and turmeronol B from the dried rhizomes of *C. longa*^[53]. The phytochemicals isolated from turmeric oil are given in **Figure 1**.



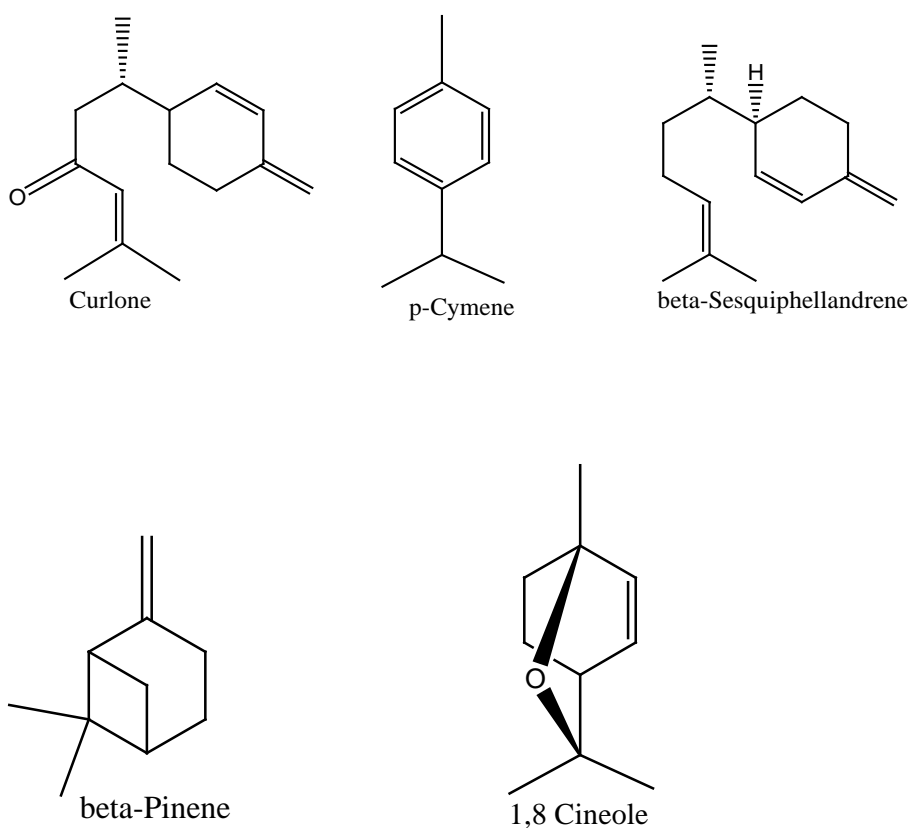


Figure 1. Phytochemicals isolated from turmeric oil.

3. Isolation of curcumin

The colouring principle of turmeric was first isolated in 1815 by Vogel and Pelletier and was named as curcumin^[54]. Curcuminoids refer to a group of phenolic compounds present in turmeric, which are chemically related to its principal ingredient curcumin. Three curcuminoids were isolated from turmeric viz., curcumin, demethoxy curcumin and bisdemethoxy curcumin (**Figure 4, Section I**). All three impart the hallmark yellow pigmentation to its rhizomes. Although the chemical structure of curcumin was determined in 1910, the potential uses of curcuminoids in medicine have been studied extensively from 1970s onwards. These studies increased interest in the isolation of curcumin and several new methods and techniques were applied to isolate curcumin from the rhizomes of turmeric^[55].

Because curcumin is nearly insoluble in water, most of these methods make use an organic solvent for its isolation. Sastry reported the isolation of curcumin and related demethoxy compounds from turmeric by extraction with organic solvents. The drawback was low recovery of the curcuminoids (1.5–2.0%)^[56]. Krishnamurthy, Mathew and Nambudiri reported the hot and cold percolation extraction methods with good yields with a high recovery of curcumin^[57]. Stransky reported that curcumin was isolated from the rhizome by the action of soap solution at 60–90°C. However, curcumin obtained by this method was found to be a paste, and keeping the solution at alkaline pH at higher temperature may bring structural changes^[45]. Tonnesen, Karlsen and Aghikary reported the isolation of curcumin by its insoluble lead salt^[45].

Recently, Baumann, Rodrigues, and Viana have claimed efficient extraction of curcuminoids using supercritical CO₂^[58]. Although supercritical fluid extraction is known to be a clean technology giving acceptable yields and purity, its major disadvantage lies in its high operating pressures. The scale up problems could also be severe when the extraction is to be done at large scales.

Dandekar and Gaikar reported microwave assisted extraction (MAE) technique for selective and rapid extraction of curcuminoids^[59]. Turmeric powder was irradiated for 2 and 4 min with microwave showed marginally higher extraction of curcuminoids. Sodium cumenesulfonate was reported to be an efficient hydrotrope for the extraction of curcuminoids.

In 2000, Anderson, Mitchell, and Mohan reported a technique for isolating curcumin from ground turmeric^[22,60]. They magnetically stirred the ground turmeric in dichloromethane and heated at reflux for 1 h. The mixture was suction-filtered, and the filtrate was concentrated in a hot-water bath maintained at 50 °C. The reddish–yellow oily residue was triturated with hexane, and the resulting solid was collected by suction filtration. Further TLC analysis (3% methanol–97% dichloromethane) showed the presence of all three

components. Preparative TLC with the crude curcuminoids gives pure curcumin.

Isolation of pure curcumin from plant material is time consuming and pure curcumin sold on the market is therefore, a purified extract containing a mixture of the three curcuminoids i.e. curcumin (75–81%), demethoxy curcumin (15–19%) and bisdemethoxy curcumin (2–6%). Now numerous companies like Sigma-Aldrich Chemicals are marketing curcumin commercially with purity up to 94%.

4. Structural characteristics of curcumin

The chemical structure of curcumin was established in 1910 by Miłobedzka, von Kostanecki and Lampe^[55]. On boiling with alkali, curcumin gave vanillic acid and ferulic acids whose structures were established. Fusion with alkali yielded protocatechuic acid and oxidation with potassium permanganate yielded vanillin. On hydrogenation, mixtures of hexahydro- and tetrahydroderivative were obtained. Based on degradative studies, these authors clearly established the identity of curcumin as diferuloylmethane or 1,7-bis(4-hydroxy-3-methoxyphenyl)-1,6-heptadiene-3,5-dione^[61].

Like acetylacetone, curcumin displays typical keto–enol tautomerism (**Figure 2**). However, unlike acetylacetone, the central beta-diketone functionality is flanked by the sterically demanding unsaturated phenolic groups, which results in an unusually wide and flat beta-diketonate ligand. Thus the overall shape of curcumin ligands with the two large wings attached to the beta-diketone unit may be compared to that of an eagle^[62].

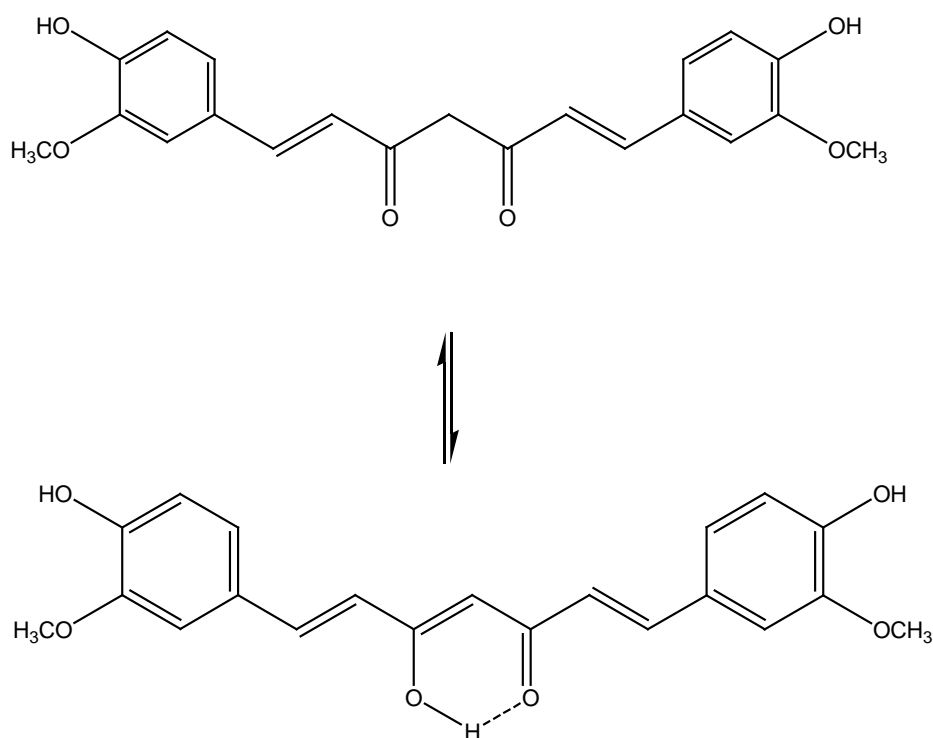


Figure 2. Tautomers of curcumin

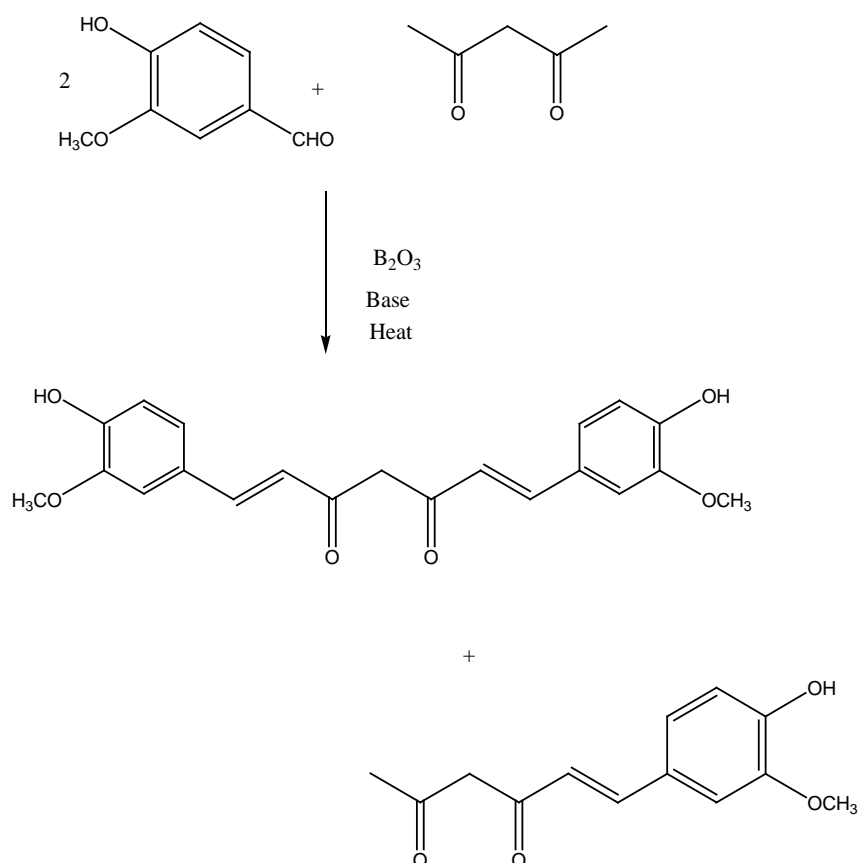
Tonnesen, Karlsen and Mostad reported the three dimensional molecular structure of curcumin from X-ray crystallographic studies^[63]. The single crystal xrd data suggest that in solid state curcumin entirely exist in the intramolecularly hydrogen bonded enol form with trans orientation of the alkenyl groups. In solution it exists as *cis-trans* isomers where the *trans*-form in which the two phenolic-methoxy groups are on the opposite sides of the curcumin backbone is slightly more stabilized than the *cis*-form^[64].

5. Synthesis of curcumin

A century after its isolation from turmeric, the first paper on synthesis of curcumin was reported by Lampe in 1918. The method involved five steps starting from carbomethoxy feruloyl chloride and ethyl acetoacetate^[65]. Later, Pabon reported a simple method for the synthesis of curcumin in high yields using acetyl acetone and substituted aromatic aldehydes in the presence of boron trioxide (B₂O₃), trialkyl borate and *n*-butylamine^[44] and with slight

modifications this method by Pabon has been adopted by several research groups for practically all subsequent curcumin syntheses. Along with the biscondensation product (major product), monocondensation product is also formed in these methods (**Scheme 1**). The desired biscondensation product can be separated by column chromatography^[44].

There are some patents indicating utilization of B₂O₃, trialkylborate and *n*-butylamine along with inert organic solvents to improve the yields. Attempts to replace boric oxide with boric acid did not prove to be successful. Rao and Sudheer proposed the use of trifluoroboronite and produced stable curcuminoid trifluoroboronites that can be hydrolysed in aqueous methanol at pH 5.8 to get curcumin^[66]. In all these methods the primary step is the reaction of acetylacetone with suitably substituted aromatic aldehydes. To prevent participation of the diketone in Knoevenagel condensations, it is complexed with boron. Anhydrous conditions and polar aprotic solvents, where curcumin can be separated easily from the reaction mixtures, are suitable for these reactions. Primary and secondary amines are used as catalysts to provide the necessary basicity to deprotonate the alkyl groups of the diketone. To remove the water produced during the condensation reaction scavengers like alkyl borates are employed. Unless removed, the water can react with the diketone complex, thereby reducing the curcumin yield. The boron complex dissociates into curcumin under slightly acidic conditions. Curcumin from this reaction mixture can be separated by repeated precipitation followed by column chromatography^[44].



Scheme 1. Synthesis of curcumin

6. Reactivity of curcumin

Important chemical reactions associated with the biological activity of curcumin are the hydrogen donation reactions leading to oxidation of curcumin, nucleophilic addition (Michael reaction) reactions, hydrolysis, degradation and enzymatic reactions. All these have significant role in different biological activities of curcumin.

Reactions with ROS

Curcumin has been found to be an excellent scavenger of most reactive oxygen species (ROS), a property that bestows curcumin with antioxidant activity in normal cells. ROS consists of both free radical oxidants and molecular oxidants. Free radical oxidants participate in hydrogen abstraction and also in electron transfer reactions. All three active sites of curcumin can undergo oxidation by electron transfer and hydrogen abstraction. Detailed

investigations by different groups have confirmed that during free radical reactions, the most easily abstractable hydrogen from curcumin is from the phenol-OH group, resulting in formation of phenoxy radicals, which are resonance stabilized across the keto-enol structure^[67-69]. The reaction of peroxy radicals with curcumin produces curcumin phenoxy radicals, which are less reactive than the peroxy radicals and thereby cause protection from ROS-induced oxidative stress. The regeneration reaction of phenoxy radicals back to curcumin by water soluble antioxidants like ascorbic acid, impart the molecule with a chain breaking antioxidant ability like vitamin E. Scavenging reactions of several other free radical ROS such as hydroxyl radicals, superoxide radicals and alkoxy radicals by curcumin has been reported^[70,71].

Among the molecular oxidants, reactions with peroxynitrite, hydrogen peroxide are the most common ones. In several biological models curcumin has been found to protect cells under conditions where there is excessive production of these molecular oxidants^[72]. However, there are not many studies elucidating the possible chemical reactions and identification of the reaction products. There are few reports in the literature on direct reaction of curcumin with peroxynitrite. The rate constants and the inhibition concentrations of curcumin to prevent nitrotyrosine formation indicate that curcumin is as powerful antioxidant against peroxynitrite-induced oxidative stress^[73].

Curcumin was found to be an effective antioxidant in different *in vitro* assays including: reducing power, DPPH[•] (2,2-diphenyl-1-picrylhydrazyl), ABTS^{•+} (2,2'-azino-bis(3-ethylbenzothiazoline-6-sulphonic acid) and O₂^{•-} radical scavenging, hydrogen peroxide scavenging and metal chelating activities^[74]. Curcumin also showed strong antioxidant activity in different *in vivo* assays like AAPH (2,2'-azobis(2-amidinopropane) dihydrochloride) induced hemolysis in erythrocytes and inhibition of erythrocyte lipid peroxidation^[75]. Studies on the ability of curcumin to inhibit lipid peroxidation in a variety of models such as rat brain homogenates, rat liver microsomes,

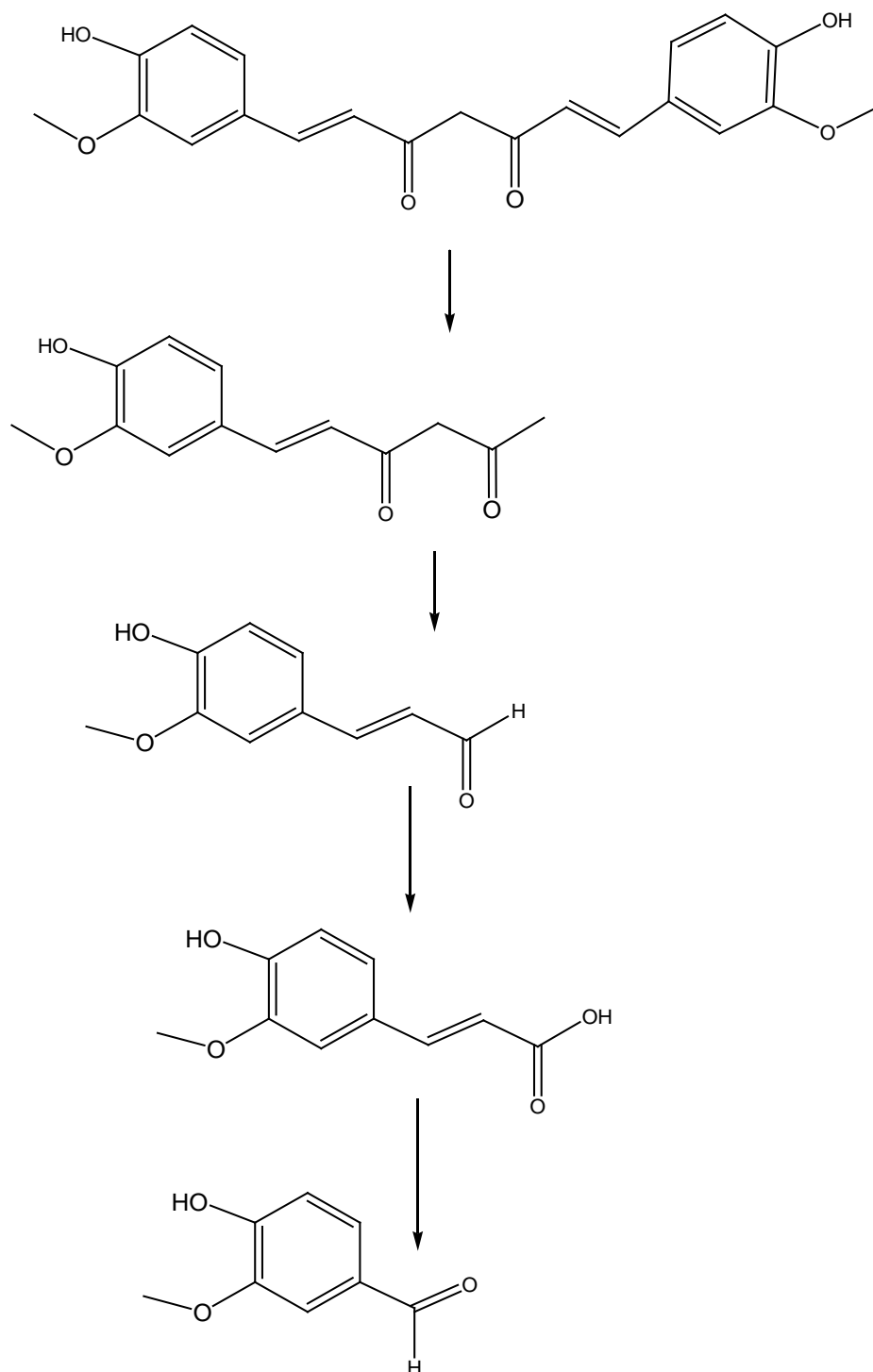
erythrocytes, liposomes, and macrophages provoked a number of recent studies of the antioxidant mechanisms by which the curcuminoids exert their activity, in an attempt to correlate activity with structural features of the molecule. The primary basis for the activity is believed to be the ability of the curcuminoids to scavenge free radicals *in vivo*, especially peroxy radicals of the form ROO^\bullet , where R is an alkyl group^[76]. Reactive radical scavenging and antioxidant activity of curcumin was interpreted as originating by H-atom abstraction from the free hydroxyl group. The phenolic group is essential for the free radical scavenging activity and that the presence of the methoxy group further increased the activity. The transient absorption at 490–500 nm, which they took to be the evidence of phenoxy radicals, and believed that these radicals were formed by a single-electron transfer (SET) mechanism in aqueous-organic solutions^[77].

In order to explain the radical scavenging property of curcumin analogues lacking both phenolic and methoxy groups, another mechanism is proposed involving H-atom transfer (HAT) from a methylene C–H bond (*i.e.*, between the diketo group)^[78]. This was in part deduced by attributing the transient peak at 490 nm to be that arising from a carbon-centered radical. Loss of a methylenic hydrogen will also cause a fully conjugated chain resulting in stabilization of the carbon-centred radical. The reactivity of curcumin and hence its efficiency as an antioxidant depends on the nature of the free radical which it encounters, as well as the mechanism (HAT or SET) by which it deactivates the free radical^[79].

Chemical degradation and metabolism

Curcumin undergoes chemical degradation in aqueous-organic solutions and the degradation increases as the pH is increased, which is of a serious concern in its applications. Most phenols in solution form polymers over time, but the degradation of curcumin is not through the phenolic group but is rather found to be through the α,β -unsaturated β -diketo moiety^[80]. In dilute solutions (*i.e.*, in micromolar solutions) 90% curcumin degrades in 30

minutes. However the percentage degradation will decrease at high concentrations. Several products like feruloylmethane, ferulic aldehyde, ferulic acid, and vanillin were identified (**Scheme 2**) from a suspension of curcumin in aqueous basic medium at pH=9^[81].

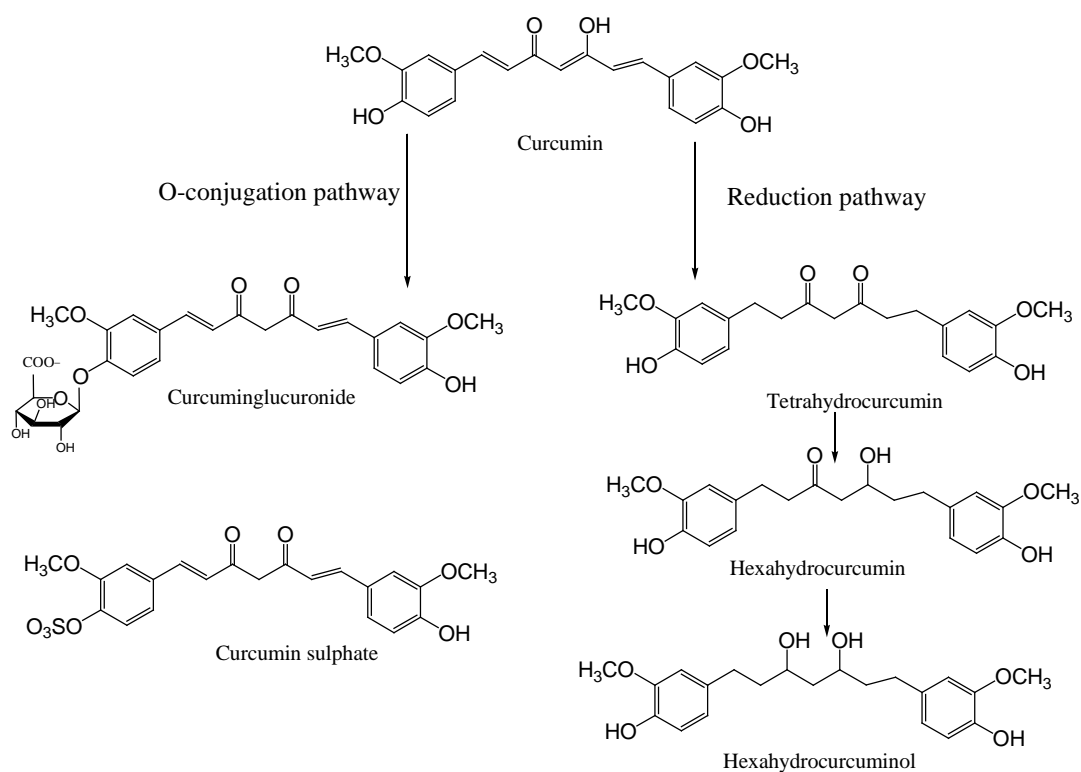


Scheme 2. Chemical degradation of curcumin

Although not fully understood, it is believed that the degradation is by hydrolysis through the diketo moiety. However the degradation is significantly decreased when curcumin is attached to lipids, liposomes, albumins, cyclodextrin, surfactants, polymers and many other macromolecular and microheterogenous systems^[82]. Thus has been found to be of great use that stable curcumin solutions could be prepared in culture medium containing 10% Fetal Bovine Serum (FBS) and also in human blood^[83].

Curcumin undergoes much faster degradation when exposed to sunlight. It is one common observation that curcumin/turmeric stains can be quickly removed on exposure to sunlight. The colourless products identified during photo degradation of curcumin are vanillin, ferullic acid, and other small phenols, indicating a similar product distribution during photochemical degradation as in chemical degradation in solution^[83,84]. This photo degradation involves formation of the excited states of curcumin. The photo degradation is accelerated in presence of TiO₂ nanoparticles, and this method can be employed to remove turmeric stains from cotton fabrics^[85].

The metabolism of curcumin in rats and humans produces different products. Two major pathways have been identified in curcumin metabolism, like O-conjugation and reduction. The O-conjugation products are curcumin glucuronide and curcumin sulfate. The reduction products are tetrahydrocurcumin, hexahydrocurcumin and octahydrocurcumin. Other minor products are dihydrocurcumin glucuronide, tetrahydrocurcumin glucuronide, ferulic acid and dihydroferulic acid^[86,87]. The formation of these products has been confirmed by HPLC and mass spectrometry. Although it has been reported that these processes occur enzymatically, the exact enzymes involved are not yet established. Sulphonation of curcumin through human phenol sulfur transferase enzymes and the formation of reduction products through alcohol dehydrogenase is the one that is widely accepted.



Scheme 3. Metabolic products of curcumin

Comparing these metabolic products (**Scheme 3**) with the degradation products (**Scheme 2**), it appears that simple hydrolytic degradation is prevented in biofluids. Since the degradation may occur through the β -diketo structure, one can presume that in these systems curcumin is not in free form but rather in conjugated form bound to some proteins or other biomolecules, and as the diketo moiety is involved in binding to the proteins, it is not available for hydrolytic degradation^[88]. It may also be implied that the specific enzymatic reactions are probably much faster and do not allow the slow hydrolytic degradation, therefore the latter process cannot compete with the former reaction. This leaves a bigger challenge for chemists to understand the differences between degradation and metabolic reactions in terms of kinetic parameters and also identify the crucial mechanism in these reactions^[28].

Nucleophilic addition reactions of curcumin

The α,β -unsaturated β -diketo moiety of curcumin participates in nucleophilic addition reactions. This reaction, known as the Michael addition,

occurs between the unsaturated ketone as an acceptor and anions of $-\text{OH}$, $-\text{SH}$, $-\text{SeH}$ as donors^[28,88-90]. It is a 1,4-addition reaction and the resultant product formations are mostly irreversible, but they can be made reversible under oxidizing and basic conditions. Since the anions only act as nucleophiles, pH conditions are very important for this reaction to take place. At physiological pH both $-\text{OH}$ and $-\text{SH}$ are protonated but $-\text{SeH}$ can easily undergo deprotonation, therefore it acts as a better nucleophile. This reaction has been reported to be extremely useful to explain the biological chemistry of curcumin in living cells^[91, 92].

Reaction of curcumin with biological thiols like glutathione having $-\text{SH}$ groups, is of special interest in explaining its bioactivities. A similar reaction has been observed during the inhibition of thioredoxin reductase by curcumin. Thioredoxin reductase is a crucial enzyme involved in maintaining cellular redox homeostasis. The active centre in this enzyme is selenocysteine. The selenol of selenocysteine, being a stronger nucleophile at physiological pH, easily undergoes 1,4-addition with curcumin, forming covalently bonded species. This reaction is speculated to be mainly responsible for the effective inhibition of the thioredoxin reductase enzyme by curcumin. The methylenic hydrogen of the diketo/enol moiety of curcumin can also act as a nucleophile and participate in Michael addition reactions with stronger electrophiles, but such reactions may not have significance in biological systems^[93].

Chemistry of curcumin-metal ion interactions

Curcumin forms coloured complexes with boron in presence of dicarboxylic acids like oxalic acid and these reactions are employed for the spectrophotometric estimation of boron as well as oxalic acid^[94]. In addition to boron, curcumin forms stable complexes with a range of metals and metalloids. The α,β -unsaturated β -diketo moiety of curcumin displays typical keto–enol tautomerism (**Figure 2**) and hence curcumin can function as an excellent chelating agent. In the last two decades, many papers and three excellent reviews have been published on metal-curcumin complexes^[47-49].

Metal complexation property of curcumin can lower metal induced toxicity. Metal complexes of curcumin have greater significance in view of the pathology of Alzheimer's disease, where it has been found that due to its lipophilic nature, curcumin can cross the blood brain barrier and chelate metal ions that are toxic to the neurons. It has also been observed that the incidence of Alzheimer's disease is significantly reduced among people that are known to regularly consume turmeric in their diet. Curcumin forms stable complexes with all the metals involved in Alzheimer's disease ^[95-98].

Metal coordination of curcumin occurs through the enolic group, where the enolic proton is replaced by the metal ion and the *o*-methoxy phenolic moiety remains intact in the complexes. The metal-oxygen bond is characterized by IR absorption at $\sim 455\text{ cm}^{-1}$ corresponding to $\nu_{(\text{C-O})}$ and the carbonyl peaks in the complexes show a small shift of $\sim 10\text{-}20\text{ cm}^{-1}$ on coordination to metals. Changes in NMR chemical shifts of curcumin have also been reported on metal coordination. The shifts however depend on the affinity and thermodynamic stability of the resulting complexes. In the case of strong complexes, the resonances of protons attached to the double bonds of the alkyl chain show significant downfield shifts, while the phenolic protons show negligible shifts in the $^1\text{H-NMR}$ spectra, and the $^{13}\text{C-NMR}$ spectrum shows down- and up-field shifts of carbons near the coordination site ^[69].

Typical structure of curcumin complex with a divalent metal ion is given in **Figure 3**

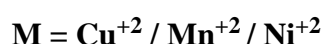
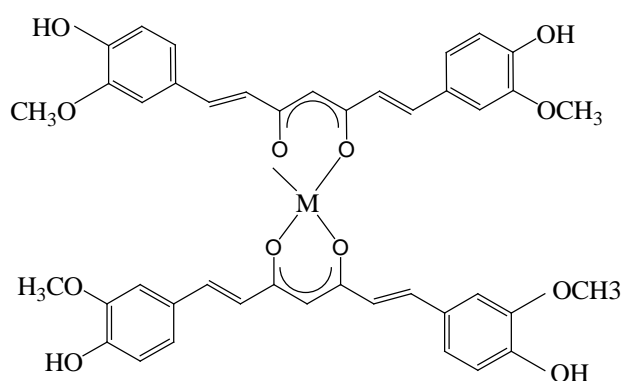


Figure 3. Curcumin complex with divalent metal ions

A variety of metal ions can be complexed by the β -diketo-moiety of curcumin. The metal complexes so formed often possess a higher stability than the easily degraded curcumin itself. The first complexes of curcumin with medically valuable transition metals, such as Pd, Pt, Rh, and In, were published in 1997^[99]. In most cases the resulting complexes exhibited favorable biological activity compared with the parent ligands for a number of molecular targets^[100].

There are several papers published in the literature on complexes of curcumin with transition metals like Fe^{3+} , Mn^{2+} , Ni^{2+} , Cu^{2+} , Zn^{2+} , Pb^{2+} , Cd^{2+} , Ru^{3+} , Re^{+3} and many others. Complexes with non-transition metal ions and rare earth ions like Al^{3+} , Ga^{3+} , Sm^{3+} , Eu^{3+} , Dy^{3+} , Y^{3+} , Se^{2+} and metal oxides like VO^{2+} have also been synthesized. The structure and physical properties of these complexes depend on the nature of the metal ion, as well as the metal-ligand stoichiometry, which in turn decides their stability and reactivity^[101].

Stable 2:1 complexes of some transition metals can be prepared by mixing stoichiometric amounts of curcumin and metal salts in suitable organic solvents and refluxing for few hours, the complex can be separated as a precipitate, and purified by repeated crystallization^[102,103].

7. Biological activities of curcumin

The biological characteristics of curcumin were scientifically identified in the mid-twentieth century. In a paper published in *Nature* in 1949, Schraufstatter and co-workers reported that curcumin is a biologically active compound that has antibacterial properties^[24]. These authors found that curcumin was active against strains of *Staphylococcus aureus*, *Salmonella paratyphi*, *Trichophyton gypseum*, and *Mycobacterium tuberculosis*. However, research on curcumin became quiet for the next two decades. Curcumin again became the subject of scientific investigation in the 1970s. During this decade, three independent groups discovered diverse characteristics of curcumin, including its cholesterol-lowering, antidiabetic, antiinflammatory, and antioxidant activities^[104].

Ghatak and Basu showed that curcumin is more potent than hydrocortisone for inhibiting formalin-induced arthritis in rats and carrageenin-induced rat paw edema^[105]. Later, Srimal and Dhawan reported that curcumin is as potent as cortisone or phenylbutazone for the inhibition of carrageenin-induced rat paw edema. These studies indicate curcumin's potential as an anti-inflammatory agent^[106]. Singh and Aggarwal demonstrated that curcumin exhibits anti-inflammatory activity by suppressing the proinflammatory transcription factor nuclear factor (NF)- κ B and outlined the molecular mechanism of the inhibition^[107]. The anticancer activity of curcumin was demonstrated in the 1980s by Kuttan and colleagues in both *in vitro* and *in vivo* models^[108]. Interest in curcumin research has increased substantially over the years.

As on January 2016, more than 6500 articles on curcumin were listed in the National Institutes of Health PubMed database (www.ncbi.nlm.nih.gov/sites/entrez). The pleiotropic activity of curcumin in animal models of many human diseases is now reported by numerous groups. In human clinical trials, curcumin has been found to be safe and efficacious,

and the U.S. Food and Drug Administration has approved curcumin as a “generally regarded as safe” compound.

Antimicrobial activity

The antimicrobial activity of α,β -unsaturated carbonyl compounds has been recognized generally due to their ability to react with sulfhydryl containing system essential for normal metabolism of microbes. Several studies have reported the broad-spectrum antimicrobial activity for curcumin including antibacterial, antiviral, and antifungal activities. Because of the extended antimicrobial activity of curcumin and safety property even at high doses assessed by clinical trials in human, mixture of curcumin with other antimicrobial agents is used for the development of antimicrobial skin gels and emulsions with improved skin protection and wound dressing properties^[109]

Composition of curcumin with hydrogel silver nanoparticles is used to increase the function of hydrogel silver nanocomposites for antimicrobial applications and wound dressing. Curcumin-loaded myristic acid micro emulsion with the 0.86 $\mu\text{g/mL}$ of curcumin suitable for skin consumption inhibited 50% of the growth of *S. epidermidis*, one of the nosocomial infectious agents. It showed 12-fold stronger inhibitory effect compared to curcumin activity dissolved in DMSO^[110].

Outburst of drug resistant microbial strains necessitates the studies for synergistic effects of antibiotics in combination with plant's derivatives to develop the antimicrobial cock tail with a wider spectrum of activity and reduction of adverse side effects of antimicrobial agents. The synergistic activity of curcuminoids and ampicillin combination demonstrated pronounced reduction in the MIC of ampicillin against clinical strain^[111]. The consumption of turmeric during the treatment of *S. aureus* infections with these antibiotics especially cefixime can be possibly helpful. Curcumin also demonstrated a synergistic effect in combination with some antibiotics, including ampicillin, oxacillin, and norfloxacin against methicillin-resistant *S. Aureus* strain (MRSA). The synergistic effect of curcumin with ciprofloxacin

against MRSA has also been reported, although there is an evidence of its antagonistic activity against *S. typhimurium* in combination with ciprofloxacin [112,113].

Complexes of curcumin with cobalt nanoparticles showed increased antibacterial activity against *E. coli*. Additionally, fabrication of silver nanocomposite films impregnated with curcumin showed the stronger antibacterial activity against *E. coli*^[114]. It was shown that the bactericidal activity of sodium carboxy methyl cellulose silver nanocomposite films (SCMC SNCFs) as an effective antibacterial material was improved by loading of curcumin with SCMC SNCFs^[115]. The novel curcumin encapsulated chitosan-[poly (vinyl alcohol)] silver nanocomposite films with pronounced antimicrobial exhibition against *E. coli* proved to be potential antibacterial material for treating infections or wound dressing^[116].

Lack of effective therapeutics for the most of viral diseases, emergence of antiviral drug resistance, and high cost of some antiviral therapies necessitate finding new effective antiviral compounds. It has been demonstrated that curcumin has a wide range of antiviral activity against different viruses. Inosine monophosphate dehydrogenase (IMPDH) enzyme is suggested as a therapeutic target for antiviral and anticancer compounds^[117] due to its rate-limiting activity in the *de novo* synthesis of guanine nucleotides. In *in vitro* studies, curcumin showed strong inhibitory activity against IMPDH suggesting that it can be a potent antiviral compound via this process. Integrase, an essential enzyme for HIV-1 replication was found to be inhibited by curcumin. The study of energy minimization and the structural analogues of curcumin elicited that an intramolecular stacking of two phenyl rings of curcumin is possibly responsible for anti-integrase activity via bringing the hydroxyl groups into close proximity. The clinical trial of ethanol extract of *C. longa* rhizome on HIV patients reduced the wound infections and considerable decrease in itching symptom and it also affected the abscess to convert to dryness scabs within two weeks^[118]. Curcumin showed the anti-influenza

activity against influenza viruses PR8, H1N1, and H6N1. The results showed more than 90% reduction in virus yield in cell culture in presence of curcumin^[119].

Substances and extracts isolated from plants have always been a rich arsenal for controlling the fungal infections and spoilage. Due to extensive traditional use of turmeric in food products, various researches have been done in order to study the turmeric and curcumin with the aspect of controlling fungal related spoilage and fungal pathogens. The study of addition the turmeric powder in plant tissue culture showed that turmeric at the 0.8 and 1.0 g/L had appreciable inhibitory activity against fungal contaminations^[120]. *In vitro* screening of the antifungal activity with curcumin against *Aspergillus niger*, *Aspergillus flavus*, *Aspergillus heteromorphus* and *Penicillium verruculosum* was reported.

Antioxidant activity of curcuminoids

The oxygen consumption inherent in cell growth leads to the generation of a series of ROS. They are continuously produced by the body's normal use of oxygen such as respiration and some cell-mediated immune functions. ROS include free radicals such as superoxide anion radicals ($O_2^{\cdot-}$), hydroxyl radicals (OH^{\cdot}) and non-free radical species such as hydrogen peroxide (H_2O_2) and singlet oxygen. ROS play a positive role in energy production, phagocytosis and regulation of cell growth, intercellular signalling, and synthesis of biologically important compounds. However, ROS may also be very damaging; they can attack the lipids of cell membranes and DNA. The oxidation induced by ROS can result in cell membrane disintegration, membrane protein damage and DNA mutation, which can further initiate or propagate the development of many diseases. ROS are continuously produced during normal physiologic events and are removed by antioxidant defence mechanisms. It is well known that ROS are closely involved in various human diseases such as Alzheimer's disease, cancer, inflammation, rheumatoid arthritis and atherosclerosis. Excessive production of the free radical NO in the

brain has been shown to induce neurotoxicity. Typical for neurodegenerative diseases is progressive loss of the structure or function of neurons and eventually even the death of neurons^[121].

Thus, antioxidants are considered to be important as neuroprotective agents. It is commonly recognized that antioxidants can neutralize potentially harmful reactive free radicals in body cells before they cause lipid and protein oxidation and may reduce potential mutation and therefore, help prevent cancer or heart diseases. Antioxidants have been widely used as food additives to provide protection against oxidative degradation of foods. Currently, synthetic antioxidants, such as butylated hydroxyanisole (BHA), butylated hydroxytoluene (BHT), and tert-butylhydroquinone (TBHQ) are widely used in the food industry. However, restriction on the synthetic antioxidants is being imposed because of their toxicity to liver and carcinogenicity. Therefore, the development and utilization of more effective antioxidants of natural origins are desired^[122,123]. Curcumin was found to be an effective antioxidant in different *in vitro* assays and *in vivo* assays.

Cytotoxic activities of curcuminoids

Cancer is the leading cause of death in developed countries and the second-largest cause of death in developing countries after cardiovascular diseases. More than 200 types of cancers are known in humans, depending on tissue and cell type. Carcinogenesis is a complex process but may be broadly considered to be comprised of three main phases: initiation, promotion, and progression. These closely related steps: going from a normal cell to a transformed initiated cell (initiation); from initiated to pre-neoplastic cell (promotion); and from preneoplastic to neoplastic (progression). There is suggestive evidence that inflammation may have a role in the three phases of carcinogenesis^[124]. Cancer initiation has been produced by oxidative stress and chronic inflammation. Inflammation acts a key regulator in promotion of these initiated cells, possibly by providing them with proliferating signals and by preventing apoptosis. Inflammatory response produces cytokines which act as

growth and/or angiogenic factors leading transformed cells to proliferate and undergo promotion. The most clinically established cancer treatment strategies are surgery, radiotherapy, and chemotherapy^[125].

The chemotherapeutic approach uses a combination of drugs with various mechanisms of action to enhance the therapeutic efficiency. Currently available monotargeted cancer therapeutics has numerous adverse effects and is expensive. Curcumin is a nontoxic natural product known to exert a wide range of pharmacological activities through its effect on several targets including transcription factors, growth regulators, adhesion molecules, apoptotic genes, angiogenesis regulators and cellular signaling molecules. These multi target interactions of curcumin form the molecular basis of anti-carcinogenic and chemopreventive effects of curcumin^[126].

The anticancer properties include suppression of cellular transformation, prevention of cancer cell proliferation, and suppression of carcinogenic effects. Recent studies have found that curcumin has a dose dependent chemopreventive effect in several animal tumour bioassay systems including colon, duodenal, stomach, esophageal and oral carcinogenesis. It has been shown to reduce tumours induced by benz(a) pyrene and 7, 12-dimethyl benz(a) anthracene, tumor promotion induced by phorbol esters on mouse skin, on carcinogen-induced tumorigenesis in the fore stomach and N-ethyl-N'-nitro-N-nitrosoguanidine-induced duodenal tumours. Curcumin administration during both the initiation and post initiation periods significantly inhibited colon tumorigenesis^[127,128]. In addition, administration of the synthetic curcumin in the diet during the promotion/progression stage significantly suppressed the incidence and multiplicity of noninvasive adenocarcinomas and also strongly inhibited the multiplicity of invasive adenocarcinomas of the colon. Curcumin has been demonstrated to induce apoptosis in a variety of cells including prostate cancer cells^[129].

Curcumin has been reported to possess anticarcinogenic properties in several experimental models. Because of its lack of toxicity, its efficacy in inhibiting tumorigenesis in several models, and its multiple mechanisms of action, curcumin has been selected for further evaluation by different investigators all over the world. In these studies curcumin and its synthetic analogues were screened for numerous cancer types found in humans ^[130]. In vitro and animal studies have revealed that curcumin suppresses carcinogenesis and inhibits the proliferation of a wide variety of tumor cells and modulates growth of tumour cells through regulation of multiple cell signaling pathways including cell proliferation pathway. It blocks transformation, tumour initiation, tumour promotion, invasion, angiogenesis, and metastasis. It has shown to display chemotherapeutic and chemopreventive effects in diverse cancers. It inhibits the cell cycle progression of colon cancer cells ^[131].

Probably the first indication of curcumin's anticancer activities in human participants was shown in 1987 by Kuttan and co-workers, who conducted a clinical trial involving 62 patients with external cancerous lesions. Topical curcumin was found to produce remarkable symptomatic relief as evidenced by reductions in smell, itching, lesion size, and pain. Although the effect continued for several months in many patients, only one patient had an adverse reaction. Since then, curcumin, either alone or in combination with other agents, has demonstrated potential against colorectal cancer, pancreatic cancer, breast cancer, prostate cancer, multiple myeloma, lung cancer, oral cancer, and head and neck squamous cell carcinoma ^[132].

Curcumin has also found to be a potential for the prevention and treatment of colorectal cancer (CRC) in combination with other agents. Curcumin was administered to patients with CRC after diagnosis and before surgery. Curcumin (360 mg in a capsule form) was given three times a day for 10–30 days. Curcumin administration increased body weight, increased the

number of apoptotic cells, and enhanced the expression in tumor tissue. The curcumin treatment can improve the general health of CRC patients^[133].

Curcumin induces cell death in numerous animal and human cell lines, including leukemia, melanoma, and carcinomas of the breast, lung, colon, kidney, ovaries and liver^[134]. Certain data have demonstrated that curcumin exhibits a biphasic action: Low doses lead to oxidative stress and apoptosis, while higher doses lead to reduced production of reactive oxygen species, reduction of ATP and necrotic cell death^[135]. It also appears to be able to cause cell death in various cell lines resistant to apoptosis, possibly by activating cell death mechanisms. Apoptosis is a process of programmed cell death through cell shrinkage, nuclear fragmentation, chromatin condensation, chromosomal DNA fragmentation and global mRNA decay that occurs in multicellular organisms. Necrosis is a form of cell injury which results in the premature death of cells in living tissue by autolysis. It is caused by factors external to the cell or tissue, such as infection, toxins, or trauma which result in the unregulated digestion of cell components.

Anti-Alzheimer's disease activity

Alzheimer's disease is the most common cause of dementia among people of age 65 or older. It appears well established that the gradual loss of brain function characteristic for Alzheimer's disease is connected to two main forms of nerve damage. It has been demonstrated that the incidents of Alzheimer's disease among elderly people of age 70–79 in rural India, who eat curry dishes on a daily basis, is about 4.4 times lower than that of Americans of the same age. Curcumin shows an array of activities that can be helpful in ameliorating Alzheimer disease symptoms acting on various target sites. The therapeutic benefits of curcumin for Alzheimer diseases appear multifactorial via regulation of transcription factors, cytokines and enzymes. It has also been shown to suppress oxidative damage, inflammation, cognitive deficits, and amyloid accumulation in Alzheimer diseases. Furthermore, various *in vivo*

studies have provided supporting evidence for the therapeutic potential of curcumin in Alzheimer diseases. These studies indicate that curcumin probably interferes with the formation of plaques and can therefore improve the disease condition ^[136,137].

The currently available treatments for this disease have numerous adverse effects, thus underscoring the need for alternative approaches. A randomized, double blind, placebo-controlled study was conducted in the United States to evaluate the safety and tolerability of curcumin in patients with mild to moderate Alzheimer's disease. This study included the safety, tolerability, pharmacokinetics, and efficiency of curcumin in patients with Alzheimer's disease, as well as the effects of curcumin on biomarkers associated with the pathology of this disease. It was found that curcumin administration was associated with an increase in vitamin E level, and curcumin did not cause any adverse effects ^[138]. The anti-oxidant activity of curcuminoids might decrease the need for anti-oxidant vitamin E. These observations support the opening of a clinical trial of curcumin against Alzheimer's disease using large numbers of patients ^[139].

Anti-inflammatory effects

Curcumin inhibits cyclooxygenase2 (COX-2) as well as lipoxygenase (LOX), two enzymes involved in inflammation. Indeed, cytokine-induced COX-2 transforms arachidonic acid in prostaglandins during acute inflammatory episodes. COX2 is also prevalent during chronic inflammations ^[140]. Lipoxygenase transforms arachidonic acid in leukotrienes, which take part in leukocytes recruiting and play a role in inflammation. Moreover, curcumin protects keratinocytes and fibroblasts against H₂O₂-induced damages and allows reduction of oxidative and inflammatory stress. Pancreatitis improves after curcumin treatment, which blocks key inflammatory signals. However, by verifying the effect of curcumin in galactose-induced cataract and discovered that small doses of curcumin (0.01%) could increase oxidative stress in hyperglycaemic rats.

Antidiabetic properties

Curcumin has been shown to be effective against diabetes in patients and in experimental animal models. In rats with alloxan-induced diabetes, in streptozotocin (STZ)-induced rats models, and in STZ-nicotinamide-induced rats models, oral administration of various dosages of curcumin was able to prevent loss of body weight; reduce levels of glucose, hemoglobin, and glycosylated hemoglobin in the blood; and improve insulin sensitivity. In rat models of high-fat diet induced insulin resistance and oral administration of curcumin showed an antihyperglycemic effect and improved insulin sensitivity, which was attributed by its anti-inflammatory properties ^[141,142]. Diabetes mellitus is a chronic metabolic disease in which a person has high concentrations of blood sugar. Because of its anti-inflammatory property, curcumin represents a promising therapeutic option for Diabetes mellitus. Curcumin's ability to decrease blood sugar levels in human patients was first reported in 1972. Injection of turmeric or curcumin along with insulin synergistically reduced the blood sugar level ^[143].

Antiarthritic/antirheumatic activity

Arthritis is a chronic disease that results from the inflammation of one or more joints. It usually results from dysregulation of pro-inflammatory cytokines and pro inflammatory enzymes that mediate the production of prostaglandins and leukotrienes, together with the expression of adhesion molecules and matrix metalloproteinases. Although more than 100 different kinds of arthritis have been reported, the three most common forms are osteoarthritis, rheumatoid arthritis, and gout.

The potential of curcumin against arthritis was first reported in 1980 curcumin's efficiency was compared with that of the prescription drug phenylbutazone ^[144]. Patients were randomly assigned to receive either curcumin (1.2 g/day) or phenylbutazone (0.3 g/day) for 2 weeks. Curcumin was well tolerated, had no adverse effects, and exerted an antirheumatic activity identical to that of phenylbutazone as shown by improvement in joint

swelling, morning stiffness, and walking time. Curcumin alone and in combination with diclofenac sodium was found to be safe and effective with rheumatoid arthritis^[145].

The water insolubility and low bioavailability of curcumin in cells have prompted researchers to develop new formulations based on biocompatible organic substances like liposomes, polyethylene glycols, biopolymers, cellulose, corn oil, hydrogels *etc.* All these systems have not only shown improved water solubility but also increased curcumin bioavailability. Interestingly the fluorescence of curcumin gets is enhanced once solubilised in any of these systems, making it easy to estimate its binding efficiency^[146].

Due to their biocompatibility all these systems could be successfully investigated for anti-cancer activity in cancer cells, and *in vivo* systems, where significant increase in the anticancer activity due to improved bioavailability of curcumin was reported. Liposomal curcumin was found to be the best for improving the bioavailability of curcumin in cells and products based on liposomal formulations are being marketed for different dietary applications of curcumin. Till recently the word nanocurcumin referred to curcumin-loaded organic formulations only. Recently, a large number of inorganic nano formulations with application in delivery of curcumin^[146].

Mesoporous silica nanoparticles (MSN) are one of the most employed nanosystems for improving the bioavailability of poorly water soluble drugs. Such systems can be easily manipulated for improved delivery, activity and specificity^[147,148]. Due to their ordered nanoporous structures, high surface areas, large pore volumes and high surface densities of hydroxyl groups, MSNs can be functionalized easily. They are biocompatible and they are commonly used in many biomedical applications. Curcumin binds covalently through a silicon-oxygen bond at the diketo moiety. Curcumin-loaded MSNs have been prepared and employed in several studies. In these systems, curcumin release could be controlled for even up to several hours along with improvement in the stability and bioavailability of curcumin^[149].

The fluorescence of curcumin is enhanced on MSN conjugation and therefore has the potential to be employed for imaging biomolecules/organelles. Novel cyclodextrin functionalized MSN have been found to be photothermally controlled on exposure to light to release curcumin on demand in zebra fish larve. Large amount of curcumin could be loaded in to spherical microcapsules containing L-lysine, trisodiumcitrate and silica sol (colloidal suspension). These microcapsules could be triggered to release curcumin by adjusting the pH to acidic conditions. MSN-curcumin conjugates, increased the cytotoxicity of curcumin in HeLa cell lines (derived from cervical cancer cells) and also in normal fibroblast cell lines. They also increased photocytotoxicity of curcumin in human oral cancer cells, on exposure to light^[150,151].

Gold nanoparticle-based curcumin formulations have been prepared and reported recently. Gold nanoparticles find application in biology and medicine, for drug delivery, diagnosis and cancer treatment. In a simple method, curcumin-gold composites were prepared by mixing alkaline curcumin solutions with gold salts, where the ionized curcumin acts both as a reducing agent and also as the capping agent. In this case, both the phenolic-OH and enolic-OH donate hydrogen for reduction of Au³⁺ ions. Such gold-curcumin conjugates were reported to be hemocompatible and non-toxic^[152].

The spectrum of beneficial biological activities of cucumin reported so far is very wide. Excellent reviews and monographs are available on this subject. Some significant biological activities reported are briefly summarized below (**Figure4**).

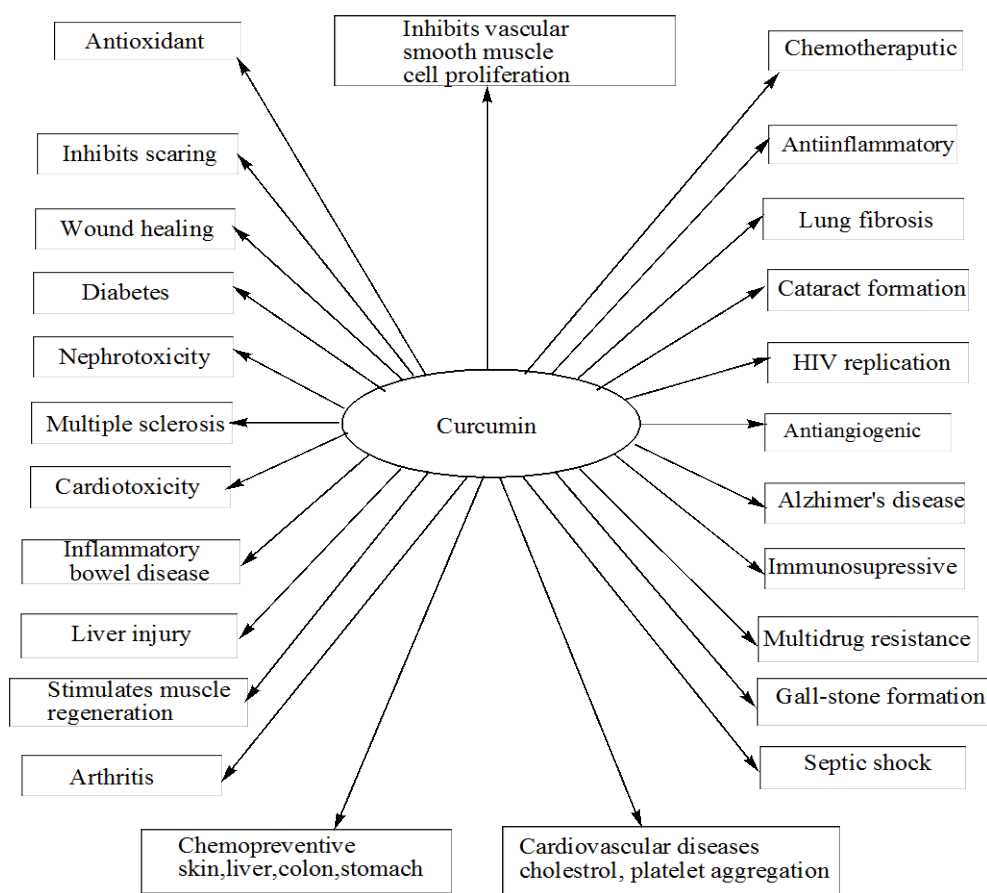
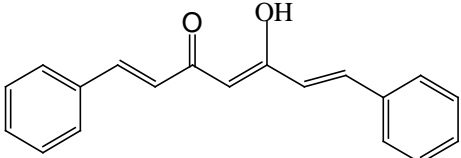
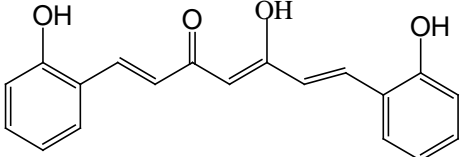
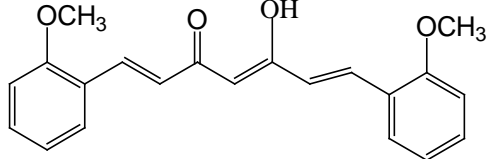
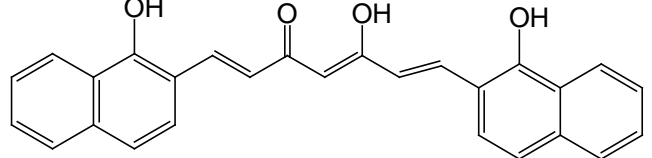
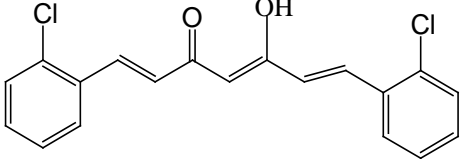
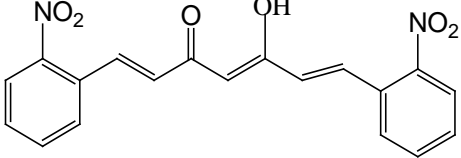
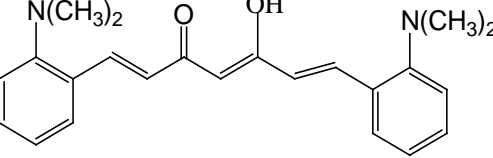
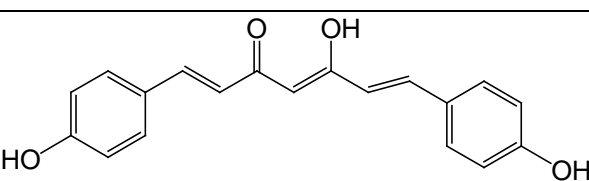


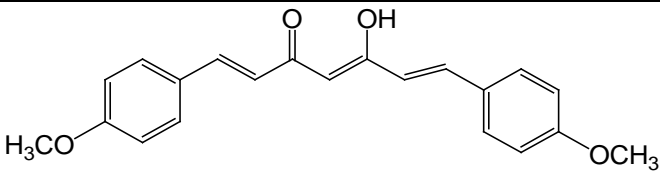
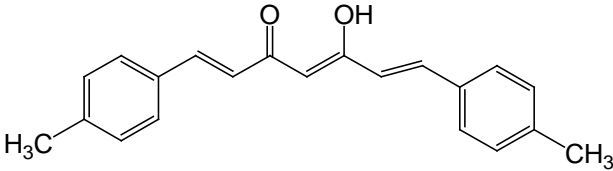
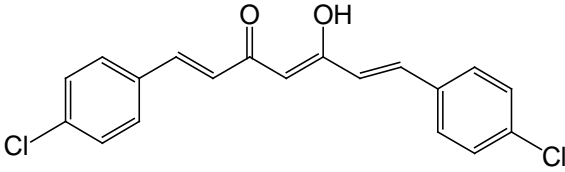
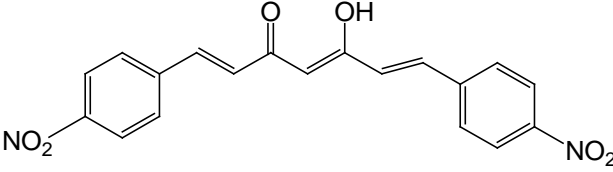
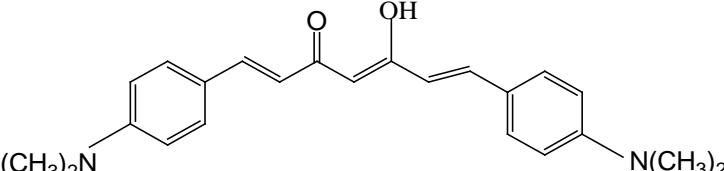
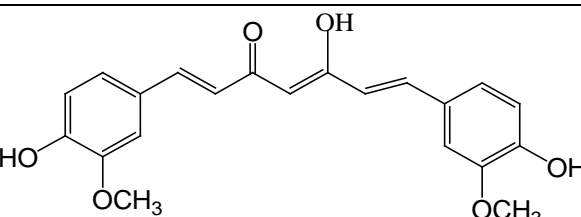
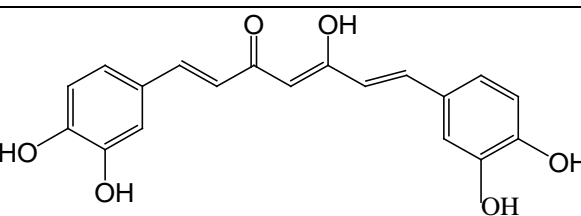
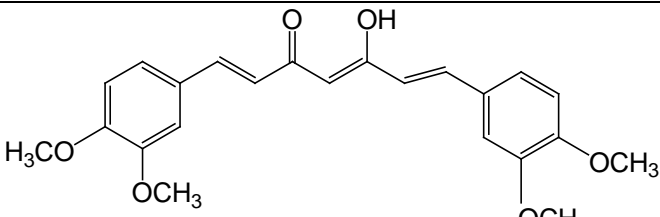
Figure 4. Biological activities of curcumin

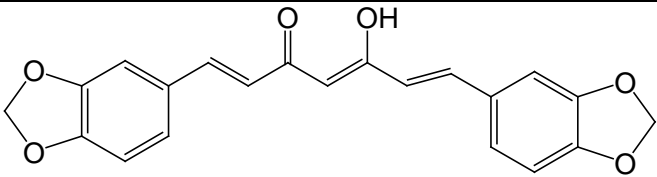
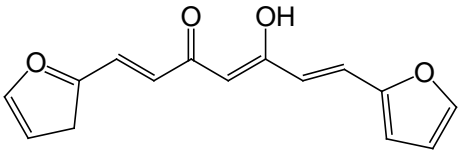
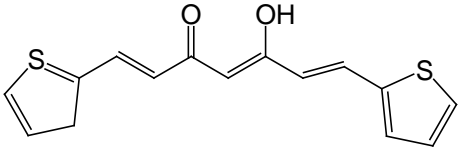
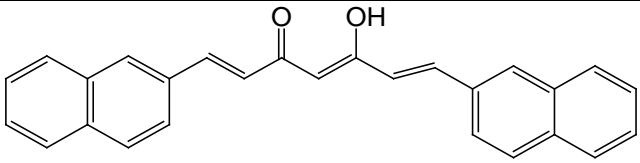
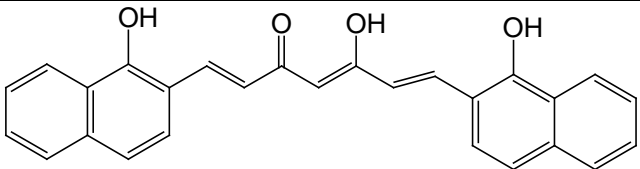
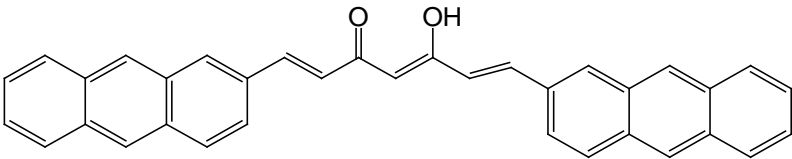
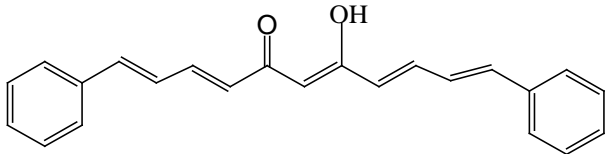
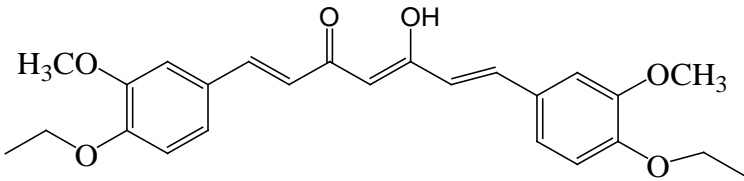
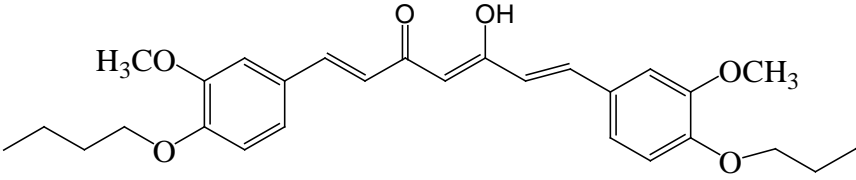
8. Synthetic analogues of curcumin

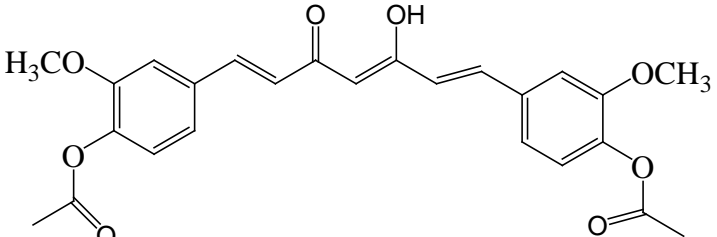
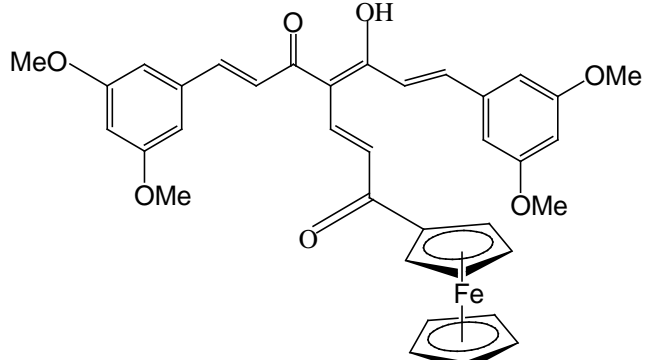
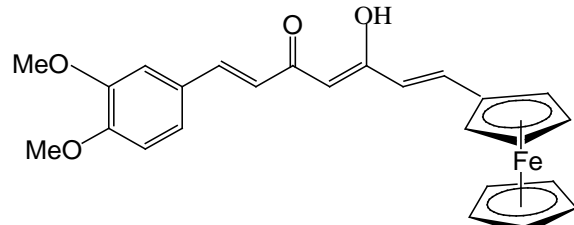
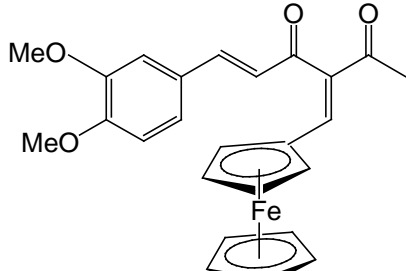
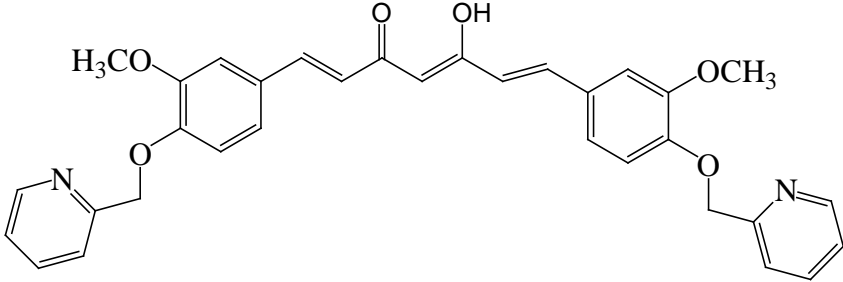
Curcumin is reported to have a large number of beneficial biological activities. Since biological activities are directly related to the molecular structure, structurally related compounds can also be ideal candidate for therapeutic applications. This aspect along with the flexibility in the structure of curcumin with two aryl groups and a seven carbon linker lead to the synthesis of a large number of synthetic analogues of curcumin with a variation in the aryl substituents / aryl rings. A large number of such compounds are reported in the past two decades (**Table 2**). Biological screening with some of these compounds and their metal derivatives gave promising results.

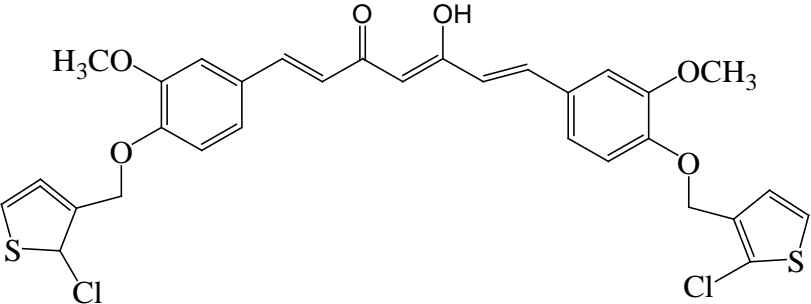
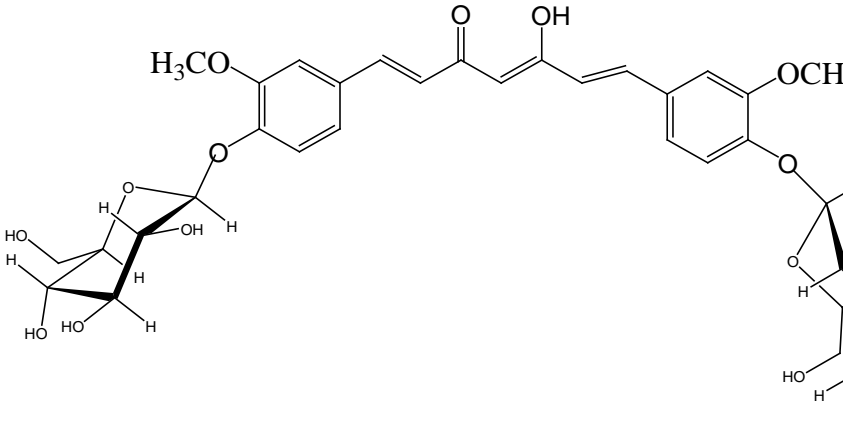
Table 2. Synthetic analogues of curcumin

Sl. No.	Structure	Reference
1		[153]
2		[153]
3		[153]
4		[155]
5		[154]
6		[154]
7		[154]
8		[155]

10	 <p>Chemical structure of a chalcone derivative. The central chalcone core consists of a propenoic acid derivative with a ketone group at the 2-position and a hydroxyl group at the 3-position. The 1-position is substituted with a trans-3-phenylprop-2-en-1-yl group. The phenyl rings are substituted with a methoxy group (H_3CO) at the para position.</p>	[155]
11	 <p>Chemical structure of a chalcone derivative. The central chalcone core consists of a propenoic acid derivative with a ketone group at the 2-position and a hydroxyl group at the 3-position. The 1-position is substituted with a trans-3-phenylprop-2-en-1-yl group. The phenyl rings are substituted with a methyl group (H_3C) at the para position.</p>	[155]
12	 <p>Chemical structure of a chalcone derivative. The central chalcone core consists of a propenoic acid derivative with a ketone group at the 2-position and a hydroxyl group at the 3-position. The 1-position is substituted with a trans-3-phenylprop-2-en-1-yl group. The phenyl rings are substituted with a chlorine atom (Cl) at the para position.</p>	[155]
13	 <p>Chemical structure of a chalcone derivative. The central chalcone core consists of a propenoic acid derivative with a ketone group at the 2-position and a hydroxyl group at the 3-position. The 1-position is substituted with a trans-3-phenylprop-2-en-1-yl group. The phenyl rings are substituted with a nitro group (NO_2) at the para position.</p>	[156]
14	 <p>Chemical structure of a chalcone derivative. The central chalcone core consists of a propenoic acid derivative with a ketone group at the 2-position and a hydroxyl group at the 3-position. The 1-position is substituted with a trans-3-phenylprop-2-en-1-yl group. The phenyl rings are substituted with a dimethylamino group ($(\text{CH}_3)_2\text{N}$) at the para position.</p>	[157]
15	 <p>Chemical structure of a chalcone derivative. The central chalcone core consists of a propenoic acid derivative with a ketone group at the 2-position and a hydroxyl group at the 3-position. The 1-position is substituted with a trans-3-phenylprop-2-en-1-yl group. The phenyl rings are substituted with a hydroxyl group (HO) at the meta position and a methoxy group (OCH_3) at the para position.</p>	[155]
16	 <p>Chemical structure of a chalcone derivative. The central chalcone core consists of a propenoic acid derivative with a ketone group at the 2-position and a hydroxyl group at the 3-position. The 1-position is substituted with a trans-3-phenylprop-2-en-1-yl group. The phenyl rings are substituted with hydroxyl groups (HO) at the meta and para positions.</p>	[156]
15	 <p>Chemical structure of a chalcone derivative. The central chalcone core consists of a propenoic acid derivative with a ketone group at the 2-position and a hydroxyl group at the 3-position. The 1-position is substituted with a trans-3-phenylprop-2-en-1-yl group. The phenyl rings are substituted with a methoxy group (H_3CO) at the meta position and another methoxy group (OCH_3) at the para position.</p>	[156]

16		[156]
17		[156]
18		[156]
19		[157]
20		[157]
21		[157]
22		[154]
23		[158]
24		[158]

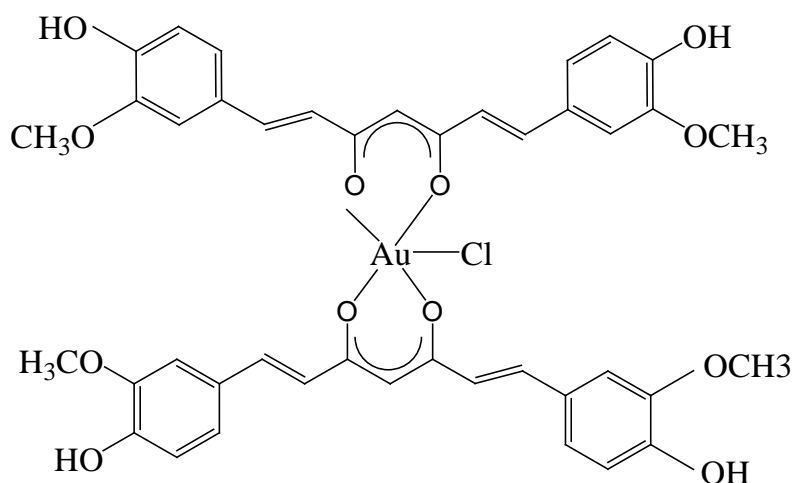
25	 <chem>CC(=O)Oc1ccc(OC)c(O)C=C/C=C/C(=O)C(O)/C=C/c2ccc(OC)c(OC)c2</chem>	[158]
26	 <chem>CC(=O)Oc1ccc(OC)c(OC)c1C=C/C=C/C(=O)C(O)/C=C/c2ccc(OC)c(OC)c2C3=CC=CC=C3FeC4=CC=CC=C4</chem>	[159]
27	 <chem>CC(=O)Oc1ccc(OC)c(OC)c1C=C/C=C/C(=O)C(O)/C=C/c2ccc(OC)c(OC)c2C3=CC=CC=C3FeC4=CC=CC=C4</chem>	[159]
28	 <chem>CC(=O)C(=O)C=C/C=C/C(=O)C(O)/C=C/c1ccc(OC)c(OC)c1</chem>	[159]
29	 <chem>CC1=CN=CC=C1COc2ccc(OC)c(O)C=C/C=C/C(=O)C(O)/C=C/c3ccc(OC)c(CO1=CN=CC=C1)c3</chem>	[160]

30		[160]
31		[160]

9. Biological activities of metal complexes of curcumin and its synthetic analogues

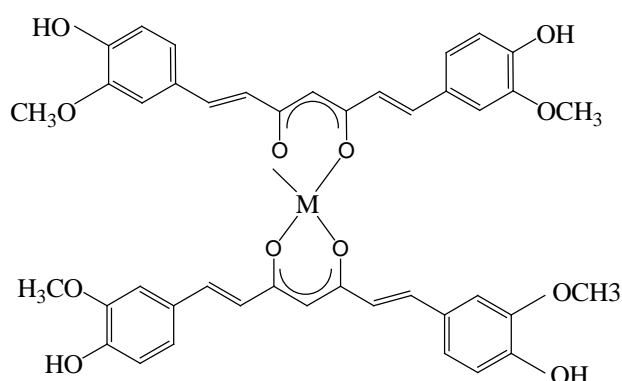
Curcumin-metal complexes not only modify the physico-chemical properties of curcumin but they also affect the biological reactivity. In general it has been observed that complexation with curcumin reduces the toxicity of the metals and some curcumin complexes with metals like Cu^{2+} , Mn^{2+} , act as new metal-based antioxidants. Due to the reversible electron transfer reactions with superoxide ions, Cu^{2+} and Mn^{2+} complexes of curcumin behaves like superoxide dismutase enzyme ^[161].

One of the first biological investigations on metal curcumin complexes was published as early as 1987 and comprises an antiarthritic study of the orally active gold(III) curcumin complex $[\text{Au}(\text{Curc})_2]\text{Cl}$ (**I**). This complex was prepared in a simple manner by mixing curcumin with gold(III) chloride in a 2 : 1 molar ratio in ethanol. *In vivo* antiarthritic activity was reported to this five co-ordinated Au^{3+} complex ^[162].



I

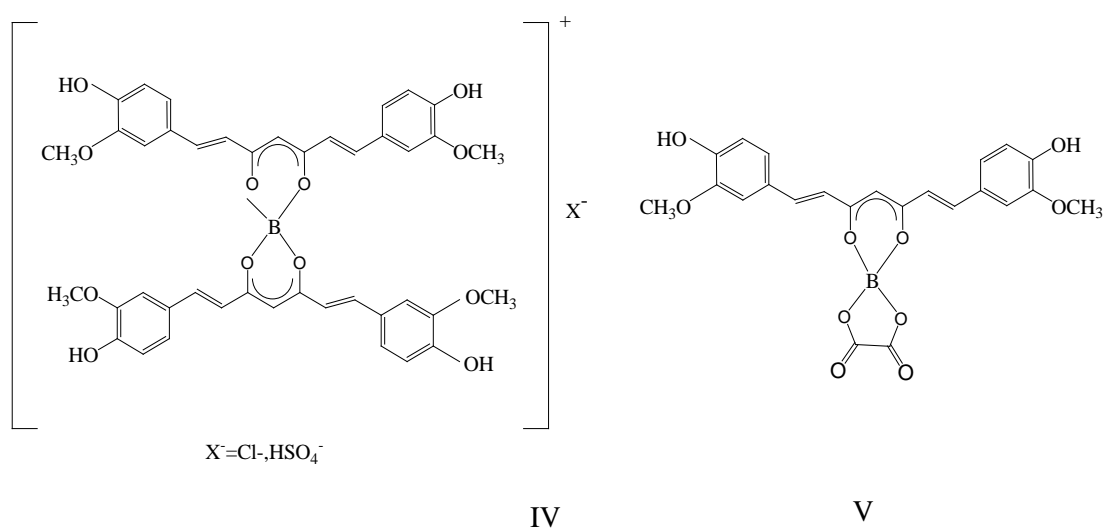
Several metal chelates of curcumin are reported to possess biological activity over that of free curcumin. Divalent and trivalent metal complexes of synthetic curcumin analogues given in **Table 2** are synthesised and characterized by our group during 1995-2010. John and Krishnankutty studied the antitumor activities of curcumin, piperonylcurcumin, 2-hydroxy naphthylcurcumin, cinnamylcurcumin, and their copper complexes^[154,157]. Copper complexes of curcumin and its derivatives were found to be better antitumor agents than were the parent compounds. Further, the curcumin-copper complex was equally effective as curcumin against cadmium induced oxidative damage in mice. Theoretical calculation of ionization energies of curcumin and curcumin-copper complex(**II**) have shown that these possess higher reactive oxygen species scavenging ability than does curcumin^[163].



II , M = Cu

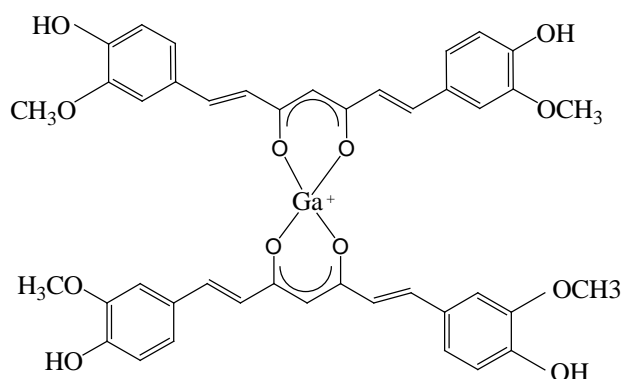
III , M = Mn

Similarly, it was demonstrated that curcumin-manganese complex (**III**) exhibited a more potent neuroprotective activity than curcumin both *in vitro* and *in vivo* suggesting that this complex may be useful as a neuroprotective agent in the treatment of acute brain pathologies associated with NO-induced neurotoxicity and oxidative stress-induced neuronal damage such as epilepsy, stroke, and traumatic brain injury^[161]. Studies by Sui, Salto and Li showed that the modest activity of curcumin as an *in vitro* inhibitor of HIV-1 and HIV-2 proteases is enhanced more than 10-fold when curcumin is complexed with boron (**IV** and **V**)^[164].



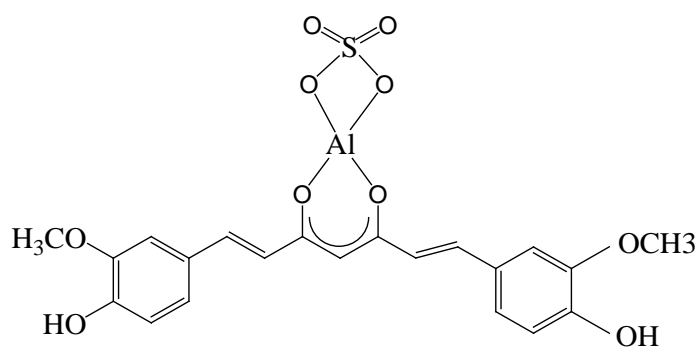
Recently 2:1 complexes of curcumin with Ga³⁺ (**VI**) have been prepared with high radiochemical purity. These compounds have also been reported to

be binding to β -amyloid fibrils very strongly, with possible applications in the diagnosis of Alzheimer's disease^[165].



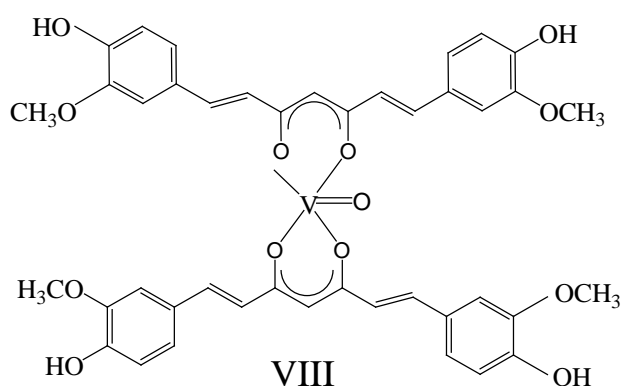
VI

It was revealed that curcumin strongly interacts with the Al^{3+} ion. Curcumin is thus capable of scavenging Al^{3+} and preventing this metal ion from interacting with proteins like β -amyloid, thereby weakening the β -amyloid toxicity and oxidative stress. 1:1 Al^{3+} -curcumin complex (**VII**) showed less affinity to DNA binding than free Al^{3+} , which has been attributed to its ability to reduce development of Al^{3+} induced Alzheimer's disease^[166, 167].

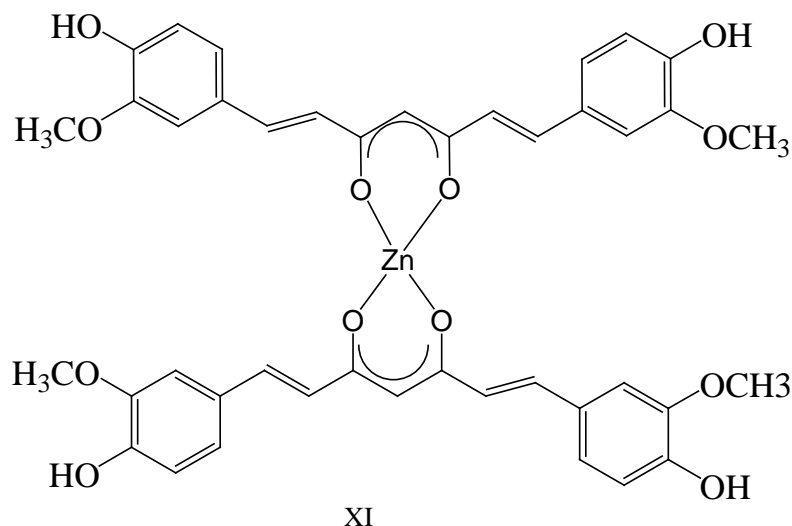


VII

A vanadylcurcumin complex [$\text{VO}(\text{Curc})_2$] (**VIII**) was reported to show a 2-fold increase in antirheumatic activity and a 4-fold increase in inhibiting smooth muscle cell proliferation as compared to free curcumin *in vitro*. Further, this complex was more effective as an anticancer agent, compared to uncomplexed curcumin^[168].

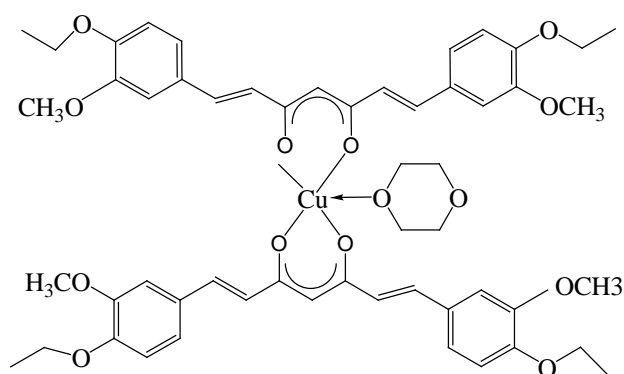
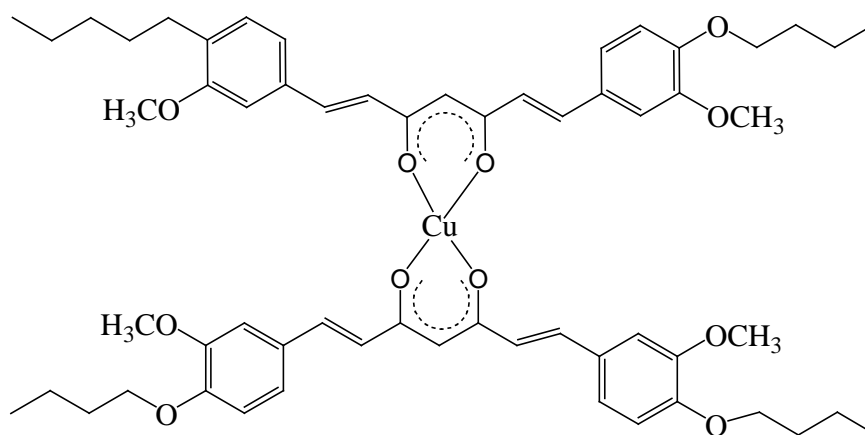


Zn^{2+} -curcumin complexes showed anti-cancer, gastro protective and antidepressant effects in rats ^[169].

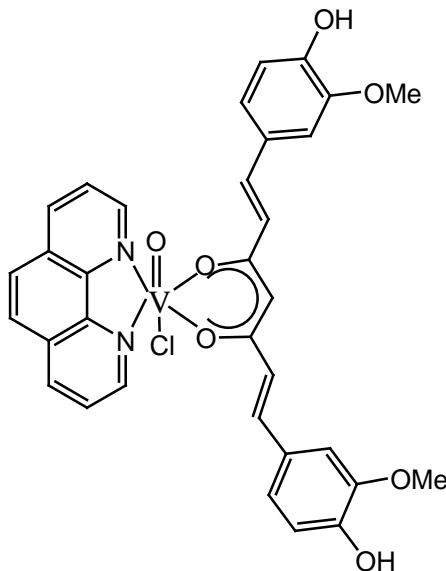


Two copper complexes $Cu(Et_2Curc)_2(\text{dioxane})$ (**X**) and $Cu(Bu_2Curc)_2$ (**XI**) have large two-photon absorption cross-sections, a property desirable for bioimaging of living cells and tissues. Compared with single-photon absorbing materials, the molecular excitation by the simultaneous absorption of two photons presents several advantages that include high confined excitation capacity, intrinsic three-dimension resolution, and the possibility of imaging at an increased penetration depth in tissue, with reduced photo-damage and background fluorescence. The experimental results showed that the complexes exhibit a large two-photon absorption cross-section in the near-infrared region,

high quantum yield and photostability and low cytotoxicity. The *in vitro* study utilized the human breast cancer MCF-7 cell line that was imaged by two-photon fluorescence microscopy^[170]. The tumor targeting capability of (**X**) and (**XI**) on tumor-bearing nude mice *in vivo* demonstrated its high targeting capability to test cancerous cells. The results suggested that these Cu(II) complexes are promising probes for *in vivo* imaging^[171].

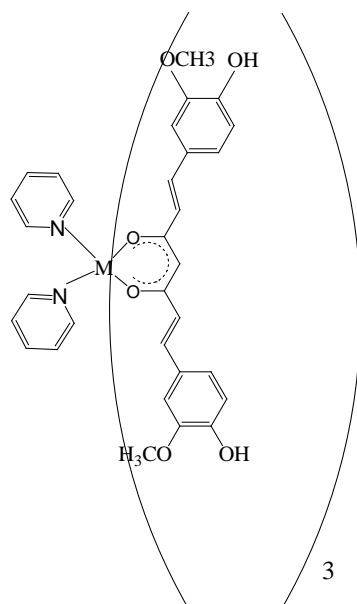
**X****XI**

Heteroleptic complexes containing suitable spectator ligands in addition to curcumin like VO(Curc)(phenanthroline)Cl (**X**) have also been reported recently found to possess more activity than VO(Curc)₂ (**XII**)^[172].

**XII**

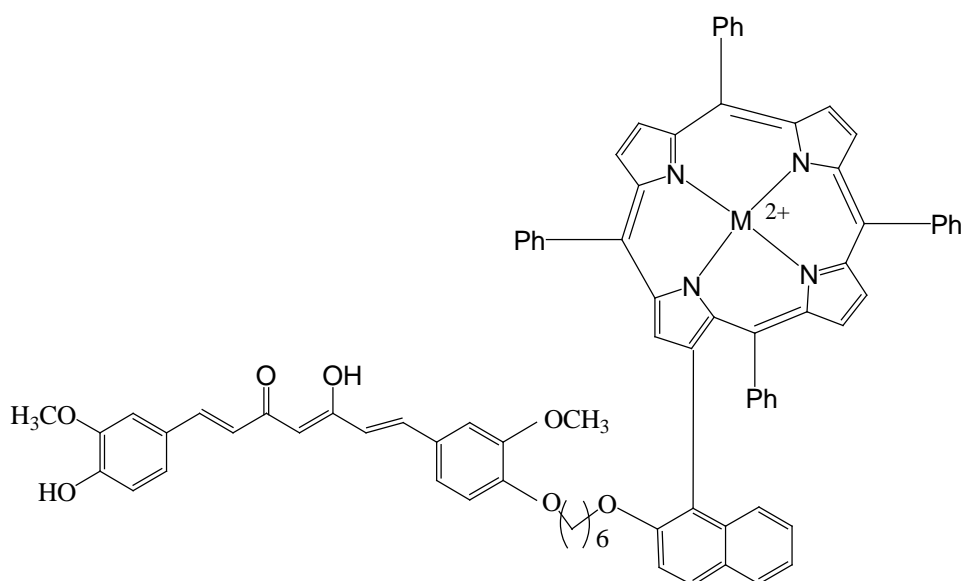
Most of these mixed ligand complexes of curcumin apparently contain only one curcumin ligand and ligands like pyridine, 2,2'-bipyridine, phenanthroline, terpyridine derivatives, tertiary phosphines, cyclopentadienyl ligands and η^6 -coordinated arenes like cymene or hexamethylbenzene as the co-ligands. A few examples of these mixed ligand complexes are summarized here.

Experimental and theoretical studies on two rare earth metal curcumin complexes, La(Curc)₃(pyridine)₂ (**XIII**) and Eu(Curc)₃(pyridine)₂ (**XIV**), revealed their potential application as a biological fluorescent probe^[173].



XIII, M=Eu (III) XIV, M=La(III)

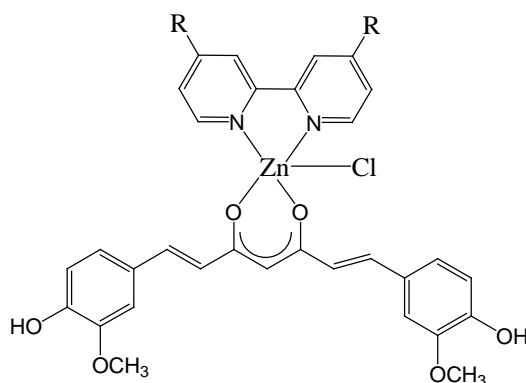
Photodynamic therapy is a modern minimally invasive technique for the treatment of cancer. It has many benefits compared with chemotherapy, radiotherapy, or surgery including reduced long-term morbidity, no resistance development and no negative consequences of repeated treatments. The three basic components of any photodynamic approach are light, oxygen, and the photosensitizer. The most widely used photosensitizer in current clinical use is photofrin, a tetrapyrrole-containing compound. However, this compound has several disadvantages, *e.g.*, long-lasting skin photosensitivity and low absorbance at $\lambda = 630$ nm. Hence there is great interest in alternatives which offer advantages over photofrin, including absorption between $\lambda = 600$ nm and 800 nm, rapid clearance from non-pathological tissue, and low toxicity in the absence of an optical trigger. Huang et al made an interesting modification of the curcumin skeleton by bridging the curcumin moiety *via* 1,6-dibromohexane and a hydroxyl naphthyl-group to a porphyrin molecule^[174,175]. The ligand and its Ni(II), Cu(II) and Zn(II) complexes (**XV-XVIII**) showed strong binding interactions with DNA and light-triggered cleavage activity^[176].



XV-XVII

M=Ni (II)
M=Cu (II)
M=Zn (II)

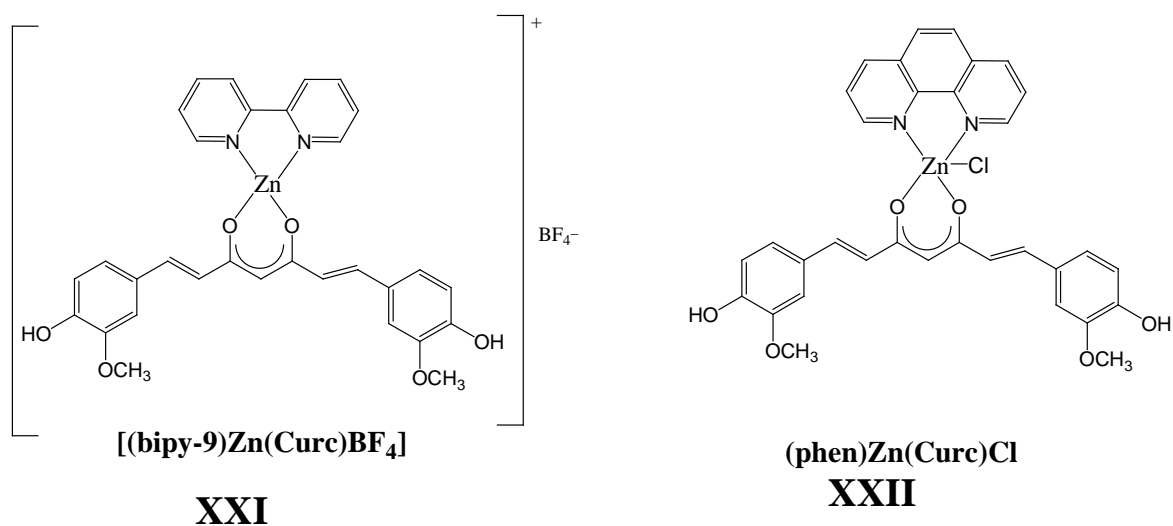
Complexes of curcumin-and 4,4'-bipyridine with Zn^{2+} were more effective than curcumin to kill neuroblastoma cells^[177]. The presence of intrinsic fluorescence in (bipy-9)Zn(Curc) (**XIX**) and (bipy-CH₂OH)Zn(Curc) (**XX**) allows the combination of anticancer properties with an excellent tool for investigating their mechanism of action through optical methods in a single molecule, without additional external agents.



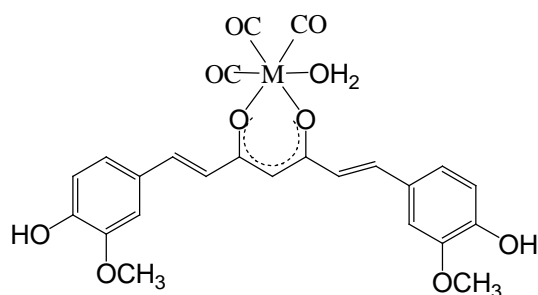
XIX (bipy-9)Zn(Curc)

XX (bipy-CH₂OH)Zn(Curc)

The ionic tetrafluoroborate Zn(II) complex [(bipy-9)Zn(Curc)]BF₄ (**XXI**) and the neutral phenanthroline based Zn(II) derivative (phen)Zn(Curc)Cl (**XXII**) also showed potential growth inhibition in *in vitro* studies^[177].



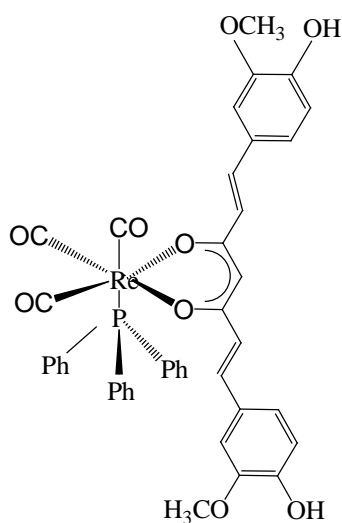
Fluorescent curcumin-metal complexes are being explored for imaging of cancer cells. Re(CO)₃(Curcumin)(H₂O) (**XXIII**) complex is fluorescent and show affinity to β -amyloid plaques, which has potential to be explored in microscopic imaging of the tissue of Alzheimer's disease patients. Similarly ⁹⁹Tc(CO)₃(curcumin)(H₂O) (**XXIV**) complexes have been produced in high radiochemical yield, and showed significant affinity to β -amyloid plaques and such systems are being developed as novel radio diagnostic agents for Alzheimer's disease^[178, 179].



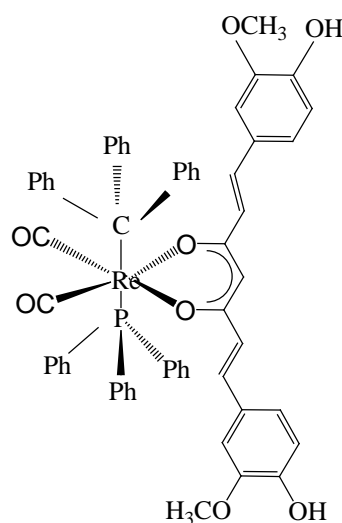
XXIII, M=Re

XXIV, M=⁹⁹Tc

Two monophosphine and bis(phosphine)curcumin rhenium carbonyl complexes *fac*-Re(CO)₃(PPh₃)(Curc) (**XXV**) and *cis*-*trans*-Re(CO)₂(PPh₃)₂(Curc) (**XXVI**) were found to show selective binding to β -amyloid plaques of Alzheimer's disease and stain the β -amyloid plaques, allowing clear visualization of the plaques^[180].



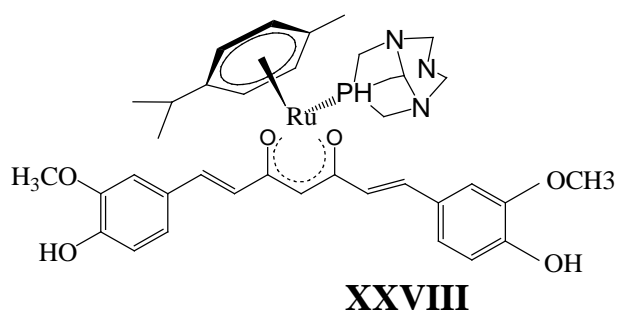
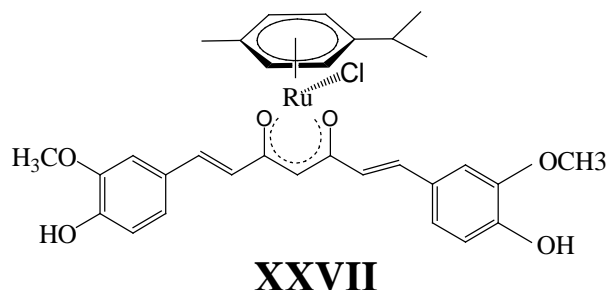
XXV



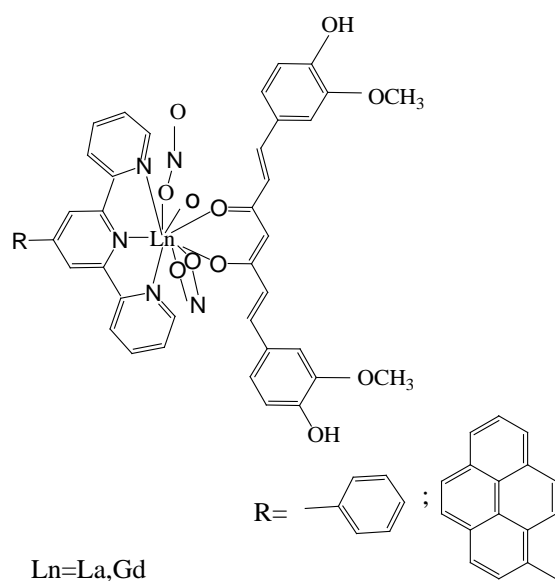
XXVI

A DNA docking study of (η^6 -*p*-cymene)RuCl(Curc) (**XXVII**) revealed the same mechanism of action that has been established in Pt chemotherapy. The ruthenium η^6 -*p*-cymene-PTA-curcumin complex (PTA = 1,3,5-triaza-7-phosphaadamantane) (**XVIII**) showed not only superior solubility properties

due to the sophisticated ligand design but also superior cytotoxicities compared to other classes of related compounds^[181].



Recently a few mixed ligand complexes of curcumin with lanthanides having unique chemical and biological activities have been reported. Curcumin-terpyridyl-lanthanide complexes (**XXIX** and **XXX**) showed enhanced photocytotoxicity in HeLa cells. Mixed ligand-curucumin complexes of ruthenium metal showed antibacterial activity. It has significant potential for photo chemotherapeutic applications and highest toxicity for the colorectal tumour cell lines^[182,183].

**XXIX-XXX**

Numerous reports on both homoleptic and heteroleptic metal complexes of synthetic analogues of curcumin are coming up, each claiming with improved biological activities or other properties that have potential applications in the diagnosis and treatment of various diseases.

MATERIALS, METHODS AND INSTRUMENTS

Materials

All chemicals used for synthesis were of analytical reagent grade procured from Merck, India and used as such. Solvents used were of commercial purity grade procured from commercial sources such as Nice/Loba Chemicals and were purified by standard procedures^[184]. For recording UV Visible spectra and for chromatographic analysis, spectroscopic grade solvents procured from Merck, India was used.

2-acetylcyclopentanone used for synthesis of ligands was procured from Sigma Aldrich, USA. Copper (II) acetate monohydrate, nickel (II) acetate tetrahydrate, and zinc (II) acetate dihydrate were used for the synthesis of metal complexes. Double distilled water collected from all glass equipment was used in all preparations.

For DNA binding studies, ethidiumbromide (EB), tris(hydroxymethyl) aminomethane(Tris) and calf thymus (CT) DNA were procured from Sigma Aldrich, USA. Tris-HCl buffer solution was prepared using de-ionized and triple distilled water using a quartz water distillation setup.

For antioxidant assay, 1,1-diphenyl-2-picrylhydrazyl (DPPH) and nitrobluetetrazolium (NBT) were procured from Sigma Aldrich, USA. Sodium dodecyl sulphate, thiobarbituric acid, ascorbic acid, deoxyribose, and riboflavin were procured Himedia Chemicals.

For screening antitumor activity, cyclophosphamide (cyclophos, Biochem. Pharmaceutical Industrial Ltd.) is used as control. Carboxymethyl cellulose and the dye trypan blue were procured from Himedia Chemicals.

Dalton's lymphoma ascites (DLA) cells were obtained from the Cancer Research Institute, Mumbai, India. DLA was maintained as ascites tumors in

Swiss albino mice, purchased from Kerala Agricultural University, Thrissur, Kerala. They were fed with normal mouse chow (Lipton India) and water *ad libitum*.

Instruments

Instruments used in this investigation are

1. Elemental Vario EL CHN analyzer
2. Heraeus Elemental analyzer
3. AAS (Perkin Elmer 2380)
4. Jasco V – 550 UV visible spectrophotometer
5. Jasco FTIR-4100 Fourier transform infrared spectrophotometer
6. Bruker Avance III, 400MHz FT NMR spectrometer
7. JEOL / SX-102 MS
8. ELICO-CM-82 T conductivity bridge
9. Varian E-12 ESR spectrometer
10. PCI-analytic sonicator
11. LG-Highwave (70W) microwave oven
12. MPF-4 fluorescence spectrophotometer
13. Ostwald's viscometer
14. ELICO SL 218 double beam UV-VISIBLE spectrophotometer
15. Rohan India Ltd. Hemocytometer
16. Gouy's type magnetic balance

Methods

Microwave assisted synthesis were carried out in a domestic microwave oven (70W) as the source of microwave. PCI-analytic sonicator (6.5L, 200W) is used for sonication.

Molecular mass of compounds reported were determined by Rast's method using camphor as medium.

Carbon and hydrogen percentages reported are by microanalysis carried out at SAIF IIT Bombay, Mumbai and at CDRI Lucknow, India.

The electronic spectra of the ligands and complexes were recorded from solutions (10^{-3} M) using CHCl_3 or DMSO as solvents.

The IR spectra were recorded in the region $4000\text{--}250\text{ cm}^{-1}$ in KBr discs from STIC, CUSAT. Bands were calibrated using the nearest polystyrene bands.

The ^1H NMR and ^{13}C NMR spectra were recorded in CDCl_3 or DMSO d_6 from SAIF-IIT Bombay and SAIF - IIT Madras, Chennai. Chemical shifts are given in ppm relative to tetramethylsilane.

FAB mass spectra were recorded at room temperature using argon (6 KV, 10 mA) as the FAB gas and 3-nitrobenzyl alcohol as the matrix. ESI-MS were recorded (scan range 30-2000) in positive ion mode with accelerating voltage 10 KV. ESR spectra of copper complexes were recorded at 77 K.

Molar conductivity measurements were recorded in DMF at $28 \pm 1^\circ\text{C}$ using solution of about 10^{-3} M in a cell having cell constant 0.51 cm^{-1} .

Magnetic susceptibility measurement on powder samples were carried out at room temperature ($28 \pm 1^\circ\text{C}$) using mercury tetrathiocyanatocobaltate (II) as standard.

The lipid peroxidation inhibitory activity was determined by the thiobarbituric acid method by recording absorbance at 532 nm.

The DPPH free radical scavenging activity was monitored by measuring the absorbance of 0.5 mM DPPH solution at 520 nm in the presence of test compounds at different concentrations ranging from 10-100 µg/ml after incubating for 30min at 37°C in the dark. The EC_{50%} (Efficient Concentration of the test compound necessary to decrease the initial DPPH radical concentration by 50%) value was determined.

The super oxide radical scavenging activity was determined by the NBT reduction method.

The hydroxyl radical scavenging was measured by studying the competition between deoxy ribose and the test compounds for hydroxyl radicals generated from Fe³⁺/ ascorbate/ EDTA/ H₂O₂ system using TBA.

UV-vis absorption spectrophotometry was used to monitor the interactions of ligand and its complexes with CT-DNA at 7.2 pH in double distilled water containing tris-(hydroxymethyl)amino methane (Tris, 10⁻² M). The binding experiments were carried out by recording the absorbance changes on adding increasing concentrations of DNA (0 – 250 µM) against a fixed concentration of the ligand and its complexes (50 µM) at room temperature (28 ± 1°C).

Viscosity measurements of 1x10⁻⁴ M CT-DNA in Tris-HCl/NaCl buffer were performed using an Ostwald viscometer at 35 ± 0.2 °C in a thermostatic water bath. Flow time was measured with a digital stopwatch. Each experiment was performed three times and an average flow time was calculated.

Since the copper(II) complexes are non-luminescent at room temperature, in fluorescence quenching studies, EB-bound CT-DNA solution in Tris–HCl/NaCl buffer is used.

In vitro cytotoxicity studies were carried out using DLA cells. The stained and unstained cells were counted using hemocytometer using trypan blue as the staining agent.

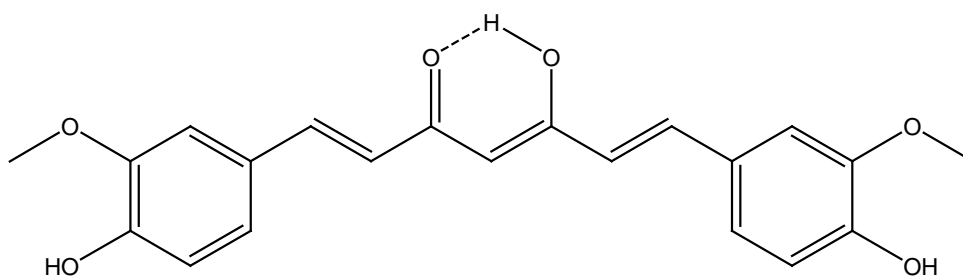
For *in vivo* studies, groups of Swiss Albino mice (female, 6 per group) were injected intraperitoneally (ip) with Dalton's lymphoma ascites tumour cells (1×10^6 cells/animal). They were injected ip with test compound suspended in carboxy methyl cellulose (CMC) and the injections of the test compounds were started 24 hours after tumor inoculation and continued for 10 consecutive days.

Solid tumors were also induced in groups of Swiss albino mice (female, 6 per group) by subcutaneous injection of DLA cells (1×10^6 cells/animal) on the right hand limb. One group was kept as control and other groups were injected intramuscularly (im) with the test compounds (25mg/kg body weight) and the injections of the test compounds were started 24 hours after inoculation and continued for 10 consecutive days. Tumor diameter was measured every third day for one month and the tumor volume was calculated

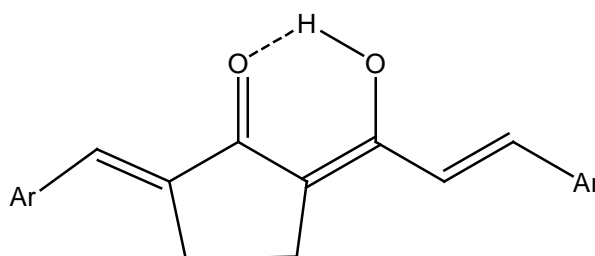
The detailed procedures of all biological studies were presented in **Results and Discussion, Part B** of the thesis.

RESULTS AND DISCUSSION
PART A
Synthesis and Characterisation

In the present investigation, the basic curcumin ligand system is modified and a series of unsymmetrical curcumin analogues were synthesized. The modification of the curcumin skeleton included both incorporation of a cyclopentane ring to the enolizable β -diketone moiety which is common to all ligands and a deviation in the nature and position of phenyl substituent, as well as replacing phenyl ring with hetero aryl and naphthyl / substituted naphthyl rings. The synthesis and characterisation of these ligands and their nickel(II), copper(II) and zinc(II) complexes are presented in five chapters with respect to the structural feature of ligands and titled accordingly.



Curcumin



(Ar = substituted phenyl / hetero aryl / naphthyl)

General structure of ligands

Results obtained from biological studies are separately detailed in **Part B**.

Chapter 1

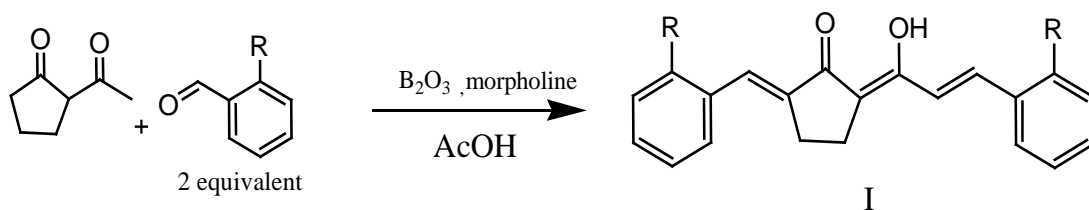
LIGANDS WITH ORTHO SUBSTITUTED PHENYL RINGS

1.1 Synthesis of ligands

Synthesis of curcumin and its synthetic analogues involves condensation between appropriate aromatic aldehyde and 2,4-pentadione - boric oxide complex in ethyl acetate medium. Use of boron-based protection of the 1,3-diketone circumvents the Knoevenagel condensation at C-3 (active methylene group) and facilitates aldol condensations at C-1 and C-5 of 2,4-pentadione successively via the dienolate^[185]. The procedure involves stirring of the reaction mixture for 3 – 4 hours and it usually gives a mixture of mono and bis condensation products from which the desired product is separated by column chromatography.

In the present investigation, ligands were synthesised by exposing a mixture of benzaldehyde or an ortho-substituted benzaldehyde and 2-acetyl cyclopentanone to microwave radiations in a domestic microwave oven for a short period of 3 minutes. The microwave assisted synthesis exclusively gave the bis condensation product in a short time. Relatively good yield are obtained in all cases. A typical procedure is given below.

2-Acetyl cyclopentanone (20mmol) was mixed with the boron oxide (20 mmol) in a 100 ml Erlenmeyer flask. The appropriate aromatic aldehyde (40 mmol), acetic acid (100 mg), and morpholine (100 mg) were then added. The reaction mixture was irradiated with the microwave at 70W for 3 minutes. The flask was cooled to room temperature and then methanol (50 ml) was added. This mixture was then sonicated for 30-40 minutes. The fine powder so obtained was filtered and washed with cold methanol. The compounds were recrystallized from hot benzene to obtain chromatographically pure material.

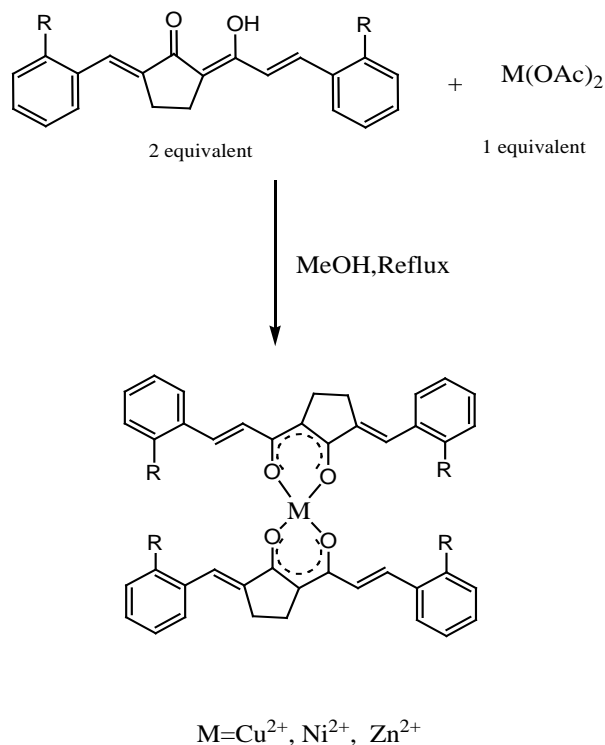


Scheme 1.1

1.2 Synthesis of Cu^{II}, Ni^{II} and Zn^{II} complexes

Copper(II), Nickel(II) and Zinc(II) complexes of the ligands were prepared by the following general method.

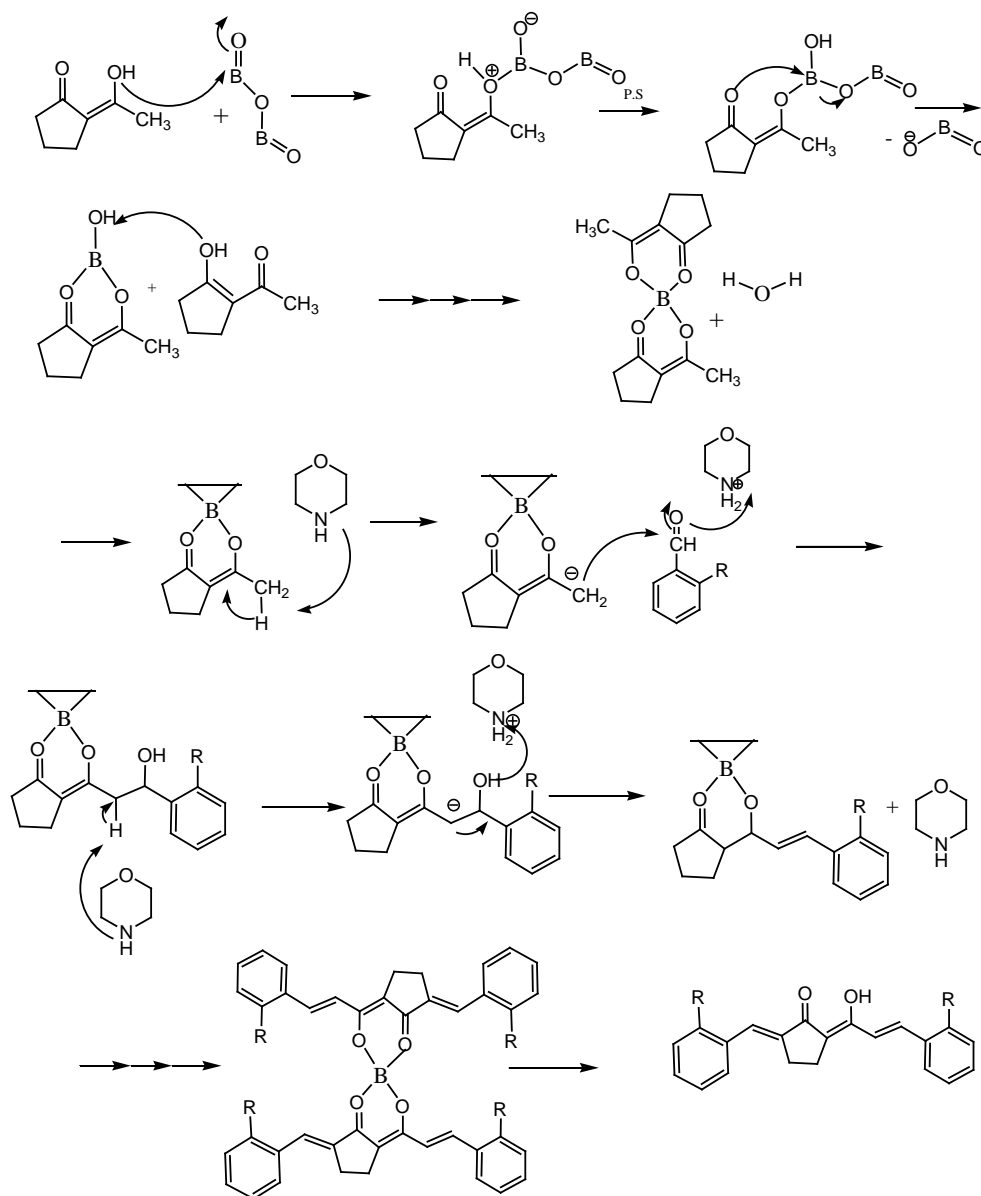
A methanolic solution of metal(II) acetate (25 ml, 1 mmol) was added with stirring to a solution of ligand (25 ml, 2 mmol) in methanol and refluxed gently for ~2 hours. The solution was concentrated to half of its volume and cooled to room temperature. The precipitated complexes were filtered, washed with methanol and recrystallized from hot methanol.



Scheme 1.2

1.3 Results and discussion

The systematic names of the ligands (**1a-1f**) and the aldehydes from which they synthesised are depicted in **Table.1.1**. A probable mechanism of the reaction is outlined in **Scheme 1.3**.

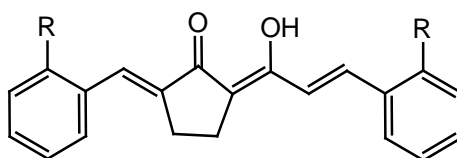


Scheme 1.3. Probable mechanism of the reaction

All the compounds are crystalline in nature and insoluble in water but freely soluble in common organic solvents like methanol, DMSO, acetone, chloroform, etc. Maximum yields are obtained with aldehydes having electron donating substituents (OH/OCH₃/CH₃) in the phenyl ring.

The results of elemental analysis and molecular weight determination of the compounds given in **Table 1.2** indicate that two equivalents of the aromatic aldehyde has condensed with one equivalent of 2-acetyl cyclopentanone in all cases and the ligands can be formulated as **I** in **Scheme1.1**.

Table 1.1 Synthetic details of the ligands



Compounds	Aldehydes used for synthesis	R	Systematic name
HL¹ (1a)	Benzaldehyde	H	(2E)-2-(phenyl methylidene)-5-((E)-3-(phenyl acryloyl) cyclopentanone
HL² (1b)	2- Hydroxybenzaldehyde	OH	(2E)-2-(2-hydroxybenzylidene)-5-((E)-3-(2-hydroxy phenyl) acryloyl) cyclopentanone
HL³ (1c)	2- Methoxybenzaldehyde	OCH ₃	(2E)-2-(2-methoxybenzylidene)-5-((E)-3-(2-methoxy phenyl) acryloyl) cyclopentanone
HL⁴ (1d)	2- Methylbenzaldehyde	CH ₃	(2E)-2-(2-methylbenzylidene)-5-((E)-3-(2-methyl phenyl) acryloyl) cyclopentanone
HL⁵ (1e)	2-chlorobenzaldehyde	Cl	(2E)-2-(2-chlorobenzylidene)-5-((E)-3-(2-chloro phenyl) acryloyl) cyclopentanone
HL⁶ (1f)	2- Nitrobenzaldehyde	NO ₂	(2E)-2-(2-nitrobenzylidene)-5-((E)-3-(2-nitro phenyl) acryloyl) cyclopentanone

1.4 Characterization of ligands

The ligands were characterised on the basis of their UV, IR, ^1H NMR, ^{13}C NMR and mass spectral data.

1.4.1 Electronic spectra

The electronic spectra of the ligands displayed two absorption maxima, the low energy band corresponds to an $n\rightarrow\pi^*$ transition (420-484 nm) and the high energy band is due to a $\pi\rightarrow\pi^*$ transitions (246-284 nm) (**Table 1.2**)^[186]. In general, the $n\rightarrow\pi^*$ absorption of the carbonyl chromophore occurs at higher wavelength in the UV absorption spectra of 1,3-diketones due to reversible enolisation and the absorption maximum (λ_{max}) depends on the degree of enolisation. It is usually observed that with increase in the percentage of enol form, λ_{max} increases. Presence of α,β -unsaturation can also lowers energy requirements and can rise the carbonyl absorption maxima. Since the ligands are typical α,β -unsaturated 1,3-diketones and their observed absorption maxima are significantly greater than those reported for simple saturated 1,3-diketones like acetylacetone. The λ_{max} values of the low energy band undoubtedly corresponds to the $n\rightarrow\pi^*$ transition of the enolised dicarbonyl function^[186] and the observed bathochromic shift of this band in **1b**, **1c** and **1d** can be correlated with the electron releasing tendencies of the substituents in the phenyl rings.

The high energy band due to the $\pi\rightarrow\pi^*$ transitions of the fully conjugated system is only marginally influenced by the aryl substituents.

Table 1.2 Analytical, UV, IR, and mass spectral data of ligands

Ligands	M. p. (⁰ C)	Elemental analysis (found /calcd) %		Colour	Yield (%)	UV λ_{\max} (nm)	IR (cm ⁻¹)			Mass spectral data (m/z)
		C	H				$\nu(\text{C}=\text{O})$	$\nu_{\text{as}}(\text{C}-\text{C}-\text{C})$	$\nu(\text{CH}=\text{CH}-)$ (trans)	
(1a) HL¹ C ₂₁ H ₁₈ O ₂ (302)	178 ⁰ C	(83.41) (83.42)	(5.99) (6.00)	Yellow solid	84	246 ($\pi \rightarrow \pi^*$), 420 ($n \rightarrow \pi^*$)	1645	1524	963	302, 285, 225, 197, 157, 103, 91, 77
(1b) HL² C ₂₁ H ₁₈ O ₄ (334)	86 ⁰ C	(75.24) (75.43)	(5.14) (5.43)	Dark red solid	71	266 ($\pi \rightarrow \pi^*$), 484 ($n \rightarrow \pi^*$)	1586	1554	963	334, 271, 202, 186, 173, 77
(1c) HL³ C ₂₃ H ₂₂ O ₄ (362)	176 ⁰ C	(76.34) (76.22)	(6.51) (6.12)	Yellow solid	74	261 ($\pi \rightarrow \pi^*$), 446 ($n \rightarrow \pi^*$)	1592	1342	941	362, 345, 213, 103, 91, 77
(1d) HL⁴ C ₂₃ H ₂₂ O ₂ (330)	172 ⁰ C	(83.51) (83.60)	(6.19) (6.71)	Yellow solid	71	257 ($\pi \rightarrow \pi^*$), 434 ($n \rightarrow \pi^*$)	1587	1435	921	330, 313, 211, 197, 171, 105, 91, 77
(1e) HL⁵ C ₂₁ H ₁₆ Cl ₂ O ₂ (371)	182 ⁰ C	(67.53) (67.94)	(4.12) (4.34)	Yellow solid	72	266 ($\pi \rightarrow \pi^*$), 456 ($n \rightarrow \pi^*$)	1583	1387	964	370, 353, 259, 231, 217, 191, 137, 125
(1f) HL⁶ C ₂₁ H ₁₆ N ₂ O ₆ (392)	138 ⁰ C	(64.02) (64.28)	(4.31) (4.11)	Brownish yellow solid	78	248 ($\pi \rightarrow \pi^*$), 434 ($n \rightarrow \pi^*$)	1611	1425	954	390, 346, 298, 270, 176, 92, 77

1.4.2 Infrared Spectra

The absence of band assignable to a normal or α,β -unsaturated carbonyl group in the region $1640\text{-}1700\text{ cm}^{-1}$ of the spectra and the presence of a strong band in the region $1590\text{-}1640\text{ cm}^{-1}$ (indicates that the ligands exist as in their enolic form) (Table 1.2)^[186]. Intramolecular hydrogen bonding can lower the carbonyl stretching frequency by about 50 cm^{-1} ^[187,188]. A broad band present in the range of $2800\text{-}3600\text{ cm}^{-1}$ is due to the stretching of the intramolecular hydrogen bonded enol group. The observed breadth and intensity of the band suggest the involvement of the enolic proton in strong intramolecular hydrogen bonding^[186]. Infrared spectra of all the ligands showed a prominent band at $\sim 975\text{ cm}^{-1}$ typical of *trans* -CH=CH- absorption as the *cis* ethylenic double bonds usually show weak intensity bands^[189]. These characteristic stretching frequencies of **1a-1f** are tabulated in Table 1.2. Since the IR spectra of the ligands are very similar, only one is reproduced here (Figure 1.1)

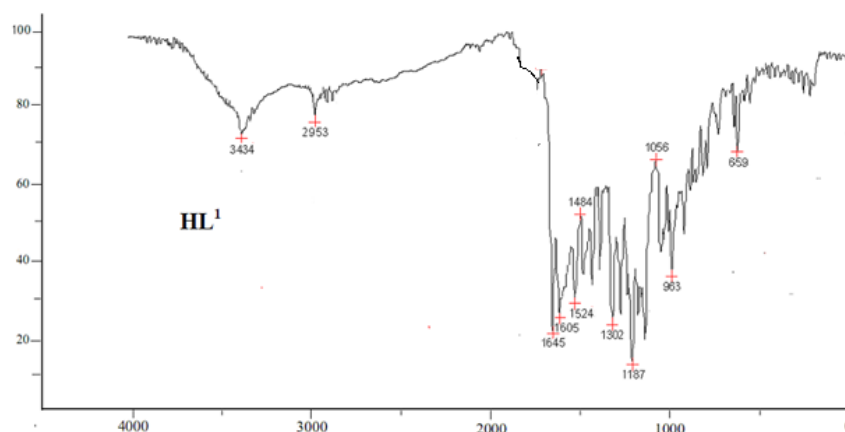


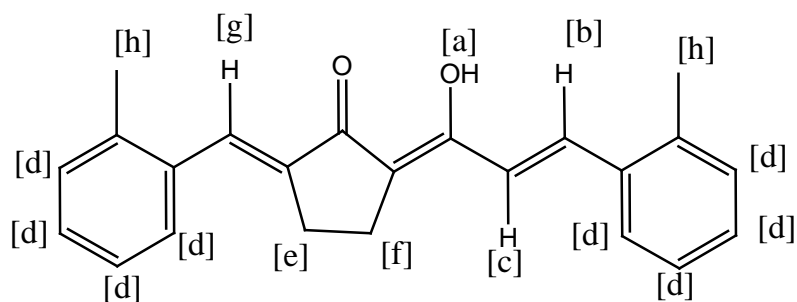
Figure 1.1. IR spectrum of the compound **HL¹** (**1a**)

The medium intensity band observed at 632 cm^{-1} in the IR spectrum of **1e** is due to the aryl $\nu_{\text{C-Cl}}$ stretching. The ligand **HL⁶** (**1f**) also showed two

intense absorption bands at 1523 cm^{-1} and at 1337 cm^{-1} are due to N–O asymmetric and symmetric stretching vibrations, respectively^[186].

1.4.3 ^1H NMR spectra

^1H NMR spectroscopy is widely adopted as the most efficient tool in studying the keto-enol tautomerism of 1,3-diketones and related compounds. The spectra usually display a downfield singlet above 10 ppm due to the enolic proton and the presence of conjugation can further cause a downfield shift^[60]. For instance, in the ^1H NMR spectrum of curcumin the enolic proton resonates at $\delta=17\text{ ppm}$ ^[152]. The ^1H NMR spectra of all the ligands showed a characteristic downfield singlet at $\delta\sim 14.5\text{ ppm}$ which can be assigned to the intramolecularly hydrogen bonded enolic proton. The ^1H NMR spectra of **HL**² showed a downfield singlet at 9.79 ppm due to phenolic proton^[186]. The ^1H NMR spectra of all the ligands shows signals δ at 2.61-2.90 ppm due to protons in the cyclopentane ring and two doublets δ at $\sim 6\text{-}7\text{ ppm}$ due to the alkenyl protons ($J=16.1\text{-}16.4\text{ Hz}$, suggest their trans orientation) and a singlet at $\delta\sim 7\text{ ppm}$ due to vinylic protons also appeared along with the aromatic protons. The integrated intensities of the aryl and alkenyl protons are in well agreement with their formulation. The ^1H NMR spectral data of the ligands are given in **Table 1.3**. The ^1H NMR spectra of all the ligands are reproduced in **Figures 1.2 – 1.7**.

Table 1.3 ^1H NMR spectral data of ligands

Chemical shift, ppm (Coupling constant, Hz)								
Compounds	[a]	[b]	[c]	[d]	[e]	[f]	[g]	[h]
HL¹	14.18	6.67 (16.2)	6.71 (16.2)	7.36-7.61	2.88 (5.2)	2.90 (5.2)	7.68	-
HL²	14.57	6.67 (16.2)	6.91 (16.2)	6.72-7.14	2.61 (5.2)	2.64 (5.3)	7.24	9.79
HL³	14.33	6.67 (16.4)	6.98 (16.4)	6.82-7.64	2.73 (5.5)	2.81 (5.6)	7.79	3.74
HL⁴	14.17	6.79 (16.3)	6.94 (16.4)	7.11-7.31	2.76 (5.4)	2.84 (5.4)	7.42	2.26
HL⁵	14.67	6.64 (16.2)	6.98 (16.3)	7.12-7.32	2.68 (5.5)	2.73 (5.5)	7.37	-
HL⁶	14.32	6.91 (16.3)	7.46 (16.2)	7.51-8.28	2.72 (5.7)	2.79 (5.7)	8.02	-

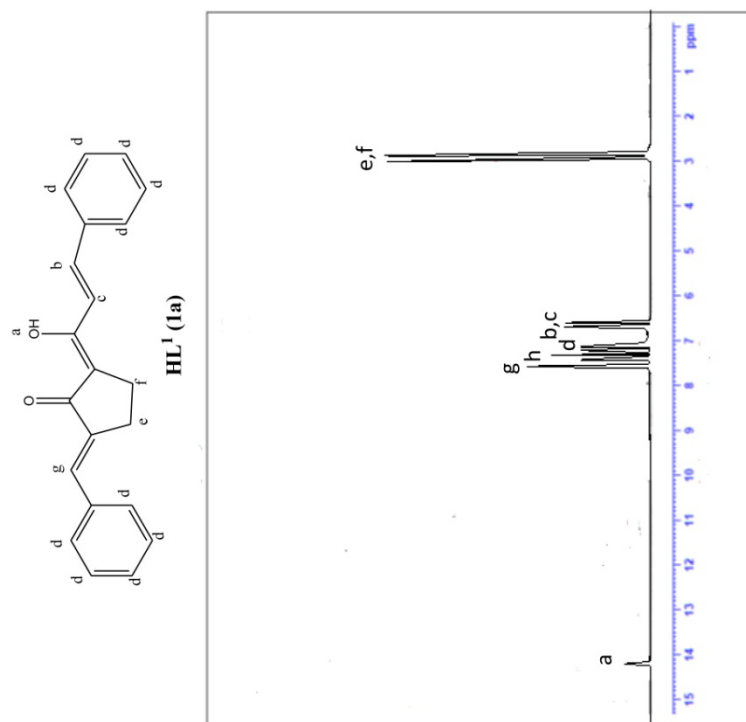
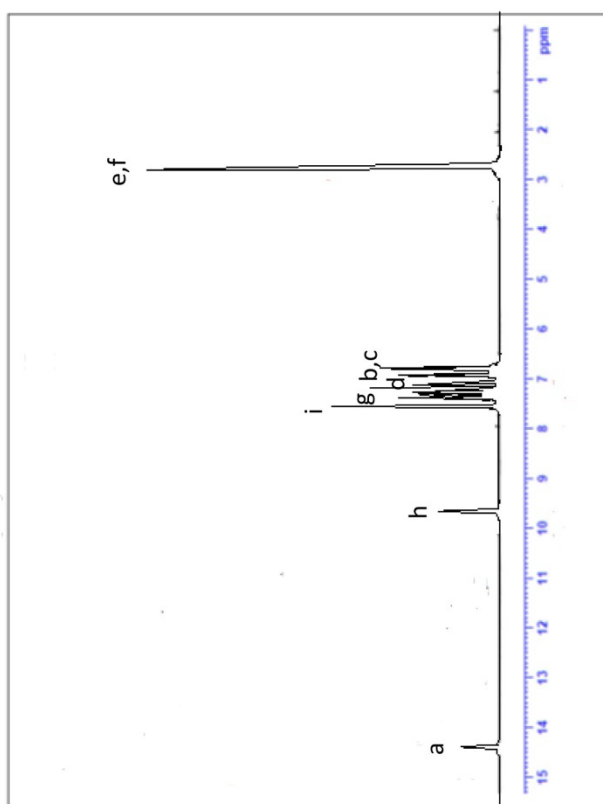
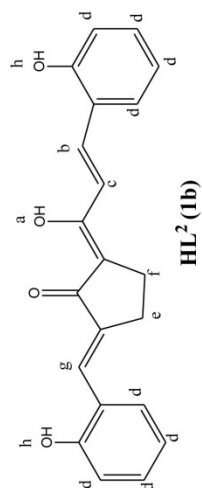


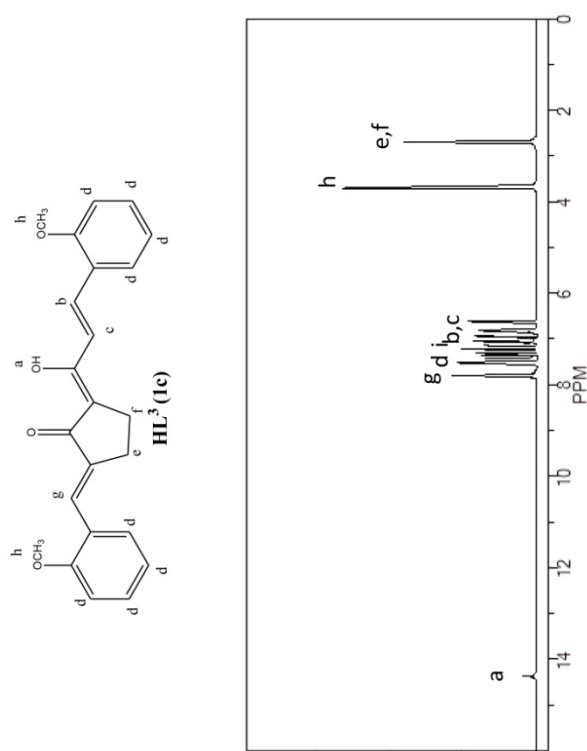
Figure 1.2 ¹H NMR spectrum of **HL¹ (1a)**

¹H NMR (400MHz, CDCl₃, ppm): δ 14.18 (s, enolic, 1H) [a], [2.88 (t, J=5.2Hz cyclopentane ring CH₂, 2H), 2.90 (t, J=5.2 Hz cyclopentane ring CH₂, 2H)] [e,f], [6.67 (d, J=16.2Hz, (E)- alkenyl, 1H), 6.71 (d, J=16.2Hz, (E)- alkenyl, 1H)] [b,c], 7.36-7.61 (m, aromatic, 10H) [d], 7.68 (s, vinylic, 1H) [g], 7.26 (solvent) [h].



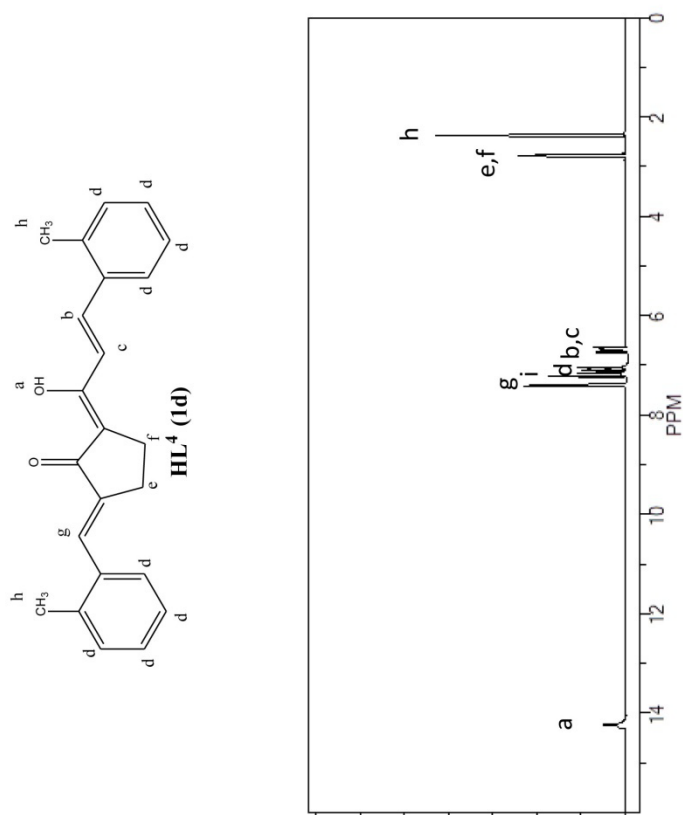
¹H NMR (400MHz, CDCl₃, ppm): δ 14.57 (s, enolic, 1H) [a], [2.61 (t, , J=5.2Hz, cyclopentane ring CH₂, 2H), 2.67 (t, , J=5.3Hz, cyclopentane ring CH₂, 2H)] [e, f], [6.67 (d, J=16.2Hz, (E)-alkenyl, 1H), 6.91 (d, J=16.2Hz, (E)-alkenyl, 1H)] [b, c], 6.72-7.14 (m, aromatic, 8H) [d], 7.24 (s, vinylic, 1H) [g], 9.79 (s, phenolic, 2H) [h], 7.26 (solvent) [i].

Figure 1.3 ¹H NMR spectrum of **HL² (1b)**



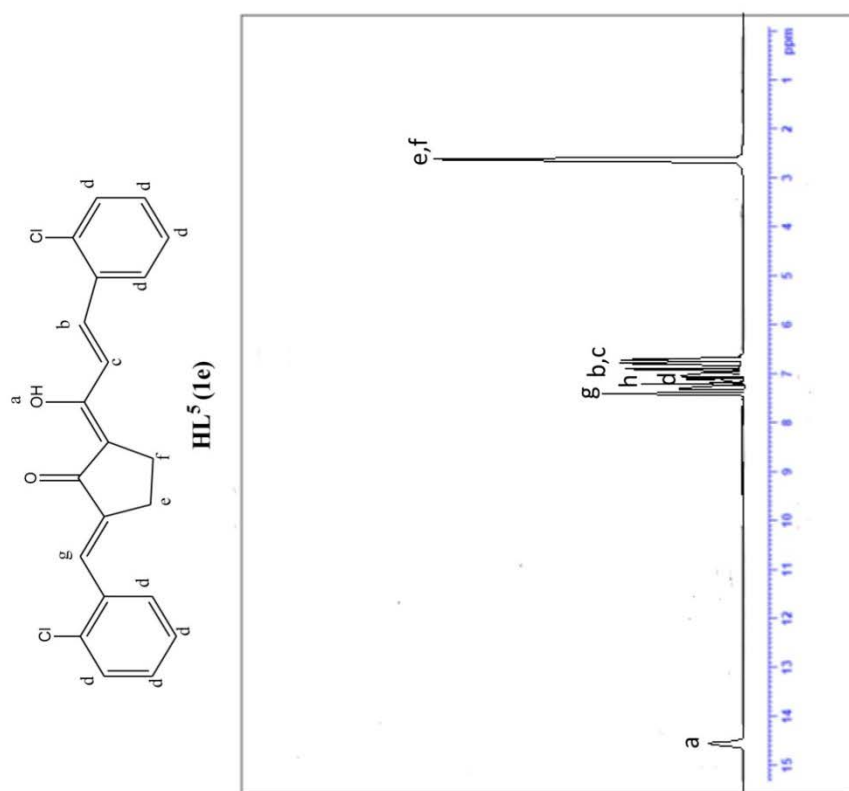
¹H NMR (400MHz, CDCl₃, ppm): δ 14.33 (s, enolic, 1H) [a], [2.73 (t, J=5.5Hz, cyclopentane ring CH₂, 2H), 2.81 (t, c, J=5.6 Hz, cyclopentane ring CH₂, 2H)] [e,f], [6.67 (d, J=16.4Hz, (E)- alkenyl, 1H), 6.98 (d, J=16.4Hz, (E)- alkenyl, 1H)] [b,c], 6.82-7.64 (m, aromatic, 8H) [d], 7.79 (s, vinylic, 1H) [g], 3.74 (s, methoxy, 6H) [h], 7.26 (solvent) [i].

Figure 1.4. ¹H NMR spectrum of **HL³ (1c)**



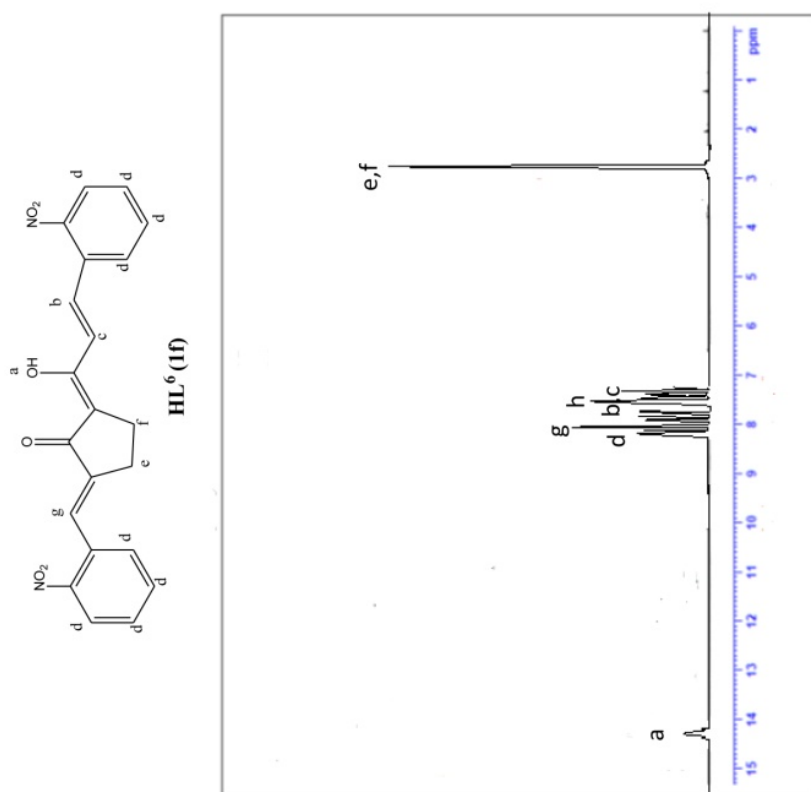
¹H NMR (400MHz, CDCl₃, ppm): δ 14.17 (s,enolic, 1H) [a], [2.76 (t, J=5.4Hz cyclopentane ring CH₂, 2H), 2.84 (t, J=5.4Hz cyclopentane ring CH₂, 2H)] [e,f], [6.79 (d, J=16.3Hz, (E)- alkenyl,1H), 6.94 (d, J=16.4Hz, (E)- alkenyl,1H)] [b,c], 7.11-7.31 (m, aromatic, 8H) [d], 7.42 (s, vinylic, 1H) [g], 2.26 (s, methyl,6H) [h], 7.26 (solvent) [i].

Figure 1.5. ¹H NMR spectrum of **HL⁴ (1d)**



¹H NMR (400MHz, CDCl₃, ppm): δ 14.67 (s, enolic, 1H) [a], [2.68 (t, J=5.5Hz cyclopentane ring CH₂, 2H), 2.73 (t, J=5.5Hz cyclopentane ring CH₂, 2H)] [e,f], [6.64 (d, J=16.2Hz, (E)- alkenyl, 1H), 6.98 (d, J=16.3Hz, (E)- alkenyl, 1H)] [b,c], 7.12-7.32 (m, aromatic, 8H) [d], 7.37 (s, vinylic, 1H) [g], 7.26 (solvent) [h].

Figure 1.6. ¹H NMR spectrum of **HL⁵ (1e)**

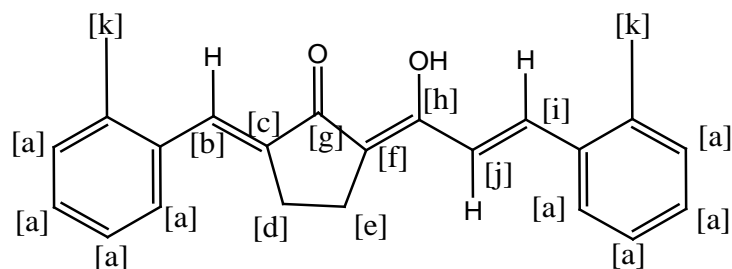


¹H NMR (400MHz, CDCl₃, ppm): δ 14.32 (s, enolic, 1H) [a], [2.72 (t, J=5.7Hz cyclopentane ring CH₂, 2H), 2.79 (t, J=5.7Hz cyclopentane ring, CH₂, 2H)] [e,f], [6.91 (d, J=16.3Hz, (E)-alkenyl, 1H), 7.46 (d, J=16.4Hz, (E)-alkenyl, 1H)] [b,c], 7.51-8.28 (m, aromatic, 8H) [d], 8.02 (s, vinylic, 1H) [g], 7.26 (solvent) [h].

Figure 1.7. ¹H NMR spectrum of **HL⁶ (1f)**

1.4.4 ^{13}C NMR spectra

The ^{13}C NMR spectrum of curcumin, a symmetric molecule, showed a singlet assignable to carbonyl groups. The identical electronic environment of both carbonyl groups is clearly indicated from the appearance of a singlet at ~ 184 ppm^[152]. The ^{13}C NMR spectral data of the ligands showed two resonance signals at ~ 197 ppm and ~ 180 ppm indicating that the two carbonyl groups have different electronic environment. The two aliphatic carbon atoms in the cyclopentanone ring show a resonance signal at ~ 24 ppm. The other two aliphatic carbon atoms in the cyclopentanone ring show a resonance signal at ~ 29 ppm. The resonance signals in the range 110-170 ppm are due to the aromatic carbon atoms (**Table 1.4**). The spectra are attached in **Figures 1.8-1.13**.

Table 1.4 ^{13}C NMR spectral data of ligands

Compounds	Chemical shift (ppm)										
	[a]	[b]	[c]	[d]	[e]	[f]	[g]	[h]	[i]	[j]	[k]
HL¹	120.35-140.10	140.72	147.89	23.08	26.58	94.85	170.82	193.17	123.18	144.62	-
HL²	115.42-128.86	145.23	141.29	25.58	29.78	96.87	180.76	195.54	118.54	133.75	-
HL³	117.89-167.25	143.12	152.21	24.37	27.61	93.64	179.83	194.77	131.12	139.12	57.88
HL⁴	121.72-147.63	144.21	141.04	23.47	28.79	96.74	187.45	195.31	115.52	137.14	18.87
HL⁵	126.35-132.54	142.84	141.86	25.41	29.24	95.75	182.33	197.21	120.97	130.58	-
HL⁶	121.54-146.84	144.64	140.98	25.94	29.25	95.36	181.34	195.98	117.54	132.45	-

1.4.5 Mass spectra

Mass spectra of all the ligands displayed an intense molecular ion peak and peaks due to the elimination of O, OH, ArCH₂, R, CH₂, C₂H₂ and Ph species from the molecular ion (M⁺)^[189,190]. The spectra are shown in **Figure 1.14-1.19**. A comparison of mass spectral data suggests a common fragmentation pattern for the compounds which is independent on the nature of phenyl substituent. Peaks having relative intensity above 50% that fit into the common fragmentation pattern are only depicted in **Table 1.2**. A probable fragmentation pattern is given in **Figure 1.20**.

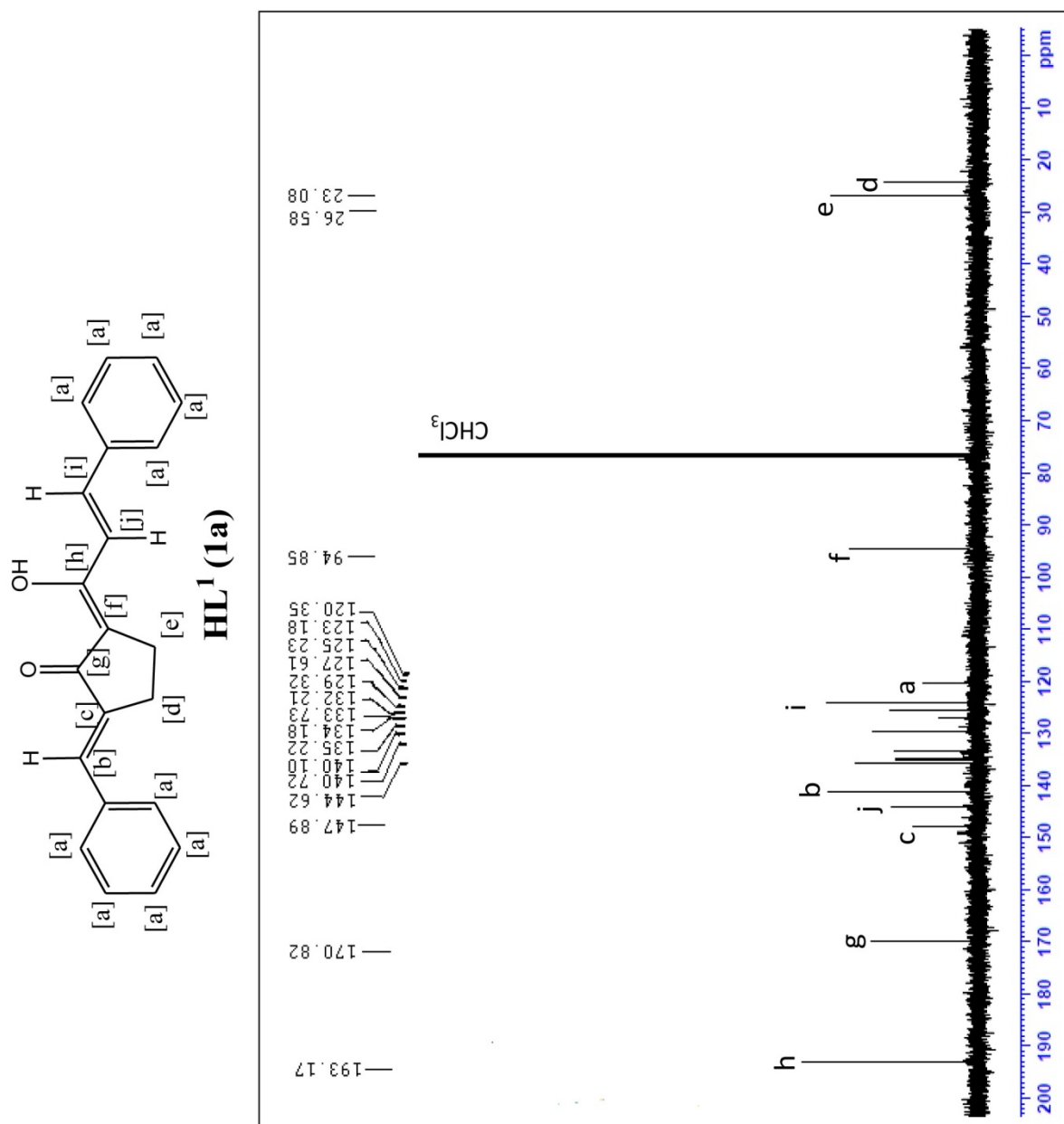


Figure 1.8. ¹³C NMR spectrum of **HL¹ (1a)**

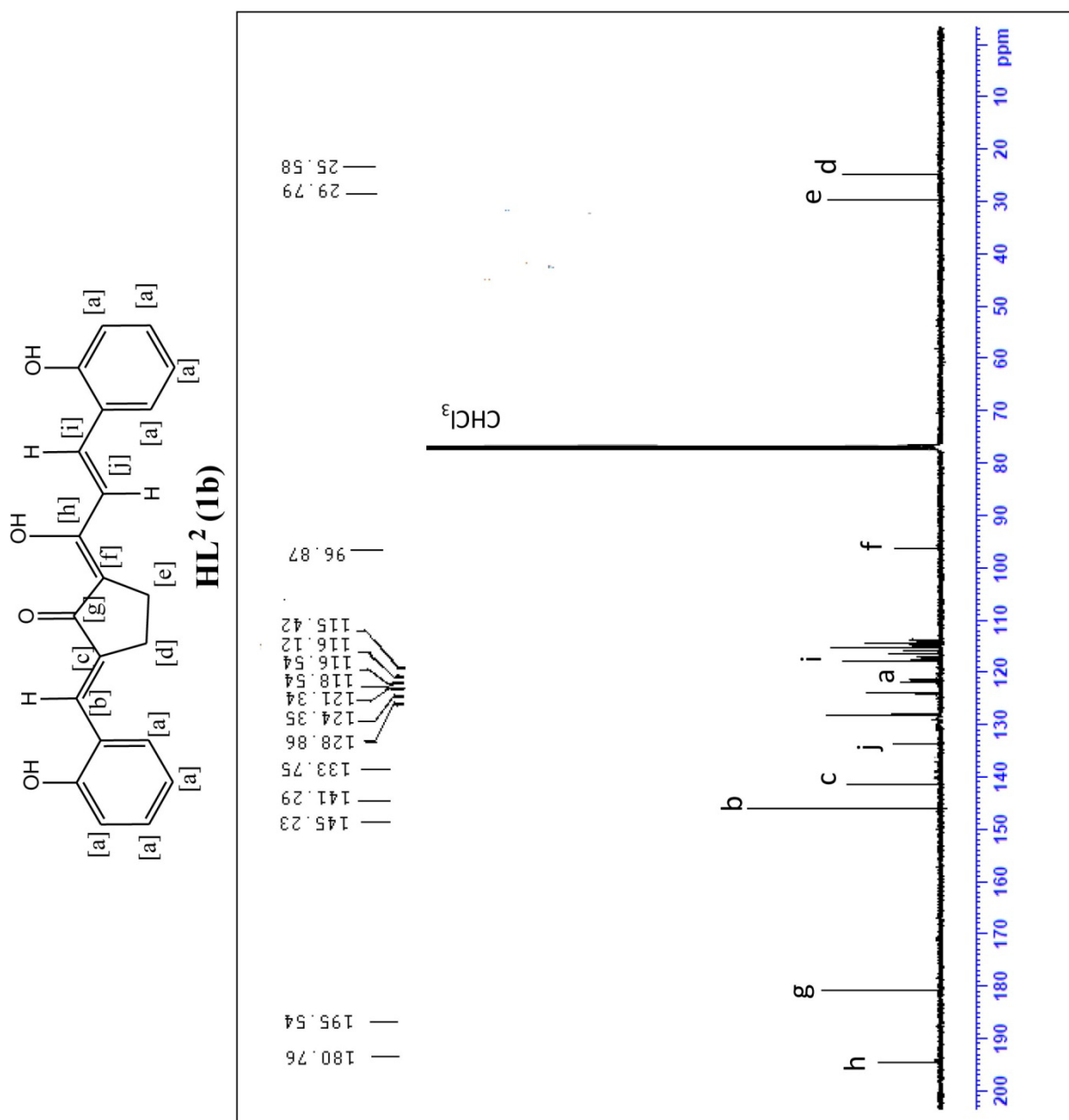


Figure 1.9. ^{13}C NMR spectrum of HL^2 (1b)

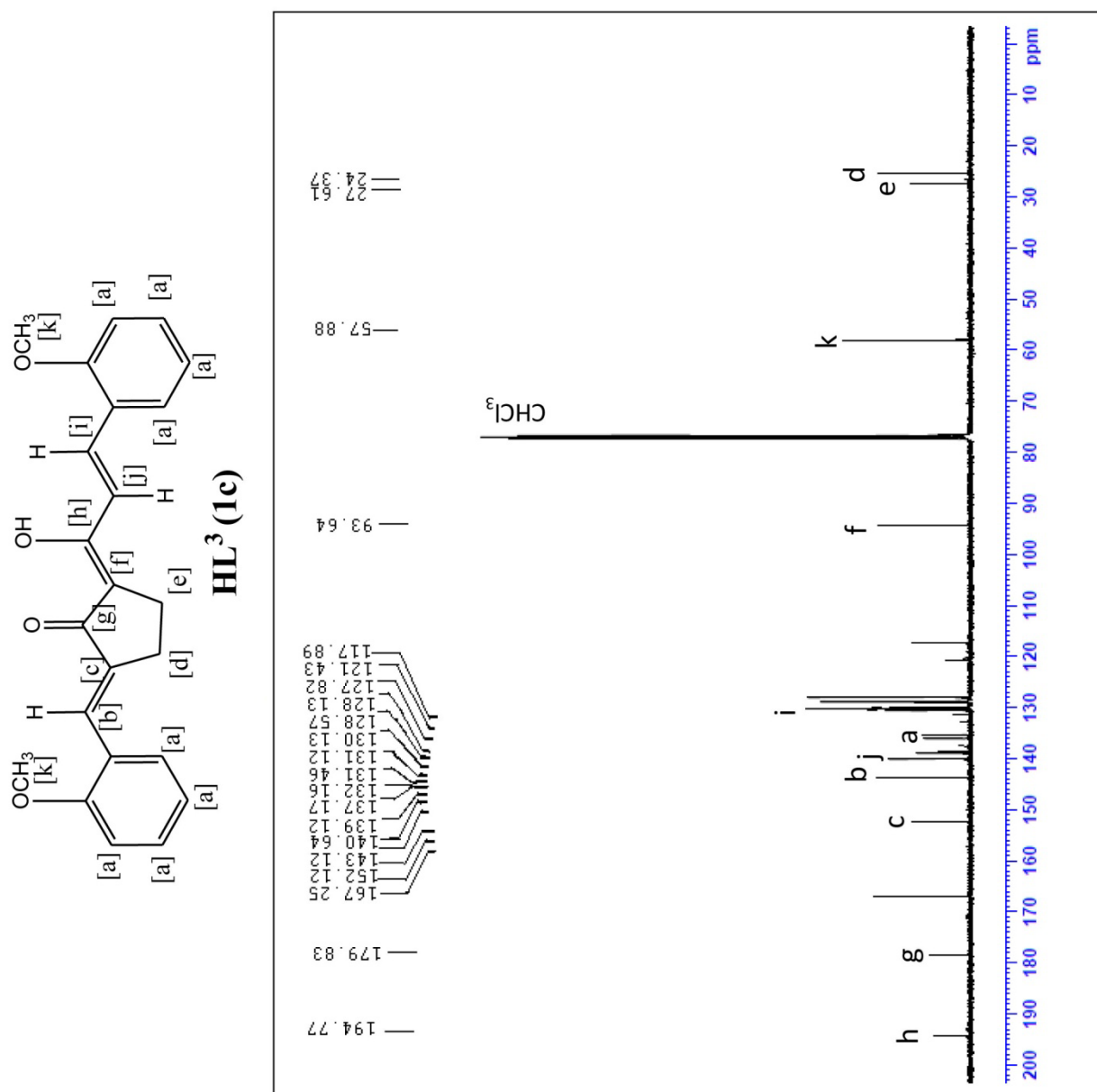


Figure 1.10. ¹³C NMR spectrum of **HL³(1c)**

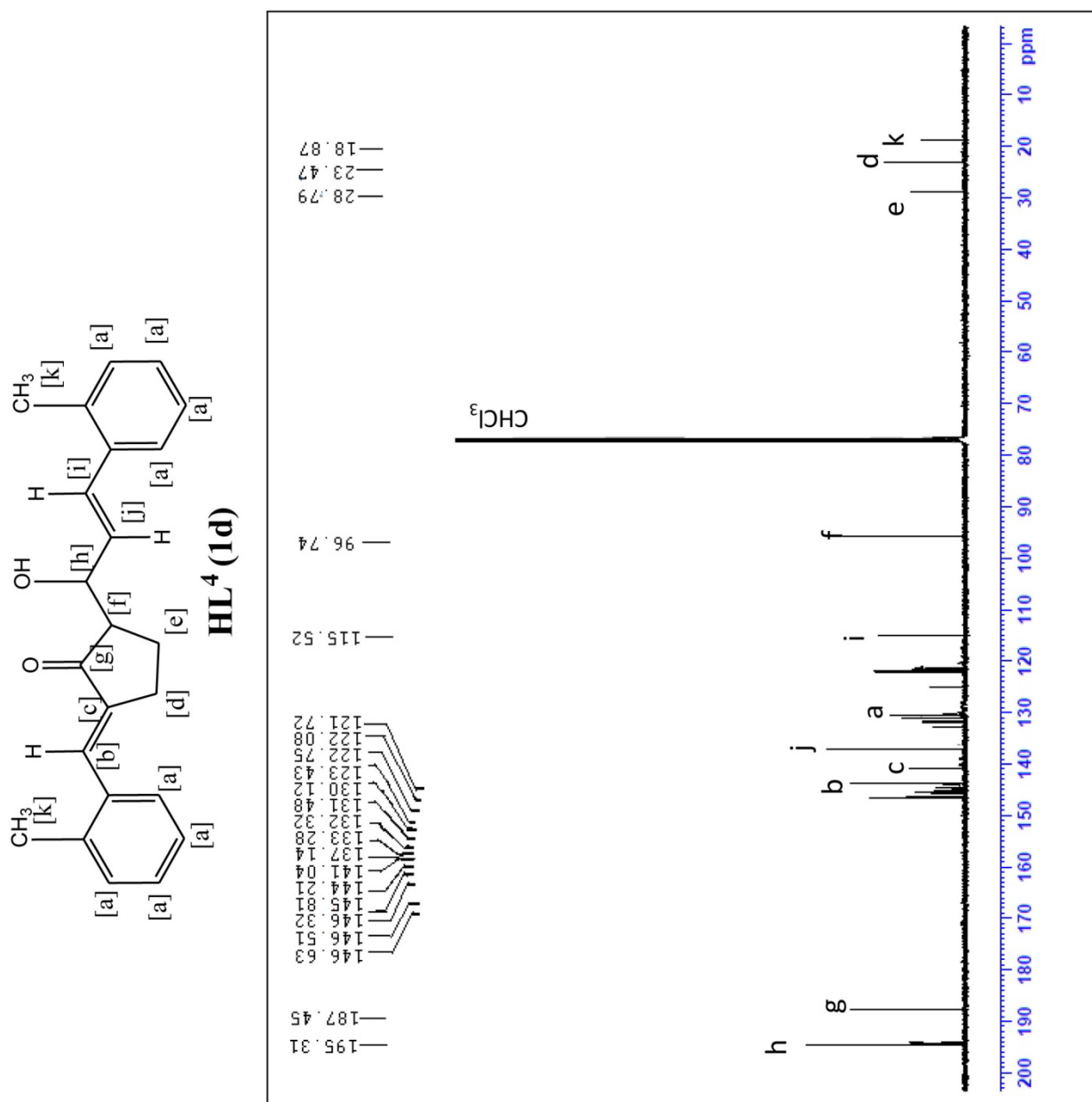


Figure 1.11. ¹³C NMR spectrum of **HL⁴ (1d)**

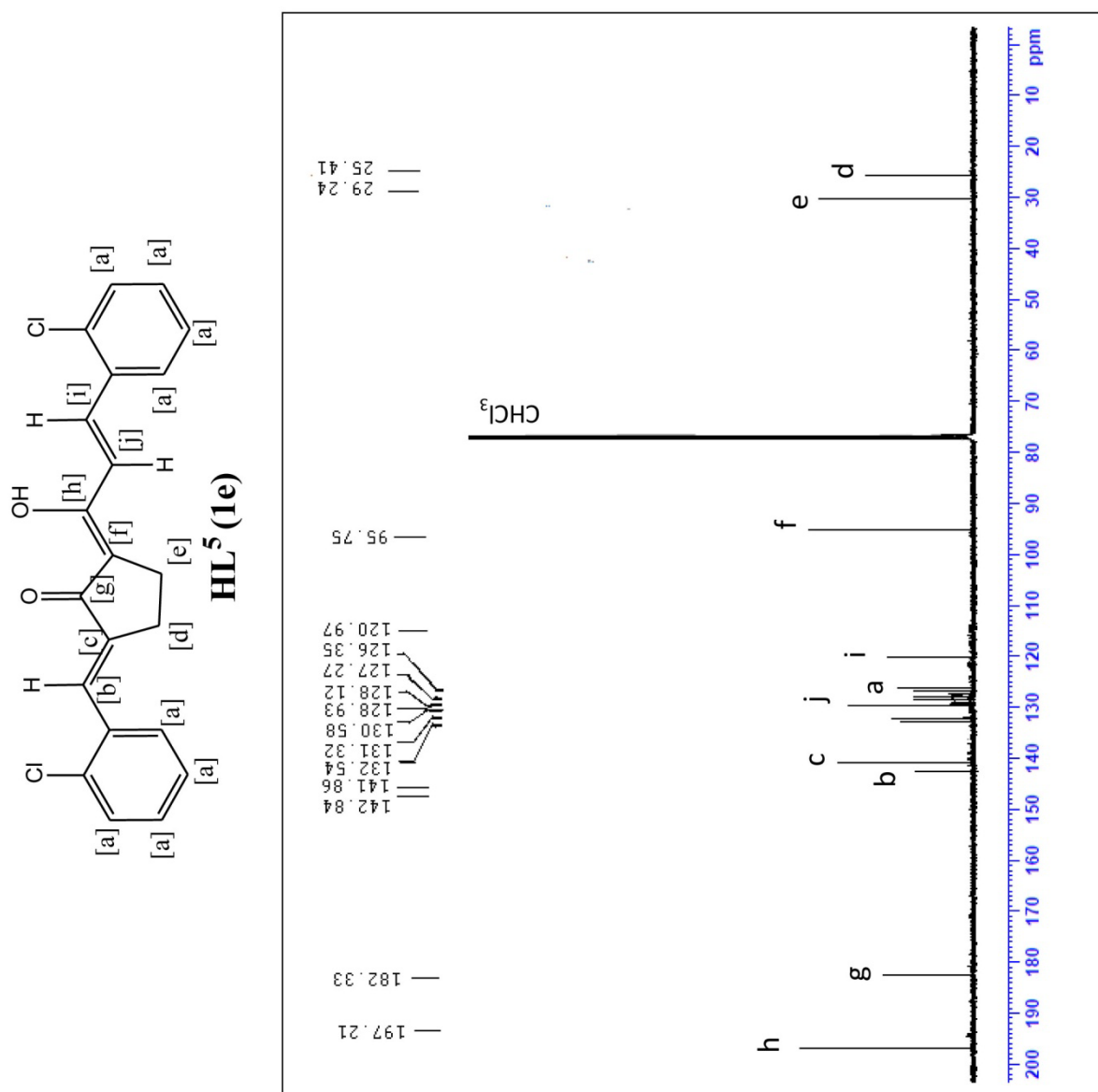


Figure 1.12. ¹³C NMR spectrum of **HL⁵ (1e)**

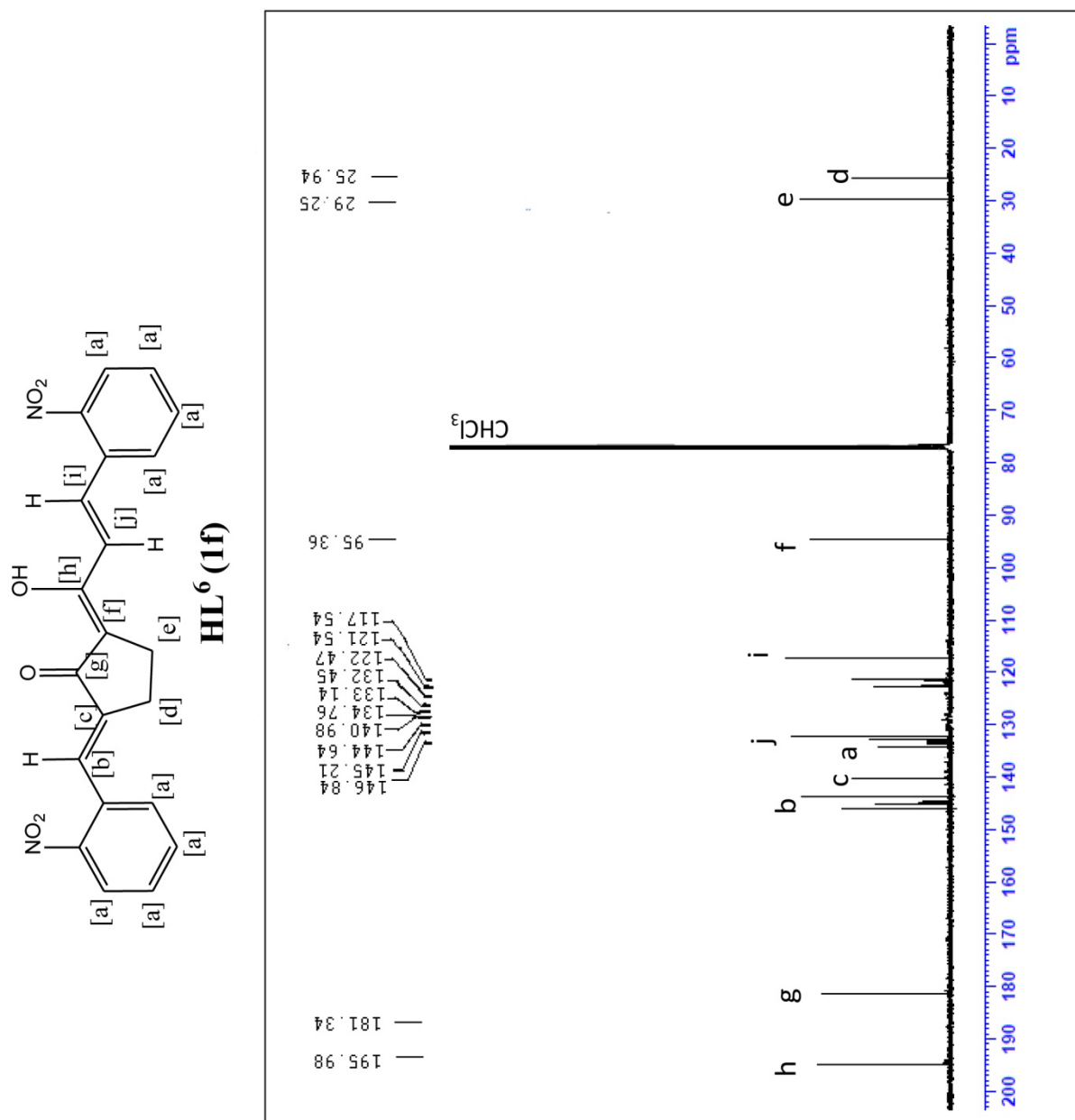


Figure 1.13. ¹³C NMR spectrum of **HL⁶ (1f)**

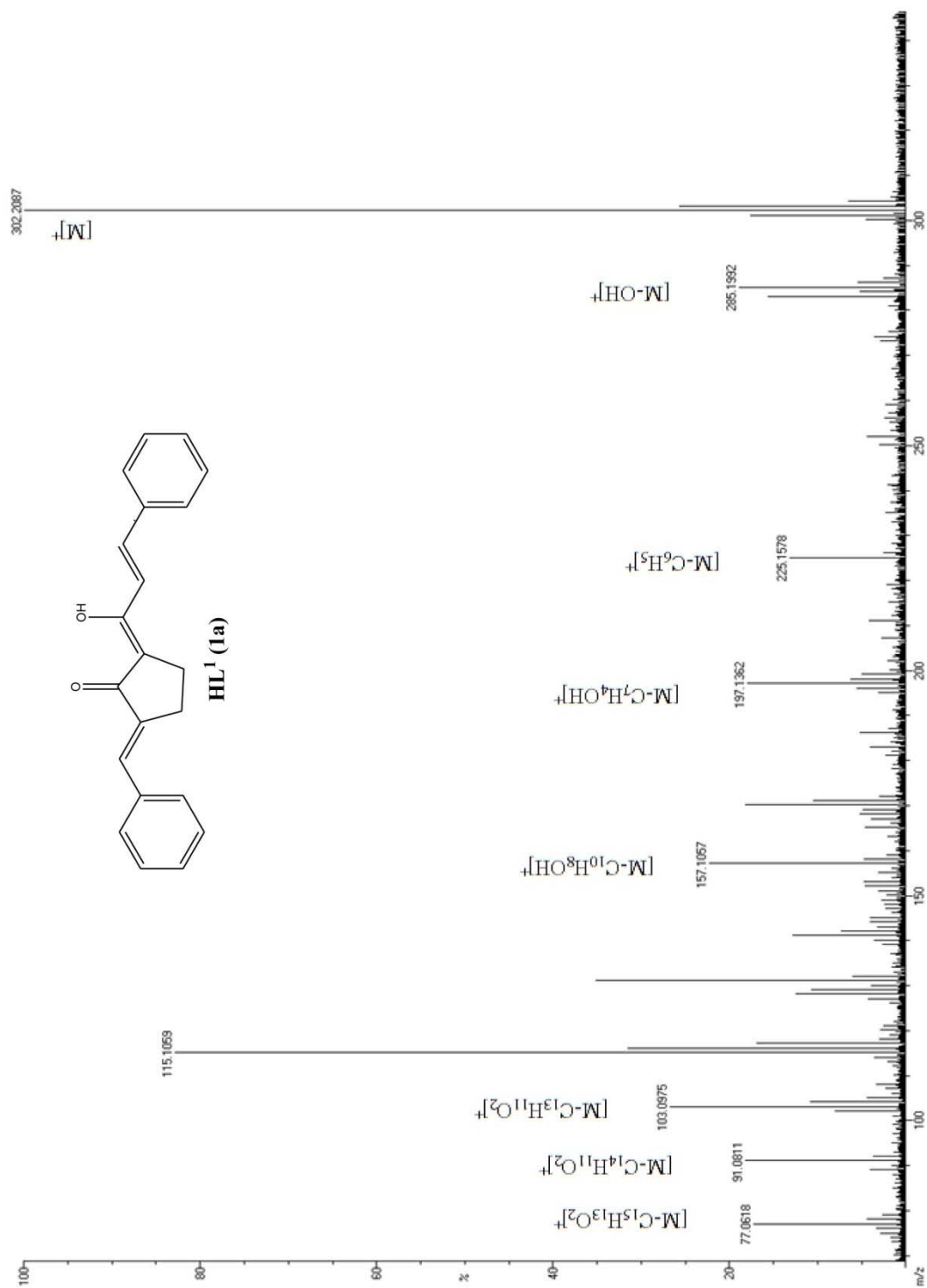


Figure 1.14. EI Mass spectrum of **HL¹ (1a)**

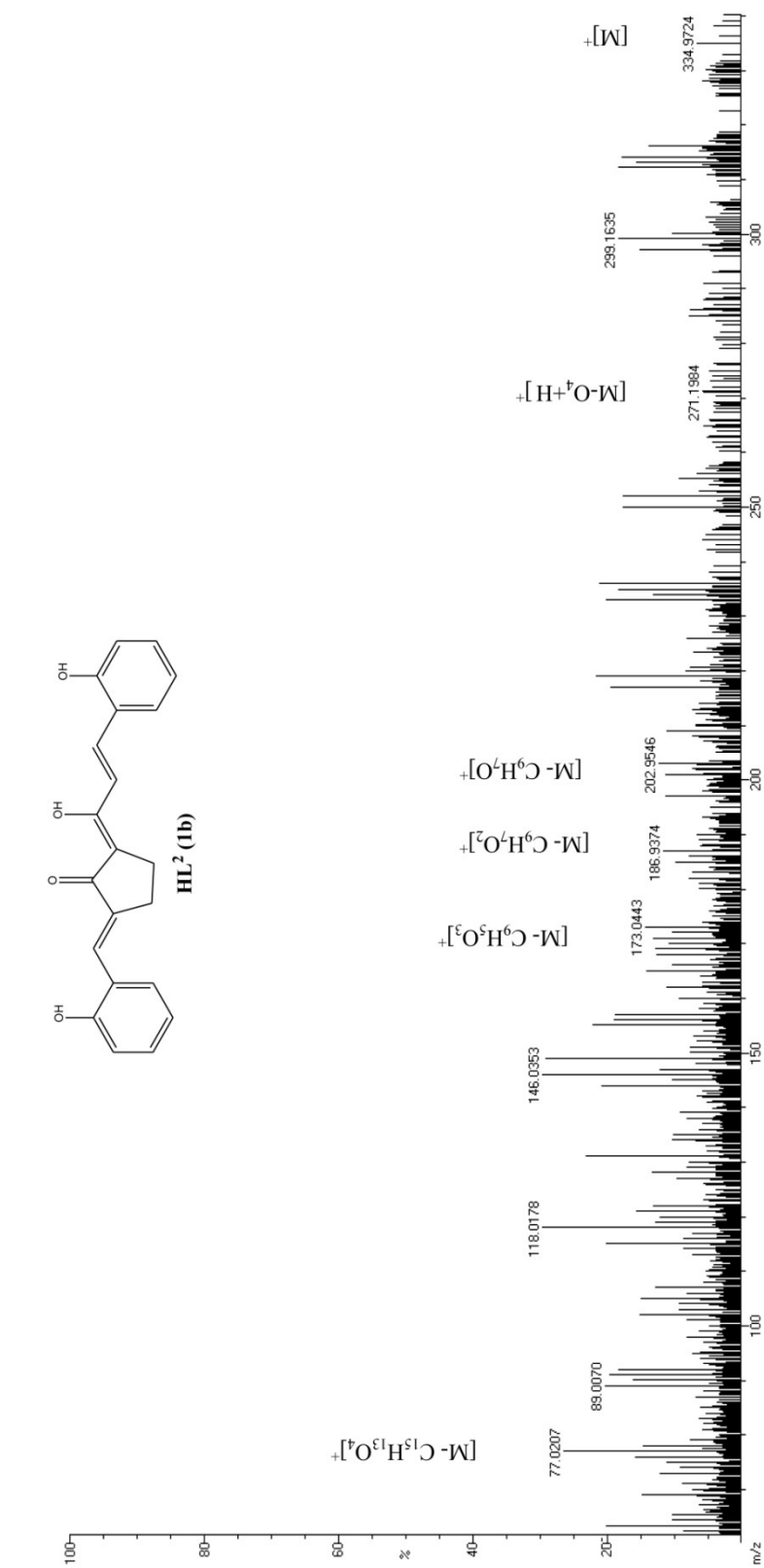


Figure 1.15. EI Mass spectrum of **HL² (1b)**

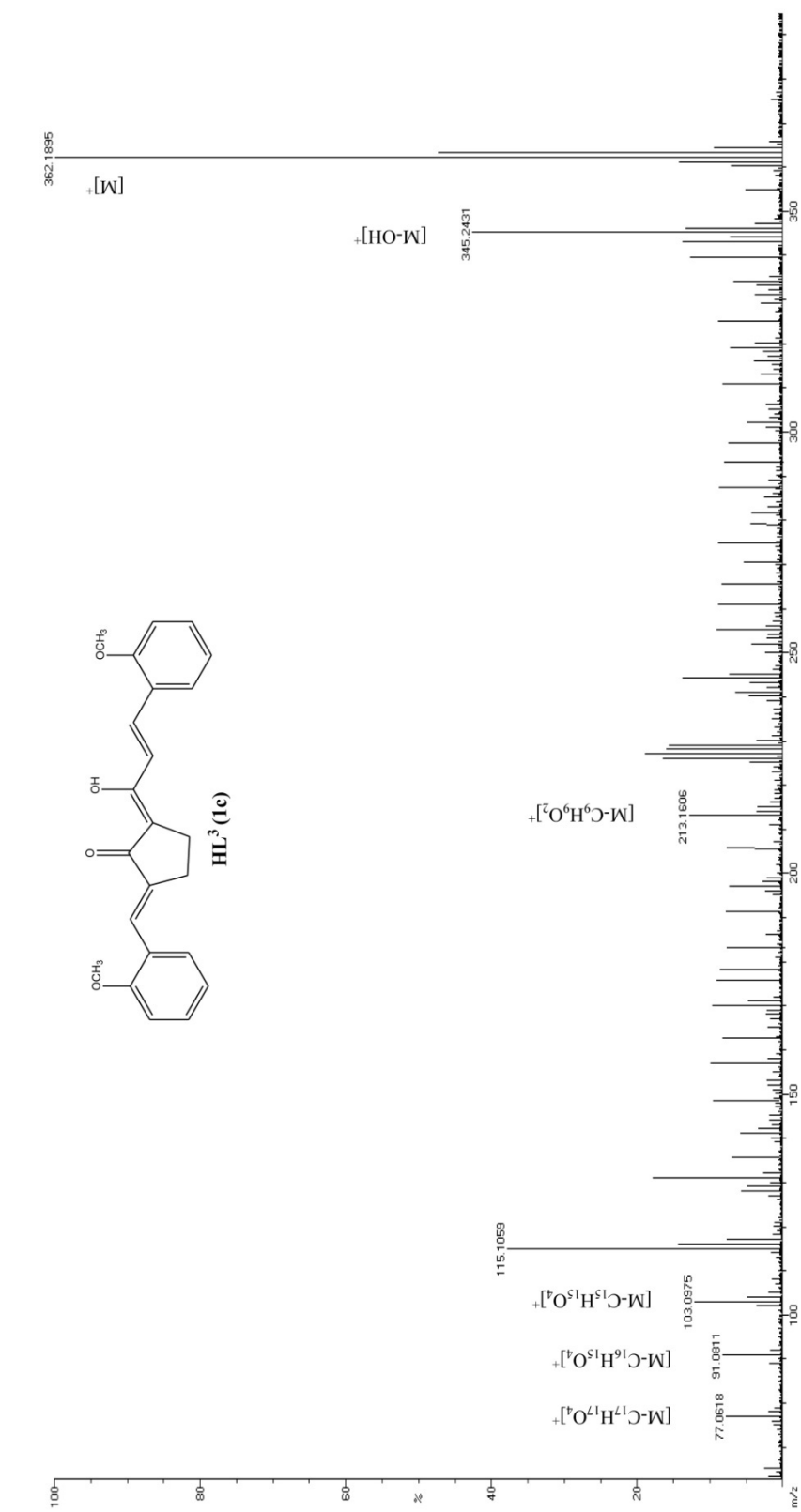


Figure 1.16. EI Mass spectrum of **HL³ (1c)**

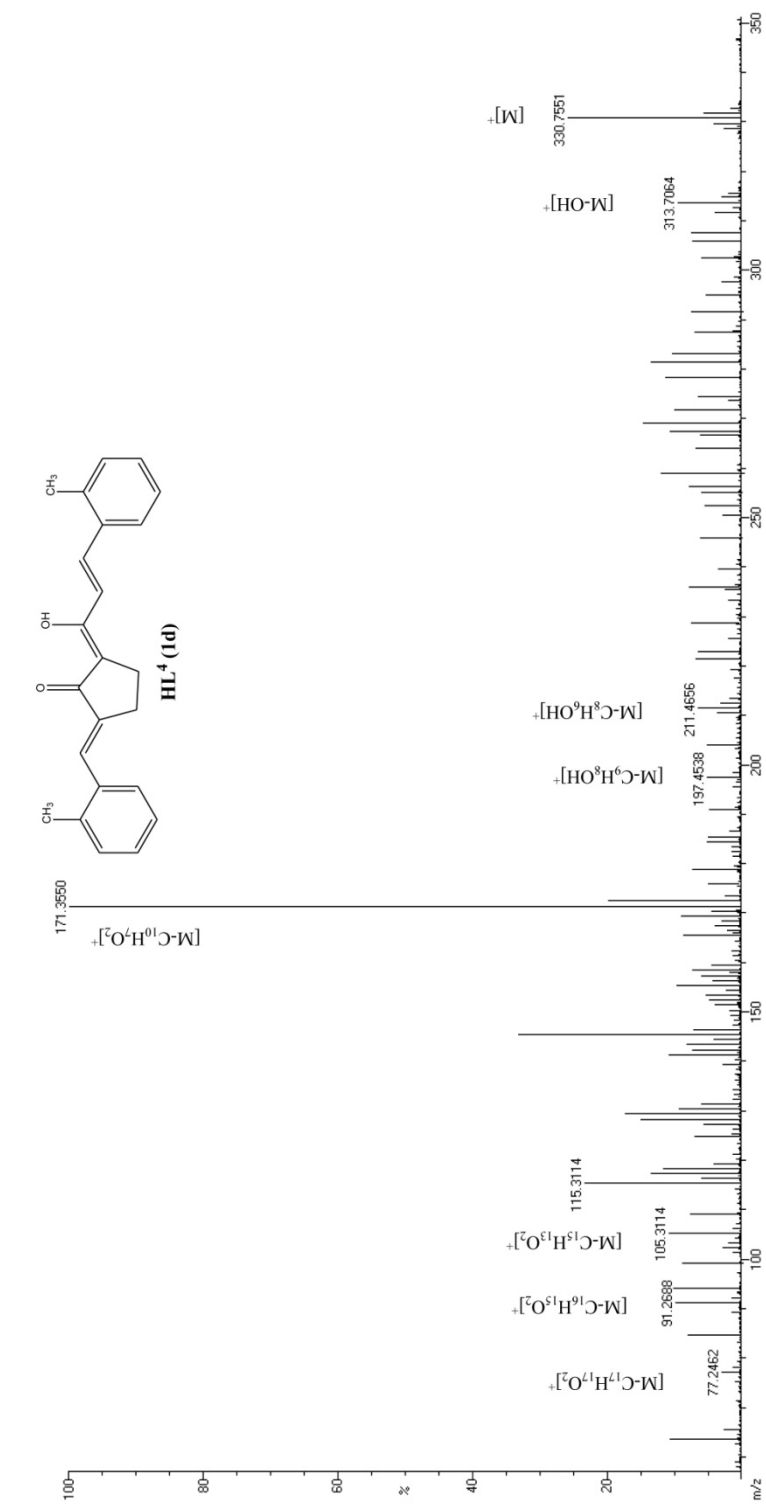


Figure 1.17. EI Mass spectrum of **HL⁴ (1d)**

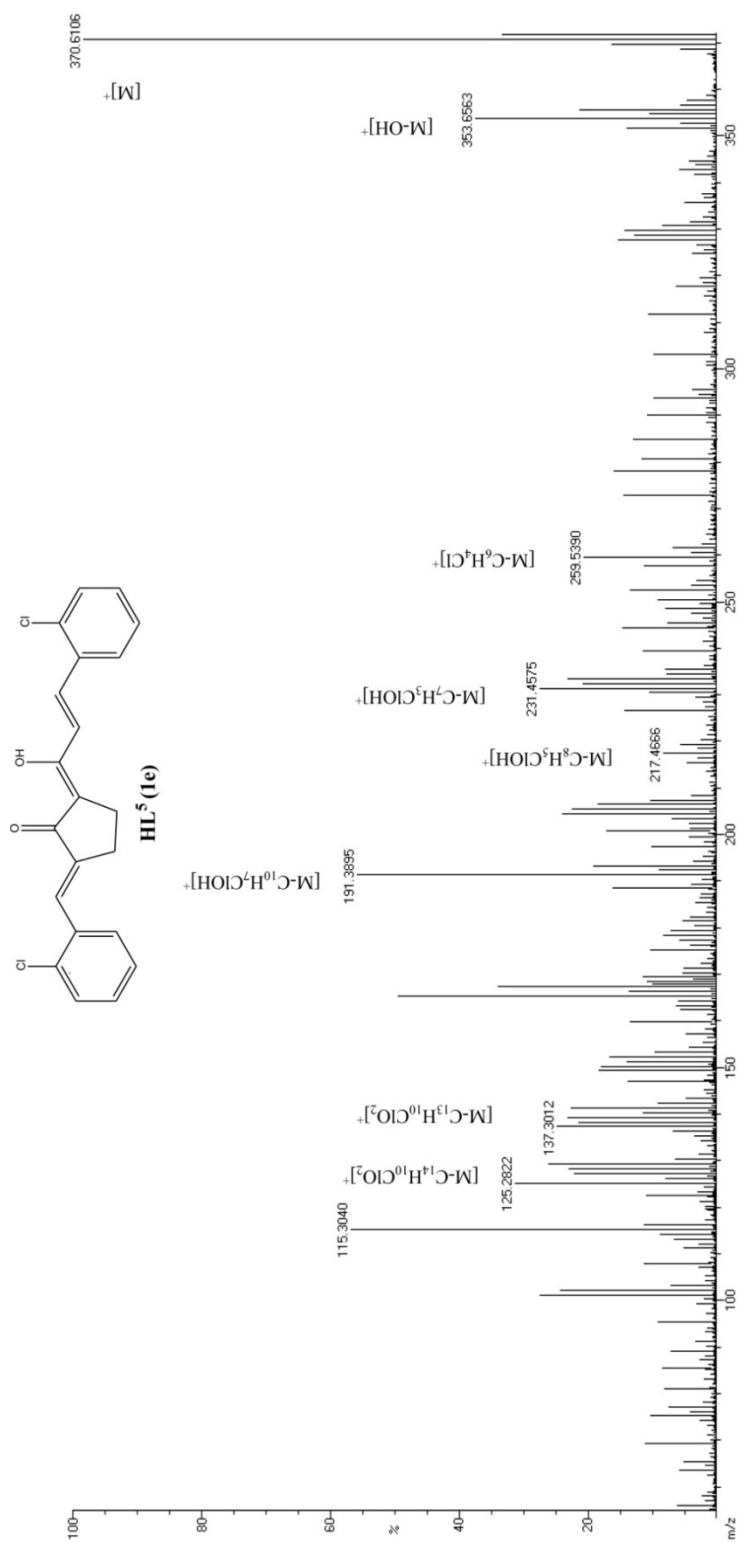


Figure 1.18. EI Mass spectrum of **HL⁵ (1e)**

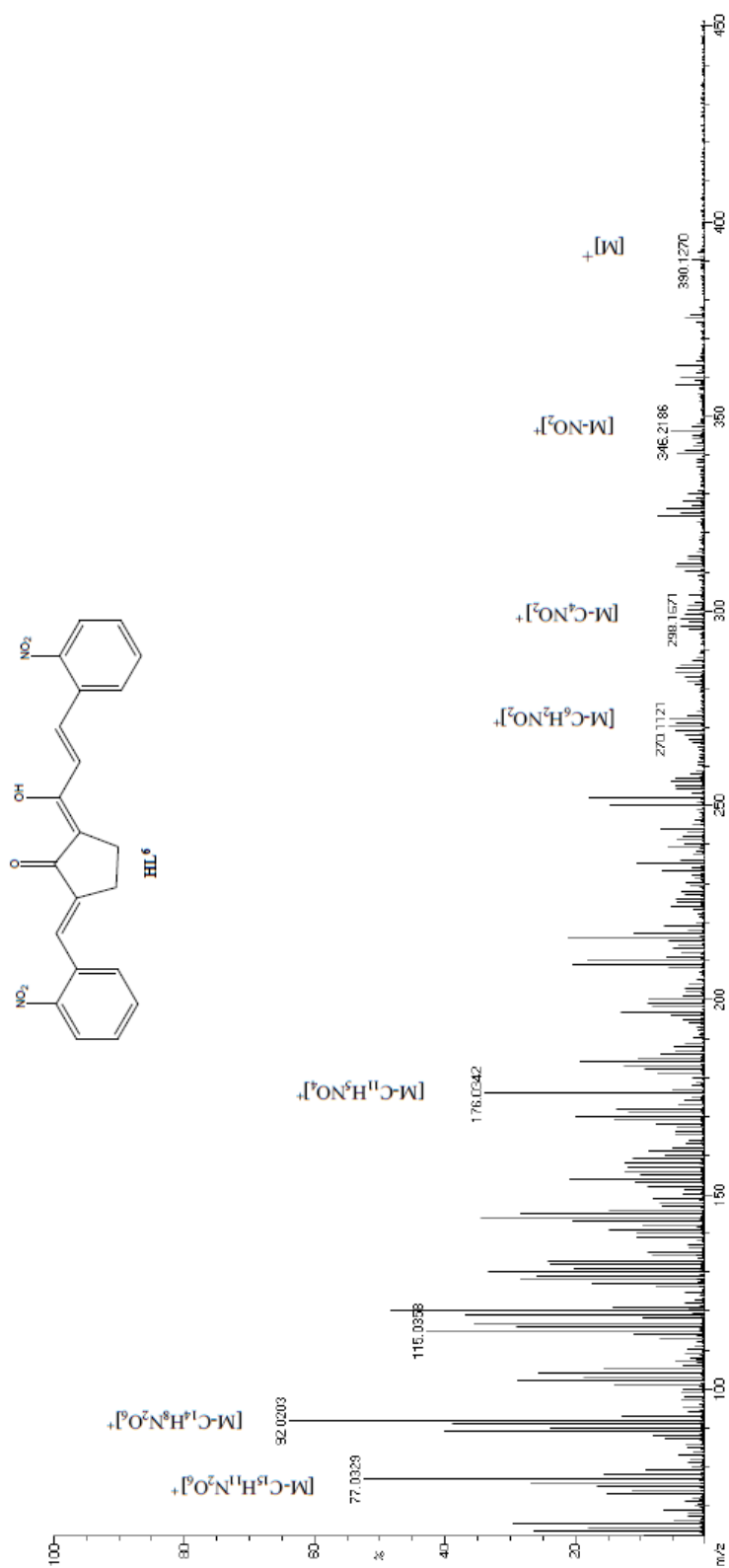


Figure 1.19. EI Mass spectrum of **HL⁶** (1f)

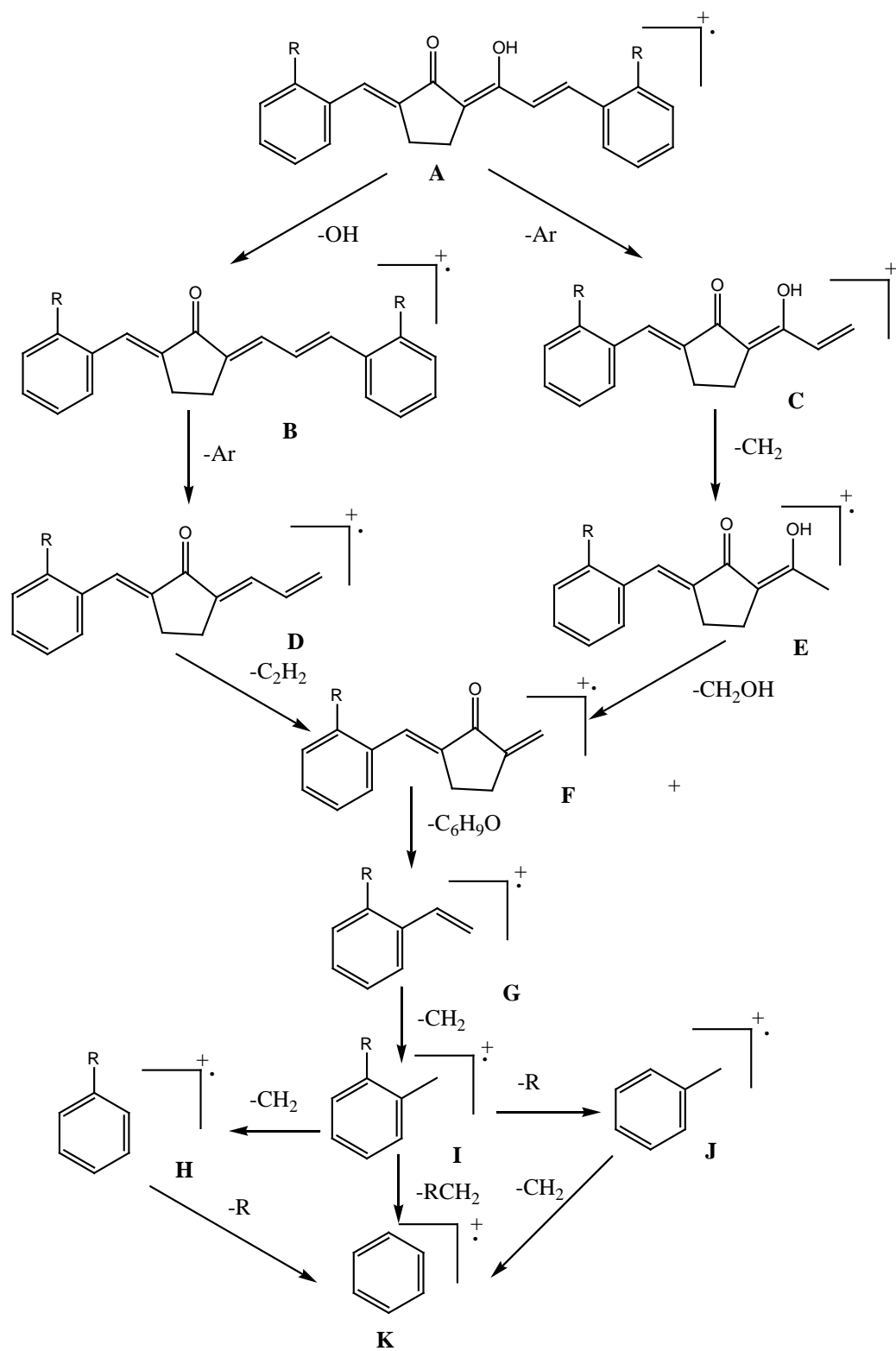


Figure 1.20. Fragmentation pattern of ligands

From the above spectral data, the probable structure of ligands can be assigned as **I** in **Scheme 1.2**.

1.5 Characterization of metal complexes

Analytical and physical data of the metal complexes are given in **Tables.1.5-1.7**. The observed carbon, hydrogen and metal percentages of the metal complexes and mass spectral data suggest their ML_2 stoichiometry. All the metal complexes behaved as non-electrolytes (specific conductance in the range 8 - 12 $\Omega^{-1} \text{ cm}^{-1}$ in DMF) and do not contain the anion of the metal salt used for their preparation. The nickel(II) and zinc(II) complexes are diamagnetic and copper(II) complexes are paramagnetic. Copper(II) complexes showed a normal magnetic moment (μ_{eff} 1.75-1.81BM). The electronic, IR, ^1H NMR, ^{13}C NMR and mass spectral data of the complexes are compatible with the structure **II** given in **Scheme 1.2**. The spectral data are discussed below.

Table 1.5 Analytical data of copper (II) complexes

Complexes (formula weight)	M.p. (°C)	Yield (%)	Elemental analysis % (found /calcd)			UV λ_{\max} (nm)	μ_{eff} BM	Mass spectral data
			C	H	Cu			
[Cu(L¹)₂] C ₄₂ H ₃₄ O ₄ Cu (666)	268	69	(75.82) 75.71	(5.43) 5.14	(9.57) 9.54	246 425	1.78	667, 665, 363, 301, 208, 194
[Cu(L²)₂] C ₄₂ H ₃₄ O ₈ Cu (730)	176	62	(69.01) 69.08	(4.62) 4.69	(8.61) 8.70	260 462	1.77	752, 731, 729, 395, 334, 224, 210
[Cu(L³)₂] C ₄₆ H ₄₂ O ₈ Cu (786)	152	67	(70.14) 70.26	(5.27) 5.38	(8.16) 8.08	251 448	1.75	787, 785, 423, 361, 238, 224
[Cu(L⁴)₂] C ₄₆ H ₄₂ O ₄ Cu (722)	162	66	(76.34) 76.48	(5.43) 5.86	(8.76) (8.80)	260 455	1.81	723, 721, 391, 330, 222, 208
[Cu(L⁵)₂] C ₄₂ H ₃₀ O ₄ Cl ₄ Cu (804)	164	63	(62.43) 62.74	(3.52) 3.76	(7.71) 7.90	252 446	1.80	826, 805, 803, 432, 370, 243, 229
[Cu(L⁶)₂] C ₄₂ H ₃₀ N ₄ O ₁₂ Cu (846)	178	68	(59.14) 59.61	(3.24) 3.57	(7.41) 7.51	245 478	1.76	847, 845, 453, 391, 253, 239

Table 1.6 Analytical data of nickel (II) complexes

Complexes (formula weight)	M.p. (°C)	Yield (%)	Elemental analysis %			UV λ_{\max} (nm)
			(found /calcd)			
			C	H	Ni	
[Ni(L¹)₂] C ₄₂ H ₃₄ O ₄ Ni (661)	112	69	(76.46) 76.27	(5.54) 5.18	(8.52) 8.87	248 484
[Ni(L²)₂] C ₄₂ H ₃₄ O ₈ Ni (724)	212	61	(69.25) 69.54	(4.67) 4.72	(8.43) 8.09	268 438
[Ni(L³)₂] C ₄₆ H ₄₂ O ₈ Ni (781)	168	63	(70.21) 70.70	(5.23) 5.42	(7.43) 7.51	254 458
[Ni(L⁴)₂] C ₄₆ H ₄₂ O ₄ Ni (717)	172	64	(77.24) 77.00	(5.68) 5.90	(8.35) 8.18	268 476
[Ni(L⁵)₂] C ₄₂ H ₃₀ O ₄ Cl ₄ Ni (779)	224	62	(63.89) 63.12	(3.84) 3.78	(7.86) 7.34)	233 458
[Ni(L⁶)₂] C ₄₂ H ₃₀ N ₄ O ₁₂ Ni (841)	234	63	(59.34) 59.95	(3.78) 3.59	(7.12) 6.98	254 474

Table 1.7 Analytical data of zinc (II) complexes

Complexes (formula weight)	M.p. (^o C)	Yield (%)	Elemental analysis %			UV λ_{\max} (nm)
			(found /calcd)			
			C	H	Zn	
[Zn(L¹)₂] C ₄₂ H ₃₄ O ₄ Zn (668)	176	68	(75.67) 75.50	(5.32) 5.13	(9.81) 9.79	262 451
[Zn(L²)₂] C ₄₂ H ₃₄ O ₈ Zn (732)	206	65	(68.54) 68.90	(4.21) 4.68	(8.14) 8.93	274 468
[Zn(L³)₂] C ₄₆ H ₄₂ O ₈ Zn (788)	210	62	(70.76) 70.09	(5.84) 5.37	(8.67) 8.30	276 472
[Zn(L⁴)₂] C ₄₆ H ₄₂ O ₄ Zn (724)	224	61	(76.81) 76.29	(5.23) 5.85	(9.68) 9.03	258 482
[Zn(L⁵)₂] C ₄₂ H ₃₀ O ₄ Cl ₄ Zn (805)	236	63	(62.19) 62.60	(3.31) 3.75	(8.86) 8.11	275 472
[Zn(L⁶)₂] C ₄₂ H ₃₀ N ₄ O ₁₂ Zn (848)	248	61	(59.94) 59.48	(3.69) 3.57	(7.46) 7.71	284 446

1.5.1 Electronic spectra

The UV spectra of the complexes displayed two absorption maxima, one low energy band in the range 425-484 nm due to an $n \rightarrow \pi^*$ transition and another high energy band in the range 233-284 nm due to a $\pi \rightarrow \pi^*$ transition^[186]. In the metal complexes these absorption bands show only a slight bathochromic shifts due to the involvement of the carbonyl group in metal complexation. Similarity in the UV absorption maxima of metal complexes with that of free ligands, show that no structural alteration of the ligand has occurred during the complex formation. (**Tables 1.3-1.5**).

In the copper(II) complexes, the presence of a broad visible band at ~665 nm and the measured μ_{eff} values (1.75–1.81 B.M.) support their square planar structure^[191]. The observed diamagnetism and broad medium-intensity band in the region 562-581 nm in the visible spectra of the nickel(II) chelates suggest their square-planar geometry. In conformity with this observation the visible spectra of the nickel chelates in pyridine solution (10^{-3} M) showed three bands corresponding to a configurational change from square-planar to octahedral due to the association of pyridine. The absorption maxima in the regions 1243-1253 nm ($\epsilon = 4.30 \times 10^4 - 4.85 \times 10^4 \text{ M}^{-1} \text{ cm}^{-1}$), 736-770 nm ($\epsilon = 5.23 \times 10^4 - 5.54 \times 10^4 \text{ M}^{-1} \text{ cm}^{-1}$) and 410-424 nm ($\epsilon = 2.43 \times 10^4 - 2.68 \times 10^4 \text{ M}^{-1} \text{ cm}^{-1}$) in the adducts can be assigned to the transitions ${}^3A_{2g} \rightarrow {}^3T_{2g}$; ${}^3A_{2g} \rightarrow {}^3T_{1g}(\text{F})$ and ${}^3A_{2g} \rightarrow {}^3T_{1g}(\text{P})$, respectively^[192].

1.5.2 Infrared Spectra

In the IR spectra of the metal complexes, the bands of diketones are absent and instead a strong band assignable to the stretching of the carbonyl moiety appeared at $\sim 1613 \text{ cm}^{-1}$. The broad free ligand band in the region at $2800-3600 \text{ cm}^{-1}$ due to the hydrogen bonded enol proton is absent in the spectra of metal complexes and weak bands attributable to various $\nu_{(\text{C-H})}$ appeared. The carbonyl groups are involved in metal complex formation is

evident from the appearance of two medium intensity bands in the region 426-507 cm^{-1} due to $\nu_{(\text{M-O})}$ vibrations^[186]. The prominent band at $\sim 975\text{ cm}^{-1}$ (**Table 1.8**) is typical of a trans $-\text{CH}=\text{CH}-$ group which remained unaltered in the spectra of metal complexes^[189].

Bands due to aromatic C-Cl stretching band in **1e** and the symmetric and asymmetric stretching due to NO_2 group in **1f** are remained unaltered in their metal complexes^[186].

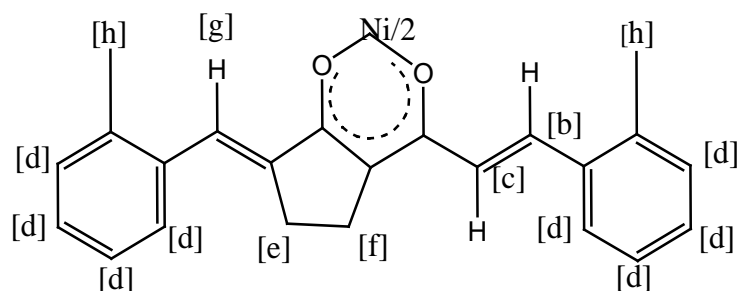
1.5.3 ^1H NMR spectra

The most characteristic feature of the ^1H NMR spectra of the diamagnetic nickel(II) and zinc(II) chelates is the absence of proton signals above $\delta\sim 10$ ppm^[186]. This strongly supports the replacement of the enolic proton by the metal ion in the complexes. The ^1H NMR spectra of $[\text{Ni}(\text{L}^2)_2]$ showed a downfield singlet at 9.92 ppm (**Table 1.9**) due to phenolic proton^[182,155]. The most characteristic feature of the ^1H NMR spectra of the diamagnetic nickel(II) and zinc(II) chelates is the absence of proton signals above $\delta\sim 9$ ppm. This strongly supports the replacement of the enolic proton by the metal ion in the complexes. Observed J value of 16.2 Hz for the alkenyl proton signals in the complexes, suggest their trans orientation as it is in the free ligands.

Table 1.8 IR spectral data of Cu^{II}, Ni^{II} and Zn^{II} complexes

IR spectral data of complexes (cm ⁻¹)							
Compounds	$\nu(\text{C}=\text{O})$ metal chelated carbonyl	$\nu(\text{C}=\text{C})$ phenyl	$\nu(\text{C}=\text{C})$ alkenyl	$\nu_{\text{as}}(\text{C}-\text{C}-\text{C})$ chelate ring	$\nu_{\text{as}}(\text{C}-\text{C}-\text{C})$ chelate ring	$\nu(\text{CH}=\text{CH}-)$ trans	$\nu(\text{M}-\text{O})$ chelate ring
[Cu(L ¹) ₂]	1619,1553	1475	1411	1296	1244	984	481
[Cu(L ²) ₂]	1547,1514	1453	1368	1252	1164	965	468
[Cu(L ³) ₂]	1602,1551	1454	1445	1284	1123	934	507
[Cu(L ⁴) ₂]	1617,1521	1464	1358	1294	1194	984	474
[Cu(L ⁵) ₂]	1594,1512	1434	1384	1254	1131	952	462
[Cu(L ⁶) ₂]	1605,1541	1474	1402	1263	1256	972	426
[Ni(L ¹) ₂]	1667,1598	1473	1415	1243	1127	958	466
[Ni(L ²) ₂]	1542,1507	1443	1384	1247	1147	972	452
[Ni(L ³) ₂]	1634,1524	1432	1272	1264	1141	963	467
[Ni(L ⁴) ₂]	1647,1538	1476	1316	1226	1138	958	458
[Ni(L ⁵) ₂]	1586,1534	1478	1386	1268	1176	972	462
[Ni(L ⁶) ₂]	1615,1574	1486	1424	1284	1246	962	454
[Zn(L ¹) ₂]	1624,1546	1442	1434	1213	1145	962	498
[Zn(L ²) ₂]	1644,1572	1452	1405	1253	1154	973	464
[Zn(L ³) ₂]	1657,1568	1467	1413	1245	1154	954	461
[Zn(L ⁴) ₂]	1653,1556	1482	1341	1234	1163	964	458
[Zn(L ⁵) ₂]	1608,1548	1463	1396	1276	1174	981	468
[Zn(L ⁶) ₂]	1634,1549	1484	1428	1251	1168	958	446

Table 1.9 ^1H NMR spectral data of Ni^{II} complexes



Chemical shift, ppm (Coupling constant, Hz)								
Compounds	[a]	[b]	[c]	[d]	[e]	[f]	[g]	[h]
$[\text{Ni}(\text{L}^1)_2]$	-	6.45 (16.1)	6.92 (16.1)	7.48-7.62	2.76 (5.4)	2.81 (5.3)	7.67	-
$[\text{Ni}(\text{L}^2)_2]$	-	6.23 (16.1)	6.38 (16.1)	6.87-7.12	2.81 (5.3)	2.88 (5.3)	6.73	9.92
$[\text{Ni}(\text{L}^3)_2]$	-	6.71 (16.4)	6.84 (16.4)	7.21-7.55	2.74 (5.6)	2.84 (5.7)	7.64	3.78
$[\text{Ni}(\text{L}^4)_2]$	-	6.28 (16.3)	6.74 (16.3)	7.34-7.69	2.81 (5.2)	2.89 (5.4)	7.85	2.25
$[\text{Ni}(\text{L}^5)_2]$	-	6.37 (16.1)	6.51 (16.2)	6.96-7.29	2.64 (5.4)	2.75 (5.5)	6.89	-
$[\text{Ni}(\text{L}^6)_2]$	-	6.47 (16.2)	6.63 (16.2)	7.57-8.21	2.73 (5.6)	2.83 (5.7)	7.35	-

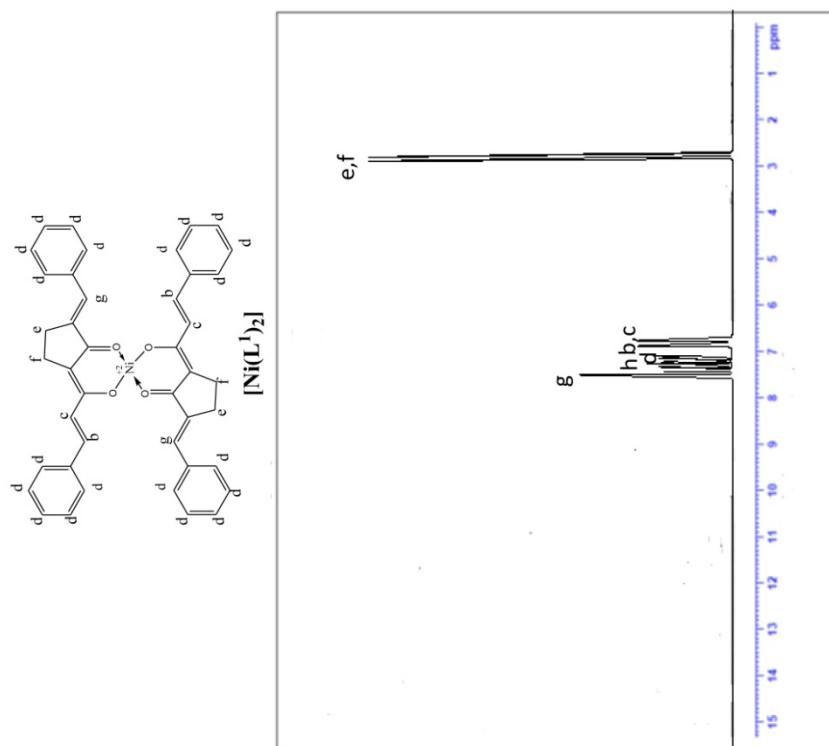
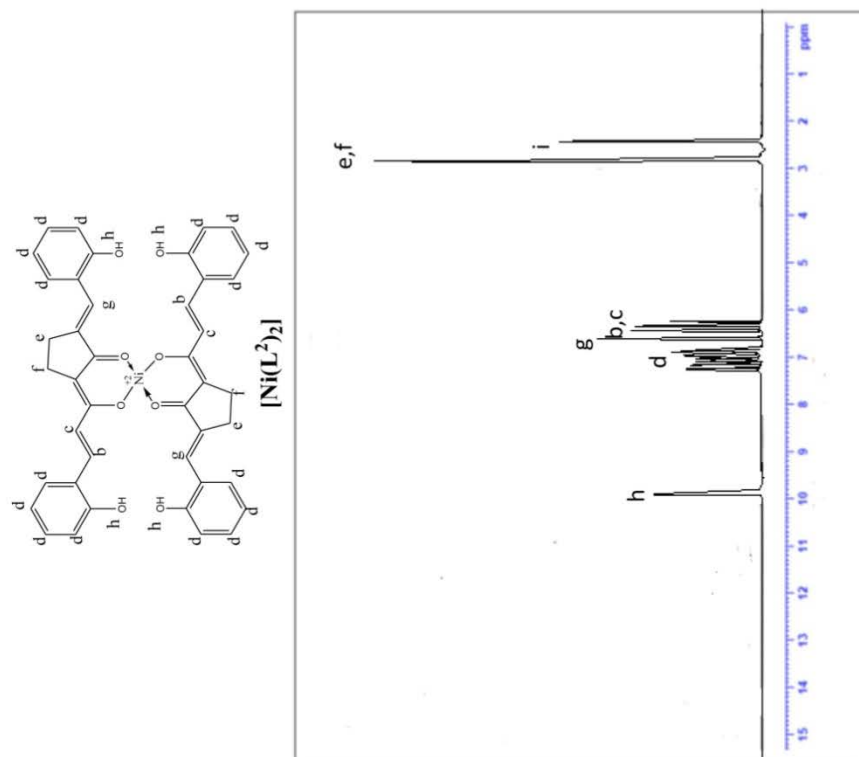


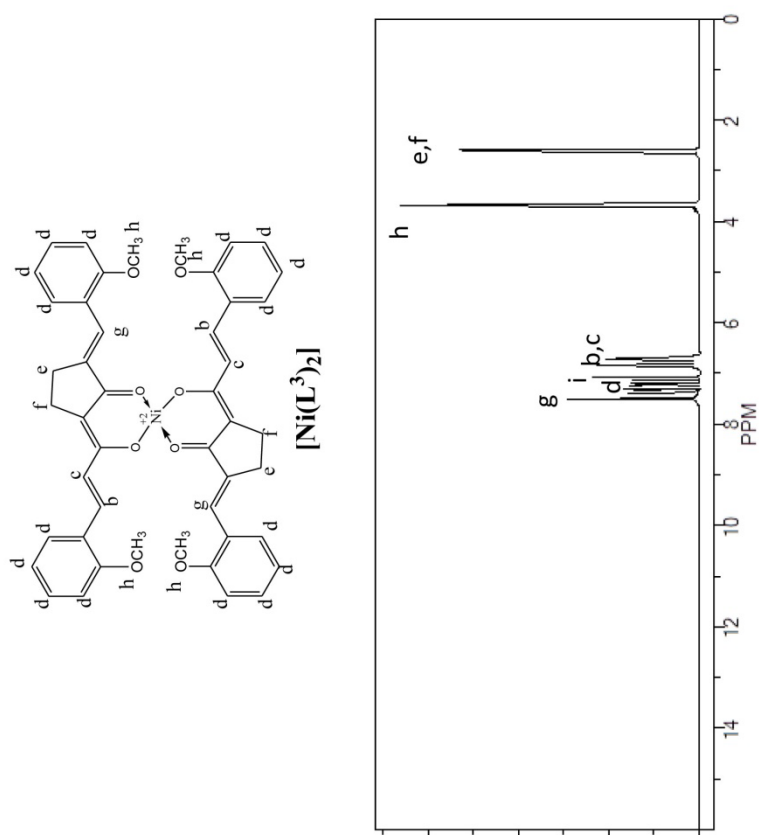
Figure 1.21. ^1H NMR spectrum of $[\text{Ni}(\text{L}^1)_2]$

^1H NMR (400MHz, CDCl_3 , ppm): δ [2.76 (t, $J=5.4$ Hz cyclopentane ring CH_2 , 4H), 2.81 (t, $J=5.3$ Hz cyclopentane ring CH_2 , 4H)] [e,f], [6.45 (d, $J=16.1$ Hz, (E)- alkenyl,2H), 6.92 (d, $J=16.1$ Hz, (E)- alkenyl,2H)] [b,c], 7.48-7.62 (m, aromatic, 20H) [d], 7.26 (s, vinylic, 2H) [g], 7.26 (solvent) [h].



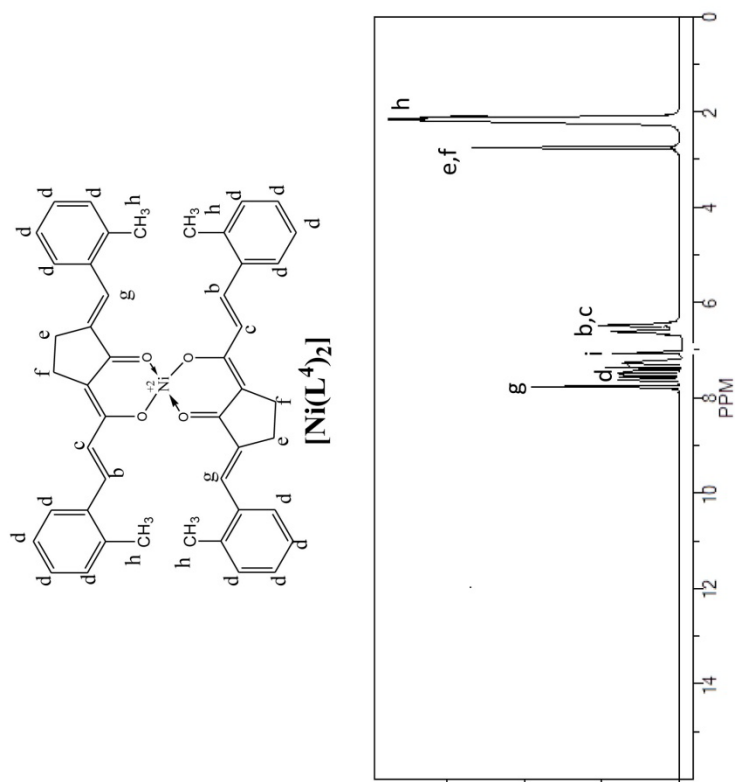
^1H NMR (400MHz, DMSO, ppm): δ [2.81 (t, $J=5.3\text{Hz}$, cyclopentane ring CH_2 , 4H), 2.88 (t, $J=5.3\text{Hz}$, cyclopentane ring CH_2 , 4H) [e,f], [6.23 (d, $J=16.1\text{Hz}$, (E)- alkenyl, 2H), 6.38 (d, $J=16.1\text{Hz}$, (E)- alkenyl, 2H)] [b,c], 6.87-7.12 (m, aromatic, 16H) [d], 6.73 (s, vinylic, 2H) [g], 9.92 (s, phenolic, 4H) [h], 2.49 (solvent) [i].

Figure 1.22. ^1H NMR spectrum of $[\text{Ni}(\text{L}^2)_2]$



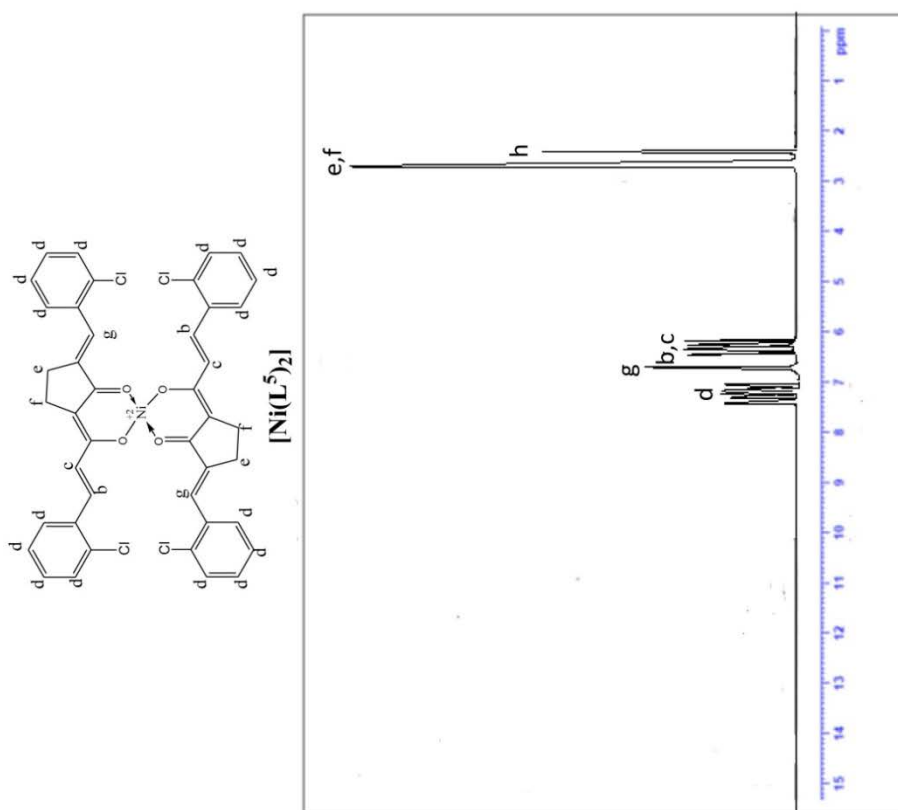
^1H NMR (400MHz, CDCl_3 , ppm): δ [2.74 (t, $J=5.6\text{Hz}$, cyclopentane ring CH_2 , 4H), 2.84 (t, $J=5.7\text{Hz}$, cyclopentane ring CH_2 , 4H) [e,f], [6.71 (d, $J=16.4\text{Hz}$, (E)- alkenyl,2H), 6.84 (d, $J=16.4\text{Hz}$, (E)- alkenyl,2H)] [b,c], 7.21-7.55 (m, aromatic, 16H) [d], 7.64 (s, vinylic, 2H) [g], 3.78 (s, methoxy,12H) [h], 7.26 (solvent) [i].

Figure 1.23. ^1H NMR spectrum of $[\text{Ni}(\text{L}^3)_2]$



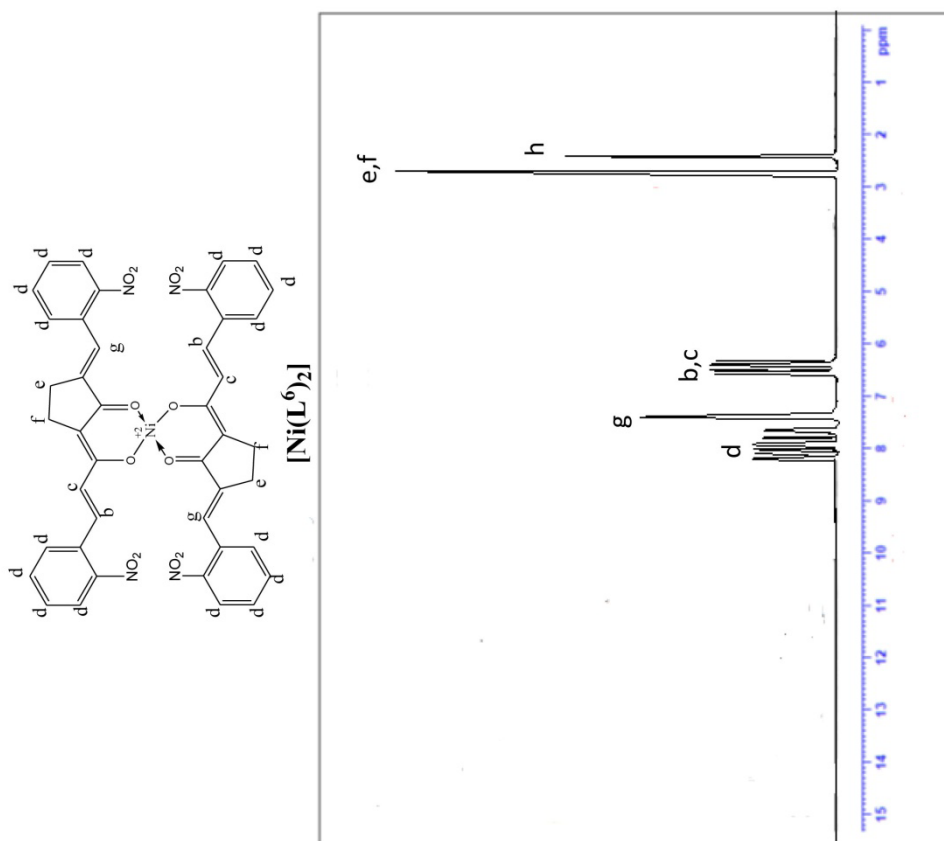
^1H NMR (400MHz, CDCl_3 , ppm): δ [2.81 (t, $J=5.2\text{Hz}$, cyclopentane ring CH_2 , 4H), 2.89 (t, $J=5.4\text{Hz}$, cyclopentane ring CH_2 , 4H)] [e,f], [6.28 (d, $J=16.3\text{Hz}$, (E)- alkenyl, 2H), 6.74 (d, $J=16.3\text{Hz}$, (E)- alkenyl, 2H)] [b,c], 7.34-7.69 (m, aromatic, 16H) [d], 7.85 (s, vinyl, 2H) [g], 2.25 (s, methyl, 12H) [h], 7.26 (solvent) [i].

Figure 1.24. ^1H NMR spectrum of $[\text{Ni}(\text{L}^4)_2]$



^1H NMR (400MHz, DMSO, ppm): δ [2.64 (t, $J=5.4\text{Hz}$, cyclopentane ring CH_2 , 4H), 2.75 (t, $J=5.5\text{Hz}$, cyclopentane ring CH_2 , 4H)] [e,f], [6.37 (d, $J=16.1\text{Hz}$, (E)-alkenyl, 2H), 6.51 (d, $J=16.2\text{Hz}$, (E)-alkenyl, 2H)] [b,c], 6.96-7.29 (m, aromatic, 16H) [d], 6.89 (s, vinylic, 2H) [g], 2.49 (solvent) [h].

Figure 1.25. ^1H NMR spectrum of $[\text{Ni}(\text{L}^5)_2]$



^1H NMR (400MHz, DMSO, ppm): δ [2.73 (t, $J=5.6\text{Hz}$, cyclopentane ring CH_2 , 4H), 2.83 (t, $J=5.7\text{Hz}$, cyclopentane ring CH_2 , 4H)] [e,f], [6.47 (d, $J=16.2\text{Hz}$, (E)- alkenyl, 2H), 6.63 (d, $J=16.2\text{Hz}$, (E)- alkenyl, 2H)] [b,c], 7.57-8.21 (m, aromatic, 16H) [d], 7.35 (s, vinylic, 2H) [g], 2.49 (solvent) [h].

Figure 1.26. ^1H NMR spectrum of $[\text{Ni}(\text{L}^6)_2]$

1.5.4 ^{13}C NMR spectra

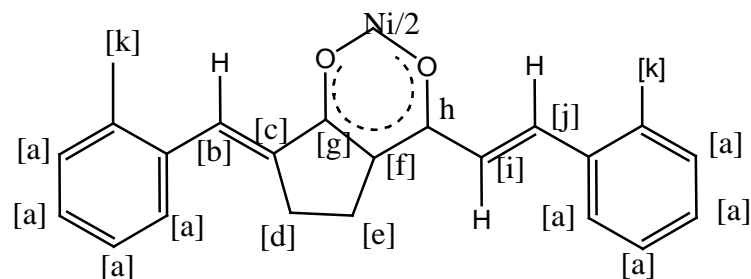
The carbonyl carbon signal of the free ligand shifted by 15- 20 ppm to low field in the spectra of nickel(II) and zinc(II) complexes^[193]. This clearly suggest the strong interaction between the metal ion and carbonyl oxygens and also more effective delocalisation that exist in the metal chelate ring compared to the free ligand.(**Table 1.10**)

1.5.5 Mass spectra

Mass spectrometry is potentially used for the establishment of stoichiometry and structural elucidation of coordination compounds. Due to the natural abundance of ^{63}Cu and ^{65}Cu isotopes in 1:3 ratio, copper containing fragments can be easily identified and hence mass spectra of copper(II) complexes of all ligands were recorded. Presence of molecular ion peak in the FAB or ESI mass spectra of the copper(II) chelates corresponding to ML_2 stoichiometry was observed in all cases. M^+ and $(\text{M}+2)^+$ with 3:1 intensity in the mass spectra of copper(II) chelates are in consistent with the natural abundance of ^{63}Cu and ^{65}Cu isotopes^[189]. The spectra are presented in **Figures 1.33-1.38**.

Peaks due to $[\text{CuL}]^+$, $[\text{CuL}-\text{ArCHCHCO}]^+$, L^+ and fragments of L^+ are common in the spectra of copper(II) complexes. Peaks corresponding to m/z $(\text{M}-\text{ArCHCHCO})^+$ and $(\text{M}-\text{ArCHCHCOCH}_2)^+$ are also present in the mass spectra of these compounds^[187]. Most of the common peaks can be assigned on the basis of common fragmentation pattern given in **Figure 1.39**.

Table 1.10 ^{13}C NMR spectral data of Ni^{II} complexes



Chemical shift (ppm)											
Compounds	[a]	[b]	[c]	[d]	[e]	[f]	[g]	[h]	[I]	[j]	[k]
$[\text{Ni}(\text{L}^1)_2]$	115.85-163.98	130.41	123.82	27.36	30.76	92.13	157.84	194.43	137.44	139.20	-
$[\text{Ni}(\text{L}^2)_2]$	114.24-148.32	123.87	132.54	31.24	32.94	94.21	124.34	138.84	111.58	138.24	-
$[\text{Ni}(\text{L}^3)_2]$	116.64-159.68	128.19	143.29	25.61	31.94	91.48	162.64	190.38	129.28	151.63	56.72
$[\text{Ni}(\text{L}^4)_2]$	114.38-159.73	122.24	148.29	26.38	32.68	94.77	163.84	194.76	127.11	139.23	18.57
$[\text{Ni}(\text{L}^5)_2]$	126.38-135.68	124.77	187.34	30.84	36.94	93.67	149.38	184.15	109.64	135.86	-
$[\text{Ni}(\text{L}^6)_2]$	122.73-138.67	125.38	138.75	30.15	37.84	92.56	148.75	177.64	110.28	134.37	-

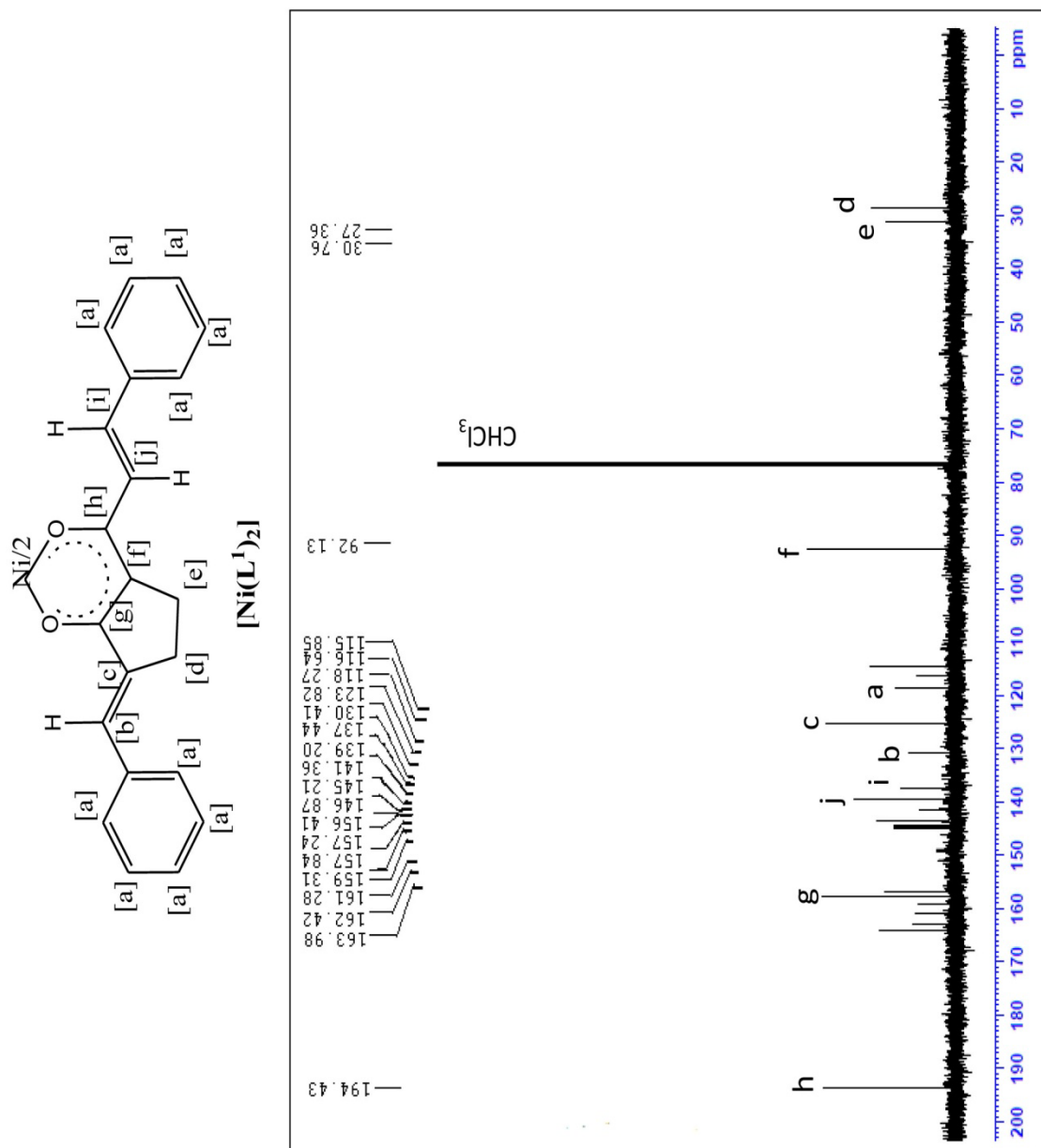


Figure 1.27. ^{13}C NMR spectrum of $[Ni(L^1)_2]$

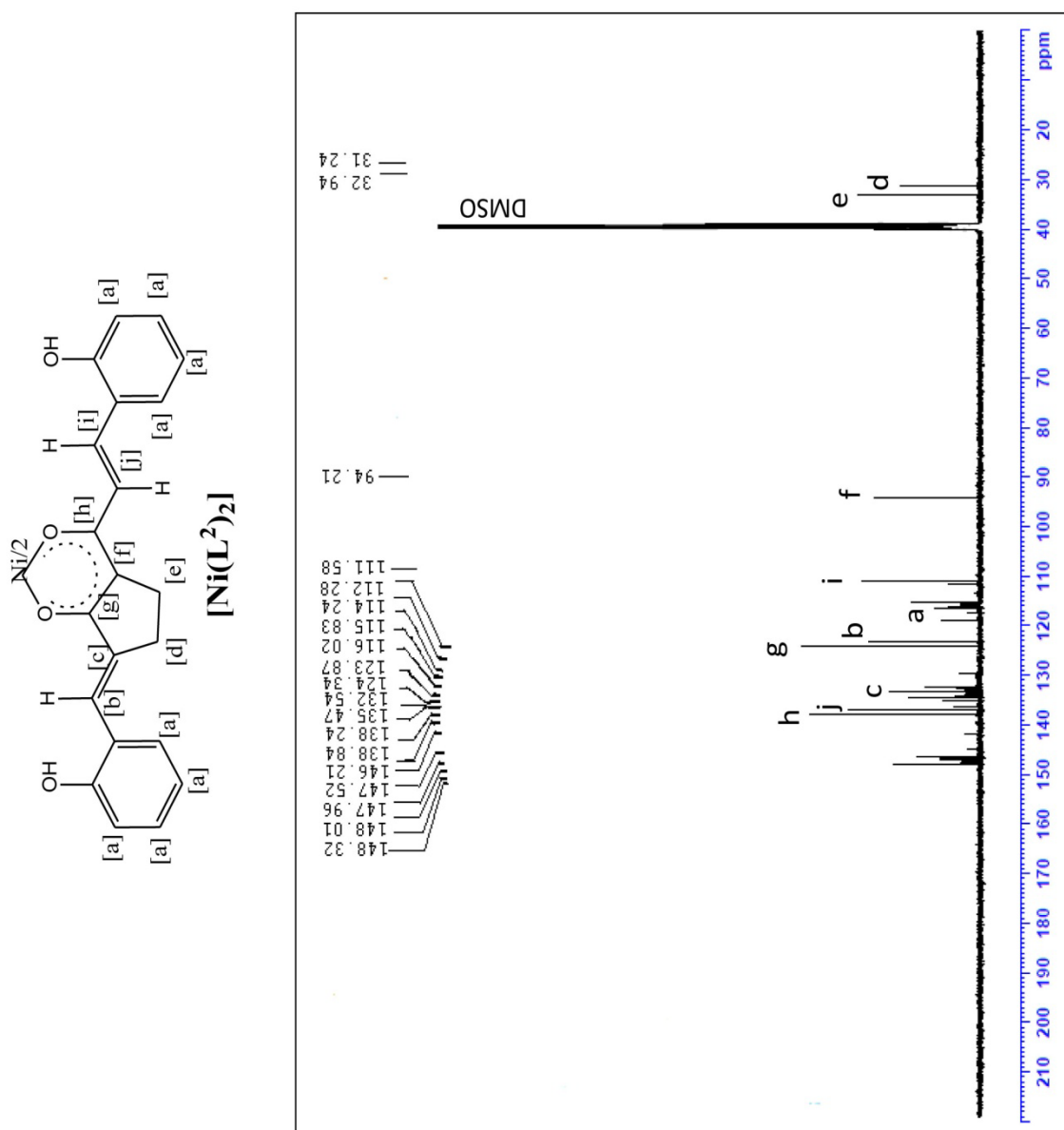


Figure 1.28. ^{13}C NMR spectrum of $[\text{Ni}(\text{L}^2)_2]$

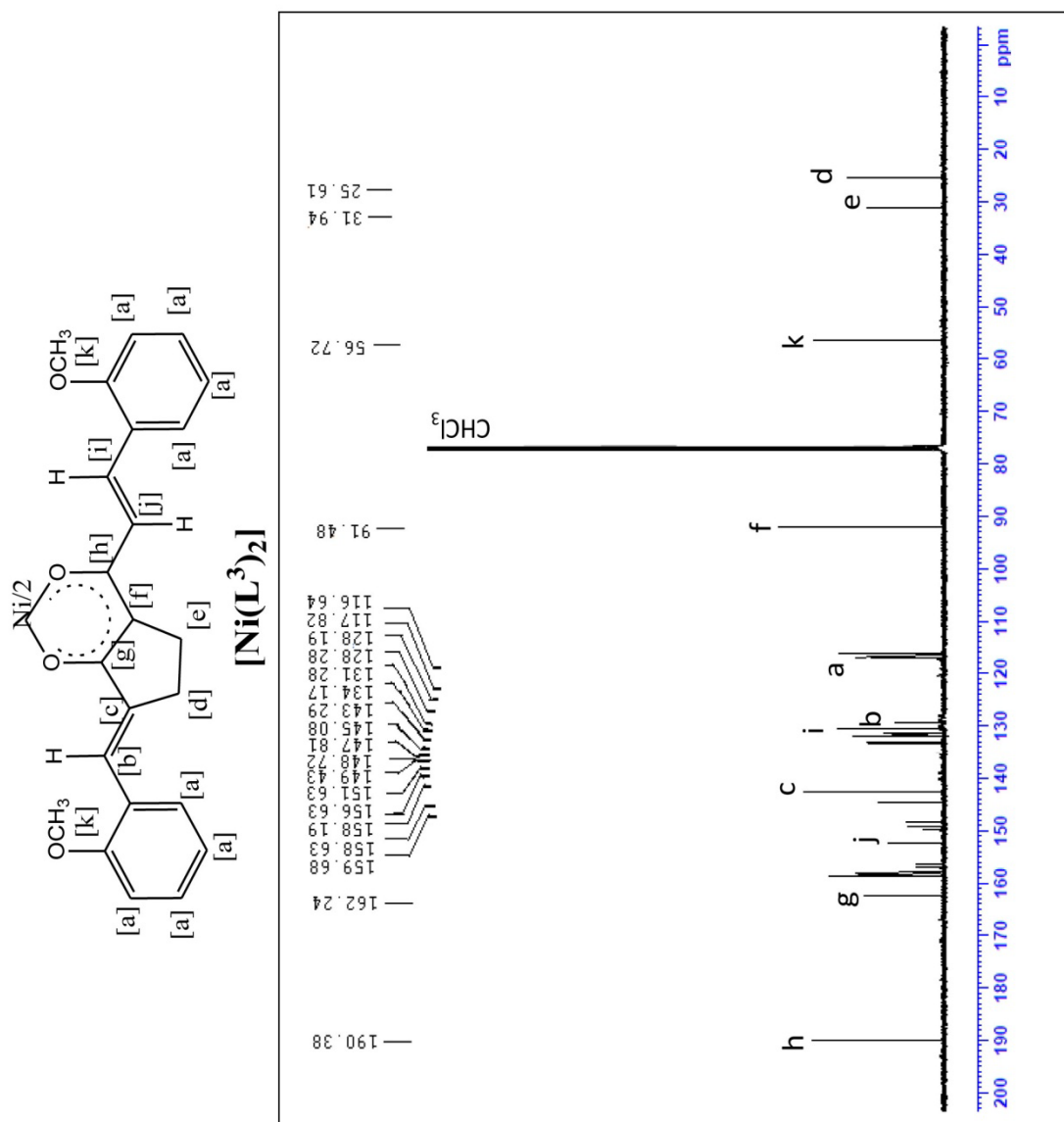


Figure 1.29. ^{13}C NMR spectrum of $[\text{Ni}(\text{L}^3)_2]$

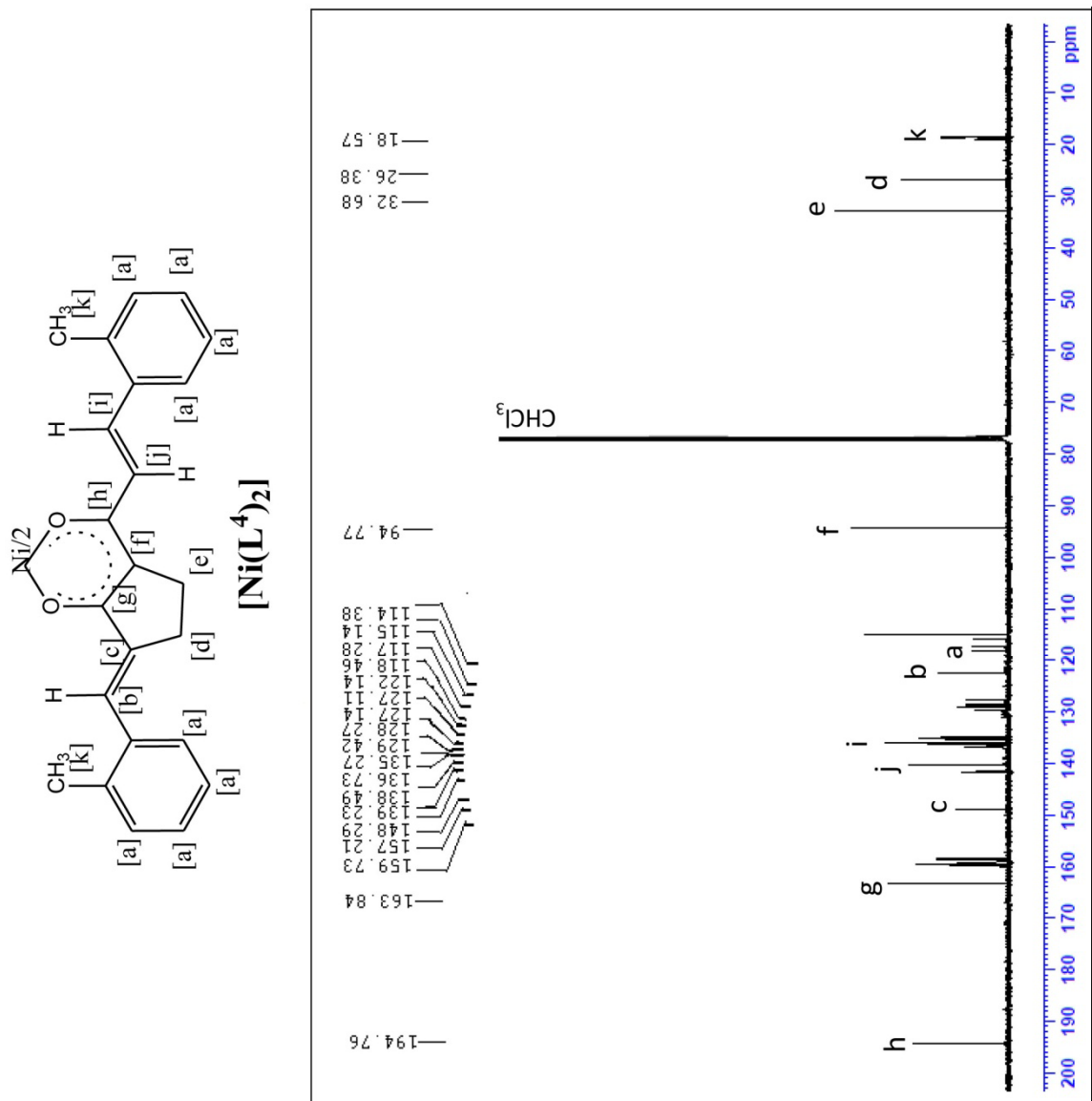


Figure 1.30. ^{13}C NMR spectrum of $[\text{Ni}(\text{L}^4)_2]$

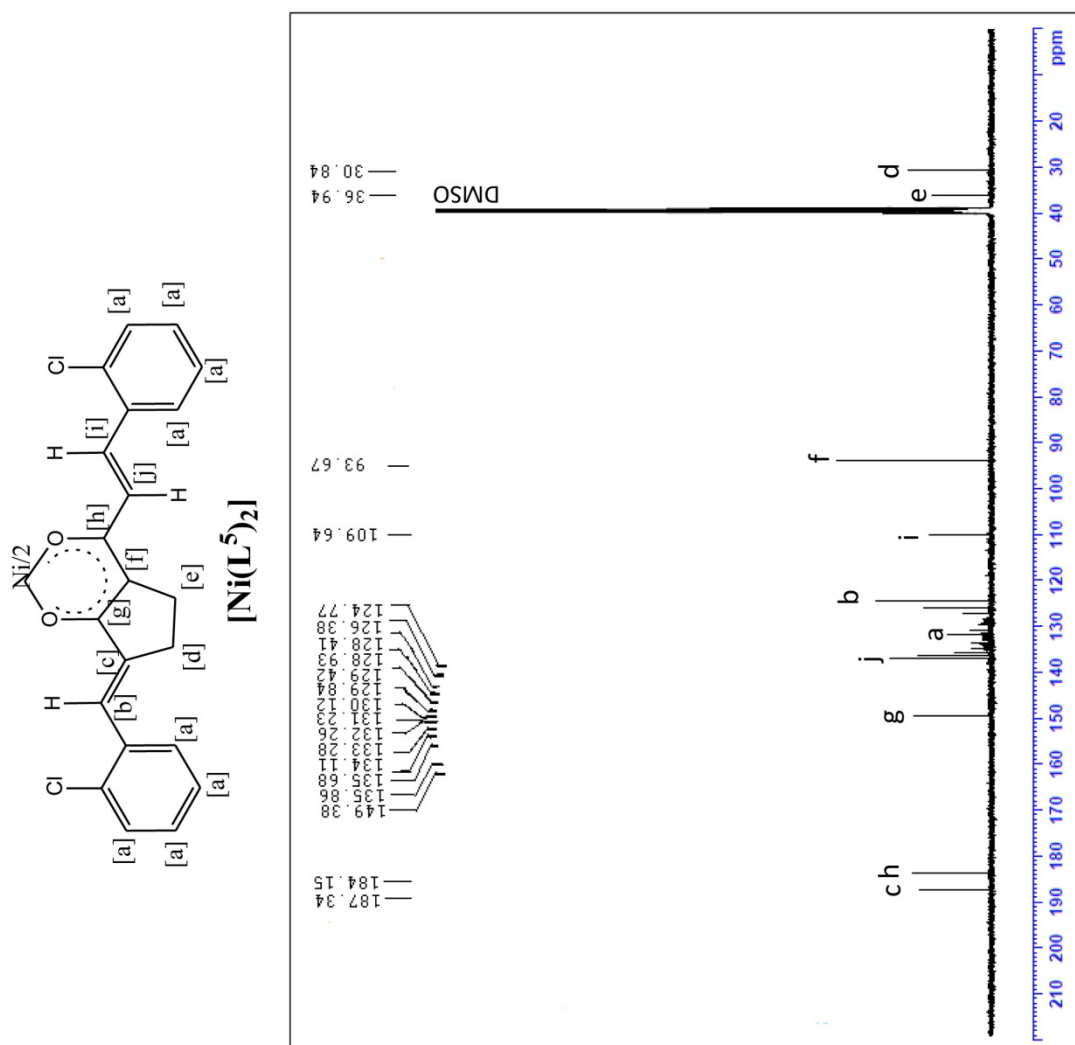


Figure 1.31. ^{13}C NMR spectrum of $[\text{Ni}(\text{L}^5)_2]$

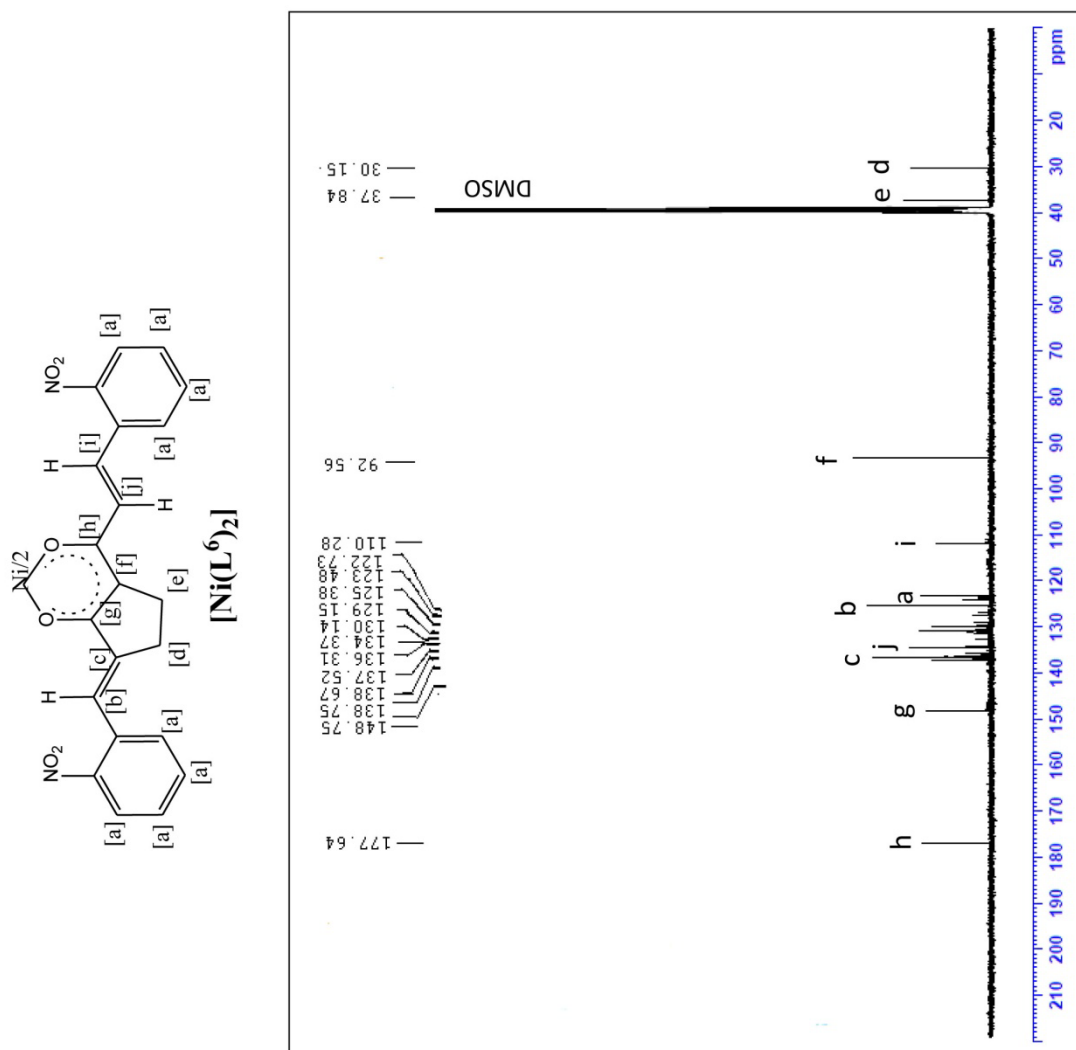


Figure 1.32. ^{13}C NMR spectrum of $[\text{Ni}(\text{L}^6)_2]$

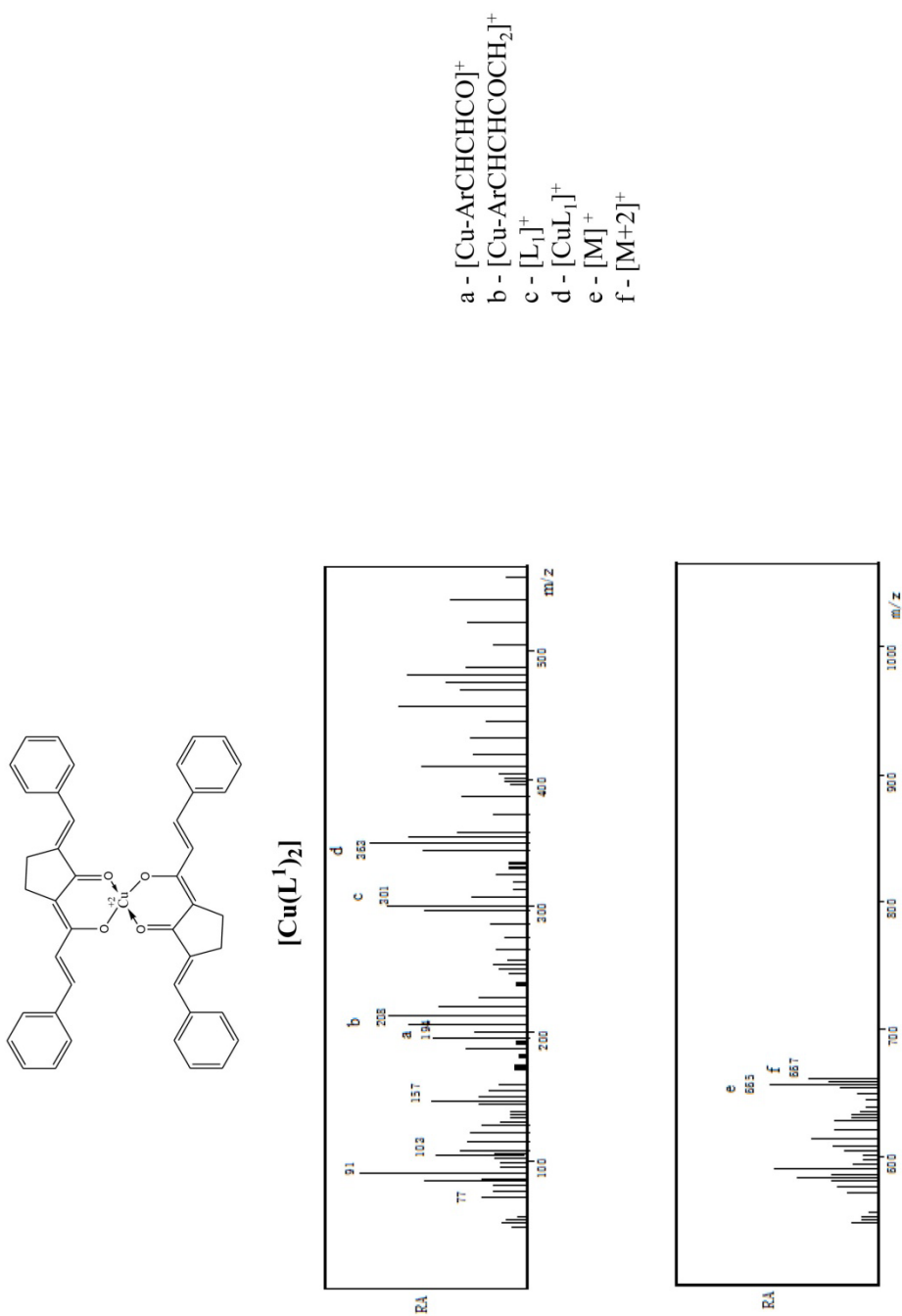


Figure 1.33. FAB Mass spectrum of $[\text{Cu}(\text{L}^1)_2]$

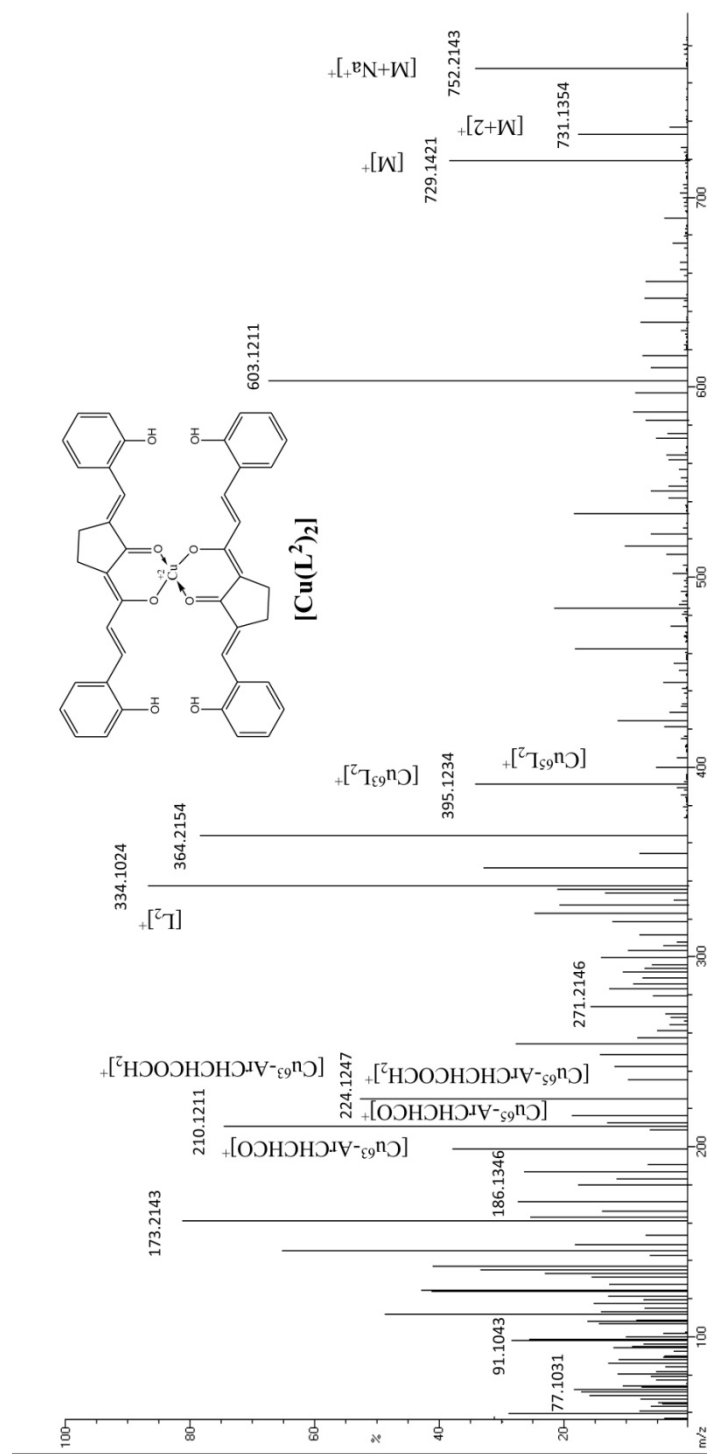


Figure 1.34. ESI Mass spectrum of $[\text{Cu}(\text{L}^2)_2]$

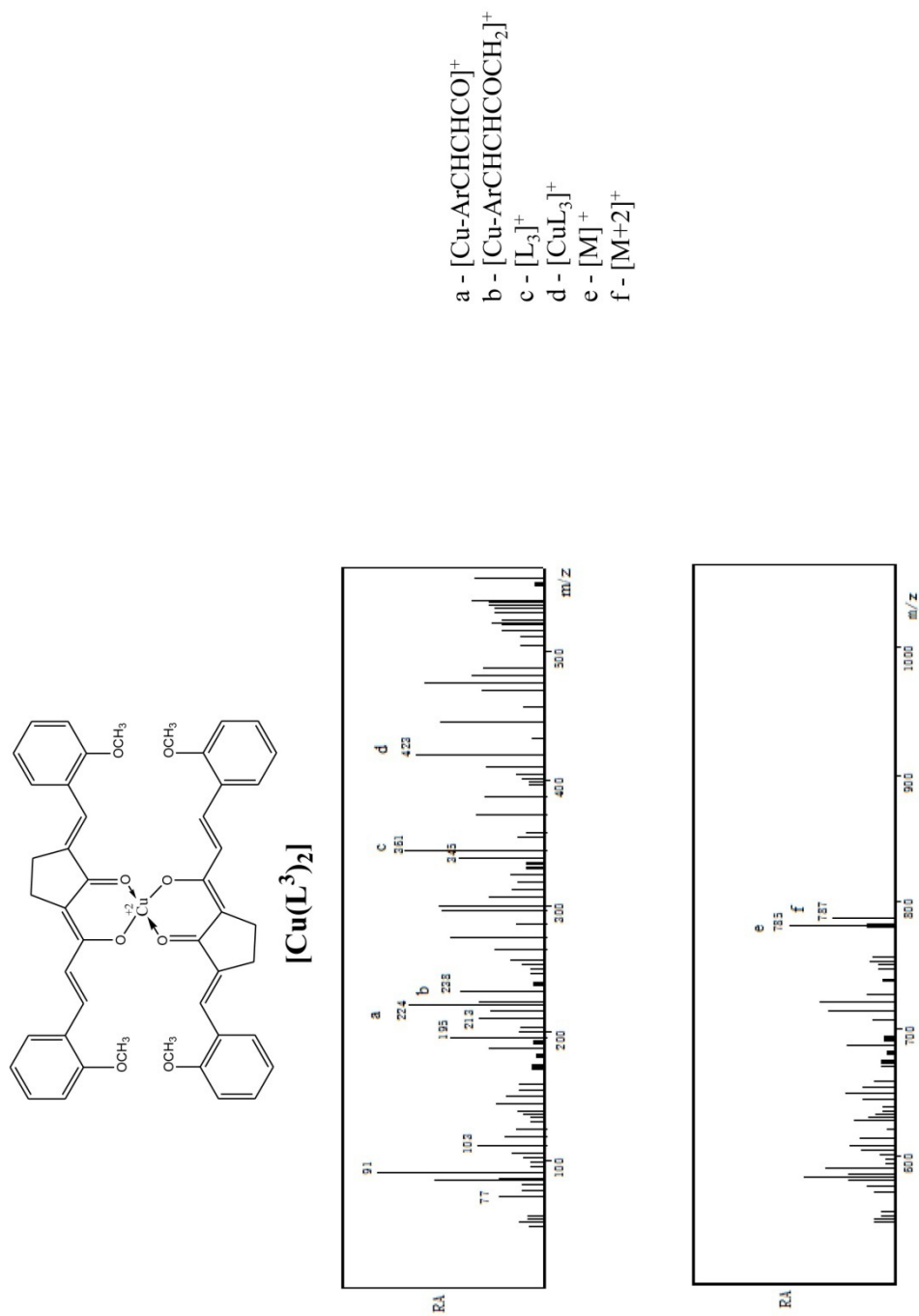


Figure 1.35 FAB Mass spectrum of $[\text{Cu}(\text{L}^3)_2]$

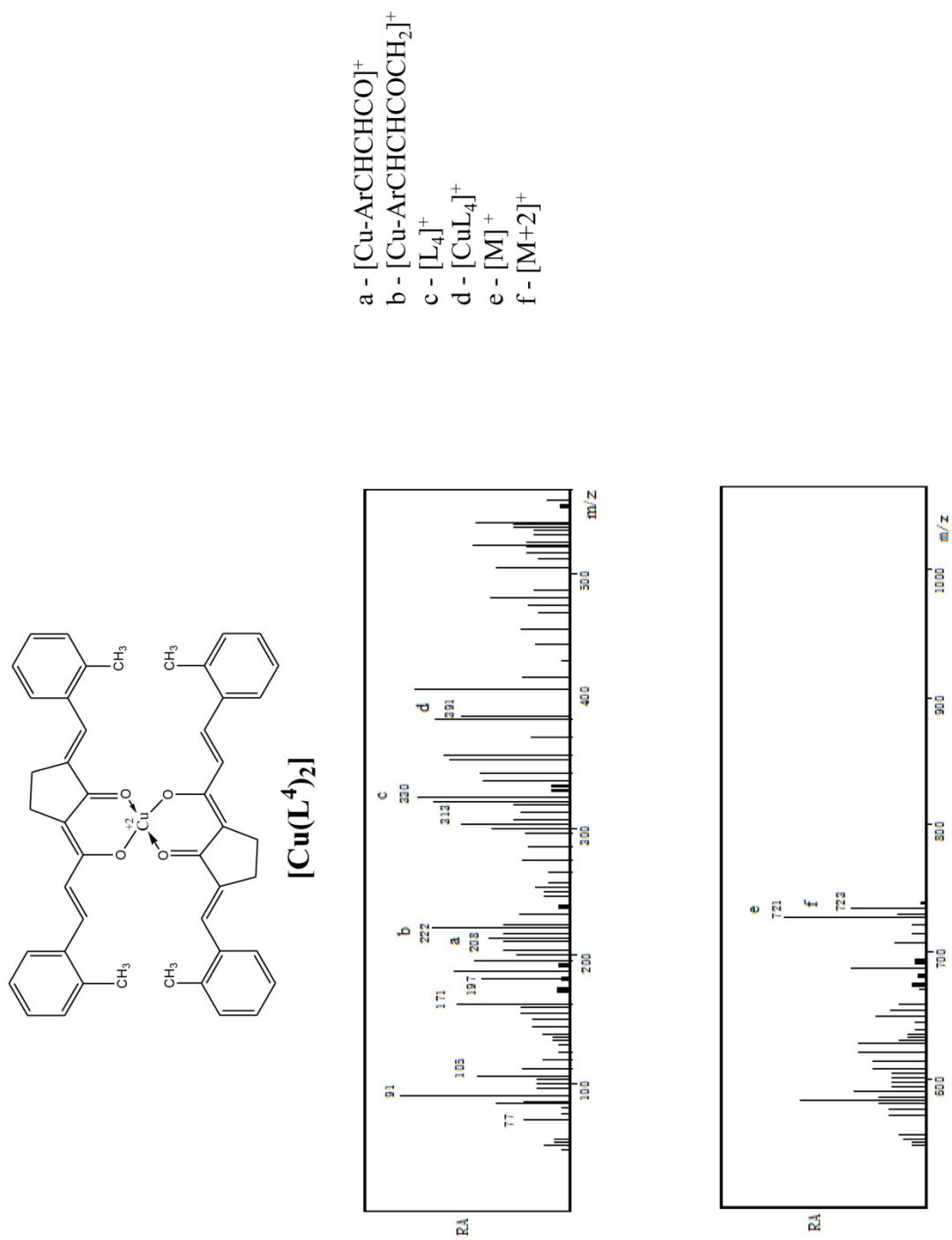


Figure 1.36 FAB Mass spectrum of [Cu(L⁴)₂]

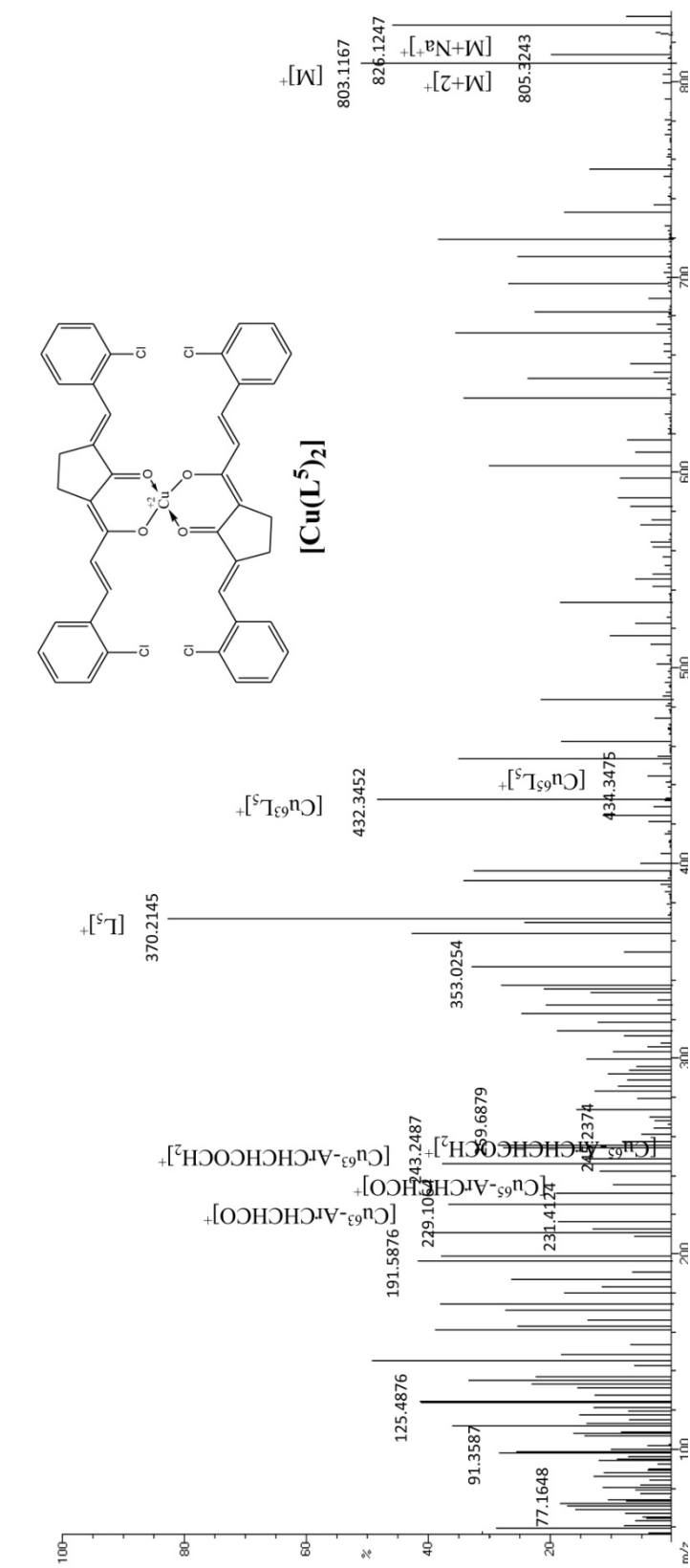


Figure 1.37. ESI Mass spectrum of $[\text{Cu}(\text{L}^5)_2]$

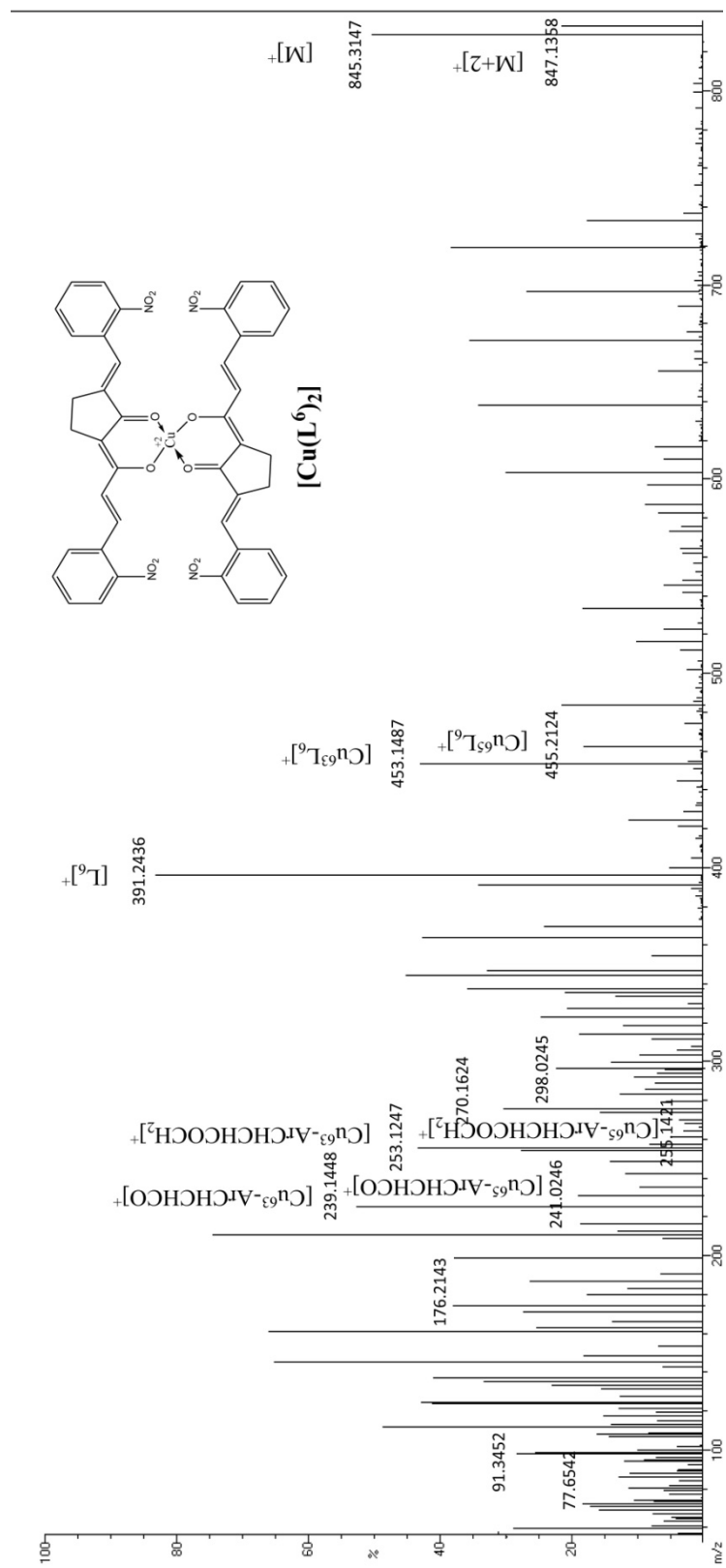


Figure 1.38. ESI Mass spectrum of [Cu(L⁶)₂]

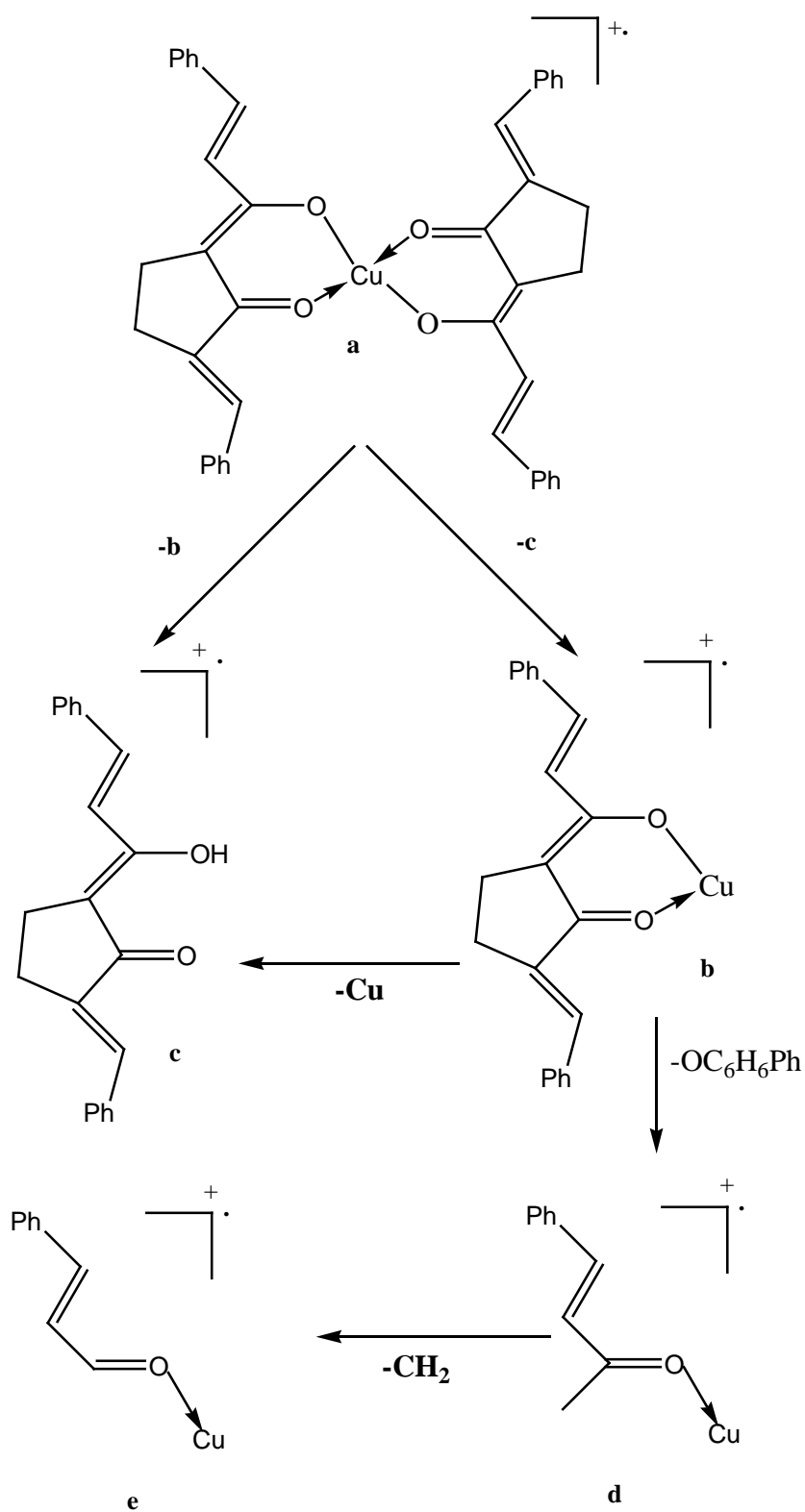
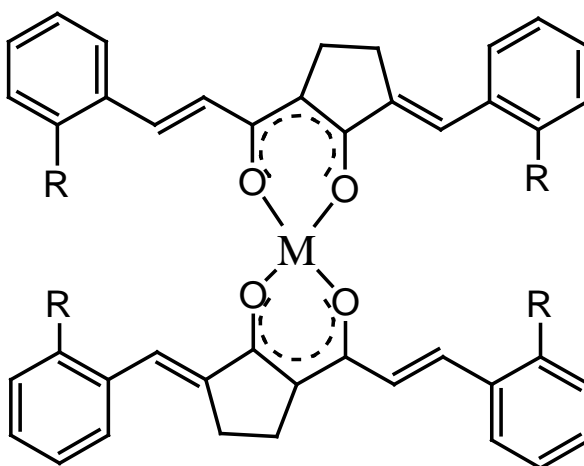


Figure 1.39. Fragmentation pattern of copper(II) complexes (Fragments ‘a’, ‘b’, ‘c’, ‘d’ and ‘e’ are marked in the MS given in **Figures 1.33-1.38**).

From the above discussion on electronic, IR, ^1H NMR, ^{13}C NMR and mass spectral data of the complexes, it follows that all the metal complexes have a 1:2 metal – ligand stoichiometry and the ligands are coordinated to metal ions through enolised β -diketone group. The probable structure of the complexes can be represented as below



Chapter 2

LIGANDS WITH PARA SUBSTITUTED PHENYL RINGS

2.1 Synthesis of ligands

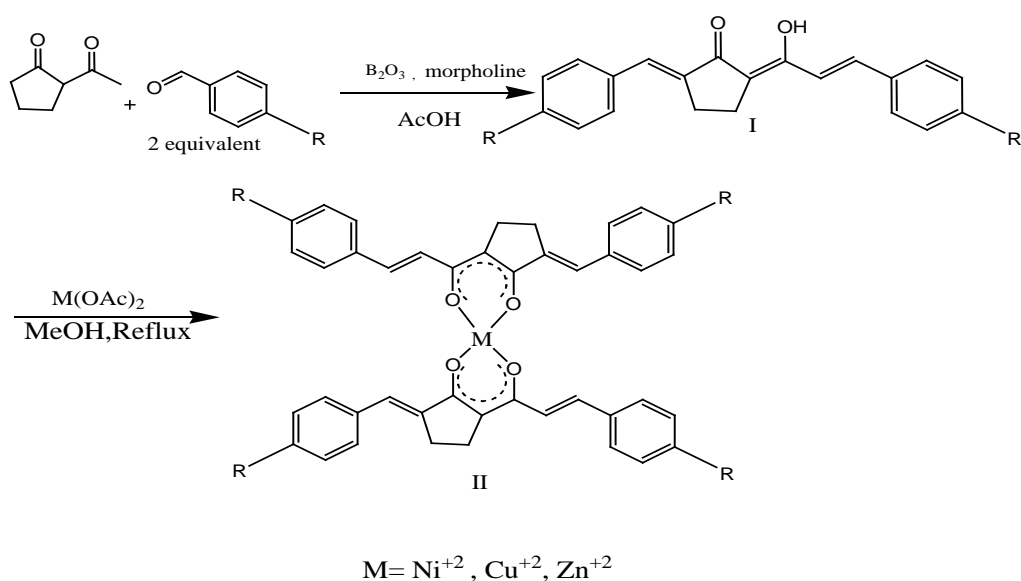
Synthesis of ligands from 2-acetyl cyclopentanone and p-substituted benzaldehyde was carried out using microwave radiations. A typical procedure for the synthesis of ligands is given below.

The cycloalkanone (20 mmol) was mixed with the boron oxide (20 mmol) in a 100 ml Erlenmeyer flask. The appropriate aromatic aldehyde (40mmol), acetic acid (100 mg), and morpholine (100 mg) were then added. The reaction was irradiated with the microwave at 70W for 3 minutes. The flask was cooled to room temperature and then methanol (50 ml) was added. This mixture was then sonicated for 30-40 minutes. The fine powder so obtained was filtered and washed with cold methanol. The compounds were recrystallized from hot benzene. The purity of sample was verified by TLC.

2.2 Synthesis of Cu^{II} , Ni^{II} and Zn^{II} complexes

Copper(II), Nickel(II) and Zinc(II) chelates of the compounds were prepared by the following general method.

Metal complexes of the ligands were prepared by refluxing a methanolic solution (25ml) of the metal(II) acetate (1 mmol) and the ligand (2 mmol, 30ml) for ~2 h. Volume of the solution was concentrated to half and cooled to room temperature. The precipitated complexes were filtered, washed with methanol and recrystallized from hot methanol. Synthesis of ligands and their metal(II) complexes are given in **Scheme 2.1**.



Scheme 2.1

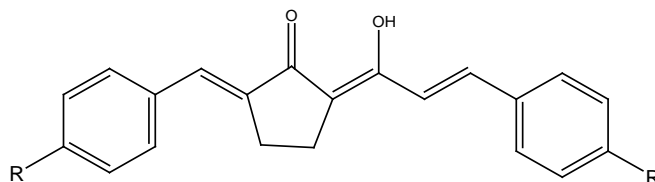
2.3 Results and discussion

The aldehydes used in the synthesis of the ligands (**2a-2e**) and their systematic names are given in **Table.2.1** All the compounds are crystalline in nature and are freely soluble in common organic solvents. Similar to *ortho*-substituted aldehydes, maximum yields are obtained when the aldehyde used contain electron donating substituent in the phenyl ring.

Elemental analysis and molecular weight determination of the compounds (**Table 2.2**) suggest that two equivalents of the aromatic aldehyde has condensed with one equivalent of 2-acetyl cyclopentanone in all cases and the ligands can be formulated as I in Scheme 2.1.

2.4 Characterization of ligands

From elemental analysis and molecular mass determination, it follows that two equivalents of aldehyde has condensed with one equivalent of 2-acetyl cyclopentanone. All the ligands are found to be existing in their intramolecularly hydrogen bonded enolic form from electronic, IR, NMR and mass spectral data.

Table 2.1 Synthetic details of ligands

Compounds	Aldehydes used for synthesis	R	Systematic name
HL¹ (2a)	4- Hydroxybenzaldehyde	OH	(2E)-2-(4-hydroxybenzylidene)-5-((E)-3-(4-hydroxy phenyl) acryloyl) cyclopentanone
HL² (2b)	4- Methoxybenzaldehyde	OCH ₃	(2E)-2-(4-methoxybenzylidene)-5-((E)-3-(4-methoxy phenyl) acryloyl) cyclopentanone
HL³ (2c)	4- Methylbenzaldehyde	CH ₃	(2E)-2-(4-methylbenzylidene)-5-((E)-3-(4-methyl phenyl) acryloyl) cyclopentanone
HL⁴ (2d)	4-chlorobenzaldehyde	Cl	(2E)-2-(4-chlorobenzylidene)-5-((E)-3-(4-chloro phenyl) acryloyl) cyclopentanone
HL⁵ (2e)	4- Nitrobenzaldehyde	NO ₂	(2E)-2-(4-nitrobenzylidene)-5-((E)-3-(4-nitro phenyl) acryloyl) cyclopentanone

2.4.1 Electronic spectra

The electronic spectra of the ligands (**2a-2e**) are similar in appearance to those of **1a-1f**. The $n \rightarrow \pi^*$ absorption of the carbonyl chromophore occurred at higher wavelength at 426-458 nm and the band corresponding to $\pi \rightarrow \pi^*$ transition occurred at 247-262 nm^[186]. The high energy band due to the $\pi \rightarrow \pi^*$ transitions of the fully conjugated system is only marginally influenced by the nature of aryl substituent.

Table 2.2 Analytical, UV, IR, and mass spectral data of ligands

Ligands	M. p. (^o C)	Elemental analysis (found/calcd) %		Colour	Yield (%)	UV λ_{\max} (nm)	IR (cm ⁻¹)			Mass spectral data (m/z)
		C	H				$\nu(\text{C}=\text{O})$	$\nu_{\text{as}}(\text{C}-\text{C}-\text{C})$	$\nu(\text{CH}=\text{CH}-)$ (trans)	
(2a) HL¹ C ₂₁ H ₁₈ O ₄ (334)	228 ^o C	(75.51) (75.43)	(5.62) (5.43)	Dark red solid	74	258 ($\pi \rightarrow \pi^*$), 451 ($n \rightarrow \pi^*$)	1591	1503	967	333, 301, 118, 91, 77
(2b) HL² C ₂₃ H ₂₂ O ₄ (362)	198 ^o C	(76.42) (76.22)	(6.18) (6.12)	Dark Yellow solid	90	251 ($\pi \rightarrow \pi^*$), 441 ($n \rightarrow \pi^*$)	1628	1589	968	362, 345, 213, 103, 91, 77
(2c) HL³ C ₂₃ H ₂₂ O ₂ (330)	223 ^o C	(83.72) (83.60)	(6.83) (6.71)	Yellow solid	81	249 ($\pi \rightarrow \pi^*$), 429 ($n \rightarrow \pi^*$)	1627	1591	947	330, 313, 211, 197, 171, 105, 91, 77
(2d) HL⁴ C ₂₁ H ₁₆ Cl ₂ O ₂ (371)	217 ^o C	(67.96) (67.94)	(4.41) (4.34)	Yellow solid	79	247($\pi \rightarrow \pi^*$), 426($n \rightarrow \pi^*$)	1627	1487	967	370, 353, 259, 231, 217, 191, 137, 125
(2e) HL⁵ C ₂₁ H ₁₆ N ₂ O ₆ (392)	213 ^o C	(64.87) (64.28)	(4.63) (4.11)	Brownish yellow solid	70	262 ($\pi \rightarrow \pi^*$), 458 ($n \rightarrow \pi^*$)	1608	1494	959	391, 375, 270, 258, 268, 228, 148, 136, 122, 91, 77

2.4.2 Infrared Spectra

The IR spectra of the ligands are characterized by the presence of a strong band at $\sim 1600\text{ cm}^{-1}$. It is well known that when a carbonyl group is involved in hydrogen bonding, its C=O stretching frequency is lowered^[186]. Intra molecular hydrogen bonding is another factor which lowers the carbonyl stretching frequency. Absence of band in the region $1680\text{-}1720\text{ cm}^{-1}$ along with a strong absorption band at 1600 cm^{-1} suggests a chelated enolised β -dicarbonyl group. A broad band present in the range of $2600\text{-}3800\text{ cm}^{-1}$ is due to the stretching of intramolecular hydrogen bonded enol group^[186]. The observed breadth and intensity of the band suggest the involvement of the enolic proton in strong intramolecular hydrogen bonding. The presence of various ring vibrations and C–H absorption makes the spectra fairly complicated for complete assignments of individual bands. The imperative absorptions corresponding to $\nu(\text{C}=\text{O})$, $\nu_{\text{as}}(\text{C}-\text{C}-\text{C})$ and $\nu(\text{CH}=\text{CH}-)$ (trans) are given in **Table 2.2**.

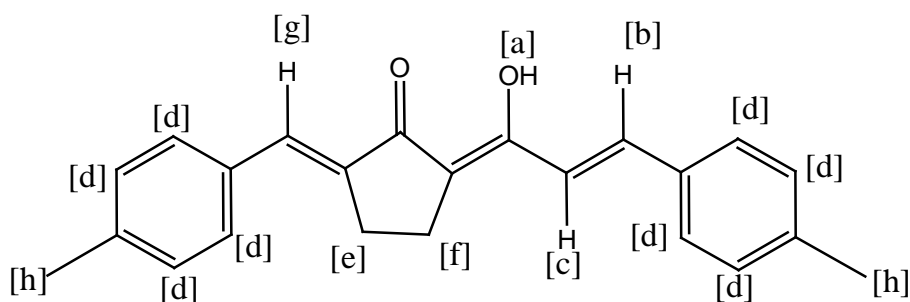
The aryl $\nu_{\text{C}-\text{Cl}}$ stretching band observed at 635 cm^{-1} (m) in the IR spectrum of **2d**. The ligand **2e** also displayed two intense absorption bands at 1525 cm^{-1} and at 1337 cm^{-1} are due to N–O asymmetric and symmetric stretching vibrations, respectively^[186].

2.4.3 ^1H NMR spectra

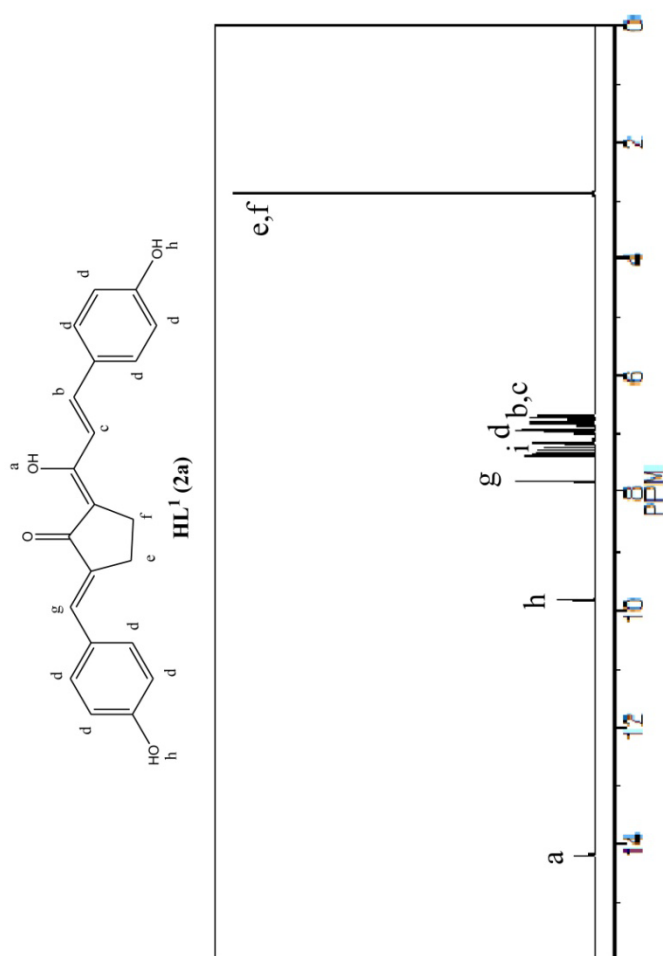
The ^1H NMR spectral data of all the ligands showed a characteristic downfield singlet at $\delta \sim 15$ ppm which can be assigned to the intramolecularly hydrogen bonded enolic proton. The ^1H NMR spectra of all the ligands shows signals at δ in the range $2.80\text{-}2.92$ ppm assignable to protons in the cyclopentane ring. Two doublets at ~ 6.67 ppm due to the alkenyl protons and a singlet at $\delta \sim 7.72$ due to vinylic protons also appeared along with the aromatic protons. The integrated intensities of the aryl and alkenyl protons are

in well agreement with their formulation. The ^1H NMR spectral data of **2a-2e** along with probable assignments are given in **Table 2.3**

Table 2.3 ^1H NMR spectral data of ligands

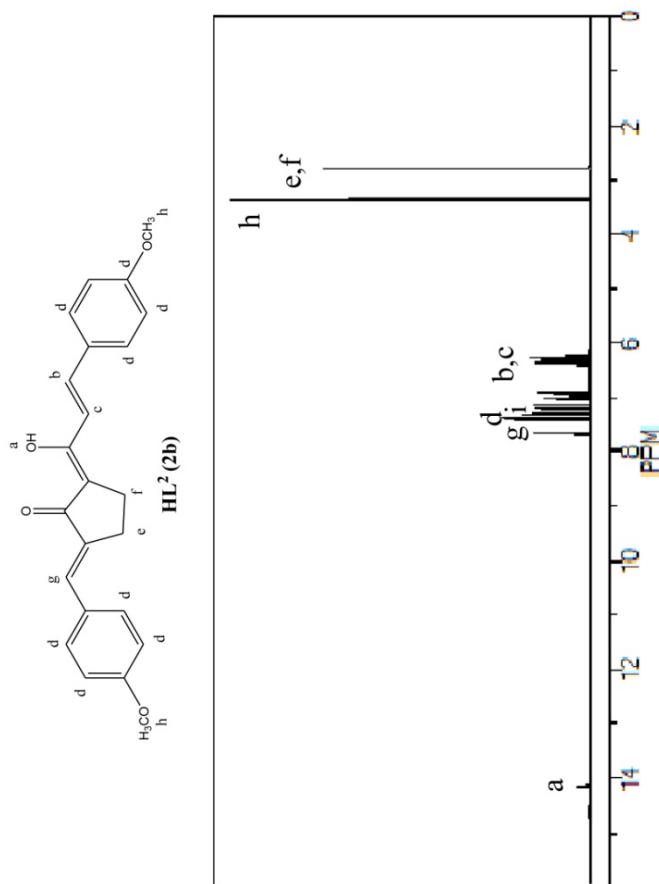


Compounds	Chemical shift, ppm (Coupling constant, Hz)							
	[a]	[b]	[c]	[d]	[e]	[f]	[g]	[h]
HL¹	14.17	6.67 (16.4)	6.71 (16.3)	6.87-7.61	2.82 (5.3)	2.92 (5.3)	7.83	9.89
HL²	14.21	6.49 (16.3)	6.49 (16.3)	7.26-7.61	2.83 (5.6)	2.89 (5.5)	7.87	3.41
HL³	14.20	6.58 (16.4)	6.62 (16.3)	7.21-7.62	2.81 (5.2)	2.85 (5.2)	7.71	2.63
HL⁴	14.09	6.62 (16.2)	6.66 (16.1)	7.30-7.61	2.86 (5.3)	2.89 (5.4)	7.79	-
HL⁵	14.32	6.71 (16.5)	6.82 (16.4)	7.11-7.43	2.80 (5.4)	2.84 (5.3)	7.68	-



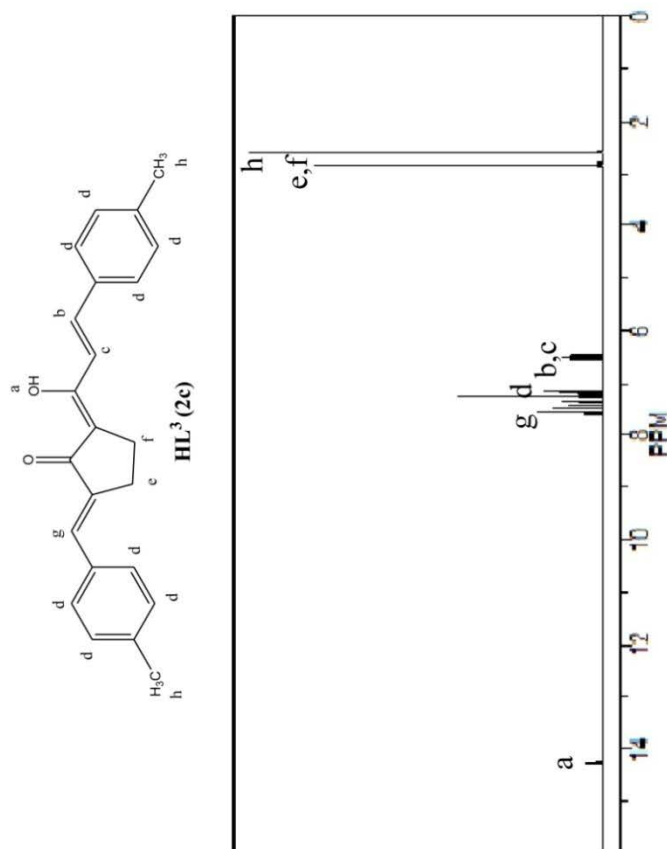
¹H NMR (400MHz, CDCl₃, ppm): δ 14.17 (1H, s, enolic -OH) [a], [2.82 (2H, t, J=5.3Hz, cyclopentane ring CH₂), 2.92 (2H, t, J=5.3Hz, cyclopentane ring CH₂)] [e,f], [6.67 (1H, d, J=16.4Hz, (E)- alkenyl H), 6.71 (1H, d, J=16.3Hz, (E)- alkenyl H)] [b,c], 6.87-7.61 (8H, m, aromatic Hs) [d], 7.83 (1H, s, vinylic H) [g], 9.89 (2H, s, phenolic H) [h], 7.26 (solvent) [i].

Figure 2.1. ¹H NMR spectrum of **HL¹ (2a)**



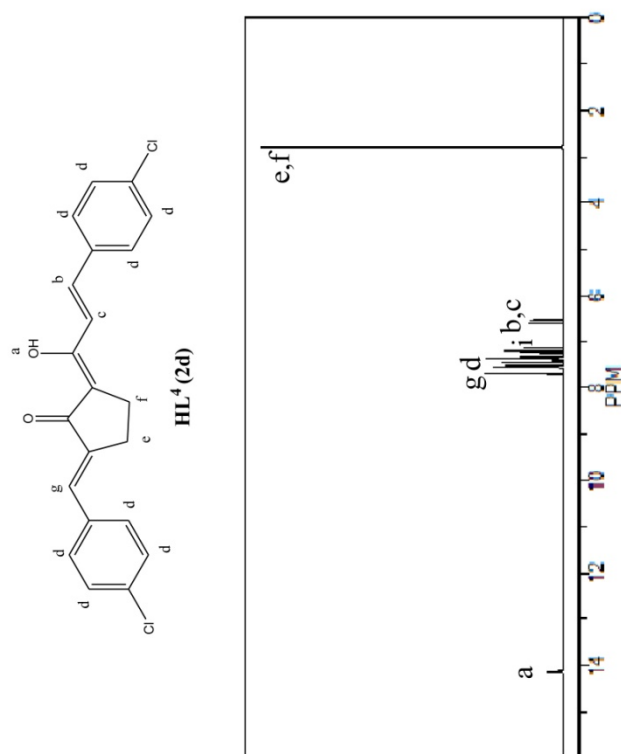
1H NMR (400MHz, $CDCl_3$, ppm): δ 14.21 (1H, s, enolic -OH) [a], [2.83 (2H, t, $J=5.6$ Hz, cyclopentane ring CH_2), 2.89 (2H, t, $J=5.5$ Hz, cyclopentane ring CH_2) [e,f], [6.49 (1H, d, $J=16.3$ Hz, (E)- alkenyl H), 6.49 (1H, d, $J=16.3$ Hz, (E)- alkenyl H)] [b,c], 7.26-7.61 (14H, m, aromatic Hs) [d], 7.87 (1H, s, vinylic H) [g], 3.41 (1H, s, methoxy H) [h], 7.26 (solvent) [i].

Figure 2.2. 1H NMR spectrum of HL^2 (2b)



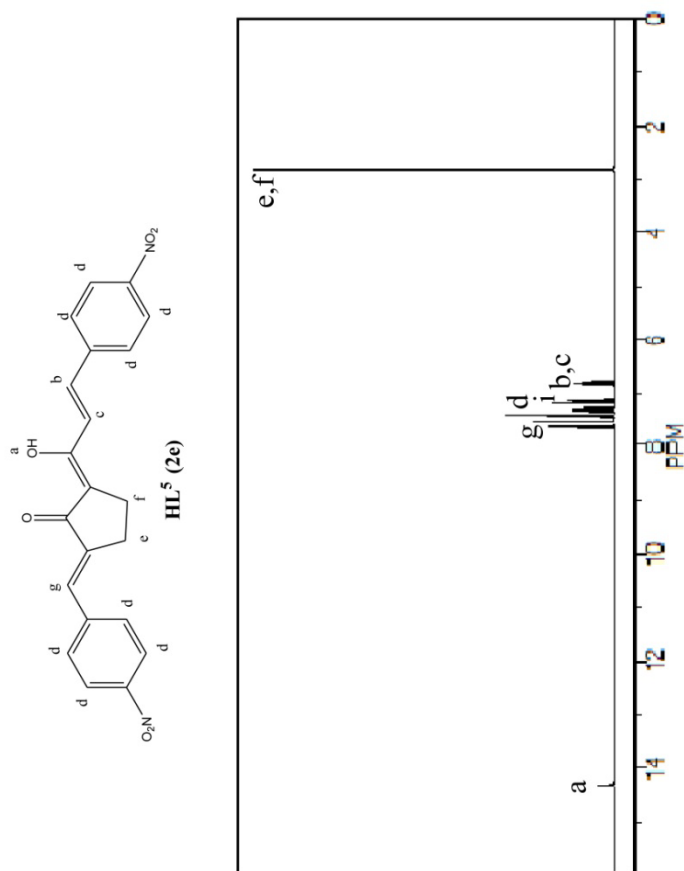
¹H NMR (400MHz, CDCl₃, ppm): δ 14.20 (1H, s, enolic -OH) [a], [2.81 (2H, t, J=5.2Hz, cyclopentane ring CH₂), 2.85 (2H, t, J=5.2Hz, cyclopentane ring CH₂)] [e,f], [6.58 (1H, d, J=16.4Hz, (E)- alkenyl H), 6.62 (1H, d, J=16.3Hz, (E)- alkenyl H)] [b,c], 7.21-7.62 (8H, m, aromatic Hs) [d], 7.71 (1H, s, vinylic H) [g], 2.63 (1H, s, methyl H) [h], 7.26 (solvent) [i].

Figure 2.3. ¹H NMR spectrum of **HL³ (2c)**



¹H NMR (400MHz, CDCl₃, ppm): δ 14.09 (1H, s, enolic -OH) [a], [2.86 (2H, t, J=5.3Hz, cyclopentane ring CH₂), 2.89 (2H, t, J=5.4Hz, cyclopentane ring CH₂) [e,f], [6.62 (1H, d, J=16.2Hz, (E)- alkenyl H), 6.66 (1H, d, J=16.1Hz, (E)- alkenyl H)] [b,c], 7.30-7.61 (8H, m, aromatic Hs) [d], 7.79 (1H, s, vinylic H) [g], 7.26 (solvent) [i].

Figure 2.4. ¹H NMR spectrum of **HL⁴ (2d)**



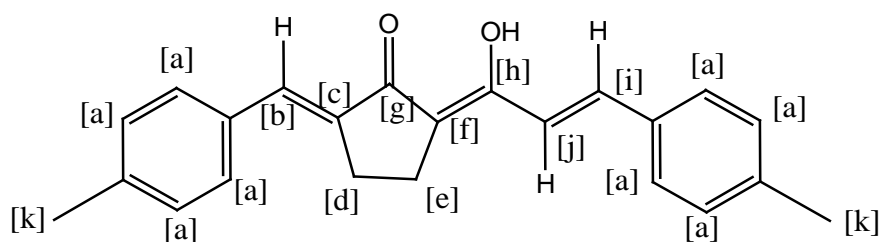
^1H NMR (400MHz, CDCl_3 , ppm): δ 14.32 (1H, s, enolic -OH) [a], [2.80 (2H, t, $J=5.4\text{Hz}$, cyclopentane ring CH_2), 2.84 (2H, t, $J=5.3\text{Hz}$, cyclopentane ring CH_2)] [e,f], [6.71 (1H, d, $J=16.5\text{Hz}$, (E)- alkenyl H), 6.82 (1H, d, $J=16.4\text{Hz}$, (E)- alkenyl H)] [b,c], 7.11-7.43 (8H, m, aromatic Hs) [d], 7.68 (1H, s, vinylic H) [g], 7.26 (solvent) [i].

Figure 2.5. ^1H NMR spectrum of **HL**⁵ (**2e**)

2.4.4 ^{13}C NMR spectra

^{13}C NMR spectral data of all ligands show two resonance signals at ~ 193 ppm and ~182 ppm indicating that the two carbonyl groups have different electronic environment. The two aliphatic carbon atoms in the cyclopentanone ring shows a resonance signal at ~ 24 ppm. The other two aliphatic carbon atoms in the cyclopentanone ring show a resonance signal at ~ 29 ppm. The resonance signals in the range 113-159 ppm are due to the aromatic carbon atoms. (Table 2.4)

Table 2.4 ^{13}C NMR spectral data of ligands



Chemical shift (ppm)											
Compounds	[a]	[b]	[c]	[d]	[e]	[f]	[g]	[h]	[I]	[j]	[k]
HL¹	113.29-159.66	149.86	147.33	22.28	25.99	97.63	169.65	193.05	121.27	132.24	-
HL²	114.37-159.90	143.28	140.32	24.71	26.70	95.28	182.28	193.75	116.28	138.74	57.38
HL³	119.30-140.38	148.49	146.57	23.04	26.57	98.51	170.65	193.32	120.47	135.67	19.34
HL⁴	129.17-139.36	146.75	141.87	23.04	26.51	97.21	170.67	192.84	127.43	137.72	-
HL⁵	120.48-146.54	149.21	140.12	25.92	28.23	93.28	178.14	195.26	123.47	131.83	-

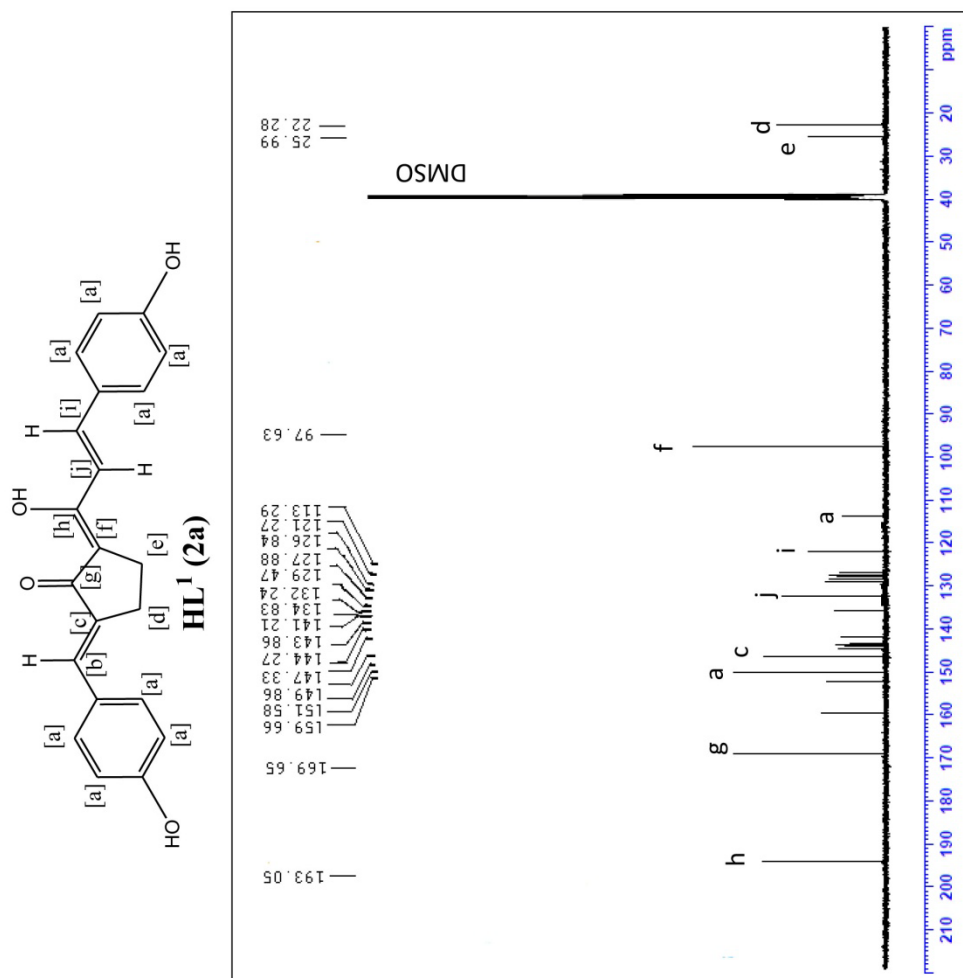


Figure 2.6. ¹³C NMR spectrum of **HL¹ (2a)**

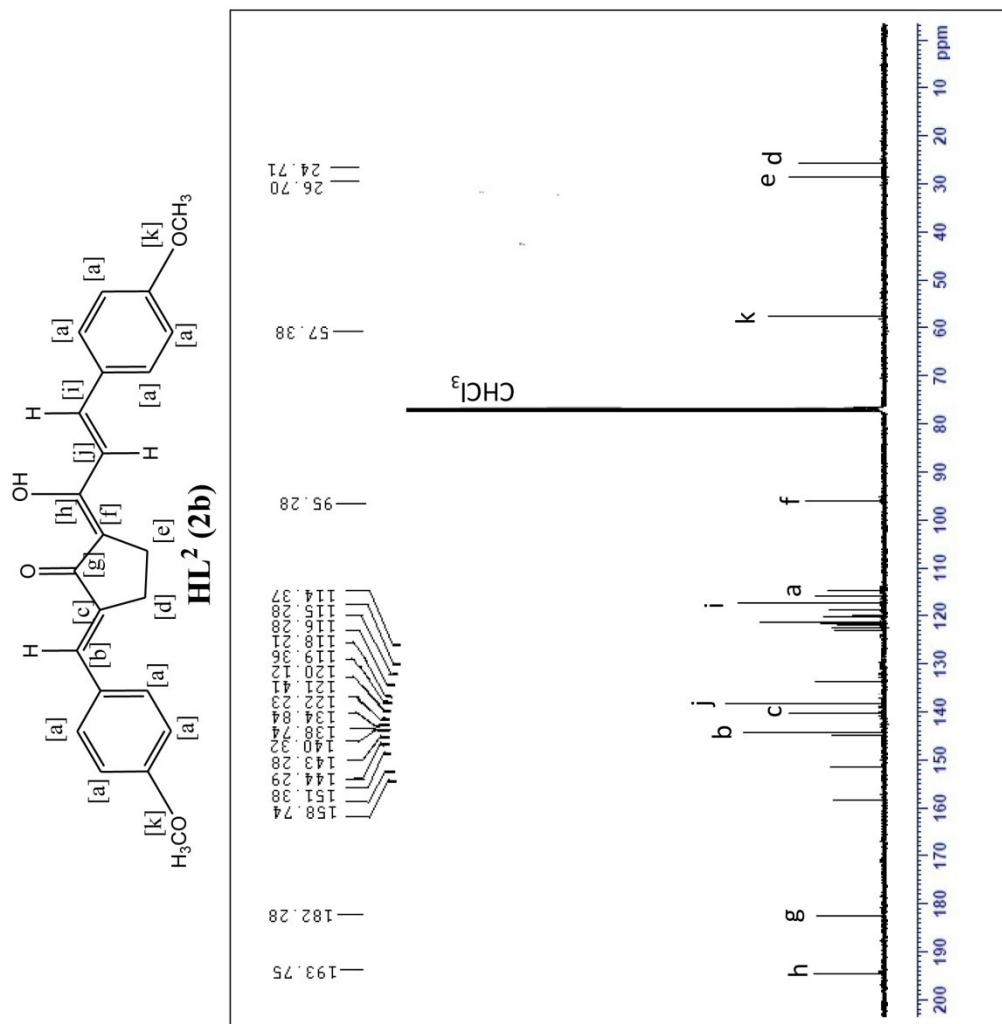


Figure 2.7. ¹³C NMR spectrum of **HL² (2b)**

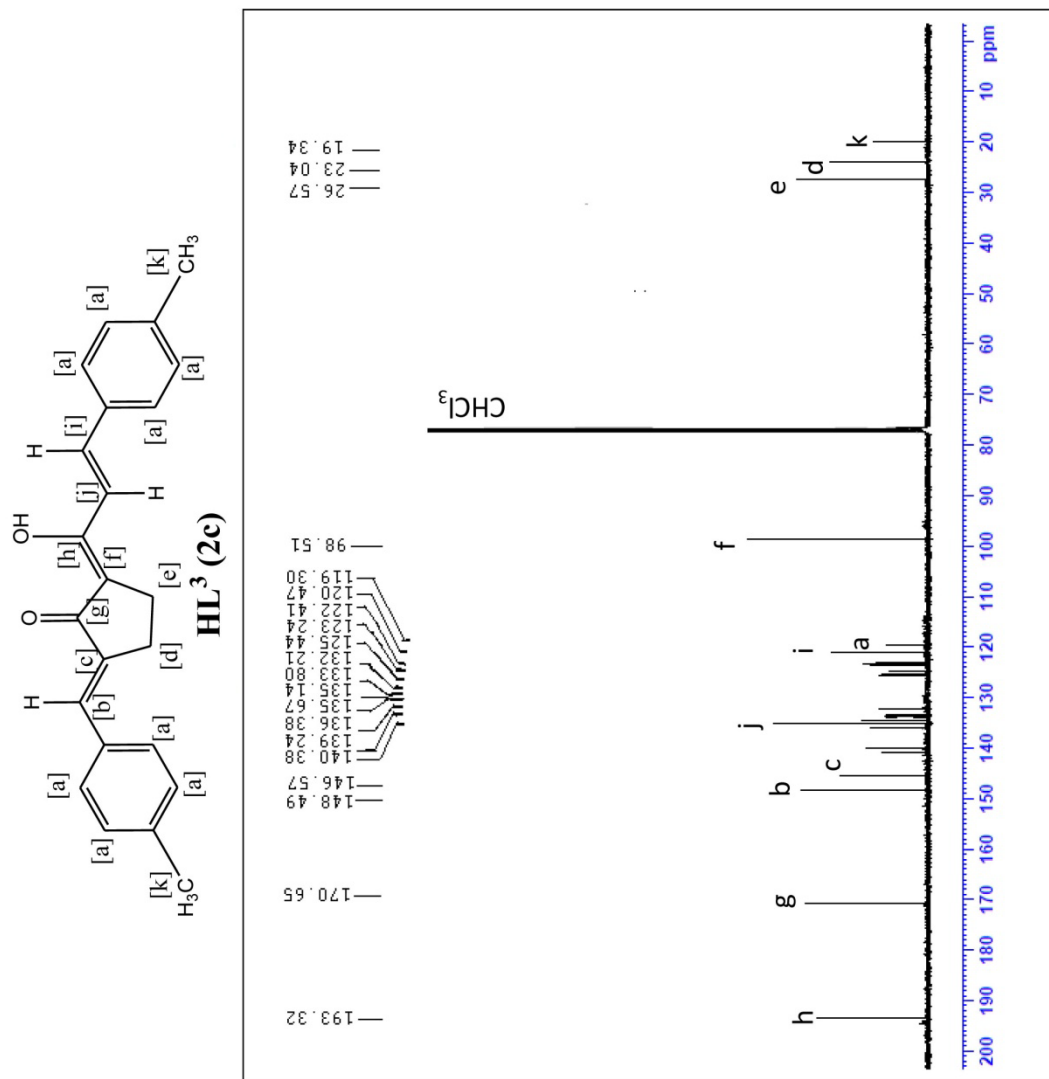


Figure 2.8. ¹³C NMR spectrum of **HL³ (2c)**

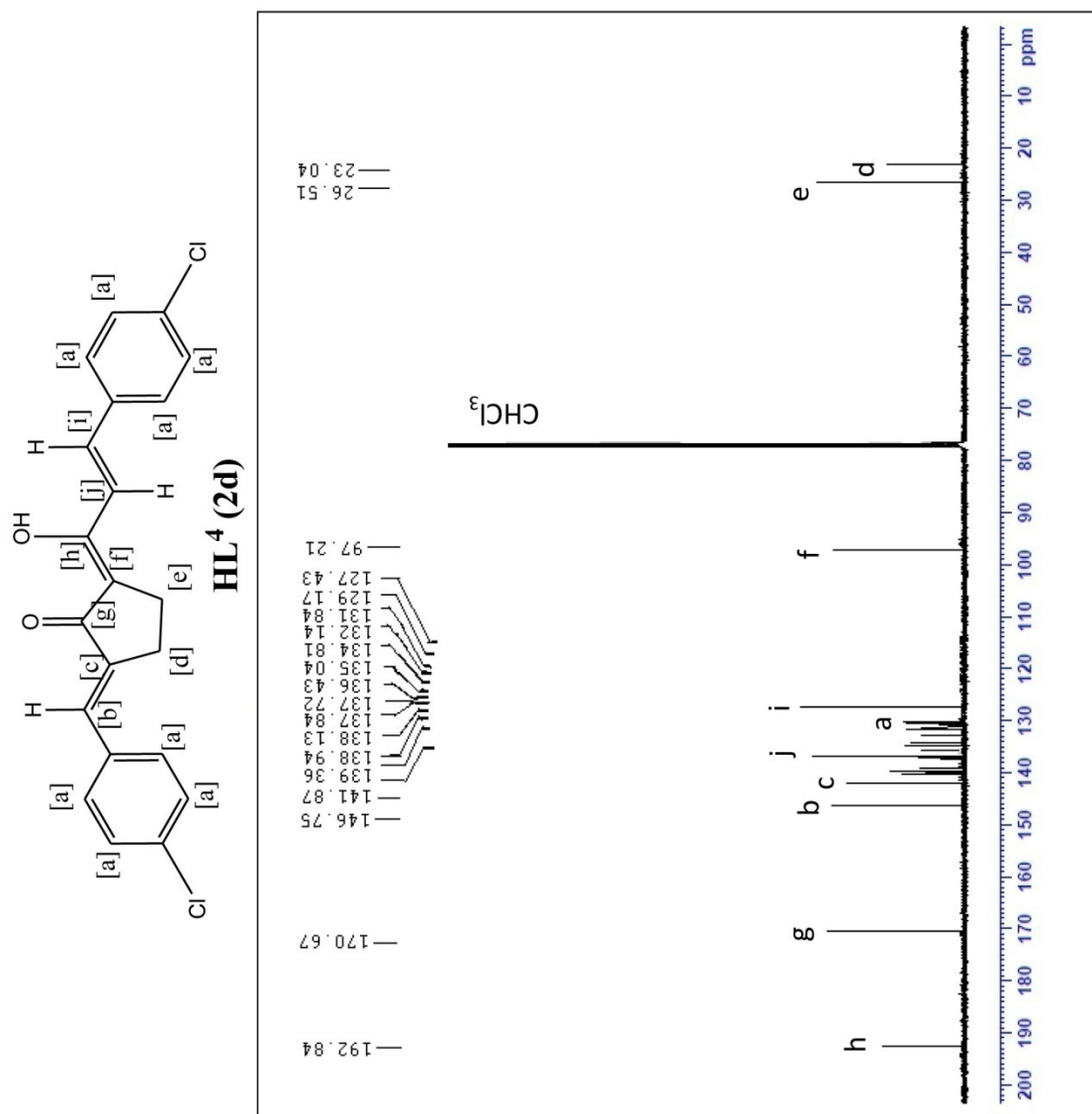


Figure 2.9. ¹³C NMR spectrum of **HL⁴ (2d)**

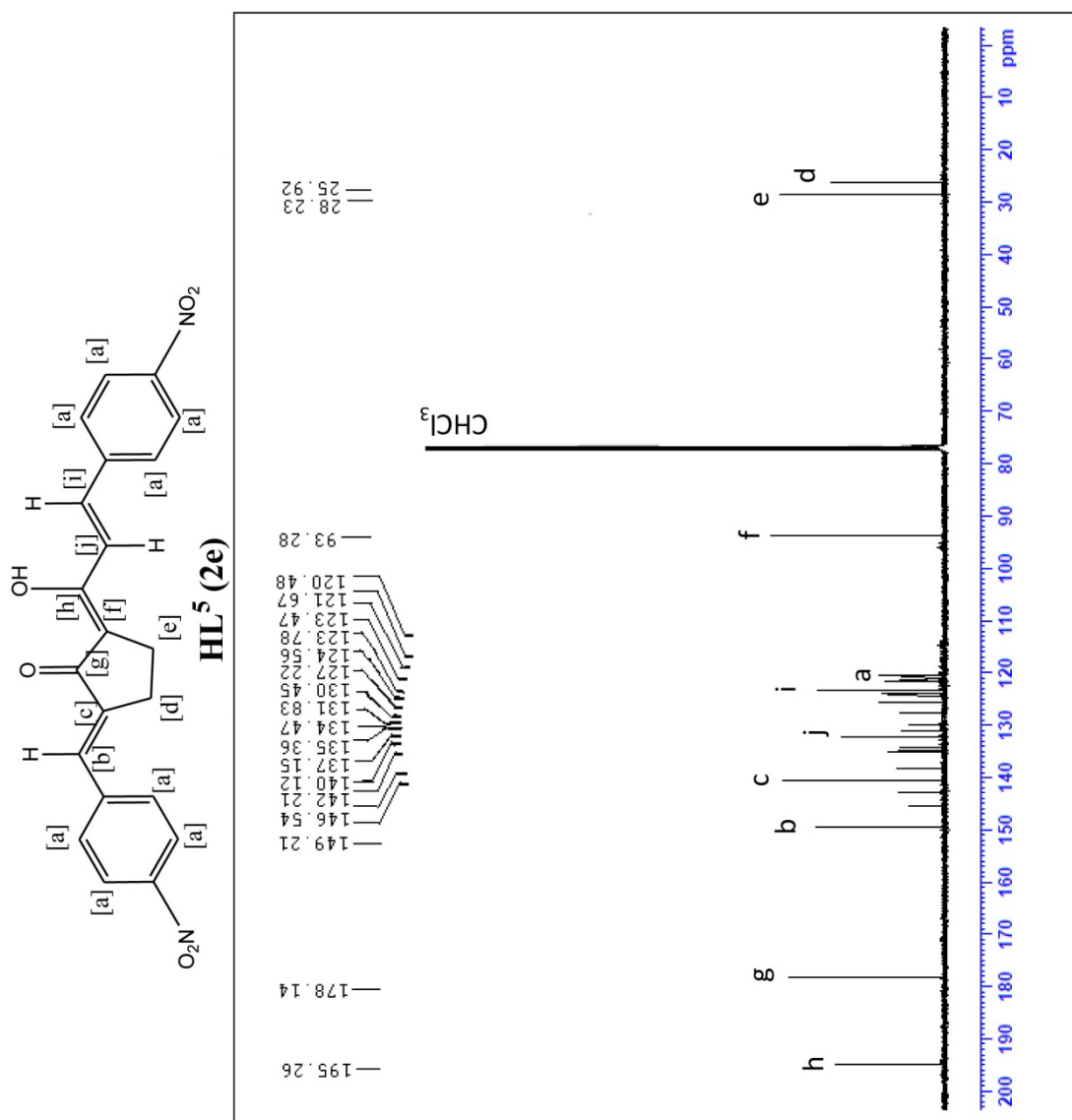


Figure 2.10. ¹³C NMR spectrum of **HL⁵ (2e)**

2.4.5 Mass spectra

The fragmentation pattern in the mass spectra of 1,3-diketones depends mainly on the nature of alkyl/ aryl substituents attached to the carbonyl groups. Mass spectra of **2a-2e** showed an intense molecular ion peak. In addition to the molecular ion peak (M^+), several other peaks are also present in the spectra. Some of the peaks can be explained on the basis of probable fragmentation pattern shown in **Figure 2.16**. These peaks are listed in **Table 2.2**. The mass spectra of the compounds are displayed below in **Figures 2.11-2.15**.

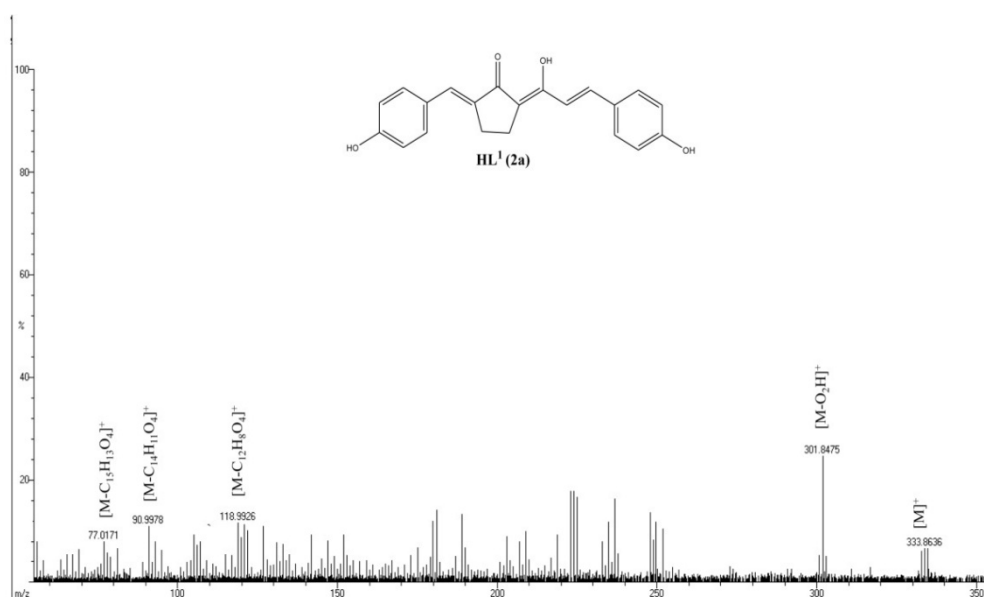


Figure 2.11. EI Mass spectrum of **HL¹ (2a)**

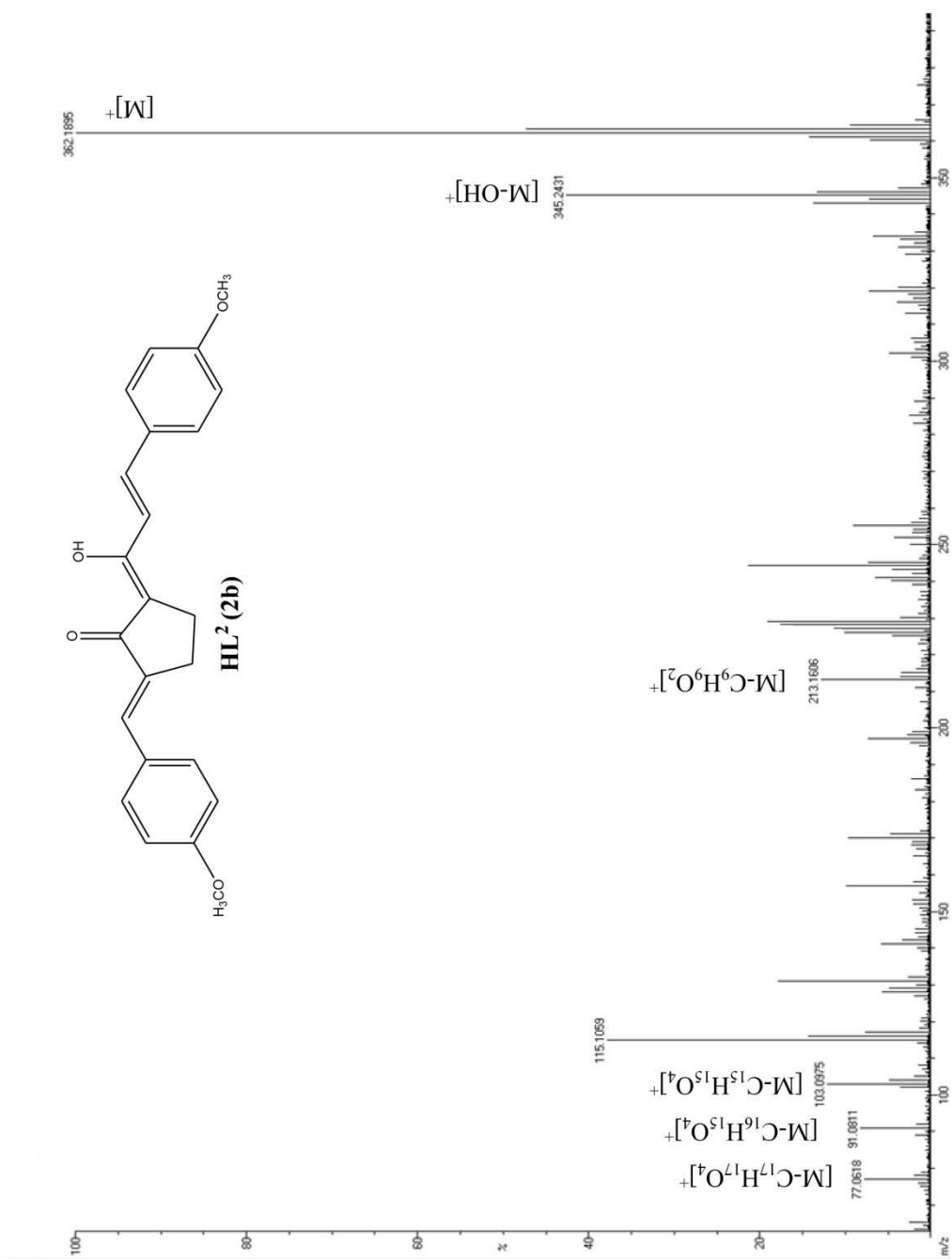


Figure 2.12. EI Mass spectrum of **HL² (2b)**

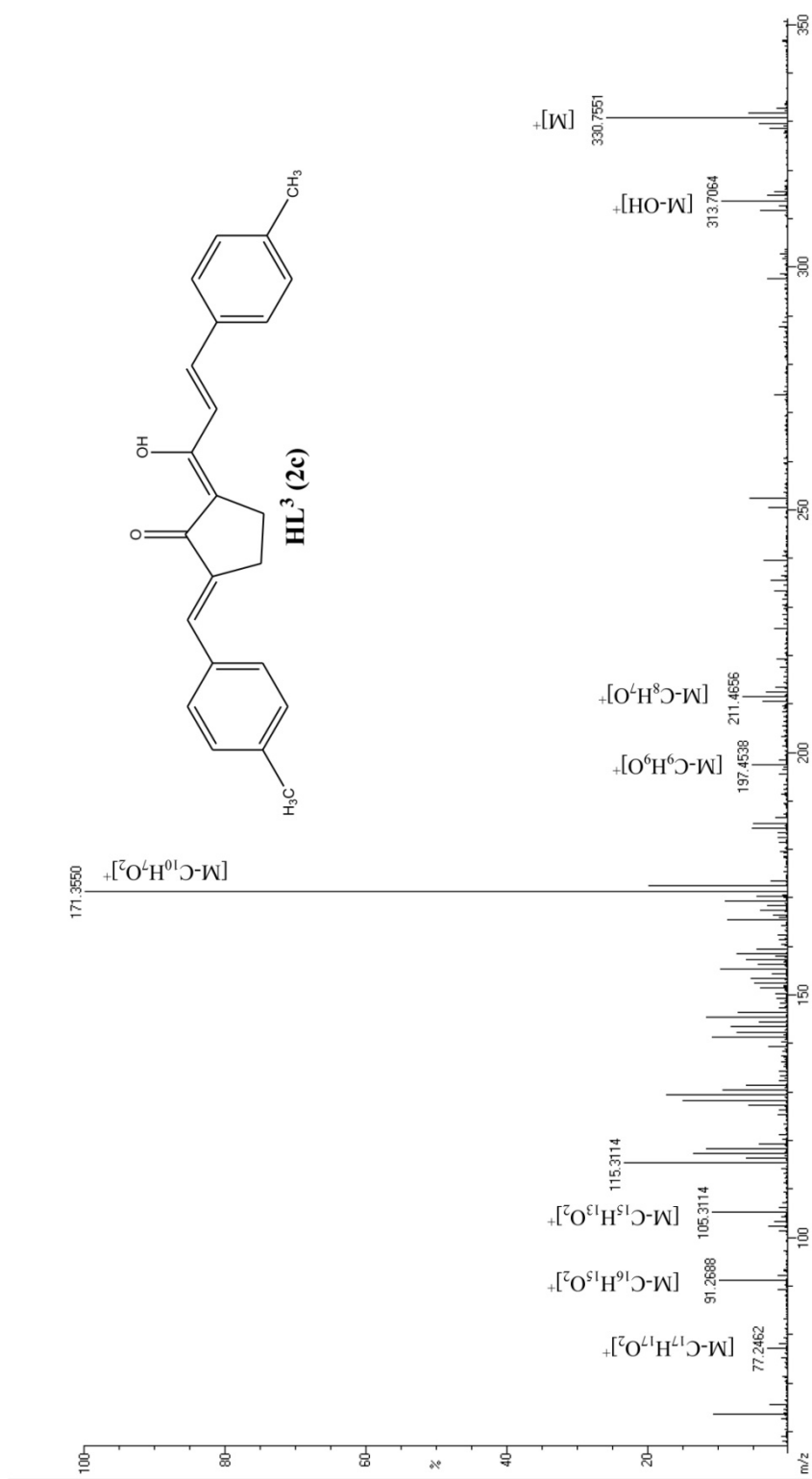


Figure 2.13. EI Mass spectrum of **HL³ (2c)**

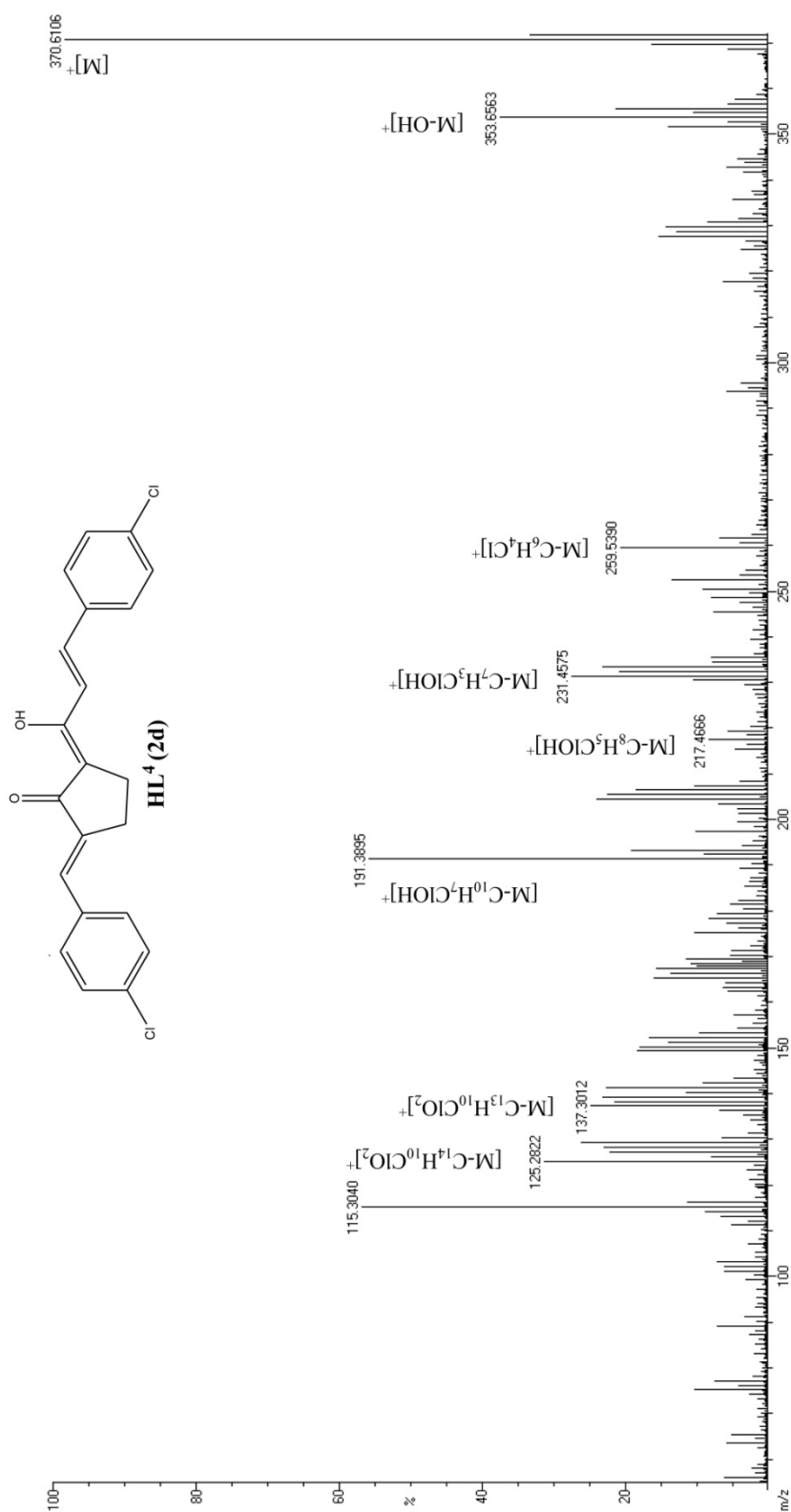


Figure 2.14. EI Mass spectrum of **HL⁴ (2d)**

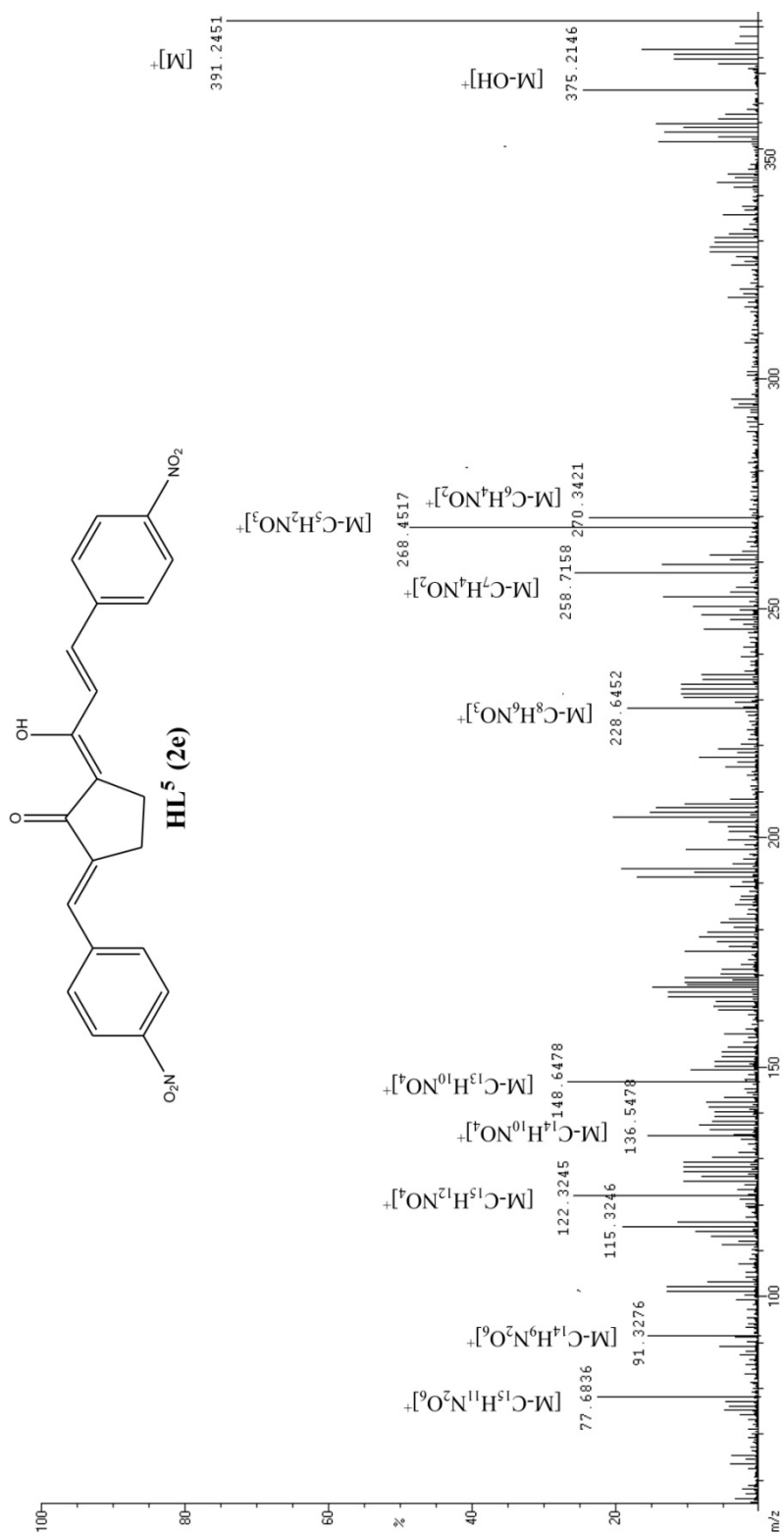


Figure 2.15. EI Mass spectrum of **HL⁵ (2e)**

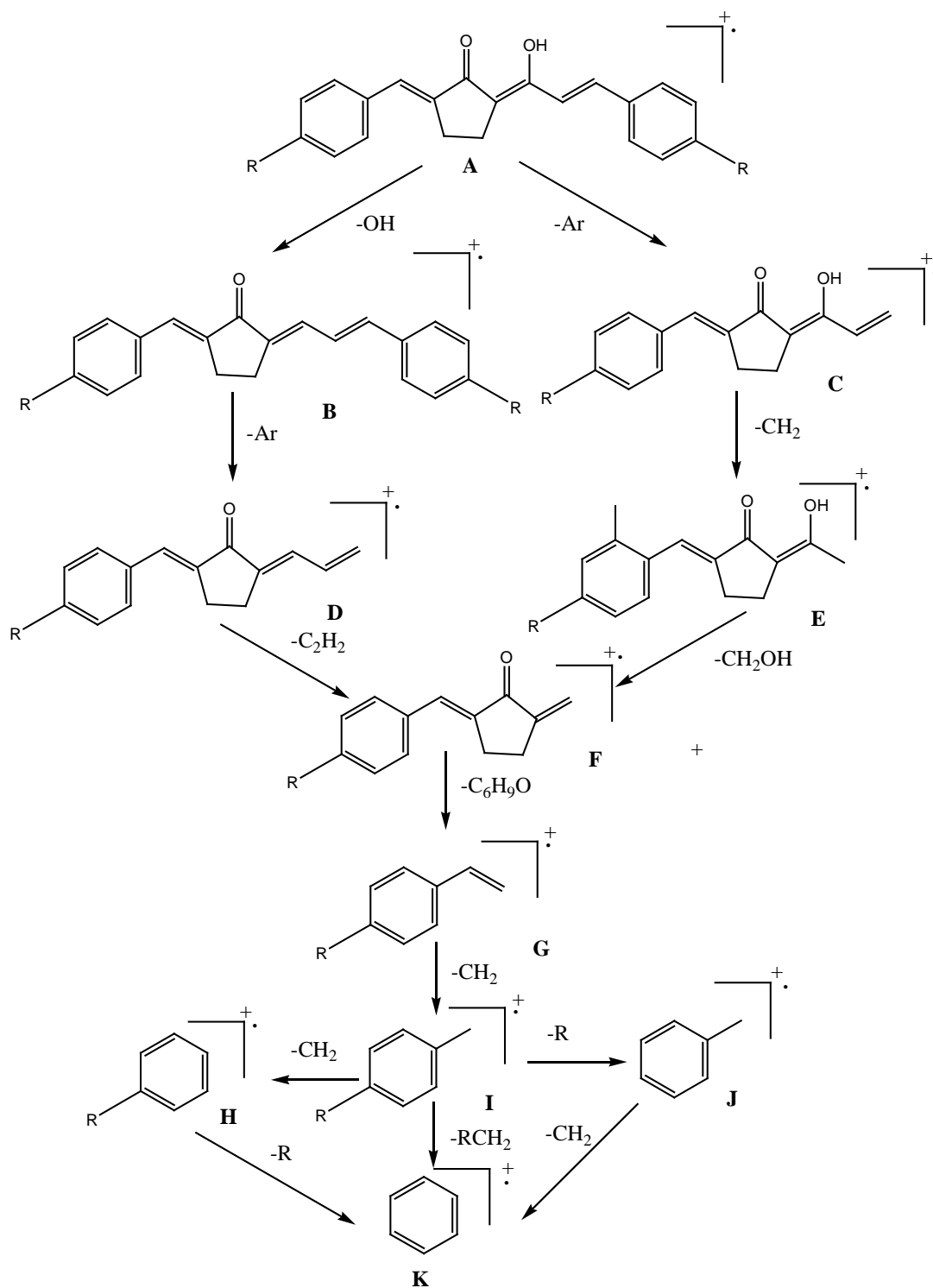


Figure 2.16. Fragmentation pattern of ligands

2.5 Characterization of metal complexes

Analytical and physical data of the metal complexes are given in **Table 2.5-2.7**. The observed carbon, hydrogen and metal percentages of the metal complexes and FAB mass spectral data suggest their ML_2 stoichiometry. All the metal complexes behave as non-electrolytes (specific conductance $< 15\Omega^{-1} \text{ cm}^{-1}$ in DMF) and do not contain the anion of the metal salt used for their preparation. The nickel(II) and zinc(II) complexes are diamagnetic and copper(II) complex is paramagnetic. The electronic, IR, ^1H NMR, ^{13}C NMR and mass spectral data of the complexes are compatible with the structure given in **Scheme 2.2**. The spectral data are discussed below.

Table 2.5 Analytical data of copper (II) complexes

Complexes (formula weight)	M.p. ($^{\circ}\text{C}$)	Yield (%)	Elemental analysis %			UV λ_{max} (nm)	μ_{eff} BM	Mass spectral data (m/z)
			(found /calcd)					
			C	H	Cu			
[Cu(L¹)₂] C ₄₂ H ₃₄ O ₈ Cu (730)	256	67	(69.25) 69.08	(4.71) 4.69	(8.86) 8.70	260 455	1.81	729, 395, 334, 224, 210
[Cu(L²)₂] C ₄₆ H ₄₂ O ₈ Cu (786)	234	72	(70.28) 70.26	(5.41) 5.38	(8.25) 8.08	252 445	1.76	785, 423, 362, 238, 224
[Cu(L³)₂] C ₄₆ H ₄₂ O ₄ Cu (722)	272	70	(76.52) 76.48	(5.94) 5.86	(8.91) (8.80)	248 434	1.75	721, 391, 330, 222, 208
[Cu(L⁴)₂] C ₄₂ H ₃₀ O ₄ Cl ₄ Cu (804)	278	69	(62.84) 62.74	(3.58) 3.76	(7.59) 7.90	246 429	1.77	803, 432, 370, 243, 229
[Cu(L⁵)₂] C ₄₂ H ₃₀ N ₄ O ₁₂ Cu (846)	246	62	(59.47) 59.61	(3.06) 3.57	(7.89) 7.51	274 458	1.76	847, 845, 453, 391, 253, 239

Table 2.6 Analytical data of nickel (II) complexes

Complexes (formula weight)	M.p. (°C)	Yield (%)	Elemental analysis %			UV λ_{\max} (nm)
			(found /calcd)			
			C	H	Ni	
[Ni(L¹)₂] C ₄₂ H ₃₄ O ₈ Ni (725)	242	63	(69.34) 69.54	(4.63) 4.72	(8.41) 8.09	264 488
[Ni(L²)₂] C ₄₆ H ₄₂ O ₈ Ni (781)	298	67	(70.58) 70.70	(5.21) 5.42	(7.22) 7.51	274 446
[Ni(L³)₂] C ₄₆ H ₄₂ O ₄ Ni (717)	104	70	(77.31) 77.00	(5.84) 5.90	(8.21) 8.18	294 467
[Ni(L⁴)₂] C ₄₂ H ₃₀ O ₄ Cl ₄ Ni (799)	166	68	(63.02) 63.12	(3.71) 3.78	(7.45) 7.34	264 484
[Ni(L⁵)₂] C ₄₂ H ₃₀ N ₄ O ₁₂ Ni (841)	240	60	(59.14) 59.95	(3.26) 3.59	(6.24) 6.98	248 472

Table 2.7 Analytical data of zinc (II) complexes

Complexes (formula weight)	M.p. (°C)	Yield (%)	Elemental analysis %			UV λ_{\max} (nm)
			(found /calcd)			
			C	H	Zn	
[Zn(L¹)₂] C ₄₂ H ₃₄ O ₈ Zn (732)	198	68	(68.16) 68.90	(4.71) 4.68	(8.97) 8.93	272 476
[Zn(L²)₂] C ₄₆ H ₄₂ O ₈ Zn (788)	202	73	(70.19) 70.09	(5.76) 5.37	(8.49) 8.30	267 464
[Zn(L³)₂] C ₄₆ H ₄₂ O ₄ Zn (724)	254	65	(76.31) 76.29	(5.88) 5.85	(9.15) 9.03	264 487
[Zn(L⁴)₂] C ₄₂ H ₃₀ O ₄ Cl ₄ Zn (805)	274	70	(62.73) 62.60	(3.22) 3.75	(8.36) 8.11	254 449
[Zn(L⁵)₂] C ₄₂ H ₃₀ N ₄ O ₁₂ Zn (848)	236	58	(59.87) 59.48	(3.71) 3.57	(7.08) 7.71	266 458

2.5.1 Electronic spectra

The UV spectra of the complexes are characterized by the presence of two absorption maxima, the low energy band corresponds to an $n \rightarrow \pi^*$ transition (429-488 nm) and the high energy band is due to a $\pi \rightarrow \pi^*$ transitions (246-294 nm) (**Table 2.5-2.7**). From a comparison of these spectra with that of free ligands, it follows that both $n \rightarrow \pi^*$ transition and $\pi \rightarrow \pi^*$ transition show only a slight bathochromic shifts, indicating the involvement of the carbonyl group in metal complexes^[186]. Similarity in the UV absorption maxima of metal complexes with that of free ligands, show that no structural variation of the ligand has occurred during the complex formation.

In the copper(II) complexes the presence of a broad visible band at ~ 665 nm and the measured μ_{eff} values (1.75–1.81 B.M.) support their square planar structure^[192]. The observed diamagnetism and broad medium-intensity band at $\sim 17,800$ cm^{-1} in the visible spectra of the nickel(II) chelates suggest their square-planar geometry. In order to establish the square planar structure of nickel(II) complexes, electronic spectra of the complexes are recorded by mixing with 10^{-3} M solution of pyridine. Square-planar nickel(II) complexes undergo a structural change to octahedral symmetry in the presence of donor solvents. In conformity with this observation the visible spectra of the nickel chelates in pyridine solution (10^{-3} M) showed three bands corresponding to a configurational change from square-planar to octahedral due to the association of pyridine. The absorption maxima at $\sim 8,040$, $\sim 13,540$ and $\sim 24,340$ cm^{-1} in the adducts can be assigned to the transitions ${}^3A_{2g} \rightarrow {}^3T_{2g}$; ${}^3A_{2g} \rightarrow {}^3T_{1g}(\text{F})$ and ${}^3A_{2g} \rightarrow {}^3T_{1g}(\text{P})$, respectively^[193].

2.5.2 Infrared Spectra

In the IR spectra of the metal complexes, strong band assignable to the stretching of the carbonyl moiety appeared at ~ 1613 cm^{-1} . The broad free

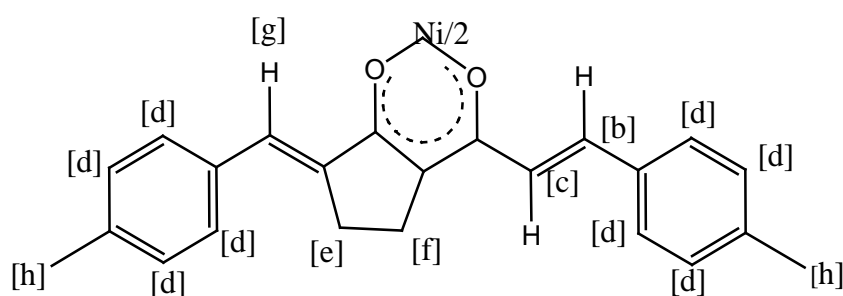
ligand band in the region at $2600\text{-}3800\text{ cm}^{-1}$ due to the hydrogen bonded enol proton is absent in the spectra of metal complexes and weak bands attributable to various $\nu(\text{C-H})$ appeared^[186]. A significant feature in the spectra of metal complexes in which the ligand contains an OH group in its phenyl ring is the presence of a relatively broad medium intensity band at 3450 cm^{-1} assignable to the $\nu(\text{O-H})$ vibration. This confirms that the phenolic OH group remains free and it is not involved in the bonding formation with metal(II) ions. The carbonyl groups are involved in metal complex formation is evident from the appearance of two medium intensity bands in the region $462\text{-}503\text{ cm}^{-1}$ due to $\nu(\text{M-O})$ vibrations^[186]. The prominent band at $\sim 975\text{ cm}^{-1}$ is typical of a trans – CH=CH– group which remained unaltered in the spectra of metal complexes (**Table 2.8**). Bands due to aryl C-Cl and NO_2 are also found in metal complexes of **2d** and **2e**.

2.5.3 ^1H NMR spectra

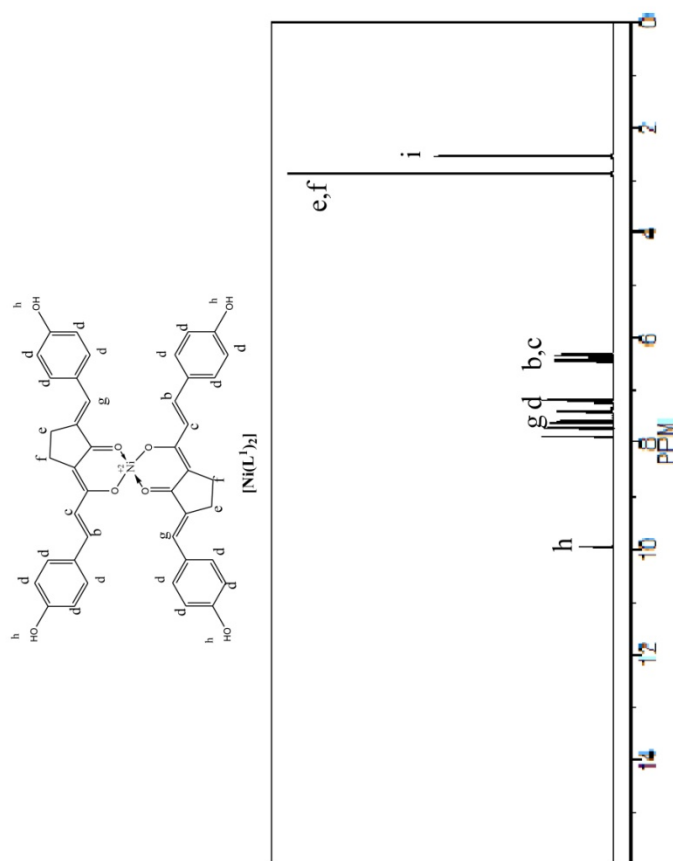
In order to establish the replacement of enolic proton in the ligands by metal ions, the ^1H NMR spectra of the diamagnetic nickel(II) complexes were recorded. The most distinguishing feature of the ^1H NMR spectra of the diamagnetic nickel(II) complexes is the absence of proton signals above $\delta \sim 10$ ppm. This strongly supports the replacement of the enolic proton by the metal ion in the complexes. In the spectra of the complexes of (**2a**), the phenolic signal appeared at $\delta \sim 9.91\text{ ppm}$ is clearly indicating that the phenolic group is not involved in bonding with the metal ions. Observed J value of 16 Hz for the alkenyl proton signals in the nickel (II) complexes suggest their trans orientation as it is in the free ligands. The integrated intensities of the aryl and alkenyl protons are in well agreement with 1:2 metal- stoichiometry. The ^1H NMR spectra of nickel(II) complexes are given in **Figures 2.17-2.21**.

Table 2.8 IR spectral data of complexes

IR spectral data of complexes (cm ⁻¹)							
Compounds	$\nu(\text{C}=\text{O})$ metal chelated carbonyl	$\nu(\text{C}=\text{C})$ phenyl	$\nu(\text{C}=\text{C})$ alkenyl	$\nu_{\text{as}}(\text{C}-\text{C}-\text{C})$ chelate ring	$\nu_{\text{as}}(\text{C}-\text{C}-\text{C})$ chelate ring	$\nu(\text{CH}=\text{CH}-)$ trans	$\nu(\text{M}-\text{O})$ chelate ring
[Cu(L ¹) ₂]	1537,1502	1448	1375	1249	1178	979	492
[Cu(L ²) ₂]	1611,1523	1467	1415	1251	1183	967	503
[Cu(L ³) ₂]	1611,1555	1487	1287	1251	1183	967	467
[Cu(L ⁴) ₂]	1539,1503	1451	1395	1271	1251	911	483
[Cu(L ⁵) ₂]	1622,1526	1472	1346	1252	1173	966	468
[Ni(L ¹) ₂]	1614,1554	1484	1324	1234	1148	968	491
[Ni(L ²) ₂]	1652,1528	1419	1413	1268	1157	951	498
[Ni(L ³) ₂]	1624,1559	1438	1269	1274	1128	965	484
[Ni(L ⁴) ₂]	1654,1533	1438	1394	1234	1241	967	488
[Ni(L ⁵) ₂]	1598,1518	1460	1362	1238	1172	978	462
[Zn(L ¹) ₂]	1614,1584	1467	1349	1268	1187	961	487
[Zn(L ²) ₂]	1621,1548	1478	1426	1231	1173	964	472
[Zn(L ³) ₂]	1678,1542	1434	1246	1224	1164	972	472
[Zn(L ⁴) ₂]	1584,1542	1464	1357	1263	1238	924	494
[Zn(L ⁵) ₂]	1632,1556	1448	1365	1236	1178	958	464

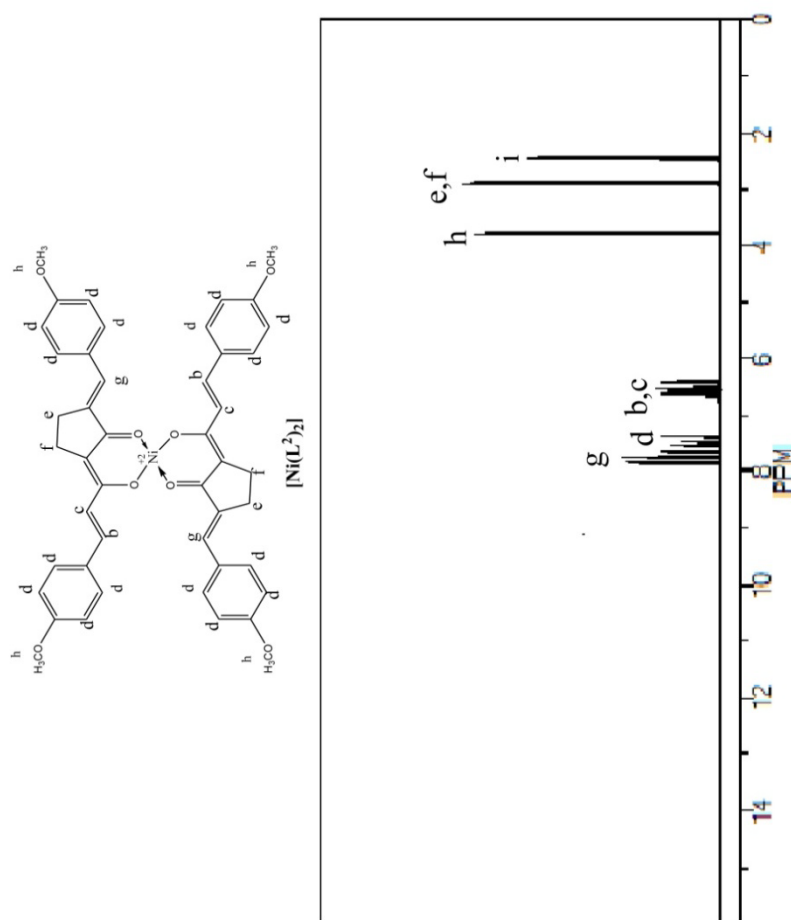
Table 2.9 ^1H NMR spectral data of Ni(II) complexes

Chemical shift, ppm (Coupling constant, Hz)								
Compounds	[a]	[b]	[c]	[d]	[e]	[f]	[g]	[h]
$[\text{Ni}(\text{L}^1)_2]$	-	6.21 (16.2)	6.69 (16.2)	7.22-7.91	2.82 (5.4)	2.87 (5.4)	7.76	9.91
$[\text{Ni}(\text{L}^2)_2]$	-	6.38 (16.4)	6.81 (16.4)	7.47-7.93	2.54 (5.5)	2.92 (5.4)	7.81	3.79
$[\text{Ni}(\text{L}^3)_2]$	-	6.75 (16.3)	6.91 (16.4)	7.27-7.89	2.78 (5.6)	2.88 (5.6)	7.92	2.82
$[\text{Ni}(\text{L}^4)_2]$	-	6.28 (16.5)	6.64 (16.4)	7.48-7.84	2.76 (5.4)	2.87 (5.4)	7.92	-
$[\text{Ni}(\text{L}^5)_2]$	-	6.69 (16.4)	6.71 (16.4)	7.19-7.44	2.73 (5.2)	2.77 (5.3)	7.63	-



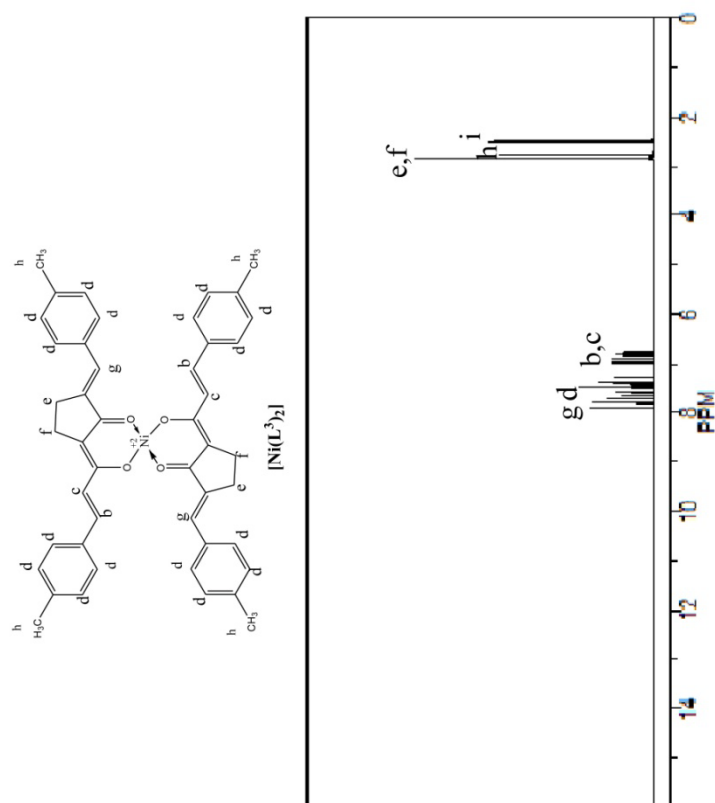
^1H NMR (400MHz, DMSO, ppm): [2.82 (4H, t, $J=5.4\text{Hz}$, cyclopentane ring CH_2), 2.87 (4H, t, $J=5.4\text{Hz}$, cyclopentane ring CH_2) [e,f], [6.21 (2H, d, $J=16.2\text{Hz}$, (E)- alkenyl H), 6.69 (2H, d, $J=16.2\text{Hz}$, (E)- alkenyl H)] [b,c], 7.22-7.91 (16H, m, aromatic Hs) [d], 7.76 (2H, s, vinylic H) [g], 9.91 (4H, s, phenolic H) [h], 2.49 (solvent) [i].

Figure 2.17. ^1H NMR spectrum of $[\text{Ni}(\text{L}^1)_2]$



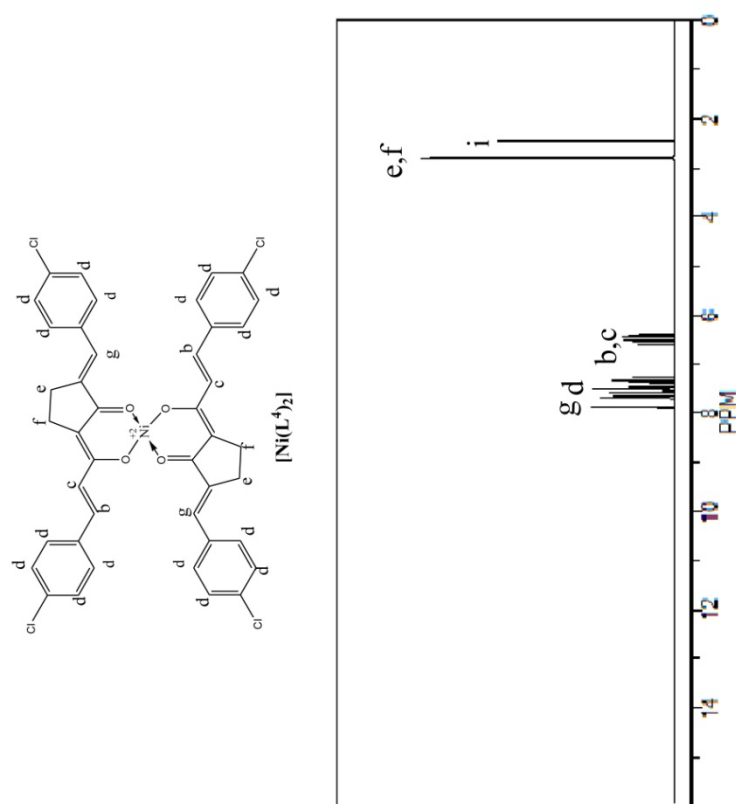
^1H NMR (400MHz, DMSO, ppm):, [2.54 (4H, t, $J=5.5\text{Hz}$, cyclopentane ring CH_2), 2.92 (4H, t, $J=5.4\text{Hz}$, cyclopentane ring CH_2)] [e,f], [6.38 (2H, d, $J=16.4\text{Hz}$, (E)- alkenyl H), 6.81 (2H, d, $J=16.4\text{Hz}$, (E)- alkenyl H)] [b,c], 7.47-7.93 (16H, m, aromatic Hs) [d], 7.81 (2H, s, vinylic H) [g], 3.79 (6H, s, methoxy H) [h], 2.49 (solvent) [i].

Figure 2.18. ^1H NMR spectrum of $[\text{Ni}(\text{L}^2)_2]$



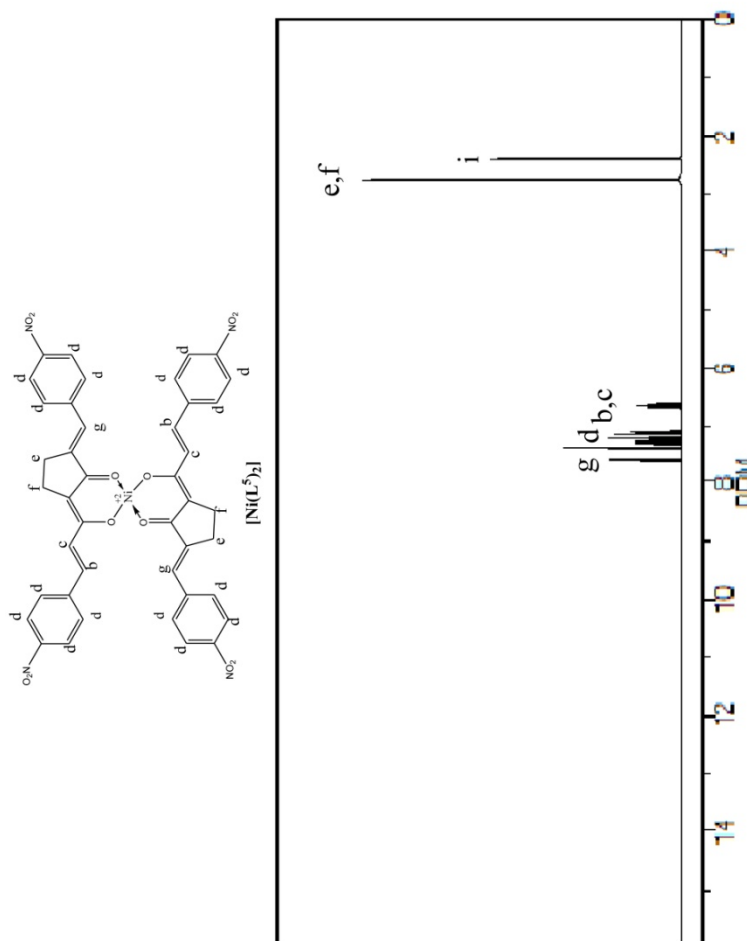
^1H NMR (400MHz, DMSO, ppm):, [2.78 (4H, t, $J=5.6\text{Hz}$, cyclopentane ring CH_2), 2.88 (4H, t, $J=5.6\text{Hz}$, cyclopentane ring CH_2) [e,f], [6.75 (2H, d, $J=16.3\text{Hz}$, (E)- alkenyl H), 6.91 (2H, d, $J=16.4\text{Hz}$, (E)- alkenyl H) [b,c], 7.27-7.89 (16H, m, aromatic Hs) [d], 7.92 (2H, s, vinylic H) [g], 2.82 (6H, s, methyl H) [h], 2.49 (solvent) [i].

Figure 2.19. ^1H NMR spectrum of $[\text{Ni}(\text{L}^3)_2]$



^1H NMR (400MHz, DMSO, ppm): [2.76 (4H, t, $J=5.4\text{Hz}$, cyclopentane ring CH_2), 2.87 (4H, t, $J=5.4\text{Hz}$, cyclopentane ring CH_2) [e,f], [6.28 (2H, d, $J=16.5\text{Hz}$, (E)- alkenyl H), 6.64 (2H, d, $J=16.4\text{Hz}$, (E)- alkenyl H)] [b,c], 7.48-7.84 (16H, m, aromatic Hs) [d], 7.92 (2H, s, vinylic H) [g], 2.49 (solvent) [i].

Figure 2.20. ^1H NMR spectrum of $[\text{Ni}(\text{L}^4)_2]$



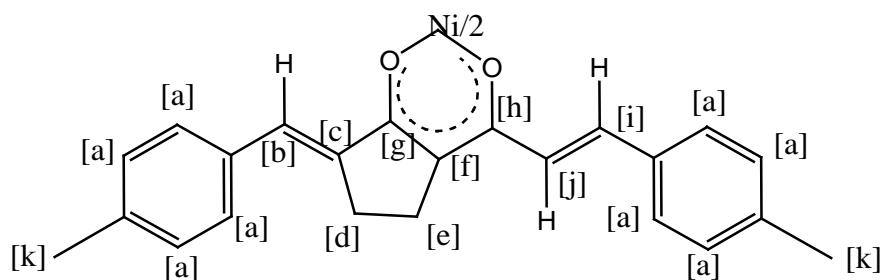
^1H NMR (400MHz, DMSO, ppm): [2.73 (4H, t, $J=5.2\text{Hz}$, cyclopentane ring CH_2), 2.77 (4H, t, $J=5.3\text{Hz}$, cyclopentane ring CH_2)] [e,f], [6.69 (2H, d, $J=16.4\text{Hz}$, (E)- alkenyl H), 6.71 (2H, d, $J=16.4\text{Hz}$, (E)- alkenyl H)] [b,c], 7.19-7.44 (16H, m, aromatic Hs) [d], 7.63 (2H, s, vinylic H) [g], 2.49 (solvent) [i].

Figure 2.21. ^1H NMR spectrum of $[\text{Ni}(\text{L}^5)_2]$

2.5.4 ^{13}C NMR spectra

The carbonyl carbon signal of the free ligand shifted by 15- 20 ppm to low field in the spectra of nickel(II) complexes (**Table 2.10**). This clearly suggest the strong interaction between the metal ion and carbonyl oxygens and also more effective delocalisation that exist in the metal chelate ring compared to the free ligand. The probable assignment of signals in the spectra is brought out in **Table 2.10**. The spectra are given in **Figures 2.22-2.26**.

Table 2.10 ^{13}C NMR spectral data of Ni (II) complexes



Compounds	Chemical shift (ppm)										
	[a]	[b]	[c]	[d]	[e]	[f]	[g]	[h]	[I]	[j]	[k]
$[\text{Ni}(\text{L}^1)_2]$	118.86-158.81	142.24	140.73	29.54	33.72	97.46	167.32	195.89	123.86	137.25	-
$[\text{Ni}(\text{L}^2)_2]$	115.67-167.64	141.49	138.26	30.24	31.54	98.73	151.42	184.32	119.21	129.84	56.37
$[\text{Ni}(\text{L}^3)_2]$	115.85-158.27	148.24	145.37	29.87	34.46	94.26	164.67	191.85	121.14	135.23	18.24
$[\text{Ni}(\text{L}^4)_2]$	117.85-160.94	147.67	141.09	28.64	30.94	96.27	158.19	188.37	123.14	132.49	-
$[\text{Ni}(\text{L}^5)_2]$	124.48-137.86	149.43	145.28	31.28	34.43	94.78	163.96	190.72	125.67	133.87	-

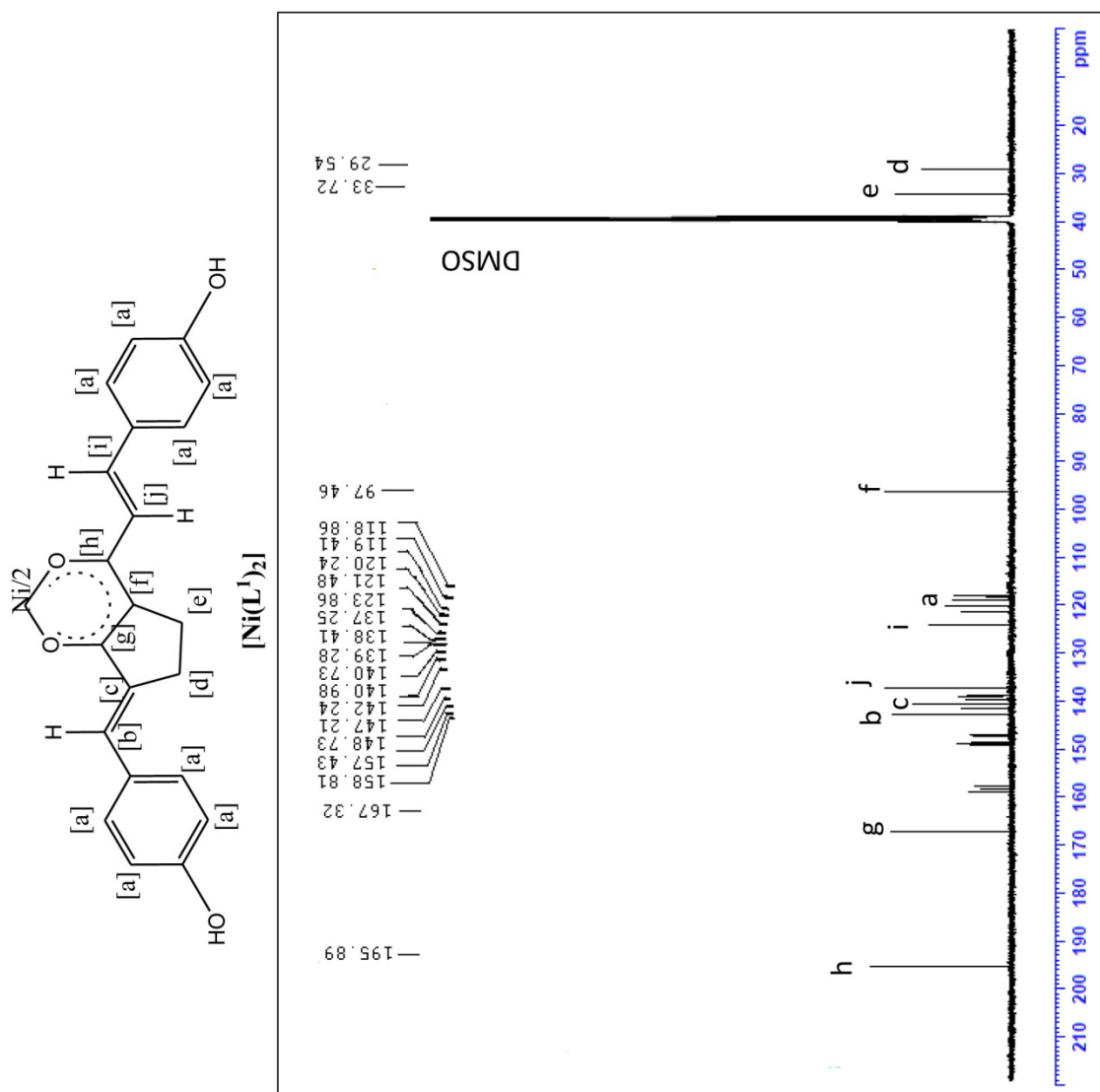


Figure 2.22. ^{13}C NMR spectrum of $[\text{NiL}_2]$

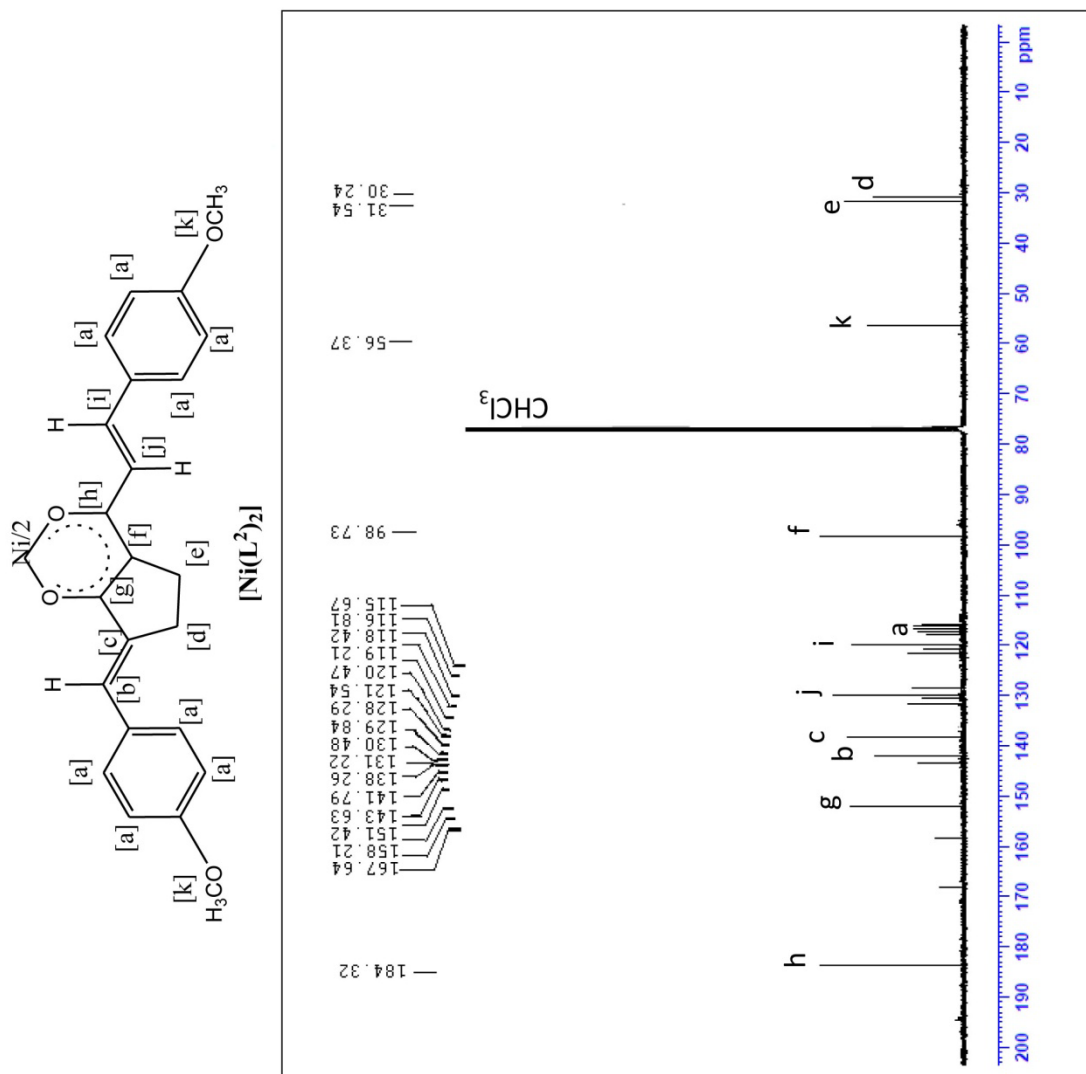


Figure 2.23. ^{13}C NMR spectrum of $[\text{Ni}(\text{L}^2)_2]$

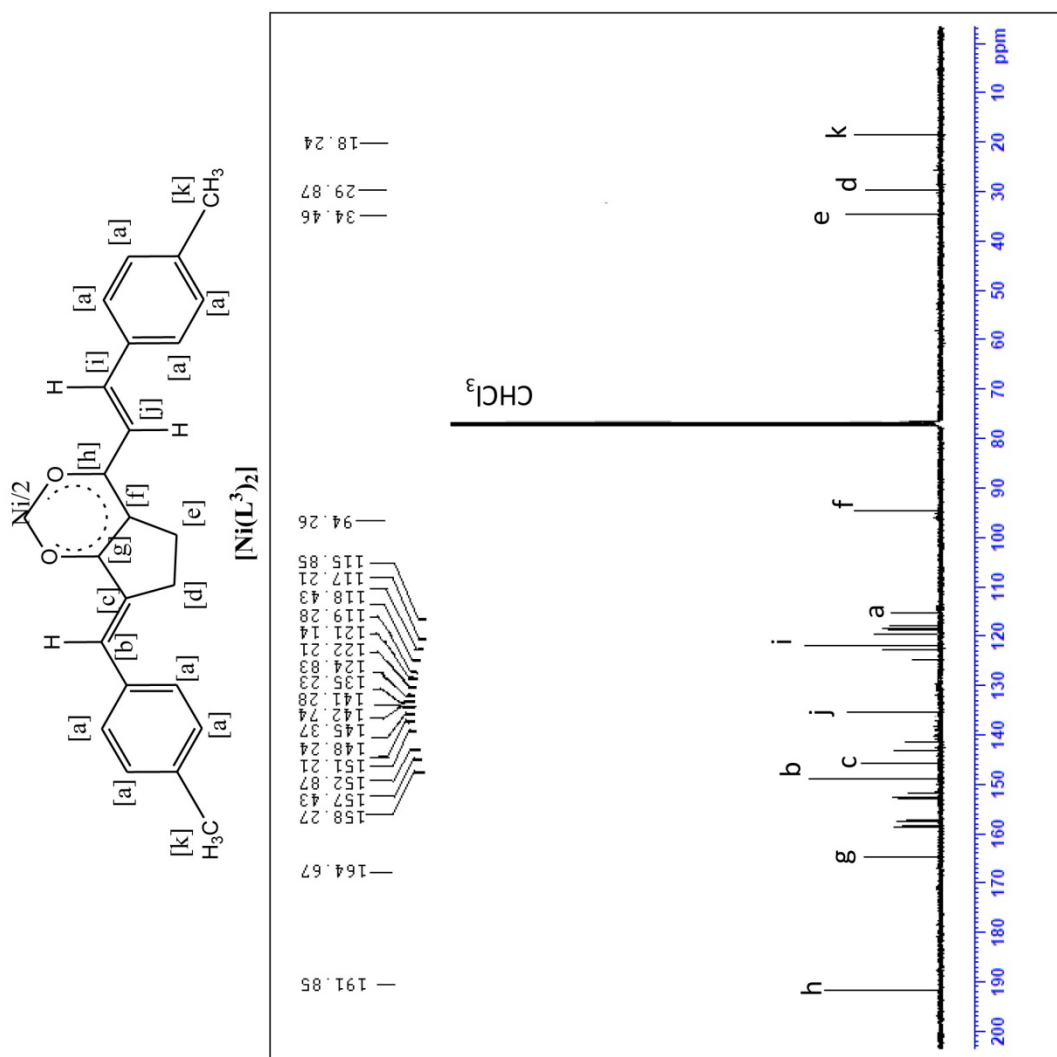


Figure 2.24. ^{13}C NMR spectrum of $[\text{Ni}(\text{L}^3)_2]$

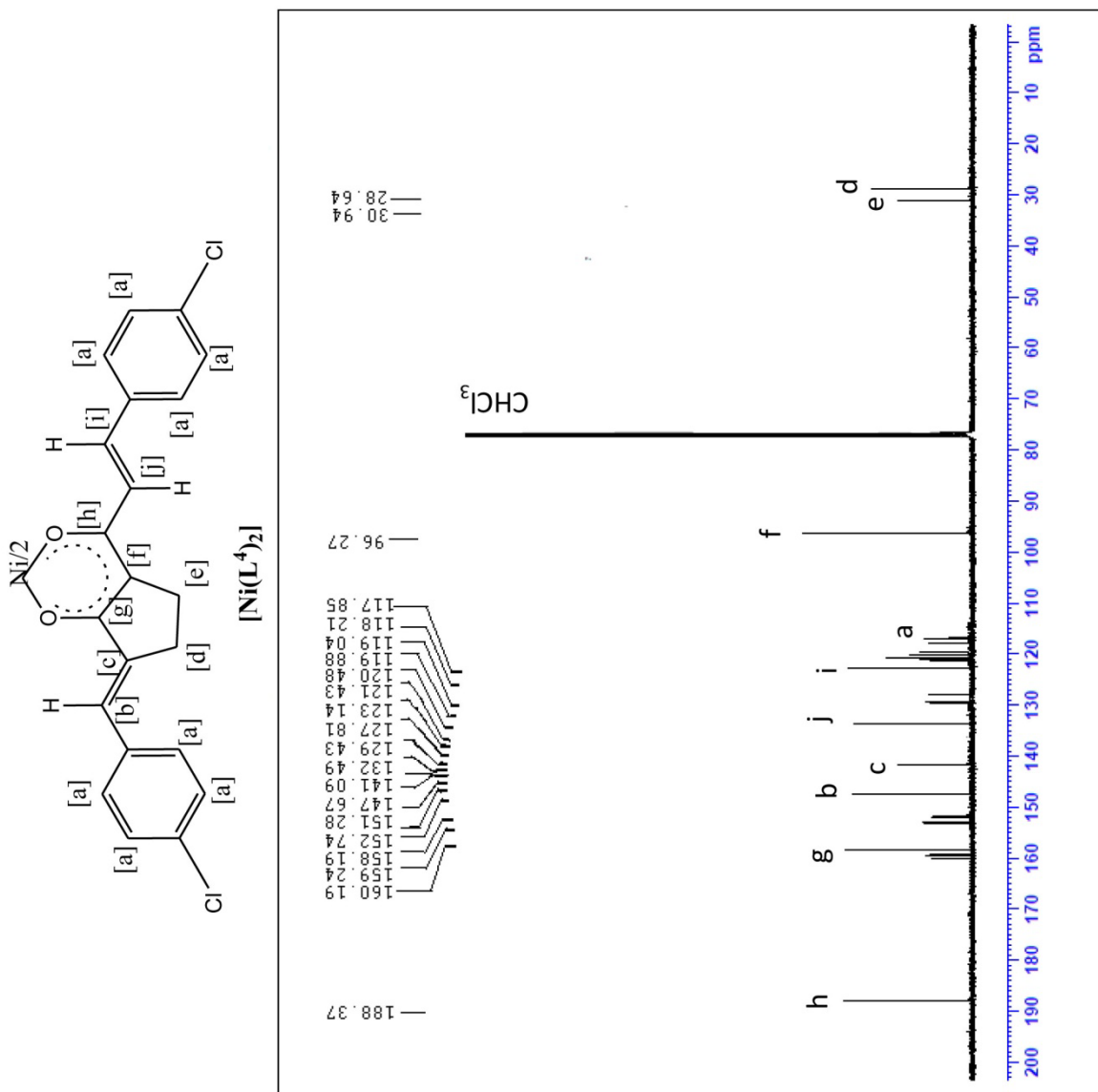


Figure 2.25. ^{13}C NMR spectrum of $[\text{Ni}(\text{L}^4)_2]$

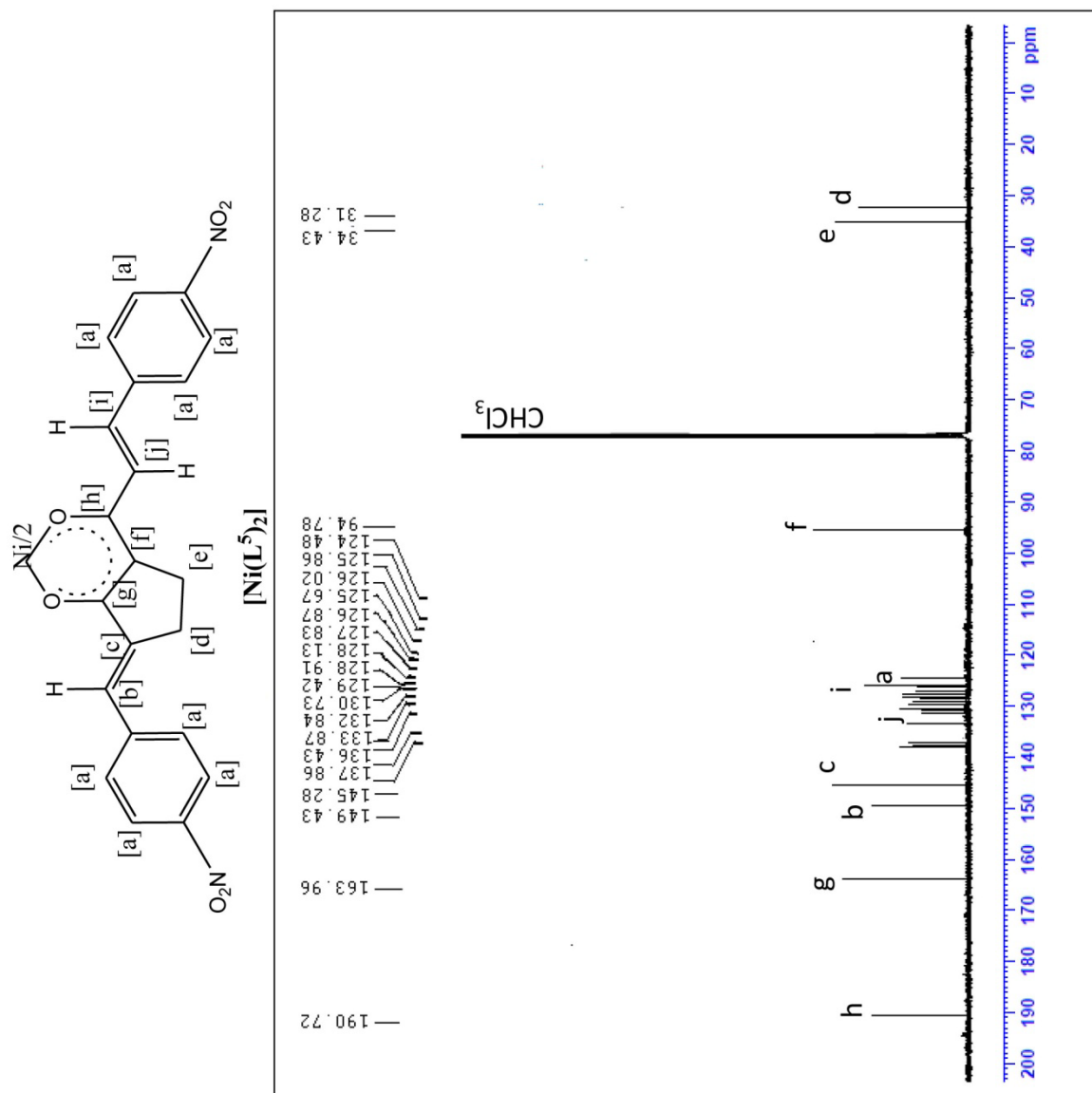


Figure 2.26. ^{13}C NMR spectrum of $[\text{Ni}(\text{L}^5)_2]$

2.5.5 Mass spectra

The FAB mass spectra of the copper(II) chelates confirm the ML_2 stoichiometry of the complexes. Peaks due to M^+ and $(M+2)^+$ are present in the FAB MS of copper(II) chelates. The relative intensity of these peaks are consistent with the natural abundance of ^{63}Cu and ^{65}Cu isotopes^[186]. The mass spectra of the copper(II) complexes showed a stepwise removal of phenyl groups as a characteristic feature. Peaks due to $[\text{CuL}]^+$, L^+ and fragments of L^+ are also present in the spectra of copper(II) complexes. The prominent peaks in the spectra are given in **Table 2.6**. The FAB MS of copper(II) complexes of **2a-2e** are given in **Figures 2.27-2.31**. A probable fragmentation pattern is also described in **Figure 2.32**.

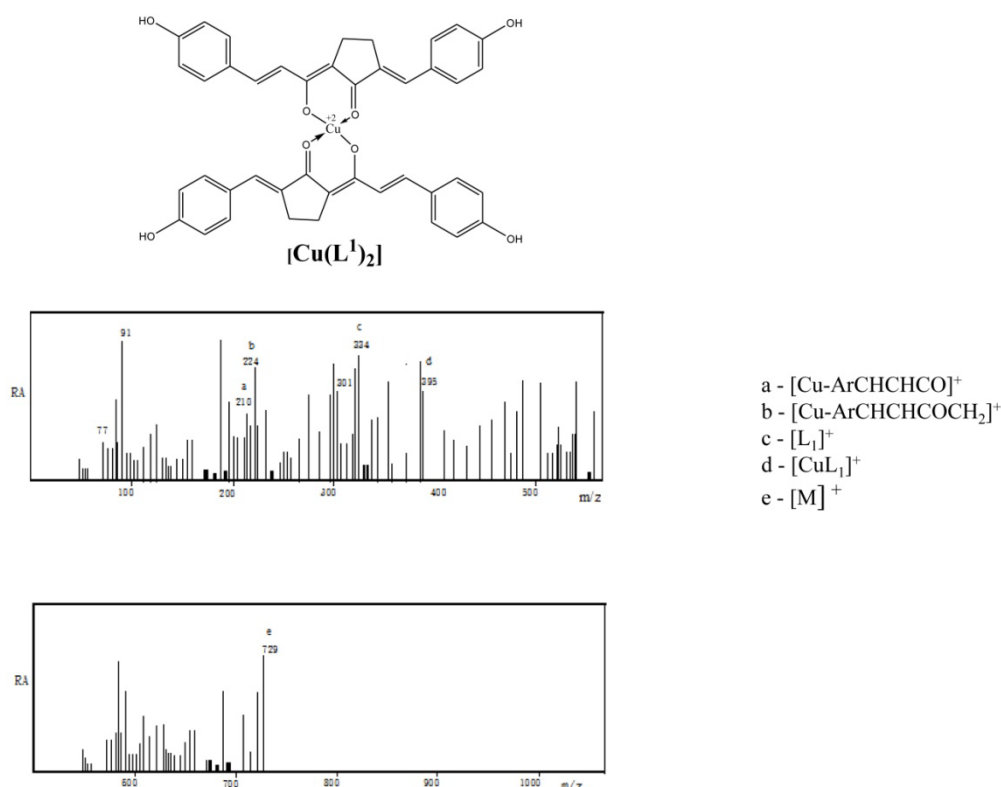


Figure 2.27. FAB Mass spectrum of **[Cu(L¹)₂]**

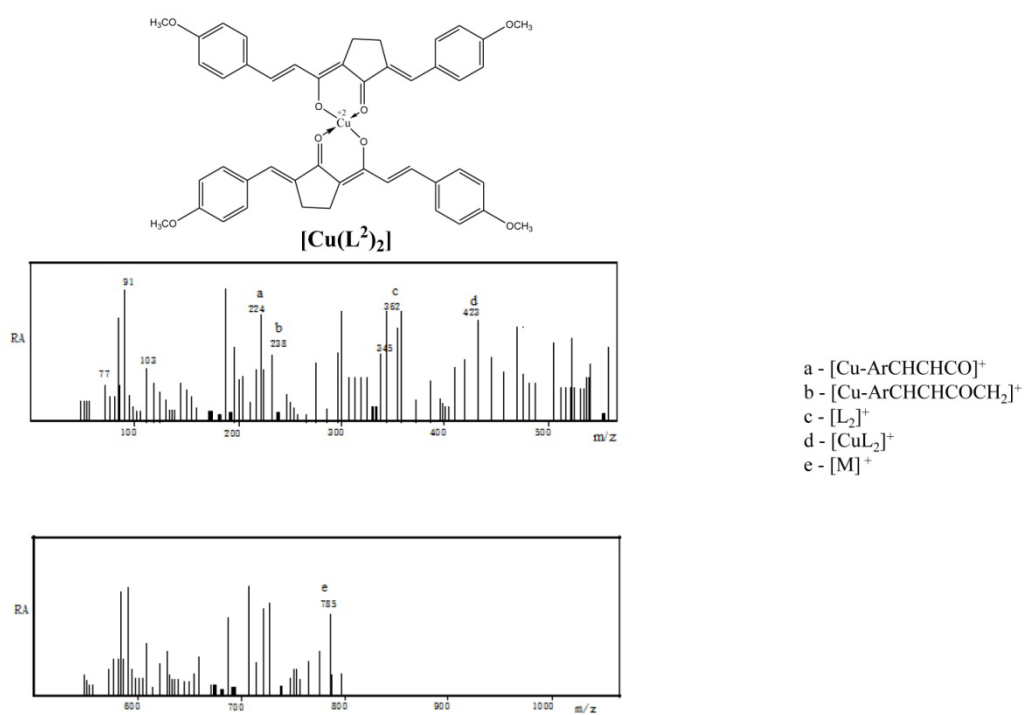


Figure 2.28. FAB Mass spectrum of $[\text{Cu}(\text{L}^2)_2]$

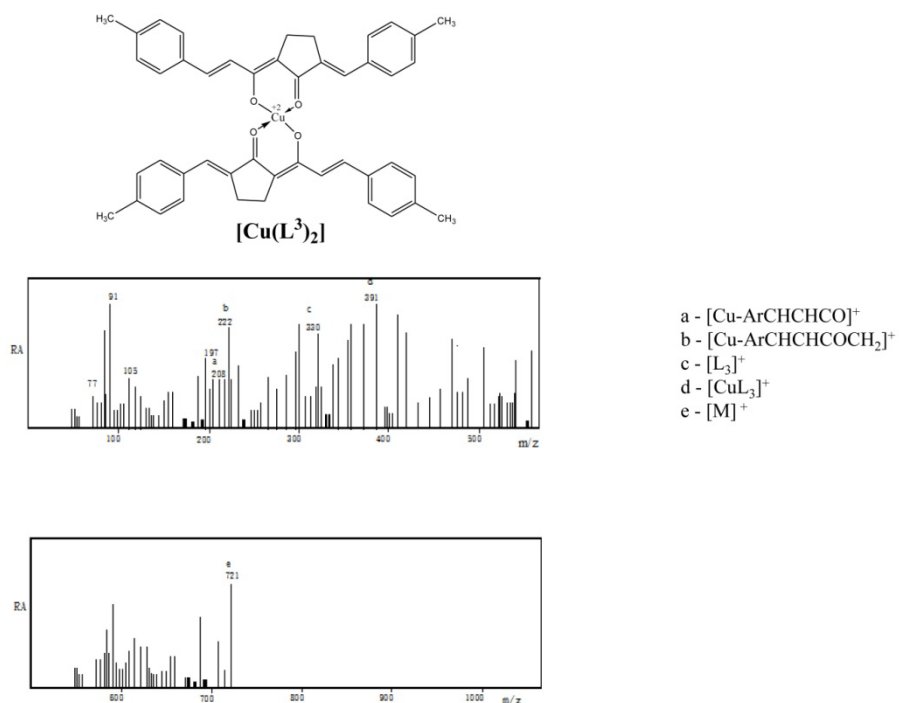


Figure 2.29. FAB Mass spectrum of $[\text{Cu}(\text{L}^3)_2]$

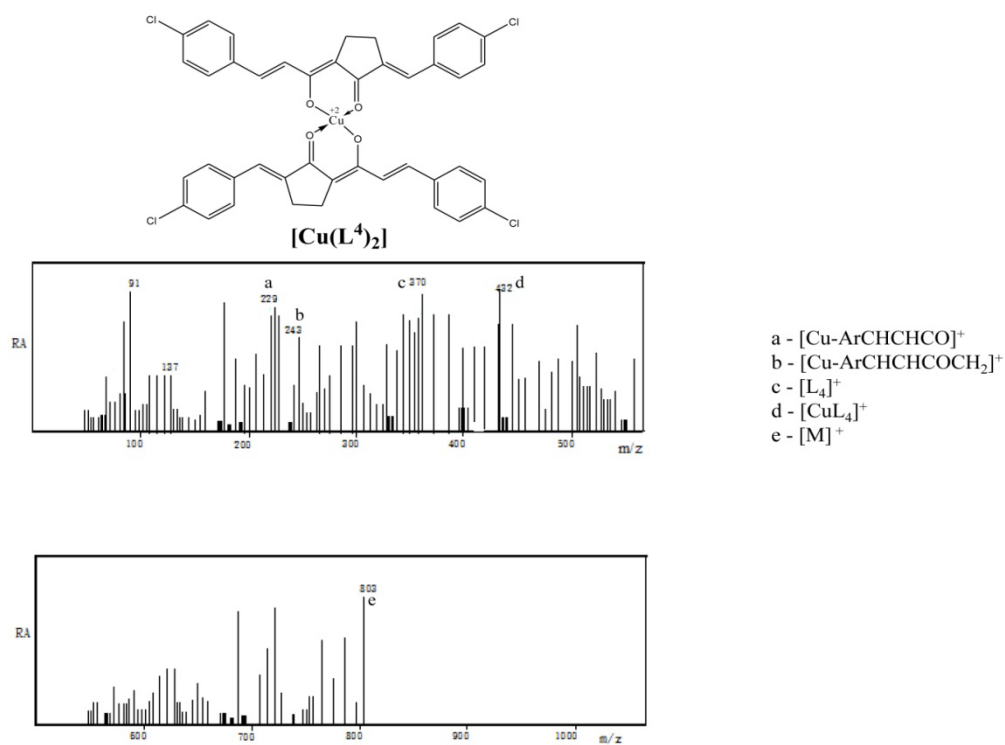


Figure 2.30. FAB Mass spectrum of [Cu(L⁴)₂]

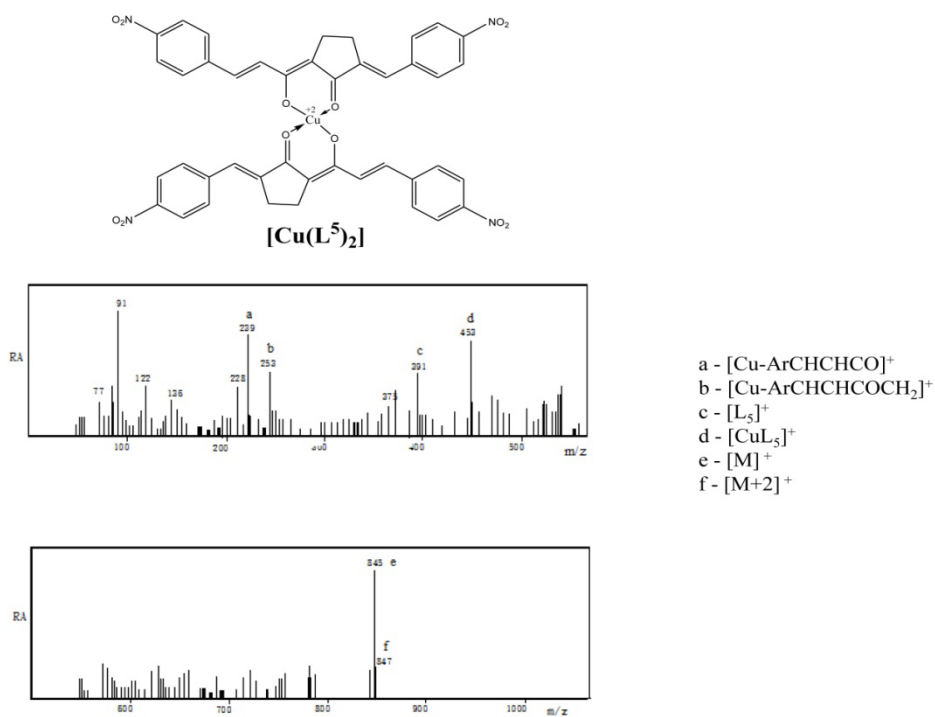


Figure 2.31. FAB Mass spectrum of [Cu(L⁵)₂]

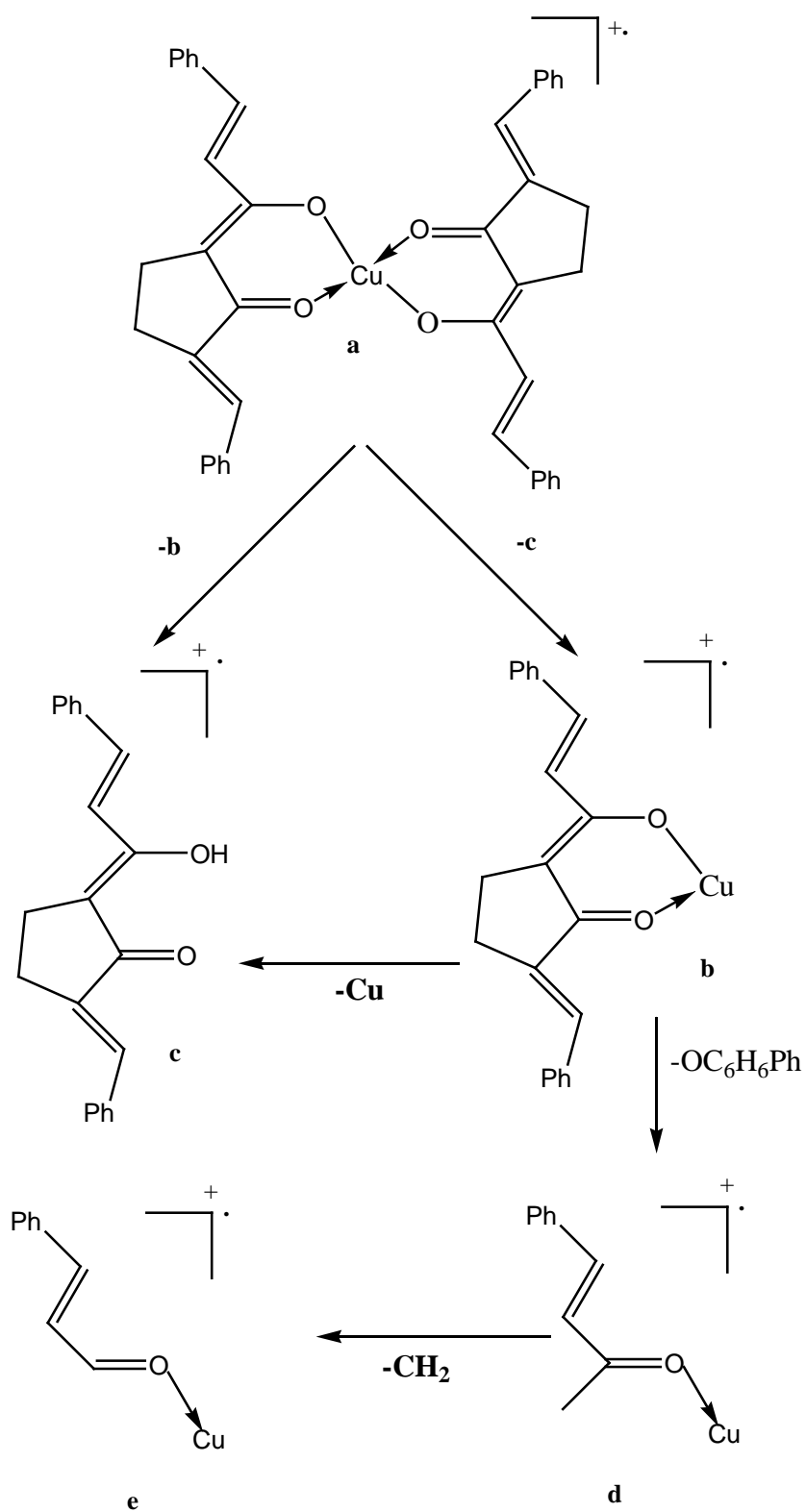
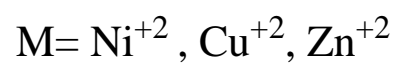
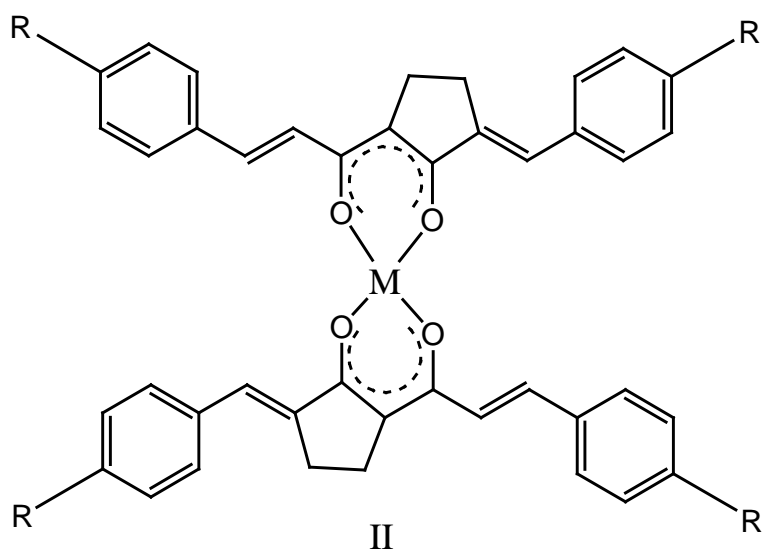


Figure 2.32. Fragmentation pattern of copper(II) complexes

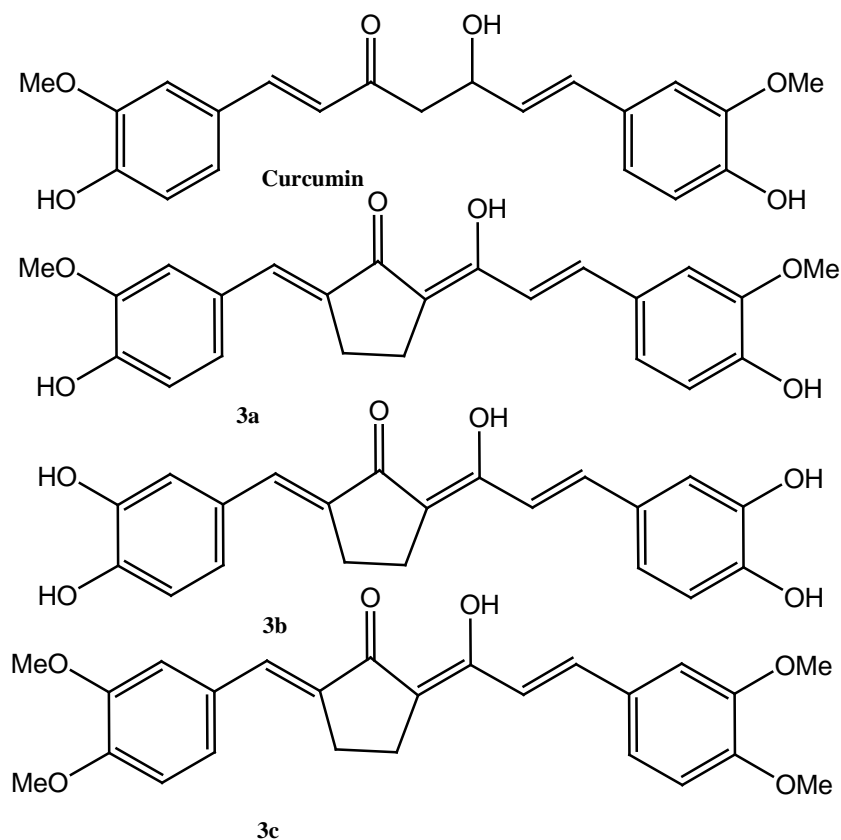
From the above discussion on various spectral data of the metal(II) complexes, the following probable structure can be assigned to the metal complexes



Chapter 3

LIGANDS WITH 3,4-DISUBSTITUTED PHENYL RINGS

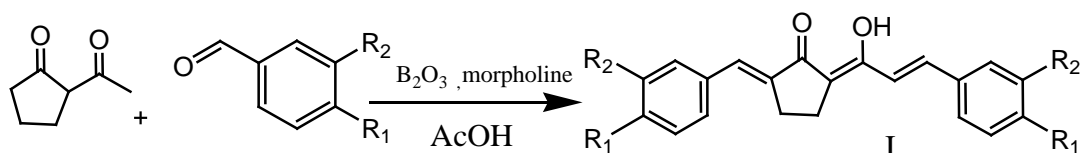
By analogy with curcumin, the following three β -diketones (**3a**, **3b** and **3c**) were synthesised from vanillin, protocatechuic aldehyde and veratraldehyde, respectively and 2-acetylcyclopentanone under microwave conditions.



From a series of experiments, the optimum conditions for the synthesis are obtained. The reaction involved is depicted in **Scheme 3.1** and the general procedure is described below.

3.1 Synthesis of ligands

2-acetylcyclopentanone (20 mmol) was mixed with boron oxide (20 mmol) in a 100 ml Erlenmeyer flask. The appropriate aromatic aldehyde (40 mmol), acetic acid (100 mg), and morpholine (100 mg) were then added. The reaction mixture was irradiated with the microwave at 70W for 3 minutes. The flask was cooled to room temperature and then methanol (50 ml) was added. This mixture was then sonicated for 20-30 minutes. The fine powder so obtained was filtered and washed with cold methanol. The compounds were recrystallized from hot benzene to obtain chromatographically pure material.



Scheme 3.1

3.2 Synthesis of Cu^{II}, Ni^{II} and Zn^{II} complexes

The Ni^{II}, Zn^{II} and Cu(II) complexes were prepared as given below. A methanolic solution of metal(II) acetate (25 ml, 1 mmol) was added with stirring to a solution of ligand (40 ml, 2 mmol) in methanol and refluxed gently for ~1 hour in a boiling water bath. After 1 hour, the volume was reduced to half and the solution was allowed to cool to room temperature. The precipitated complex was filtered, washed with cold methanol and recrystallized from hot methanol.

3.3 Results and discussion

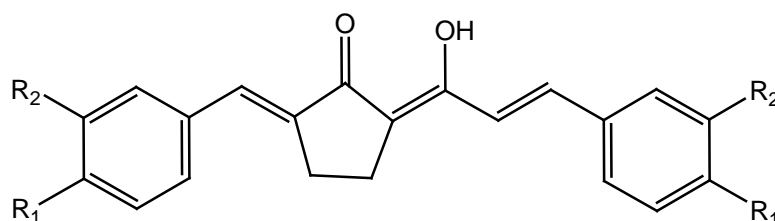
The ligands were synthesized by the condensation of 3,4-disubstituted benzaldehyde with 2-acetylcyclopentanone (**Scheme 3.1**). The systematic

names of the ligands (**3a-3c**) are given in **Table.3.1**. All the compounds are crystalline in nature and are freely soluble in common organic solvents.

The results of elemental analysis and molecular weight determination of the compounds are given in **Table 3.2**. The UV, IR, ^1H NMR, ^{13}C NMR and mass spectral data of the compounds discussed below are in agreement with the structure **I** given in **Scheme 3.1**.

3.4 Characterization of ligands

Table 3.1 Synthetic details of ligands



Compounds	Aldehydes used for synthesis	R ₁	R ₂	Systematic name
HL¹ (3a)	4-hydroxy-3-methoxy benzaldehyde (vanillin)	OH	OCH ₃	(2E)-2-(4-hydroxy-3-methoxybenzylidene)-5-((E)-3-(4-hydroxy-3-methoxyphenyl) acryloyl) cyclopentanone
HL² (3b)	3,4-dihydroxy benzaldehyde (protocatechualdehyde)	OH	OH	(2E)-2-(3,4-dihydroxybenzylidene)-5-((E)-3-(3,4-dihydroxyphenyl) acryloyl) cyclopentanone
HL³ (3c)	3,4- dimethoxy benzaldehyde (veratraldehyde)	OCH ₃	OCH ₃	(2E)-2-(3,4-dimethoxy benzylidene)-5-((E)-3-(3,4-dimethoxy phenyl) acryloyl) cyclopentanone

Table 3.2 Analytical, UV, IR, and mass spectral data of ligands

Ligands	M. p. (°C)	Elemental analysis (found /calcd) %		Colour	Yield (%)	UV λ_{\max} (nm)	IR (cm ⁻¹)			Mass spectral data (m/z)
		C	H				$\nu(\text{C}=\text{O})$	$\nu_{\text{as}}(\text{C}-\text{C}-\text{C})$	$\nu(\text{CH}=\text{CH}-)$ (trans)	
(3a) HL¹ C ₂₃ H ₂₂ O ₆ (394)	164 °C	(69.84) (70.04)	(5.76) (5.62)	Orange yellow solid	74	263 ($\pi \rightarrow \pi^*$), 448 ($n \rightarrow \pi^*$)	1614	1526	962	394,377, 271, 255,243,229, 149, 137, 91,77
(3b) HL² C ₂₁ H ₁₈ O ₆ (366)	148 °C	(68.37) (68.85)	(4.84) (4.95)	Reddish brown solid	70	257 ($\pi \rightarrow \pi^*$), 471 ($n \rightarrow \pi^*$)	1564	1546	968	366,349,317, 257, 241,231, 215,135, 123,91,77
(3c) HL³ C ₂₅ H ₂₆ O ₆ (422)	132 °C	(71.54) (71.07)	(6.12) (6.20)	Orange yellow solid	72	260 ($\pi \rightarrow \pi^*$), 472 ($n \rightarrow \pi^*$)	1593	1497	966	422,405,269,257, 243,231,191,151, 91,77

3.4.1 Electronic spectra

The UV absorption spectrum of curcumin shows two bands – one low energy band at 360-430 nm corresponding to $n \rightarrow \pi^*$ transition and high energy band at ~ 240 -290 nm corresponding to $\pi \rightarrow \pi^*$ transition^[189]. The UV spectra of the ligands **3a** - **3c** (10^{-3} M; CHCl_3) also displayed two absorption maxima which can be easily interpreted as follows- the low energy band corresponds to an $n \rightarrow \pi^*$ transition (448–472 nm) and the high energy band is due to a $\pi \rightarrow \pi^*$ transitions (257-263 nm) (**Table 3.2**)^[186]. The high energy band due to the $\pi \rightarrow \pi^*$ transitions of the fully conjugated system is not much influenced by the nature of substituent in the phenyl rings.

3.4.2 Infrared Spectra

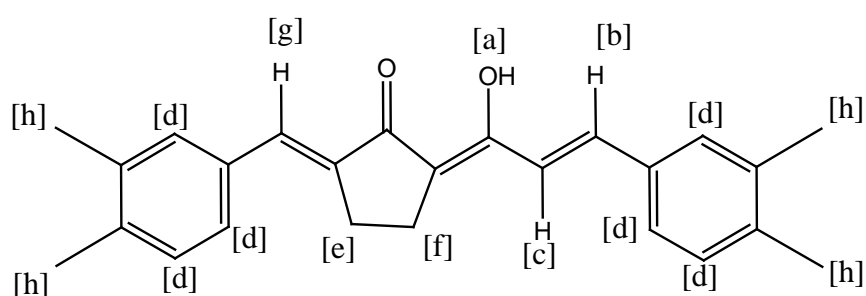
The strong intensity bands centered at 1614 cm^{-1} , 1564 cm^{-1} and 1593 cm^{-1} in **3a**, **3b** and **3c**, respectively, can be assigned to $\nu_{(\text{C}=\text{O})}$ stretching of the enolised diketo group. It is well known that both α , β - unsaturation and intramolecular hydrogen bonding can lower C=O stretching frequency by about 50 cm^{-1} . A broad band present in the range of 2800 - 3500 cm^{-1} is due to the stretching of the enol group. The observed breadth and intensity of the band suggest the involvement of the enolic proton in strong intramolecular hydrogen bonding. The absence of band assignable to a normal or α , β -unsaturated carbonyl group in the region 1640 - 1740 cm^{-1} of the spectra indicates that these ligands exist in the enolic form. The presence of various ring vibrations and C–H absorption makes the spectra fairly complicated for complete assignments of individual bands^[152,189,193]. The important absorptions corresponding to $\nu_{(\text{C}=\text{O})}$, $\nu_{\text{as}(\text{C}-\text{C}-\text{C})}$ and $\nu_{(\text{CH}=\text{CH}-)}$ (trans) are given in **Table 3.2**. The intense band at 1293 cm^{-1} in the IR spectrum of **3a** and at 1287 cm^{-1} in the IR spectrum of **3b** may be assigned to phenolic (O-H) stretching mode, according to the previous assignments^[191].

3.4.3 ^1H NMR spectra

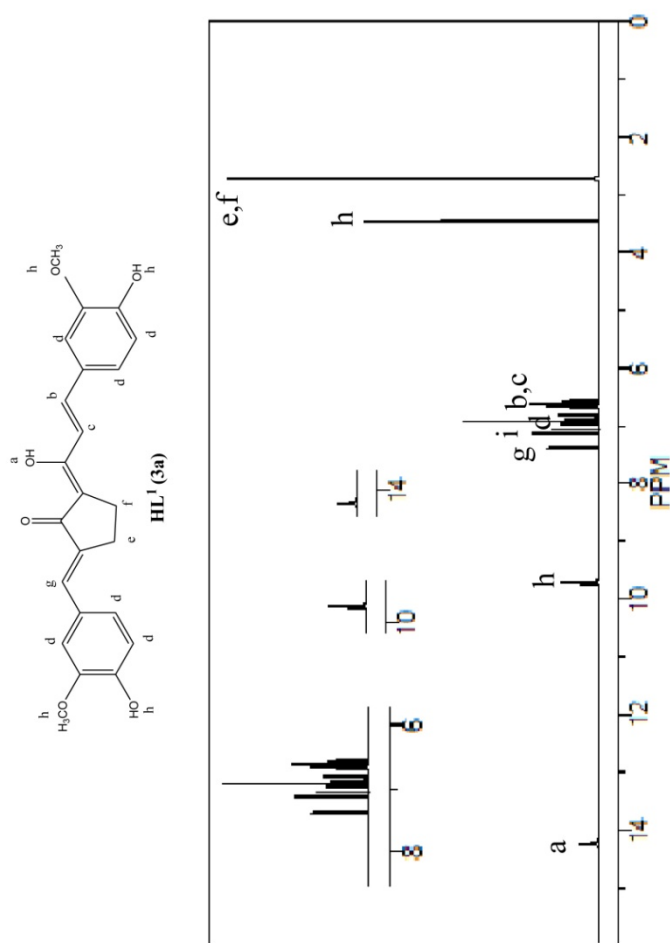
The downfield signals at δ 14.28, 14.37 and 14.33 ppm in the ^1H NMR spectra of **3a**, **3b** and **3c**, respectively can be assigned undoubtedly to the enolic proton. The downfield singlet at ~ 15 ppm is a characteristic feature of the ^1H NMR spectral data of 1,3-diketones arising from the intramolecularly hydrogen bonded enolic proton. The broad singlet observed at δ 9.78 and at δ 9.87 in **3a** and **3b** is presumably due to the phenolic protons^[152,189]. The ^1H NMR spectra of **3c** do not have any signals in the region 8-11 due to the absence of phenolic proton (**Table 3.3**).

The ^1H NMR spectra of all the ligands shows signals δ at 2.57-2.79 ppm due to protons in the cyclopentane ring and two doublets δ at ~ 6.67 ppm due to the alkenyl protons and a singlet at $\delta \sim 7.72$ due to vinylic protons also appeared along with the aromatic protons. Observed J values of 16.2 Hz for the alkenyl protons suggest their trans orientation. The ^1H NMR spectra of the ligands are given **Figures 3.1-3.3**.

Table 3.3 ^1H NMR spectral data of ligands

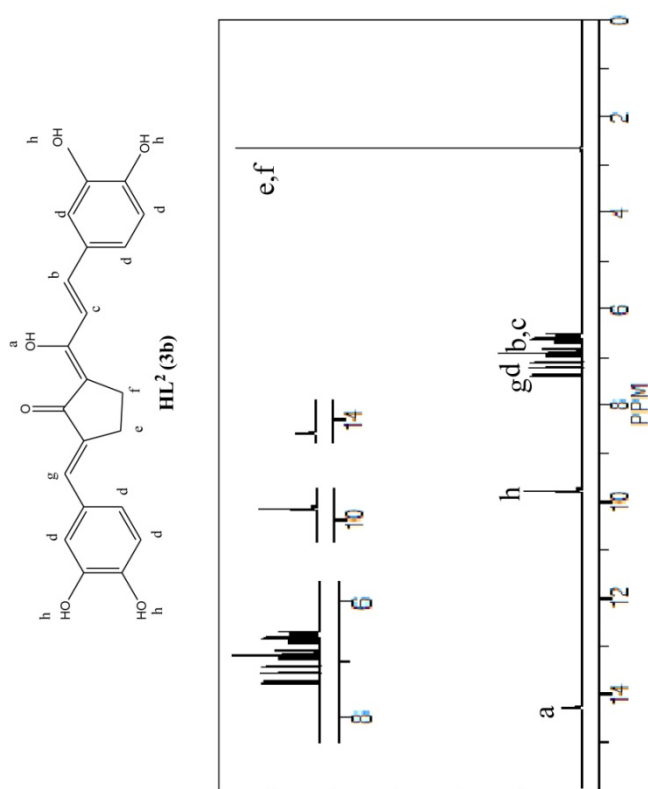


Compounds	Chemical shift, ppm (Coupling constant, Hz)							
	[a]	[b]	[c]	[d]	[e]	[f]	[g]	[h]
HL¹	14.28	6.67 (16.4)	6.49 (16.4)	6.54-7.23	2.64 (5.4)	2.76 (5.3)	7.41	9.78,3.57
HL²	14.37	6.67 (16.5)	6.87 (16.3)	6.52-7.11	2.57 (5.5)	2.65 (5.5)	7.43	9.87
HL³	14.33	6.68 (16.4)	6.83 (16.5)	6.69-7.28	2.71 (5.6)	2.79 (5.7)	7.51	3.72



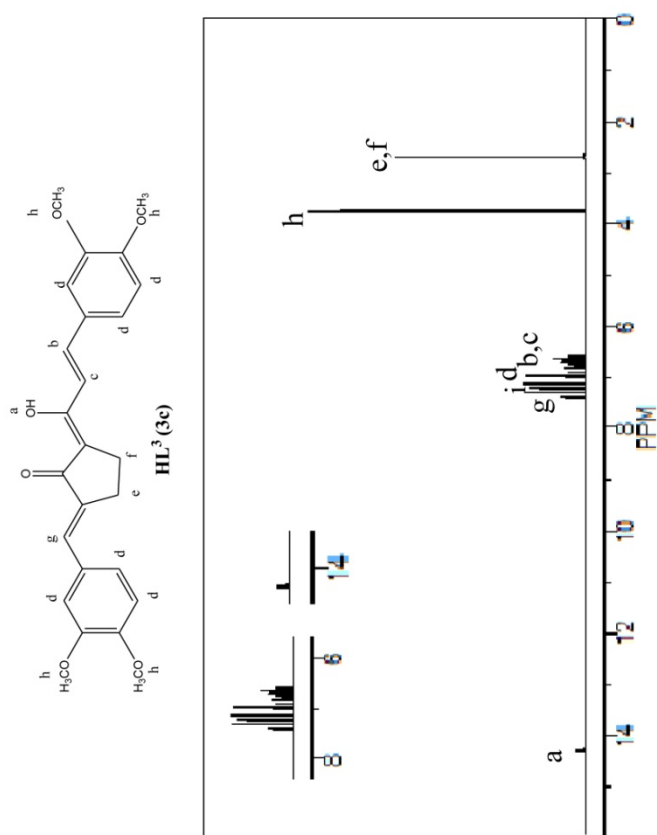
¹H NMR (400MHz, CDCl₃, ppm): δ 14.28 (1H, s, enolic -OH) [a], [2.64 (2H, t, J=5.4Hz, cyclopentane ring CH₂), 2.76 (2H, t, J=5.3Hz, cyclopentane ring CH₂) [e, f], [6.67 (1H, d, J=16.4Hz, (E)- alkenyl H), 6.49 (1H, d, J=16.4Hz, (E)- alkenyl H)] [b, c], 6.54-7.23 (6H, m, aromatic Hs) [d], 7.41 (1H, s, vinylic H) [g], 9.78 (2H, s, phenolic H), 3.57 (6H, s, methoxy H) [h], 7.26 (solvent) [i].

Figure 3.1. ¹H NMR spectrum of **HL¹ (3a)**



¹H NMR (400MHz, CDCl₃, ppm): δ 14.37 (1H, s, enolic -OH) [a], [2.57 (2H, t, J=5.5Hz, cyclopentane ring CH₂), 2.65 (2H, t, J=5.5Hz, cyclopentane ring CH₂)] [e,f], [6.67 (1H, d, J=16.5Hz, (E)- alkenyl H), 6.87 (1H, d, J=16.3Hz, (E)- alkenyl H)] [b,c], 6.52-7.11 (6H, m, aromatic Hs) [d], 7.43 (1H, s, vinylic H) [g], 9.87 (4H, s, phenolic H) [h], 7.26 (solvent) [i].

Figure 3.2. ¹H NMR spectrum of **HL² (3b)**



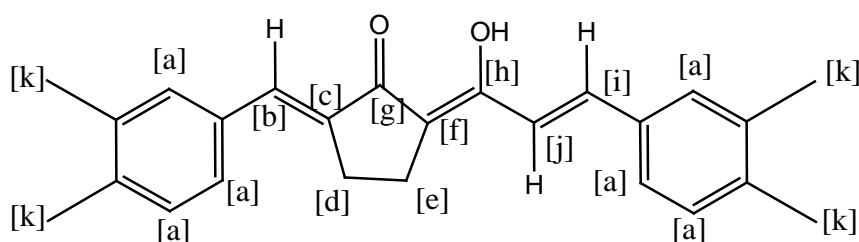
¹H NMR (400MHz, CDCl₃, ppm): δ 14.33 (1H, s, enolic -OH) [a], [2.71 (2H, t, J=5.6Hz, cyclopentane ring CH₂), 2.79 (2H, t, J=5.7Hz, cyclopentane ring CH₂)] [e,f], [6.68 (1H, d, J=16.4Hz, (E)- alkenyl H), 6.83 (1H, d, J=16.5Hz, (E)- alkenyl H)] [b,c], 6.69-7.28 (6H, m, aromatic Hs) [d], 7.51 (1H, s, vinylic H) [g], 3.72 (12H, s, methoxy H) [h], 7.26 (solvent) [i].

Figure 3.3. ¹H NMR spectrum of **HL³ (3c)**

3.4.4 ^{13}C NMR spectra

^{13}C NMR spectral data of all ligands show two resonance signals in the range 193.32–196.37 ppm and in the range 181.29–181.94 ppm indicating that the two carbonyl groups have different electronic environment. The two aliphatic carbon atoms in the cyclopentanone ring show a resonance signal at 25–29 ppm. The carbon atoms in the methoxy substituent show a resonance signal at 58.37 ppm. The resonance signals in the range 111.38–152.78 ppm are due to the aromatic carbon atoms (**Table 3.4**). The ^{13}C NMR spectra of the ligands are reproduced in **Figures 3.4-3.6**.

Table 3.4 ^{13}C NMR spectral data of ligands



Compounds	Chemical shift (ppm)										
	[a]	[b]	[c]	[d]	[e]	[f]	[g]	[h]	[I]	[j]	[k]
HL¹	112.38- 152.78	142.46	139.81	25.57	29.68	94.27	181.94	196.37	120.12	136.84	58.47
HL²	113.28- 146.27	147.26	138.27	25.36	29.72	97.46	181.29	193.32	126.18	133.21	-
HL³	111.38- 149.38	146.37	131.62	25.76	29.47	95.48	181.43	196.36	129.79	138.85	57.27

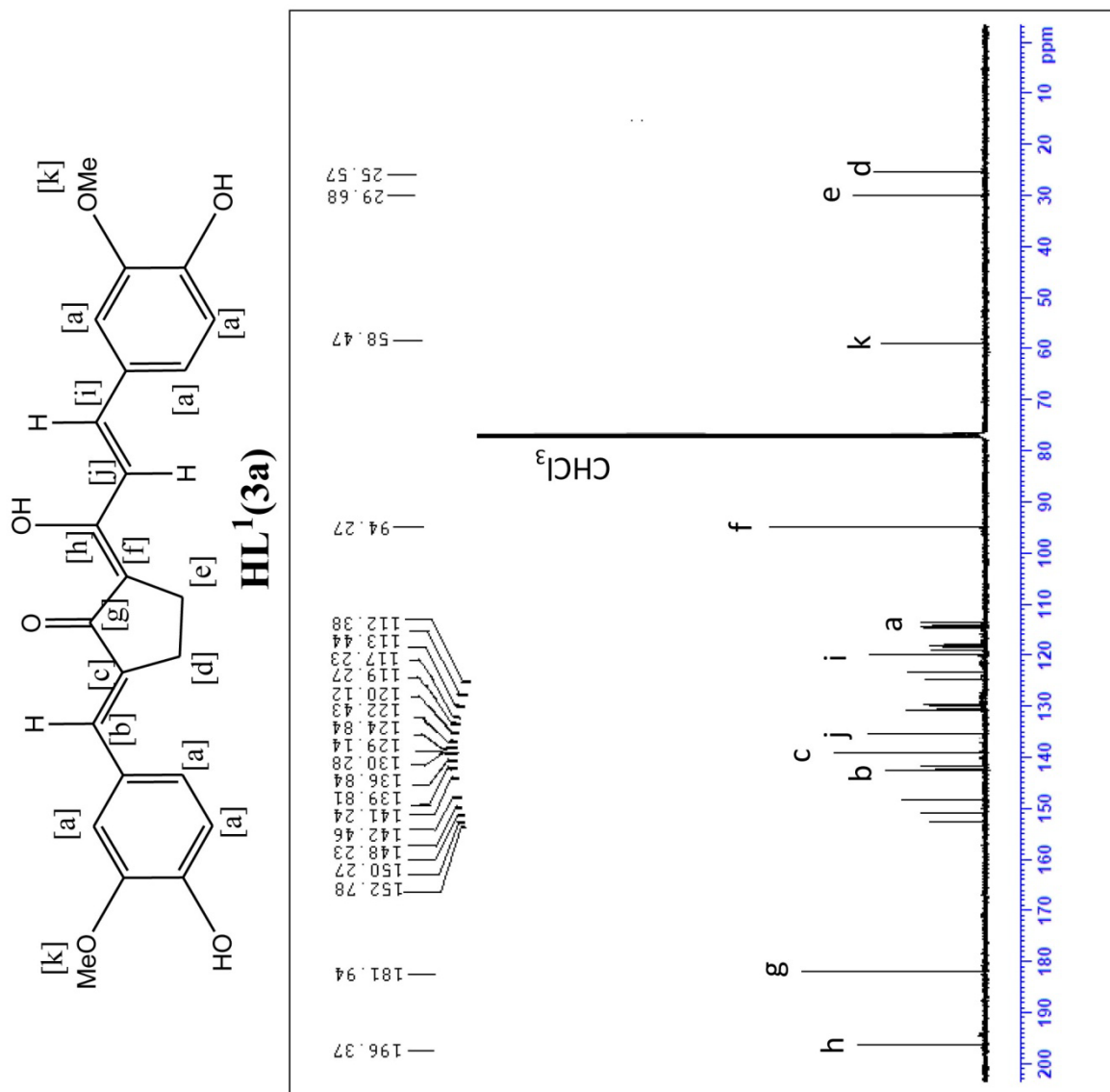


Figure 3.4. ¹³C NMR spectrum of **HL¹(3a)**

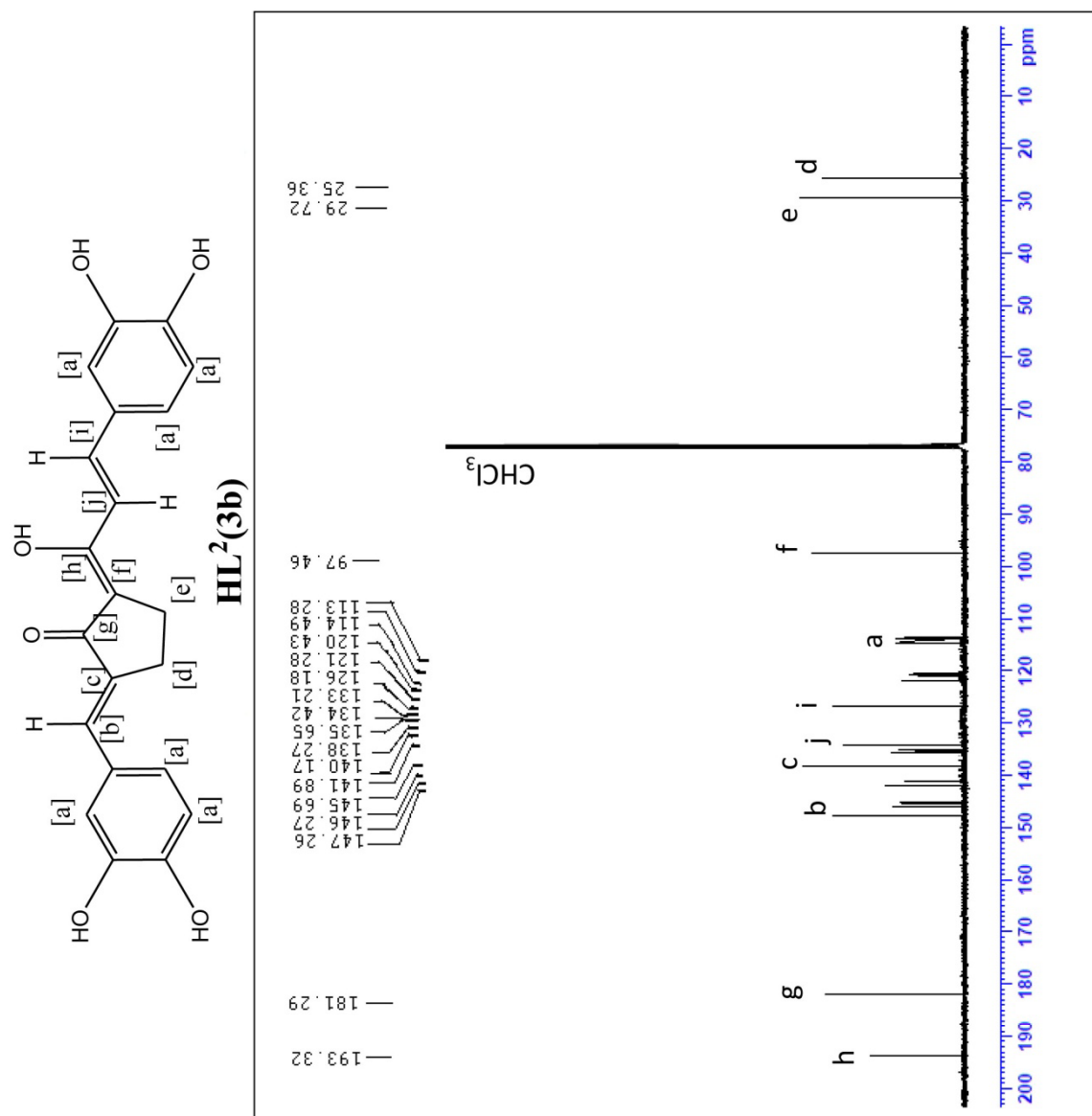


Figure 3.5. ¹³C NMR spectrum of **HL²(3b)**

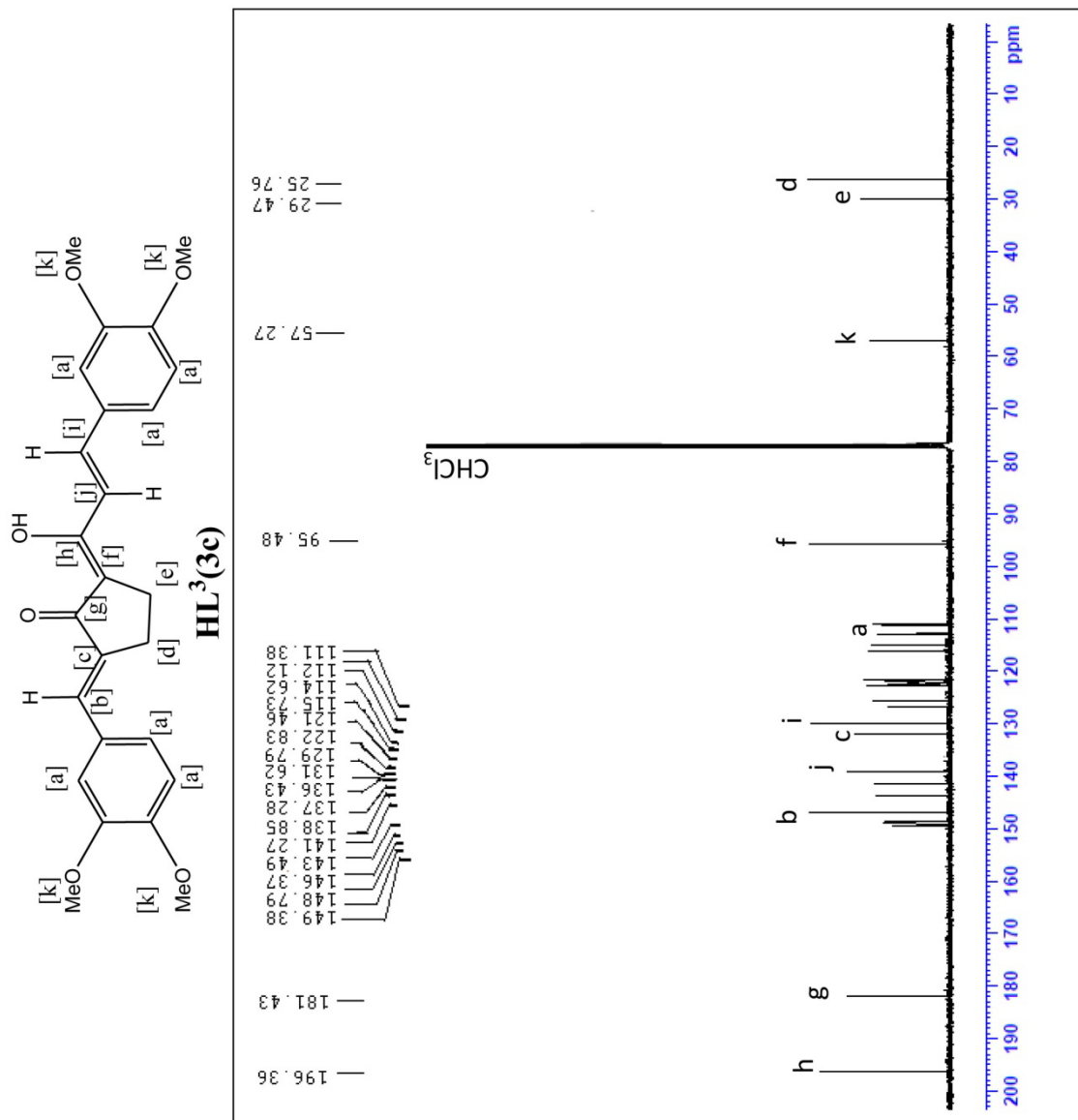


Figure 3.6. ¹³C NMR spectrum of **HL³(3c)**

3.4.5 Mass spectra

The EI mass spectra of the ligands contain molecular ion peak and a large number of peaks at lower m/z than the molecular ion. The spectra are reproduced in **Figures 3.7-3.9**. From a comparison of the spectra of the three compounds, a few prominent peaks can be identified in accordance with the common fragmentation pattern depicted in **Figure 3.10**.

Most of the peaks having relative intensity 50% have been identified and marked in the mass spectra given in **Figures 3.7-3.9**. They are also listed in **Table 3.2**.

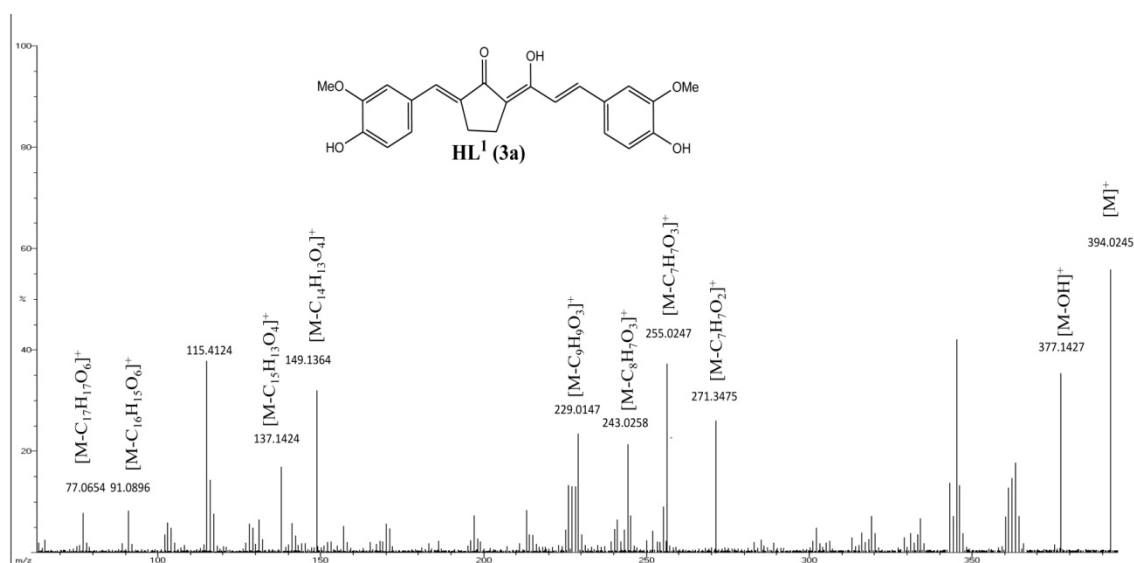


Figure 3.7. EI mass spectrum of **HL¹ (3a)**

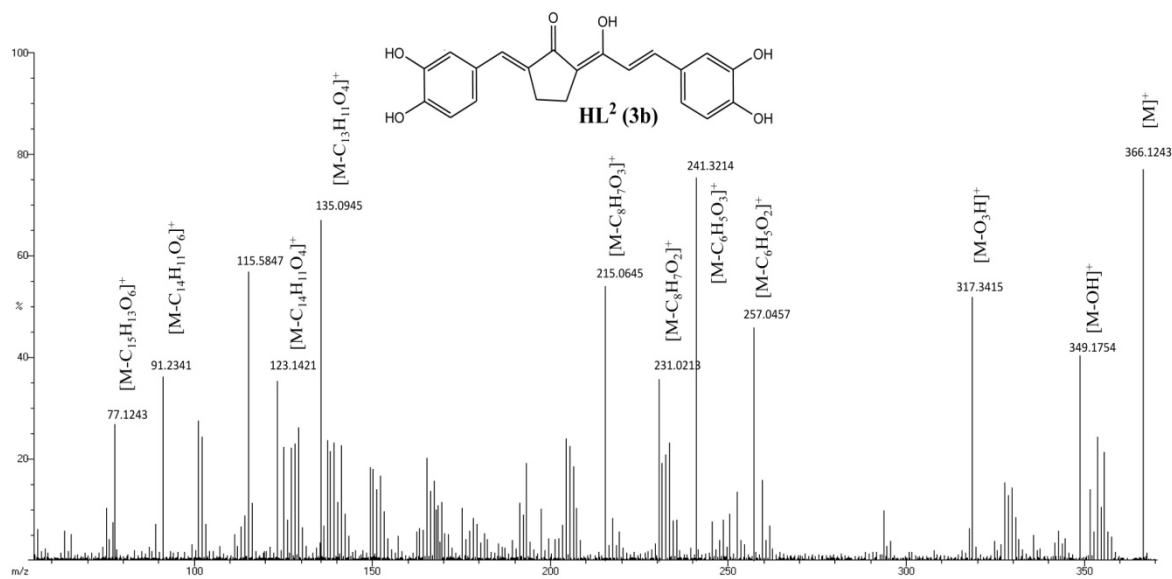


Figure 3.8. EI mass spectrum of **HL² (3b)**

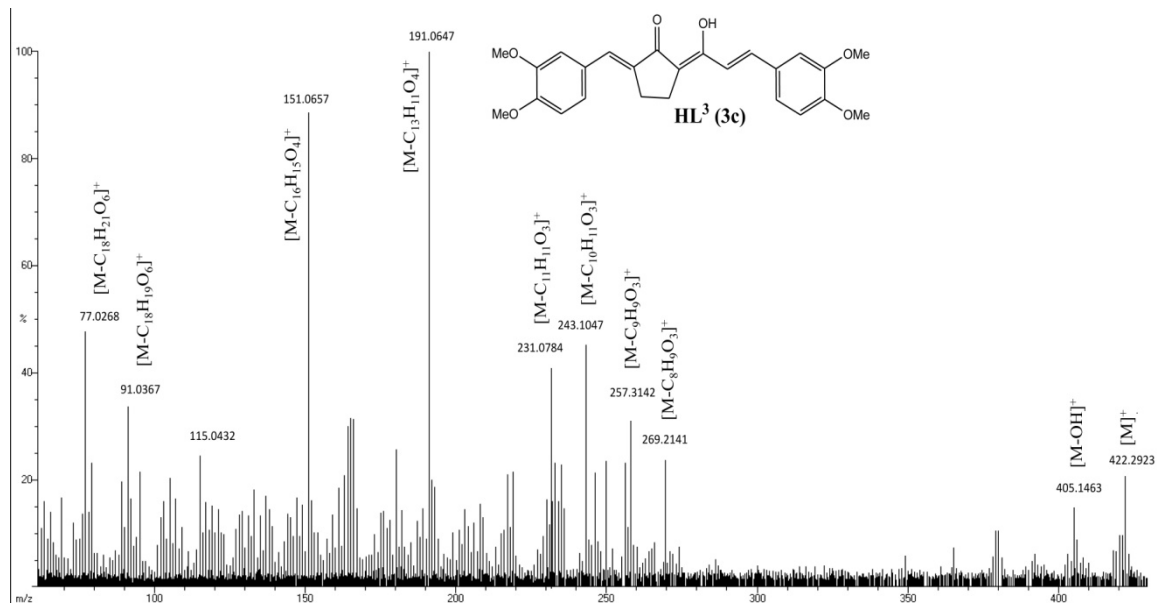


Figure 3.9. EI mass spectrum of **HL³ (3c)**

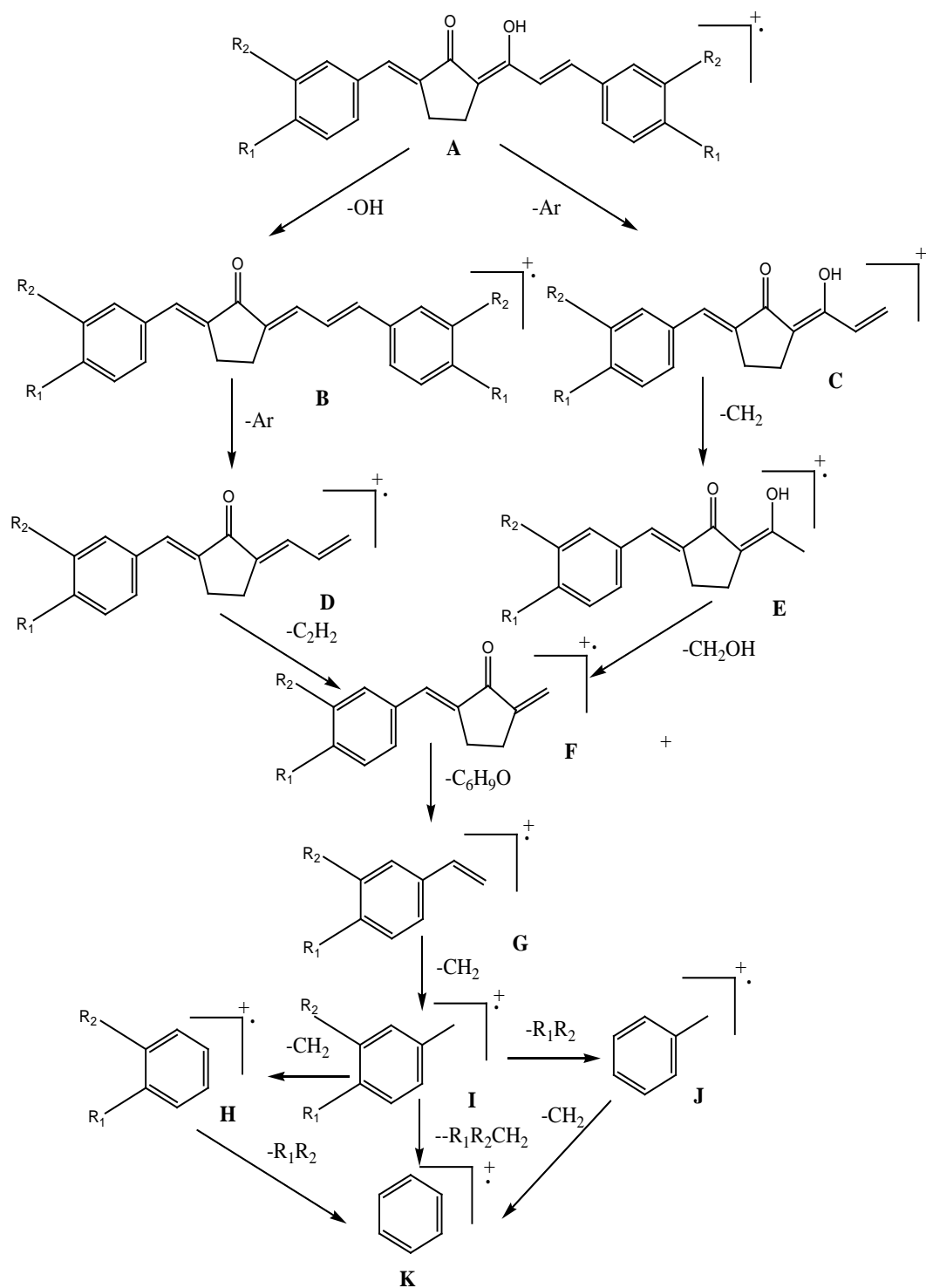
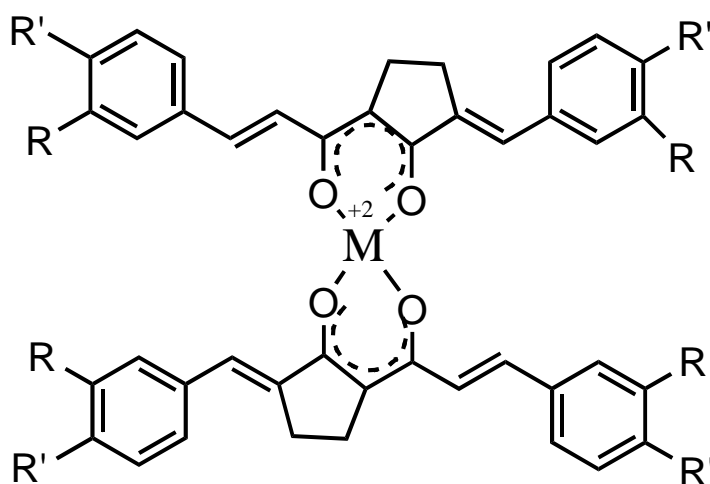


Figure 3.10. Fragmentation pattern of ligands

From the above spectral data, it follows that all the three synthetically modified curcumin analogues are typical 1,3-diketones existing in their intramolecularly hydrogen bonded enol form. The enolised 1,3-diketo moiety in the structure of ligands suggest that they can form stable complexes with metal ions.

3.5 Characterization of metal complexes

Analytical and physical data of the metal complexes are given in **Table 3.5**. The observed carbon, hydrogen and metal percentages of the metal complexes and ESI mass spectral data suggest their ML_2 stoichiometry. All the metal complexes have a specific conductance $< 15\Omega^{-1} \text{ cm}^{-1}$ in DMF. The nickel(II) and zinc(II) complexes are diamagnetic copper(II) complex is paramagnetic. The electronic, IR, ^1H NMR, ^{13}C NMR, mass and ESR spectral data of the complexes are compatible with the structure given in **Figure 3.11**. The spectral data are discussed below.



3.5.1 Electronic spectra

The observed bathochromic shifts in the $n \rightarrow \pi^*$ transition (448-484 nm) and the $\pi \rightarrow \pi^*$ transitions (249-286 nm) (**Table 3.5**) in the UV absorption spectra of the complexes indicating the involvement of the 1,3-dicarbonyl group in metal complexation^[186]. Similarity in the UV absorption maxima of metal complexes with that of free ligands, show that no structural alteration of the ligand has occurred during the complex formation.

In the copper(II) complexes the presence of a broad visible band at ~665 nm and the measured μ_{eff} values (1.75–1.81 B.M.) support their square planar structure.

The observed diamagnetism and broad medium-intensity band in the region 562-581 nm in the visible spectra of the nickel(II) chelates suggest their square-planar geometry. In conformity with this observation the visible spectra of the chelates in pyridine solution (10^{-3} M) showed three bands corresponding to a configurational change from square-planar to octahedral due to the association of pyridine. The absorption maxima in the regions 1243-1253 nm ($\epsilon = 4.30 \times 10^4 - 4.85 \times 10^4 \text{ M}^{-1} \text{ cm}^{-1}$), 736-770 nm ($\epsilon = 5.23 \times 10^4 - 5.54 \times 10^4 \text{ M}^{-1} \text{ cm}^{-1}$) and 410-424 nm ($\epsilon = 2.43 \times 10^4 - 2.68 \times 10^4 \text{ M}^{-1} \text{ cm}^{-1}$) in the adducts can be assigned to the transitions ${}^3A_{2g} \rightarrow {}^3T_{2g}$; ${}^3A_{2g} \rightarrow {}^3T_{1g}(\text{F})$ and ${}^3A_{2g} \rightarrow {}^3T_{1g}(\text{P})$, respectively^[193].

Table 3.5 Analytical data of copper (II), nickel (II) and Zinc (II) complexes

Complexes (formula weight)	M.p. (°C)	Yield (%)	Elemental analysis % (found /calcd)			UV λ_{\max} (nm)	μ_{eff} BM	Mass spectral data (m/z)
			C	H	Cu			
[Cu(L¹)₂] C ₄₆ H ₄₂ O ₁₂ Cu (850)	264	70	(64.11) 64.97	(5.41) 4.98	(7.85) 7.47	266 471	1.81	895,872,849,455,393 , 254, 240
[Cu(L²)₂] C ₄₂ H ₃₄ O ₁₂ Cu (794)	234	68	(62.98) 63.51	(4.65) 4.31	(8.61) 8.00	249 465	1.75	839,816,793,427,365 , 240, 226
[Cu(L³)₂] C ₅₀ H ₅₀ O ₁₂ Cu (906)	278	69	(66.87) 66.25	(5.04) 5.56	(7.67) 7.01	263 474	1.79	951,928,905,484,421 , 268, 254
[Ni(L¹)₂] C ₄₆ H ₄₂ O ₁₂ Ni (845)	248	63	(65.91) 65.34	(5.78) 5.01	(7.43) 6.94	286 484	-	-
[Ni(L²)₂] C ₄₂ H ₃₄ O ₁₂ Ni (789)	224	62	(63.12) 63.90	(4.97) 4.34	(7.86) 7.44	278 477	-	-
[Ni(L³)₂] C ₅₀ H ₅₀ O ₁₂ Ni (901)	262	64	(66.94) 66.61	(5.04) 5.59	(6.87) 6.51	249 463	-	-
[Zn(L¹)₂] C ₄₆ H ₄₂ O ₁₂ Zn (852)	218	61	(65.47) 64.83	(5.31) 4.97	(7.62) 7.67	249 476	-	-
[Zn(L²)₂] C ₄₂ H ₃₄ O ₁₂ Zn (796)	246	58	(63.69) 63.36	(4.77) 4.30	(8.93) 8.21	273 452	-	-
[Zn(L³)₂] C ₅₀ H ₅₀ O ₁₂ Zn (908)	268	60	(66.71) 66.12	(4.98) 5.55	(7.64) 7.20	256 448	-	-

3.5.2 Infrared Spectra

The intense band at 1293 cm^{-1} in the IR spectrum of HL^1 and at 1287 cm^{-1} in the IR spectrum of HL^2 due to phenolic (O–H) stretching mode remains unaffected in the spectrum of complexes of HL^1 and HL^2 , suggesting that oxygen atom of the phenolic group(s) is not coordinated to the metal ion. In the IR spectra of all complexes, a strong band assignable to the stretching of the coordinated dicarbonyl moiety appeared at $\sim 1590\text{ cm}^{-1}$. The broad band in the region at $2800\text{--}3600\text{ cm}^{-1}$ due to the hydrogen bonded enol proton present in the free ligands is absent in the spectra of metal complexes and weak bands attributable to various $\nu_{\text{(C-H)}}$ appeared^[189]. The carbonyl groups are involved in metal complex formation is evident from the appearance of two medium intensity bands in the region $458\text{--}492\text{ cm}^{-1}$ due to $\nu_{\text{(M-O)}}$ vibrations. The prominent band at $\sim 975\text{ cm}^{-1}$ is typical of a trans –CH=CH– group which remained unaltered in the spectra of metal complexes^[189]. The significant IR band are brought out in **Table 3.6**.

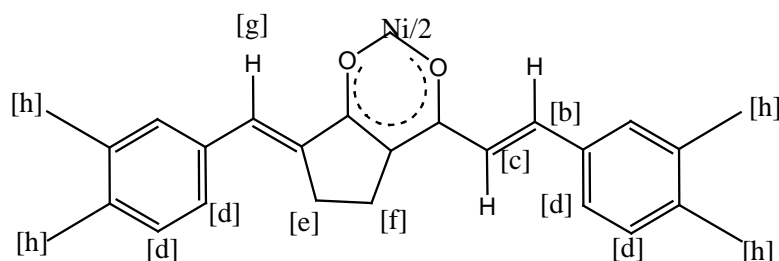
Table 3.6 IR spectral data of complexes

IR spectral data of complexes (cm^{-1})							
Compounds	$\nu(\text{C=O})$ metal chelated carbonyl	$\nu(\text{C=C})$ phenyl	$\nu(\text{C=C})$ alkenyl	$\nu_{\text{as}}(\text{C-C-C})$ chelate ring	$\nu_{\text{as}}(\text{C-C-C})$ chelate ring	$\nu(\text{CH=CH-})$ trans	$\nu(\text{M-O})$ chelate ring
$[\text{Cu}(\text{L}^1)_2]$	1617,1538	1487	1408	1276	1238	972	458
$[\text{Cu}(\text{L}^2)_2]$	1571,1527	1467	1397	1275	1157	961	476
$[\text{Cu}(\text{L}^3)_2]$	1576,1534	1437	1376	1268	1151	958	472
$[\text{Ni}(\text{L}^1)_2]$	1611,1547	1443	1337	1231	1138	963	492
$[\text{Ni}(\text{L}^2)_2]$	1607,1536	1422	1294	1252	1146	974	464
$[\text{Ni}(\text{L}^3)_2]$	1634,1521	1434	1364	1279	1174	982	468
$[\text{Zn}(\text{L}^1)_2]$	1629,1538	1456	1423	1214	1168	959	487
$[\text{Zn}(\text{L}^2)_2]$	1646,1562	1429	1368	1227	1124	966	473
$[\text{Zn}(\text{L}^3)_2]$	1616,1574	1458	1351	1243	1165	952	475

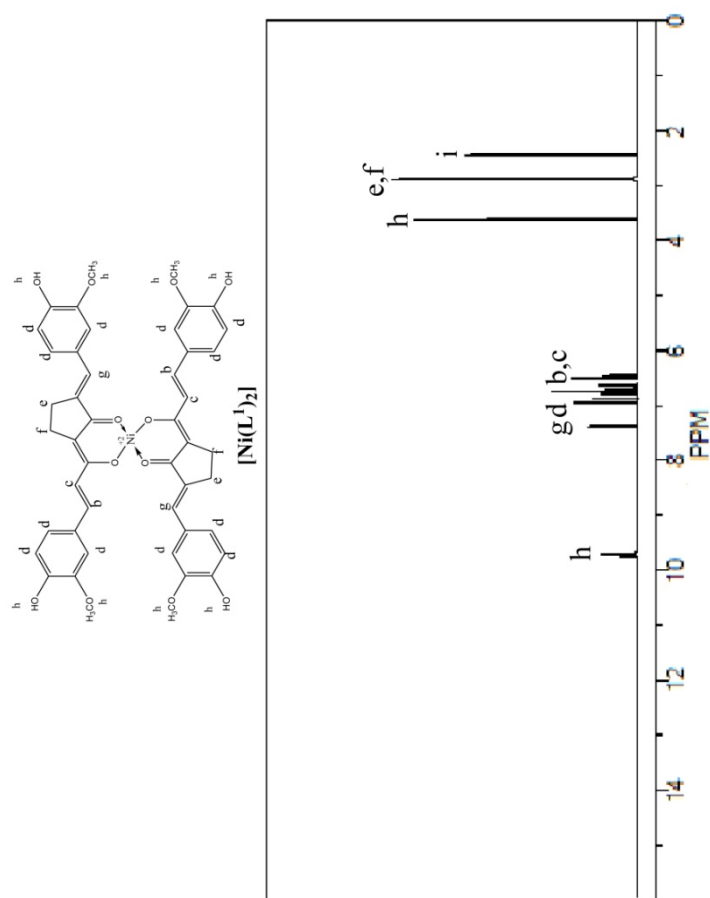
3.5.3 ^1H NMR spectra

The most characteristic feature of the ^1H NMR spectra of the diamagnetic nickel(II) chelates is the absence of proton signals above $\delta \sim 11$ ppm. This strongly supports the replacement of the enolic proton by the metal ion in the complexes. In the spectra of the complexes of HL^1 (**3a**) and HL^2 (**3b**), the phenolic signal remains unaltered at $\delta \sim 9.72$ ppm is clearly indicating that the phenolic group is not involved in bonding with the metal ions. Observed J value of 16 Hz for the alkenyl proton signals in the nickel (II) and zinc(II) complexes suggest their trans orientation as it is in the free ligands. The integrated intensities of the aryl and alkenyl protons are in well agreement with the structure of metal chelates given in **Figure 3.11-3.13**.

Table 3.7 ^1H NMR spectral data of Ni(II) complexes

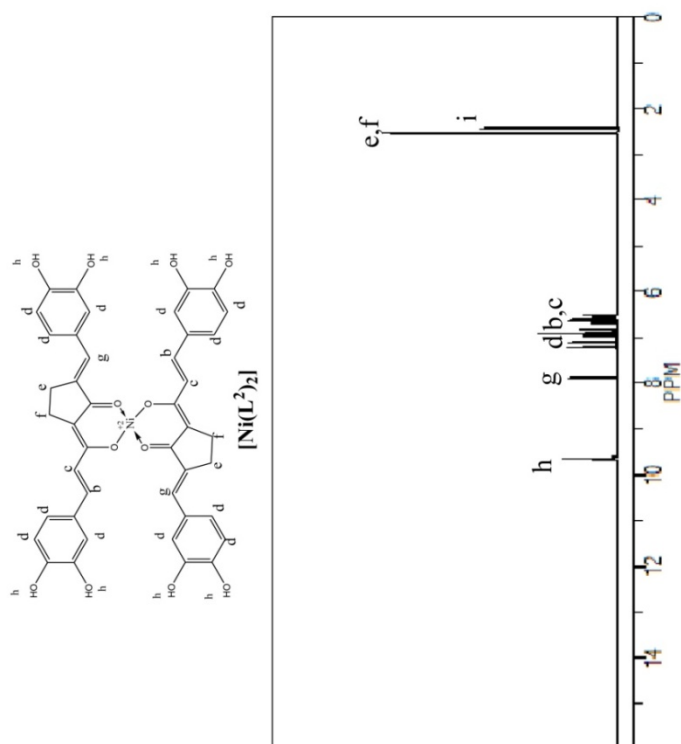


Compounds	Chemical shift, ppm (Coupling constant, Hz)							
	[a]	[b]	[c]	[d]	[e]	[f]	[g]	[h]
$[\text{Ni}(\text{L}^1)_2]$	-	6.54 (16.3)	6.48 (16.2)	6.84- 6.97	2.76 (5.4)	2.81 (5.5)	7.43	9.88,3.62
$[\text{Ni}(\text{L}^2)_2]$	-	6.61 (16.2)	6.76 (16.2)	6.81- 7.06	2.62 (5.1)	2.71 (5.2)	7.86	9.76
$[\text{Ni}(\text{L}^3)_2]$	-	6.58 (16.4)	6.46 (16.3)	7.02- 7.27	2.73 (5.3)	2.82 (5.3)	7.67	3.84



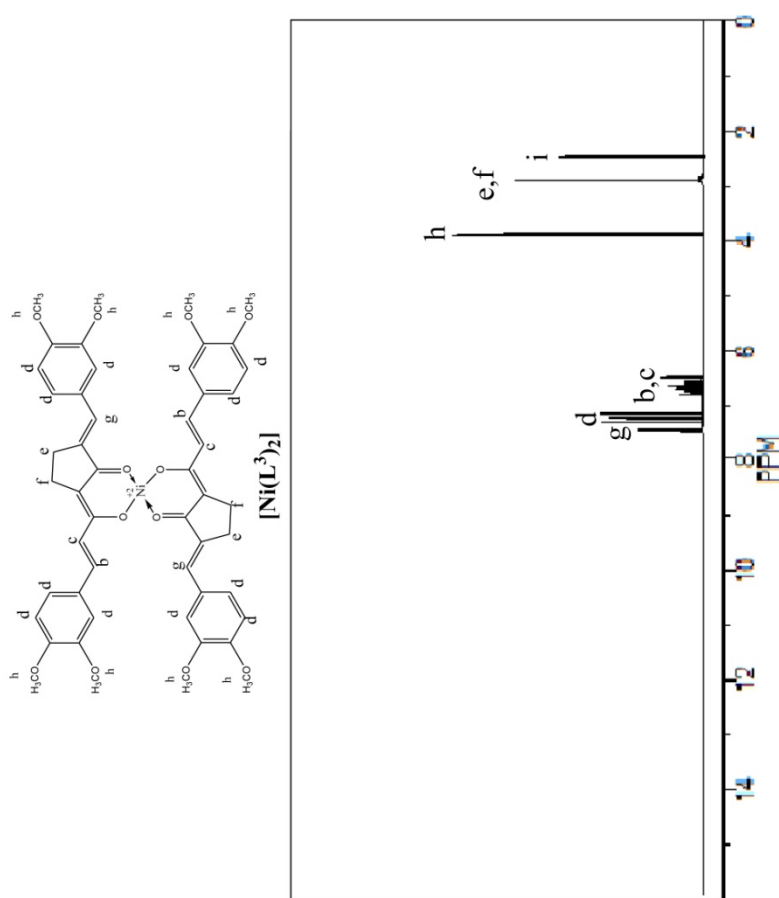
^1H NMR (400MHz, DMSO, ppm): [2.76 (4H, t, $J=5.4\text{Hz}$, cyclopentane ring CH_2), 2.81 (4H, t, $J=5.5\text{Hz}$, cyclopentane ring CH_2) [e,f], [6.54 (2H, d, $J=16.3\text{Hz}$, (E)- alkenyl H), 6.48 (2H, d, $J=16.2\text{Hz}$, (E)- alkenyl H)] [b,c], 6.84-6.97 (12H, m, aromatic Hs) [d], 7.43 (2H, s, vinylic H) [g], 9.88 (4H, s, phenolic H), 3.62 (12H, s, methoxy H) [h], 2.49 (solvent) [i].

Figure 3.11. ^1H NMR spectrum of $[\text{Ni}(\text{L}^1)_2]$



^1H NMR (400MHz, DMSO, ppm): [2.62 (4H, t, $J=5.1\text{Hz}$, cyclopentane ring CH_2), 2.71 (4H, t, $J=5.2\text{Hz}$, cyclopentane ring CH_2)] [e,f], [6.61 (2H, d, $J=16.2\text{Hz}$, (E)- alkenyl H), 6.76 (2H, d, $J=16.2\text{Hz}$, (E)- alkenyl H)] [b,c], 6.81-7.06 (12H, m, aromatic Hs) [d], 7.86 (2H, s, vinylic H) [g], 9.76 (8H, s, phenolic H) [h], 2.49 (solvent) [i].

Figure 3.12. ^1H NMR spectrum of $[\text{Ni}(\text{L}^2)_2]$



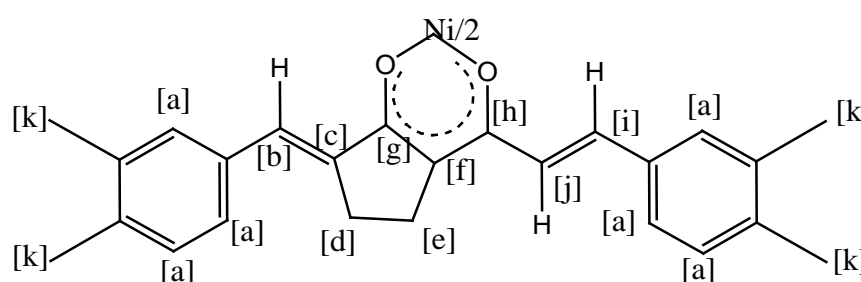
^1H NMR (400MHz, DMSO, ppm): [2.73 (4H, t, $J=5.3\text{Hz}$, cyclopentane ring CH_2), 2.82 (4H, t, $J=5.3\text{Hz}$, cyclopentane ring CH_2) [e,f], [6.58 (2H, d, $J=16.4\text{Hz}$, (E)- alkenyl H), 6.46 (2H, d, $J=16.3\text{Hz}$, (E)- alkenyl H)] [b,c], 7.02-7.27 (12H, m, aromatic Hs) [d], 7.67 (2H, s, vinylic H) [g], 3.84 (24H, s, methoxy H) [h], 2.49 (solvent) [i].

Figure 3.13. ^1H NMR spectrum of $[\text{Ni}(\text{L}^3)_2]$

3.5.4 ^{13}C NMR spectra

The carbonyl carbon signal in the free ligands shifted by 15- 20 ppm to low field in the spectra of nickel(II) complexes (**Table 3.8**). This clearly suggest the strong interaction between the metal ion and carbonyl oxygens and also more effective delocalisation that exist in the metal chelate ring compared to the free ligand.

Table 3.8 ^{13}C NMR spectral data of Ni(II) complexes



Chemical shift (ppm)											
Compounds	[a]	[b]	[c]	[d]	[e]	[f]	[g]	[h]	[I]	[j]	[k]
$[\text{Ni}(\text{L}^1)_2]$	117.21- 151.29	143.67	134.82	28.43	34.24	93.24	183.24	197.21	124.32	137.28	54.23
$[\text{Ni}(\text{L}^2)_2]$	116.78- 149.23	145.38	138.49	27.43	32.78	92.47	180.29	195.43	128.63	132.43	-
$[\text{Ni}(\text{L}^3)_2]$	124.12- 153.81	144.25	141.45	29.47	36.84	95.92	185.38	194.29	127.14	139.48	58.23

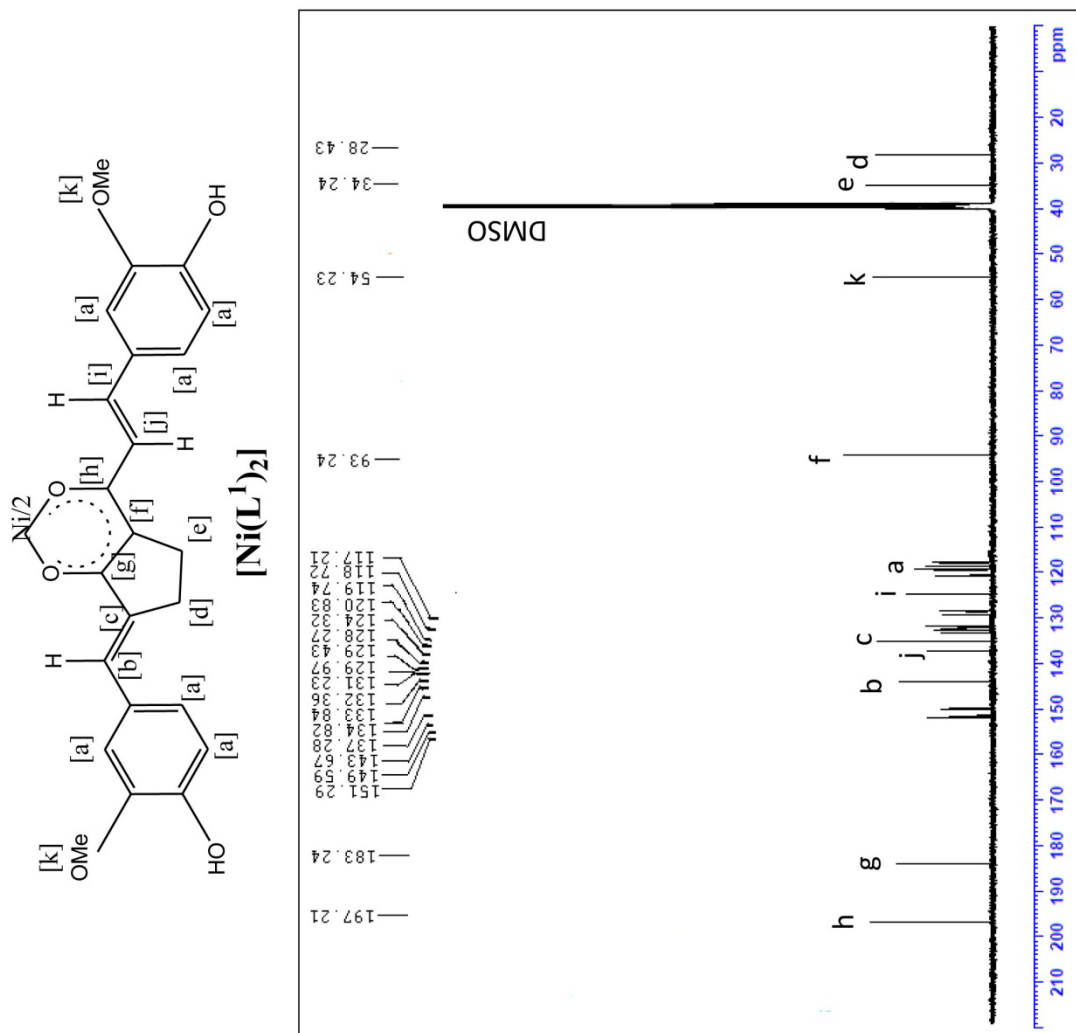


Figure 3.14 ^{13}C NMR spectrum of $[\text{Ni}(\text{L}^1)_2]$

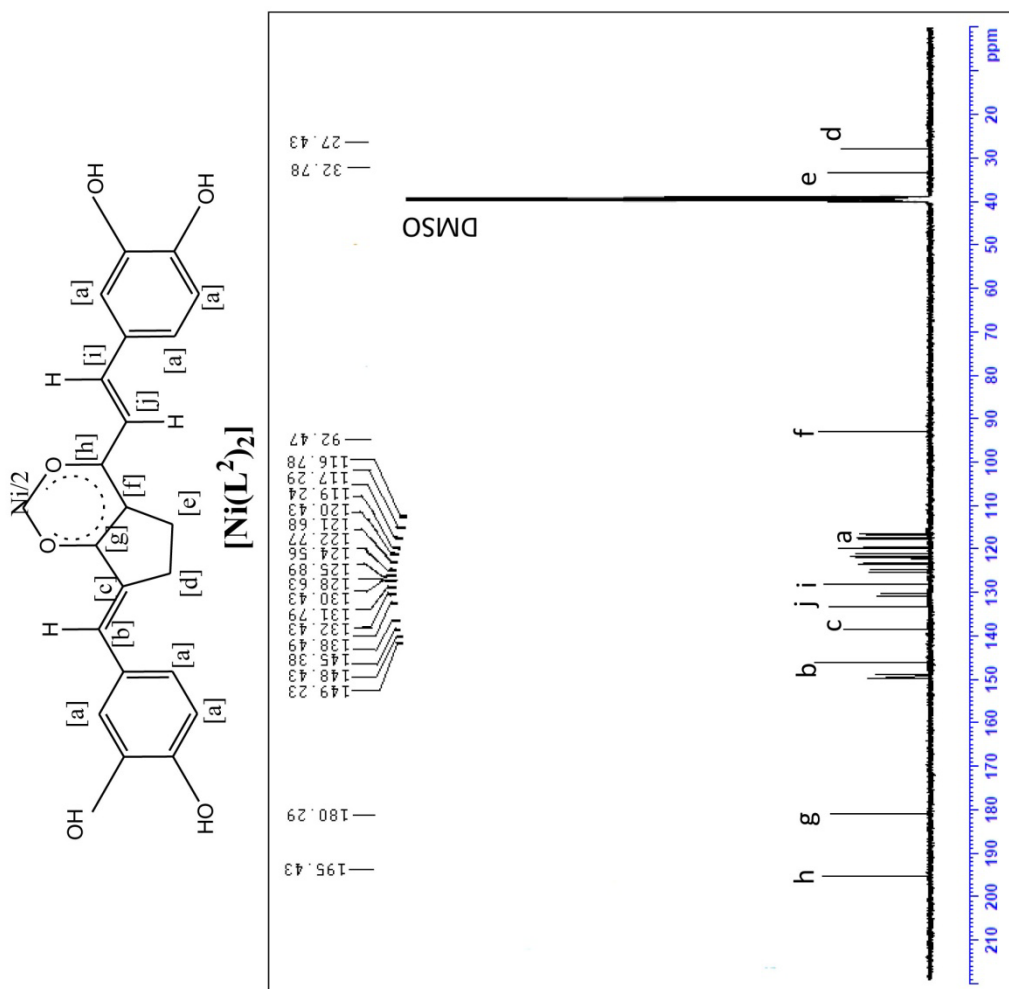


Figure 3.15 ^{13}C NMR spectrum of $[\text{Ni}(\text{L}^2)_2]$

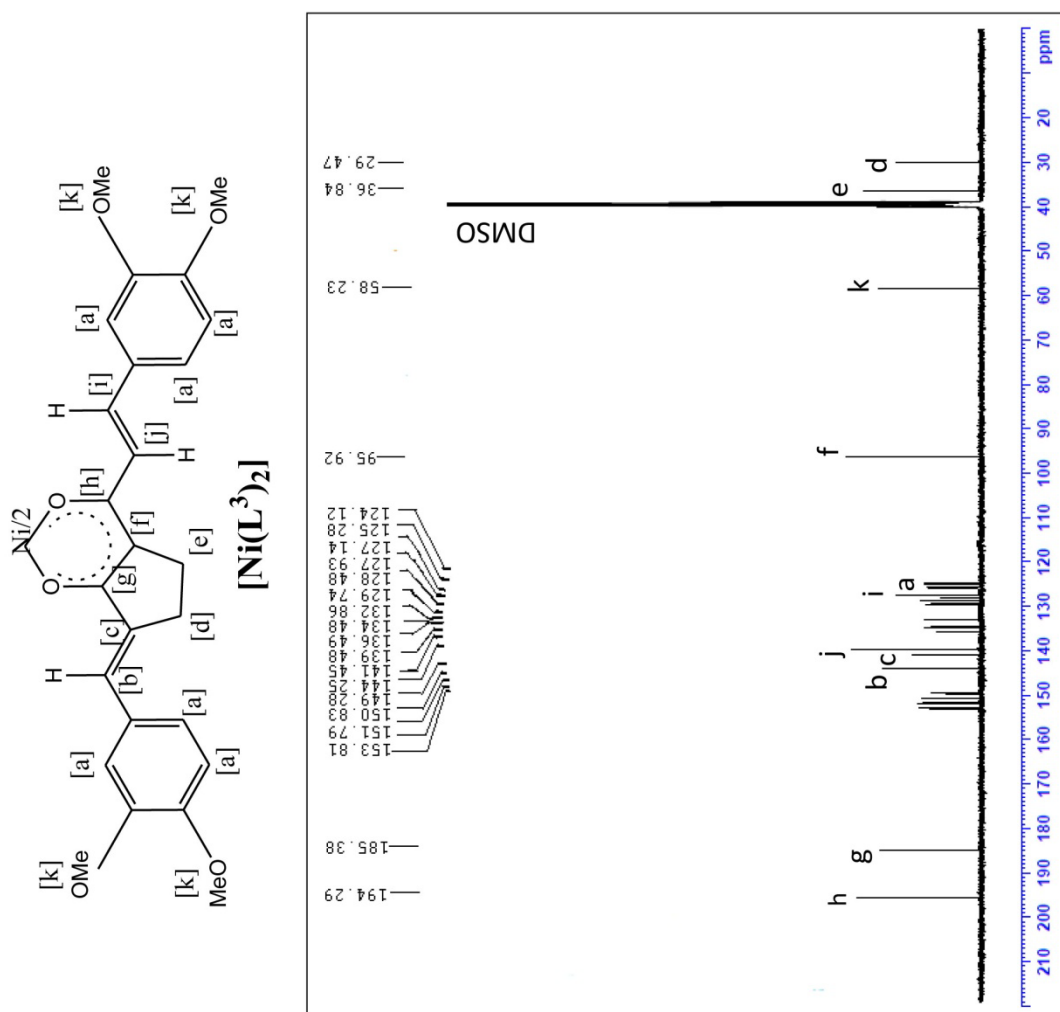


Figure 3.16 ^{13}C NMR spectrum of $[Ni(L^3)_2]$

3.5.5 Mass spectra

The ESI mass spectra of the copper(II) chelates confirm the $[ML_2]$ stoichiometry of the complexes. Peaks due to M^+ and $(M+2)^+$ with 3:1 intensity are present in the ESI MS of copper(II) chelates in consistent with the natural abundance of ^{63}Cu and ^{65}Cu isotopes. The mass spectra of the copper(II) chelates show that stepwise removal of aryl groups is a characteristic feature of these complexes. Peaks due to $[\text{CuL}]^+$, $[\text{CuL-ArCHCHCO}]^+$, $[\text{CuL-ArCHCHCOCH}_2]^+$, L^+ and fragments of L^+ are common in the spectra of copper(II) complexes^[186,187]. The ESI mass spectra of the copper(II) complexes are shown in **Figures 3.17-3.19**. The major peaks in the spectra can be explained on the basis of probable fragmentation pattern illustrated in **Figure 3.20**.

3.5.6 ESR spectra

In order to establish the involvement of 1,3-diketo moiety in the complex formation and to assess the covalent character of metal – ligand bonds, the ESR spectra of the copper (II) complexes were recorded at 77 K in DMF solution and the spectra are reproduced in **Figure 3.21 - 3.23**. The observed g_{\parallel} , g_{\perp} , A_{\parallel} and A_{\perp} values given in **Table 3.9** are comparable with that reported for copper(II) complexes of simple 1,3-diketones, indicating extensive delocalization in the pseudo aromatic metal–chelate ring system and significant covalent character for the metal–ligand bonds^[194,195].

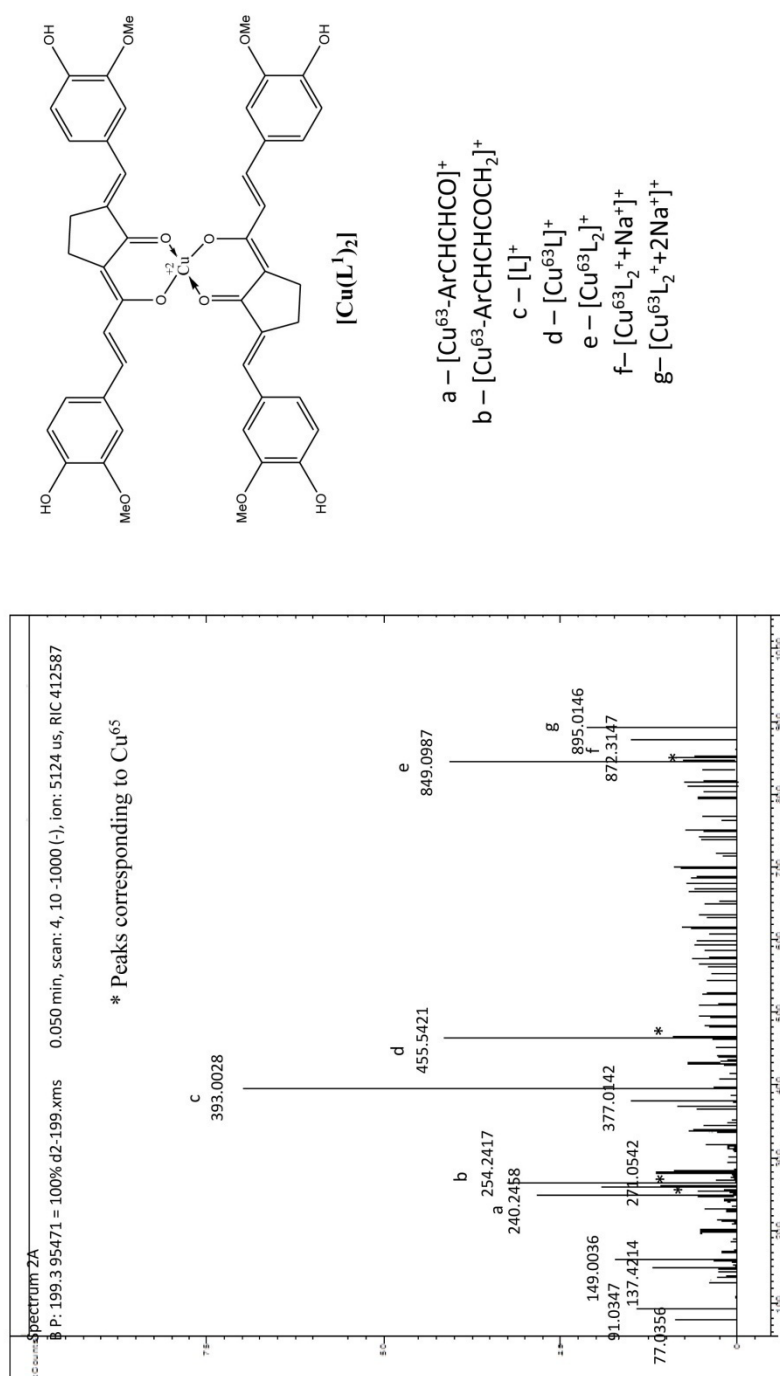


Figure 3.17. The ESI mass spectrum of [Cu(L¹)₂]

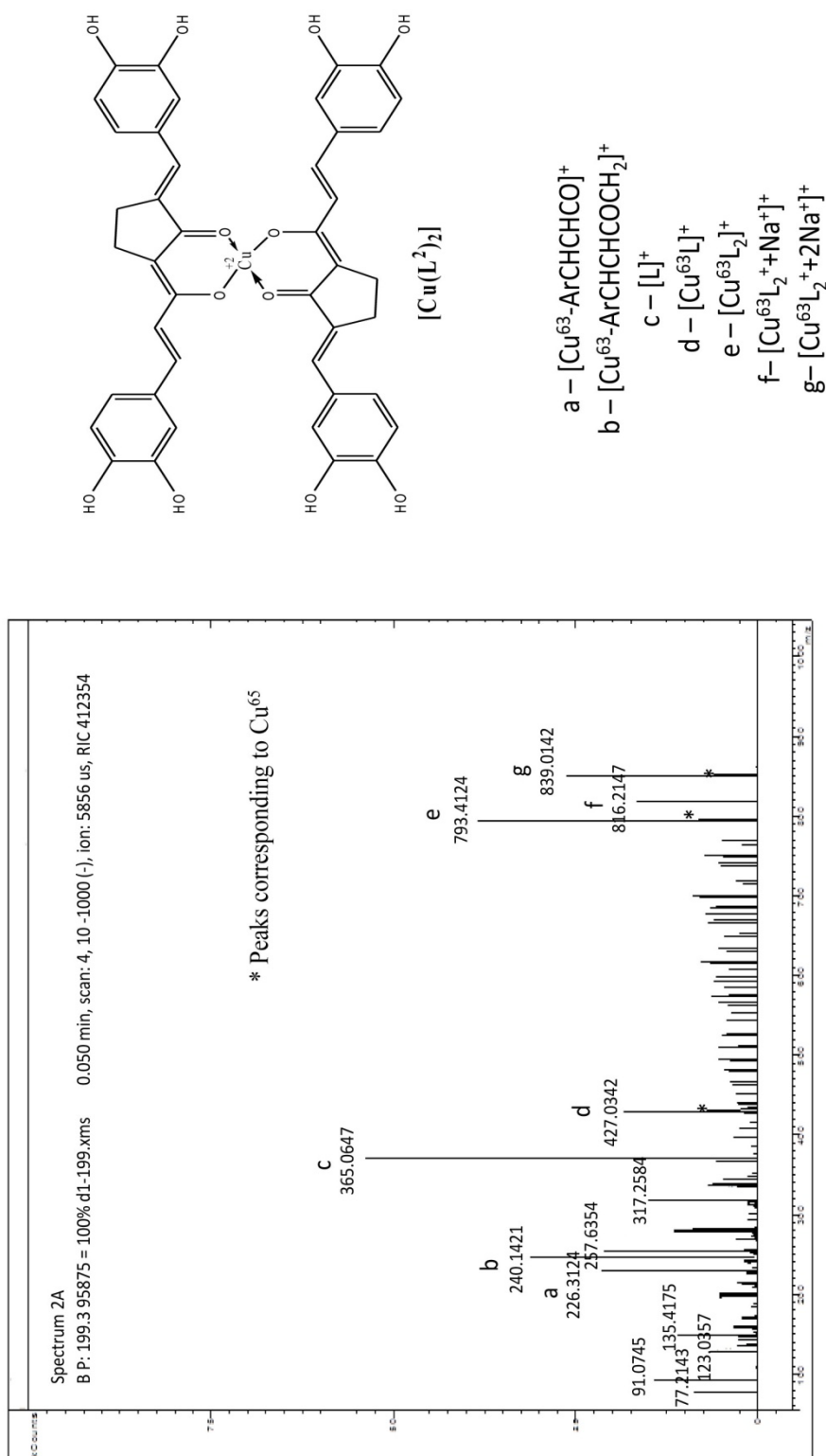


Figure 3.18. The ESI mass spectrum of [Cu(L²)₂]

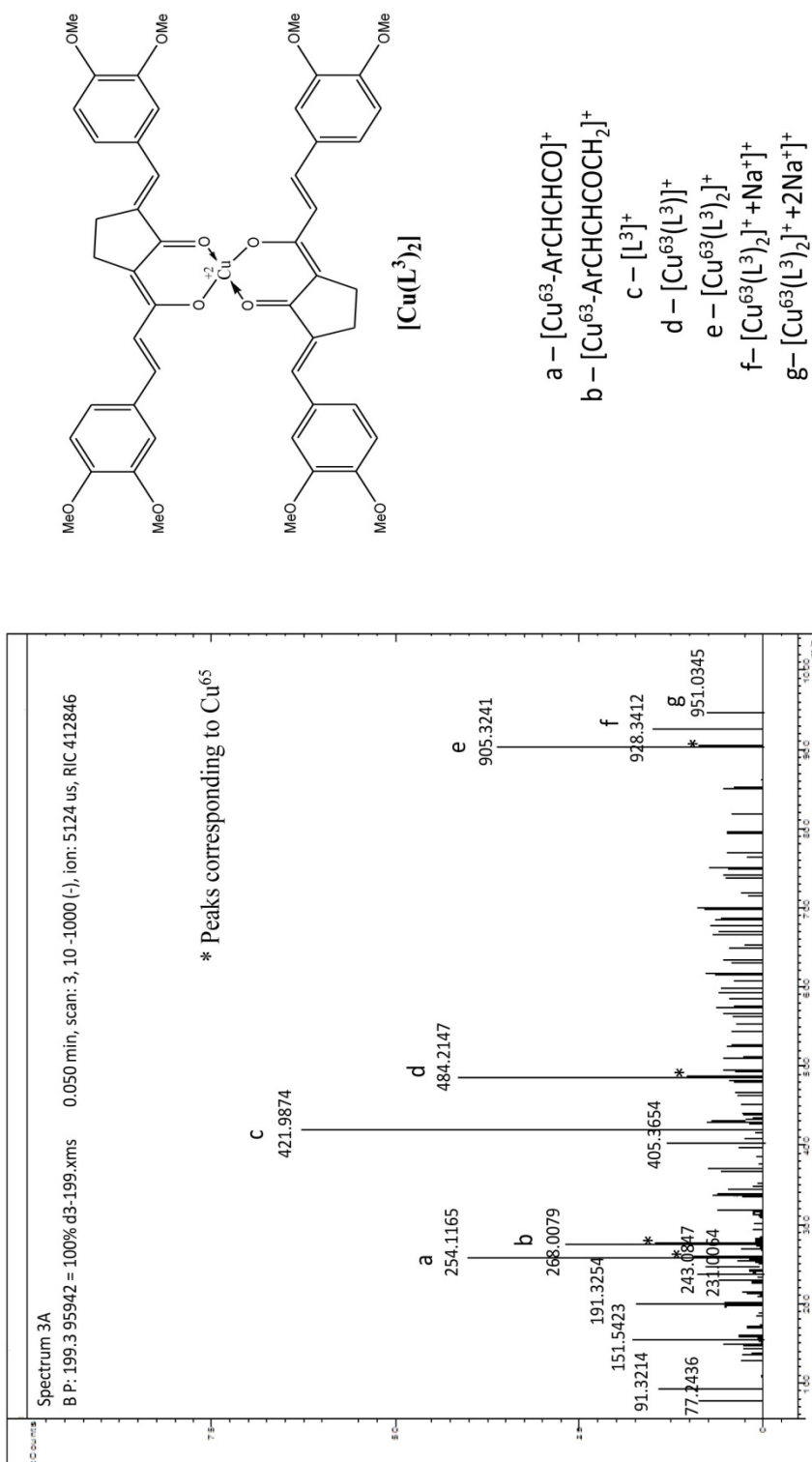


Figure 3.19. The ESI mass spectrum of [Cu(L³)₂]

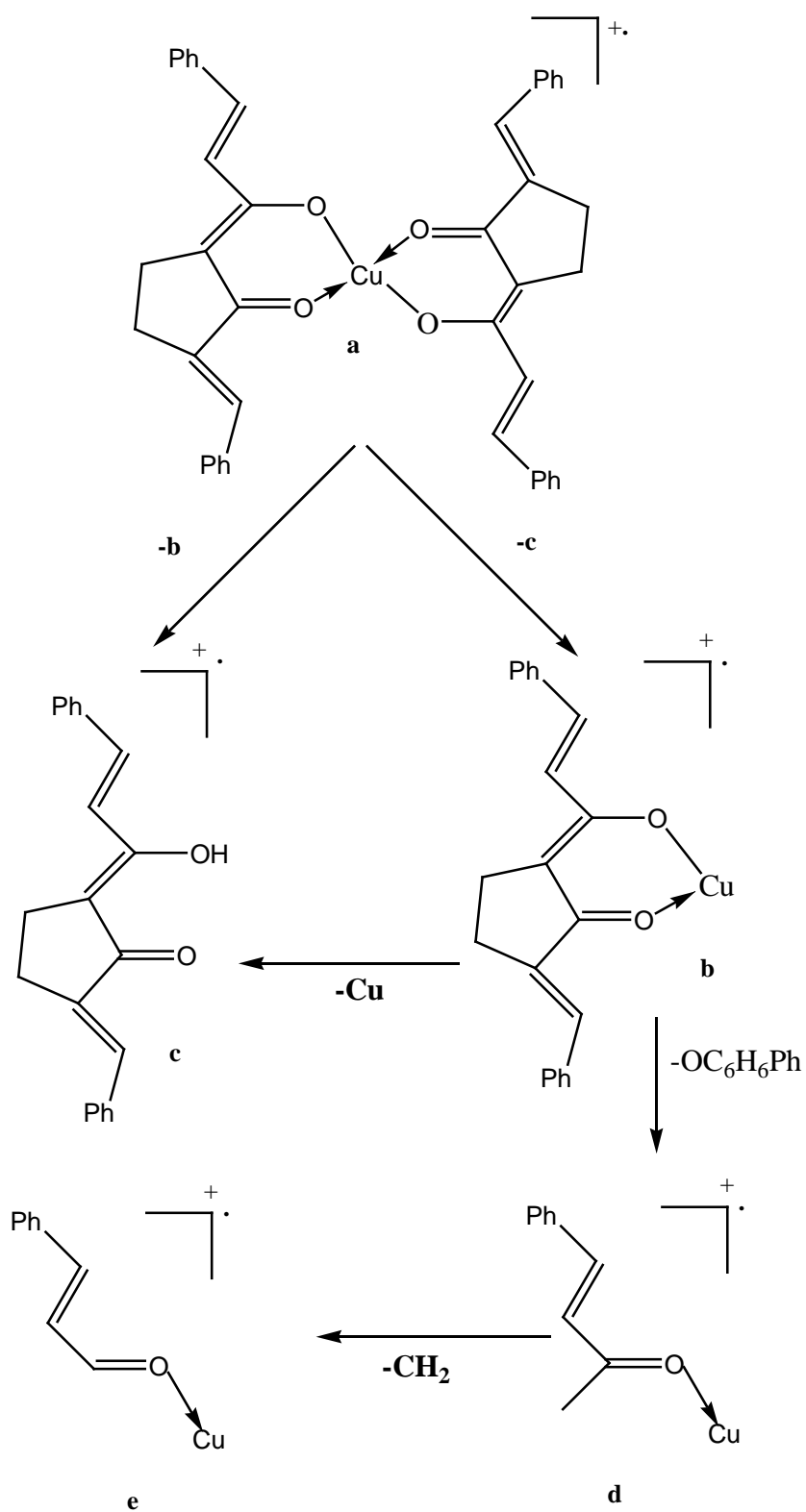
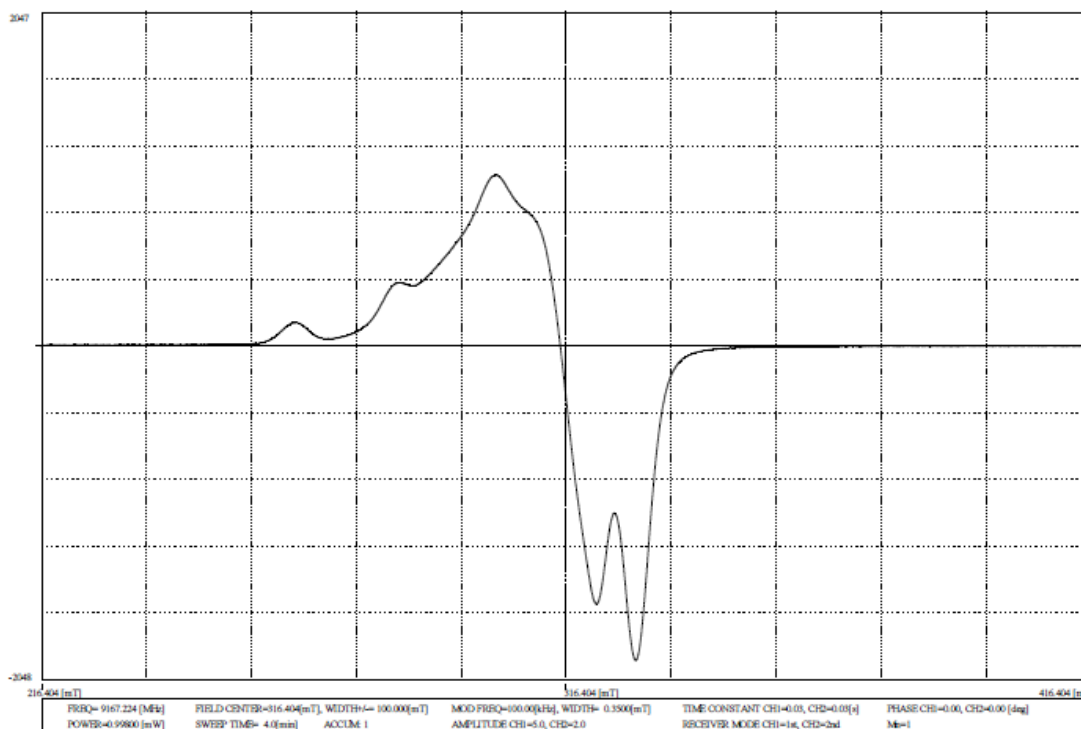


Figure 3.20. Fragmentation pattern of copper (II) complexes

Table 3.9. ESR parameters of Cu(II) complexes in DMF at 77 K

Complexes	g_{\parallel}	g_{\perp}	$A_{\parallel} \times 10^{-4} \text{ cm}^{-1}$	$A_{\perp} \times 10^{-4} \text{ cm}^{-1}$
1a	2.262	2.052	163	44.6
2a	2.258	2.053	161	45.3
3a	2.256	2.056	159	44.8

ESR spectra of the complexes in DMF shows two bands located at $g = 2.6$ and $g = 2.05$ corresponding to the $\Delta M_S = \pm 1$ transition. This feature is typical for square planar copper(II) complexes. $g_{\parallel} > g_{\perp} > 2.0023$ also exhibit large parallel hyperfine splitting and are associated with the dx^2-y^2 ground state. In the spectrum of complex, the parallel region is clearly resolved, and all four transitions derived from the Cu ($I = 3/2$) hyperfine splitting can be directly observed. These hyperfine lines for complexes split the g_{\parallel} signal with an average spacing of $160 \times 10^{-4} \text{ cm}^{-1}$.

**Figure 3.21.** ESR spectrum of $[\text{Cu}(\text{L}^1)_2]$

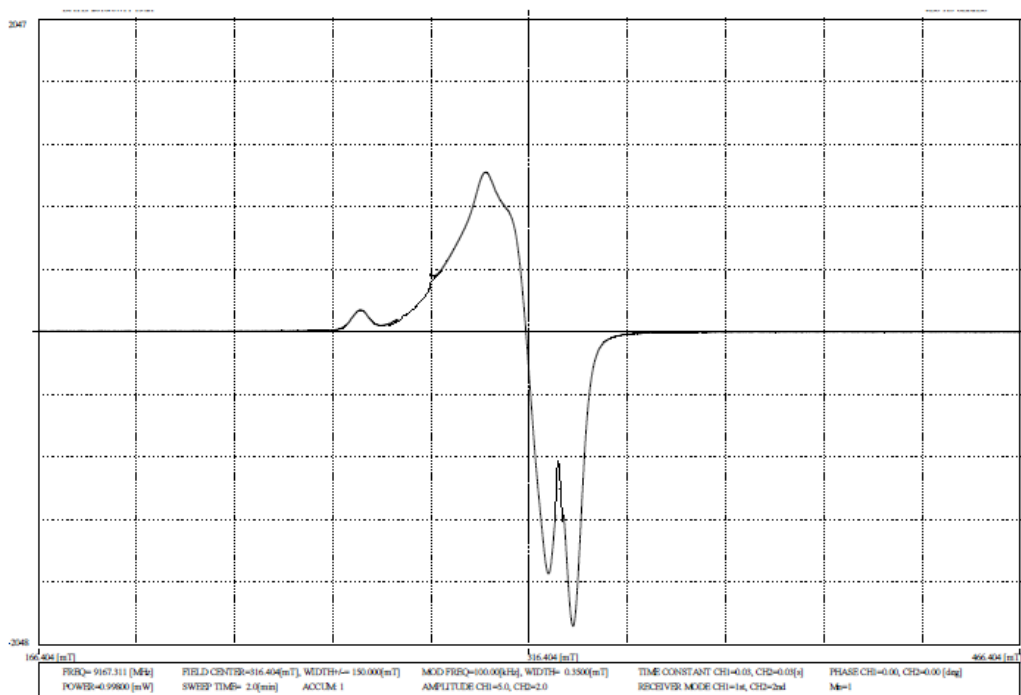


Figure 3.22. ESR spectrum of $[\text{Cu}(\text{L}^2)_2]$

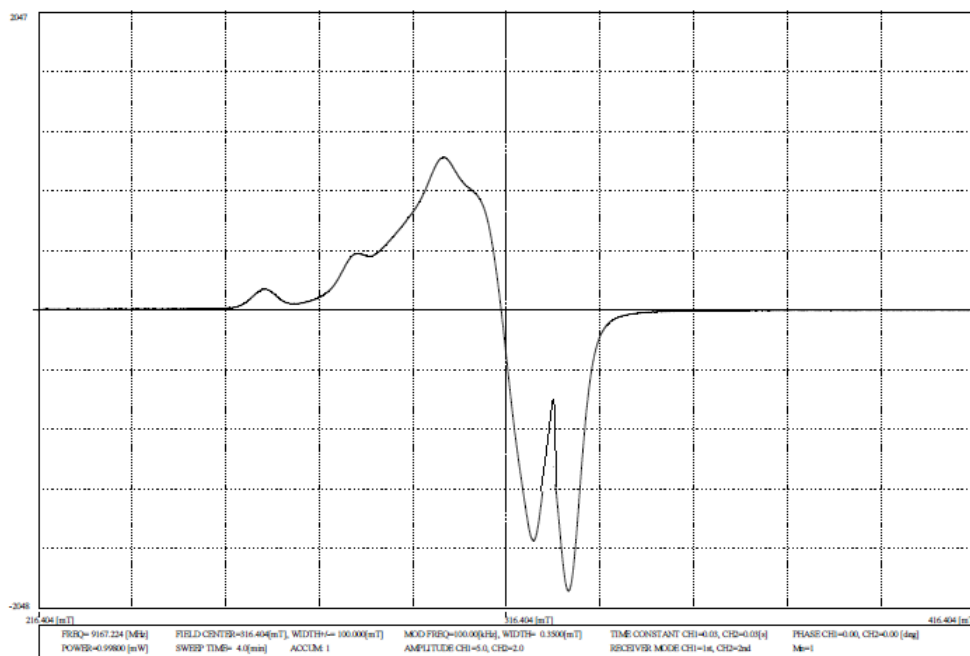


Figure 3.23. ESR spectrum of $[\text{Cu}(\text{L}^3)_2]$

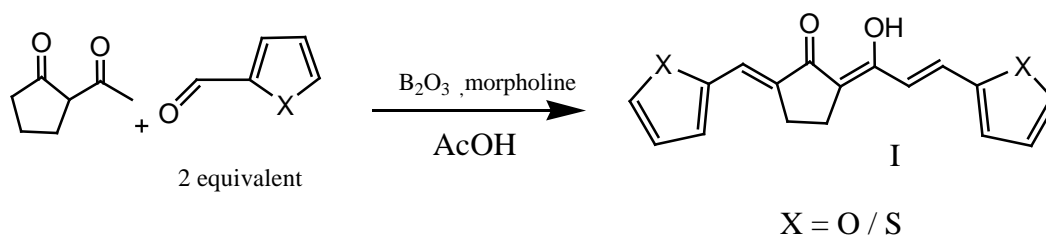
Chapter 4

LIGANDS WITH HETEROCYCLIC ARYL RINGS

In the previous chapters curcumin analogues having phenyl or substituted phenyl rings are discussed. In this chapter, two ligands having hetero aryl rings are discussed.

4.1 Synthesis of ligands

The ligands were synthesised from 2-Acetylcyclopentanone and furan-2-carbaldehyde or thiophene-2-carbaldehyde by following the same procedure described in the previous chapters. The reaction involved is depicted in **Scheme 4.1**



Scheme 4.1

4.2 Synthesis of Cu^{II}, Ni^{II}, Zn^{II} complexes

The Ni^{II}, Zn^{II}, Cu^{II} complexes were prepared from corresponding metal(II) acetate using the general procedure given below. A methanolic solution of metal(II) acetate (25 ml, 1 mmol) was added with stirring to a solution of ligand (50 ml, 2 mmol) in methanol and refluxed gently for ~3 hours. After ~3 hours, the volume of reaction mixture was reduced to nearly half and the solution was allowed to cool to room temperature. The precipitated complex was filtered, washed 3-4 times using methanol and dried in vacuum. A few mg of sample were recrystallized from hot methanol for elemental analysis and other spectral analysis.

4.3 Results and discussion

The ligands were synthesized by the condensation of heteroaromatic aldehyde with 2-acetylcyclopentanone. The yield of product is slightly lower than that obtained with benzaldehyde or substituted benzaldehyde (**Table 4.1**). Both compounds are crystalline in nature and are freely soluble in common organic solvents.

4.4 Characterization of ligands

The results of elemental analysis and molecular weight determination of the compounds are given in **Table 4.1**. The ligands **4a** and **4b** are characterised using UV, IR, ^1H NMR, ^{13}C NMR and mass spectral studies detailed below.

Table 4.1 Analytical, UV, IR, and mass spectral data of ligands

Ligands	M. p. (⁰ C)	Elemental analysis (found /calcd) %		Colour	Yield (%)	UV λ_{\max} (nm)	IR (cm ⁻¹)			Mass spectral data (m/z)
		C	H				$\nu(\text{C}=\text{O})$	$\nu_{\text{as}}(\text{C}-\text{C}-\text{C})$	$\nu(\text{CH}=\text{CH}-)$ (trans)	
(4a) HL¹ C ₁₇ H ₁₄ O ₄ (282)	102	(72.84) (72.33)	(5.34) (5.00)	Brownish yellow solid	71	235($\pi \rightarrow \pi^*$), 468 ($n \rightarrow \pi^*$)	1575	1534	978	281,265,229,2 15,199,187,17 3, 93,81, 67
(4b) HL² C ₁₇ H ₁₄ O ₂ S ₂ (314)	128	(64.14) (64.94)	(4.85) (4.49)	Reddish brown solid	68	234($\pi \rightarrow \pi^*$), 476 ($n \rightarrow \pi^*$)	1568	1534	972	313,297,245,2 19, 215,205, 203,189,177, 109, 97,83

4.4.1 Electronic spectra

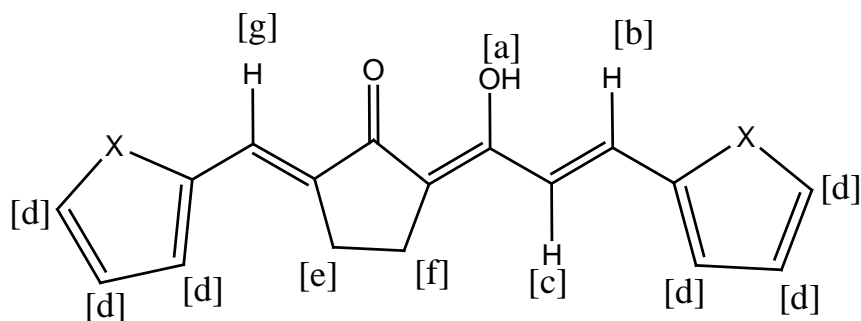
Similar to the ligands described in previous chapters, the UV spectra of the ligands showed two absorption maxima, corresponding to $n \rightarrow \pi^*$ and $\pi \rightarrow \pi^*$ transitions (**Table 4.1**).

4.4.2 Infrared Spectra

The IR spectra of the compounds displayed a strong intensity band at $\sim 1575 \text{ cm}^{-1}$ corresponding to the C=O stretching of intramolecularly hydrogen bonded dicarbonyl function. A broad band present in the range of $2600\text{-}3600 \text{ cm}^{-1}$ is due to the stretching of OH in the chelated carbonyl group. The observed breadth and intensity of the band suggest the involvement of the enolic proton in strong intramolecular hydrogen bonding. The absorptions corresponding to $\nu(\text{C=O})$, $\nu_{\text{as}}(\text{C-C-C})$ and $\nu(\text{CH=CH-})$ (trans) are given in **Table 4.1**.

4.4.3 ^1H NMR spectra

The ^1H NMR spectral data of both ligands show a characteristic downfield singlet at $\delta \sim 14.5$ ppm which can be assigned to the intramolecularly hydrogen bonded enolic proton. The multiplet signals at δ 2.54-2.82 ppm due to protons in the cyclopentane ring and two doublets δ at ~ 6.67 ppm due to the alkenyl protons and a singlet at $\delta \sim 7.72$ due to vinylic protons also appeared along with the aromatic protons. Observed J value of 16.2 Hz and 16.3 Hz for the alkenyl proton suggests their trans orientation (**Table 4.2**). The ^1H NMR spectra are shown in **Figures 4.1** and **4.2**.

Table 4.2 ^1H NMR spectral data of ligands

Chemical shift, ppm (Coupling constant, Hz)							
Compounds	[a]	[b]	[c]	[d]	[e]	[f]	[g]
HL¹	14.64	6.71 (16.3)	6.89 (16.3)	6.97- 7.87	2.54 (5.2)	2.61 (5.2)	7.28
HL²	14.46	6.69 (16.2)	6.93 (16.2)	7.12- 7.76	2.71 (5.3)	2.82 (5.3)	7.52

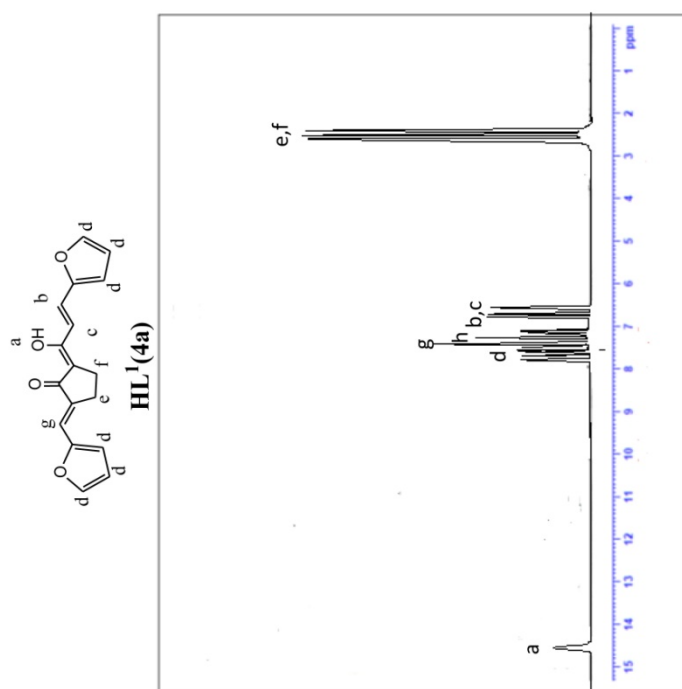


Figure 4.1. ¹H NMR spectrum of **HL¹(4a)**

¹H NMR (400MHz, CDCl₃, ppm): δ 14.64 (1H, s, enolic -OH) [a], [2.54 (2H, t, J=5.2Hz, cyclopentane ring CH₂), 2.61 (2H, t, J=5.2Hz, cyclopentane ring CH₂)] [e, f], [6.71 (1H, d, J=16.3Hz, (E)- alkenyl H), 6.89 (1H, d, J=16.3Hz, (E)- alkenyl H)] [b, c], 6.97-7.87 (6H, m, hetero aryl H) [d], 7.28 (1H, s, vinylic H) [g], 7.26 (solvent) [h].

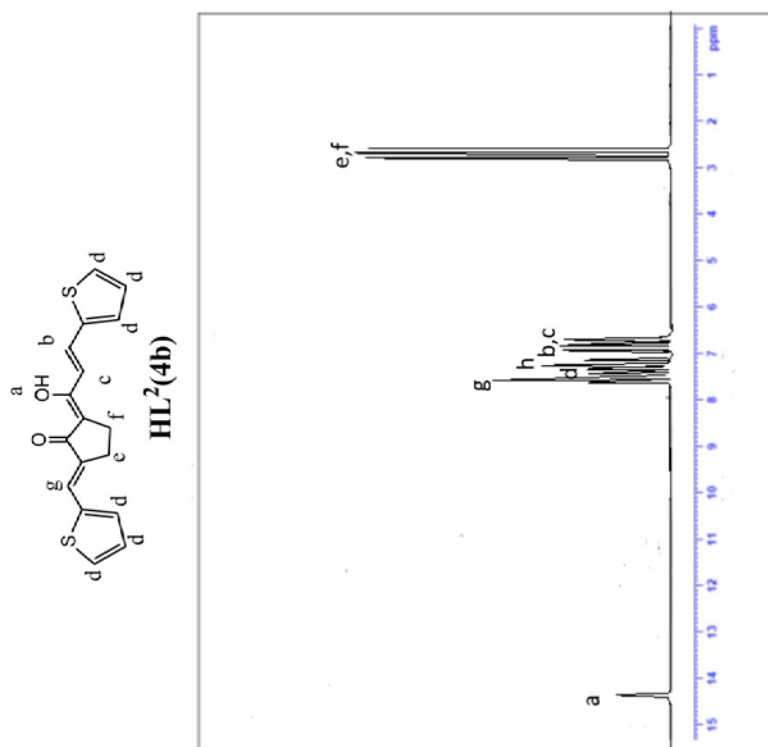


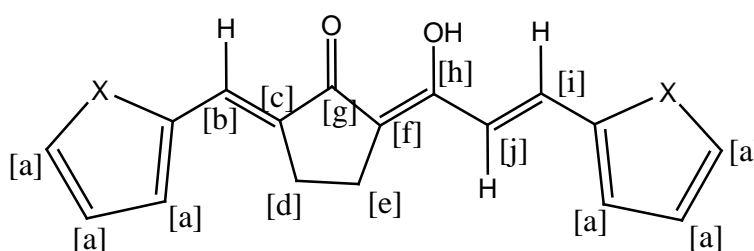
Figure 4.2. ¹H NMR spectrum of **HL²(4b)**

¹H NMR (400MHz, CDCl₃, ppm): δ 14.46 (1H, s, enolic -OH) [a], [2.71 (2H, t, J=5.3Hz, cyclopentane ring CH₂), 2.82 (2H, t, J=5.3Hz, cyclopentane ring CH₂) [e,f], [6.69 (1H, d, J=16.2Hz, (E)- alkenyl H), 6.93 (1H, d, J=16.2Hz, (E)- alkenyl H)] [b,c], 7.12-7.76 (6H, m, hetero aryl H) [d], 7.52 (1H, s, vinylic H) [g], 7.26 (solvent) [h].

4.4.4 ^{13}C NMR spectra

The ^{13}C NMR spectra of **4a** and **4b**, given in **Figures 4.3** and **4.4**, showed two resonance signals in the range 195.34–195.93 ppm and in the range 184.64–186.37 ppm indicating that the two carbonyl groups have different electronic environment. The two aliphatic carbon atoms in the cyclopentanone ring show a resonance signal at 25–29 ppm. The resonance signals in the range 111.64–149.86 ppm are due to the hetero aryl carbon atoms (**Table 4.3**).

Table 4.3 ^{13}C NMR spectral data of ligands



Chemical shift (ppm)										
Compounds	[a]	[b]	[c]	[d]	[e]	[f]	[g]	[h]	[I]	[j]
HL¹	111.64-149.86	148.34	132.04	25.42	29.67	98.47	184.64	195.34	116.32	152.67
HL²	120.61-149.12	143.76	135.45	25.94	29.84	95.89	186.37	195.93	121.34	138.64

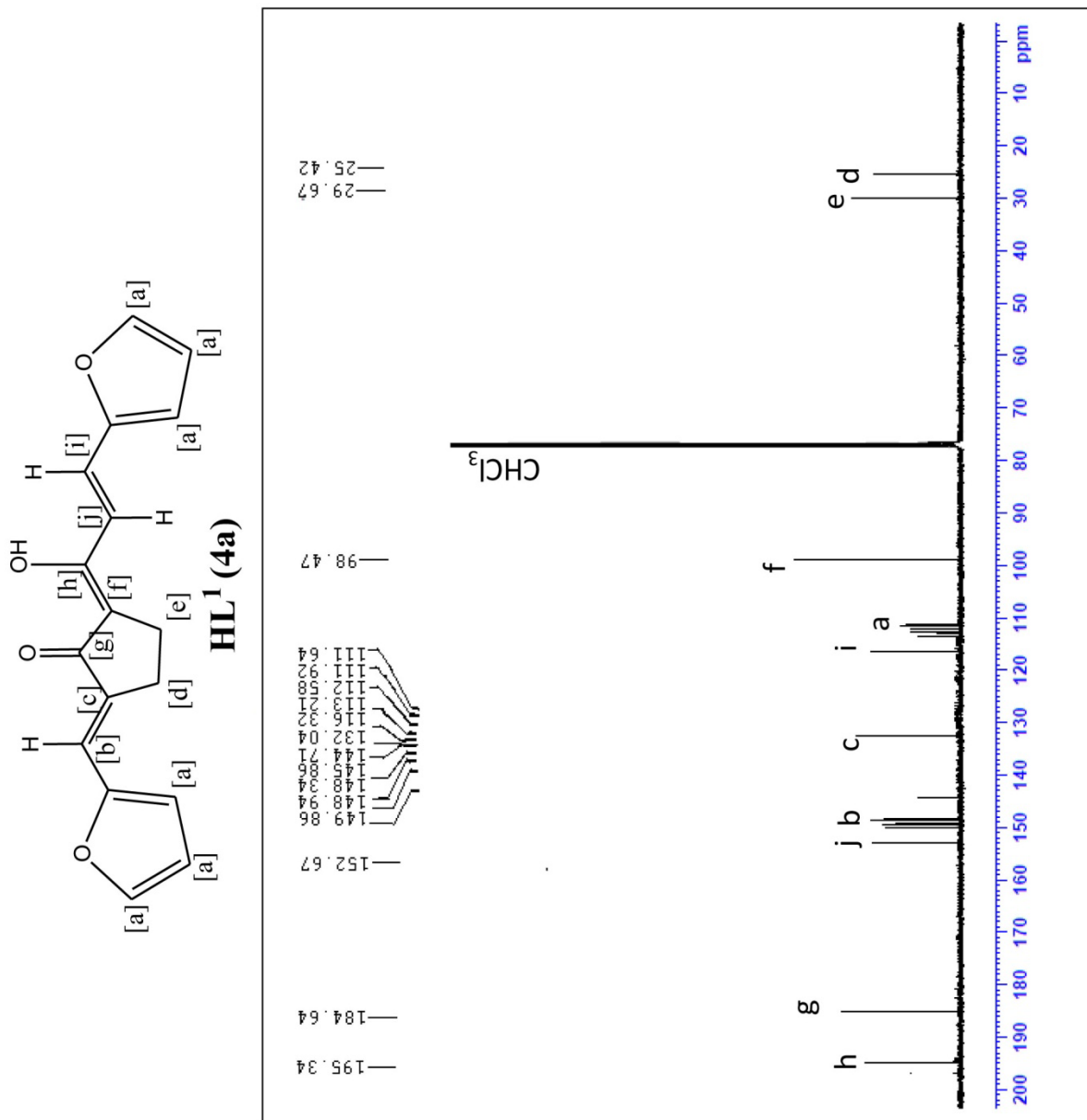


Figure 4.3. ¹³C NMR spectrum of **HL¹ (4a)**

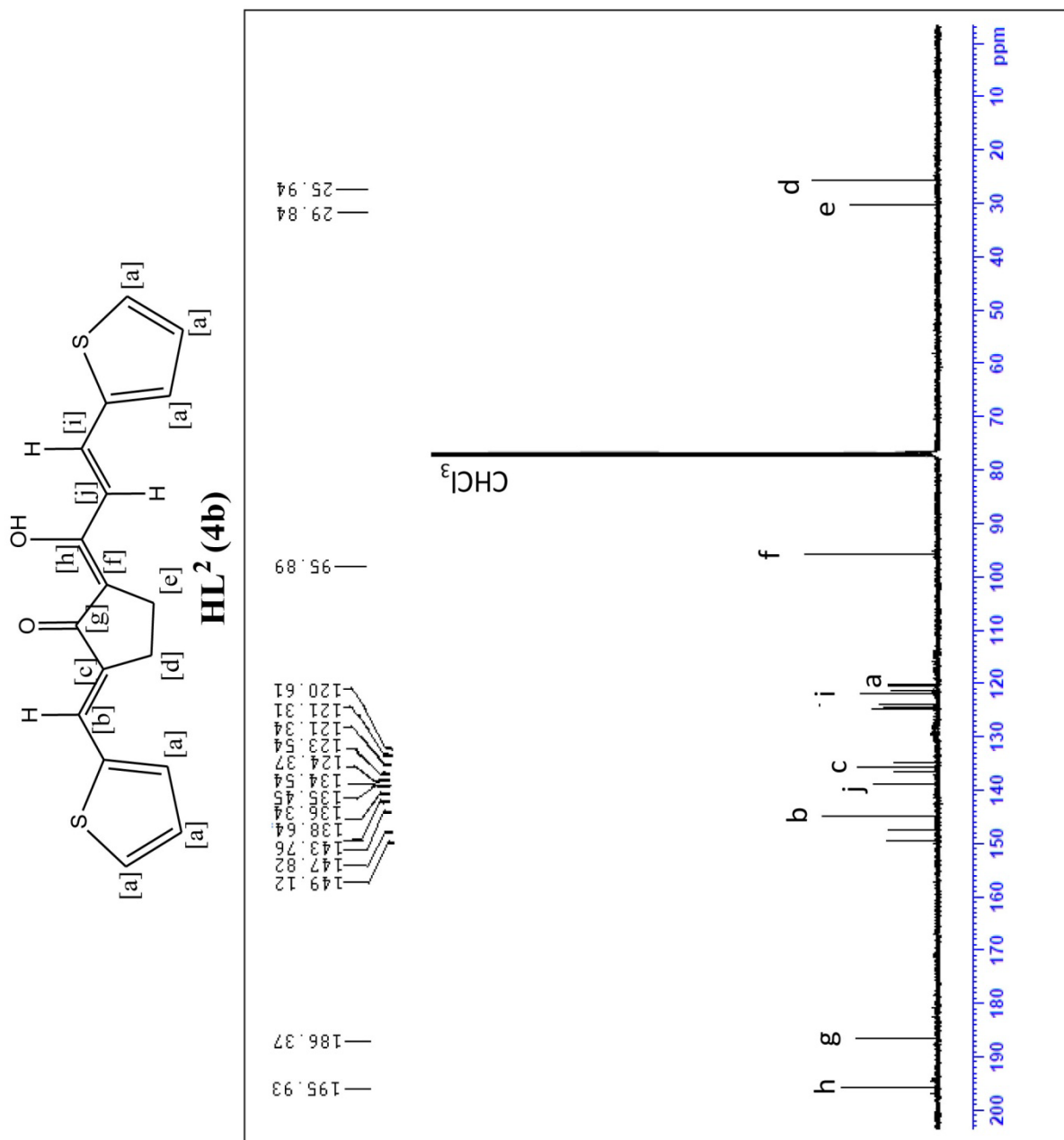


Figure 4.4. ¹³C NMR spectrum of **HL² (4b)**

4.4.5 Mass spectra

The ESI mass spectra of the compounds are given in **Figures 4. 5** and **4.6**. Intense molecular ion peak is present in both cases. The major peaks having relative intensity above 50% are marked in the spectra (**Figures 4.5-4.6**). A probable fragmentation pattern is shown in **Figure 4.7**.

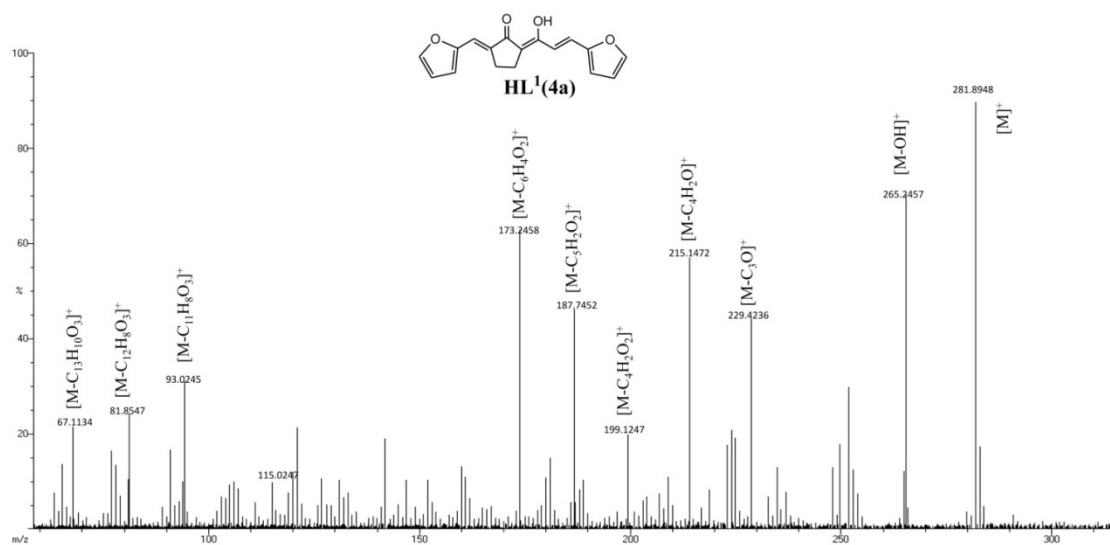


Figure 4.5. EI mass spectrum of HL¹ (4a)

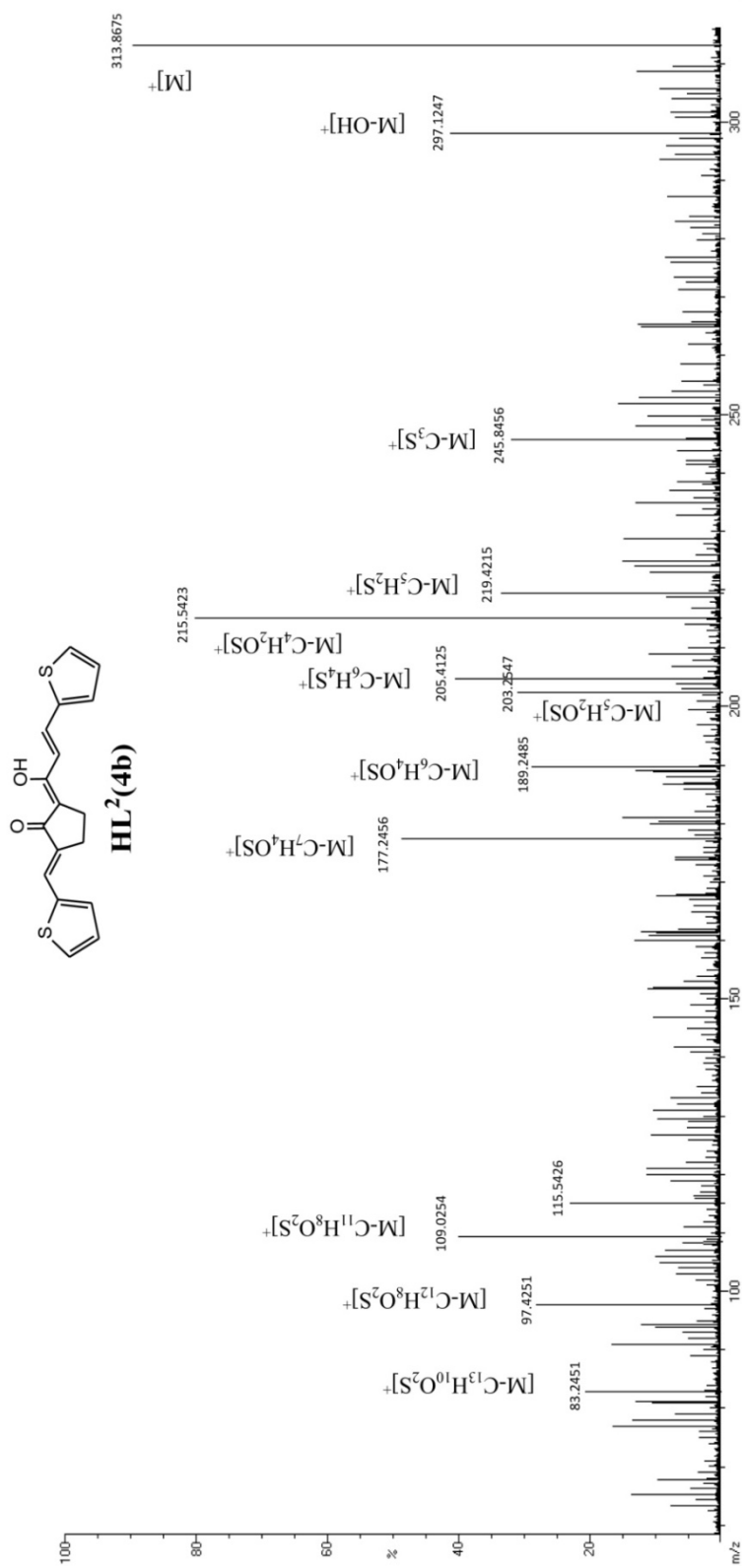


Figure 4.6. EI mass spectrum of **HL² (4b)**

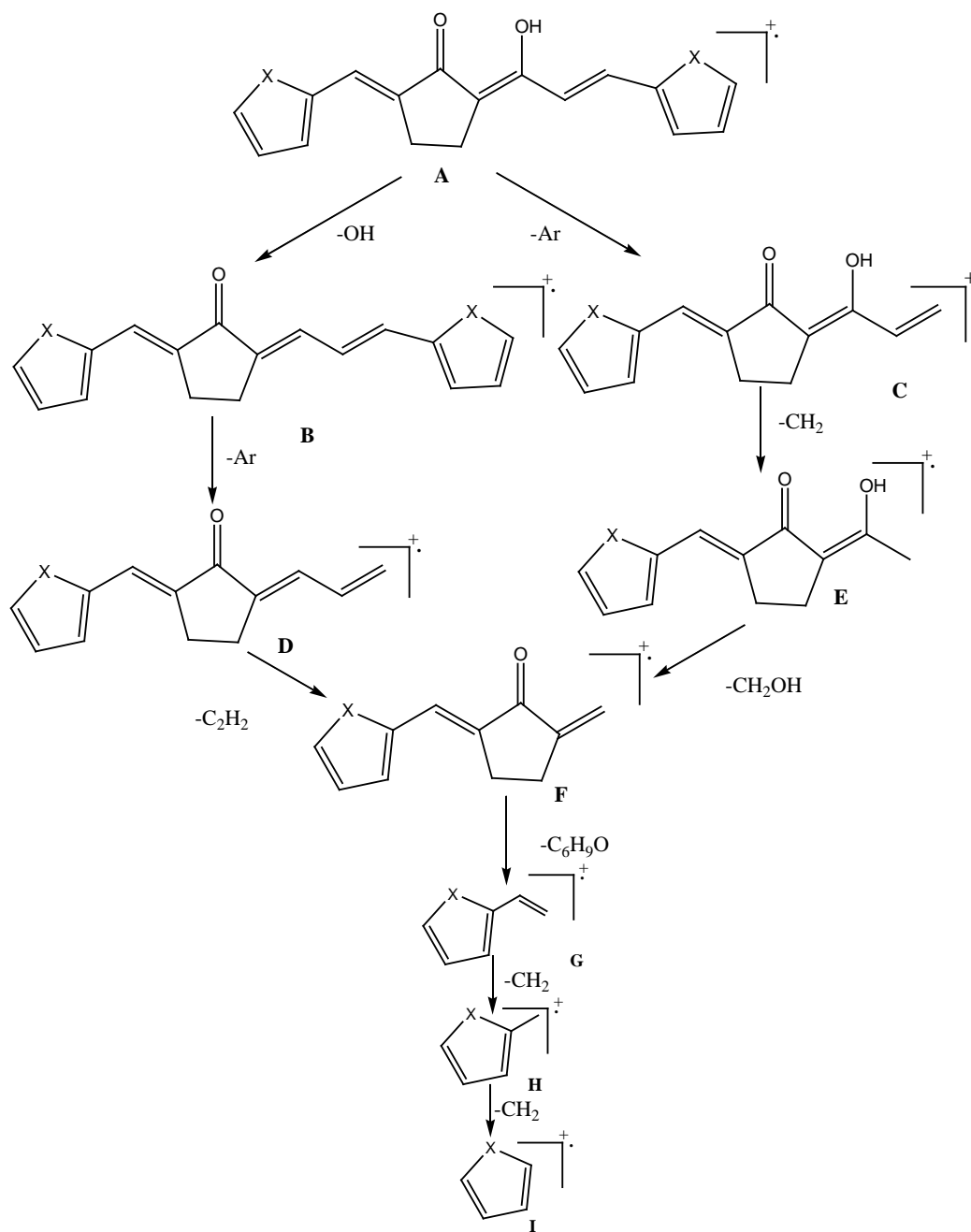
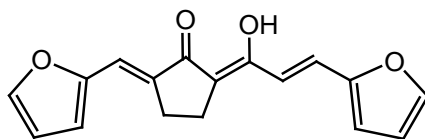


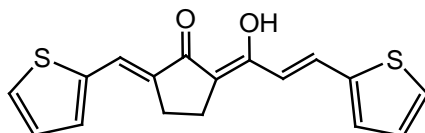
Figure 4.7. Fragmentation pattern of the ligands

From the above discussion, both the ligands can be formulated as below.



HL¹ (4a)

(2E)-2-(2-furyl)-5-((E)-3-(2-furyl) acryloyl) cyclopentanone



HL² (4b)

(2E)-2-(2-thiophenyl)-5-((E)-3-(2-thiophenyl) acryloyl) cyclopentanone

4.5 Characterization of metal complexes

Analytical and physical data of the metal complexes are given in **Table 4.4**. The observed carbon, hydrogen and metal percentages of the metal complexes and ESI mass spectral data suggest their ML₂ stoichiometry. All the metal complexes behave as non-electrolytes (specific conductance < 15Ω⁻¹ cm⁻¹ in DMF) and do not contain the anion of the metal salt used for their preparation. The nickel(II) and zinc(II) complexes are diamagnetic and other is paramagnetic. The electronic, IR, ¹H NMR, ¹³C NMR and mass spectral data of the complexes are discussed below.

4.5.1 Electronic spectra

The electronic spectra of the complexes showed a bathochromic shift in the low energy band due to n→π* transition (453-482 nm) and the high energy band due to π→π* transitions remains unaltered (233-258 nm) (**Table 4.4**).

Table 4.4 Analytical data of copper (II), nickel (II) and Zinc (II) complexes

Complexes (formula weight)	M.p. (°C)	Yield (%)	Elemental analysis %			UV λ_{\max} (nm)	μ_{eff} BM	Mass spectral data (m/z)
			(found /calcd)					
			C	H	Cu			
[Cu(L¹)₂] C ₃₄ H ₂₆ O ₈ Cu (626)	218	62	(65.97) 65.22	(4.64) 4.19	(10.67) 10.15	234 459	1.81	671,648,625,343, 281,198 ,184
[Cu(L²)₂] C ₃₄ H ₂₆ O ₄ S ₄ Cu (690)	236	61	(58.76) 59.15	(3.97) 3.80	(9.67) 9.20	248 454	1.75	735,712,689,375, 313,214,200
[Ni(L¹)₂] C ₃₄ H ₂₆ O ₈ Ni (621)	218	57	(65.97) 65.73	(4.64) 4.22	(9.84) 9.45	233 464	-	-
[Ni(L²)₂] C ₃₄ H ₂₆ O ₄ S ₄ Ni (685)	232	59	(59.31) 59.57	(3.41) 3.82	(8.24) 8.56	240 482	-	-
[Zn(L¹)₂] C ₃₄ H ₂₆ O ₈ Zn (627)	202	55	(65.98) 65.03	(4.87) 4.17	(10.87) 10.41	258 453	-	-
[Zn(L²)₂] C ₃₄ H ₂₆ O ₄ S ₄ Zn (692)	216	53	(58.18) 58.99	(3.24) 3.79	(9.09) 9.45	246 478	-	-

In the copper(II) complexes the presence of a broad visible band at ~665 nm and the measured μ_{eff} values (1.75–1.81 B.M.) support their square planar structure. The nickel(II) chelates are found to be diamagnetic and appearance of a broad medium-intensity band at $\sim 17,800 \text{ cm}^{-1}$ in the visible spectra suggest their square-planar geometry. Three absorption bands at $\sim 8,090$, $\sim 13,570$ and $\sim 24,390 \text{ cm}^{-1}$ were observed in the spectra of nickel(II) chelates recorded in presence of pyridine solution which can be assigned to the transitions ${}^3A_{2g} \rightarrow {}^3T_{2g}$; ${}^3A_{2g} \rightarrow {}^3T_{1g}(\text{F})$ and ${}^3A_{2g} \rightarrow {}^3T_{1g}(\text{P})$, respectively, in an octahedral environment due to the association of pyridine.. These observations suggest square planar structure of nickel complexes.

4.5.2 Infrared Spectra

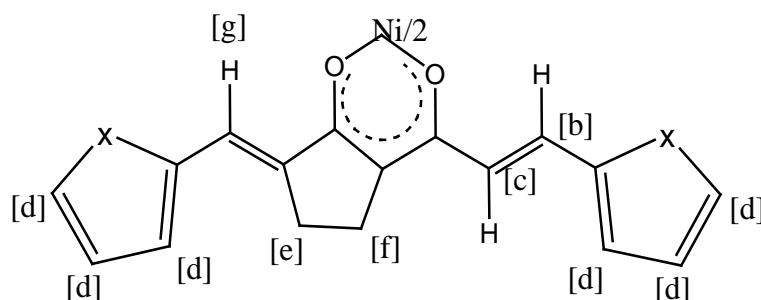
In the IR spectra of all complexes, the band due to the stretching of the coordinated carbonyl moiety appeared at $\sim 1590 \text{ cm}^{-1}$. The broad band in the region at $2800\text{--}3600 \text{ cm}^{-1}$ due to the hydrogen bonded enol proton present in the free ligands is absent in the spectra of metal complexes and weak bands attributable to various $\nu(\text{C-H})$ appeared. The appearance of two medium intensity bands in the region $459\text{--}482 \text{ cm}^{-1}$ due to $\nu(\text{M-O})$ vibrations indicate that carbonyl oxygen atoms are involved in metal complex formation. The prominent band at $\sim 975 \text{ cm}^{-1}$ is typical of a trans $-\text{CH}=\text{CH}-$ group which remained unaltered in the spectra of metal complexes (**Table 4.5**).

4.5.3 ${}^1\text{H}$ NMR spectra

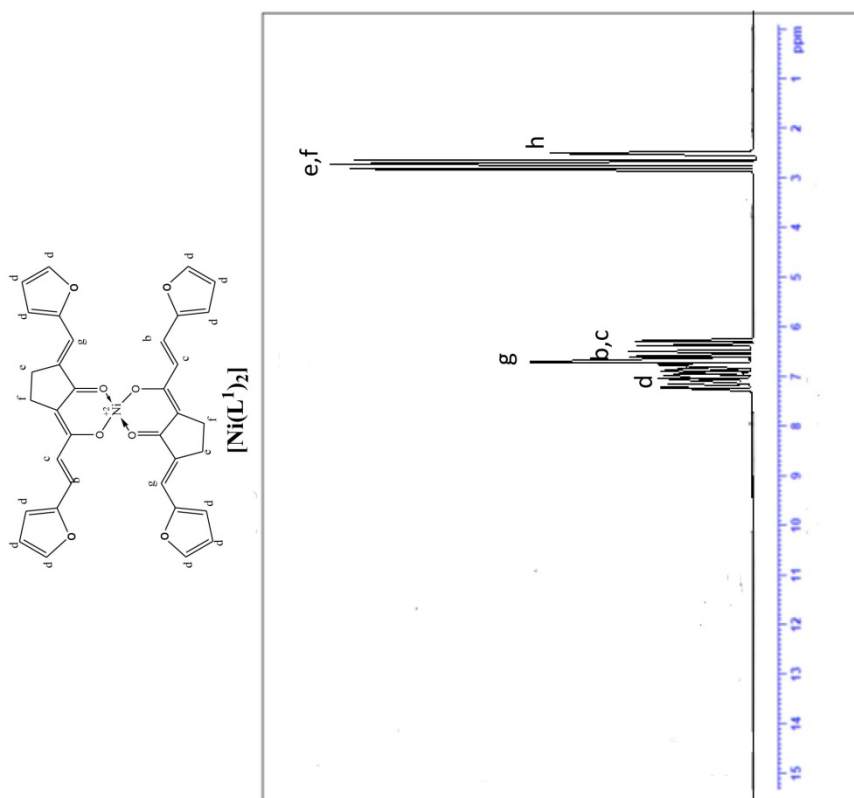
The replacement of the enolic proton by the metal ion in the complexes is confirmed by the absence of proton signals above $\delta \sim 11 \text{ ppm}$ in the ${}^1\text{H}$ NMR spectra of the diamagnetic nickel(II) chelates. The spectra are given in **Figures 4.8** and **4.9**. Observed J value of 16 Hz for the alkenyl proton signals in the nickel (II) complexes suggest their trans orientation as it is in the free ligands (**Table 4.6**).

Table 4.5 IR spectral data of complexes

IR spectral data of complexes (cm ⁻¹)							
Compounds	$\nu(\text{C}=\text{O})$ metal chelated carbonyl	$\nu(\text{C}=\text{C})$ phenyl	$\nu(\text{C}=\text{C})$ alkenyl	$\nu_{\text{as}}(\text{C}-\text{C}-\text{C})$ chelate ring	$\nu_{\text{as}}(\text{C}-\text{C}-\text{C})$ chelate ring	$\nu(\text{CH}=\text{CH}-)$ trans	$\nu(\text{M}-\text{O})$ chelate ring
[Cu(L ¹) ₂]	1576,1534	1446	1364	1264	1167	964	478
[Cu(L ²) ₂]	1613,1558	1434	1413	1274	1236	972	482
[Ni(L ¹) ₂]	1572,1531	1424	1324	1243	1128	976	480
[Ni(L ²) ₂]	1605,1564	1428	1411	1264	1243	976	472
[Zn(L ¹) ₂]	1617,1542	1464	1419	1238	1184	958	464
[Zn(L ²) ₂]	1626,1574	1451	1427	1252	1174	978	459

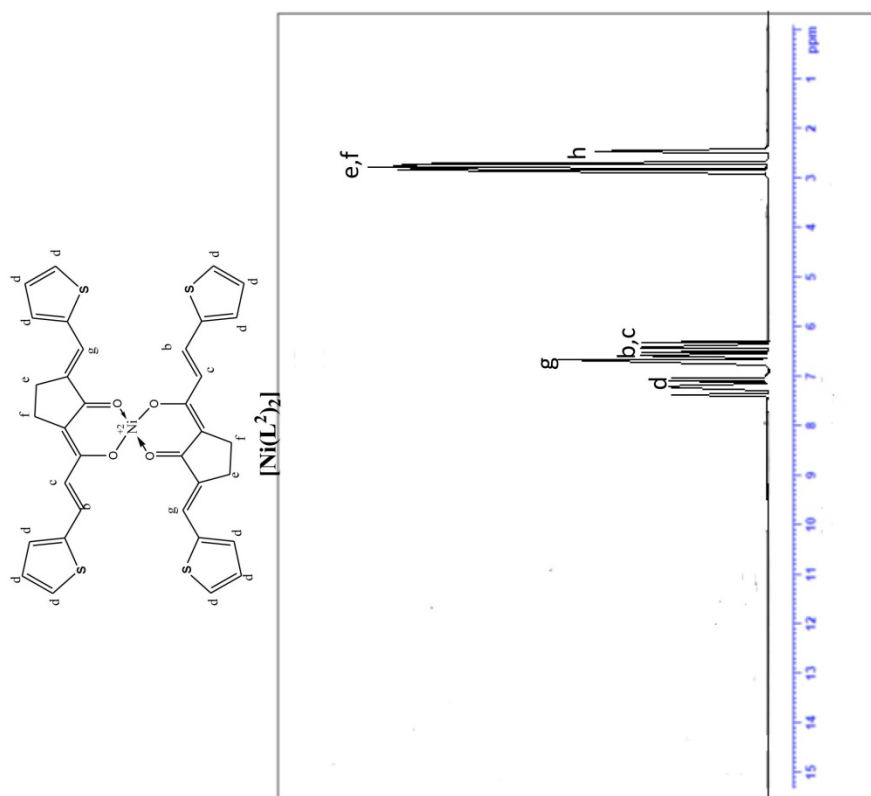
Table 4.6 ¹H NMR spectral data of Ni (II) complexes

Compounds	Chemical shift, ppm (Coupling constant, Hz)						
	[a]	[b]	[c]	[d]	[e]	[f]	[g]
[Ni(L ¹) ₂]	-	6.48 (16.2)	6.57 (16.2)	6.62-7.41	2.69 (5.4)	2.72 (5.4)	6.64
[Ni(L ²) ₂]	-	6.29 (16.4)	6.43 (16.4)	7.11-7.42	2.74 (5.7)	2.85 (5.7)	6.62



^1H NMR (400MHz, DMSO, ppm): δ [2.69 (4H, t, $J=5.4\text{Hz}$, cyclopentane ring CH_2s), 2.72 (4H, t, $J=5.4\text{Hz}$, cyclopentane ring CH_2s) [e,f], [6.48 (2H, d, $J=16.2\text{Hz}$, (E)- alkenyl Hs), 6.57 (2H, d, $J=16.2\text{Hz}$, (E)- alkenyl Hs)] [b,c], 6.62-7.41 (12H, m, hetero aryl Hs) [d], 6.64 (2H, s, vinylic Hs) [g], 2.49 (solvent) [h].

Figure 4.8. ^1H NMR spectrum of $[\text{Ni}(\text{L}^1)_2]$



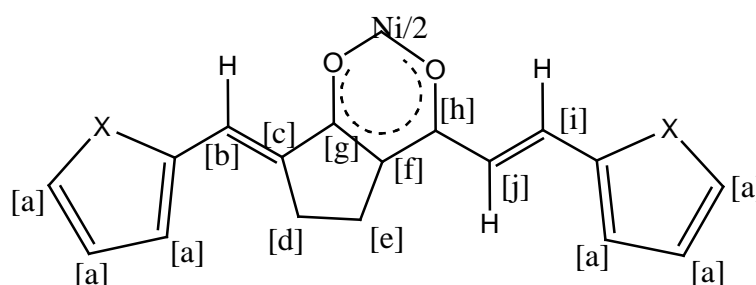
^1H NMR (400MHz, DMSO, ppm): δ [2.74 (4H, t, cyclopentane ring CH_2s), 2.85 (4H, t, $J=5.7\text{Hz}$, cyclopentane ring CH_2s)] [e,f], [6.29 (2H, d, $J=16.4\text{Hz}$, (E)- alkenyl Hs), 6.43 (2H, d, $J=16.4\text{Hz}$, (E)- alkenyl Hs)] [b,c], 7.11-7.42 (12H, m, hetero aryl Hs) [d], 6.62 (2H, s, vinylic Hs) [g], 2.49 (solvent) [h].

Figure 4.9. ^1H NMR spectrum of $[\text{Ni}(\text{L}^2)_2]$

4.5.4 ^{13}C NMR spectra

The ^{13}C NMR spectra of the nickel(II) complexes are given in **Figures 4.10** and **4.11**. The low field shift carbonyl carbon signal of the free ligand by 15- 20 ppm in the spectra of nickel(II) complexes suggest the involvement of carbonyl groups in metal complex formation(**Table 4.7**).

Table 4.7 ^{13}C NMR spectral data of Ni(II) complexes



Chemical shift (ppm)										
Compounds	[a]	[b]	[c]	[d]	[e]	[f]	[g]	[h]	[i]	[j]
$[\text{Ni}(\text{L}^1)_2]$	110.31- 149.64	147.34	109.34	23.28	32.54	97.76	181.38	192.65	119.34	124.91
$[\text{Ni}(\text{L}^2)_2]$	126.94- 139.82	147.64	124.34	22.34	35.64	98.16	183.41	194.64	117.79	128.67

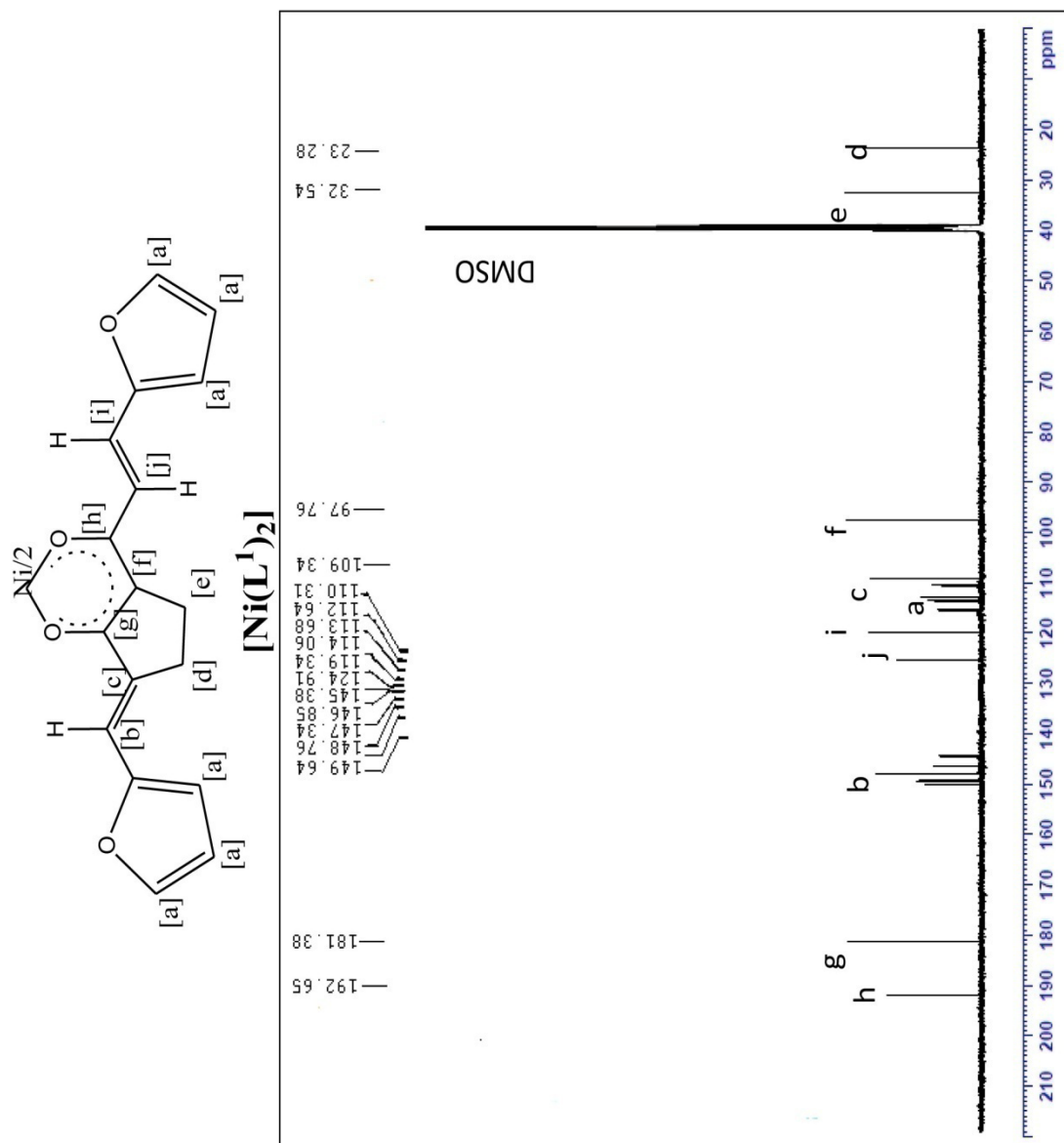


Figure 4.10. ^{13}C NMR spectrum of $[\text{Ni}(\text{L}^1)_2]$

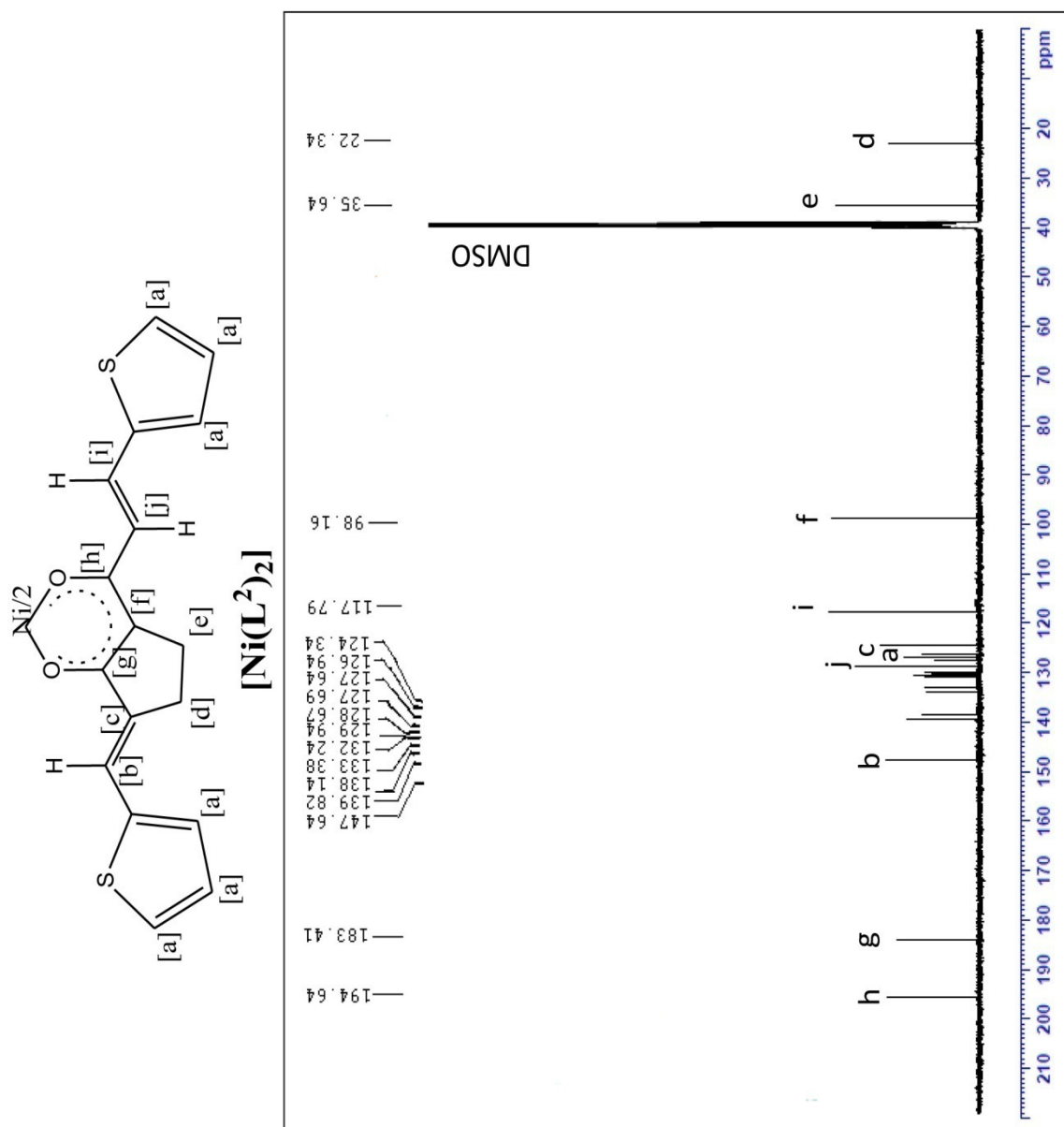


Figure 4.11. ^{13}C NMR spectrum of $[\text{Ni}(\text{L}^2)_2]$

4.5.5 Mass spectra

The ESI mass spectra of the copper(II) chelates confirm the $[ML_2]$ stoichiometry of the complexes. Peaks due to M^+ and $(M+2)^+$ with 3:1 intensity are present in the ESI MS of copper(II) chelates in consistent with the natural abundance of ^{63}Cu and ^{65}Cu isotopes^[186,187]. Several peaks containing Cu can be identified in the spectra given in **Figures 4.12** and **4.13**.

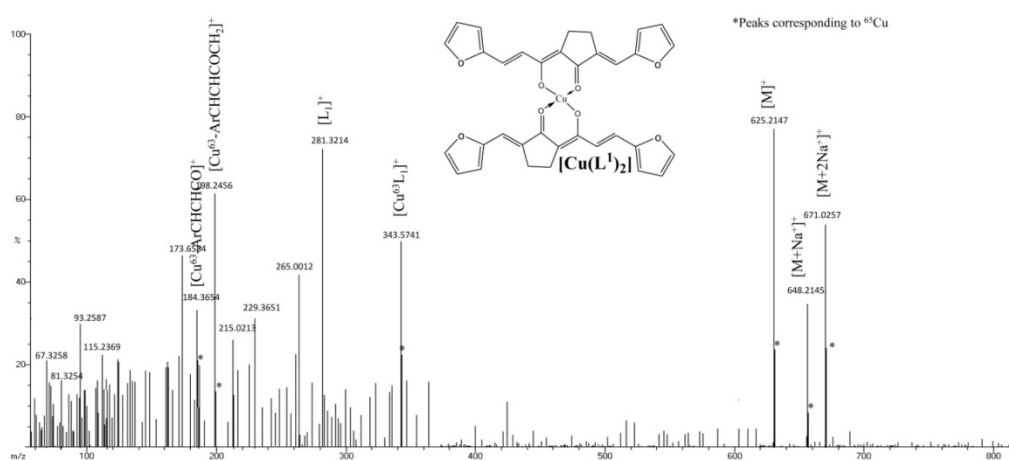


Figure 4.12. ESI mass spectrum of $[\text{Cu}(\text{L}^1)_2]$

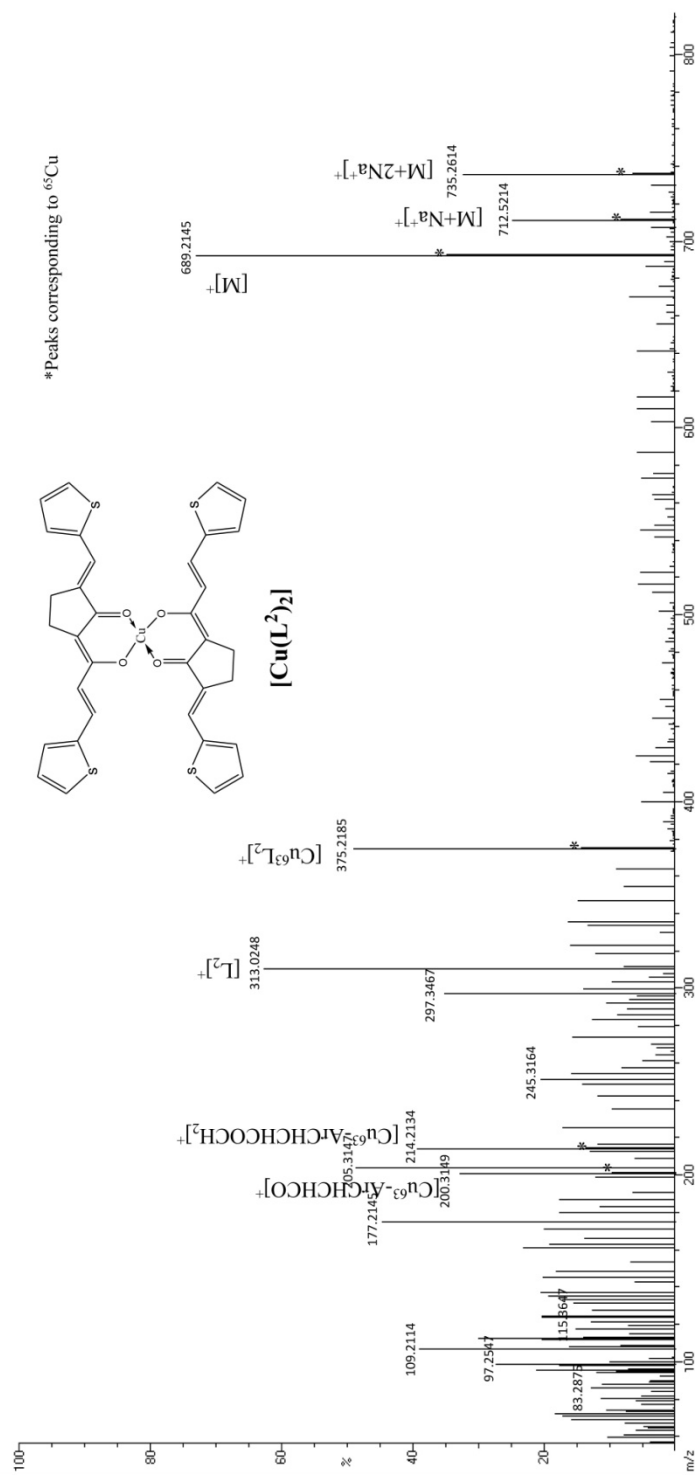


Figure 4.13. ESI mass spectrum of [Cu(L²)₂]

The electronic, IR, ^1H NMR, ^{13}C NMR and mass spectral data of the complexes are compatible with the structure given in **Figure 4.14**.

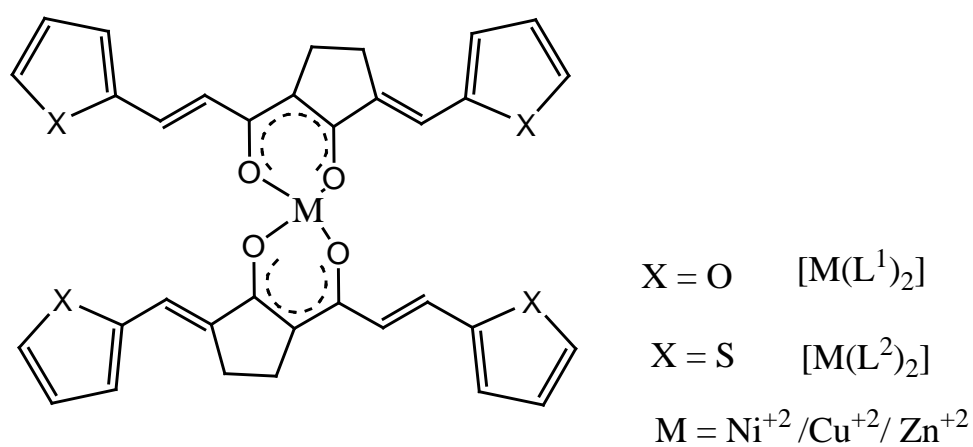


Figure 4.14. Proposed structure of metal complexes

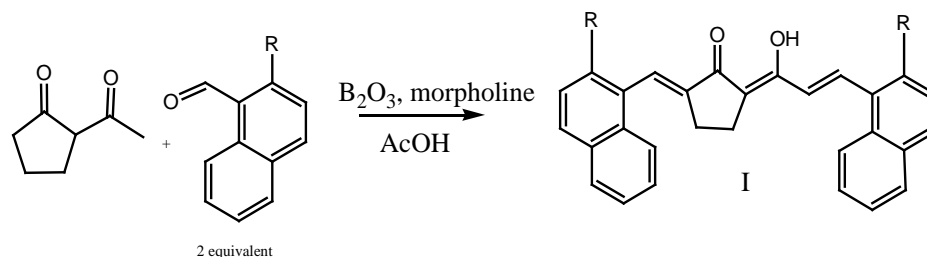
Chapter 5

LIGANDS WITH NAPHTHYL RINGS

Two synthetic analogues of curcumin with naphthyl rings synthesised from 2-acetylcyclopentanone using naphthalene-1-carbaldehyde and 2-hydroxy naphthalene-1-carbaldehyde are presented in this chapter.

5.1 Synthesis of ligands

The ligands were synthesized by exposing a mixture of 2-acetyl cyclopentanone, B_2O_3 and 1-naphthaldehyde / 2-hydroxy-1-naphthaldehyde in 1:1:2 molar ratios with catalytic amount of morpholine to microwave radiations in a domestic microwave oven. The procedure is same as that described in **Chapter 3**. The reaction is depicted in **Scheme 5.1**.



Scheme 5.1

5.2 Synthesis of Cu^{II} , Ni^{II} and Zn^{II} complexes

The metal complexes were prepared from ligands by direct interaction with metal (II) ions in methanol under reflux conditions. A typical procedure is given below. A methanolic solution of metal(II) acetate (25 ml, 1 mmol) was added with stirring to a solution of ligand (40 ml, 2 mmol) in methanol-acetone mixture (1:1 v/v) and refluxed gently for ~4 hours. After reducing the volume to half, the solution was cooled to room temperature. The precipitated complex was filtered, repeatedly washed with cold methanol and dried in vacuum.

5.3 Results and discussion

The results of elemental analysis and molecular weight determination of the compounds given in **Table 5.1** indicate that two equivalents of the aromatic aldehyde has condensed with one equivalent of 2-acetyl cyclopentanone in both cases.

5.4 Characterization of ligands

5.4.1 Electronic spectra

Compared to the UV absorption maxima of ligands discussed in the previous chapters, the significant red shift in the absorption maxima of $n \rightarrow \pi^*$ transition (484-492 nm) in the UV spectra of **5a** and **5b** is due to extended conjugation with π electrons in the naphthyl rings. The $\pi \rightarrow \pi^*$ transition also slightly shifted to longer wavelength (282-290 nm) (**Table 5.1**).

5.4.2 Infrared Spectra

The IR spectral bands of **5a** and **5b** are given in **Table 5.1**. Similar to the ligand systems described in the previous chapters, bands due to chelated C=O stretching and stretching of the intramolecular hydrogen bonded enol group indicates extensive enolisation in both cases.

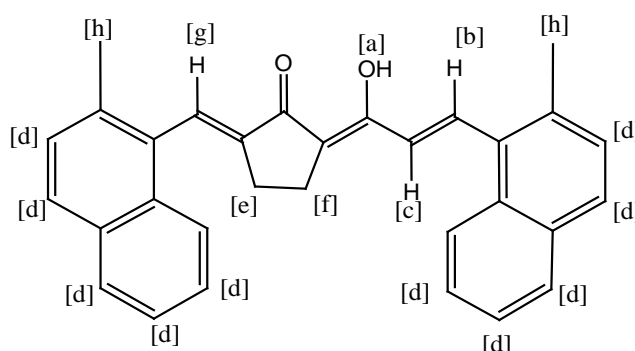
Table 5.1 Analytical, UV, IR, and mass spectral data of ligands

Ligands	M. p. (^o C)	Elemental analysis (found /calcd) %		Colour	Yield (%)	UV λ_{\max} (nm)	IR (cm ⁻¹)			Mass spectral data (m/z)
		C	H				$\nu(\text{C}=\text{O})$	$\nu_{\text{as}}(\text{C}-\text{C}-\text{C})$	$\nu(\text{CH}=\text{CH}-)$ (trans)	
(5a) HL¹ C ₂₉ H ₂₂ O ₂ (402)	176	(86.84) 86.54	(5.76) 5.51	Dark green solid	72	282($\pi \rightarrow \pi^*$), 484 ($n \rightarrow \pi^*$)	1585	1562	968	401,385,335, 289, 273, 259,195,153, 127,77
(5b) HL² C ₂₉ H ₂₂ O ₄ (434)	168	(80.67) (80.17)	(5.54) (5.10)	Dark green solid	70	290($\pi \rightarrow \pi^*$), 492 ($n \rightarrow \pi^*$)	1584	1552	974	433,417,291, 279, 275,263, 197,169, 143, 127,77

5.4.3 ^1H NMR spectra

The ^1H NMR spectral data of both ligands show a characteristic downfield singlet at $\delta \sim 15$ ppm which can be assigned to the intramolecularly hydrogen bonded enolic proton. The ^1H NMR spectra also shows signals at $\delta \sim 2.57$ - 2.69 ppm due to protons in the cyclopentane ring and two doublets at $\delta \sim 6.67$ ppm due to the alkenyl protons and a singlet at $\delta \sim 7.72$ due to vinylic protons. Observed J value of 16.4 Hz and 16.3 Hz for the alkenyl proton suggests their trans orientation (**Table 5.2**). The ^1H NMR spectra are shown in Figures 5.1 and 5.2.

Table 5.2 ^1H NMR spectral data of ligands



Chemical shift, ppm (Coupling constant, Hz)								
Compounds	[a]	[b]	[c]	[d]	[e]	[f]	[g]	[h]
HL¹	14.51	7.24 (16.4)	7.47 (16.4)	7.49-7.91	2.63 (5.1)	2.69 (5.1)	6.84	-
HL²	14.67	7.36 (16.3)	7.54 (16.3)	7.62-7.87	2.57 (5.4)	2.69 (5.4)	6.72	9.83

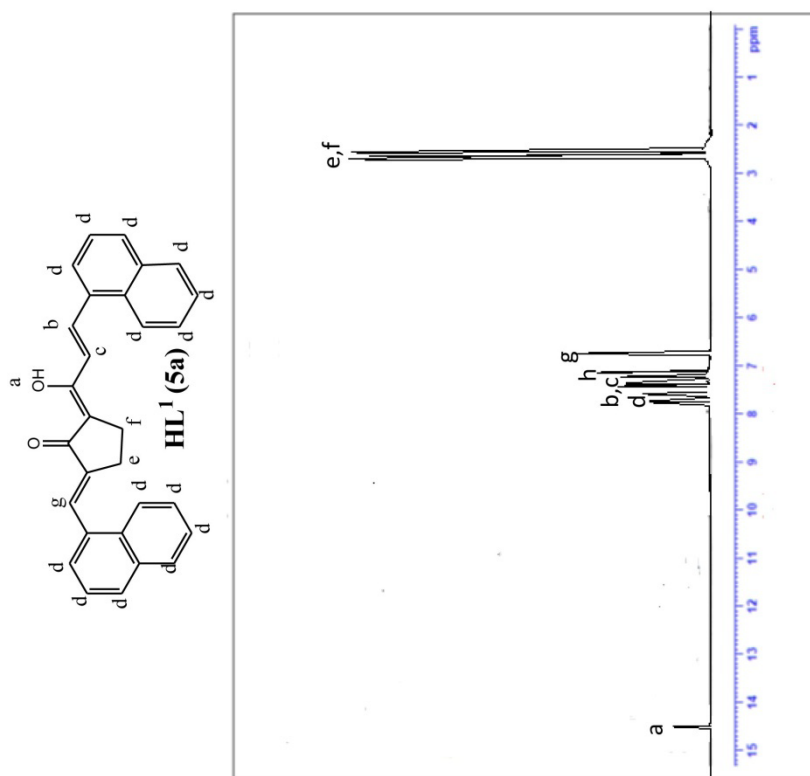
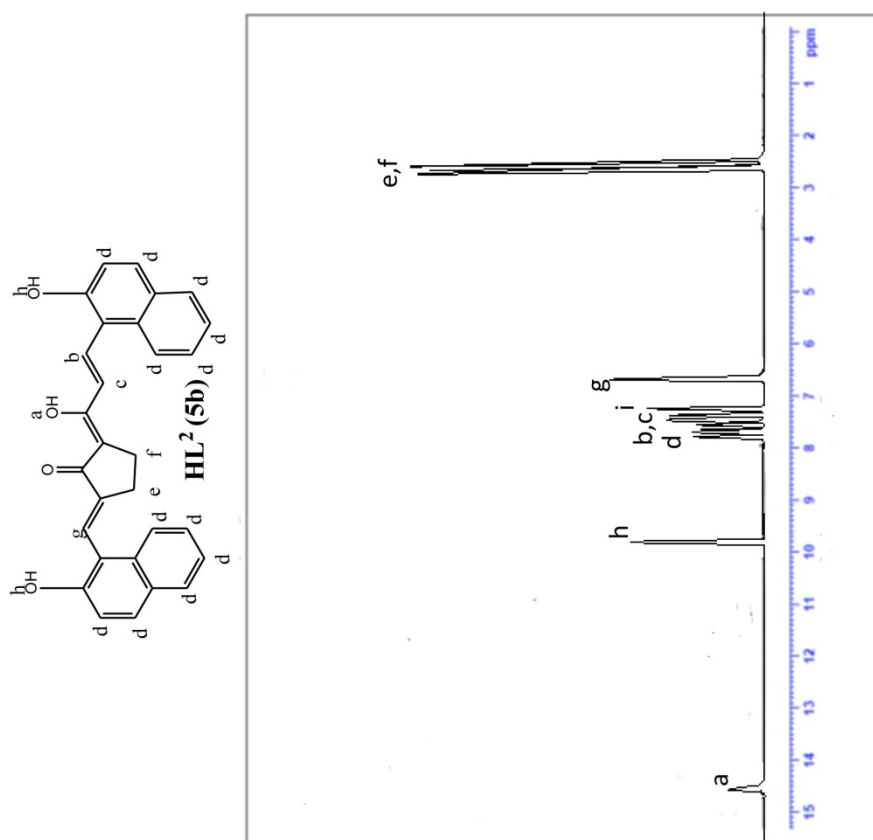


Figure 5.1. ¹H NMR spectrum of **HL¹ (5a)**

¹H NMR (400MHz, CDCl₃, ppm); δ 14.51 (1H, s, enolic -OH) [a], [2.63 (2H, t, J=5.1Hz, cyclopentane ring CH₂), 2.69 (2H, t, J=5.1Hz, cyclopentane ring CH₂) [e,f], [7.24 (1H, d, J=16.4Hz, (E)- alkenyl H), 7.47 (1H, d, J=16.4Hz, (E)- alkenyl H)] [b,c], 7.49-7.91 (14H, m, naphthyl Hs) [d], 6.84 (1H, s, vinylic H) [g], 7.26 (solvent) [h].



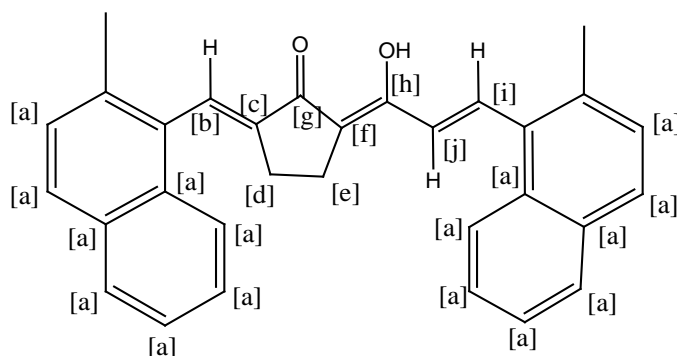
¹H NMR (400MHz, CDCl₃, ppm): δ 14.67 (1H, s, enolic -OH) [a], [2.57 (2H, t, J=5.4Hz, cyclopentane ring CH₂), 2.69 (2H, t, J=5.4Hz, cyclopentane ring CH₂) [c,f], [7.36 (1H, d, J=16.3Hz, (E)- alkenyl H), 7.54 (1H, d, J=16.3Hz, (E)- alkenyl H)] [b,c], 7.62-7.87 (12H, m, naphthyl Hs) [d], 6.72 (1H, s, vinylic H) [g], [9.83 (1H, s, phenolic), 9.78 (1H, s, phenolic)] [h], 7.26 (solvent) [i].

Figure 5.2. ¹H NMR spectrum of **HL² (5b)**

5.4.4 ^{13}C NMR spectra

Two resonance signals in the range 192.14–196.84 ppm and in the range 185.84–194.46 ppm present in the ^{13}C NMR spectra (**Figures 5.3** and **5.4**) indicate that the two carbonyl groups have different electronic environment. The resonance signals in the range 118.91–139.28 ppm are due to the naphthyl carbon atoms. The probable assignment of signals appeared in the spectra are given below (**Table 5.3**).

Table 5.3 ^{13}C NMR spectral data of ligands



Chemical shift (ppm)										
Compounds	[a]	[b]	[c]	[d]	[e]	[f]	[g]	[h]	[I]	[j]
HL¹	121.36-139.28	149.54	128.67	21.98	29.57	98.54	185.84	196.84	125.83	153.61
HL²	118.91-131.58	141.75	126.46	22.64	28.42	96.67	194.46	192.14	123.81	149.42

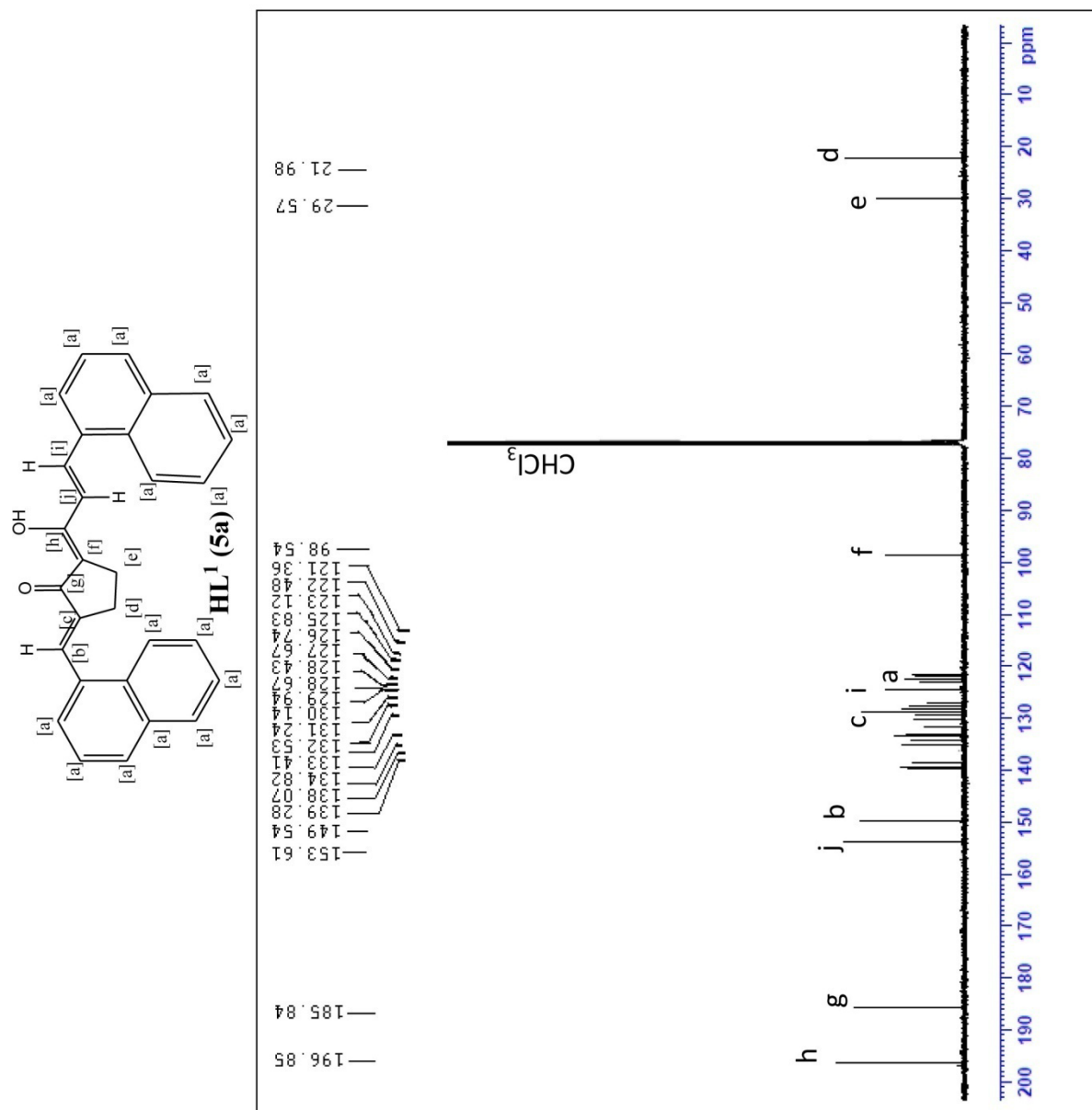


Figure 5.3. ¹³C NMR spectrum of **HL¹ (5a)**

5.4.5 Mass spectra

The ESI spectra of the ligands have molecular ion peaks at $m/z = 401.89$ for **5a** and at 275.34 for **5b** (Figure 5.5 and 5.6). Prominent peaks having relative intensity above 50% can be interpreted from the fragmentation pattern given in Figure 5.6 as in previous cases. They are listed in Table 5.1.

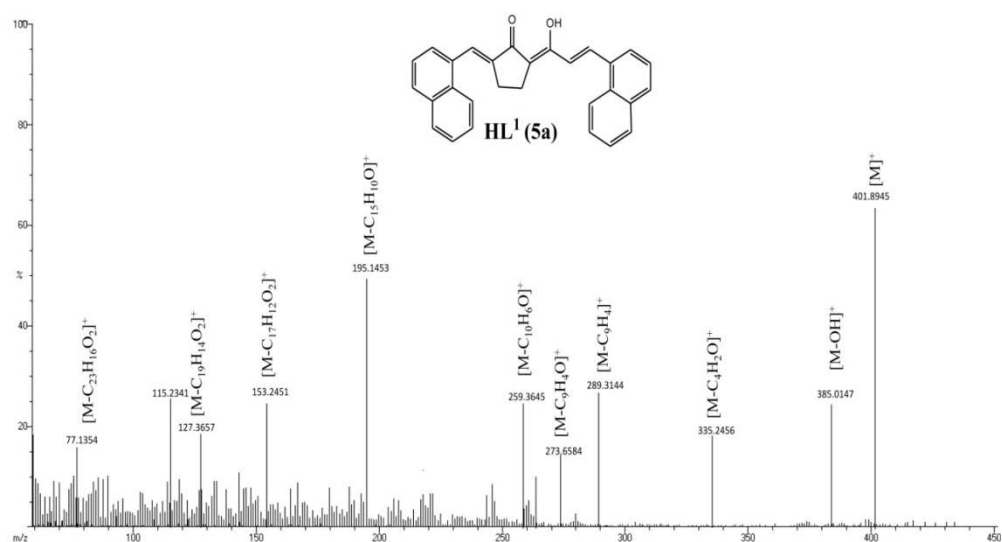


Figure 5.5 EI Mass spectrum of HL¹ (5a)

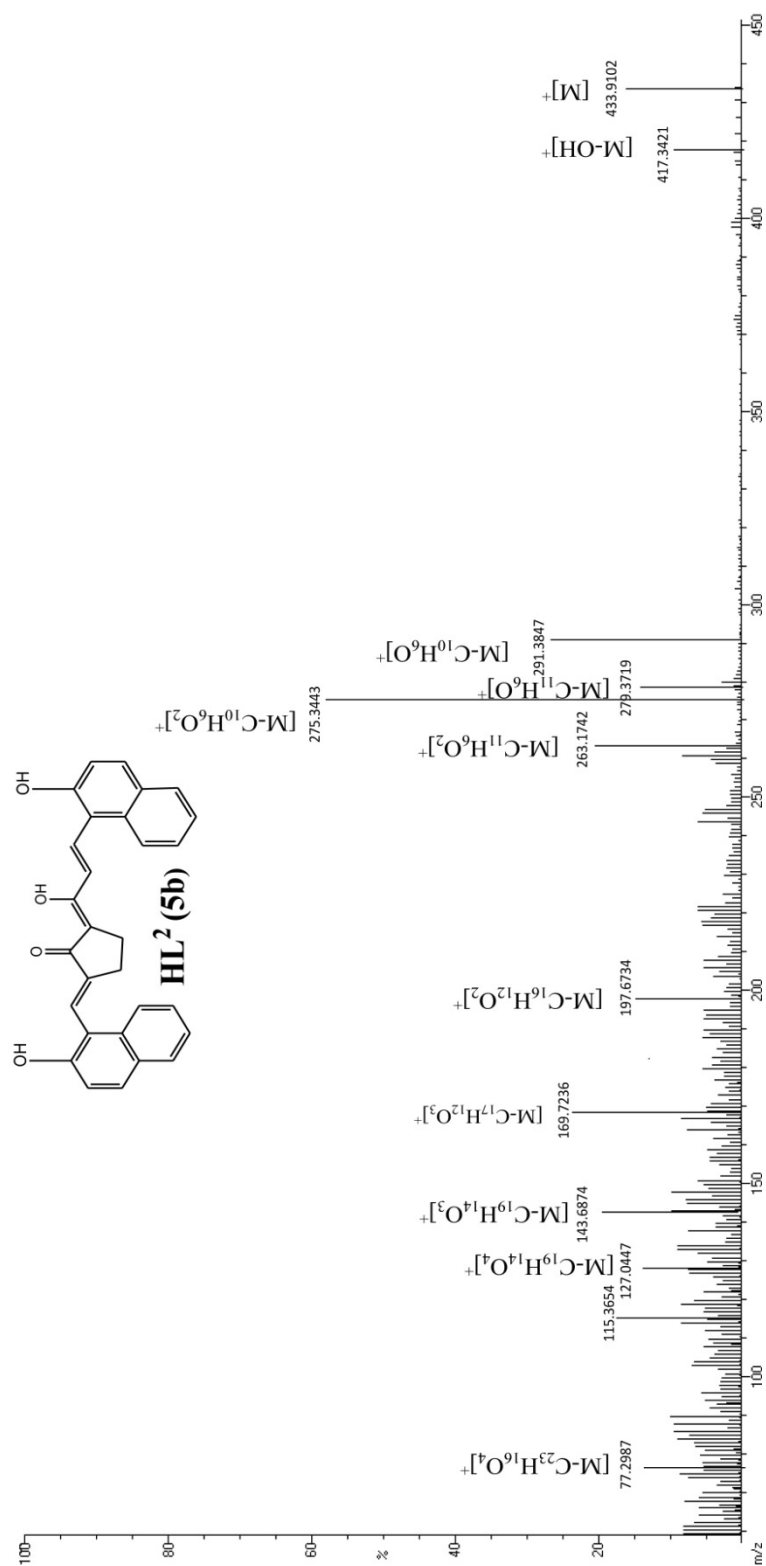


Figure 5.6 EI Mass spectrum of **HL² (5b)**

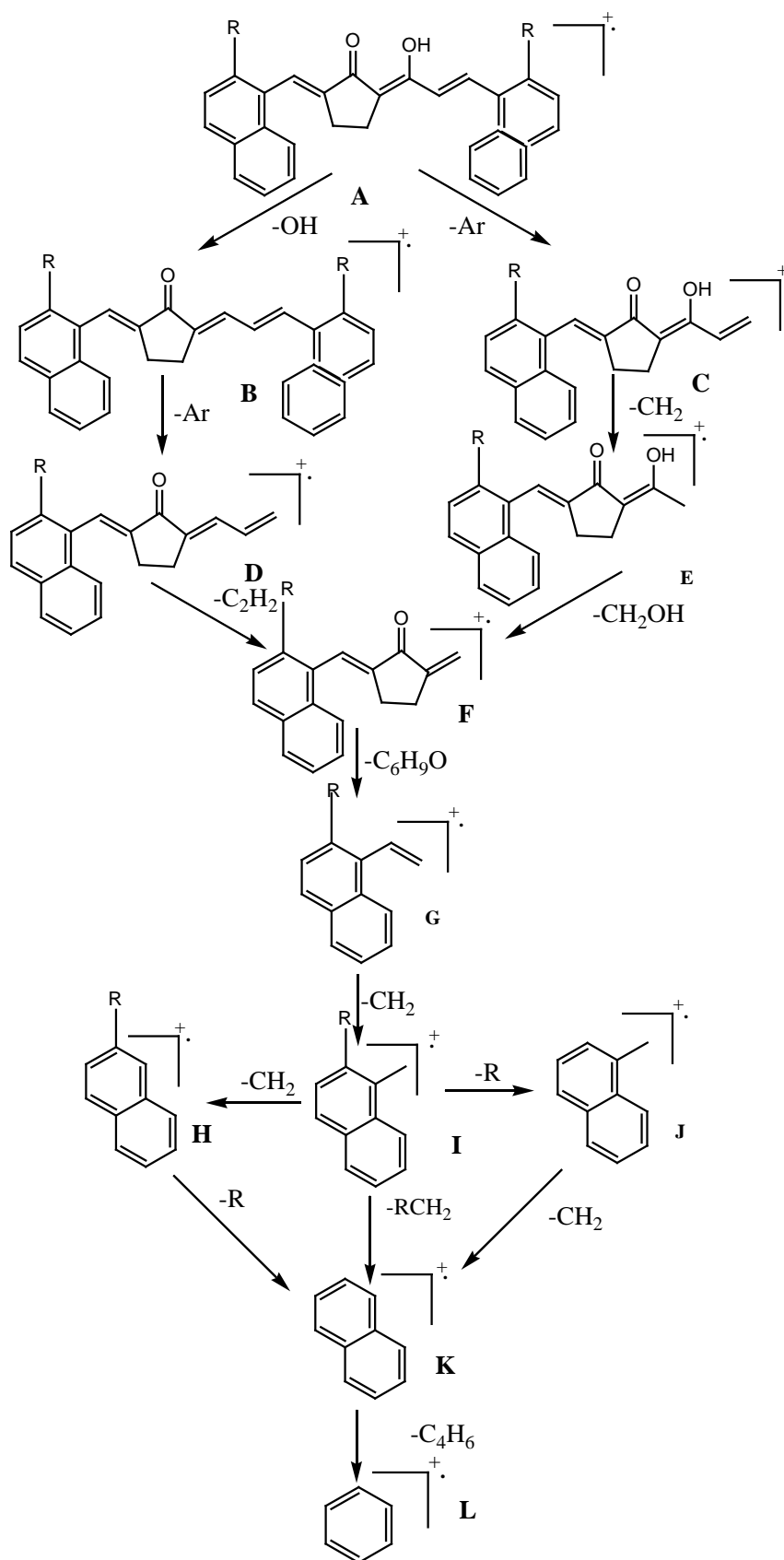
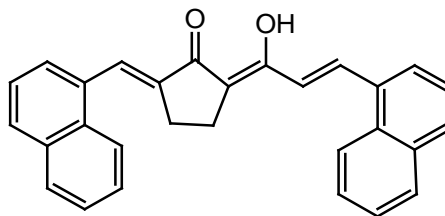


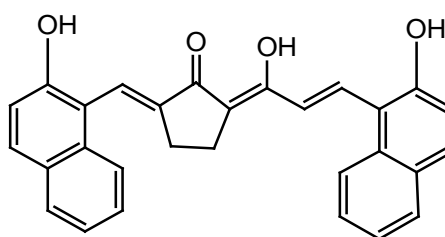
Figure 5.7. Fragmentation pattern of ligands

From the UV, IR, ^1H NMR, ^{13}C NMR and mass spectral data of the compounds, **5a** and **5b** can be formulated as



(2E)-2-(1-naphthyl)-5-((E)-3-(1-naphthyl)acryloyl)cyclopentanone

HL¹ (5a)



(2E)-2-(2-hydroxy-1-naphthyl)-5-((E)-3-(2-hydroxy-1-naphthyl)acryloyl)cyclopentanone

HL² (5b)

From the above structure of ligands, it follows that they can form stable complexes by replacing enolic proton with a metal ion.

5.5 Characterization of metal complexes

Analytical and physical data of the metal complexes are given in **Table 5.4**. The observed carbon, hydrogen and metal percentages of the metal complexes and ESI mass spectral data suggest 1:2 metal-ligand stoichiometry for the complexes.

The specific conductance ($\sim 11 \Omega^{-1} \text{ cm}^{-1}$ in DMF) of metal complexes suggests that they do not contain the anion of the metal salt used for their preparation and they are non-electrolytes. The nickel(II) and zinc(II) complexes are diamagnetic while copper(II) is paramagnetic.

5.5.1 Electronic spectra

The UV spectra of the complexes are characterized by the presence of two absorption maxima, the low energy band corresponds to an $n \rightarrow \pi^*$ transition (486-498 nm) and the high energy band is due to a $\pi \rightarrow \pi^*$ transitions (287-296 nm) (**Table 5.1**). In the metal complexes these absorptions show only a slight bathochromic shifts due the involvement of the carbonyl group in metal complexation (**Table 5.4**). Similarity in the UV absorption maxima of metal complexes with that of free ligands, show that no structural alteration of the ligand has occurred during the complex formation.

In the copper(II) complexes the presence of a broad visible band at ~ 665 nm and the measured μ_{eff} values (1.77–1.83 B.M.) support their square planar structure. The observed diamagnetism and broad medium-intensity band in the region 556-561 nm in the visible spectra of the nickel(II) chelates suggest their square-planar geometry. In conformity with this observation the visible spectra of the nickel chelates in pyridine solution (10^{-3} M) showed three bands corresponding to a configurational change from square-planar to octahedral due to the association of pyridine. The absorption maxima in the regions 1283-1293 nm ($\epsilon = 4.24 \times 10^4 - 4.35 \times 10^4 \text{ M}^{-1} \text{ cm}^{-1}$), 736-770 nm ($\epsilon = 5.34 \times 10^4 - 5.64 \times 10^4 \text{ M}^{-1} \text{ cm}^{-1}$) and 415-429 nm ($\epsilon = 2.34 \times 10^4 - 2.58 \times 10^4 \text{ M}^{-1} \text{ cm}^{-1}$) in the adducts can be assigned to the transitions ${}^3A_{2g} \rightarrow {}^3T_{2g}$; ${}^3A_{2g} \rightarrow {}^3T_{1g}(\text{F})$ and ${}^3A_{2g} \rightarrow {}^3T_{1g}(\text{P})$, respectively.

Table 5.4 Analytical data of copper (II), nickel (II) and Zinc (II) complexes

Complexes (formula weight)	M.p. (°C)	Yield (%)	Elemental analysis % (found /calcd)			UV λ_{\max} (nm)	μ_{eff} BM	Mass spectral data (m/z)
			C	H	Cu			
[Cu(L¹)₂] C ₅₈ H ₄₂ O ₄ Cu (866)	252	61	(80.24) 80.39	(4.58) 4.89	(7.64) 7.33	295 489	1.77	911, 888, 865, 464, 401, 258, 244
[Cu(L²)₂] C ₅₈ H ₄₂ O ₈ Cu (930)	268	63	(74.52) 74.87	(4.39) 4.55	(6.12) 6.83	296 497	1.83	975,952,929,496, 433,274, 260
[Ni(L¹)₂] C ₅₈ H ₄₂ O ₄ Ni (861)	242	68	(80.42) 80.85	(4.84) 4.91	(6.57) 6.81	288 486	-	-
[Ni(L²)₂] C ₅₈ H ₄₂ O ₈ Ni (925)	240	67	(75.94) 75.26	(4.68) 4.57	(6.86) 6.34	292 494	-	-
[Zn(L¹)₂] C ₅₈ H ₄₂ O ₄ Zn (868)	246	54	(80.94) 80.22	(4.12) 4.88	(7.27) 7.53	287 496	-	-
[Zn(L²)₂] C ₅₈ H ₄₂ O ₈ Zn (932)	262	55	(74.06) 74.72	(4.19) 4.54	(6.58) 7.01	294 498	-	-

5.5.2 Infrared Spectra

In the IR spectra of all complexes, the band due to hydrogen bonded carbonyl function in the region 1594-1619 cm^{-1} disappeared and instead a strong band assignable to the stretching of the coordinated carbonyl moiety appeared at $\sim 1590 \text{ cm}^{-1}$. Along with the absence of broad band in the region at 2800-3600 cm^{-1} due to the hydrogen bonded enol proton present in the free ligands and the appearance of two medium intensity bands in the region 464-486 cm^{-1} due to $\nu(\text{M-O})$ vibrations strongly suggest the ligands bind to metal ion through the dicarbonyl moiety. The strong band at $\sim 975 \text{ cm}^{-1}$ is typical of a trans $-\text{CH}=\text{CH}-$ group which remained unaltered in the spectra of metal complexes (Table 5.5).

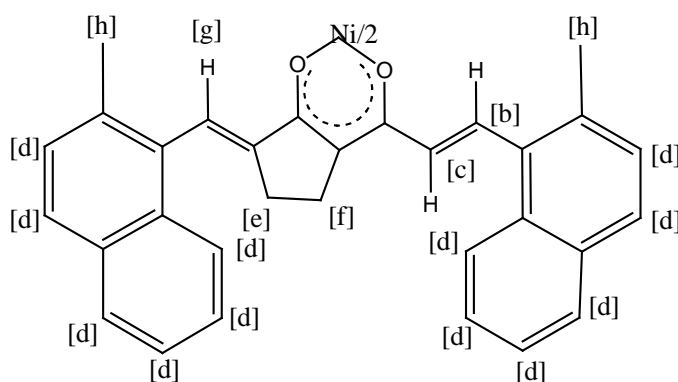
Table 5.5 IR spectral data of complexes

IR spectral data of complexes (cm^{-1})							
Compounds	$\nu(\text{C=O})$ metal chelated carbonyl	$\nu(\text{C=C})$ phenyl	$\nu(\text{C=C})$ alkenyl	$\nu_{\text{as}}(\text{C-C-C})$ chelate ring	$\nu_{\text{as}}(\text{C-C-C})$ chelate ring	$\nu(\text{CH=CH-})$ trans	$\nu(\text{M-O})$ chelate ring
[Cu(L ¹) ₂]	1536,1524	1451	1343	1268	1176	974	482
[Cu(L ²) ₂]	1561,1543	1421	1405	1264	1224	964	464
[Ni(L ¹) ₂]	1544,1521	1412	1346	1252	1143	974	476
[Ni(L ²) ₂]	1542,1534	1428	1426	1284	1276	974	486
[Zn(L ¹) ₂]	1624,1574	1439	1404	1257	1169	956	467
[Zn(L ²) ₂]	1626,1519	1433	1425	1267	1157	968	472

5.5.3 ^1H NMR spectra

The most distinguishing feature of the ^1H NMR spectra of the diamagnetic nickel(II) chelates is the absence of proton signals above $\delta \sim 11$ ppm. This strongly supports the replacement of the enolic proton by the metal ion in the complexes. The ^1H NMR spectra of $[\text{Ni}(\text{L}^2)]_2$ showed a singlet at $\delta = 9.81$ ppm, indicating that the phenolic group is not involved in the metal complex formation. The ^1H NMR spectra are given in **Figures 5.8** and **5.9**. Observed J value approximately 16 Hz for the alkenyl proton signals in the nickel (II) complexes suggest their trans orientation as it is in the free ligands. (**Table 5.6**).

Table 5.6 ^1H NMR spectral data of Ni(II) complexes



Compounds	Chemical shift, ppm (Coupling constant, Hz)							
	[a]	[b]	[c]	[d]	[e]	[f]	[g]	[h]
$[\text{Ni}(\text{L}^1)]_2$	-	6.12 (16.2)	6.46 (16.2)	7.38-7.64	2.59 (5.3)	2.67 (5.3)	7.74	-
$[\text{Ni}(\text{L}^2)]_2$	-	6.32 (16.4)	6.53 (16.4)	7.18-7.69	2.72 (5.3)	2.89 (5.3)	6.71	9.81

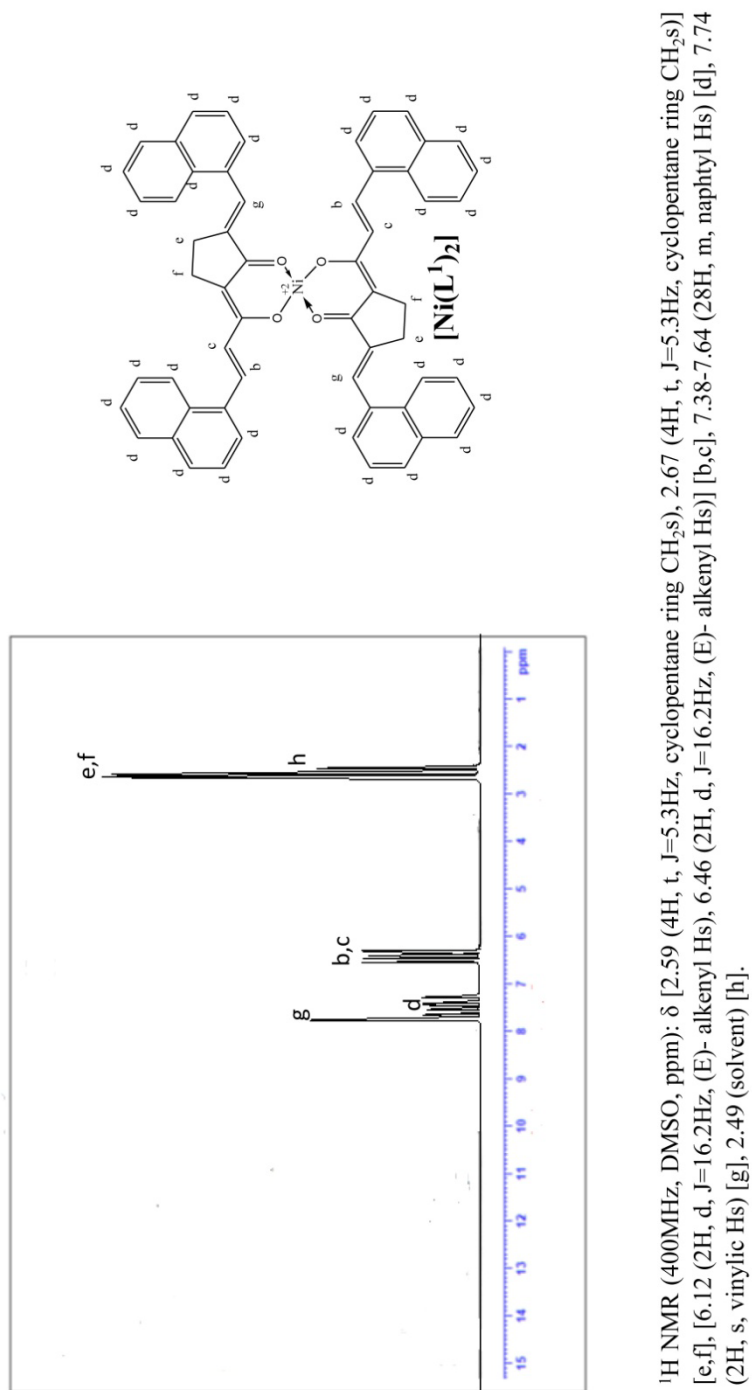


Figure 5.8. ¹H NMR spectrum of [Ni(L)₂]

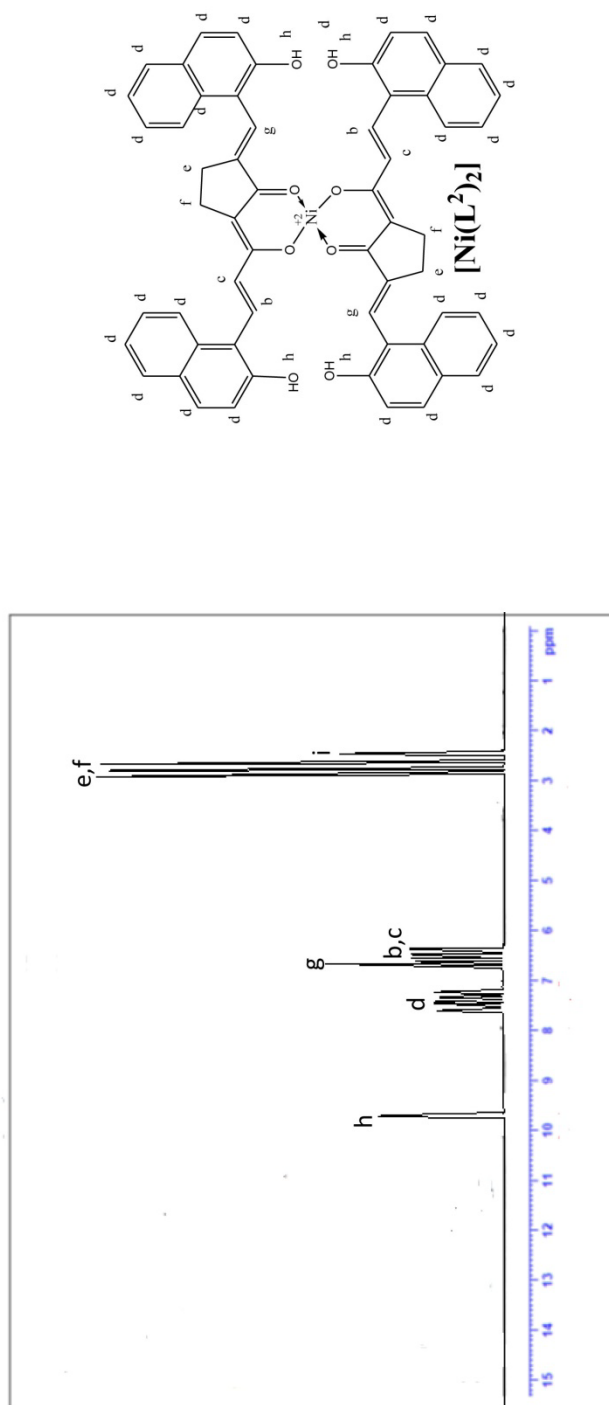
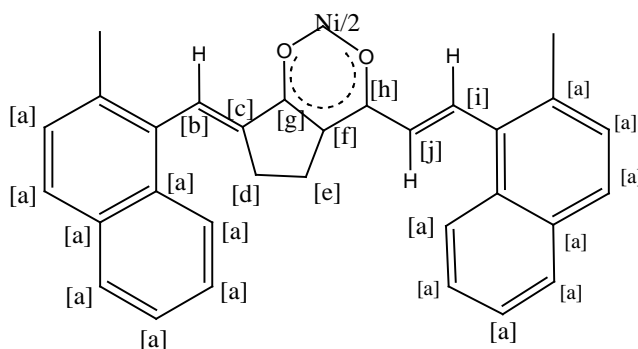


Figure 5.9. ¹H NMR spectrum of [Ni(L²)₂]

5.5.4 ^{13}C NMR spectra

Downfield shift of signal due to the carbonyl carbon resonance by 15-20 ppm is observed in the ^{13}C NMR spectra of nickel(II) complexes (**Table 5.7**) can be correlated with the involvement of carbonyl oxygens in the metal complex formation. The ^{13}C NMR spectra of $[\text{Ni}(\text{L}^1)_2]$ and $[\text{Ni}(\text{L}^2)_2]$ are given in **Figures 5.10** and **5.11**, respectively.

Table 5.7 ^{13}C NMR spectral data of Ni(II) complexes



Compounds	Chemical shift (ppm)									
	[a]	[b]	[c]	[d]	[e]	[f]	[g]	[h]	[I]	[j]
$[\text{Ni}(\text{L}^1)_2]$	123.54-138.67	143.57	129.72	22.54	36.84	96.68	182.46	189.37	115.43	138.18
$[\text{Ni}(\text{L}^2)_2]$	117.38-157.27	142.38	125.67	24.46	36.35	97.28	184.83	193.41	116.54	138.75

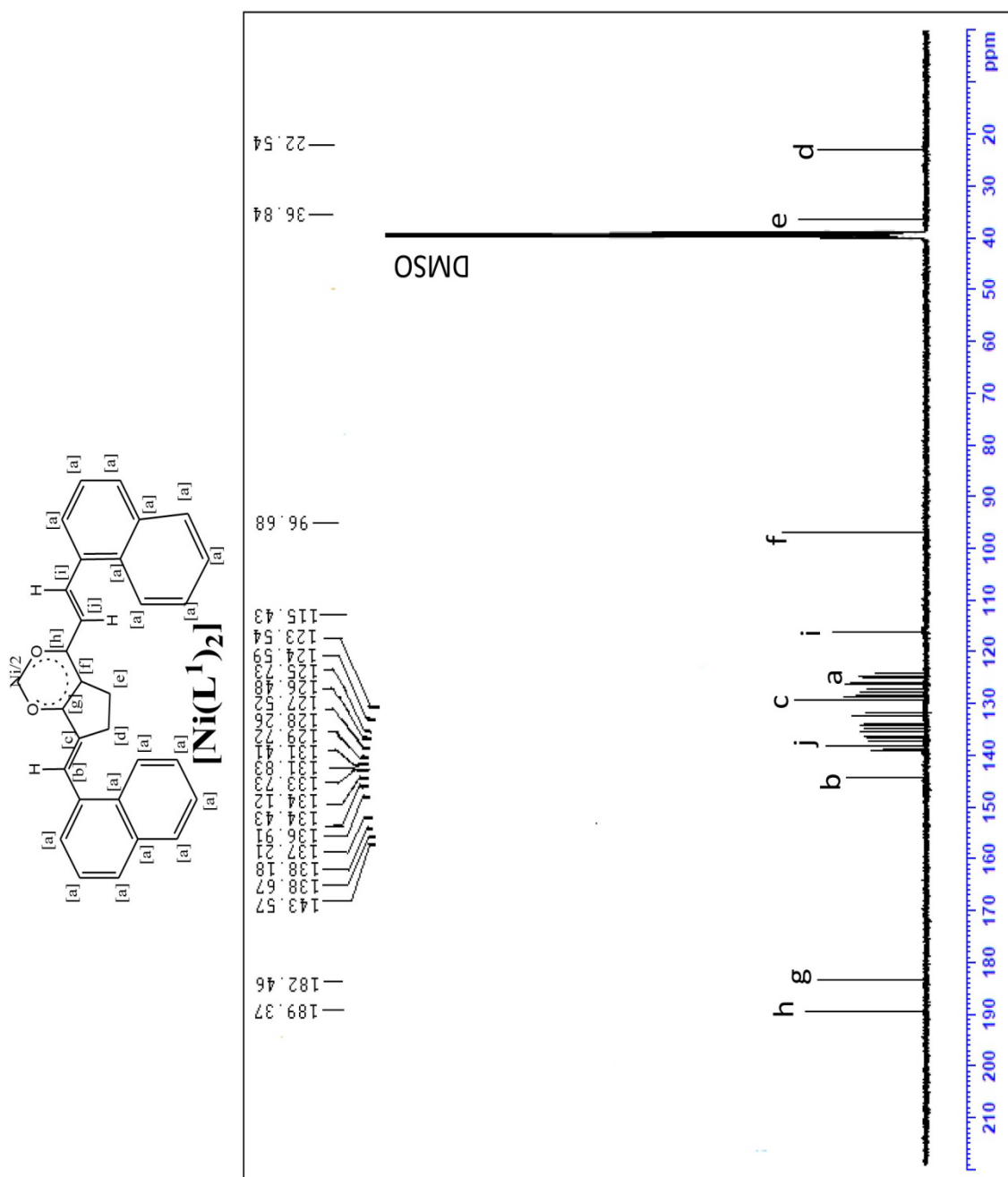


Figure 5.10. ^{13}C NMR spectrum of $[\text{Ni}(\text{L}^1)_2]$

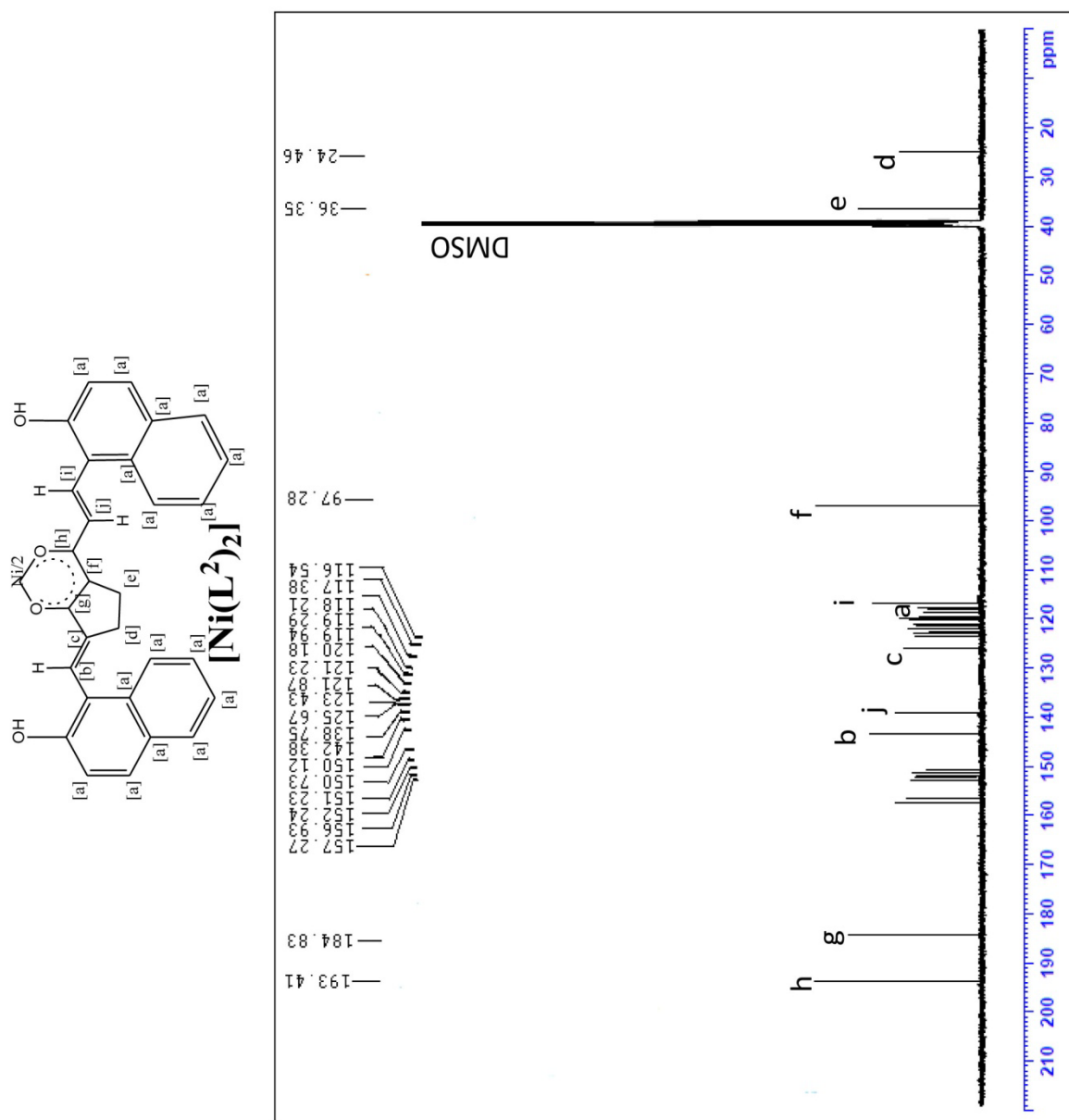
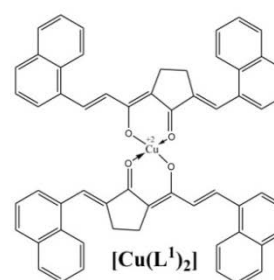
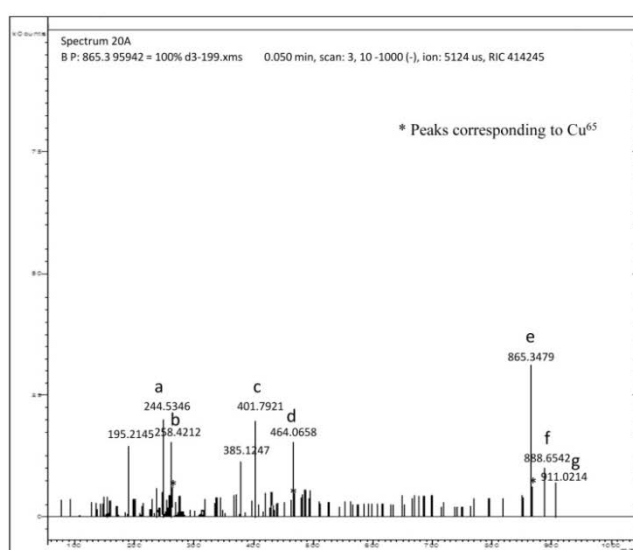


Figure 5.11. ^{13}C NMR spectrum of $[\text{Ni}(\text{L}^2)_2]$

5.5.5 Mass spectra

The ESI mass spectra of the copper(II) chelates confirm the $[ML_2]$ stoichiometry of the complexes. Peaks due to M^+ and $(M+2)^+$ with 3:1 intensity are present in the ESI MS of copper(II) chelates in consistent with the natural abundance of ^{63}Cu and ^{65}Cu isotopes. The mass spectra of the copper(II) chelates are shown in **Figures 5.12** and **5.13**. Peaks due to $[\text{CuL}]^+$, $[\text{CuL-ArCHCHCO}]^+$, $[\text{CuL-ArCHCHCOCH}_2]^+$, L^+ and fragments of L^+ are common to both spectra.



- a – $[\text{Cu}^{63}\text{-ArCHCHCO}]^+$
- b – $[\text{Cu}^{63}\text{-ArCHCHCOCH}_2]^+$
- c – $[\text{L}^1]^+$
- d – $[\text{Cu}^{63}\text{L}^1]^+$
- e – $[\text{Cu}^{63}\text{L}_2]^+$
- f – $[\text{Cu}^{63}\text{L}_2^+ + \text{Na}^+]^+$
- g – $[\text{Cu}^{63}\text{L}_2^+ + 2\text{Na}^+]^+$

Figure 5.12. ESI mass spectrum of $[\text{Cu}(\text{L}^1)_2]$

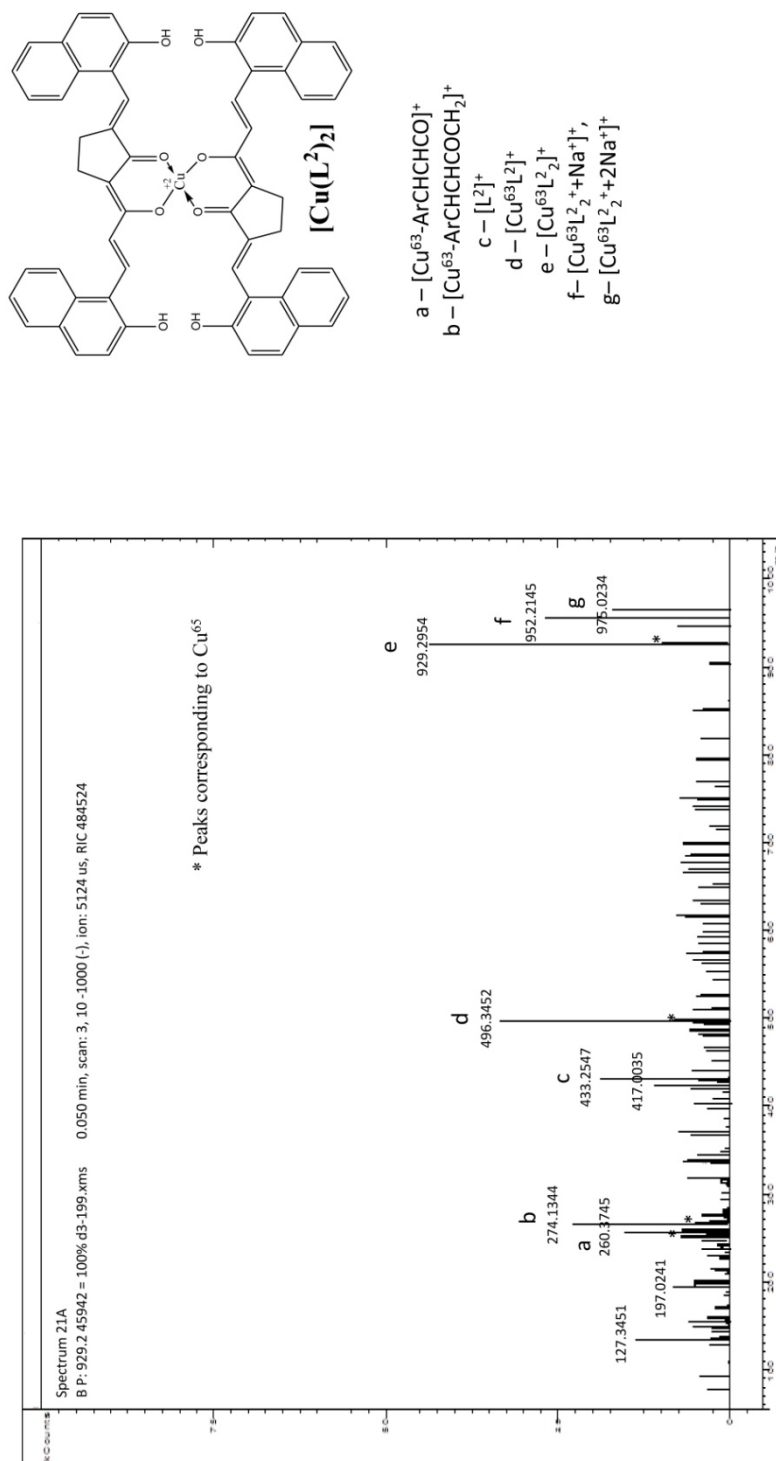
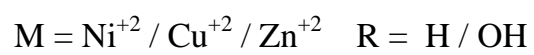
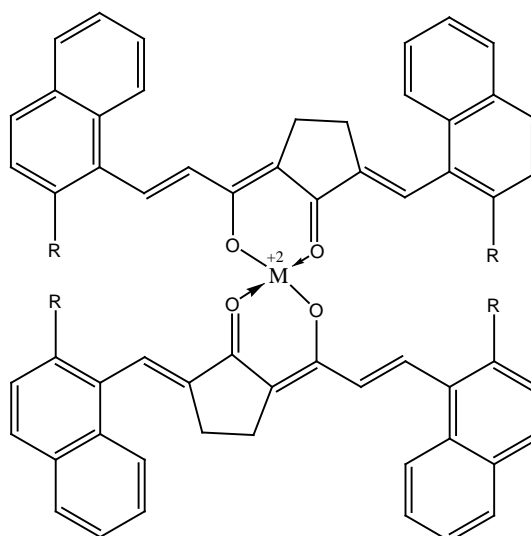


Figure 5.13. ESI mass spectrum of $[\text{Cu}(\text{L}^1)_2]$

Based on the above spectral data, the following structure can be assigned to the metal complexes with ML_2 composition.



RESULTS AND DISCUSSION
PART B
Biological Studies

Curcumin, some of its synthetic analogues and their metal complexes are known to exert a large number of beneficial biological activities. In this context, the possible antioxidant, DNA binding and antitumor activities of curcumin analogues synthesised and their metal complexes described in **Part A** were studied by reported methods. The results obtained are presented here, in three chapters. A comparison of activities is included in each chapter.

The antioxidant activities of all the ligands and their copper(II) and nickel(II) complexes were studied against lipid peroxidation, DPPH scavenging, super oxide scavenging and hydroxyl scavenging. DNA binding properties and cytotoxic activities are performed only with free ligands and their copper(II) complexes.

The same symbolic representation of ligands used in **Part A**, are as such followed in this section. For the sake of convenience, however, representation of metals complexes are slightly modified as **Cu-1a**, **Ni-1a**, etc. instead of $[\text{Cu}(\text{L}^1)_2]$, $[\text{Ni}(\text{L}^1)_2]$, etc.

Chapter 6

STUDIES ON ANTIOXIDANT ACTIVITY

Atmospheric oxygen is an indispensable element for life and oxidative property of oxygen plays a vital role in various biological phenomena. At the same time it has also been recognized as the principal agent responsible for the deterioration of organic materials exposed to air. The parallel role of oxygen, a molecule essential for many forms of life and as a destructive toxic agent for living tissues has been discovered much more recently^[196].

Oxygen is used by the cell to generate energy and free radicals are formed as a consequence of Adenosine Tri Phosphate (ATP) production by the mitochondria. Reactive Oxygen Species (ROS) and Reactive Nitrogen Species (RNS) are the by-products resulting from the cellular redox processes. These reactive species play a dual role in human as both toxic and beneficial compounds. The delicate balance between their two opposite effects is undoubtedly a key aspect of life. At low or moderate levels, reactive species exert beneficial effects on cellular redox signalling and immune function, but at high concentrations, they produce oxidative stress, a harmful process that can damage cell function and structures.^[197]

Free radicals are molecules or molecular fragments containing one or more unpaired electrons and this unpaired electron(s) give a significant degree of reactivity to them. ROS includes superoxide ($O_2^{\cdot-}$), hydroxyl ($\cdot OH$), peroxy ($ROO\cdot$), lipid peroxy ($LOO\cdot$), alkoxy ($RO\cdot$) radicals. Nitrogen free radicals include nitric oxide ($NO\cdot$) and nitrogen dioxide ($NO_2\cdot$). Oxygen and nitrogen free radicals can be readily converted to other non-radical reactive species which are also dangerous for health. Hydrogen peroxide (H_2O_2), ozone

(O₃), singlet oxygen (¹O₂), hypochlorous acid (HOCl), nitrous acid (HNO₂), peroxyxynitrite (ONOO⁻), dinitrogen trioxide (N₂O₃), lipid peroxide (LOOH) are not free radicals and generally named oxidants and can readily lead to free radical reactions in living organisms. Oxidants are also capable of nitrosylating proteins thereby disrupting biological function ^[198,199]. Thus, ROS and RNS include radical and non-radical species; these reactive species are produced in animals and humans under physiologic and pathologic conditions.

Free radicals induced oxidative stress is now believed to be a fundamental mechanism underlying a number of human cardiovascular, neurologic and other disorders. It has been estimated that approximately 5% of inhaled oxygen is converted into several damaging ROS. These ROS may oxidise nucleic acids, proteins, lipids or DNA and can initiate degenerative diseases ^[200].

The mechanism of lipid peroxidation in model systems such as linoleic acid and its esters were well established. The formation of lipid peroxide is given in **Figure 6.1**.

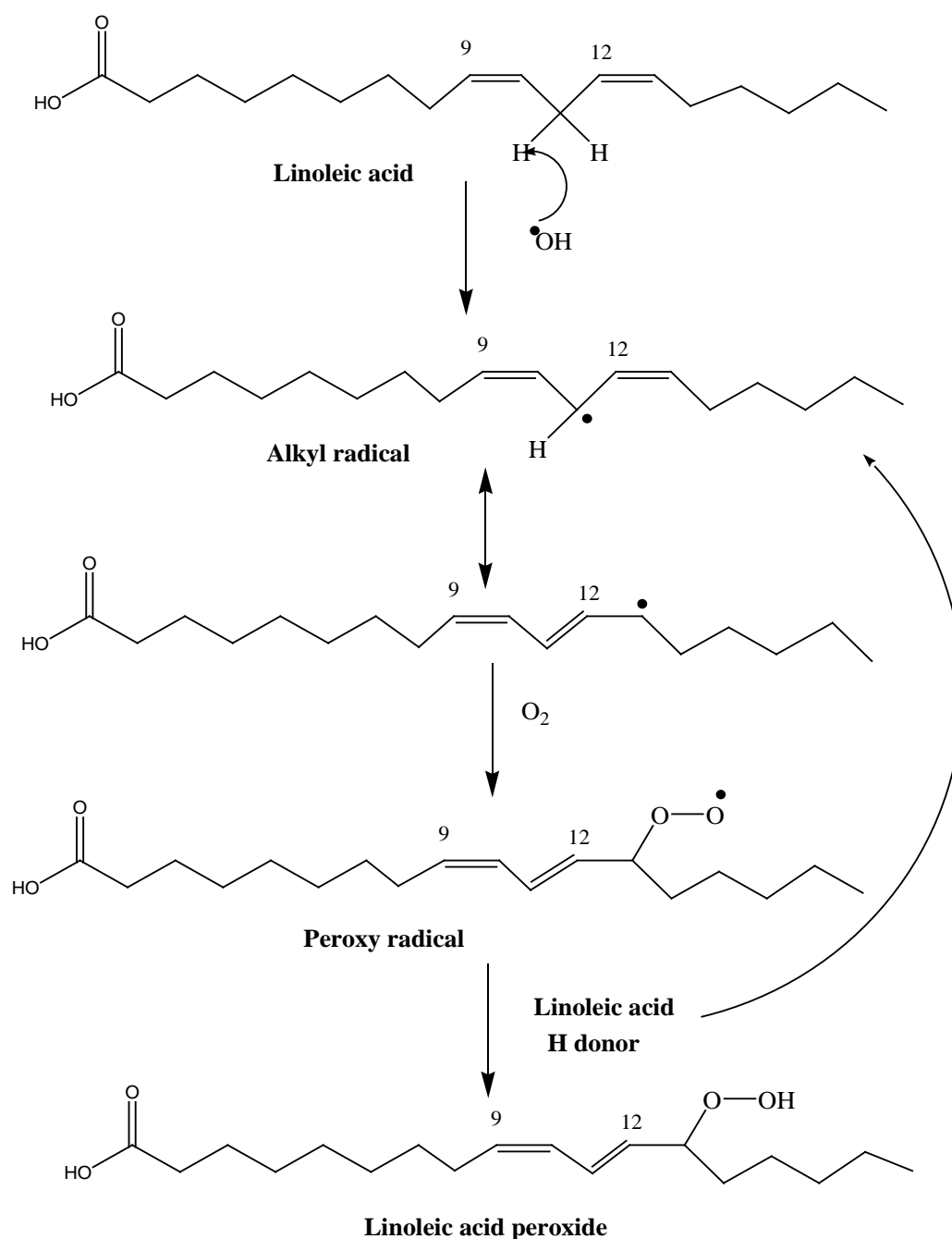


Figure 6.1 Formation of lipid peroxide

An antioxidant is a molecule capable of inhibiting the oxidation of other molecules. The main characteristic of an antioxidant is its ability to trap free radicals. Antioxidants in the diet like vitamin C, vitamin E, carotenes, phenolic acids, and phytoestrogens scavenge free radicals such as peroxide,

hydroperoxide or lipid peroxy and thus inhibit the oxidative mechanisms that lead to degenerative diseases including cancer [201]. They can eliminate free radical induced damage, and are critical for maintaining optimum health and well-being.

Various antioxidant activity methods have been used to monitor and compare the antioxidant activity of compounds. These analytical methods measure the radical scavenging activity of antioxidants against free radicals like the 1,1-diphenyl-2-picrylhydrazyl (DPPH) radical, the superoxide anion radical ($O_2^{\cdot-}$), the hydroxyl radical ($\cdot OH$), or the peroxy radical ($ROO\cdot$) [202]. The various methods used to measure antioxidant activity of compounds can give varying results depending on the specific free radical being used as a reactant.

The different methods adopted to evaluate antioxidant activity of ligands and their metal(II) complexes reported in **Chapters 1-5** are described below.

6.1. DPPH scavenging method

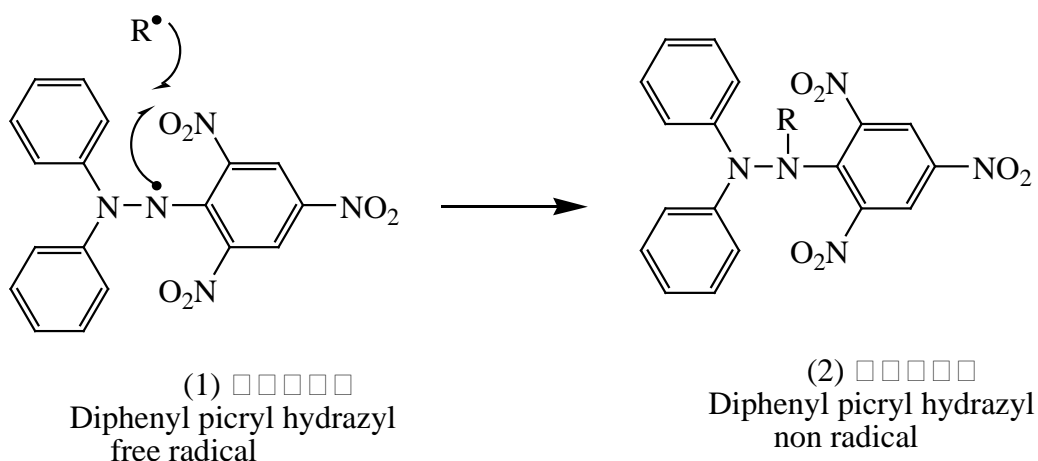
Scavenging of DPPH free radical is a rapid and simple method to monitor the antioxidant activity of chemical compound. The molecule DPPH or 1, 1-diphenyl-2-picrylhydrazyl (1) is characterised as a stable free radical by virtue of the delocalization of the spare electron over the molecule as a whole, so that the molecules do not dimerise, as would be the case with most other free radicals. The delocalisation also gives rise to the deep violet colour characterised by an absorption band in solution centred at about 520nm.

When a solution of DPPH is mixed with that of a substance that can donate a hydrogen atom, then this gives rise to the reduced form (2) with the loss of this violet colour. Representing the DPPH radical by $Z\cdot$ and the donor molecule by AH, the primary reaction is



Where ZH is the reduced form and A[•] is the free radical produced in this first step. This latter radical will then undergo further reactions which control the overall stoichiometry that is the number of molecules of DPPH reduced (decolourised) by one molecule of the reductant

The reaction [1] is therefore intended to provide the link with the reactions taking place in an oxidising system, such as the auto oxidation of a lipid or other unsaturated substance; the DPPH molecule (Z[•]) is thus intended to represent the free radicals formed in the system whose activity is to be suppressed by the substance AH.



DPPH radical scavenging activity was assessed by mixing various concentrations of the sample ranging from 10-100 mg/ml with 5ml of freshly prepared 0.5mM DPPH in DMSO solution. After incubating the mixture at 37°C in the dark for 30 min, the absorbance was measured at 520nm. Lower absorbance at 520nm represents higher DPPH scavenging activity. The % DPPH radical scavenging activity of sample was calculated from the decrease in absorbance at 520nm.

Determination of DPPH free radical scavenging activity

The scavenging activity of the test samples on 1,1-diphenyl-2-picrylhydrazyl (DPPH) analysed by the following general method.^[203]

DPPH solution was incubated at 37°C in the presence of test compounds at different concentrations ranging from 10-100 µg/ml for 30min in the dark and the absorbance at 520 nm was then read. All determinations were performed in triplicate. The DPPH radical scavenging activity ($S\%$) was calculated using the following equation:

$$S\% = ((A_{\text{control}} - A_{\text{sample}})/A_{\text{control}}) \times 100$$

Where A_{control} is the absorbance of the blank control (containing all reagents except the sample solution) and A_{sample} is the absorbance of the test sample.

The $EC_{50\%}$ value (concentration of the test compound decrease the initial DPPH radical concentration by 50%) was determined by plotting $S\%$ against concentration of the test compound (ligand or metal complex).

6.2. Lipid peroxidation method

The effect of all the ligands and their metal complexes on the inhibition of lipid peroxidation was determined by the thiobarbituric acid method. The thiobarbituricacid-reactive-substances (TBARS) assays have been used extensively since the 1950's to estimate the peroxidation of lipids in membrane and biological systems. TBARS are naturally present in biological specimens and include lipid hydroperoxides and aldehydes which increase in concentration as a response to oxidative stress. This assay is based on the reaction of a chromogenic reagent, 2-thiobarbituric acid, with malonaldehyde (malondialdehyde, MDA), a compound that results from the decomposition of polyunsaturated fatty acid lipid peroxides. One molecule of MDA reacts with 2 molecules of 2-thiobarbituric acid *via* a Knoevenagel-type condensation to

yield a chromophore with absorbance maximum at 532 nm, as shown below in **Figure 6.2**.

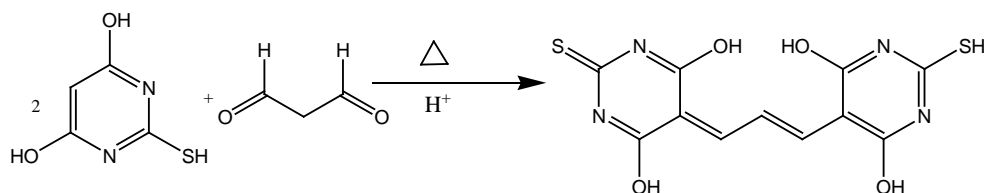


Figure 6.2 Reaction between 2-thiobarbituric acid and MDA under acidic conditions.

Determination of lipid peroxidation inhibitory activity

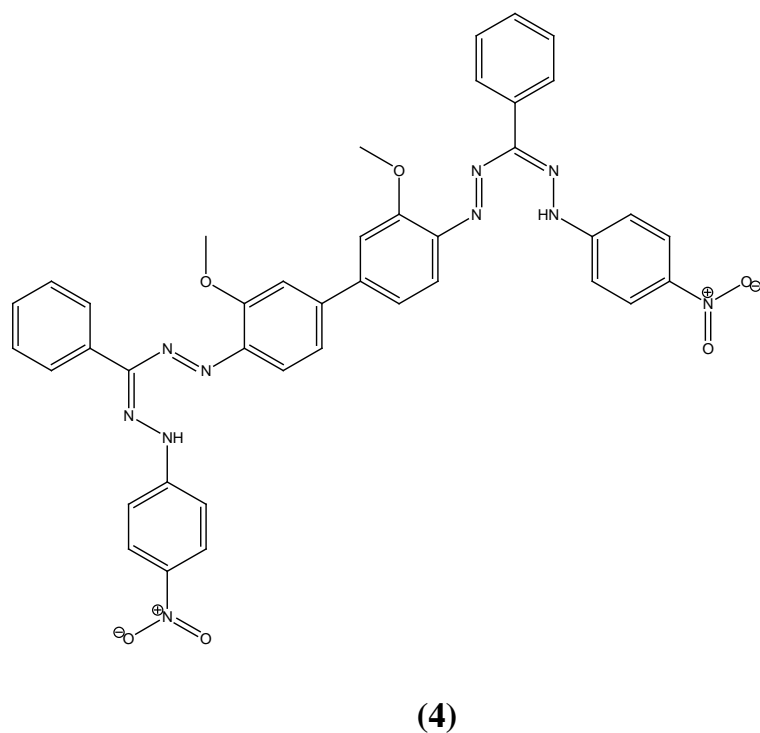
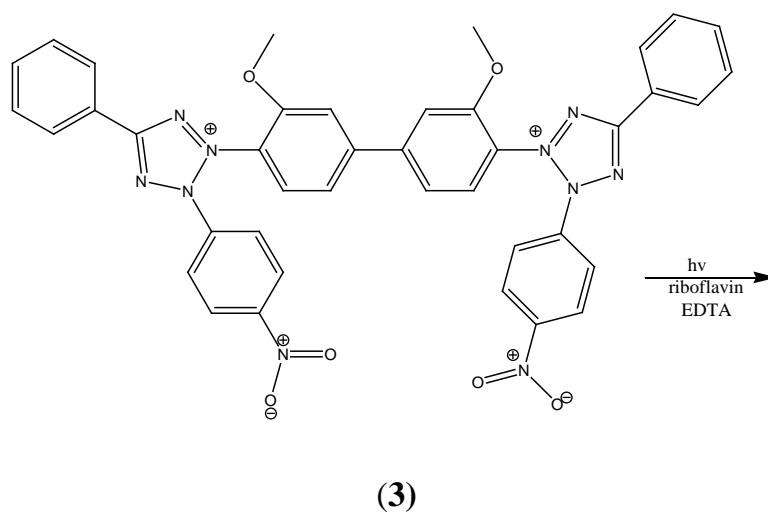
Different concentrations of the test compounds were incubated at 37⁰C with a 25% mice liver homogenate (0.1ml) containing 150mM KCl, tris-HCl buffer (0.2M, pH 7.6), ammonium ferrous sulphate (0.8mM), ascorbic acid (0.3mM) for 1hr. At the end of incubation period, 0.4ml of the reaction mixture was treated with 0.2ml sodium dodecyl sulphate (8%), 1.5ml TBA (0.8%) and 1.5ml acetic acid (20%, pH 3.5). The total volume was made up to 4ml by adding distilled water and kept it in a water bath at 80⁰C for 1hr. After cooling, 1ml distilled water and 5ml butanol –pyridine mixture (15:1 v/v) were added. After vigorous shaking, the tubes were centrifuged and the absorbance of upper layer was read at 532nm ^[204]. The percentage inhibition of lipid peroxidation by the compounds was determined by comparing the absorbance of the control and experimental tubes. The lipid peroxidation inhibitory activity (*S*%) was calculated using the following equation:

$$S\% = ((A_{\text{control}} - A_{\text{sample}})/A_{\text{control}}) \times 100$$

Where A_{control} is the absorbance of the blank control (containing all reagents except the sample solution) and A_{sample} is the absorbance of the test sample. From a plot of *S*% against concentration of test sample, the EC_{50%} value can be obtained.

6.3. Superoxide scavenging method

Super oxide scavenging was determined by the NBT(3) reduction method using riboflavin [205]. Illumination of riboflavin solution in the presence of EDTA causes a reduction of riboflavin. It then re-oxidizes and simultaneously reduces oxygen to O^{2-} , which reduces NBT to NBT-diformazan(4), which absorbs light at 560 nm. The inhibition of formazan production can be monitored by measuring the absorbance at 560 nm.



Determination of super oxide radical scavenging activity

Super oxide scavenging activity of all the ligands and their metal complexes were determined by the NBT reduction method. The reaction mixture contained EDTA (6 μ M) containing 3 μ g NaCN, riboflavin (12 μ M), NBT (50 μ M), various concentration of the test compound and phosphate buffer (67mM, pH 7.8) in a final volume of 3ml. The tubes were uniformly illuminated with an incandescent lamp for 15 min and the absorbance was measured at 560 nm before and after illumination. The percentage inhibition of super oxide generation was evaluated by comparing the absorbance value of the control and experimental tubes. All determinations were performed in triplicate. The super oxide radical scavenging activity ($S\%$) was calculated using the following equation:

$$S\% = ((A_{\text{control}} - A_{\text{sample}})/A_{\text{control}}) \times 100$$

Where A_{control} is the absorbance of the blank control (containing all reagents except the sample solution) and A_{sample} is the absorbance of the test sample. $EC_{50\%}$ values are calculated for the compounds.

6.4. Hydroxy radical method

Hydroxy radical scavenging was measured by studying the competition between deoxy ribose and the test compounds for hydroxyl radicals generated from Fe^{3+} / ascorbate/ EDTA/ H_2O_2 system^[204]. The hydroxyl radical attacks deoxyribose which eventually results in TBARS (Thiobarbituric acid reactive substance) formation as described above.

Determination of hydroxyl radical scavenging activity

Hydroxyl radical scavenging activity was measured by the ability of the ligands and complexes to scavenge the hydroxyl radicals generated by the Fe^{3+} -ascorbate-EDTA- H_2O_2 system. The reaction mixture in a final volume of

1.0 ml contained 100 μ l of 2-deoxyribose (28 mM in 20 mM KH_2PO_4 buffer, pH 7.4), 500 μ l of the test compounds at various concentrations (10-100 μ g/ml) in DMSO, 200 μ l of 1.04 mM EDTA and 200 μ M FeCl_3 (1:1, v/v), 100 μ l of 1.0 mM hydrogen peroxide (H_2O_2) and 100 μ l of 1.0 mM ascorbic acid. The reaction mixture was kept at 37°C for 1 h. The free radical damage imposed on the substrate, 2-deoxyribose was measured using the thiobarbituric acid test. One ml of 1% thiobarbituric acid and 1.0 ml 2.8% trichloroacetic acid were added to the test tubes and was incubated at 100°C for 20 min. After cooling, the absorbance was measured at 532 nm against a blank containing 2-deoxyribose, DMSO and buffer. The percentage inhibition ($S\%$) was calculated using the following equation:

$$S\% = ((A_{\text{control}} - A_{\text{sample}}) / A_{\text{control}}) \times 100$$

Where A_{control} is the absorbance of the blank control (containing all reagents except the sample solution) and A_{sample} is the absorbance of the test sample. $\text{EC}_{50\%}$ values are calculated for each compound.

6.5. Comparison of antioxidant activities

All the four methods described above are spectrophotometric methods^[206]. From a plot of %S activity against the concentration of test sample, concentration of test sample which causes 50% inhibition of free radicals ($\text{EC}_{50\%}$) was calculated. To illustrate the procedure, one plot for each type of study is presented in **Figures 6.3-6.6**. In other cases also similar plots are drawn and the $\text{EC}_{50\%}$ values obtained were tabulated below (**Tables 6.1-6.5**).

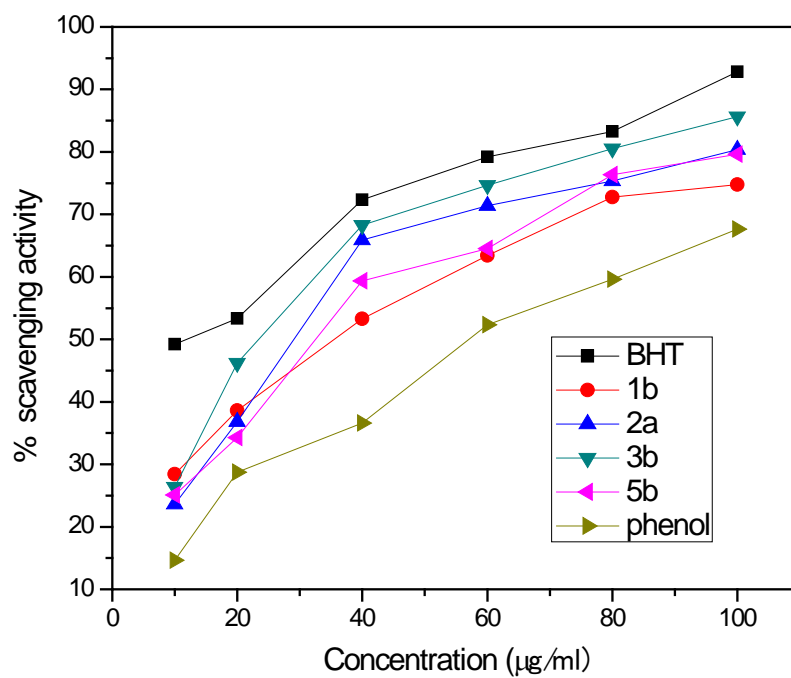


Figure 6.3. DPPH radical scavenging activity of selected ligands; BHT as control and phenol for comparison

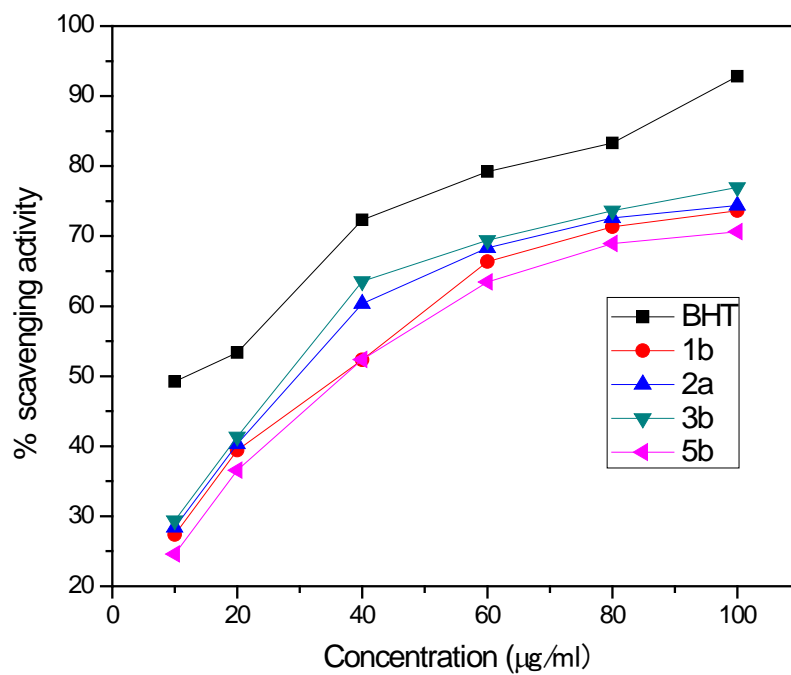


Figure 6.4. Super oxide radical scavenging activity of selected ligands

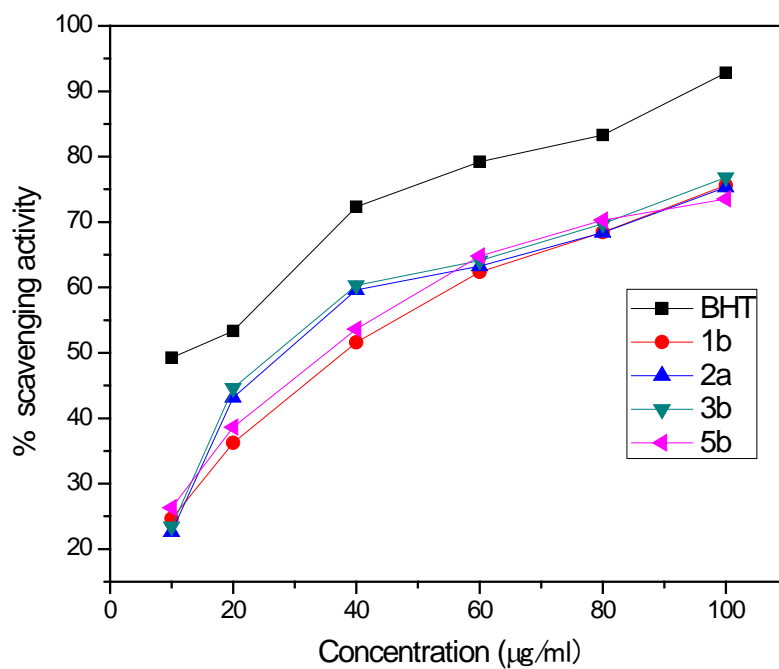


Figure 6.5. Lipid peroxidation activity of selected ligands

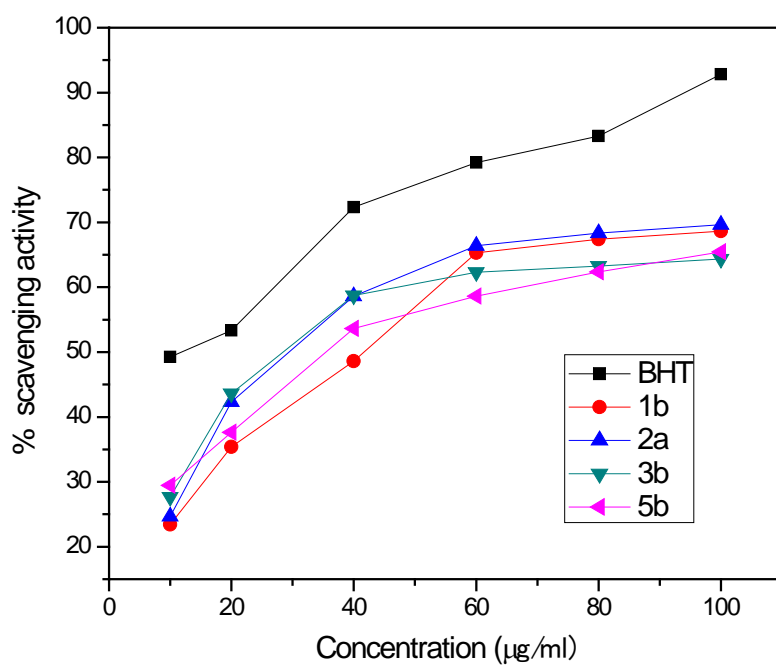


Figure 6.6. Hydroxyl radical scavenging activity of selected ligands

Table 6.1. Antioxidant activity of compounds (**1a-1c**) and their Cu(II) and Ni(II) complexes

Compounds	EC ₅₀ value ^a (μgml^{-1})			
	DPPH radical scavenging activity	Super oxide radical scavenging activity	Lipid peroxidation Inhibitory activity	Hydroxy radical scavenging activity
BHT	12±1.3	14±2.7	17±1.6	18±2.1
1a	54±2.6	57±2.4	58±1.8	59±2.3
Cu-1a	68±2.2	74±2.6	82±2.9	85±2.8
Ni-1a	61±3.2	67±2.4	68±2.3	71±2.4
1b	36±2.7	37±1.9	38±1.8	39±2.7
Cu-1b	64±1.4	67±2.7	69±3.1	70±2.3
Ni-1b	57±3.5	58±3.8	59±2.9	58±2.6
1c	42±1.3	47±2.7	43±1.7	48±2.6
Cu-1c	67 ±3.1	68±3.3	75±3.1	78±3.3
Ni-1c	58±2.4	61±2.5	62±1.8	63±2.1
Phenol	57±3.2	53±3.3	59±3.1	61±3.4

^aEach value represents mean of three different observations \pm S.D.

Table 6.2. Antioxidant activity of compounds (**1d-1f**) and their Cu(II) and Ni(II) complexes

Compounds	EC ₅₀ value ^a (μgml^{-1})			
	DPPH radical scavenging activity	Super oxide radical scavenging activity	Lipid peroxidation Inhibitory activity	Hydroxy radical scavenging activity
1d	52±1.8	53±2.1	57±3.4	54±2.3
Cu-1d	74±3.4	77±3.2	81±2.6	87±3.7
Ni-1d	59±2.3	63±2.4	67±2.6	66±2.7
1e	59±2.3	61±2.4	67±2.9	69±2.8
Cu-1e	84±2.5	86±2.3	84±2.2	91±3.3
Ni-1e	64±3.6	65±2.9	71±2.8	73±3.4
1f	61±2.1	63±2.6	67±1.8	72±1.6
Cu-1f	86±2.9	87±3.1	94±3.9	96±3.4
Ni-1f	71±2.3	74±2.6	75±2.8	78±2.4

^aEach value represents mean of three different observations \pm S.D.

Table 6.3. Antioxidant activity of compounds (**2a-2e**) and their Cu(II) and Ni(II) complexes

Compounds	EC ₅₀ value ^a (μgml^{-1})			
	DPPH radical scavenging activity	Super oxide radical scavenging activity	Lipid peroxidation Inhibitory activity	Hydroxy radical scavenging activity
2a	28 \pm 2.6	29 \pm 2.8	30 \pm 1.4	31 \pm 2.4
Cu-2a	63 \pm 2.4	64 \pm 2.1	67 \pm 2.7	69 \pm 2.6
Ni-2a	42 \pm 3.4	47 \pm 2.3	50 \pm 2.7	51 \pm 2.3
2b	29 \pm 2.1	28 \pm 1.9	27 \pm 1.5	30 \pm 2.3
Cu-2b	64 \pm 1.4	67 \pm 2.1	69 \pm 3.3	70 \pm 2.4
Ni-2b	44 \pm 3.2	46 \pm 2.8	53 \pm 1.9	56 \pm 2.3
2c	30 \pm 1.3	31 \pm 2.2	34 \pm 1.8	37 \pm 2.3
Cu-2c	66 \pm 3.5	65 \pm 3.7	69 \pm 3.7	75 \pm 3.2
Ni-2c	47 \pm 2.8	49 \pm 2.5	57 \pm 1.6	59 \pm 1.9
2d	38 \pm 1.5	39 \pm 2.6	41 \pm 3.5	40 \pm 1.3
Cu-2d	69 \pm 3.4	74 \pm 3.1	78 \pm 2.9	79 \pm 3.7
Ni-2d	57 \pm 2.5	56 \pm 2.3	61 \pm 2.8	63 \pm 2.9
2e	41 \pm 2.3	43 \pm 2.5	46 \pm 2.9	48 \pm 2.8
Cu-2e	70 \pm 2.4	73 \pm 2.8	76 \pm 2.9	81 \pm 3.4
Ni-2e	61 \pm 3.2	62 \pm 2.7	67 \pm 2.6	68 \pm 3.4

^aEach value represents mean of three different observations \pm S.D.

Table 6.4. Antioxidant activity of compounds (**3a-3c**) and their Cu(II) and Ni(II) complexes

Compounds	EC ₅₀ value ^a (μgml^{-1})			
	DPPH radical scavenging activity	Super oxide radical scavenging activity	Lipid peroxidation Inhibitory activity	Hydroxy radical scavenging activity
3a	26 \pm 2.1	27 \pm 3.2	28 \pm 1.7	30 \pm 2.6
Cu-3a	61 \pm 2.5	63 \pm 2.6	64 \pm 2.8	65 \pm 2.3
Ni-3a	43 \pm 3.1	45 \pm 2.4	47 \pm 2.6	49 \pm 2.2
3b	24 \pm 2.4	27 \pm 1.9	26 \pm 1.7	29 \pm 2.8
Cu-3b	41 \pm 1.2	40 \pm 2.1	42 \pm 2.3	44 \pm 2.7
Ni-3b	42 \pm 3.3	44 \pm 2.7	46 \pm 1.8	48 \pm 1.3
3c	30 \pm 1.5	34 \pm 2.6	33 \pm 1.9	35 \pm 2.4
Cu-3c	68 \pm 3.5	71 \pm 3.7	74 \pm 3.7	76 \pm 3.3
Ni-3c	68 \pm 3.5	71 \pm 3.7	74 \pm 3.7	76 \pm 3.3

^aEach value represents mean of three different observations \pm S.D.

Table 6.5. Antioxidant activity of compounds (**4a-5b**) and their Cu(II) and Ni(II) complexes

Compounds	EC ₅₀ value ^a (μgml^{-1})			
	DPPH radical scavenging activity	Super oxide radical scavenging activity	Lipid peroxidation Inhibitory activity	Hydroxy radical scavenging activity
4a	32 \pm 2.1	37 \pm 2.3	40 \pm 2.2	41 \pm 2.6
Cu-4a	73 \pm 3.7	76 \pm 3.2	77 \pm 3.8	79 \pm 3.6
Ni-4a	47 \pm 2.8	49 \pm 2.1	46 \pm 1.4	44 \pm 1.3
4b	27 \pm 2.6	31 \pm 2.2	34 \pm 1.9	37 \pm 2.8
Cu-4b	68 \pm 3.3	67 \pm 2.3	69 \pm 2.8	70 \pm 2.3
Ni-4b	41 \pm 3.6	37 \pm 2.4	39 \pm 1.7	45 \pm 2.6
5a	34 \pm 2.7	38 \pm 2.2	39 \pm 1.6	42 \pm 2.6
Cu-5a	68 \pm 3.9	70 \pm 3.2	71 \pm 3.1	76 \pm 3.7
Ni -5a	43 \pm 3.3	45 \pm 2.6	49 \pm 1.3	49 \pm 1.8
5b	32 \pm 2.4	37 \pm 2.4	35 \pm 1.8	36 \pm 3.2
Cu-5b	63 \pm 3.8	66 \pm 2.8	67 \pm 2.7	69 \pm 2.4
Ni-5b	40 \pm 3.1	39 \pm 2.4	42 \pm 1.6	44 \pm 1.3

^aEach value represents mean of three different observations \pm S.D.

From the data, it follows that ligands having hydroxyl group in the phenyl rings are more active than the parent unsubstituted ligand. The presence of electron releasing groups also increased activity. Among the ligands **1a-1f**, **1b** with hydroxyl group at *ortho* position and among the ligands **2a-2e**, **2a** with hydroxy group at *para* position are nearly 2 times more active than their unsubstituted counter part **1a**. A similar comparison can be drawn from the EC_{50%} values of **5b** and **5a**. These results show that the lipid peroxidation activity of ligands is through the formation of relatively stable phenoxy radical.

However, the activities of ligands with no phenolic group are greater than phenol suggesting the involvement of enolic proton in the radical formation and the stability of resulting free radical may be due to conjugation. Among the ligands **3a-3c**, **3b** with two hydroxyl groups is found to be more active than the others. The activity of **3c** having no phenolic groups suggest that enolic proton abstraction is also possible as in the case of ligands like **1a**. Therefore, it can be concluded that free radical is generated from enolic proton if phenolic OH group is not present in the ligand and in the case of ligand having phenolic OH groups, both phenolic and enolic hydrogen abstraction are possible. A comparison of activity of free ligands having hydroxyl group against DPPH scavenging activity is shown in **Figure 6.7**. Similar results are also obtained from the other three methods. The ligand **3b** with two phenolic OH groups is found to have highest activity in all the four methods.

Metal complexation has been reduced activity in all cases irrespective on the nature of ligands or metal ions. It is presumably due to replacement of enolic proton and this observation also indicating that the complexes are stable under the conditions employed for the assay. Complexes of ligands having phenolic OH group (**1b**, **2a**, **3a**, **3b** and **5b**) have activity, but the magnitude is slightly lower than the corresponding free ligands. It may probably due to the absence of enolic proton in the complex. Another major conclusion that can be

drawn from the $EC_{50\%}$ values is that the presence of nitro and chloro functionalities in the phenyl rings very little influence on antioxidant activities. It is interesting to note that these functional groups are not common in natural or synthetic antioxidants like BHT.

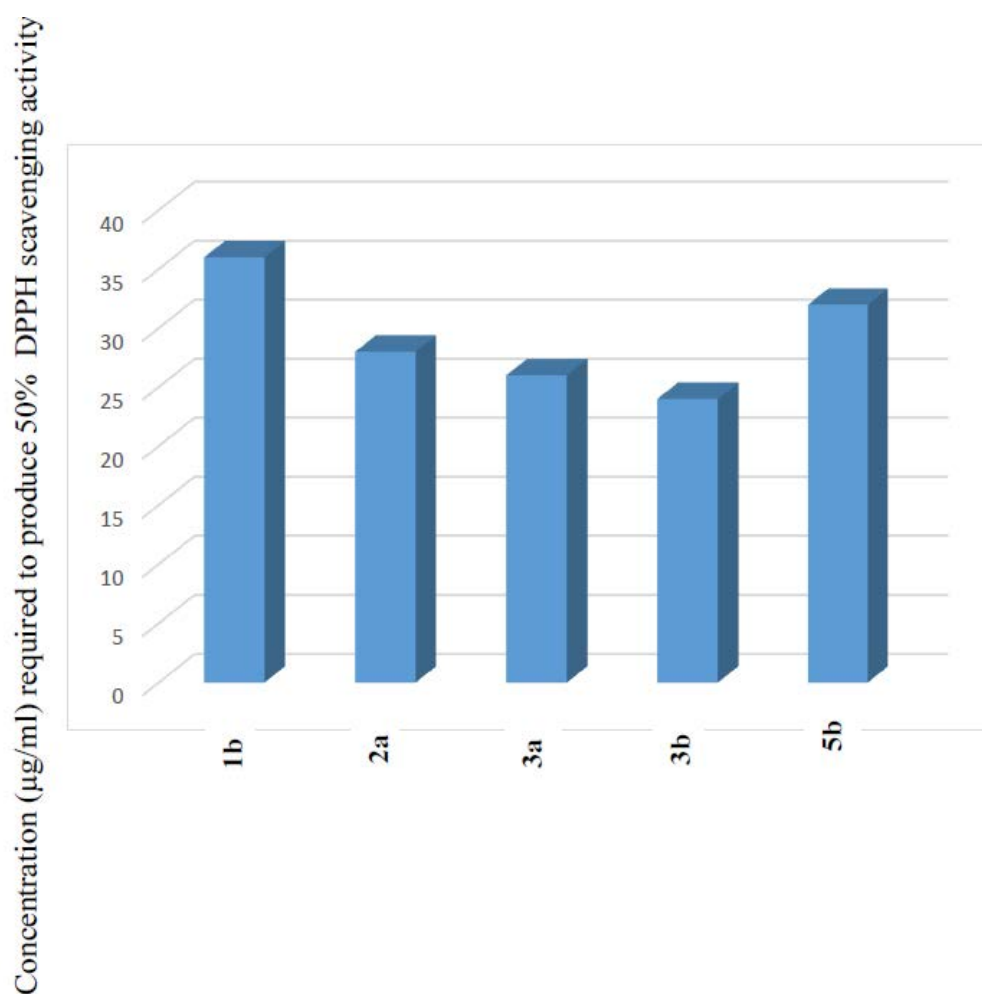


Figure 6.7. $EC_{50\%}$ values of DPPH radical scavenging activity for selected ligands having phenolic OH group(s)

Chapter 7

STUDIES ON DNA BINDING PROPERTIES

The mode of action of anticancer drugs including cisplatin involves an irreversible binding with DNA, usually to two adjacent nitrogen bases like guanine, and the cell, unable to replicate, defaults to apoptosis (that is, controlled cell death)^[207]. In the development of anticancer drugs, interest in copper complexes has been raised recently due to many reasons. The prominent among them are broader spectrum of activity, a lower toxicity profile than platinum drugs and their ability to bind with DNA through covalent/ non-covalent interactions. According to these observations, a high number of copper complexes has been and is still being tested as DNA-targeting agents.

Strong affinities towards DNA and DNA binding capacity is of great significance in their role as anticancer drugs. In order to study the binding affinity of the synthetic analogues of curcumin and their metal (II) complexes reported here, they were subjected to DNA binding studies at room temperature by taking CT-DNA as model DNA^[17].

The following three methods were adopted to evaluate the capability of compounds to bind with DNA.

7.1. UV spectrometric method

UV-vis absorption spectrophotometry was used to monitor the interactions of ligand and copper complexes with CT-DNA at 7.2 pH in double distilled water containing tris-(hydroxymethyl)amino methane (Tris, 10^{-2} M). The ratio of UV absorbance of the stock solution of CT-DNA in 5 mM Tris-HCl/50 mM NaCl buffer (pH 7.2) at 260 and 280 nm gives a ratio of 1.7–1.8, indicating that CT-DNA was sufficiently free of protein^[208,209].The

concentration of the freshly prepared CT-DNA solution was determined spectrophotometrically at 260 nm ($\epsilon = 6600 \text{ M}^{-1} \text{ cm}^{-1}$)^[13].

Adsorption spectral studies

The binding experiments were carried out by recording the absorbance changes on adding increasing concentrations of DNA (0 – 250 μM) against a fixed concentration of the ligand and copper complexes (50 μM); λ_{max} and absorbance values of pure DNA, ligand, and copper complexes in buffer solutions were recorded. An amount of 2.0 ml of each solution of DNA and ligand or metal complex were mixed together and their λ_{max} and absorbance values were recorded. The absorption spectra were recorded after each addition of different concentrations of DNA solution^[210].

DNA binding properties

The changes in the spectral absorbance of DNA in the presence of ligands and complexes are the evidences for their interactions with DNA. The DNA binding affinities of free ligands and their complexes were quantitatively studied by calculating the intrinsic binding constants (K_b) from the changes in absorbance of $\pi \rightarrow \pi^*$ spectral band (254–268 nm) with increasing concentration of DNA, by using the equation^[211]

$$[\text{DNA}]/(\epsilon_a - \epsilon_f) = [\text{DNA}]/(\epsilon_b - \epsilon_f) + 1/K_b(\epsilon_b - \epsilon_f)$$

where [DNA] is the concentration of DNA in base pairs, the apparent absorption coefficients ϵ_a , ϵ_f , and ϵ_b correspond to $A_{\text{obs}}/[\text{Compound}]$, the extinction coefficient for the free compound, and the extinction coefficient for the compound in the fully bound form, respectively. From the slope and the intercept of the linear fit of the plot of $[\text{DNA}]/[\epsilon_a - \epsilon_f]$ versus [DNA], the intrinsic binding constant, K_b , can be obtained.

Intercalation of foreign molecules into DNA usually results in hypochromism or hyperchromism as the intercalation involves some kind of interaction between the molecule and the DNA base pairs^[212]. Hypochromism arises from the contraction of CT-DNA in the helix axis and its conformational changes. Meanwhile, hyperchromism results from the secondary damage of the DNA double helix structure, in which the extent of hyperchromism is indicative of partial or non-intercalative binding modes. The observed hypochromism is due to the interaction between the π^* orbitals of the intercalated compounds with the π orbitals of the DNA base pairs, thereby decreasing the $\pi \rightarrow \pi^*$ transition energies^[213]. The hypochromism of the metal complexes are greater than that of free ligands and it is due to additional interaction with positively charged metal ion or even due to the replacement of a ligand with nitrogen bases of DNA. In addition, OH, as an electron donating group, will increase the electron density on the intercalating ligands, hence reinforcing the repulsion between the complex and DNA with the negatively charged phosphate backbone, and consequently destabilize the DNA-complex system, causing a decrease in the DNA-binding affinity^[214].

The absorption spectra of 50 μM test compounds were recorded in the absence and presence of CT-DNA (0–250 μM). Since the absorption spectra obtained are very similar probably due to the similarity in the molecular structure, the absorption spectra of representative ligands and their copper(II) complexes are only presented here. Among the set of ligands studied, those having electron releasing group(s) have higher binding constant than the others.

Absorption spectra display clear hypochromism with slight red shift of 3–9 nm. The observed hypochromism is due to the interaction between the π^* orbitals of the intercalated compounds with the π orbitals of the DNA base pairs, thereby decreasing the $\pi \rightarrow \pi^*$ transition energies^[215]. In our studies, it is found that the hypochromism of the copper complexes are greater than that of

free ligands and it may be due to additional interaction with positively charged metal ion or even due to the replacement of a ligand with nitrogen bases of DNA. Even though the exact reason is not known, it may probably due to the involvement of copper(II) ions^[216,217]. The intrinsic binding constants (K_b) obtained for free ligands and their metal complexes are given in **Table 7.1**. The values are comparable to that reported for DNA intercalative complexes. We propose that the weak hypochromism observed in UV-vis spectra probably arises from the partial intercalation of complexes into CT-DNA, in which the planarity of pseudo aromatic metal- chelate ring and the steric hindrance of the phenyl substituent might reduce the inserting degree of complex to DNA. In addition, presence of electron donating groups (OH and OCH_3), will increase the electron density on the intercalating ligands. The absorption spectra of all ligands and their copper(II) complexes having either OH/ OCH_3 groups or both are shown in **Figures 7.1-7.16**.

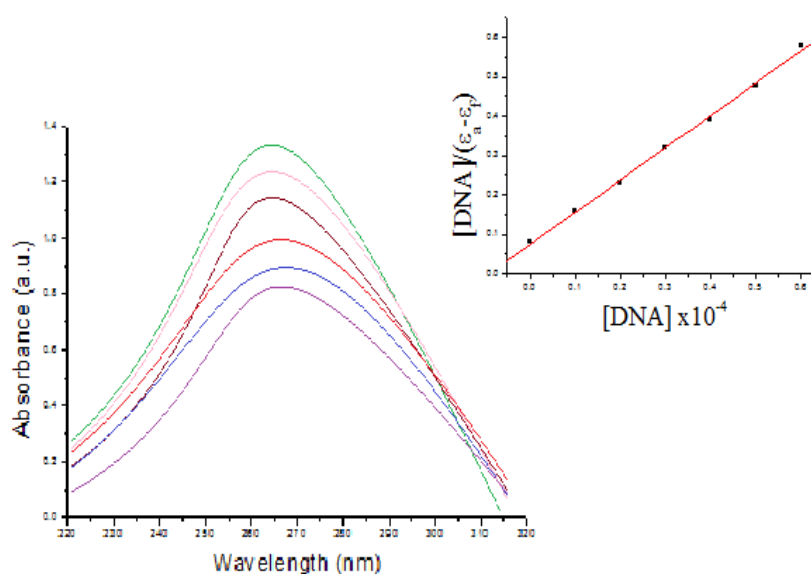


Figure 7.1. Absorption spectra of **1b** ($50 \mu\text{M}$) in the absence and presence of increasing amounts of CT-DNA ($0 - 250 \mu\text{M}$) at room temperature in Tris-HCl/NaCl buffer (pH 7.2). Inset: plot of $[\text{DNA}]/(\epsilon_a - \epsilon_f)$ vs. $[\text{DNA}]$ for absorption titration of CT-DNA with **1b**

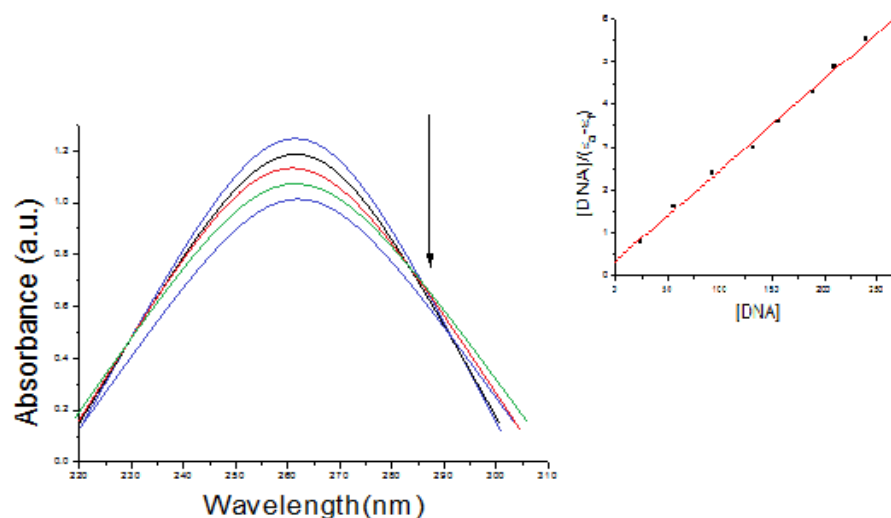


Figure 7.2. Absorption spectra of **Cu-1b** (50 μM) in the absence and presence of increasing amounts of CT-DNA (0 – 250 μM) at room temperature in Tris-HCl/NaCl buffer (pH 7.2). The arrow shows the effect of increasing of CT-DNA concentration on the absorption intensity. Inset: plot of $[\text{DNA}]/(\epsilon_a - \epsilon_f)$ vs. $[\text{DNA}]$ for absorption titration of CT-DNA with **Cu-1b**

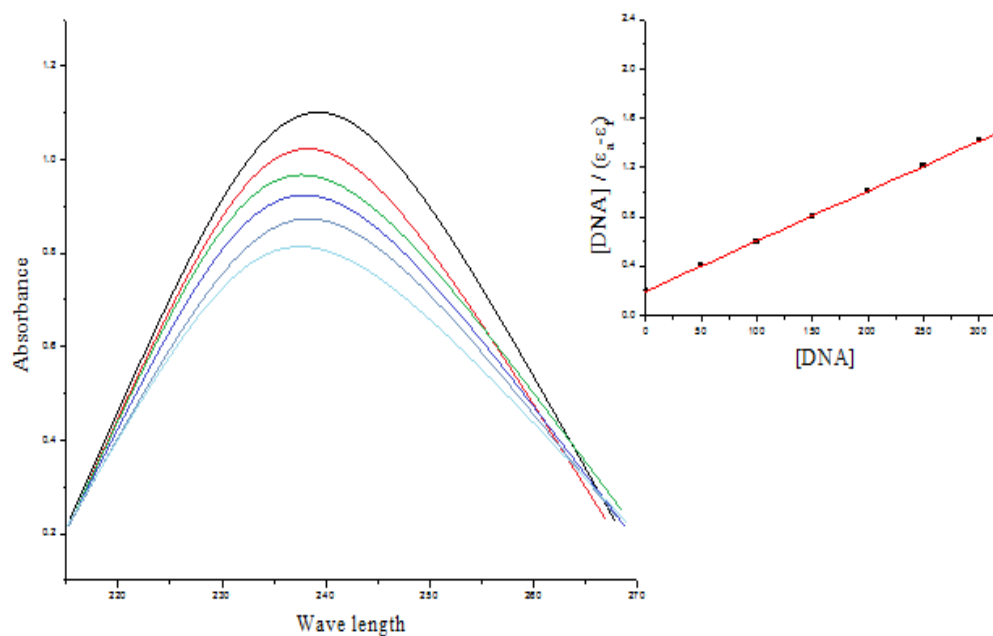


Figure 7.3. Absorption spectra of **1c** (50 μM) in the absence and presence of increasing amounts of CT-DNA (0 – 250 μM) at room temperature in Tris-HCl/NaCl buffer (pH 7.2). Inset: plot of $[\text{DNA}]/(\epsilon_a - \epsilon_f)$ vs. $[\text{DNA}]$ for absorption titration of CT-DNA with **1c**

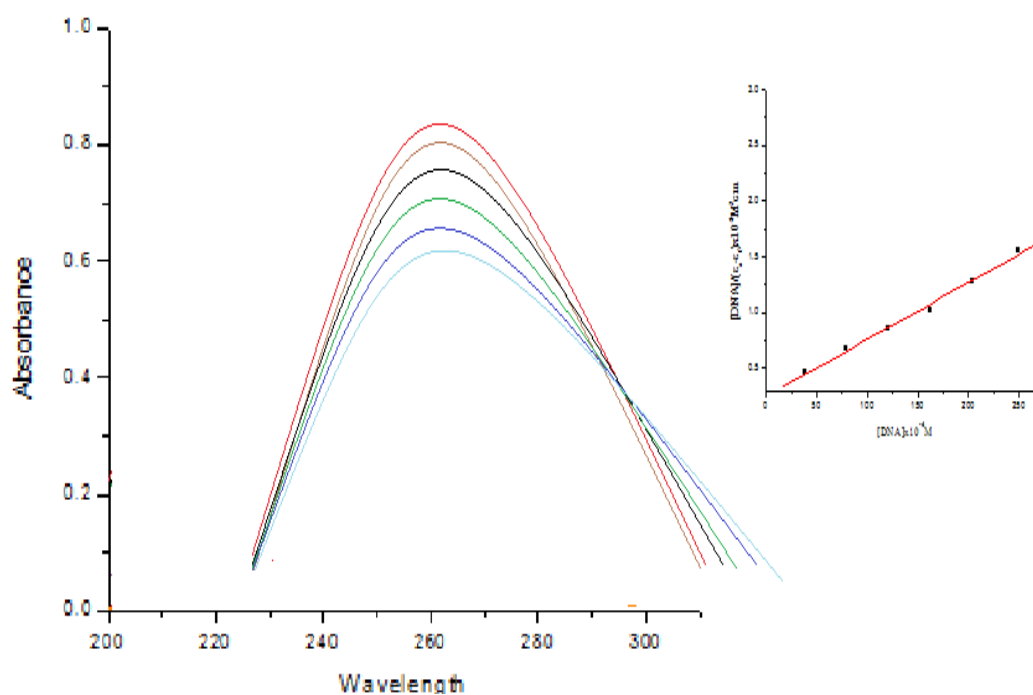


Figure 7.4. Absorption spectra of **Cu-1c** (50 μM) in the absence and presence of increasing amounts of CT-DNA (0 – 250 μM) at room temperature in Tris-HCl/NaCl buffer (pH 7.2). Inset: plot of $[\text{DNA}]/(\epsilon_a - \epsilon_f)$ vs. $[\text{DNA}]$ for absorption titration of CT-DNA with **Cu-1c**

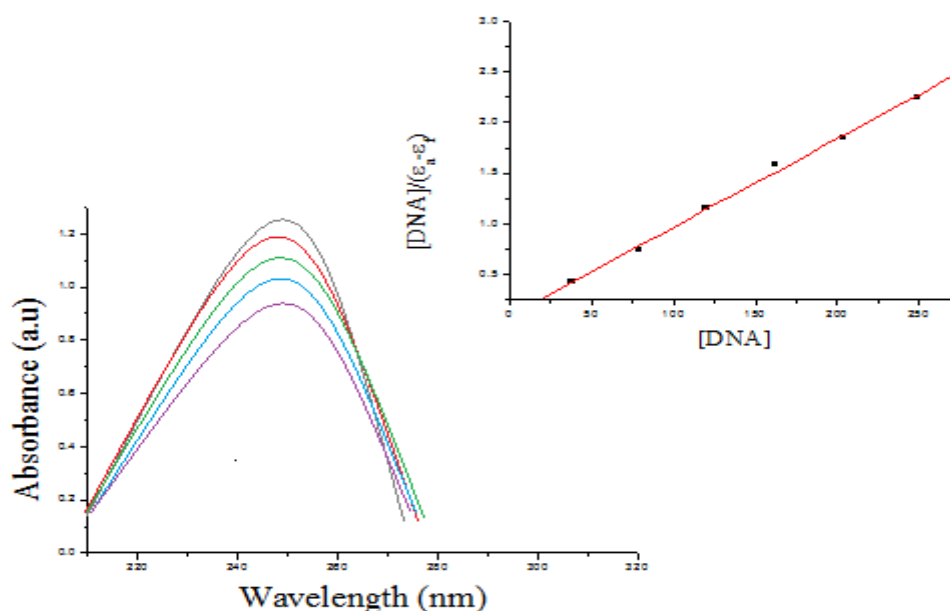


Figure 7.5. Absorption spectra of **2a** (50 μM) in the absence and presence of increasing amounts of CT-DNA at room temperature in Tris-HCl/NaCl buffer (pH 7.2). Inset: plot of $[\text{DNA}]/(\epsilon_a - \epsilon_f)$ vs. $[\text{DNA}]$ for absorption titration of CT-DNA with **2a**

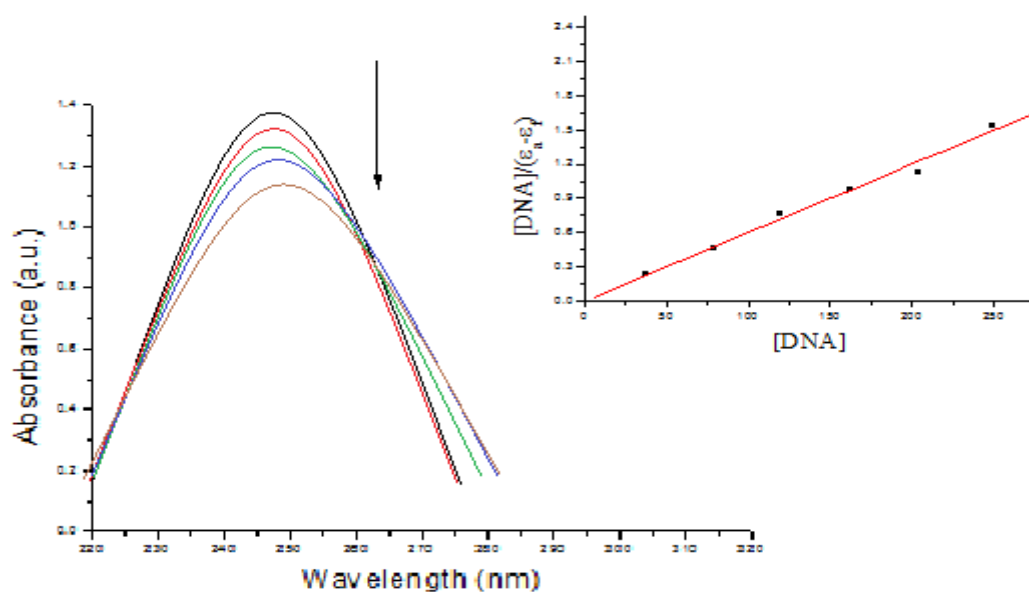


Figure 7.6. Absorption spectra of **Cu-2a** (50 μM) in the absence and presence of increasing amounts of CT-DNA at room temperature in Tris-HCl/NaCl buffer (pH 7.2). The arrow shows the effect of increasing of CT-DNA concentration on the absorption intensity. Inset: plot of $[DNA]/(\epsilon_a - \epsilon_f)$ vs. $[DNA]$ for absorption titration of CT-DNA with complex, **Cu-2a**

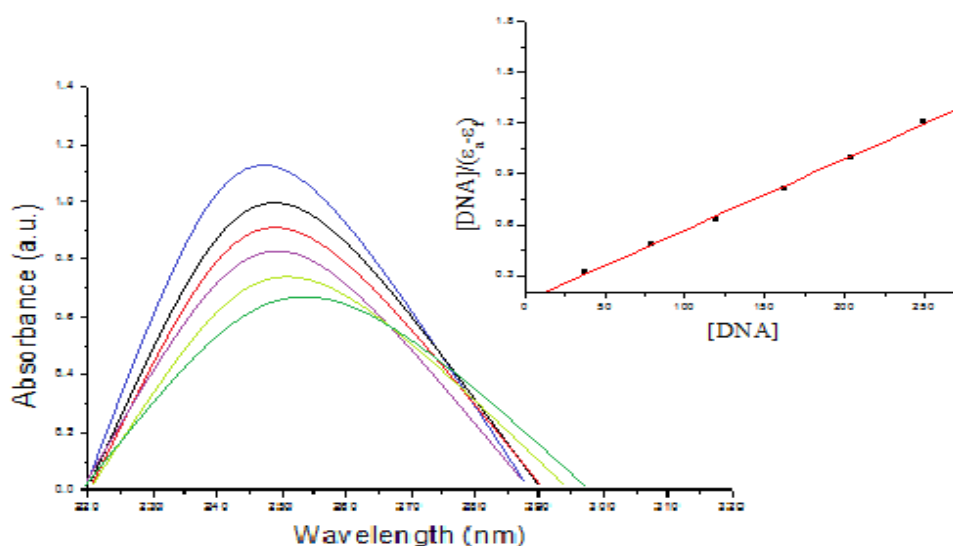


Figure 7.7. Absorption spectra of **2b** (50 μM) in the absence and presence of increasing amounts of CT-DNA (0 - 250 μM) at room temperature in Tris-HCl/NaCl buffer (pH 7.2). Inset: plot of $[DNA]/(\epsilon_a - \epsilon_f)$ vs. $[DNA]$ for absorption titration of CT-DNA with **2b**.

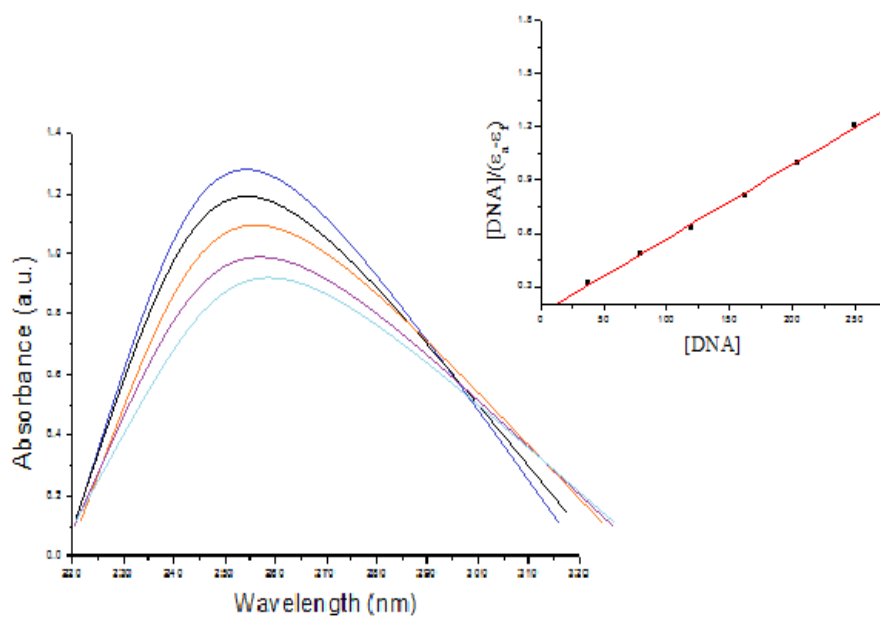


Figure 7.8. Absorption spectra of **Cu-2b** (50 μM) in the absence and presence of increasing amounts of CT-DNA (0 – 250 μM) at room temperature in Tris–HCl/NaCl buffer (pH 7.2). Inset: plot of $[\text{DNA}]/(\epsilon_a - \epsilon_f)$ vs. $[\text{DNA}]$ for absorption titration of CT-DNA with **Cu-2b**

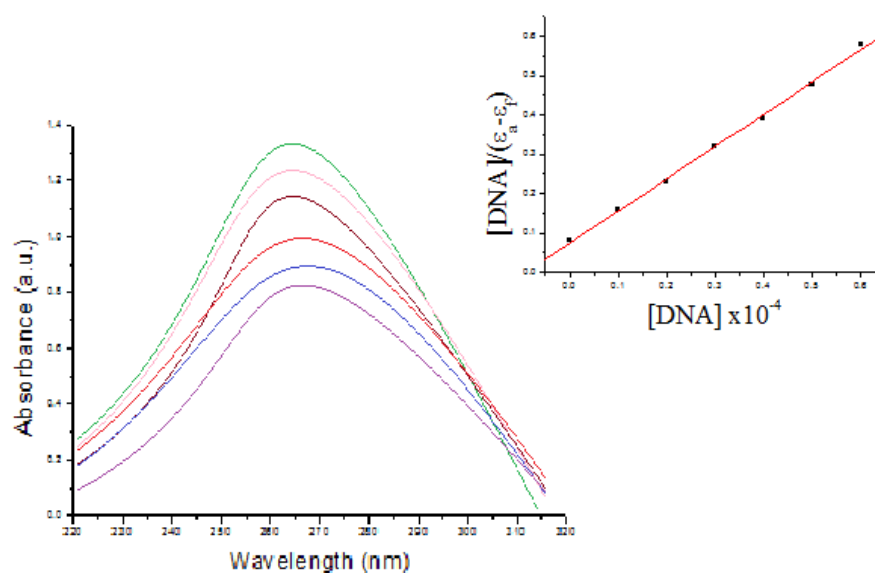


Figure 7.9. Absorption spectra of **3a** (5×10^{-5} M) in the absence and presence of increasing amounts of CT-DNA (0 – 2.5×10^{-4} M) at room temperature in Tris–HCl/NaCl buffer (pH 7.2). Inset: plot of $[\text{DNA}]/(\epsilon_a - \epsilon_f)$ vs. $[\text{DNA}]$ for absorption titration of CT-DNA with **3a**

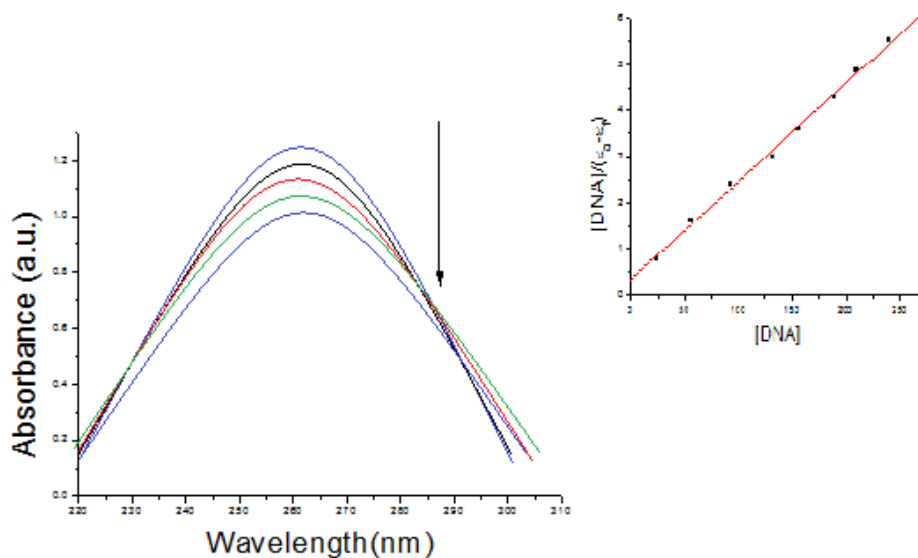


Figure 7.10. Absorption spectra of **Cu-3a** (5×10^{-5} M) in the absence and presence of increasing amounts of CT-DNA ($0 - 2.5 \times 10^{-4}$ M) at room temperature in Tris-HCl/NaCl buffer (pH 7.2). The arrow shows the effect of increasing of CT-DNA concentration on the absorption intensity. Inset: plot of $[\text{DNA}]/(\epsilon_a - \epsilon_f)$ vs. $[\text{DNA}]$ for absorption titration of CT-DNA with **Cu-3a**.

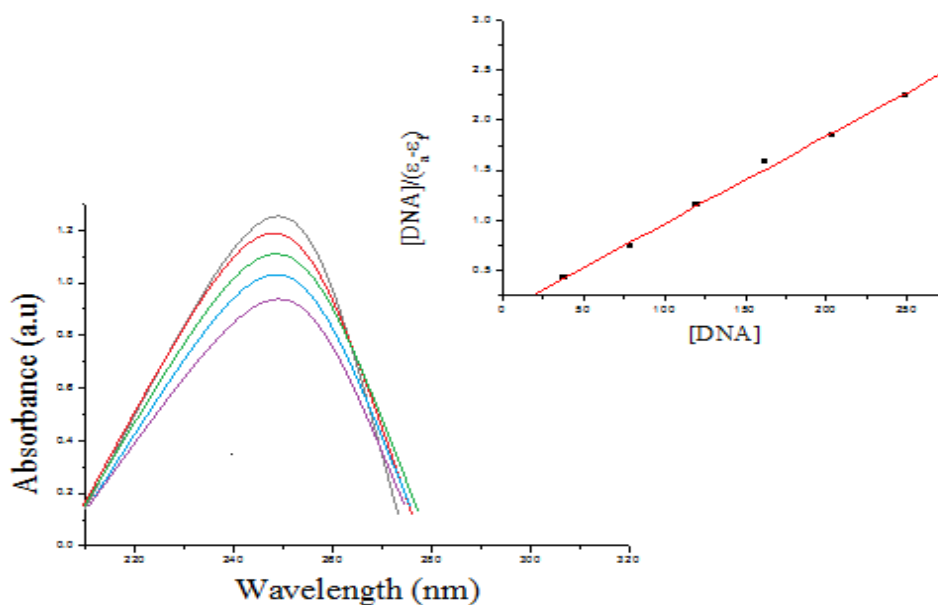


Figure 7.11. Absorption spectra of **3b** ($50 \mu\text{M}$) in the absence and presence of increasing amounts of CT-DNA at room temperature in Tris-HCl/NaCl buffer (pH 7.2). Inset: plot of $[\text{DNA}]/(\epsilon_a - \epsilon_f)$ vs. $[\text{DNA}]$ for absorption titration of CT-DNA with **3b**.

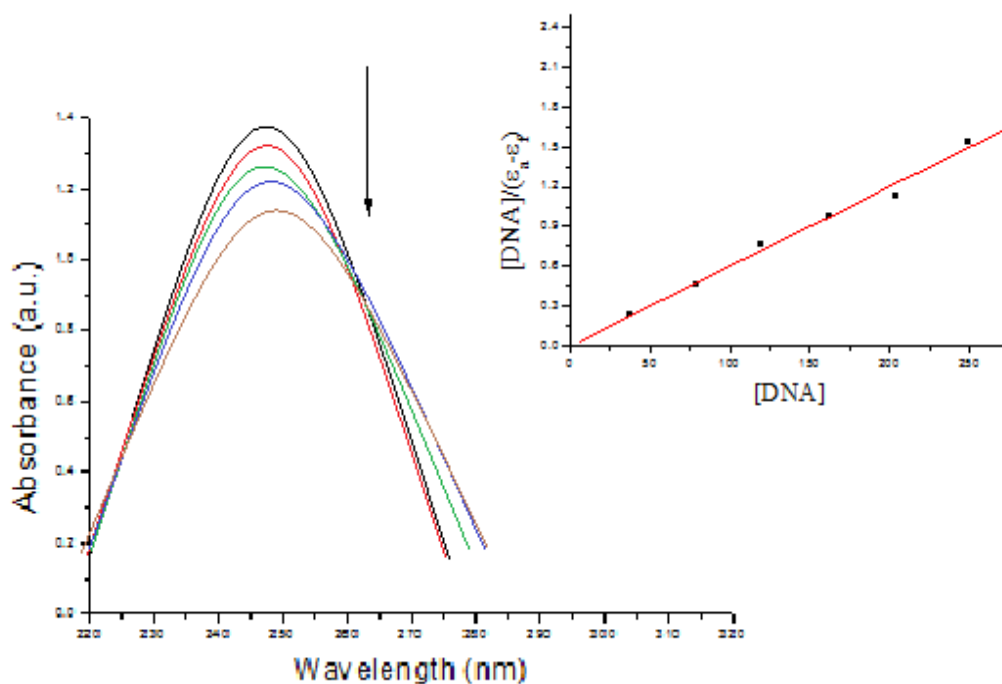


Figure 7.12. Absorption spectra of **Cu-3b** ($50\mu\text{M}$) in the absence and presence of increasing amounts of CT-DNA at room temperature in Tris-HCl/NaCl buffer (pH 7.2). The arrow shows the effect of increasing of CT-DNA concentration on the absorption intensity. Inset: plot of $[\text{DNA}]/(\epsilon_a - \epsilon_f)$ vs. $[\text{DNA}]$ for absorption titration of CT-DNA with **Cu-3b**.

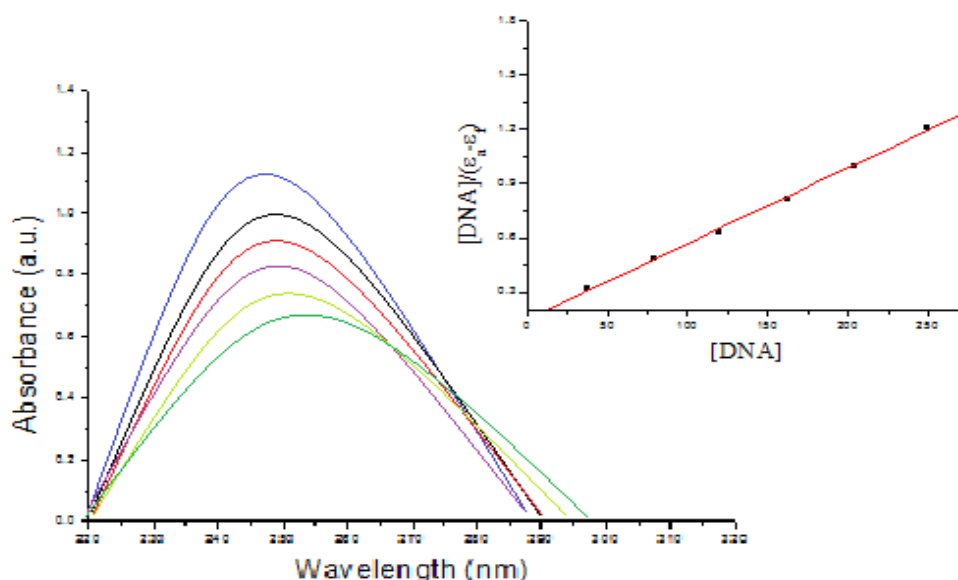


Figure 7.13. Absorption spectra of **3c** ($50\mu\text{M}$) in the absence and presence of increasing amounts of CT-DNA at room temperature in Tris-HCl/NaCl buffer (pH 7.2). Inset: plot of $[\text{DNA}]/(\epsilon_a - \epsilon_f)$ vs. $[\text{DNA}]$ for absorption titration of CT-DNA with **3c**.

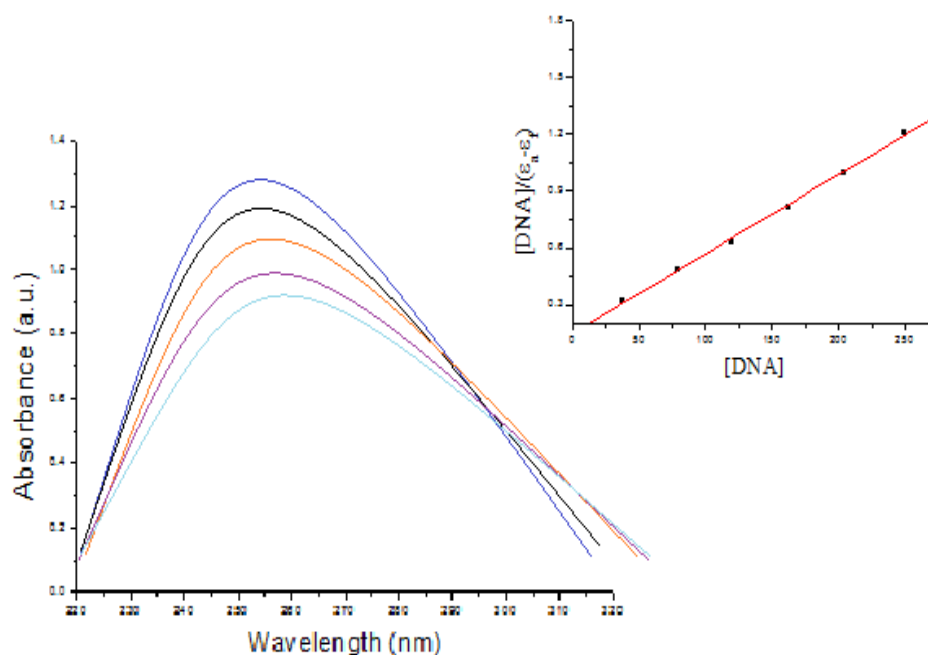


Figure 7.14. Absorption spectra of **Cu-3c** (50 μM) in the absence and presence of increasing amounts of CT-DNA at room temperature in Tris-HCl/NaCl buffer (pH 7.2). Inset: plot of $[\text{DNA}]/(\epsilon_a - \epsilon_f)$ vs. $[\text{DNA}]$ for absorption titration of CT-DNA with **Cu-3c**.

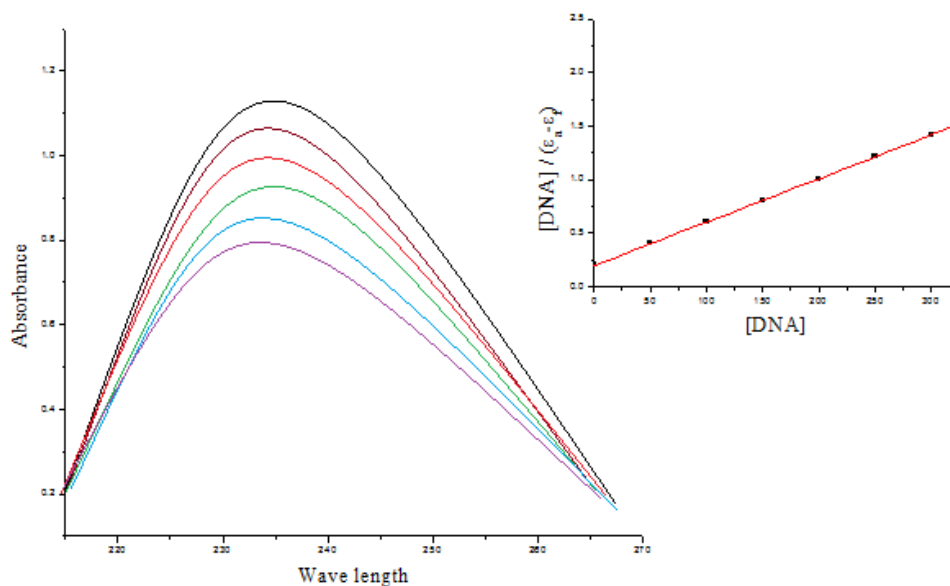


Figure 7.15. Absorption spectra of **5b** (50 μM) in the absence and presence of increasing amounts of CT-DNA at room temperature in Tris-HCl/NaCl buffer (pH 7.2). Inset: plot of $[\text{DNA}]/(\epsilon_a - \epsilon_f)$ vs. $[\text{DNA}]$ for absorption titration of CT-DNA with **5b**.

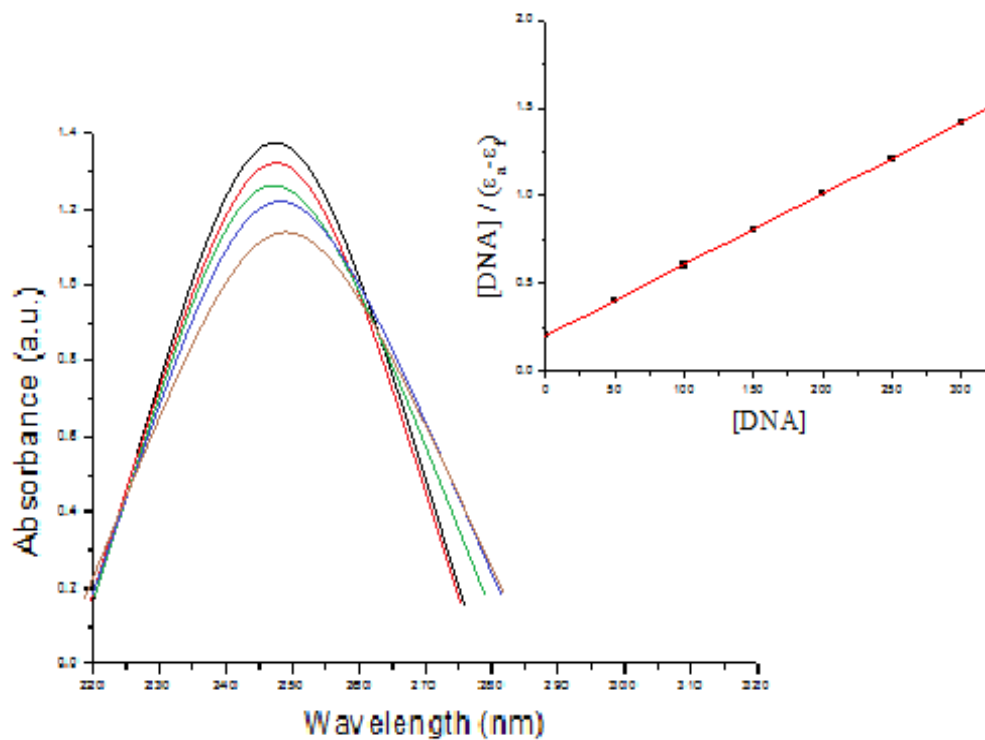


Figure 7.16. Absorption spectra of **Cu-5b** (50 μM) in the absence and presence of increasing amounts of CT-DNA at room temperature in Tris-HCl/NaCl buffer (pH 7.2). Inset: plot of $[\text{DNA}]/(\epsilon_a - \epsilon_f)$ vs. $[\text{DNA}]$ for absorption titration of CT-DNA with **Cu-5b**.

Table 7.1 DNA binding constants of ligands and their copper(II) complexes

Ligands	DNA binding constants (K_b) ^a ($\times 10^4 M^{-1}$)	Copper(II) complexes	DNA binding constants (K_b) ^a ($\times 10^4 M^{-1}$)
1a	1.07± 0.3	Cu-1a	1.64± 0.2
1b	1.54± 0.2	Cu-1b	5.42± 0.5
1c	2.23± 0.3	Cu-1c	7.42± 0.4
1d	1.34± 0.4	Cu-1d	5.31± 0.3
1e	1.23± 0.3	Cu-1e	2.47± 0.2
1f	1.01± 0.2	Cu-1f	2.28± 0.3
2a	1.67± 0.4	Cu-2a	3.23± 0.2
2b	1.24± 0.5	Cu-2b	4.72± 0.3
2c	1.25± 0.2	Cu-2c	xx
2d	1.02± 0.4	Cu-2d	xx
2e	1.05± 0.4	Cu-2e	xx
3a	1.34± 0.3	Cu-3a	3.42± 0.4
3b	1.73±0.3	Cu-3b	5.47± 0.4
3c	1.14± 0.3	Cu-3c	3.18± 0.4
4a	1.64± 0.4	Cu-4a	2.73± 0.4
4b	1.93± 0.3	Cu-4b	4.54± 0.4
5a	2.08 ± 0.2	Cu-5a	5.18 ± 0.3
5b	2.23 ± 0.2	Cu-5b	6.42 ± 0.2

^aEach value represents mean of three different observations ± S.D.

xx Not determined

From the binding constant data it follows that ligands or complexes having either OH groups or OCH₃ groups have greater affinity towards CT DNA. These functionalities are quite common in biologically active natural products. The highest value for binding constant is obtained for **Cu-1c**. It may probably due to some steric factors.

7.2. Viscosity method

In order to establish the nature of binding between the complexes and DNA, viscosity studies were also carried out. In intercalative mode due to increase in the separation of base pairs at intercalation site and the unwinding of DNA helix will increase the DNA length and cause a significant increase in viscosity of DNA solution. On the other hand, a groove binding and electrostatic interaction reduces its effective length resulting in a slight decrease of viscosity ^[218].

Viscosity measurements

The viscosity experiments were carried out in triplicate on CT-DNA by varying the concentration of the ligands or copper (II) complexes [compound]/[DNA] = 0.0–0.6. Viscosity measurements of 1×10^{-4} M CT-DNA in Tris–HCl/NaCl buffer were performed using an Ostwald viscometer at 35 ± 0.2 °C in a thermostatic water bath. Flow time was measured with a digital stopwatch, and each sample was measured three times, and an average flow time was calculated. Data are presented as $(\eta/\eta^0)^{1/3}$ versus binding ratio [Complex]/[DNA], where η and η^0 indicate the viscosity of DNA solutions in the presence and absence of complex, respectively. The relative viscosity was calculated according to the relation $\eta = (t - t_0)/t_0$, where t is the flow time of DNA solution in the presence or absence of complex and t_0 is the flow time of the buffer alone ^[219].

DNA binding properties

Both the ligands and complexes show an increase in specific viscosity with increase in concentration of compounds, obviously indicating the binding involves intercalative mode. The complexes were found to be more strongly bind with DNA than free ligands. It may probably due to the presence of metal ion which can interact with the nitrogen bases of DNA and negatively charged oxygen of phosphodiester linkages of DNA ^[220].

Change in viscosity with the free ligands having either free OH groups or OCH₃ groups or both and their copper(II) complexes are given in **Figures 6.17 - 6.20**. It can be seen that copper(II) complexes have increased relative viscosity of CT DNA all cases than their corresponding uncomplexed ligand. These results also in agreement with the results obtained from spectral titrations, that the copper(II) complexes have more affinity towards DNA than the corresponding free ligands.

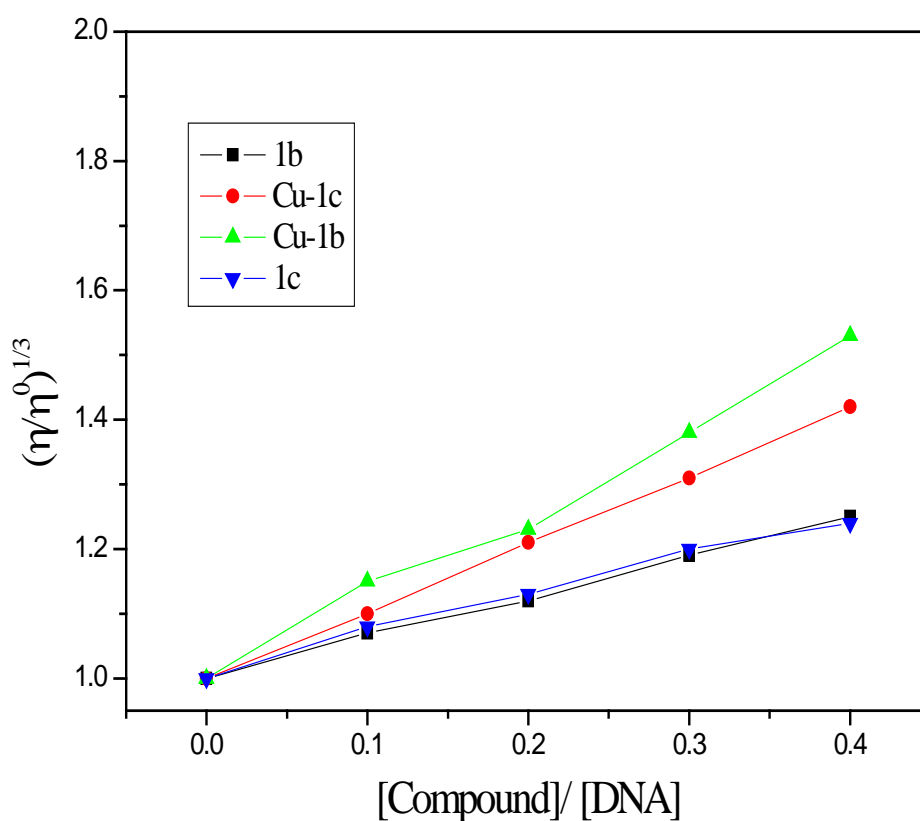


Figure 7.17. Effect of increasing concentration of the ligands and corresponding copper(II) complexes on the relative viscosities of CT-DNA at 35.0 ± 0.2 °C.

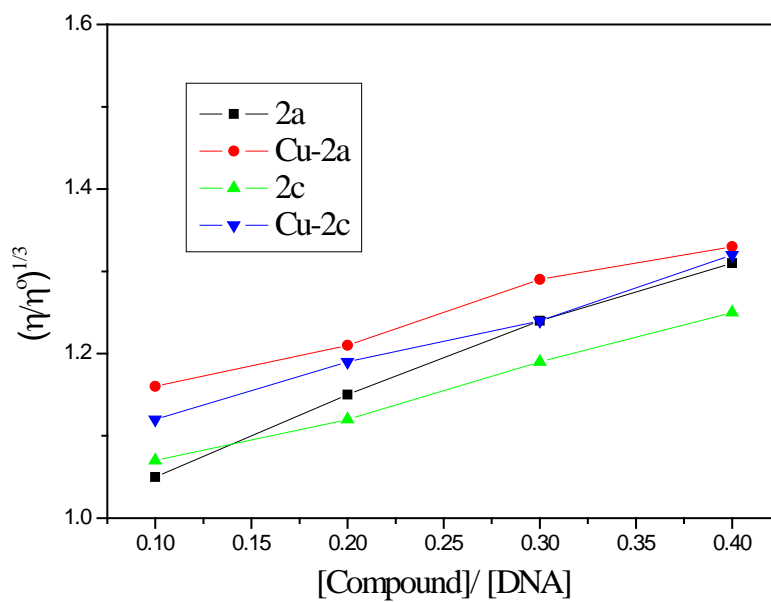


Figure 7.18. Effect of increasing concentration of ligands and complexes on the relative viscosities of CT-DNA at 32.0 ± 0.2 °C.

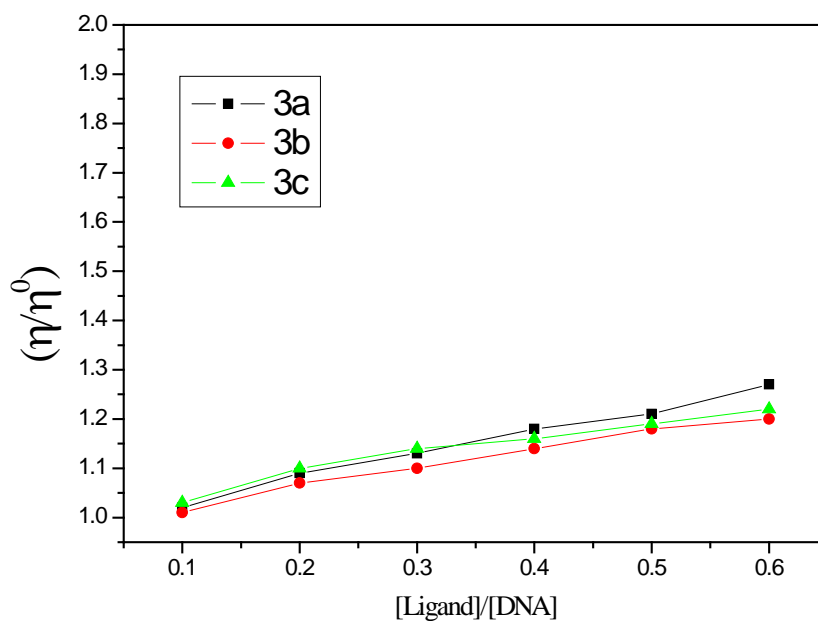


Figure 7.19. Effect of increasing concentration of the ligands (3a, 3b, and 3c) on the relative viscosities of CT-DNA at 35.0 ± 0.2 °C.

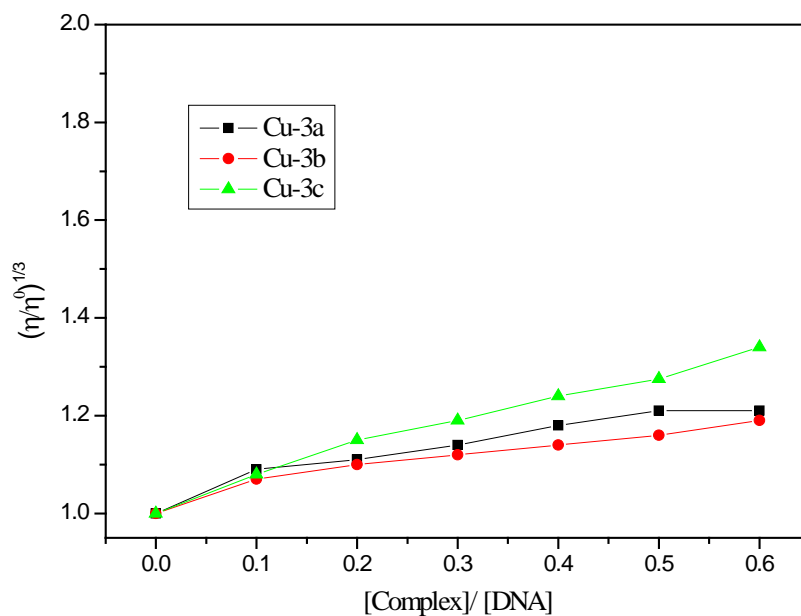


Figure 7.20. Effect of increasing concentration of **Cu-3a**, **Cu-3b** and **Cu-3c** on the relative viscosities of CT-DNA at 35.0 ± 0.2 °C.

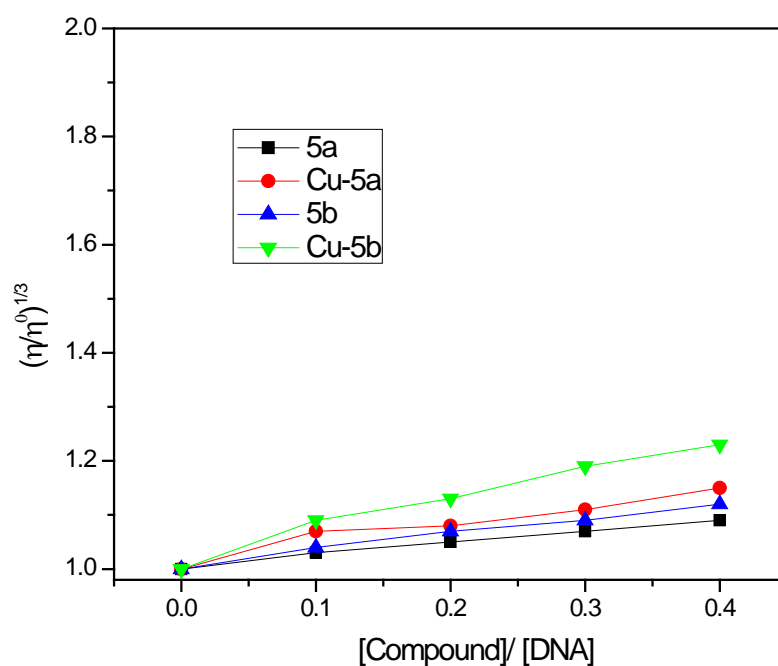


Figure 7.21. Effect of increasing concentration of ligands and complexes on the relative viscosities of CT-DNA at 35.0 ± 0.2 °C.

7.3 Fluorescence quenching method

Fluorescence quenching studies were carried out only with copper(II) complexes of ligands having disubstituted phenyl rings described in **Chapter 3, Part A**.

Fluorescence measurements

Fluorescence measurements were performed to understand the nature of binding of complexes with DNA using a MPF-4 fluorescence spectrophotometer. Since the complexes are non-luminescent at room temperature, the binding of copper(II) complexes to DNA is evaluated by the fluorescence emission intensity of EB-DNA solution as a probe. The competitive binding experiments were carried out with an EB-bound CT-DNA solution in Tris–HCl/NaCl buffer ^[221]. Fluorescence intensities at 598 nm (510 nm excitation) were measured after addition of different concentrations of copper(II) complexes of **3a** which suggested the complex could compete with EB to bind to DNA with similar intercalating fashion. Similarly, fluorescence intensities at 608 nm (502 nm excitation) and at 623 nm (490 nm excitation) were measured after addition of different concentrations of copper(II) complexes of **3b** and **3c**, respectively.

DNA binding properties

The fluorescence quenching curves are shown in **Figures 7.22-7.24**. The curves clearly suggesting that the quenching of EB-DNA system by the complexes are in agreement with the classical Stern–Volmer equation ^[222]

$$I_0/I = 1 + K[Q]$$

Where I_0 is the intensity of fluorescence without a quencher, I is the intensity of fluorescence with a quencher and $[Q]$ is the concentration of the quencher, K being the quencher rate coefficient.

From the equation

$$K_{EB}[EB] = K_{app}[\text{complex}]$$

where [complex] is the value at a 50% reduction of the fluorescence intensity of EB, $K_{EB} = 1.0 \times 10^7 \text{ M}^{-1}$, and $[EB] = 5 \mu\text{M}$, the value of apparent binding constants (K_{app}) were calculated to be $5.82(\pm 0.4) \times 10^5$, $3.22 (\pm 0.5) \times 10^5$ and $2.08(\pm 0.4) \times 10^5 \text{ M}^{-1}$ for copper(II) complexes of **3a**, **3b** and **3c** respectively. These results are consistent with some earlier reports on quenching fluorescence of EB-DNA for Cu complexes with similar K_{app} value^[223-226], suggesting that the interaction of the complexes with DNA is an intercalative mode. The modes and affinities of DNA binding of these copper(II) complexes mainly depend on the nature of the ligands.

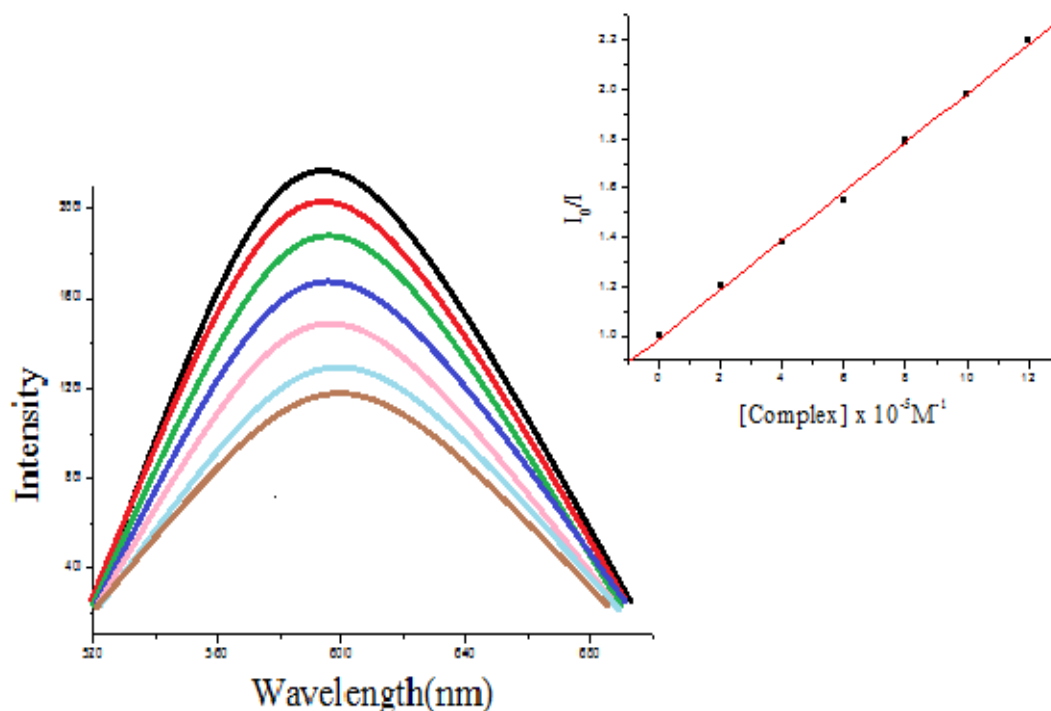


Figure 7.22. Fluorescence quenching curves of EB bound to DNA by **Cu-3a** ($[\text{complex}] = 0-3 \times 10^{-5} \text{ M}$) Inset: plot of I_0/I vs. $[\text{complex}]$, $\lambda_{ex} = 510 \text{ nm}$.

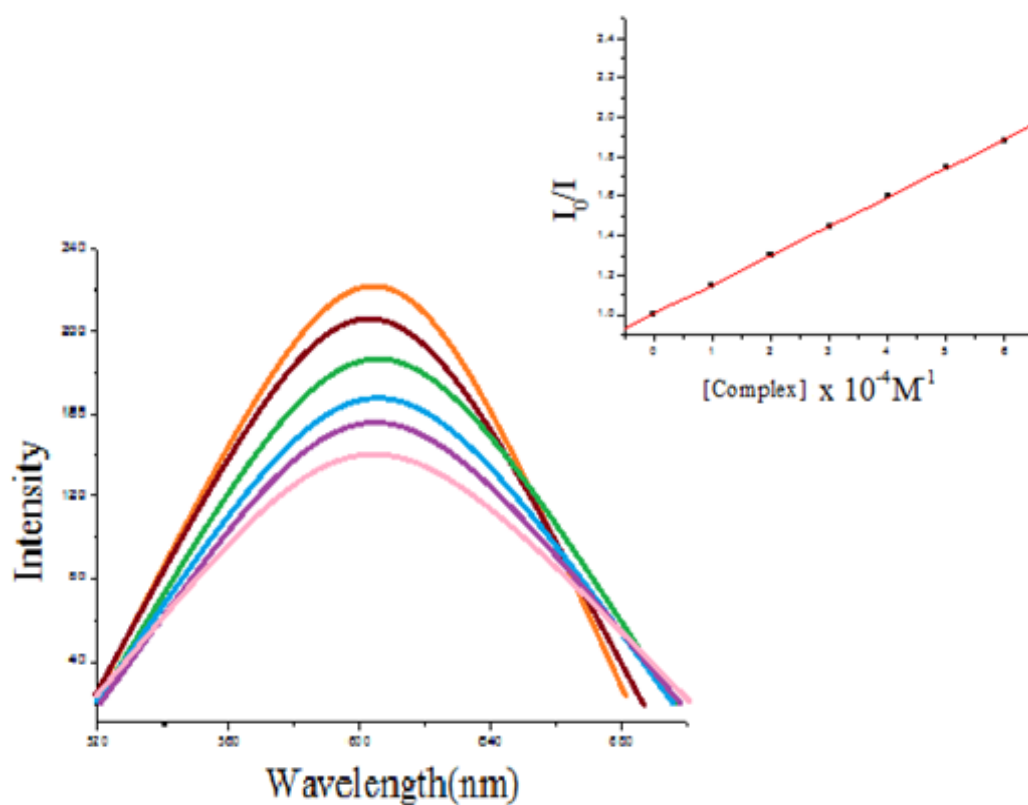


Figure 7.23. Fluorescence quenching curves of EB bound to DNA by **Cu-3b** ($[\text{complex}] = 0\text{--}3 \times 10^{-5} \text{ M}$) Inset: plot of I_0/I vs. $[\text{complex}]$, $\lambda_{\text{ex}} = 502 \text{ nm}$.

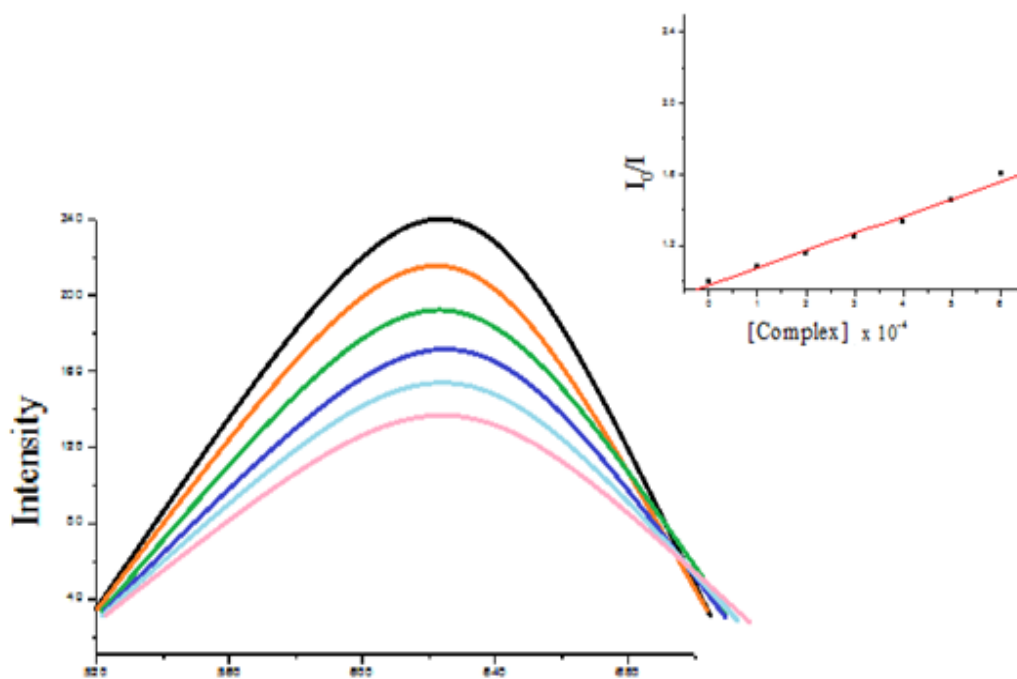


Figure 7.24. Fluorescence quenching curves of EB bound to DNA by **Cu-3c** ($[\text{complex}] = 0\text{--}3 \times 10^{-5} \text{ M}$) Inset: plot of I_0/I vs. $[\text{complex}]$, $\lambda_{\text{ex}} = 490 \text{ nm}$.

The DNA binding activity of copper(II) complexes is found to be greater than free ligands. The intrinsic binding constant obtained from fluorescent quenching studies were found to be comparable with other complexes reported in the literature ^[227-229]. The binding involves intercalative mode through non covalent interactions and produced conformational changes in the structure of DNA via moderate interaction as evidenced from fluorescence quenching experiments and viscosity measurements. Introduction of cyclopentane ring to modify the basic skeleton of curcumin and the presence of two hydroxylic groups in the aryl rings significantly increased the DNA binding properties of compounds. Strong interaction of copper complexes with DNA suggests that they may have cytotoxic effects against tumour cells.

Chapter 8

STUDIES ON ANTITUMOR ACTIVITIES

Several *in vivo* and *in vitro* studies revealed that curcumin, some of its synthetic analogues and their metal complexes have antitumor activities against different types of cancer cell lines. In some cases, the activity of synthetic analogues and metal complexes of curcumin based ligands have more activity than the parent curcumin^[230]. Copper(II) complexes have attracted considerable attention as antitumor candidates in recent years because copper is an essential micronutrient that participates in several biological processes like mitochondrial respiratory reactions, cellular stress response, antioxidant, etc and hence it may be less toxic than non-essential metals like platinum^[17]. In our studies, it is found that the ligands as well as their copper(II) complexes have strong interaction with CT DNA and this observation along with the profound interest in copper(II) complexes as potential anticancer agents, provoked us to evaluate their antitumor activities. The free ligands and their copper(II) complexes were screened for both the *in vitro* and *in vivo* antitumor activity against Daltons lymphoma ascites cells. The experimental details and results obtained are described below.

8.1. *In vitro* studies

Determination of the effect of compounds on ascites tumour model

In vitro cytotoxicity studies were carried out using DLA cells. The tumour cells were aspirated from the peritoneal cavity of tumor bearing mice. It was washed thrice with phosphate buffered saline. Cell viability was determined by trypan blue exclusion method^[231]. Viable cell suspension (1×10^6 cells in 0.1ml) was added to tubes containing various concentrations of the test compounds (200 μ g/ml, 100 μ g/ml, 50 μ g/ml, 20 μ g/ml, and 10 μ g/ml)

dissolved in the minimum quantity of DMSO and the volume was made up to 1ml using phosphate buffered saline. Control tube contains only cell suspension. These assay mixture were incubated for 3hrs at 37⁰C. Further cell suspension was mixed with 100µl of 1% trypan blue and kept for 2-3 minutes. Dead cells take up the blue colour of trypan blue while the live cells do not take up the dye. The number of stained and unstained cells was counted separately counted using heamocytometer.

Effect of compounds on short-term *in vitro* cytotoxic activity

The results of short-term *in vitro* cytotoxic activity of the ligands and their metal chelates (**Table 8.1**) against Dalton's lymphoma ascites indicate that metal complexation enhances the cytotoxicity of compounds considerably. Among the ligands **1a-1f**, concentrations required to produce 50% cell death are in the range 108-62 µg/ml in the case of free ligands. The copper chelates produced the same effect at remarkably lower concentrations of 86-23 µg/ml. The presence of functional groups like NO₂, CH₃ or Cl in the phenyl rings did not significantly increased activity. However, presence of OH and OCH₃ groups significantly contributed to improve the antitumor activity. Even though the exact role of OH and OCH₃ groups are not known, these groups are very common in many antitumor drugs isolated from natural sources.

Among the set of ligands **2a-2e**, concentrations required to produce 50% cell death ranges from 116 to 57 µg/ml. The copper chelates produced the same effect at much lower concentrations (86-23 µg/ml). The copper chelate of **2a** (ligand having OH group in the para position of phenyl rings) showed maximum activity than the others. Among the ligands **3a-3c**, **3b** with two hydroxyl groups is found to be more active than the others. A concentration of 27µg/ml of **3b** produced 50% activity where as only 10 µg/ml of **Cu-3b** is found to be sufficient to produce the same effect.

Ligands having hetero aryl groups (**4a** and **4b**) or naphthyl groups (**5a** and **5b**) did not show any significant activity. However, it can be concluded that copper chelation drastically increased the antitumor activity. A direct comparison of concentration required to produce 50% activity in the case of each ligands and corresponding copper complexes are shown in **Figures 8.1-8.4**.

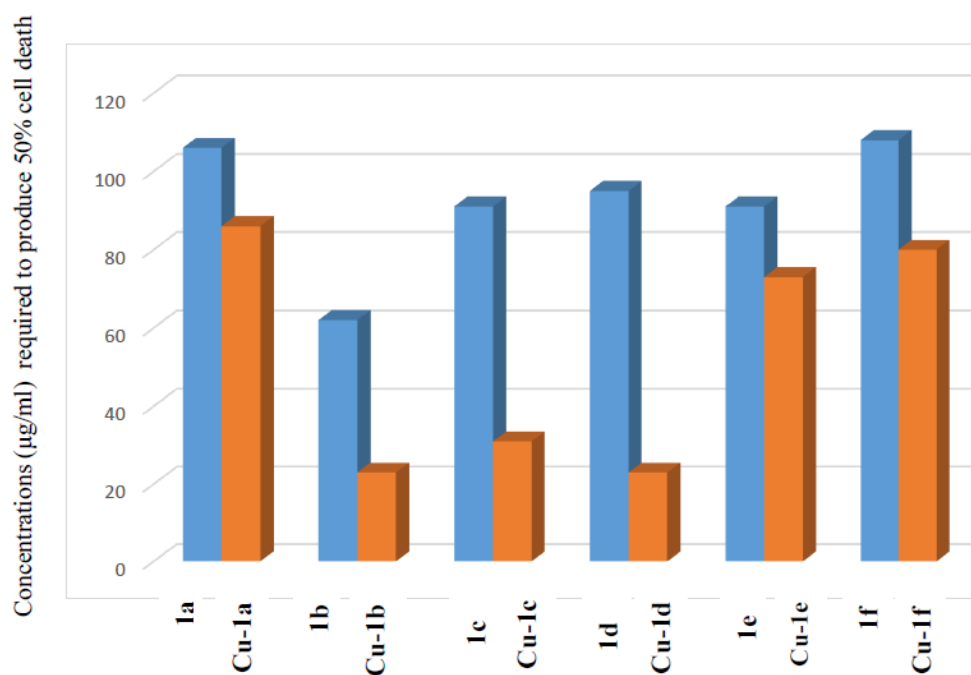


Figure 8.1 Cytotoxic activity of ligands (**1a-1f**) and their copper(II) complexes

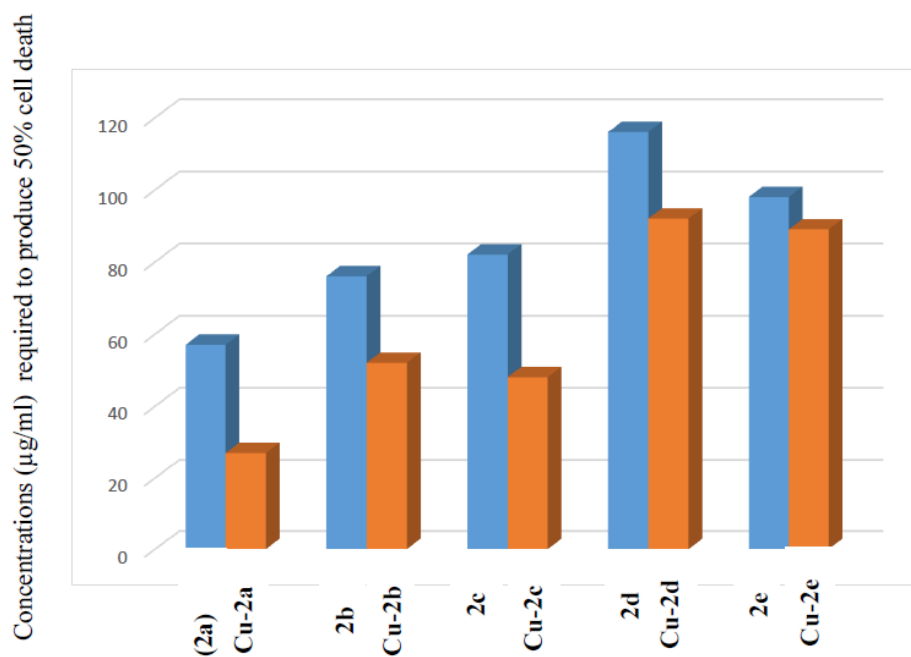


Figure 8.2 Cytotoxic activity of ligands (2a-2e) and their copper(II) complexes

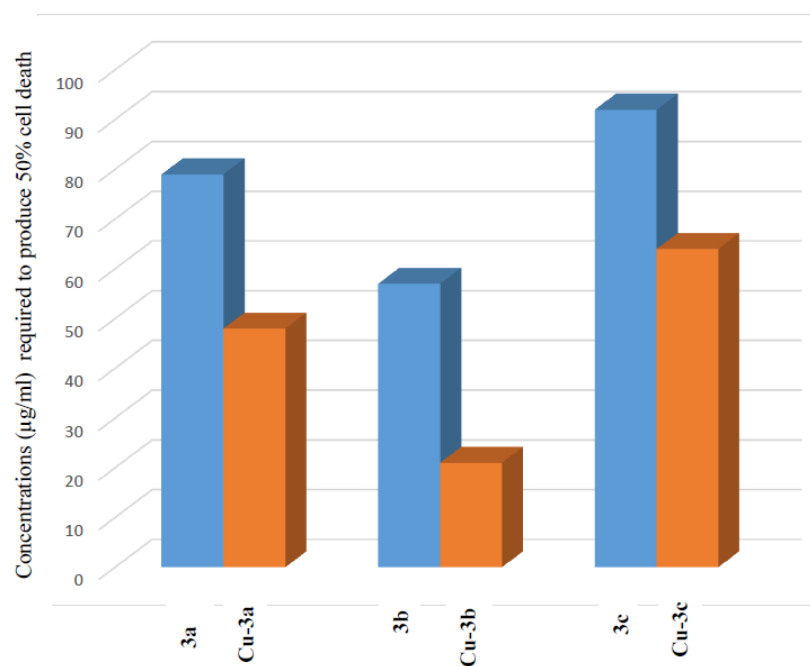


Figure 8.3 Cytotoxic activity of ligands (3a-3c) and their copper(II) complexes

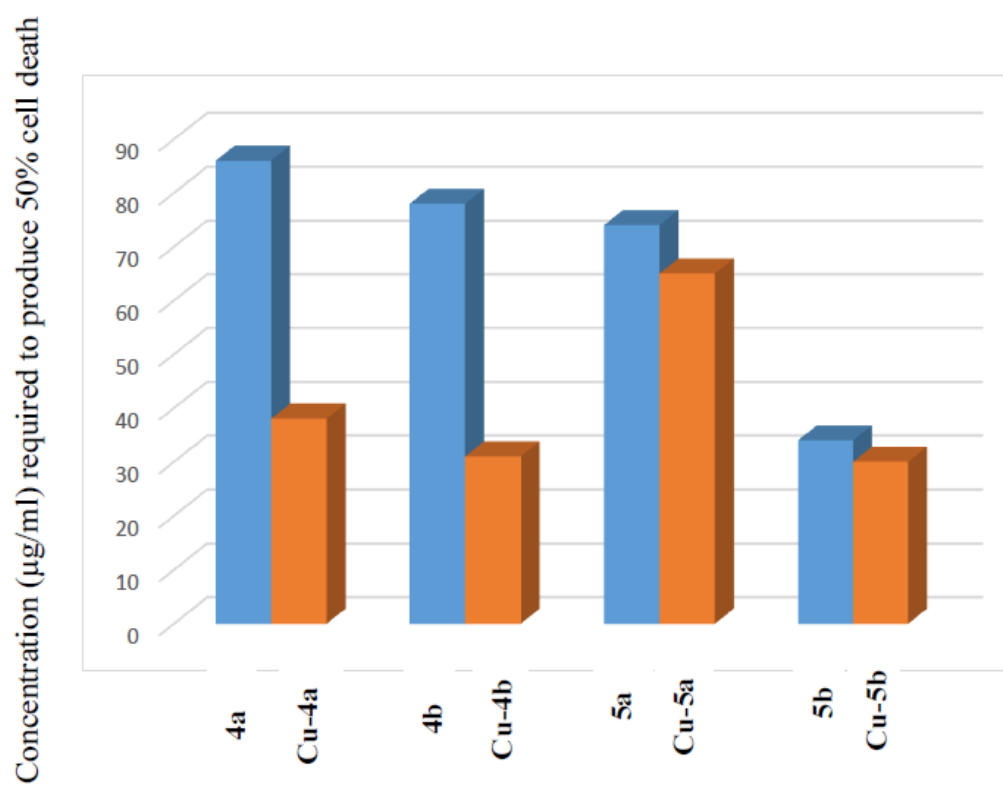


Figure 8.4 Cytotoxic activity of ligands and their copper(II) complexes

Table 8.1. *In vitro* and *in vivo* antitumor activity of compounds

Compounds	Concentrations ($\mu\text{g/ml}$) required to produce 50% cell death	No.of days survived ^a	Increase in life span (%)
Control		17.29 \pm 1.1	
1a	106	20.41 \pm 1.6	18.04
1b	62	27.43 \pm 1.8	58.67
1c	91	27.36 \pm 2.1	36.80
1d	95	27.68 \pm 2.1	37.53
1e	91	23.28 \pm 1.6	34.64
1f	108	22.93 \pm 1.4	32.62
Cu-1a	86	26.87 \pm 2.2	55.40
Cu-1b	23	30.21 \pm 2.4	74.72
Cu-1c	31	34.46 \pm 2.6	49.82
Cu-1d	23	36.96 \pm 2.8	53.21
Cu-1e	73	28.15 \pm 2.2	38.57
Cu-1f	80	27.35 \pm 2.1	36.78

^aEach value represents mean of three different observations \pm S.D.

Table 8.2. *In vitro* and *in vivo* antitumor activity of compounds

Compounds	Concentrations ($\mu\text{g/ml}$) required to produce 50% cell death	No.of days survived ^a	Increase in life span (%)
Control		18.34 ± 1.3	
2a	57	26.24 ± 2.1	43.07
2b	76	25.68 ± 2.1	40.02
2c	82	24.64 ± 1.9	34.35
2d	116	22.33 ± 1.8	21.75
2e	98	22.12 ± 1.9	20.61
Cu-2a	27	33.14 ± 2.8	80.69
Cu-2b	52	32.75 ± 2.6	78.57
Cu-2c	48	31.68 ± 2.4	72.73
Cu-2d	92	28.96 ± 2.4	57.90
Cu-2e	89	27.43 ± 2.3	49.56

^aEach value represents mean of three different observations \pm S.D.

Table 8.3. *In vitro* and *in vivo* antitumor activity of compounds

Compounds	Concentrations ($\mu\text{g/ml}$) required to produce 50% cell death	No.of days survived ^a	Increase in life span (%)
Control		19.02 \pm 1.1	
3a	38	27.42 \pm 1.7	44.16
3b	27	29.75 \pm 1.9	56.41
3c	52	26.54 \pm 1.6	39.53
Cu-3a	18	31.57 \pm 2.4	65.98
Cu-3b	10	33.84 \pm 2.6	77.91
Cu-3c	22	30.46 \pm 2.1	60.14

^aEach value represents mean of three different observations \pm S.D.

Table 8.4 *In vitro* and *in vivo* antitumor activity of compounds

Compounds	Concentrations ($\mu\text{g/ml}$) required to produce 50% cell death	No.of days survived ^a	Increase in life span (%)
Control		18.82 \pm 1.1	
4a	74	26.21 \pm 1.4	39.26
4b	70	27.02 \pm 1.7	43.57
Cu-4a	34	30.54 \pm 1.9	62.27
Cu-4b	32	31.13 \pm 2.1	65.40
5a	86	25.42 \pm 1.4	35.06
5b	78	26.74 \pm 1.7	42.08
Cu-5a	38	30.05 \pm 1.9	59.67
Cu-5b	31	31.61 \pm 2.1	67.95

^aEach value represents mean of three different observations \pm S.D.

8.2. *In vivo* studies

Toxicity studies

For *in vivo* studies, Swiss Albino mice (female, 3 weighed mice for 1 group) were injected intraperitoneally with Dalton's lymphoma ascites tumour cells. The injections of the test compounds (single dose) were started 24 hours after tumour inoculation and continued for 5 consecutive days. Toxicity studies showed that the drug has no lethal effect for Swiss Albino mice.

Determination of the effect of compounds on DLA cell induced ascites tumour

For *in vivo* studies, groups of Swiss Albino mice (female, 6 per group) were injected intraperitoneally with Dalton's lymphoma ascites tumour cells (1×10^6 cells/animal). Group I kept as control (without any treatment). Group III, IV, V and VI were treated with vehicle control (CMC), standard, 12.5mg/kg body weight, 25mg/kg body weight, 50mg/kg body weight respectively. Cyclophosphamide (20mg/kg) was used as the standard drug. They were injected (ip) with (12.5mg/kg body weight, 25mg/kg body weight, 50mg/kg body weight) test compound suspended in carboxy methyl cellulose (CMC). The injections of the test compounds were started 24 hours after tumour inoculation and continued for 10 consecutive days. The death pattern of the animals due to tumour burden was noted and expressed as mean of survival time in days^[232].

The percentage increase in lifespan (% ILS) was calculated using the formula

$$\% \text{ ILS} = [(T-C)/C \times 100]$$

Where T and C represent the mean number of days survived by the treated and control animals respectively.

Effect of compounds on DLA cell induced ascites tumour model

Experiments in which mice injected (ip) with 25mg/kg body weight of test compounds showed maximum antitumour activity. The incorporation of metal ion enhanced the antitumor activity of the ligands. Among **1a-1f** and their copper chelates, Copper chelate of **1b** is found to be more effective than other copper chelates and it may probably due to the presence of hydroxy group in the *ortho* position of aryl ring that can produce a phenoxy free radical. Life span of ascites tumour bearing animals induced by DLA cells was found to be increased by treatment with copper complexes. The animals inoculated with DLA cell lines alone survived for a period of 17.29 ± 1.1 days (**Table 8.1**). Treatment with copper(II) complexes increased the average life span of tumour bearing mice than the free ligands (**Table 8.1**). Among the copper(II) complexes of **1a-1f**, **Cu-1b** and **Cu-1d** found to be more effective in increasing the life span of animals with an average of 30.05 and 36.96 days for **Cu-1b** and **Cu-1d** respectively. **Cu-2a** and **Cu-2b** shows maximum increase in life span with an average of 33.14 and 32.75 days among the **2a-2e** ligands and their copper complexes. It is due to the presence of phenoxy and methoxy groups in the aryl ring. Among **3a-3c** and their copper chelates, **Cu-3a** and **Cu-3b** shows highest activity because of the two OH groups and OH and OCH₃ groups as the substituents. **Cu-3a** and **Cu-3b** are found to be more effective in increasing the life span of animals with an average of 31.57 and 33.84 days for **Cu-3b** and **Cu-3d** respectively. Ligands and complexes with naphthyl and aryl rings show least activity compared to the others. **Cu-5b** found to be more effective in increasing the life span of animals with an average of 31.61 days.

Determination of the effect of compounds on DLA cell induced solid tumour model

Solid tumours were also induced in groups of Swiss albino mice (female, 6 per group) by subcutaneous injection of DLA cells (1×10^6 cells/animal) on the right hand limb. Group I was kept as control (without any treatment). Groups III, IV, V and VI were treated with vehicle control (CMC), standard, 12.5mg/kg body weight, 25mg/kg body weight, 50mg/kg body weight respectively. Cyclophosphamide (20mg/kg) was used as the standard drug. They were injected intramuscularly (im) with the test compounds (12.5mg/kg body weight, 25mg/kg body weight, 50mg/kg body weight) and the injections of the test compounds were started 24 hours after inoculation and continued for 10 consecutive days. Tumour diameter was measured every third day for one month and the tumour volume was calculated using the formula; $V = \frac{4}{3}\pi r_1^2 r_2$ where r_1 and r_2 are the minor and major radii respectively [233].

Effect of compounds on DLA cell induced solid tumour model

Reductions of solid tumour volume in mice by the intraperitoneal administration of compounds are given in **Figures 8.5-8.11**. Results of concentration with 25mg/kg body weight were discussed here. Compared with free ligands, their respective copper(II) complexes are remarkably active in reducing tumour volume. Tumour volumes were respectively 5.94, 3.51, 3.18, 3.29, 3.36, 3.76 and 2.46 on 30th day for control, **1a**, **1b**, **1c**, **1d**, **1e**, **1f** and standard respectively. Tumour volumes of copper chelates of **1a-1f** were 3.42, 3.09, 3.21, 3.22, 3.57 and 3.68 on 30th day. The results clearly reveal that **Cu-1b** with hydroxy groups on the phenyl rings show the maximum activity towards cytotoxicity on DLA cells, reduction of solid tumour volume in mice (**Figures 8.5-8.6**). The copper complexes dramatically enhanced the activity as evident from the data. Among the set **2a-2e** and their copper chelates, **Cu-2a**

shows maximum activity (**Figure 8.7-8.8**) than the other chelates that is tumour volume is 3.08 on 30th day of observation. It may be due to the OH group in the para position and copper chelation. In the case of ligands having disubstituted phenyl rings and their copper complexes, tumour volume is reduced to 3.41, 3.12, 3.51, 3.19, 3.07 and 3.29 on 30th day for **3a, 3b, 3c, and Cu-3a, Cu-3b and Cu-3 c**. It clearly evidenced that **Cu-3b** showed maximum tumour reduction (**Figure 8.9**) compared to the other compounds. It may presumably due to the presence of two hydroxyl groups in the aryl ring. Among the set **4a, 4b, 5a and 5b** and their copper(II) chelates, **Cu-5b** shows maximum tumour reduction volume 3.11 on 30th day due to the presence of hydroxyl group in the naphthyl ring (**Figures 8.10-8.11**).

A general observation is that copper complexation enhanced the activity in all cases. Earlier studies have shown that curcumin with methoxy and hydroxyl groups in the aryl ring, is an inhibitor of lipid peroxidation which promotes anticancer properties of the compound ^[234-236]. The present study suggests that metal complexation significantly increased the cytotoxic and antitumor activities of compounds. Both the phenolic OH groups and methoxy groups in the aryl ring enhanced the antitumor activity.

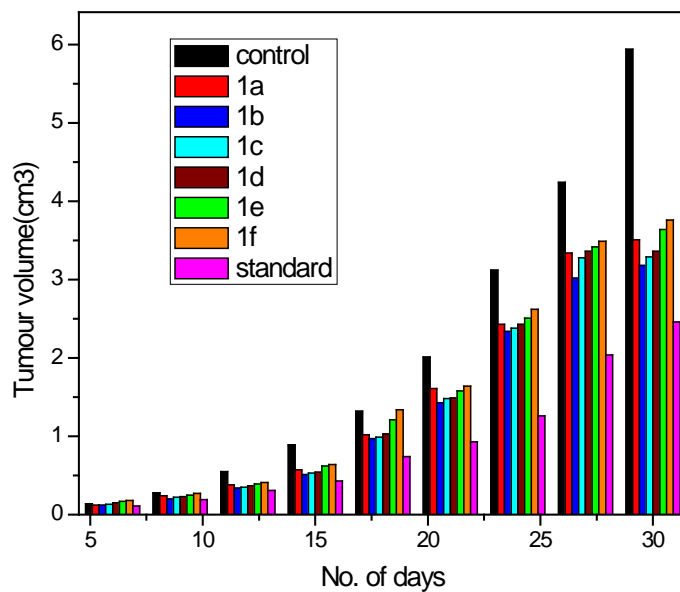


Figure 8.5 Effect of compounds (1a-1f) on solid tumour development.

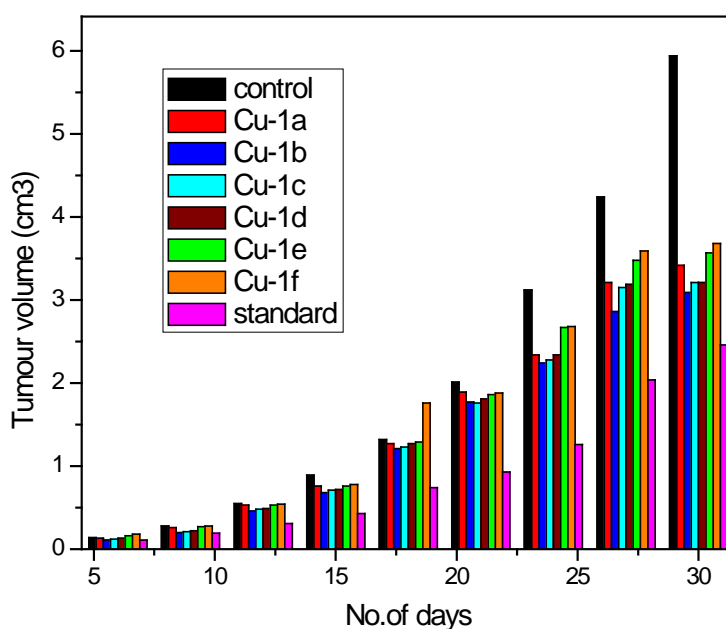


Figure 8.6 Effect of compounds (Cu-1a–Cu-1f) on solid tumour development.

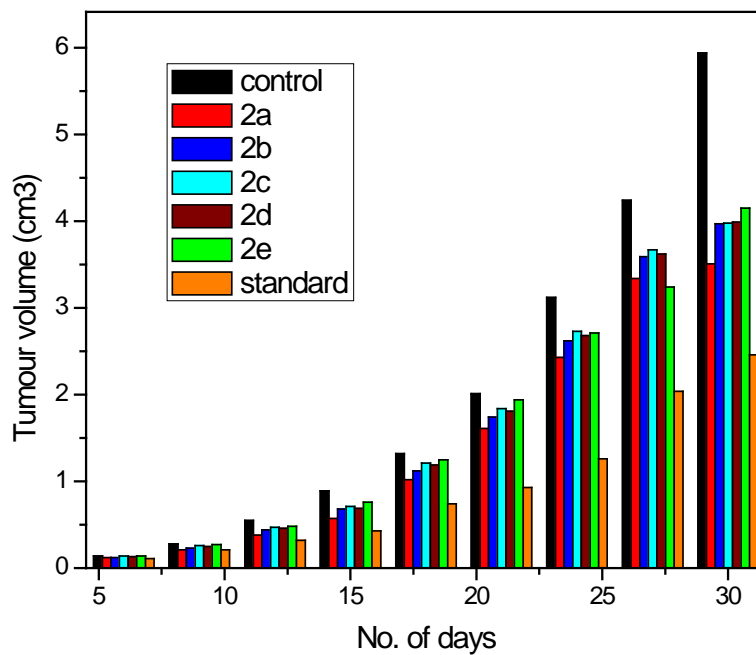


Figure 8.7 Effect of compounds (2a–2e) on solid tumour development.

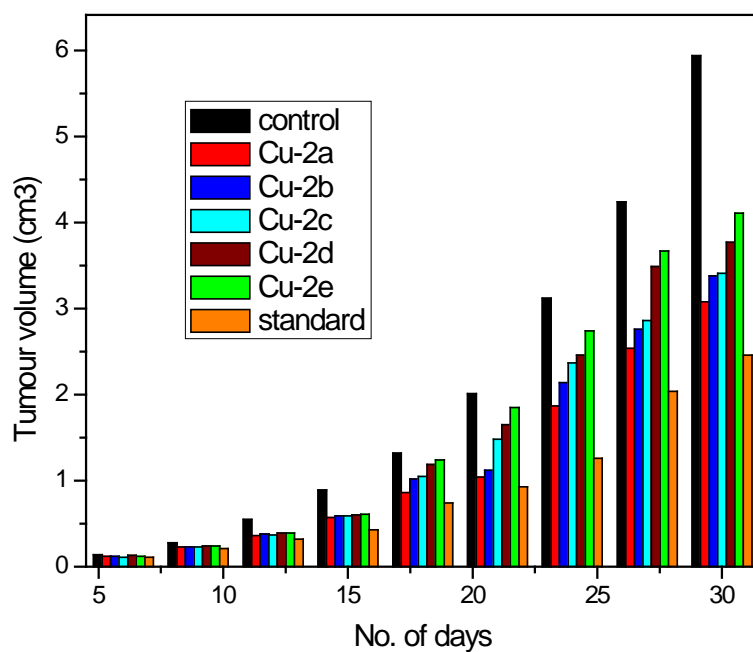


Figure 8.8 Effect of compounds (Cu-2a –Cu-2e) on solid tumour development

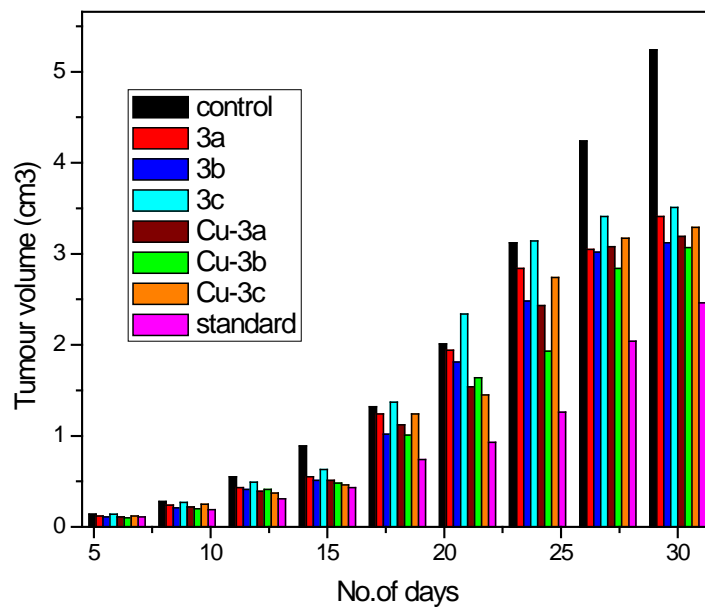


Figure 8.9 Effect of compounds (3a, 3b, 3c, Cu-3a, Cu-3b and Cu-3c) on solid tumour development.

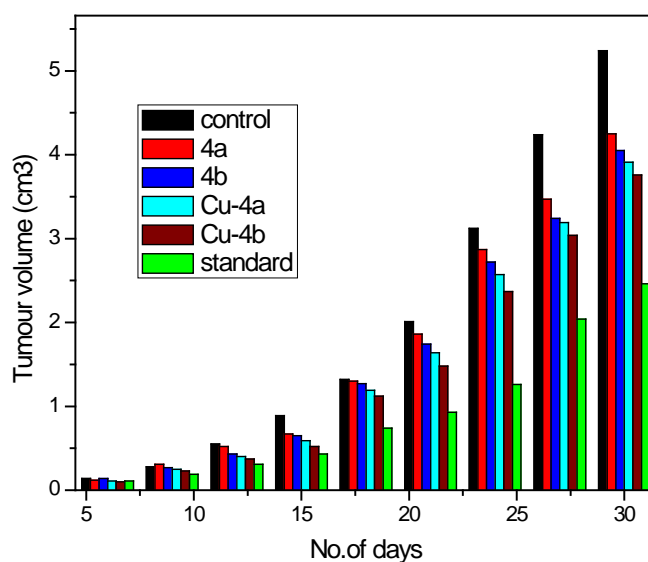


Figure 8.10 Effect of compounds (4a, 4b, Cu-4a and Cu-4b) on solid tumour development.

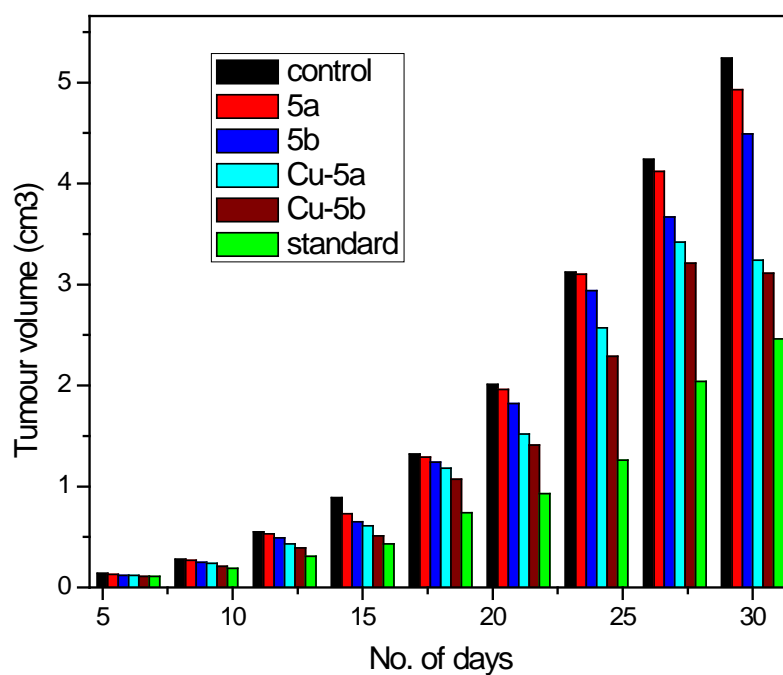


Figure 8.11.Effect of compounds (**5a**, **5b**, **Cu-5a** and **Cu-5b**) on solid tumour development.

CONCLUSIONS

Curcumin, a natural product isolated from the rhizomes of turmeric, is reported to have a large number of beneficial biological activities. The pharmacological safety and efficacy of curcumin makes it a potential compound for treatment and prevention of a wide variety of human diseases. Unfortunately, its clinical application is restricted by its poor solubility in water, light sensitivity, low absorption, high rate of metabolism, inactivity of metabolic products and/or rapid elimination and clearance from the body. Studies over the past three decades related to absorption, distribution, metabolism and excretion of curcumin have revealed that poor bioavailability of curcumin severely curtail its therapeutic applications.

Since biological activities are directly related to the molecular structure, structurally related compounds can also be ideal candidate for therapeutic applications. Synthesis of compounds structurally related to curcumin by new methods or by reported methods with varying structural features not encountered in natural sources is an active area of research and such studies developed a large number of products with greater beneficial properties than curcumin. Recently there is a surge of activity on preparation and characterization of curcumin-metal complexes due to the strong affinity of β -diketo moiety as an efficient metal chelator.

In the present investigation, the basic curcumin ligand system is modified and a series of unsymmetrical curcumin analogues were synthesized. The modification of the curcumin skeleton included both incorporation of a cyclopentane ring to the enolizable β -diketone moiety which is common to all ligands and a deviation in the nature and position of phenyl substituent, as well as replacing phenyl ring with hetero aryl and naphthyl / substituted naphthyl rings.

Copper(II), nickel(II) and zinc(II) complexes of all these ligands were also synthesised. The ligands and their metal complexes were characterized by various physico-chemical methods including electronic, IR, ^1H NMR, ^{13}C NMR and mass spectral studies. The ligands were found to be existing in their enolic form and the metal complexes have 1:2 metal ligand stoichiometry.

In view of reported biological activities of curcumin, its synthetic analogues and their metal complexes, the antioxidant activity of ligands and their metal complexes were studied by DPPH radical scavenging, super oxide radical scavenging, hydroxyl radical scavenging and lipid peroxidation inhibitory methods. The $\text{EC}_{50\%}$ values suggest that ligands having hydroxyl group in the phenyl rings are more active than the parent unsubstituted ligand. These results show that the lipid peroxidation activity of ligands is through the formation of relatively stable phenoxy radical. The presence of electron releasing groups also increased activity.

Metal complexation has been reduced activity in all cases irrespective on the nature of ligands or metal ions. It is presumably due to replacement of enolic proton and this observation also indicating that the complexes are stable under the conditions employed for the assay. Complexes of ligands having phenolic OH group have activity, but the magnitude is slightly lower than the corresponding free ligands. It may probably due to the absence of enolic proton in the complex. Another major conclusion that can be drawn from the $\text{EC}_{50\%}$ values is that the presence of nitro and chloro functionalities in the phenyl rings very little influence on antioxidant activities.

The DNA binding properties of ligand and metal complexes were studied by absorption titrations, fluorescence quenching experiments and by viscosity measurements with calf thymus DNA. From the binding constant data obtained from absorption titrations it follows that ligands or complexes having either OH groups or OCH_3 groups have greater affinity towards CT DNA. Both the ligands and complexes show an increase in specific viscosity with increase in concentration of compounds, obviously indicating the binding

involves intercalative mode. The copper complexes were found to be more strongly bind with DNA than free ligands and it can be attributed to the presence of metal ion which can interact with the nitrogen bases of DNA and negatively charged oxygen of phosphodiester linkages of DNA. These results also in agreement with the results obtained from spectral titrations, that the copper(II) complexes have more affinity towards DNA than the corresponding free ligands.

The intrinsic binding constant obtained from fluorescence quenching studies were found to be comparable with other complexes reported in the literature. The binding involves intercalative mode through non covalent interactions and produced conformational changes in the structure of DNA via moderate interaction as evidenced from fluorescence quenching experiments and viscosity measurements. Introduction of cyclopentane ring to modify the basic skeleton of curcumin and the presence of two hydroxylic groups in the aryl rings significantly increased the DNA binding properties of compounds. Strong interaction of copper complexes with DNA suggests that they may have cytotoxic effects against tumour cells.

Both *in vitro* and *in vivo* antitumor studies of free ligands and their copper(II) chelates against Daltons lymphoma ascites cell lines suggests that metal complexation significantly increased the cytotoxic and antitumor activities of compounds. Both the phenolic OH groups and methoxy groups in the aryl ring also have significant contribution to the antitumor activity.

Introduction of cyclopentane ring to modify the basic skeleton of curcumin the presence of hydroxylic and methoxy groups in the aryl rings and complexation with copper(II) ions significantly increased the DNA binding properties and antitumor activities of compounds. Interaction of copper complexes with DNA may be correlated with their cytotoxic effects against tumour cells. Studies on emerging targets for anticancer drugs such as cytotoxicity against other tumour cells, the rate of metabolism, absorption and stability *in vivo* should be further investigated.

REFERENCES

1. Roat-Malone, Rosette M, Bioinorganic Chemistry: A Short Course; 2nd Edn. John Wiley & Sons, Inc., Hoboken, New Jersey (2007) ISBN 978-0-471-76113-6
2. G. Fermi, J. Mol. Biol., 97 (2), 237 – 256 (1975)
3. T. A. Melenteva N. D. Pekel and V. M. Berezovskii, Russ.Chem.Rev., 38, 926-943 (1969)
4. Y. Mawani and C. Orvig, J. Inorg. Biochem., 132, 52–58 (2014)
5. R. A. Festa and D. J. Thiele, Curr. Biol. 21, 877–883 (2011)
6. J. Anastassopoulou and T. Theophanides, Bioinorg. Chem., 459, 209-218 (1995)
7. J. D. Helmann, L. M. Shewchuck, and C. T. Walsh, Adv. Inorg. Biochem., 8, 33-61(1990)
8. Geoffrey A. Lawrance, Introduction to Coordination Chemistry, Wiley, New Jersey (2009) ISBN: 978-0-470-51930-1
9. I. Bertini, H.B. Gray, S.J. Lippard and J. S. Valentine, Bioinorganic Chemistry, University Science Books, Mill Valley, USA, (1994) ISBN 0-935702-57-1
10. J. R. Glusker, Adv. Protein Chem., 42, 1-73 (1991)
11. J. Vidgren, L. A. Svensson and A. Liljas, Nature, 368, 354-358 (1994)
12. C. Moncharmont, P. Auberdiac, A. Melis, S. Afqir, C. Pacaut, C. Chargari, Y. Merrouche, and N. Magne, Bull.Cancer., 98(2), 164-175 (2011)
13. R. B. Weiss and M. C. Christian, Drugs, 46, 360–377 (1993)
14. S. Dasari and P. B. Tchounwou, Eur. J. Pharmacol., 740, 364–378 (2014)
15. J. H. Burcheranal, K. Kalaher and K. Dew, Biochemie, 60, 961-965 (1978)

16. C. Marzano, M. Pellei, F. Tisato and C. Santini, *Anticancer Agents Med. Chem.*, 9, 185-211 (2009)
17. Z. Xiao-Tong, M. Zhong-Ying, Z. Chuan, Z. Qi-Ji, X. Cheng-Zhi and X. Jing-Yuan, *J. Coord. Chem.*, 68(3), 2307–2323 (2015)
18. P. M. Takahara, C. A. Frederick and S. J. Lippard, *J. Am. Chem. Soc.*, 118, 12309-12321 (1996)
19. C. Santini, M. Pellei, V. Gandin, M. Porchia, F. Tisato and C. Marzano, *Chem. Rev.*, 114, 815-862 (2014)
20. D. M. Katja and O. Chris, *Chem. Rev.*, 114 (8), 4540–4563 (2014)
21. V.S. Govindarajan and W.H. Stahl. *Crit. Rev. Food. Sci. Nutr.*, 12, 199-301 (1980)
22. A. M. Anderson, M. S. Mitchell, and R. S. Mohan, *J. Chem. Ed.*, 77(3), 359-360 (2000)
23. G.K. Jayaprakasha, L. Jagan Mohan Rao and K. K. Sakariah, *J. Agric. Food Chem.*, 50(13), 3668-3672 (2002)
24. E. Schraufstatter and H. Bernt, *Nature*, 164, 456-457 (1949)
25. S.C. Gupta, S. Patchva and B. B. Aggarwal, *The AAPS J.*, 15(1), 195–218 (2013)
26. P. Anand, A.B. Kunnumakkara, R.A. Newman and B.B. Aggarwal. *Mol. Pharm.*, 4, 807-818 (2007)
27. T. N. Shankar, N. V. Shantha, H. P. Ramesh, I. A. Murthy and V. S. Murthy, *Indian J. Exp. Biol.*, 18 (1), 73–75 (1980)
28. K.I. Priyadarsini. *Curr. Pharm. Des.*, 19, 2093-2100 (2013)
29. S. Prasad, S. C. Gupta, A. K. Tyagi and B. B. Aggarwal, *Biotechnol. Adv.*, 32, 1053–1064 (2014)
30. R. Sakey, A.F. Bafubiandi-Mulaba, V. Rajnikanth, K. Varaprasad, N.N. Reddy and K.M. Raju, *J. Inorg. Organomet. Polym. Mat.*, 22, 1254–1262 (2012)

31. R.K. Gangwar, G.B. Tomar, V.A. Dhumale, S. Zinjarde, R.B. Sharma and S. Datar, *J. Agric. Food Chem.*, 61, 9632–9637 (2013)
32. K.I. Priyadarsini, *Free Radic. Biol. Med.*, 23, 838–884 (1997)
33. B. B. Aggarwal, C. Sundaram, N. Malani and H. Ichikawa, *Vol. 595*, 1- 75 (2007)
34. B. Wahlstrom and G. Blennow, *Acta Pharmacol. Toxicol.*, 43 (2), 86– 92 (1972)
35. Z. Ma, A. Shayeganpour, D.R. Brocks, A. Lavasanifar and J. Samuel, *Biomed. Chromatogr.*, 21, 546-552 (2007)
36. L. Jun-Ling, J. Lin, L. Si-Tong, T. Jin-Lei, G. Wen, L. Xin and Y. Shi-Ping, *J. Coord. Chem.*, 67(22), 3598–3612 (2014)
37. Q. Shi K., Wada, E. Ohkoshi, L. Lin, R. Huang, S.L. Morris-Natschke, M. Goto and K.H. Lee, *Bioorg. Med. Chem.* 20, 4020–4031 (2012)
38. H. J. Roth and B. Miller, *Arch. Pharm.*, 297, 660–673 (1964)
39. K. Krishnankutty and M.B. Ummathur, *Russian J. Coord. Chem.*, 34, 502-510 (2008)
40. B. Samya and R. C. Akhil, *Accounts of Chemical Research*, 48 (7), 2075-2083 (2015)
41. W. A. Wani, Z. Al-Othman, I. Ali, K. Saleem and M.F. Hsieh, *J. Coord. Chem.*, 67(12), 2110-2130 (2014)
42. R. Pallikkavil, M.B. Ummathur, S. Sreedharan and K. Krishnankutty, *Main Group Metal Chem.*, 36, 123–127 (2013)
43. J. Sheikh, H. Juneja, V. Ingle, P. Ali and T. B. Hadda, *J. Saudi Chem. Soc.*, 17(3), 269-276 (2013)
44. H. J. J. Pabon, *Rec. Trav. Chim. Pays Bas*, 83, 379-386 (1964)
45. G.K. Jayaprakasha, L. Jagan Mohan Rao and K.K. Sakariah, *Trends Food Sci. Tech.*, 16, 533–548 (2005)

46. H. P. T. Ammon, M. I. Anazoda, H. Safayhi, B. N. Dhawan and R. C. Srimal, *Planta Medica*, 58, 26–28 (1992)
47. W. Simon, L. Volker, S. Abdus and T.E. Frank, *Chem. Soc. Rev.*, 44, 4986-5002 (2015)
48. M.H.M. Leung, T. Harada and T.W. Kee, *Curr. Pharm. Des.*, 19, 2070-2083 (2013)
49. B.S. Mendiguchia, I. Aiello and A. Crispini, *Dalton Trans.*, 44, 9321-9334 (2015)
50. N.C. Kelkar and B. Sanjeev Rao, *J. Indian Inst. Sci.*, 17A, 7–10 (1933)
51. Y.Kiso, Y.Suzuki, Y.Oshima, and H.Hikino, *Phytochemistry*, 22, 596–597 (1983)
52. N. F. Cooray, E.R. Jansz, J. Ranatunga, and S. Wimalasena, *Journal of the National Science Council of Sri Lanka*, 16, 39–51 (1988)
53. S.Imai, M.Morikiyo, K.Furihata, Y. Hayakawa, and H. Seto, *Agric. Biol. Chem.*, 54, 2367–2371 (1990)
54. H.A Vogel and J. Pelletier, *J. Pharma.*, 2, 50, (1815)
55. J. Milobedzka, V. Kostanecki and V. Lampe, *Ber. Dtsch. Chem. Ges.*, 43, 2163-2170 (1910)
56. B. S. Sastry, *Research and Industry*, 15, 258–260 (1970)
57. N. Krishnamurthy, A.G. Mathew, E.S. Nambudiri, S.Shivashankar, Y.S. Lewis and C. P. Natarajan, *Tropical Science*, 18, 37–39 (1976)
58. W.Baumann, S. V. Rodrigues and L. M. Viana, *Braz. J. Chem. Eng.*, 17, 323–328 (2000)
59. D. V. Dandekar and V. G. Gaikar, *Sep. Sci. Tech.*, 37, 2669–2690 (2002)
60. A. Bagchi, *J. Environ. Sci. Toxicol. Food Technol.*, 1, 1–16 (2012)
61. K.R. Srinivasan, *J. Pharm. Pharmacol.*, 5, 448–457 (1953)

62. S. Kawano, Y. Inohana, Y. Hashi and J. Lin, *Chin. Chem. Lett.*, 24, 685–687 (2013)
63. H.H. Tonnesen, J. Karlsen and A. Mostad, *Acta Chem. Scand. B*, 36, 475–480 (1982)
64. Y. Ishigami, M. Goto, T. Masuda, Y. Takizawa and S. Suzum, *J. Jpn. Soc. Colour Mater.*, 72(2), 71-77 (1999)
65. V. Lampe, *Eur. J. Inorg. Chem.*, 51(2), 1347–1355 (1918)
66. E. Venkata Rao and P. Sudheer, *Indian J. Pharm Sci.*, 73(3), 262–270 (2011)
67. M.O. Iwunze and D. McEwan, *Cell. Mol. Biol.*, 50, 749–752 (2004)
68. J.E. Kim, A.R. Kim, H.Y.Chung, S.Y. Han and B.S. Kim, J.S.Choi, *Phytother. Res.*, 17, 481–484 (2003)
69. M. Borsari, E. Ferrari, R. Grandi and M. Saladini, *Inorg. Chim. Acta*, 328, 61–68 (2002)
70. Y.M. Sun, H.Y. Zhang, D.Z. Chen and C.B. Liu, *Org. Lett.*, 4, 2909–2911 (2002)
71. K.I. Priyadarsini, D.K. Maity, G.H. Naik, M.S. Kumar, M.K. Unnikrishnan, J.G. Satav and H. Mohan, *Free Radic. Biol. Med.*, 35, 475–484 (2003)
72. B. Mishra, K.I Priyadarsini, M.K. Bhide, R.M. Kadam and H. Mohan, *Free Radic. Res.*, 38, 355–362 (2004)
73. S.V. Jovanovic, C.W. Boone, S. Steenken, M. Trinoga and R.B. Kaskey, *J. Am. Chem. Soc.*, 12, 3064–3068 (2001)
74. O.P. Sharma, *Biochem. Pharmacol.*, 25, 1811-1812 (1976)
75. G. Cao, C.P. Verdon, A.H.B. Wu, H. Wang and R.L. Prior, *Clin. Chem.*, 41, 1738-1744 (1995)
76. H.H. Tonnesen, A.F. Arrieta and D. Lerner, *Pharmazie*, 50, 689-693 (1995)
77. H.H. Tonnesen, and J.V. Greenhill, *Int. J. Pharmacol.*, 87, 79-87 (1992)

78. L.R.C. Barclay and M. Vinqvist, *Org. Lett.*, 2, 2841- 2843 (2000)
79. J.S. Wright, E.R. Johnson and G.A. Dilabio, *J. Am. Chem. Soc.*, 123 (6), 1173-1183 (2001)
80. M.V. Canamares, J.V Garcia-Ramos and S. Sanchez-Cortes, *Appl. Spectrosc.*, 60, 1386–1391 (2006)
81. Y.J. Wang, M.H. Pan, A.L.Cheng, L.I. Lin, Y.S. Ho, C.Y. Hsieh and J.K. Lin, *J. Pharm. Biomed. Anal.*, 15, 1867–1876 (1997)
82. A. Khurana and C.T. Ho, *J. Liquid Chromatogr.*, 11, 2295–2304 (1988)
83. K.I. Priyadarsini, *J. Photochem. Photobiol. C*, 10, 81–96 (2009)
84. H.H. Tonnesen, H. de Vries, J. Karlsen and B.V. Henegouwen, *J. Pharm. Sci.*, 76, 371–373 (1987)
85. U. Singh, S.Verma, H.N. M.C. Ghosh Rath, K.I.Priyadarsini, A. Sharma, K.K. Pushpa, S.K. Sarkar and Mukherjee, *J. Mol. Catal. A*, 318, 106–111 (2010)
86. A.Asai and T.Miyazawa, *Life Sci.*, 67, 2785–2793 (2000)
87. C.R. Ireson, D.J.L. Jones, S. Orr, M.W.H. Coughtrie, D.J. Boocock, M.L.Williams, P.B. Farmer, W.P. Steward and A.J. Gesher, *Cancer Epidemiol. Biomark. Prev.*, 11, 105–111 (2002)
88. S. Gupta, S. Prasad, H.K. Ji, S. Patchva, L.J.Webb, K.I. Priyadarsini and B.B. Aggarwal, *Nat. Prod. Rep.*, 28, 1937–1955 (2011)
89. G. Grykiewicz and P. Silfirski, *Acta Biochim. Pol.*, 59, 201–212 (2012)
90. S. Awasthi, U. Pandya, S.S. Singhal, J.T. Lin, V. Thiviyathan, W.E. Seifert, Y.C. Awasthi and G.A. Ansari, *Chem. Biol. Int.*, 128, 19–38 (2000)
91. J. Fang, L. Jun and A. Holmegren, *J. Biol. Chem.*, 280, 25284–25290 (2005)
92. Y. Jung, W. Xu, H. Kim, N. Ha and L. Neckers, *Biochim. Biophys. Acta Mol. Cell Res.*, 1773, 383–390 (2007)

93. W. Li, W. Wu, F. Yu, H. Huang, X. Liang and J. Ye, *Org. Biomol. Chem.*, 9, 2505–2511 (2011)
94. P.S. Ramanjaneyulu, Y.S. Sayi, V.A. Raman and K.L. Ramakumar, *J. Radioanal. Anal. Nucl. Chem.*, 274, 109–114 (2007)
95. L. Baum and A. Ng, *J. Alzheimer's Dis*, 6, 367–377 (2004)
96. T. Jiang, X. Zhi, Y. Zhang, L. Pan and P. Zhou, *Biochim. Biophys. Acta Mol. Basis Dis.*, 1822, 1207–1215 (2012)
97. T. Jiang, L. Wang, S. Zhang, P.C. Sun, C.F. Ding, Y.Q. Chu and P. Zhou, *J. Mol. Struct.*, 1004, 163–173 (2011)
98. M.H.M. Leung, T. Harada and T. W. Kee, *Curr. Pharm. Des.*, 19, 2070–2083 (2013)
99. F. Kuhlwein, K. Polborn and W. Beck, *Z. Anorg. Allg. Chem.*, 623, 1211–1219 (1997)
100. O. Vajragupta, P. Boonchoong, H. Watanabe, Y. Wongkrajang and N. Kammasud, *Free Radic. Biol. Med.*, 35, 1632–1644 (2003)
101. O. Vajragupta, P. Boonchoong and L.J. Berliner, *Free Radic. Res.*, 38, 303–314 (2004)
102. A. Barik, B. Mishra, L. Shen, H. Mohan, R.M. Kadam, S. Dutta, H. Zhang and K.I. Priyadarsini, *Free Radic. Biol. Med*, 39, 811–822 (2005)
103. A. Barik, B. Mishra, A. Kunwar, R.M. Kadam, L. Shen, S. Dutta, S. Padhye, A.K. Satpati, H.Y. Zhang and K.I. Priyadarsini, *Eur. J. Med. Chem.* 42, 431–439 (2007)
104. S.C. Gupta, S. Patchva, W. Koh, and B.B. Aggarwal, *Clin. Exp. Pharmacol. Physiol.*, 39(3), 283–299 (2012)
105. N. Ghatak and N. Basu *Indian J. Exp. Biol.*, 10, 235–236 (1972)
106. R.C. Srimal and B.N. Dhawan, *J. Pharm. Pharmacol.*, 25, 447–452 (1973)
107. S. Singh and B.B. Aggarwal, *J. Biol. Chem.*, 270, 4995–5000 (1995)

108. R. Kuttan, P. Bhanumathy, K. Nirmala and M.C. George, *Cancer Lett.*, 29,197–202 (**1985**)
109. K. Varaprasad, K. Vimala, S. Ravindra, N. Narayana Reddy, G. Venkata Subba Reddy and K. Mohana Raju, *J. Mater. Sci.Mater. Med.*, 22 (8), 1863–1872 (**2011**)
110. C.H. Liu and H. Y. Huang, *Chem. Pharm. Bull.*, 60(9), 1118–1124 (**2012**)
111. T. Amrouche, K.S. Noll, Y. Wang, Q. Huang, and M. L. Chikindas, *Probiotics and Antimicrobial Proteins*, 2(4), 250–257 (**2010**)
112. S. H. Mun, D. K. Joung and Y.S. Kim, *Phytotherapy Research*, 19 (7), 599–604 (**2013**)
113. S. A. Marathe, R. Kumar, P. Ajitkumar, V. Nagaraja, and D. Chakravortty, *J. Antimicro. Chemo.*, 68(1), 139–152 (**2013**)
114. S. Hatamie, M. Nourian and S. K. Karandikar., *Mate. Sci. and Eng.*, 32(2), 92–97(**2012**)
115. K. Varaprasad, Y. M. Mohan, K. Vimala, and K. Mohana Raju, *J. Appl. Polym. Sci.*, 12 (2), 784–796 (**2011**)
116. K. Vimala, Y. M. Mohan and K. Varaprasad, *J. Biomater. Nanobiotech.*, 2(1), 55–64 (**2011**)
117. I. Dairaku, Y. Han, N. Yanaka, and N. Kato, *Biosci. Biotechnol. Biochem.*, 74(1), 185–187 (**2010**)
118. A. Mazumder, K. Raghavan, J. Weinstein, K. W. Kohn, and Y. Pommier, *Biochem. Pharmacol.*, 49(8), 1165–1170 (**1995**)
119. D.Y. Chen, J.H. Shien and L. Tiley, *Food Chem.*, 119(4), 1346–1351 (**2010**)
120. R. S. Upendra, P. Khandelwal and A. H. M. Reddy, *Int. J. Eng. Sci.*, 3(11), 7899–7904 (**2011**)
121. B. Uttara, A.V. Singh, P. Zamboni and R. T. Mahajan, *Curr. Neuropharmacol.*, 7, 65–74 (**2009**)
122. R. Kahl, *Toxicol.*, 33, 185–228 (**1984**)

123. M.S. Kozarski, A.S. Klaus, M.P. Niksic, L.J.L.D. van Griensven, M.M. Vrvic and D.M. Jakovljevic, *Chem. Ind.*, 68, 305–320 (2014)
124. F. Balkwill, K.A. Charles and A. Mantovani, *Cancer Cell.*, 7, 211-217 (2005)
125. M. Philip, D.A. Rowley and H. Schreiber, *Semin. Cancer Biol.*, 14, 433-439 (2004)
126. B.B. Aggarwal, A. Kumar and A.C.Bharti, *Anticancer Res.*, 23 (1A), 363–398 (2003)
127. S.V. Singh, X. Hu, S.K. Srivastava, M. Singh, H. Xia, J.L. Orchard and H.A. Zaren, *Carcinogenesis*, 19 (8), 1357–1360 (1998)
128. M.T. Huang, Y.R. Lou, W. Ma, H.L. Newmark, K.R. Reuhl and A.H. Conney, *Cancer Res.*, 54 (22), 5841–5847 (1994)
129. T. Kawamori, R. Lubet, V.E. Steele, G.J. Kelloff, R.B. Kaskey, C.V. Rao and B.S. Reddy, *Cancer Res.*, 59 (3), 597–601 (1999)
130. G. Kelloff, J.Crowell and E. Hawk, *J. Cell. Biochem.*, 26 S, 72–85 (1996)
131. H.W. Chen, and H.C. Huang, *Br. J. Pharmacol.*, 124 (6), 1029–1040 (1998)
132. R. Kuttan, P.C. Sudheeran and C.D. Josph, *Tumori*, 73, 29–31 (1987)
133. Z.Y. He, C.B. Shi, H. Wen, F.L. Li, B.L. Wang and J. Wang , *Cancer Investig.*, 29(3), 208–213 (2011)
134. D. Karunakaran, R. Rashmi and T.R. Kumar, *Curr. Cancer Drug Targets.*, 5, 117–129 (2005)
135. L .Helson, *Biofactors*, 39, 21-26 (2013)
136. G. P. Lim, T. Chu, F. Yang, W. Beech, S. A. Frautschy and G. M. Cole, *J. Neurosci.*, 21, 8370–8377 (2001)
137. M. P. Mattson and R.E. Rydel, *Nature*, 382(6593), 674–675 (1996)
138. L. Baum, C.W. Lam, S.K. Cheung, T .Kwok, V. Lui and J. Tsoh, *J. Clin. Psychopharmacol.*, 28(1), 110–113 (2008)

139. J.M. Ringman, S.A. Frautschy, G.M. Cole, D.L. Masterman and J.L. Cumming, *Curr. Alzheimer Res.* 2(2), 131–136 (2005)
140. J. Hong, M. Bose, J. Ju, J.H. Ryu, X. Chen, S. Sang, M.J. Lee and C.S. Yang, *Carcinogenesis*, 25(9), 1671–1679 (2004)
141. L. Pari and P. Murugan, *J. Med. Food*, 10, 323–329 (2007)
142. M.A. El-Moselhy, A. Taye, S.S. Sharkawi, S.F. El-Sisi and A.F. Ahmed, *Food Chem. Toxicol.*, 49, 1129–1140 (2011)
143. M. Srinivasan, *Indian J. Med. Sci.*, 26(4), 269–270 (1972)
144. S.D. Deodhar, R. Sethi and R.C. Srimal, *Indian J. Med. Res.*, 71, 632–634 (1980)
145. B. Chandran and A. Goel, *Phytother. Res.* 26(11), 1719–1725 (2012)
146. A. Kunwar, A. Barik, R. Pandey and K.I. Priyadarsini, *Biochim. Biophys. Acta (Gen.)*, 1760, 1513–1520 (2006)
147. S.F. Chin, K.S. Iyer, M. Saunders, G. Tim, C. Buckley, M. Paskevicious, and C.L. Raston, *Chemistry*, 15, 5661–5665 (2009)
148. D. Jin, K.W. Park, J.H. Lee, K. Song, J.G. Kim, M.L. Seo and J.H. Jung, *J. Mat. Chem.*, 21, 3641–3645 (2011)
149. A.K. Dinda, C.K. Prashant and S. Naqvi, *Int. J. Nanotechnol.*, 9, 862–871 (2012)
150. R.K. Gangwar, G.B. Tomar, V.A. Dhumale, S. Zinjarde, R.B. Sharma and S. Datar, *J. Agric. Food Chem.*, 61, 9632–9637 (2013)
151. S.P. Singh, M. Sharma and P.K. Gupta, *Lasers Med. Sci.*, 29, 645–652 (2014)
152. R.K. Gangwar, V.A. Dhumale, D. Kumari, U.T. Nakate, S.W. Gosavi, R.B. Sharma, S.N. Kale and S. Datar, *Mater. Sci. Eng.*, 32, 2659–2663 (2012)
153. K. Krishnankutty and P. Venugopalan, *Synth. React. Inorg. Met.-Org. Chem.*, 28, 1313–1325 (1998)

154. V.D. John and K. Krishnankutty, *Main Group Met. Chem.*, **33**, 157-165 (2010)
155. K. Krishnankutty and V.D. John, *Synth. React. Inorg.Met.-Org. Chem.*, **33**, 343-358 (2003)
156. V. D. John and K. Krishnankutty, *Appl. Organometal. Chem.*, **20**, 477–482 (2006)
157. V.D. John, G. Kuttan and K. Krishnankutty, *J. Exp. Clin. Cancer Res.*, **21**, 219–224 (2002)
158. J. Wang, D. Wei, B. Jiang, T. Liu, J. Ni, and S. Zhou, *Transition Met. Chem.*, **39**(5), 553-558 (2014)
159. A. Anusch, G.C. Guy, Q. Lionel, S. Daniel, J. Gerard and B. Emilie, *Med. Chem. Commun.*, **2**, 190-195 (2011)
160. E. Ferrari, B. Arezzini, M. Ferrali, S. Lazzari, F. Pignedoli, F. Spagnolo and M. Saladini, *BioMetals*, **22**, 701–710 (2009)
161. Y. Sumanont, Y. Murakami, M. Tohda, O. Vajragupta, H. Watanabe and K. Matsumoto, *Biol. Pharm. Bull.*, **30**, 1732–1739 (2007)
162. K. K. Sharma, S. Chandra and D. K. Basu, *Inorg. Chim. Acta*, **135**, 47–48 (1987)
163. S. Daniel, J.L. Limson, A. Dairam, G.M. Watkins and S. Daya, *J. Biol. Inorg. Chem.*, **98**, 266–275 (2004)
164. Z. Sui, R. Salto, J. Li, C. Craik and P. R. Ortiz de Montellano, *Bioorg. Med. Chem.*, **1**, 415–422 (1993)
165. E. Ferrari, R. Benassi, S. Sacchi, F. Pignedoli, M. Asti and M. Saladini, *J. Inorg. Biochem.*, **139**, 38–48 (2014)
166. T. Jiang, L. Wang, S. Zhang, P.C. Sun, C.F. Ding, Y.Q. Chu and P. Zhou, *J. Mol. Struct.*, **1004**, 163–173 (2014)
167. F. Ahmadi, A.A. Alizadeh, N. Shahabadi and M. Rahimi-Nasrabadi, *Spectrochim. Acta, Part A*, **79**, 1466–1474 (2011)

168. K. H. Thompson, K. Bohmerle, E. Polishchuk, C. Martins, P. Toleikis, J. Tse, V. Yuen, J. H. McNeill and C. Orvig, *Inorg. Biochem.*, 98, 2063–2070 (2004)
169. M. I. Khalil, M.M. Al-Qunaibit, A.M. Al-zahem and J.P. Labis, *Arabian J. Chem.*, 7, 1178–1184 (2014)
170. Z. Pi, J. Wang, B. Jiang, G. Cheng and S. Zhou, *Mater. Sci Eng.*, 46, 565–571 (2015)
171. S.S. Zhou, X. Xue, J.F. Wang, Y. Dong, B. Jiang, D. Wei, M.L. Wan and Y. Jia, *J. Mater. Chem.*, 22, 22774–22780 (2012)
172. B. Banik, K. Somyajit, G. Nagaraju and A. R. Chakravarty, *Dalton Trans.*, 43, 13358–13369 (2014)
173. S.S. Zhou, X. Xue, J.F. Wang, Y. Dong, B. Jiang, D. Wei, M.L. Wan and Y. Jia, *J. Mater. Chem.*, 22, 22774–22780 (2012)
174. P. Agostinis, K. Berg, K.A. Cengel, T.H. Foster, A.W. Girotti, S.O. Gollnick, S.M. Hahn, M.R. Hamblin, A. Juzeniene, D. Kessel, M. Korbelik, J. Moan, P. Mroz, D. Nowis, J. Piette, B.C. Wilson and J. Golab, *Cancer J. Clin.*, 61, 250–281 (2011)
175. L.B. Josefsen and R.W. Boyle, *Met-Based Drugs*, 1–24 (2008)
176. T. K. Goswami, S. Gadadhar, B. Gole, A.A. Karande and A. R. Chakravarty, *Eur. J. Med. Chem.*, 63, 800–810 (2013)
177. D. Pucci, T. Bellini, A. Crispini, I.D. Agnano, P.F. Liguori, P. Garcia-Orduna, S. Pirillo, A. Valentini and G. Zanchetta, *Med. Chem. Commun.*, 3, 462–468 (2012)
178. C. Triantis, T. Tsokatos, C. Tsoukalas, M. Sagnou, C. Raptopoulou, A. Terzis, V. Psycharis, M. Pelecanou, I. Pirmettis and M. Papadopoulos, *Inorg. Chem.*, 52, 12995–13003 (2013)
179. C.F. Ramogida and C. Orvig, *Chem. Commun.*, 49, 4720–4739 (2013)

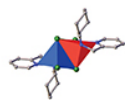
180. M. Sagnou, D. Benaki, C. Triantis, T. Tsotakos, V. Psycharis, C.P. Raptopoulou, I. Pirmettis, M. Papadopoulos and M. Pelecanou, *Inorg. Chem.*, 50(4), 1295-1303 (2011)
181. F. Caruso, M. Rossi, A. Benson, C. Opazo, D. Freedman, E. Monti, M. B. Gariboldi, J. Shaulky, F. Marchetti, R. Pettinari and C. Pettinari, *J. Med. Chem.*, 55, 1072–1081 (2012)
182. A. Hussain, K. Somyajit, B. Banik, S. Banerjee, G. Nagaju and A. R. Chakravarty, *Dalton Trans.*, 42, 182–195 (2013)
183. Y.M. Song, J.P. Xu, L. Ding, Q. Hou, J.W. Liu and Z.L. Zhu, *J. Inorg. Biochem.*, 103, 396–400 (2009)
184. W.L.F. Armarego and D.D. Perrin, *Purification of Laboratory Chemicals*, 3rd Edn, Pergamon Press Inc., New York (1988)
185. K.V.D. Babu and K.N. Rajasekharan, *Org. Prep. Proc. Int'l.*, 26, 674–677 (1994)
186. K. Nakamoto, *Advances in the Chemistry of Coordination Compounds*, S. Kirschner Edn. Mc Millan, New York (1961)
187. K.C. Joshi and V.N. Pathak, *Coord. Chem. Rev.*, 22, 37-122 (1977)
188. P.J. Roughley and D.A. Whiting, *J. Chem. Soc. Perkin Trans. I.*, 2379-2388 (1973)
189. V.D. John and K. Krishnankutty, *Trans. Met. Chem.*, 30, 229-233 (2005)
190. C.G. Macdonald and J.S. Shannon, *Aust. J. Chem.*, 19, 1545-1566 (1966)
191. R.S. Drago, *Physical Methods for Chemists*, 2nd Edn, Surfside Scientific Publishers, Gainesville, (1992) ISBN 0-03-075176-4
192. A.D. Naik, S.M. Annigeri, U.B. Gangadharmath, V.K. Revankar and V.B. Mahale, *Trans. Met. Chem.*, 27, 333-336 (2002)
193. R. Atkins, G. Brewer and E. Kokot. *Inorg. Chem.*, 24, 127-134 (1985)

194. S. Chandra, D. Jain and A.K. Sharma, *Spectrochim. Acta Part A*, 71, 1712-1719 (2009)
195. I. Adato and I. Eliezer, *J. Chem. Phys.*, 54, 1472-1476 (1971)
196. L. A. Pham-Huy, H. He and C. Pham-Huy, *Int. J. Biomed. Sci.*, 4, 89–96 (2008)
197. S. Sen, R. Chakraborty, C. Sridhar, Y.S.R. Reddy and B. De, *Int. J. Pharma. Sci. Rev. Res.*, 3, 91–100 (2010)
198. M. Valko, D. Leibfritz, J. Moncol, M.T.D. Cronin, M. Mazur and J. Telser, *Int. J. Biochem., Cell Biol.*, 39, 44–84 (2007)
199. B. Halliwell and J.M.C. Gutteridge, *Free Rad. Biol. Med.*, 3rd edn. Oxford University Press: New York, USA, 10-121(1999)
200. V. K. Gupta and S.K. Sharma, *Nat. Prod. Radiance*, 5, 326–334 (2006)
201. G. S. Rathore, M. Suthar, A. Pareek and R.N. Gupta, *J. Nat. Pharmaceuticals*, 2, 2–14 (2011)
202. R. Choudhary, V. K. Chawala, N. D. Soni, J. Kumar and R. K. Vyas, *Pak. J. Physiol.*, 6, 54–59 (2010)
203. R. Aquino, S. Morelli, M. R. Lauro, S. Abdo, A. Saija and A. Tomaino, *J. Nat. Prod.*, 64, 1019-1023 (2001)
204. H. Ohkawa, N. Ohishi and K. Yagi, *Anal. Biochem.*, 95, 351-358 (1979)
205. J.M. McCord and I. Fridovich, *J. Biol. Chem.*, 244(22), 6049-6055 (1969)
206. A.J. Ruby, G. Kuttan, K.V.D. Babu, K.N. Rajasekharan and R. Kuttan, *Cancer Lett.*, 94, 79-83 (1995)
207. J. Marmur, *J. Mol. Biol.*, 3, 208-218 (1961)
208. N. Mahalakshmi and R. Rajavel, *Asian J. Biochem. Pharm. Res.*, 2, 525-543 (2011)
209. W.C. Chen, L.D. Wang, Y.T. Li, Z.Y. Wu and C.W. Yan, *Transition Met. Chem.*, 37, 569-577 (2012)

210. L. Leelavathy, S. Anbu, M. Kandaswamy, N. Karthikeyan and N. Mohan, *Polyhedron*, 28, 903-910 (2009)
211. A. Wolfe, G.H.J. Shimer and T. Meehan, *Biochemistry*, 26, 6392-6396 (1987)
212. C.Z. Xie, M.M. Sun, S.H. Li, X.T. Zhang, X. Qiao, Y. Ouyang and J.Y. Xu, *J. Coord. Chem.*, 66, 3891-3905 (2013)
213. D.D. Li and Z.W. Tao, *J. Coord. Chem.*, 66, 4237-4254 (2013)
214. D.S. Raja, N.S.P. Bhuvanesh and K. Natarajan, *Inorg. Chim. Acta.*, 385, 81-93 (2012)
215. P. Jaividhya, R. Dhivya, M.A. Akbarsha and M. Palaniandavar, *J. Inorg. Biochem.*, 114, 94-105 (2012)
216. S. Anbu, A. Killivalavan, E.C. Alegria, G. Mathan and M. Kandaswamy, *J. Coord. Chem.*, 66, 3989-4003 (2013)
217. Z.L. Hua, W.W. Na, W. Yuan and S. Guang, *J. Coord. Chem.*, 66, 227-242 (2013)
218. X.L. Wang, M. Jiang, Y.T. Li, Z.Y. Wu and C.W. Yan, *J. Coord. Chem.*, 66, 1985-2003 (2013)
219. S. Thalamuthu, B. Annaraj, S. Vasudevan, S. Sengupta and M.A. Neelakantan, *J. Coord. Chem.*, 66, 1805-1820 (2013)
220. M. Ganeshpandian, S. Ramakrishnan, M. Palaniandavar, E. Suresh, A. Riyasdeen and M.A. Akbarsha, *J. Inorg. Biochem.*, 140, 202-212 (2014)
221. P. Kalaivani, R. Prabhakaran, E. Vaishnavi, T. Rueffer, H. Lang, P. Poornima, R. Renganathan, V.V. Padmad and K. Natarajan, *Inorg. Chem. Front.*, 1, 311-324 (2014)
222. D. Lawrence, V.G. Vaidyanathan and B.U. Nair, *J. Inorg. Biochem.*, 100, 1244-1251 (2006)
223. J. Li, Y.L. Wei, L.M. Guo, C.H. Zhang and Y. Jiao, *Talanta*, 76, 34 (2008)

224. C.A. Mitsopoulou, C.E. Dagas and C. Makedonas, *Inorg. Biochem.*, 102, 77-86 (2008)
225. R.C. Santra, K. Sengupta, R. Dey, T. Shireen, P. Das, P.S. Guin, K. Mukhopadhyay and S. Das, *J. Coord. Chem.*, 67, 265-285 (2014)
226. F. Gao, H. Chao, F. Zhou, Y.X. Yuan, B. Peng and L.N. Ji, *J. Inorg. Biochem.*, 100, 1487-1494 (2006)
227. J. Rajesh, M. Rajasekaran, G. Rajagopal and P. Athappan, *Spectrochim. Acta Part A*, 97, 223-230 (2012)
228. S.A. Altman, L. Randers and G. Rao, *Biotechnol. Prog.*, 9, 671-674 (1993)
229. H. Benezra, V.C. da Silveira, J.S. Luz, R.C. Georg, C.C. Oliveira and A.M. Ferreira, *J. Inorg. Biochem.*, 105, 1692-1703 (2011)
230. J.A. Ruby, M.N.A. Rao, G. Kuttan, R. Kuttan, K. Satyanarayana and M.N.A. Rao, *J. Clin. Biochem. Nutr.*, 17, 73-80 (1994)
231. J.A. Ruby, G. Kuttan, K.V.D. Babu, K.N. Rajasekharan and R. Kuttan, *Int. J. Pharm.*, 132(1), 1-7 (1996)
232. J.R. Anto, K.V.D. Babu, K.N. Rajasekharan and R. Kuttan, *Cancer Lett.*, 94, 79-83 (1995)
233. J.E. Moulder and S. Rockwell, *Int. J. Radiat., Oncol. Biol. Phys.*, 10, 695-712 (1984)
234. W.M. Weber, L.A. Hunsaker, S.F. Abcouwer, L.M. Deck and D.L. Vander-Jagt, *Bioorg. Med. Chem.*, 13, 3811-3820 (2005)
235. U. Jungwirth, C.R. Kowol, B.K. Keppler, C.G. Hartinger, W. Berger and P. Heffeter, *Antioxid. Redox Signal*, 15, 1085-1127 (2011)
236. N. Sreejayan and M.N.A. Rao, *Int. J. Pharm.*, 100, 93-97 (1993)

PUBLICATIONS



ISSN: 0095-8972 (Print) 1029-0389 (Online) Journal homepage: <http://www.tandfonline.com/loi/gcoo20>


Synthesis, DNA-binding, and cytotoxic studies on three copper(II) complexes of unsymmetrical synthetic analogues of curcumin

T. V. Deepthi & P. Venugopalan

To cite this article: T. V. Deepthi & P. Venugopalan (2016) Synthesis, DNA-binding, and cytotoxic studies on three copper(II) complexes of unsymmetrical synthetic analogues of curcumin, Journal of Coordination Chemistry, 69:22, 3403-3416, DOI: [10.1080/00958972.2016.1227973](https://doi.org/10.1080/00958972.2016.1227973)


To link to this article: <http://dx.doi.org/10.1080/00958972.2016.1227973>

 View supplementary material 

 Accepted author version posted online: 26 Aug 2016.
Published online: 12 Sep 2016.

 Submit your article to this journal 

 Article views: 89

 View related articles 

 View Crossmark data 

Synthesis, DNA-binding, and cytotoxic studies on three copper(II) complexes of unsymmetrical synthetic analogues of curcumin

T. V. Deepthi and P. Venugopalan

Department of Chemistry, Sree Neelakanta Government Sanskrit College (Affiliated to the University of Calicut), Pattambi, Kerala, India

ABSTRACT

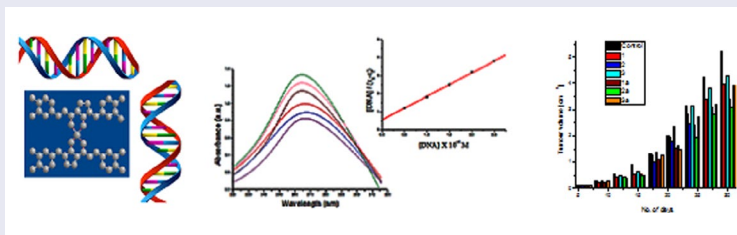
Copper(II) chelates of three unsymmetrical synthetic analogs of curcumin, namely (2E)-2-(4-hydroxy-3-methoxybenzylidene)-5-((E)-3-(4-hydroxy-3-methoxyphenyl)acryloyl)cyclopentanone (**1**), (2E)-2-(3,4-dihydroxybenzylidene)-5-((E)-3-(3,4-dihydroxyphenyl)acryloyl)cyclopentanone (**2**), and (2E)-2-(3,4-dimethoxybenzylidene)-5-((E)-3-(3,4-dimethoxyphenyl)acryloyl)cyclopentanone (**3**) have been synthesized and characterized by physicochemical and spectroscopic methods. The ligands were in their enolic form and metal complexes have 1 : 2 metal:ligand stoichiometry. The DNA-binding properties of the ligands and their metal complexes were studied by absorption titrations, fluorescence quenching experiments, and viscosity measurements with calf-thymus DNA. The interactions of copper(II) complexes were higher than that of free ligands. The observed intrinsic binding constants reveal moderate interaction of copper(II) complexes with calf-thymus DNA. The binding involves intercalative mode through non-covalent interactions and produced conformational changes in the structure of DNA. The compounds were investigated for their possible cytotoxic and antitumor activities. All the compounds were cytotoxic towards Dalton's lymphoma ascites cells. It was found that copper chelates are remarkably active compared to free curcumin analogs. Concentrations needed for 50% cell death were 10–22 $\mu\text{g mL}^{-1}$ for copper complexes and 27–52 $\mu\text{g mL}^{-1}$ for curcumin analogs. Copper complex of **2** with two hydroxyl groups in the phenyl ring was most active towards Dalton's lymphoma ascites cells (increase in life span 77.91%). Copper(II) complex of **3**, which possesses methoxy groups in the phenyl ring system, showed the lowest activity towards increase in lifespan of tumor-bearing mice (increase in lifespan 60.14%). Copper chelates of all curcuminoid analogs showed a significant reduction in solid tumor volume in mice.

ARTICLE HISTORY


Received 4 May 2016
Accepted 27 July 2016

KEYWORDS

Synthetic curcuminoids;
DNA-binding; cytotoxicity;
copper(II) complexes;
intercalative activity



CONTACT P. Venugopalan  venugpamrita@gmail.com

 Supplemental data for this article can be accessed at <http://dx.doi.org/10.1080/00958972.2016.1226503>.

1. Introduction

The yellow pigment curcumin present in the roots and shoots of herbaceous plant *Curcuma Longa L* (turmeric) and several other related curcuma species of the family *Zingiberaceae* is a 1,7-diaryl substituted α,β -unsaturated 1,3-diketone exerting a wide range of pharmacological activities including anti-oxidative, anti-inflammatory, and anticancer activities [1–4]. However, clinical application of curcumin in antitumor therapy has been limited by its rapid metabolism, low absorption, and poor stability *in vivo* [5, 6]. Chemically, curcumin is a diferuloylmethane molecule [1,7-bis(4-hydroxy-3-methoxyphenyl)-1,6-heptadiene-3,5-dione] containing two ferulic acid residues joined by a methylene bridge. It has three important functionalities: an aromatic *o*-methoxy phenolic group, an α,β -unsaturated β -diketo moiety, and a seven-carbon linker. Extensive research has provided evidence for the role of these different functional groups in its biological activities [7, 8]. The *o*-methoxy-phenol group and methylenic hydrogen are responsible for the antioxidant activity of curcumin, and curcumin donates an electron/hydrogen to reactive oxygen species [9, 10]. Curcumin interacts with a number of biomolecules through non-covalent and covalent binding. The hydrogen bonding and hydrophobicity of curcumin, arising from aromatic and tautomeric structures along with the flexibility of the linker group are responsible for the non-covalent interactions [11–14]. The β -diketo group forms chelates with transition metals, thereby reducing the metal-induced toxicity and some of the metal complexes exhibit improved antitumor activity [15, 16]. To enhance the biological properties and antitumor activity of curcumin, a number of curcumin derivatives and analogs have been synthesized through structural modifications such as variation of the aromatic rings and their substituents or replacing the heptadione bridge chain of curcumin and other linkers [17–19]. Metal chelation can cause changes in the biological activity of many organic compounds and metal complexes of biologically active ligands [20–22] have received much attention. In the present investigation, three α,β -unsaturated 1,3-diketones (**1–3**) with a cyclopentane ring incorporated into enolizable β -diketone moiety synthesized from 2-acetylcyclopentanone and substituted benzaldehyde by exposing to microwave radiation and their [ML₂] mononuclear Cu^{II} complexes were characterized by different physicochemical methods. Copper(II) complexes have attracted attention as antitumor candidates because copper is an essential micronutrient that participates in several biological processes like mitochondrial respiratory reactions, cellular stress response, antioxidant, etc. [23, 24], and, hence, it may be less toxic than non-essential metals like platinum [25]. In view of the increasing interest in copper(II) complexes [26–31], the free ligands and their copper(II) complexes were screened for *in vitro* and *in vivo* antitumor activity against Dalton's lymphoma ascites (DLA) cells. The DNA-binding properties of ligand and metal complexes were also studied by absorption spectral titrations, fluorescence quenching experiments and viscosity measurements with calf-thymus DNA.

2. Experimental

2.1. Materials and instrumentation

Ethidium bromide, 2-acetylcyclopentanone, and calf-thymus DNA were procured from Sigma–Aldrich, USA. Solvents and other chemicals used were of analytical reagent grade procured from commercial sources and used without purification. Solvents used were purified by standard procedures [32]. DLA cells were obtained from the Cancer Research Institute, Mumbai, India. DLA was maintained as ascites tumors in Swiss albino mice, purchased from Kerala Agricultural University, Thrissur, Kerala, India. They were fed with normal mouse chow (Lipton India) and water *ad libitum*. The complexes were analyzed for their metal content using AAS (Perkin Elmer 2380). Carbon and hydrogen percentages were determined by micro analysis (Heraeus Elemental analyzer) from CDRI Lucknow, India. The UV–vis spectra of the compounds were recorded on a Shimadzu UV–vis 1601 spectrophotometer. The IR spectra were recorded using KBr disks on an 8101 Shimadzu FT IR spectrophotometer. ¹H NMR spectra were recorded in CDCl₃ or DMSO-*d*₆ on a Varian 300 NMR spectrometer. The ESI-mass spectra were recorded on a Jeol SX-102 mass spectrometer operated in positive ion mode and ESR spectra of copper complexes were

recorded using a Varian E-12 ESR spectrometer at 77 K. Fluorescence measurements were performed on a MPF-4 fluorescence spectrophotometer.

2.2. Synthesis of ligands

2-Acetylcyclopentanone (20 mmol) was mixed with boron oxide (20 mmol) in a 100-mL Erlenmeyer flask. Appropriate amounts of aromatic aldehyde (40 mmol), acetic acid (100 mg), and morpholine (100 mg) were then added. The reaction mixture was irradiated with the microwave at 70 W for 3 min. The flask was cooled to room temperature and then methanol (50 mL) was added. This mixture was sonicated for 20–30 min. The so-obtained fine powder was filtered and washed with cold methanol. The compounds were recrystallized from hot benzene to obtain chromatographically pure material.

1: 74%, MW = 394, m.p. 164 °C, Orange yellow solid, Anal. Calcd for $C_{23}H_{22}O_6$ (%): C (70.04), H (5.62); Found: C (69.84), H (5.76); IR (KBr pellets, cm^{-1}): 1614 $\nu(C=O)$, 1526 $\nu_{as}^{carbonyl}$ (C–C–C), 962 $\nu(CH=CH-)$ $trans'$; UV-vis ($CHCl_3$, nm): 265 ($\pi \rightarrow \pi^*$), 470 ($n \rightarrow \pi^*$); 1H NMR (400 MHz, $CDCl_3$, δ ppm $^{-1}$): 14.28 (s, $-OH_{enolic'}$ 1H), 2.64–2.76 (s, ring, 4H), 6.67, 6.78 (d, alkenyl, 2H), 6.54–7.41 (m, aromatic, vinylic, 11H), 9.65, 9.78 (s, $-OH_{phenolic'}$ 2H); ^{13}C NMR (400 MHz, $CDCl_3$, δ ppm $^{-1}$): 25.57, 29.68 (aliphatic), 181.94, 196.37 (carbonyl), 112.38–152.78 (aromatic); ESI-MS, m/z : 394.02 $[M]^+$, 377.14 $[M-OH]^+$, 271.34 $[M-C_7H_7O_2]^+$, 255.02 $[M-C_7H_7O_3]^+$, 243.02 $[M-C_8H_7O_3]^+$, 229.01 $[M-C_9H_9O_3]^+$, 149.13 $[M-C_{14}H_{13}O_4]^+$, 137.14 $[M-C_{15}H_{13}O_4]^+$, 91.08 $[M-C_{16}H_{15}O_6]^+$, 77.06 $[M-C_{17}H_{17}O_6]^+$.

2: 70%, MW = 366, m.p. 148 °C, Reddish brown solid, Anal. Calcd for $C_{21}H_{18}O_6$ (%): C (68.85), H (4.95); Found: C (68.37), H (4.84); IR (KBr pellets, cm^{-1}): 1564 $\nu(C=O)$, 1546 $\nu_{as}^{carbonyl}$ (C–C–C), 968 $\nu(CH=CH-)$ $trans'$; UV-vis (DMSO, nm): 244 ($\pi \rightarrow \pi^*$), 476 ($n \rightarrow \pi^*$); 1H NMR (400 MHz, $CDCl_3$, δ ppm): 14.37 (s, $-OH_{enolic'}$ 1H), 2.57–2.65 (s, ring, 4H), 6.67, 6.87 (d, alkenyl, 2H), 6.52–7.43 (m, aromatic, vinylic, 11H) 9.81–9.87 (s, $-OH_{phenolic'}$ 4H) ^{13}C NMR (400 MHz, $CDCl_3$, δ ppm): 25.36, 29.72 (aliphatic), 181.29, 196.46 (carbonyl), 113.28–146.27 (aromatic); ESI-MS, m/z : 366.12 $[M]^+$, 349.17 $[M-OH]^+$, 317.34 $[M-O_3H]^+$, 257.04 $[M-C_6H_5O_2]^+$, 241.32 $[M-C_6H_5O_3]^+$, 231.02 $[M-C_8H_7O_2]^+$, 215.06 $[M-C_8H_7O_3]^+$, 135.09 $[M-C_{13}H_{11}O_4]^+$, 123.14 $[M-C_{14}H_{11}O_4]^+$, 91.23 $[M-C_{14}H_{11}O_6]^+$, 77.12 $[M-C_{15}H_{13}O_6]^+$.

3: 72%, MW = 422, m.p. 132 °C, Orange yellow solid, Anal. Calcd for $C_{25}H_{26}O_6$ (%): C (71.07), H (6.20); Found: C (71.54), H (6.12); IR (KBr pellets, cm^{-1}): 1593 $\nu(C=O)$, 1497 $\nu_{as}^{carbonyl}$ (C–C–C), 966 $\nu(CH=CH-)$ $trans'$; UV-vis ($CHCl_3$, nm): 249 ($\pi \rightarrow \pi^*$), 478 ($n \rightarrow \pi^*$); 1H NMR (400 MHz, $CDCl_3$, δ ppm $^{-1}$): 14.33 (s, $-OH_{enolic'}$ 1H), 2.71–2.79 (s, ring, 4H), 6.68, 6.83 (d, alkenyl, 2H), 6.69–7.51 (m, aromatic, vinylic, 11H) ^{13}C NMR (400 MHz, $CDCl_3$, δ ppm $^{-1}$): 25.76, 29.47 (aliphatic), 181.43, 196.36 (carbonyl), 111.38–149.38 (aromatic); ESI-MS, m/z : 422 $[M]^+$, 405.14 $[M-OH]^+$, 269.21 $[M-C_8H_9O_3]^+$, 257.31 $[M-C_9H_9O_3]^+$, 243.10 $[M-C_{10}H_{11}O_3]^+$, 231.07 $[M-C_{11}H_{11}O_3]^+$, 191.06 $[M-C_{13}H_{11}O_4]^+$, 151.06 $[M-C_{16}H_{15}O_4]^+$, 91.03 $[M-C_{18}H_{19}O_6]^+$, 77.02 $[M-C_{18}H_{21}O_6]^+$.

2.3. Preparation of copper complexes

The copper(II) complexes were prepared as described below. A methanolic solution of copper(II) acetate (25 mL, 1 mmol) was added by stirring with a solution of ligand (25 mL, 2 mmol) in methanol and refluxed gently for ~1 h. After reducing the volume to half, the solution was cooled to room temperature. The precipitated complex was filtered and recrystallized from hot methanol.

1a: 70%, MW = 850, m.p. 264 °C, Brown solid, Anal. Calcd for $C_{46}H_{42}O_{12}Cu$ (%): C (64.97), H (4.98), Cu (7.47); Found: C (64.11), H (5.41), Cu (7.85); IR (KBr pellets, cm^{-1}): 1617, 1538 $\nu(C=O)$, 1487 $\nu(C=C)$ $metal\ chelated\ carbonyl'$, 1408 $\nu(C=C)$ $phenyl'$, 1276 $\nu_{as}^{alkenyl'}$ (C–C–C) $chelate\ ring'$, 1238 $\nu_{as}^{metal\ chelated\ carbonyl'}$ (C–C–C) $chelate\ ring'$, 972 $\nu(CH=CH-)$ $trans'$, 458 $\nu(M-O)$ $chelate\ ring'$; UV-vis ($CHCl_3$, nm): 262 ($\pi \rightarrow \pi^*$), 478 ($n \rightarrow \pi^*$); ESI-MS, m/z : 895.01 $[CuL_2^+ + 2Na^+]^+$, 872.31 $[CuL_2^+ + Na^+]^+$, 849.09 $[CuL_2^+]^+$, 455.54 $[Cu(L)^+]$, 393.00 $[L]^+$, 254.24 $[Cu-ArCHCHCOCH_2]^+$, 240.24 $[Cu-ArCHCHCO]^+$.

2a: 68%, MW = 79, m.p. 234 °C, Brown solid, Anal. Calcd for $C_{42}H_{34}O_{12}Cu$ (%): C (63.51), H (4.31), Cu (8.00); Found: C (62.98), H (4.65), Cu (8.61); IR (KBr pellets, cm^{-1}): 1571, 1527 $\nu(C=O)$, 1467 $\nu(C=C)$ $metal\ chelated\ carbonyl'$, 1397 $\nu(C=C)$ $phenyl'$, 1275 $\nu_{as}^{alkenyl'}$ (C–C–C) $chelate\ ring'$, 1157 $\nu_{as}^{metal\ chelated\ carbonyl'}$ (C–C–C) $chelate\ ring'$, 961 $\nu(CH=CH-)$ $trans'$, 476 $\nu(M-O)$ $chelate\ ring'$; UV-vis (DMSO, nm): 248 ($\pi \rightarrow \pi^*$), 482 ($n \rightarrow \pi^*$); ESI-MS, m/z : 839.01 $[CuL_2^+ + 2Na^+]^+$,

816.21 $[\text{CuL}_2^+ + \text{Na}^+]^+$, 793.41 $[\text{CuL}_2]^+$, 427.03 $[\text{CuL}]^+$, 365.06 $[\text{L}]^+$, 240.14 $[\text{Cu-ArCHCHCOCH}_2]^+$, 226.31 $[\text{Cu-ArCHCHCO}]^+$.

3a: 69%, MW = 906, m.p. 278 °C, Brown solid, Anal. Calcd for $\text{C}_{50}\text{H}_{50}\text{O}_{12}\text{Cu}$ (%): C (66.25), H (5.56), Cu (7.01); Found: C (66.87), H (5.04), Cu (7.67); IR (KBr pellets, cm^{-1}): 1576, 1534 $\nu(\text{C}=\text{O})$ metal chelated carbonyl, 1437, $\nu(\text{C}=\text{C})$ phenyl, 1376, $\nu(\text{C}=\text{C})$ alkenyl, 1268, $\nu_{\text{as}}(\text{C}-\text{C})$ chelate ring, 1151, $\nu_{\text{as}}(\text{C}-\text{C})$ chelate ring 958 $\nu(\text{CH}=\text{CH}-)$ trans, 472, $\nu(\text{M}-\text{O})$ chelate ring; UV-vis (CHCl_3 , nm) 252 ($\pi \rightarrow \pi^*$), 487 ($n \rightarrow \pi^*$); ESI-MS, m/z : 951.03 $[\text{CuL}_2^+ + 2\text{Na}^+]^+$, 928.34 $[\text{CuL}_2^+ + \text{Na}^+]^+$, 905.32 $[\text{CuL}_2]^+$, 484.21 $[\text{CuL}]^+$, 421.98 $[\text{L}]^+$, 268.00 $[\text{Cu-ArCHCHCOCH}_2]^+$, 254.11 $[\text{Cu-ArCHCHCO}]^+$.

2.4. DNA-binding studies

UV-vis absorption spectrophotometry and viscosity measurements were used to assess the interaction of ligands and their copper(II) complexes with CT-DNA at 7.4 pH in double-distilled water containing tris-(hydroxymethyl)-amino methane (Tris, 10^{-2} M). The ratio of UV absorbance of the stock solution of CT-DNA in 5 mM Tris-HCl/50 mM NaCl buffer (pH 7.2) at 260 and 280 nm gives a ratio of 1.7–1.8, indicating that CT-DNA was sufficiently free of protein [33]. The concentration of CT-DNA was determined from its absorption intensity at 260 nm with a molar extinction coefficient of $6600 \text{ M}^{-1} \text{ cm}^{-1}$ [34]. The binding experiments were carried out by recording the absorbance changes on adding increasing concentrations of DNA ($0-2.5 \times 10^{-4}$ M) against a fixed concentration of the ligand and its complexes (5×10^{-5} M). Equal volumes (2.0 mL) of each solution of DNA and ligand or metal complex were mixed together and their λ_{max} and absorbance values were recorded. The absorption spectra were recorded after each addition of different concentrations of DNA solution.

The relative binding abilities of copper(II) complexes to CT-DNA were also studied by fluorescence quenching experiments [35] using Ethidium bromide(EB)-bound CT-DNA solution in 5 mM Tris-HCl/50 mM NaCl buffer (pH 7.2). The fluorescence spectra were recorded at room temperature with excitation at 490–510 nm and emission at 592–623 nm. The experiments were carried out by titrating complex into EB-DNA solution containing 1×10^{-6} M EB and 4×10^{-5} M CT-DNA.

Viscosity measurements of 100 μM CT-DNA in Tris-HCl/NaCl buffer were performed using an Ostwald viscometer at 35 ± 0.5 °C in a thermostatic water bath. Flow time was measured with a digital stopwatch, and each sample was measured three times, and an average flow time was calculated. Data are presented as $(\eta/\eta_0)^{1/3}$ versus binding ratio $[\text{Complex}]/[\text{DNA}]$, where η and η_0 indicate the viscosity of DNA solutions in the presence and absence of complex, respectively. The relative viscosity was calculated according to the relation $\eta = (t - t_0)/t_0$, where t is the flow time of DNA solution in the presence or absence of ligand or complex and t_0 is the flow time of the buffer alone [36].

2.5. Cytotoxic studies

2.5.1. Determination of the effect of compounds on ascites tumor model

In vitro cytotoxicity studies were carried out using DLA cells. The tumor cells were aspirated from the peritoneal cavity of tumor-bearing mice and washed twice with phosphate buffered saline (PBS). Cell viability was determined by trypan blue exclusion method [37]. Viable cell suspension (1×10^6 cells in 0.1 mL) was added to tubes containing various concentrations of the test compounds (200, 100, 50, 20, and 10 $\mu\text{g}/\text{mL}^{-1}$) in DMSO was made up to 1 mL using PBS. Control tube contains only cell suspension and solvent mixture. These assay mixtures were incubated for 3 h at 37 °C. Further cell suspension was mixed with 100 μL of 1% trypan blue and kept for 2–3 min. Dead cells take up the blue color of trypan blue while the live cells do not take up the dye. The numbers of stained and unstained cells were counted using a hemocytometer.

2.5.2. Determination of the effect of compounds on DLA cell induced ascites tumor

For *in vivo* studies, groups of Swiss Albino mice (female, 6 per group) were injected intraperitoneally with Dalton's lymphoma ascites tumor cells (1×10^6 cells/animal). They were injected (ip) with (25 mg/kg

body weight) test compound suspended in carboxy methyl cellulose and the injections of the test compounds were started 24 h after tumor inoculation and continued for 10 consecutive days. The death pattern of animals due to tumor burden was noted. The percentage increase in lifespan (% ILS) was calculated using the formula $\% \text{ ILS} = [(T - C)/C \times 100]$, where T and C represent the mean number of days survived by the treated and control animals, respectively [38].

2.5.3. Determination of the effect of compounds on DLA cell induced solid tumor model

Solid tumors were also induced in groups of Swiss albino mice (female, 6 per group) by subcutaneous injection of DLA cells (1×10^6 cells/animal) on the right hand limb. One group was kept as control and other groups were injected intramuscularly (im) with the test compounds (25 mg kg^{-1} body weight) and the injections of the test compounds were started 24 h after inoculation and continued for 10 consecutive days. Tumor diameter was measured every third day for one month and the tumor volume was calculated using the formula; $V = 4/3\pi r_1^2 r_2$ where r_1 and r_2 are the minor and major radii, respectively [39].

3. Results and discussion

3.1. Synthesis and structural characterization of the compounds

The ligands were synthesized by condensation of substituted benzaldehyde with 2-acetyl cyclopentanone as per the scheme given in figure 1. The metal complexes were prepared from ligands by direct interaction with copper(II) in methanol under reflux. UV, IR, ^1H NMR, ^{13}C NMR, and mass spectral data of the compounds are in agreement with structure I given in figure 1. All the ligands formed well-defined and crystalline complexes having sharp melting points with copper(II) ions. The observed carbon, hydrogen, and metal percentages of the metal complexes and ESI mass spectral data suggest their ML_2 stoichiometry. All the metal complexes behave as non-electrolytes (specific conductances of $8\text{--}13 \Omega^{-1} \text{ cm}^{-1}$ in DMF) and do not contain the anion of the metal salt used for their preparation. The electronic, IR, and mass spectral data of the complexes are compatible with structure II given in figure 1. In order to study the stability of complexes in aqueous solution at physiological pH, the complexes were dissolved in minimum quantity of DMSO, diluted with PBS, and UV-vis absorption spectra were recorded at intervals of 4–6 h for 24 h. All the complexes displayed similar spectra in PBS with no hypsochromic or bathochromic shifts in their bands indicating that the complexes are stable even after 24 h and also resisted precipitation over this time period, a desirable property for therapeutically active compounds.

IR spectra of the ligands are characterized by the presence of a strong band at $1594\text{--}1619 \text{ cm}^{-1}$. Intramolecular hydrogen bonding can lower the carbonyl stretching frequency by 50 cm^{-1} [40]. The absence of band assignable to a normal or α,β -unsaturated carbonyl group at $1640\text{--}1740 \text{ cm}^{-1}$ indicates that the ligands exist in their enolic form [41]. A broad band present at $2800\text{--}3600 \text{ cm}^{-1}$ is due to

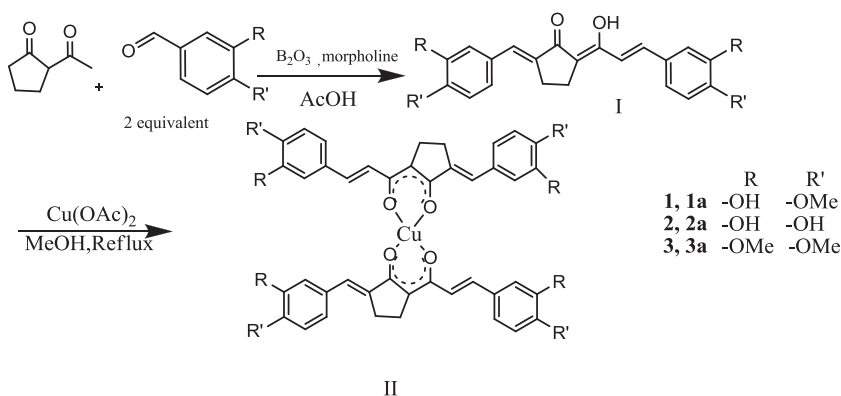


Figure 1. Synthesis of ligands and copper(II) complexes.

stretching of the chelated carbonyl group and the intramolecular hydrogen bonded enol group [42]. The intense band at 1293 cm^{-1} in the IR spectrum of **1** and at 1287 cm^{-1} in the IR spectrum of **2** may be assigned to phenolic (C–O) stretch, according to previous assignments [43]. In the spectrum of **1** and **2**, the above bands for the phenolic group do not shift, suggesting that oxygen of the phenolic group(s) is not coordinated to the metal ion [44]. In IR spectra of all complexes, the band due to hydrogen bonded carbonyl at $1594\text{--}1619\text{ cm}^{-1}$ disappeared and instead a strong band assignable to stretch of the coordinated carbonyl [45] appeared at $\sim 1590\text{ cm}^{-1}$. The broad band at $2800\text{--}3600\text{ cm}^{-1}$ due to the hydrogen-bonded enol proton present in the free ligands is absent in spectra of metal complexes and weak bands attributable to various $\nu_{(\text{C-H})}$ appeared. The fact that the carbonyl groups are involved in metal complex formation is evident from the appearance of two medium intensity bands at $458\text{--}476\text{ cm}^{-1}$ due to $\nu_{(\text{M-O})}$ vibrations [46]. The prominent band at $\sim 975\text{ cm}^{-1}$ is typical of a trans –CH = CH– group which remained unaltered in spectra of metal complexes [47].

The ^1H NMR spectral data of all the ligands show a characteristic downfield singlet at $\delta\sim 14.5$ ppm which could be assigned to intramolecularly hydrogen-bonded enolic proton [48]. The ^1H NMR spectra of **1** and **2** showed a downfield singlet at 9.72 ppm due to phenolic proton [48, 49]. The ^1H NMR spectra of all the ligands show signal at 2.57–2.79 ppm due to protons in the cyclopentanone ring and two singlets at ~ 6.67 ppm due to the alkenyl protons. Observed J value of 16.2 Hz for the alkenyl protons suggests their trans orientation. ^{13}C NMR spectral data of all ligands show two resonances at 196.36–195.46 ppm and 181.29–181.94 ppm indicating that the two carbonyl groups have different environments. The two aliphatic carbons in the cyclopentanone ring show a resonance at 25–29 ppm. The resonances from 111.38–152.78 ppm are due to aromatic carbons.

Mass spectra of all ligands show an intense molecular ion peak. In addition to the molecular ion peak (M^+), peaks due to the elimination of O, OH, ArCH_2^+ and Ar^+ from the molecular ion are the most significant features of the mass spectra of curcuminoids [50]. Peaks corresponding to m/z $(\text{M}-\text{ArCHCHCO})^+$ and $(\text{M}-\text{ArCHCHCOCH}_2)^+$ are also present in the mass spectra of these compounds. The ESI mass spectra of the copper(II) chelates confirm the $[\text{ML}_2]$ stoichiometry of the complexes. Peaks due to M^+ and $(\text{M} + 2)^+$ with 3 : 1 intensity are present in the ESI-MS of copper(II) chelates consistent with the natural abundance of ^{63}Cu and ^{65}Cu isotopes. The mass spectra of the copper(II) chelates show that stepwise removal of aryl groups is a characteristic feature of these complexes [51]. Peaks due to $[\text{CuL}]^+$, $[\text{CuL}-\text{ArCHCHCO}]^+$, $[\text{CuL}-\text{ArCHCHCOCH}_2]^+$, L^+ and fragments of L^+ are common in spectra of copper(II) complexes. The ESI-MS of free ligands and their copper(II) complexes are provided as Supplementary files **S1–S6**.

ESR spectra of the copper(II) complexes were measured at 77 K in DMF solution. The observed g_{\parallel} , g_{\perp} , A_{\parallel} and A_{\perp} values are given in table 1. The g -values are comparable to that reported for copper acetylacetonates [52, 53] for which $g_{\parallel} = 2.186$ and $g_{\perp} = 2.058$. This suggests extensive delocalization in the pseudo-aromatic metal chelate ring system and significant covalent character for the metal–ligand bonds.

The UV–vis spectra of the ligands have two absorption maxima; the low-energy band corresponds to an $n \rightarrow \pi^*$ transition (438–486 nm) and the high-energy band is due to a $\pi \rightarrow \pi^*$ transition (245–268 nm). In the metal complexes, these absorptions show only slight bathochromic shifts due to involvement of the carbonyl group in metal complexation. Similarity in the UV–vis absorption maxima of metal complexes with that of free ligands show that no structural alteration of the ligand has occurred during complex formation.

In the copper(II) complexes, the presence of a broad visible band at ~ 665 nm and the measured μ_{eff} values (1.75–1.81 B.M.) support square planar structures [54]. Square-planar copper(II) complexes undergo a change to octahedral symmetry in the presence of donor solvents. The electronic spectra

Table 1. ESR parameters of Cu(II) complexes in DMF at 77 K.

Complexes	g_{\parallel}	g_{\perp}	$A_{\parallel} \times 10^{-4} (\text{cm}^{-1})$	$A_{\perp} \times 10^{-4} (\text{cm}^{-1})$
1a	2.262	2.052	163	44.6
2a	2.258	2.053	161	45.3
3a	2.256	2.056	159	44.8

of the copper(II) complexes when recorded in pyridine (10^{-3} M) showed two low-energy weak bands at 674.3–664.8 nm and 523.5–519.5 nm ($\epsilon = 2.30 \times 10^4 - 2.85 \times 10^4 \text{ M}^{-1} \text{ cm}^{-1}$) and a strong high energy band at 332.4–332.3 nm ($\epsilon = 6.20 \times 10^4 - 6.48 \times 10^4 \text{ M}^{-1} \text{ cm}^{-1}$) which may be assigned to ${}^2B_{1g} \rightarrow {}^2A_{1g}$ and ${}^2B_{1g} \rightarrow {}^2E_g$ transitions, respectively [55]. The strong high-energy band, in turn, is assigned to (metal \rightarrow ligand) charge transfer.

3.2. DNA-binding activity

3.2.1. UV-vis absorption spectroscopy

A large number of anticancer drugs have affinity towards DNA and DNA-binding capacity is of significance in their mode of action [56–59]. Ligands and transition metal complexes bind with DNA through covalent and/or non-covalent interactions [60–62]. In the case of covalent binding, one of the labile ligands of the complexes is replaced by nitrogen bases of DNA and the non-covalent interactions generally include intercalative and electrostatic interactions with the major or minor grooves of DNA [63]. Changes in the spectral absorbance of DNA in the presence of ligands and complexes are evidence of their interaction with DNA [64, 65]. The DNA-binding affinity of free ligands and their complexes was quantitatively studied by calculating the intrinsic binding constants (K_b) from the changes in absorbance of $\pi \rightarrow \pi^*$ spectral band (254–268 nm) with increasing concentration of DNA, by using the equation [66]

$$[\text{DNA}] / (\epsilon_a - \epsilon_f) = [\text{DNA}] / (\epsilon_b - \epsilon_f) + 1 / K_b (\epsilon_b - \epsilon_f)$$

where [DNA] is the concentration of DNA in base pairs, the apparent absorption coefficients ϵ_a , ϵ_f and ϵ_b correspond to $A_{\text{obs}} / [\text{compound}]$, the extinction coefficient for the free compound, and the extinction coefficient for the compound in the fully bound form, respectively. From the slope and the intercept of the linear fit of the plot of $[\text{DNA}] / [\epsilon_a - \epsilon_f]$ versus [DNA], the intrinsic binding constant, K_b , can be obtained.

Intercalation of molecules into DNA usually results in hypochromism or hyperchromism as the intercalation involves some kind of interaction between the molecule and the DNA base pairs [67]. Hypochromism arises from contraction of CT-DNA in the helix axis and its conformational changes [68]. Meanwhile, hyperchromism results in secondary damage to the DNA double-helix structure [69, 70], in which the extent of hyperchromism is indicative of partial or non-intercalative binding mode [71]. The absorption spectra of **1** and **1a** (5×10^{-5} M) in the absence and presence of CT-DNA (0 – 2.5×10^{-4} M) are given in figures 2 and 3, respectively. Absorption spectra of **1a** display clear hypochromism with slight red shift of 3–6 nm. The observed hypochromism is due to interaction between the π^* orbitals

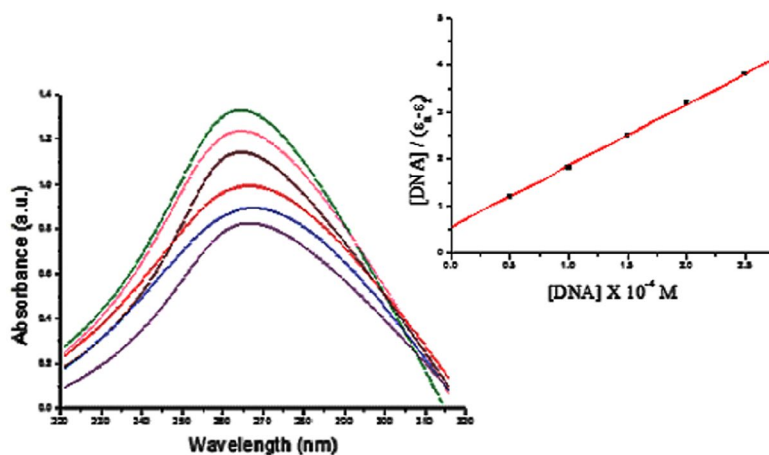


Figure 2. Absorption spectra of **1** (5×10^{-5} M) in the absence and presence of increasing amounts of CT-DNA (0 – 2.5×10^{-4} M) at room temperature in Tris-HCl/NaCl buffer (pH 7.2). Inset: plot of $[\text{DNA}] / (\epsilon_a - \epsilon_f)$ vs. [DNA] for absorption titration of CT-DNA with **1**.

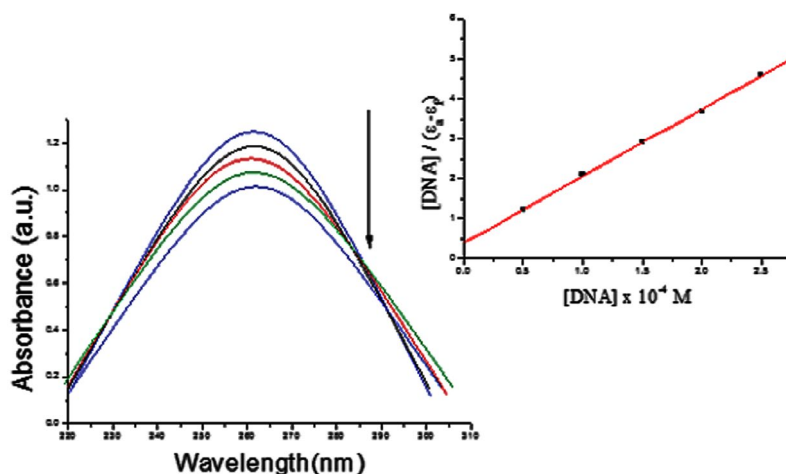


Figure 3. Absorption spectra of **1a** (5×10^{-5} M) in the absence and presence of increasing amounts of CT-DNA (0 – 2.5×10^{-4} M) at room temperature in Tris–HCl/NaCl buffer (pH 7.2). Inset: plot of $[\text{DNA}]/(\epsilon_a - \epsilon_f)$ vs. $[\text{DNA}]$ for absorption titration of CT-DNA with **1a**.

Table 2. DNA binding constants, *in vitro* and *in vivo* antitumor activity of compounds.

Compounds	DNA-binding constants (K_b) ^a ($\times 10^4$ M ⁻¹)	Concentrations ($\mu\text{g mL}^{-1}$) required to produce 50% cell death	No. of days survived ^a	Increase in life-span (%)
Control			19 \pm 1	
1	1.3 \pm 0.3	38	27 \pm 2	44.16
2	1.7 \pm 0.3	27	30 \pm 2	56.41
3	1.1 \pm 0.3	52	27 \pm 2	39.53
1a	3.4 \pm 0.4	18	32 \pm 2	65.98
2a	5.5 \pm 0.4	10	34 \pm 3	77.91
3a	3.2 \pm 0.4	22	30 \pm 2	60.14

^aEach value represents mean of three different observations \pm S.D.

of the intercalated compounds with the π orbitals of the DNA base pairs, thereby decreasing the $\pi \rightarrow \pi^*$ transition energies [72]. The hypochromism of the metal complexes are greater than that of free ligands due to additional interaction with positively charged metal ion or even due to the replacement of a ligand with nitrogen bases of DNA. In our studies, hypochromism of **1a** is higher than free **1**. Even though the exact reason is not known, it may be due to the involvement of copper(II) ions as it is involved in many natural processes. The intrinsic binding constants (K_b) obtained for free ligands and their metal complexes are given in table 2. The values are slightly lower than that reported for DNA intercalative complexes [73–80]. We propose that the weak hypochromism observed in UV–vis spectra probably arises from partial intercalation of **1a** into CT-DNA, in which the planarity of pseudo-aromatic metal-chelate ring and the steric hindrance of the phenyl substituent might reduce the insertion degree of complex to DNA. In addition, OH, as an electron donating group, will increase the electron density on the intercalating ligands, hence, reinforcing the repulsion between the complex and DNA with the negatively charged phosphate backbone, and consequently destabilize the DNA complex system, causing a decrease in the DNA-binding affinity [81]. Absorption spectra of **2**, **3** and their complexes in the absence and presence of CT-DNA (0 – 2×10^{-5} M) also showed a weak hypochromism. The absorption spectra of **2**, **2a**, **3**, and **3a** are shown in the Supplementary files **S7–S10**.

3.2.2. Fluorescence quenching studies

Fluorescence measurements were performed to understand the nature of binding of complexes with DNA. Since the complexes are non-luminescent at room temperature, the binding of copper(II)

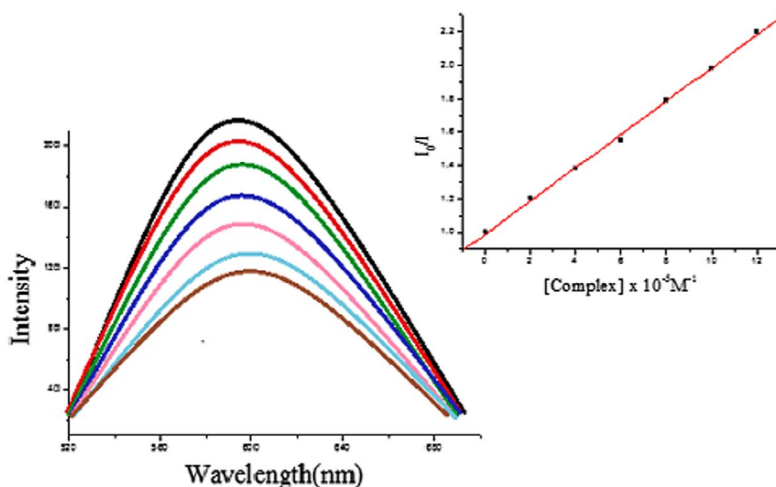


Figure 4. Fluorescence quenching curves of EB bound to DNA by **1a** ($[\text{complex}] = 0\text{--}3 \times 10^{-5} \text{ M}$). Inset: plot of I_0/I vs. $[\text{complex}]$, $\lambda_{\text{ex}} = 510 \text{ nm}$.

complexes to DNA is evaluated by the fluorescence emission intensity of EB-DNA solution as a probe. Competitive binding experiments were carried out with an EB-bound CT-DNA solution in Tris-HCl/NaCl buffer. As shown in figure 4, fluorescence intensities at 598 nm (510 nm excitation) were measured after addition of different concentrations of **1a** which suggested the complex could compete with EB to bind to DNA with similar intercalating fashion. Similarly, fluorescence intensities at 608 nm (502 nm excitation) and at 623 nm (490 nm excitation) were measured after addition of different concentrations of **1b** and **1c**, respectively. As shown in figure 4, the fluorescence quenching curves showed that quenching of the EB-DNA system by the complexes are in agreement with the classical Stern–Volmer equation [82] $I_0/I = 1 + K[Q]$. From the equation $K_{\text{EB}}[\text{EB}] = K_{\text{app}}[\text{complex}]$ (where $[\text{complex}]$ is the value at a 50% reduction of the fluorescence intensity of EB, $K_{\text{EB}} = 1.0 \times 10^7 \text{ M}^{-1}$, and $[\text{EB}] = 5 \mu\text{M}$), the value of apparent binding constants (K_{app}) was calculated to be $5.82(\pm 0.4) \times 10^5$, $3.22(\pm 0.5) \times 10^5$ and $2.08(\pm 0.4) \times 10^5 \text{ M}^{-1}$ for **1a**, **1b** and **1c**, respectively (Supplementary files **S11** and **S12**). These results are consistent with some earlier reports on quenching fluorescence of EB–DNA for Cu complexes with similar K_{app} values, suggesting that the interaction of the complexes with DNA is through an intercalative mode [83–87]. The modes and affinity of DNA-binding of these copper(II) complexes mainly depend on the nature of the ligands.

3.2.3. Viscosity measurements

In order to establish the nature of binding between the complexes and DNA, viscosity studies were also carried out. In intercalative mode due to increase in the separation of base pairs at intercalation sites, the unwinding of DNA-helix will increase the DNA length and cause a significant increase in viscosity of DNA solution [88]. On the other hand, groove-binding and electrostatic interactions reduce its effective length resulting in a slight decrease in viscosity [89]. The viscosity experiments were carried out in triplicate on CT-DNA by varying the concentration of the ligands or copper(II) complexes ($[\text{compound}]/[\text{DNA}] = 0.0\text{--}0.6$), and the corresponding data are illustrated in figure 5 (Change in viscosity with the free ligands is given in supplementary file **S13**). Both the ligands and complexes show an increase in specific viscosity with increase in concentration of compounds, obviously indicating the binding involves intercalation [90, 91]. The complexes were more strongly bound to DNA than free ligands, probably due to the presence of metal ion which can interact with the nitrogen bases of DNA.

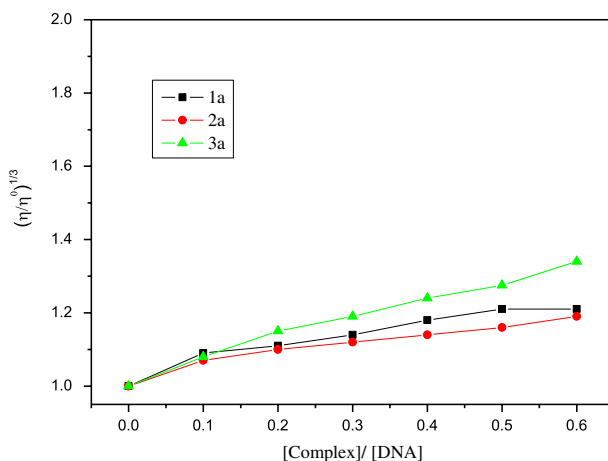


Figure 5. Effect of increasing concentration of the complexes on the relative viscosities of CT-DNA at 35.0 ± 0.2 °C.

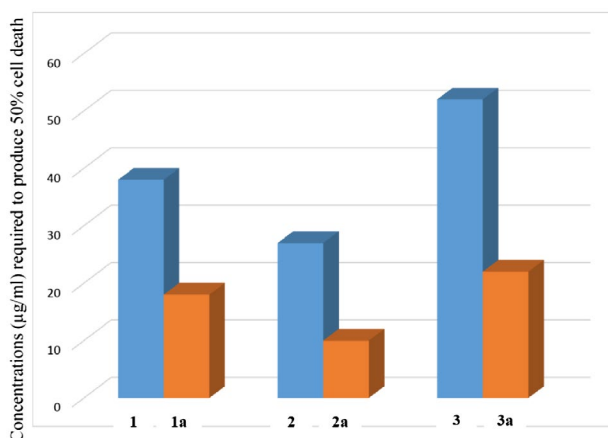


Figure 6. Cytotoxic activity of ligands and their copper(II) complexes.

3.3. Antitumor activity

Besides cisplatin, many transition metal complexes are known for their antitumor activity and many of such metallodrugs have cleared their clinical trials. Antitumor activity of curcumin, the active component of turmeric [92–95], its synthetic analogs [2, 5, 96, 97], and their metal complexes has been reported [15, 16, 96–102]. A large number of copper(II) complexes have been investigated as potential anticancer agents and copper(II) ion is an essential cofactor in a number of enzymes [19]. In our studies, copper chelates were more active than free ligands.

3.3.1. Effect of compounds on ascites tumor model

The results of short-term *in vitro* cytotoxic activity of the ligands and their metal chelates (table 2) against DLA indicate that metal complexation enhances the cytotoxicity of compounds considerably. Concentrations required to produce 50% cell death are 27–52 $\mu\text{g mL}^{-1}$ in the case of free ligands. The copper chelates produced the same effect at concentrations of 10–22 $\mu\text{g mL}^{-1}$ (figure 6).

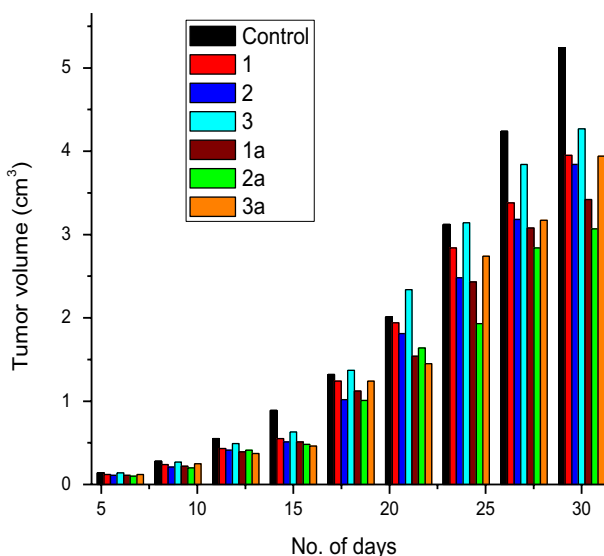


Figure 7. Effect of compounds on solid tumor development.

3.3.2. Effect of compounds on DLA cell-induced ascites tumor

The incorporation of metal ion enhanced the antitumor activity of the ligands. Copper chelate of **2** is more effective than other copper chelates, probably due to the presence of two hydroxyl groups in the aryl ring that can produce a diphenoxy free radical which can interact with reactive oxygen species. Lifespan of ascites tumor-bearing animals induced by DLA cells increased upon treatment with copper complexes. The animals inoculated with DLA cell lines alone survived for a period of 19 ± 1 days (table 2). Copper(II) complexes were effective in increasing the lifespan of animals with an average of 31.57, 33.84, and 30.46 days for **1a**, **2a**, and **3a**, respectively.

3.3.3. Effect of compounds on DLA cell-induced solid tumor model

Reductions of solid tumor volume in mice by intraperitoneal administration of compounds are given in figure 6. Compared with free ligands, their respective copper(II) complexes are active in reducing tumor volume. Tumor volumes were 5.24, 3.42, 3.07, and 3.94 cm³ on 30th day for control, **1a**, **2a**, and **3a**, respectively. The results clearly reveal that **2a** with two hydroxyl groups on the phenyl rings shows the maximum cytotoxicity on DLA cells, percentage increase in lifespan (table 2), and reduction in solid tumor volume in mice (figure 7). The copper complexes enhanced the activities in both cases. Earlier studies have shown that curcumin with methoxy- and hydroxy-groups in the aryl ring, is an inhibitor of lipid peroxidation [9, 10, 103], which promotes anticancer properties of the compound. The present study suggests that metal complexation significantly increased the cytotoxic and antitumor activities of compounds. Phenolic compounds are antioxidants and as reported earlier [104, 105], the hydroxyl group in the phenyl ring can enhance the antitumor activity. This may be the reason for the exceptional activity of the copper complex of **2**.

4. Conclusion

Three α,β -unsaturated-1,3-diketones structurally related to curcuminoids were synthesized from 2-acetylcyclopentanone and disubstituted benzaldehyde by exposing to microwave radiation. Their mononuclear copper(II) complexes having ML₂ stoichiometry were characterized by different physicochemical methods. The DNA-binding activity of copper(II) complexes is higher than free ligands. The intrinsic binding constants obtained from absorption titrations were comparable with other complexes

reported in the literature. The binding involves intercalative mode through non-covalent interactions and produced conformational changes in the structure of DNA via moderate interaction. Introduction of cyclopentane ring to modify the basic skeleton of curcumin and the presence of two hydroxylic groups in the aryl rings significantly increased the cytotoxic and antitumor activities. Interaction of copper complexes with DNA may be correlated with their cytotoxic effects against tumor cells. Studies on emerging targets for anticancer drugs such as cytotoxicity against other tumors cells, the rate of metabolism, absorption, and stability *in vivo* should be further investigated.

Supplementary material

Supplementary information contains ESI MS of free ligands and their copper(II) chelates (**S1–S6**), absorption spectra of **2**, **2a**, **3**, **3a** (5×10^{-5} M) in the absence and presence of increasing amounts of CT-DNA ($0–2.5 \times 10^{-5}$ M) at room temperature in Tris–HCl/NaCl buffer, pH = 7.2 (**S7–S10**), fluorescence quenching curves of EB bound to DNA by **2a** and **3a** with [complex] = $0–3 \times 10^{-5}$ M (**S11–S12**) and effect of increasing concentration of the ligands on the relative viscosities of CT-DNA at 35.0 ± 0.2 °C (**S13**).

Acknowledgements

We thank Dr. Ramadasan Kuttan, the Director of the Cancer Research Centre, Amala Institute of medical Sciences, Thrissur, Kerala, India for their help in the *in vivo* and *in vitro* antitumor studies and SAIF IIT Madras, SAIF IIT Bombay, STIC CUSAT, and CDRI Lucknow for spectral analysis.

Disclosure statement

No potential conflict of interest was reported by the authors.

Funding

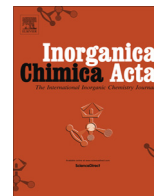
This work was supported by the Department of Higher Education, Government of Kerala [grant number H-15446/15].

References

- [1] V.S. Govindarajan, W.H. Stahl. *Crit. Rev. Food. Sci. Nutr.*, **12**, 199 (1980).
- [2] P. Anand, S.G. Thomas, A.B. Kunnumakkara, C. Sundaram, K.B. Harikumar, B. Sung, S.T. Tharakan, K. Misra, I.K. Priyadarsini, K.N. Rajasekharan. *Biochem. Pharmacol.*, **76**, 1590 (2008).
- [3] H. Itokawa, Q. Shi, T. Akiyama, S.L. Morris-Natschke, K.-H. Lee, L. Kuo-Hsiung. *Chin Med*, **3**, 11 (2008).
- [4] B.B. Aggarwal, C. Sundaram, N. Malani, H. Ichikawa. *Adv. Exp. Med. Biol.*, **595**, 1 (2007).
- [5] P. Anand, A.B. Kunnumakkara, R.A. Newman, B.B. Aggarwal. *Mol Pharm*, **4**, 807 (2007).
- [6] I. Junko, H. Ohtsu, T. Yoko, Y. Tachibana, Y. Nakanishi, K.F. Bastow, M. Nagi, H.K. Wang, H. Itokowa, K.H. Lee. *Bioorg. Med. Chem.*, **10**, 3481 (2002).
- [7] E. Ferrari, S. Lazzari, G. Marverti, F. Pignedoli, F. Spagnolo, M. Saladini. *Bioorg. Med. Chem.*, **17**, 3043 (2009).
- [8] K.I. Priyadarsini. *Curr. Pharm. Des.*, **19**, 2093 (2013).
- [9] W.M. Weber, L.A. Hunsaker, S.F. Abcouwer, L.M. Deck, D.L. Vander-Jagt. *Bioorg. Med. Chem.*, **13**, 3811 (2005).
- [10] U. Jungwirth, C.R. Kowol, B.K. Keppler, C.G. Hartinger, W. Berger, P. Heffeter. *Antioxid. Redox Signal*, **15**, 1085 (2011).
- [11] G. Liang, L. Shao, Y. Wang, C. Zhao, Y. Chu, J. Xiao, Y. Zhao, X. Li, S. Yang. *Bioorg. Med. Chem.*, **17**, 2623 (2009).
- [12] N. Handler, W. Jaeger, H. Puschacher, K. Leisser, T. Erker. *Chem. Pharm. Bull.*, **55**, 64 (2007).
- [13] S.K. Sandur, M.K. Pandey, B. Sung, K.S. Ahn, A. Murakami, G. Sethi, P. Limtrakul, V. Badmaev, B.B. Aggarwal. *Carcinogenesis*, **28**, 1765 (2007).
- [14] F. Zsila, Z. Bikádi, M. Simonyi. *Org. Biomol. Chem.*, **2**, 2902 (2004).
- [15] S. Wanninger, V. Lorenz, A. Subhan, F.T. Edelman. *Chem. Soc. Rev.*, **44**, 4986 (2015).
- [16] M. Pröhl, U.S. Schubert, W. Weigand, M. Gottschaldt. *Coord. Chem. Rev.*, **307**, 32 (2016).
- [17] L. Lin, Q. Shi, A.K. Nyarko, K.F. Bastow, C.C. Wu, C.Y. Su, C.C. Shih, K.H. Lee. *J. Med. Chem.*, **49**, 3963 (2006).
- [18] S. Venkateswarlu, M.S. Ramachandra, G.V. Subbaraju. *Bioorg. Med. Chem.*, **13**, 6437 (2005).
- [19] S. Manju, K. Sreenivasan. *J. Pharm Sci.*, **100**, 504 (2011).
- [20] P. Sengupta, S. Ghosh, T.C.W. Mak. *Polyhedron*, **20**, 975 (2001).
- [21] B. Keppler. *Metal Complexes in Cancer Chemotherapy*, VCH, Basel (1993).

- [22] H. Sigel, A. Sigel (Eds.). *Metal Ions in Biological Systems*, Vol. 31, Marcel Dekker, New York (1995).
- [23] R. Loganathan, S. Ramakrishnan, E. Suresh, A. Riyasdeen, M.A. Akbarsha, M. Palaniandavar. *Inorg. Chem.*, **51**, 5512 (2012).
- [24] K. Saleem, W.A. Wani, A. Haque, M.N. Lone, M.F. Hsieh, M.A. Jairajpuri, I. Ali. *Future Med. Chem.*, **5**, 135 (2013).
- [25] C. Marzano, M. Pellei, F. Tisato, C. Santini. *Anticancer Agents Med. Chem.*, **9**, 185 (2009).
- [26] R. Prabhakaran, P. Kalaivani, R. Huang, P. Poornima, V. Vijaya Padma, F. Dallemer, K. Natarajan. *J. Biol. Inorg. Chem.*, **18**, 233 (2013).
- [27] P.P. Silva, W. Guerra, G.C. dos Santos, N.G. Fernandes, J.N. Silveira, A.M. da Costa Ferreira, T. Bortolotto, H. Terenzi, A.J. Bortoluzzi, A. Neves, E.C.P. Maia. *J. Inorg. Biochem.*, **132**, 67 (2014).
- [28] C. Santini, M. Pellei, V. Gandin, M. Porchia, F. Tisato, C. Marzano. *Chem. Rev.*, **114**, 815 (2014).
- [29] P.U. Maheswari, S. Roy, H. den Dulk, S. Barends, G. van Wezel, B. Kozlevčar, P. Gamez, J. Reedijk. *J. Am. Chem. Soc.*, **128**, 710 (2006).
- [30] K. Ghosh, P. Kumar, V. Mohan, U.P. Singh, S. Kasiri, S.S. Mandal. *Inorg. Chem.*, **51**, 3343 (2012).
- [31] C. Rajarajeswari, R. Loganathan, M. Palaniandavar, E. Suresh, A. Riyasdeen, M.A. Akbarsha. *Dalton Trans.*, **42**, 8347 (2013).
- [32] W.L.F. Armarego, D.D. Perrin. *Purification of Laboratory Chemicals*, 3rd Edn, Pergamon Press Inc., New York (1988).
- [33] J. Marmur. *J. Mol. Biol.*, **3**, 208 (1961).
- [34] M.F. Reichmann, S.A. Rice, C.A. Thomas, P. Doty. *J. Am. Chem. Soc.*, **76**, 3047 (1954).
- [35] P. Kalaivani, R. Prabhakaran, E. Vaishnavi, T. Rueffer, H. Lang, P. Poornima, R. Renganathan, V.V. Padmad, K. Natarajan. *Inorg. Chem. Front.*, **1**, 311 (2014).
- [36] S. Thalamuthu, B. Annaraj, S. Vasudevan, S. Sengupta, M.A. Neelakantan. *J. Coord. Chem.*, **66**, 1805 (2013).
- [37] S.A. Altman, L. Randers, G. Rao. *Biotechnol. Prog.*, **9**, 671 (1993).
- [38] J.R. Anto, K.V.D. Babu, K.N. Rajasekharan, R. Kuttan. *Cancer Lett.*, **94**, 79 (1995).
- [39] J.E. Moulder, S. Rockwell. *Int. J. Radiat. Oncol. Biol. Phys.*, **10**, 695 (1984).
- [40] K. Nakamoto, *Advances in the Chemistry of Coordination Compounds*, S. Kirschner (Ed.). Mc Millan, New York (1961).
- [41] K.C. Joshi, V.N. Pathak. *Coord. Chem. Rev.*, **22**, 37 (1977).
- [42] P.J. Roughley, D.A. Whiting. *J. Chem. Soc. Perkin Trans. I.*, 2379 (1973). doi:10.1039/P19730002379.
- [43] R.L. Lintvedt, H.F. Holtzclaw. *J. Am. Chem. Soc.*, **88**, 2713 (1966).
- [44] D.C. Nonhebel. *Tetrahedron*, **24**, 1869 (1968).
- [45] K. Krishnankutty, P. Venugopalan. *Synth. React. Inorg. Met.-Org. Chem.*, **28**, 1313 (1998).
- [46] R. Atkins, G. Brewer, E. Kokot. *Inorg. Chem.*, **24**, 127 (1985).
- [47] V.D. John, K. Krishnankutty. *Trans. Met. Chem.*, **30**, 229 (2005).
- [48] A.M. Anderson, M.S. Mitchell, R.S. Mohan. *J. Chem. Educ.*, **77**, 359 (2000).
- [49] V.D. John, K. Krishnankutty. *Main Group Met. Chem.*, **33**, 157 (2010).
- [50] C.G. Macdonald, J.S. Shannon. *Aust. J. Chem.*, **19**, 1545 (1966).
- [51] K. Krishnankutty, V.D. John. *Synth. React. Inorg. Met.-Org. Chem.*, **33**, 343 (2003).
- [52] S. Chandra, D. Jain, A.K. Sharma. *Spectrochim. Acta Part A*, **71**, 1712 (2009).
- [53] I. Adato, I. Eliezer. *J. Chem. Phys.*, **54**, 1472 (1971).
- [54] R.S. Drago. *Physical Methods for Chemists*, 2nd Edn, Saunders College Pub, New York, 426 (1992).
- [55] A.D. Naik, S.M. Annigeri, U.B. Gangadharmath, V.K. Revankar, V.B. Mahale. *Trans. Met. Chem.*, **27**, 333 (2002).
- [56] H.T. Chifotides, K.R. Dunbar. *Acc. Chem. Res.*, **38**, 46 (2005).
- [57] K.E. Erkkila, D.T. Odom, J.K. Barton. *Chem. Rev.*, **99**, 2777 (1999).
- [58] H.K. Liu, P.J. Sadler. *Acc. Chem. Res.*, **44**, 349 (2011).
- [59] G. Psomas. *J. Inorg. Biochem.*, **102**, 1798 (2008).
- [60] M. Carter, M. Rodriguez, A.J. Bard. *J. Am. Chem. Soc.*, **111**, 8901 (1989).
- [61] A.M. Pyle, J.P. Rehmann, R. Meshoyrer, C.V. Kumar, N.J. Turro, J.K. Barton. *J. Am. Chem. Soc.*, **111**, 3051 (1989).
- [62] Y. Wang, Z.Y. Yang. *Trans. Met. Chem.*, **30**, 902 (2005).
- [63] W.A. Wani, Z. Al-Othman, I. Ali, K. Saleem, M.-F. Hsieh. *J. Coord. Chem.*, **67**, 2110 (2014).
- [64] M. Baldini, M. Belicchi-Ferrari, F. Bisceglie, P.P. Dall'Aglio, G. Pelosi, S. Pinelli, P. Tarasconi. *Inorg. Chem.*, **43**, 7170 (2004).
- [65] P. Kalaivani, R. Prabhakaran, F. Dallemer, P. Poornima, E. Vaishnavi, E. Ramachandran, V.V. Padma, R. Renganathan, K. Natarajan. *Metalomics*, **4**, 101 (2012).
- [66] A. Wolfe, G.H.J. Shimer, T. Meehan. *Biochemistry*, **26**, 6392 (1987).
- [67] C. Zhou, J. Zhao, Y.B. Wu, C.X. Yin, Y. Pin. *J. Inorg. Biochem.*, **101**, 10 (2007).
- [68] N. Lingthoingambi, N. Rajen Singh, M. Damayanti. *J. Chem. Pharm. Res.*, **3**, 187 (2011).
- [69] R. Eshkourfu, B. Čobeljčić, M. Vujčić, I. Turel, A. Pevec, K. Sepčić, M. Zec, S. Radulović, T. Srdić-Radić, D. Mitić, K. Andjelković, D. Sladić. *J. Inorg. Biochem.*, **105**, 1196 (2011).
- [70] S. Rajalakshmi, T. Weyhermüller, A.J. Freddy, H.R. Vasanthi, B.U. Nair. *Eur. J. Med. Chem.*, **46**, 608 (2011).
- [71] S. Saha, R. Majumdar, M. Roy, R.R. Dighe, A.R. Chakravarty. *Inorg. Chem.*, **48**, 2652 (2009).
- [72] L. Leelavathy, S. Anbu, M. Kandaswamy, N. Karthikeyan, N. Mohan. *Polyhedron*, **28**, 903 (2009).
- [73] C.Z. Xie, M.M. Sun, S.H. Li, X.T. Zhang, X. Qiao, Y. Ouyang, J.Y. Xu. *J. Coord. Chem.*, **66**, 3891 (2013).
- [74] D.D. Li, Z.W. Tao. *J. Coord. Chem.*, **66**, 4237 (2013).

- [75] T.T. Xing, S.H. Zhan, Y.T. Li, Z.Y. Wu, C.W. Yan. *J. Coord. Chem.*, **66**, 3149 (2013).
- [76] D.S. Raja, N.S.P. Bhuvanesh, K. Natarajan. *Inorg. Chim. Acta.*, **385**, 81 (2012).
- [77] P. Jaividhya, R. Dhivya, M.A. Akbarsha, M. Palaniandavar. *J. Inorg. Biochem.*, **114**, 94 (2012).
- [78] S. Anbu, A. Killivalavan, E.C. Alegria, G. Mathan, M. Kandaswamy. *J. Coord. Chem.*, **66**, 3989 (2013).
- [79] Z.L. Hua, W.W. Na, W. Yuan, S. Guang. *J. Coord. Chem.*, **66**, 227 (2013).
- [80] X.L. Wang, M. Jiang, Y.T. Li, Z.Y. Wu, C.W. Yan. *J. Coord. Chem.*, **66**, 1985 (2013).
- [81] H. Benezra, V.C. da Silveira, J.S. Luz, R.C. Georg, C.C. Oliveira, A.M. Ferreira. *J. Inorg. Biochem.*, **105**, 1692 (2011).
- [82] D. Lawrence, V.G. Vaidyanathan, B.U. Nair. *J. Inorg. Biochem.*, **100**, 1244 (2006).
- [83] J. Li, Y.L. Wei, L.M. Guo, C.H. Zhang, Y. Jiao. *Talanta*, **76**, 34 (2008).
- [84] C.A. Mitsopoulou, C.E. Dagas, C. Makedonas. *Inorg. Biochem.*, **102**, 77 (2008).
- [85] R.C. Santra, K. Sengupta, R. Dey, T. Shireen, P. Das, P.S. Guin, K. Mukhopadhyay, S. Das. *J. Coord. Chem.*, **67**, 265 (2014).
- [86] F. Gao, H. Chao, F. Zhou, Y.X. Yuan, B. Peng, L.N. Ji. *J. Inorg. Biochem.*, **100**, 1487 (2006).
- [87] J. Rajesh, M. Rajasekaran, G. Rajagopal, P. Athappan. *Spectrochimica Acta Part A*, **97**, 223 (2012).
- [88] C. Iysel, V.T. Yilmaz, A. Golcu, E. Ulukaya, O. Buyukgungor. *Bioorg. Med. Chem. Lett.*, **23**, 2117 (2013).
- [89] J. Zhao, K. Peng, Y. Guo, J. Zhang, D. Zhao, S. Chen, J. Hu. *J. Coord. Chem.*, **67**, 2344 (2014).
- [90] M. Ganeshpandian, S. Ramakrishnan, M. Palaniandavar, E. Suresh, A. Riyasdeen, M.A. Akbarsha. *J. Inorg. Biochem.*, **140**, 202 (2014).
- [91] L.H. Zhi, W.N. Wu, Y. Wang, G. Sun. *J. Coord. Chem.*, **66**, 227 (2013).
- [92] R. Kuttan, P. Bhanumathy, K. Nirmala, M.C. George. *Cancer Lett.*, **29**, 197 (1985).
- [93] K.K. Soudamini, R. Kuttan. *J. Ethnopharmacol.*, **27**, 227 (1989).
- [94] A. Duvoix, R. Blasius, S. Delhalle, M. Schnekenburger, F. Morceau, E. Henry, M. Dicato, M. Diederich. *Cancer Lett.*, **223**, 181 (2005).
- [95] B.B. Aggarwal, A. Kumar, A.C. Bharti. *Anticancer Res.*, **23**, 363 (2003).
- [96] V.D. John, G. Kuttan, K. Krishnankutty. *J. Exp. Clin. Cancer Res.*, **21**, 219 (2002).
- [97] V.D. John, K. Krishnankutty. *Appl. Organomet. Chem.*, **20**, 477 (2006).
- [98] H. Otori, H. Yamakoshi, M. Tomizawa, M. Shibuya, Y. Kakudo, A. Takahashi, S. Takahashi, S. Kato, T. Suzuki, C. Ishioka, Y. Iwabuchi, H. Shibata. *Mol. Cancer Ther.*, **5**, 2563 (2006).
- [99] C. Marzano, M. Pellei, F. Tisato, C. Santini. *Anticancer Agents Med. Chem.*, **9**, 185 (2009).
- [100] I. Warad, A.F. Eftaiha, M.A. Al-Nuri, A.I. Husein, M. Assal, A. Abdu-Obaid, N. Al-Zaqri, T.B. Hadda, B. Hammouti. *J. Mater. Environ. Sci.*, **4**, 542 (2013).
- [101] S. Banerjee, A.R. Chakravarty. *Acc. Chem. Res.*, **48**, 2075 (2015).
- [102] A. Barik, B. Mishra, A. Kunwar, R.M. Kadam, L. Shen, S. Dutta, S. Padhye, A.K. Satpati, H.Y. Zhang, K.I. Priyadarsini. *Eur. J. Med. Chem.*, **42**, 431 (2007).
- [103] N. Sreejayan, M.N.A. Rao. *Int. J. Pharm.*, **100**, 93 (1993).
- [104] J.A. Ruby, M.N.A. Rao, G. Kuttan, R. Kuttan, K. Satyanarayana, M.N.A. Rao. *J. Clin. Biochem. Nutr.*, **17**, 73 (1994).
- [105] J.A. Ruby, G. Kuttan, K.V.D. Babu, K.N. Rajasekharan, R. Kuttan. *Int. J. Pharm.*, **132**, 1 (1996).



Research paper

Synthesis, characterization and biological studies on Ni^{II} and Cu^{II} complexes of two novel α,β -unsaturated 1,3-diketones related to curcuminoids



T.V. Deepthi, P. Venugopalan*

Department of Chemistry, Sree Neelakanta Government Sanskrit College, Pattambi 679306, Kerala, India

ARTICLE INFO

Article history:

Received 27 March 2016
 Received in revised form 18 May 2016
 Accepted 19 May 2016
 Available online 27 May 2016

Keywords:

α,β -Unsaturated 1,3-diketones
 Curcuminoids
 Antitumor activity
 DNA binding
 1,7-Diarylheptanoids

ABSTRACT

Microwave assisted synthesis of two novel α,β -unsaturated 1,3-diketones, their mononuclear Ni^{II} and Cu^{II} complexes, characterization, results on DNA binding activities, short term *in vitro* and *in vivo* antitumor activities were reported. The ligands are structurally related to curcuminoids and exhibited significant antitumor activity against Dalton's lymphoma ascites cells. The ligands were found to be existing in their enolic form and metal complexes have 1:2 metal ligand stoichiometry evidenced by electronic, IR, ¹H NMR, ¹³C NMR and FAB mass spectral data. The DNA binding properties of ligand and metal complexes were studied by absorption titrations and by viscosity measurements with calf thymus DNA. The intrinsic binding constants of copper(II) complexes are slightly higher than complexes of same metals reported in the literature. Interaction of copper(II) complexes were found to be higher than that of nickel(II) complexes and free ligands. The copper(II) complexes of the ligands were found to be more effective towards Dalton's lymphoma ascites cells in both *in vitro* and *in vivo* studies.

© 2016 Elsevier B.V. All rights reserved.

1. Introduction

Literature is extensive on the chemistry and application of 1,3-diketones and their metal chelates [1,2]. The application of certain lanthanide 1,3-diketonates as NMR shift reagents has become an extremely useful technique to organic chemists for structural elucidation. The yellow pigment curcumin present in the roots and shoots of herbaceous plant *Curcuma Longa* L (turmeric) and several other related curcuma species of the family *Zingiberaceae* is a typical 1,7-diaryl substituted α,β -unsaturated 1,3-diketone exerting a wide range of pharmacological activities including antioxidative, anti-inflammatory and anticancer activities [3–7]. However, clinical application of curcumin in antitumor therapy has been greatly limited by its rapid metabolism, low absorption and poor stability *in vivo* [8]. In order to enhance the biological properties and antitumor activity of curcumin, a large number of curcumin derivatives and analogues have been designed and synthesized through structural modifications such as variation of the aromatic rings and their substituents or replacing the heptadione bridge chain of curcumin by other linkers [9–11]. Metal chelation can cause drastic

changes in the biological activity of many organic compounds and during recent years, metal complexes of biologically active ligands [12–14] have received much attention. In the present investigation, two novel α,β -unsaturated 1,3-diketones with a cyclopentane ring incorporated to enolizable β -diketone moiety synthesized from 2-acetylcyclopentanone and *o*-substituted benzaldehyde by exposing to microwave radiation and their [ML₂] mononuclear Ni^{II} and Cu^{II} complexes were characterized by different physicochemical methods. Copper(II) complexes have attracted considerable attention as antitumor candidates in recent years because copper is an essential micronutrient that participates in several biological processes like mitochondrial respiratory reactions, cellular stress response, antioxidant, etc., [15,16] and hence it may be less toxic than non-essential metals like platinum [17]. Nickel(II) forms an essential component of several enzymes, viz. urease, carbon monoxide dehydrogenase and hydrogenase [18]. In view of the increasing interest in copper(II) and nickel(II) complexes [19–24], the free ligands and their complexes were analysed for their DNA binding properties with calf thymus DNA and screened for both *in vitro* and *in vivo* antitumor activity against Dalton's lymphoma ascites cells.

* Corresponding author. Tel.: +91 9447301283.

E-mail address: venugpamrita@gmail.com (P. Venugopalan).

2. Experimental

2.1. Materials and methods

2-Acetylcyclopentanone, tris(hydroxymethyl)aminomethane (Tris) and Calf thymus (CT) DNA were procured from Sigma Aldrich, USA. Solvents and other chemicals used were of analytical reagent grade procured from commercial sources and used without any further purification. Solvents used were purified by standard procedures [25].

Carbon and hydrogen were analyzed on an Elemental Vario EL CHN analyzer and metal contents of the complexes were determined using standard methods. The electronic spectra of the ligands and complexes and other UV–Vis measurements were recorded using model Jasco V – 550 UV visible spectrophotometer in CHCl₃ and DMSO. The IR spectra were recorded in the region 4000–250 cm⁻¹ on a model Jasco FTIR-4100 Fourier transform infrared spectrophotometer in KBr discs. The ¹H NMR and ¹³C NMR spectra were recorded in CDCl₃ on a model Bruker Avance III, 400 MHz FT NMR spectrometer. Mass spectra were recorded on a model JEOL/SX-102 MS (FAB using argon and 3-nitrobenzyl alcohol as the matrix). The mass spectrometer was operated with accelerating voltage 10 kV in the positive ion mode. Molar conductivity measurements were recorded on an ELICO-CM-82 T conductivity bridge with a cell having cell constant 0.51 cm⁻¹.

Dalton's lymphoma ascites (DLA) cells were obtained from the Cancer Research Institute, Mumbai, India. DLA was maintained as ascites tumours in Swiss albino mice, purchased from Kerala Agricultural University, Thrissur, Kerala. They were fed with normal mouse chow (Lipton India) and water *ad libitum*.

2.2. Preparation of ligands

The conventional synthesis of curcumin derivative involves condensation between aromatic aldehyde and 2,4-pentadione – boric oxide complex in ethyl acetate medium [26]. Use of boron-based protection of the 1,3-diketone circumvents the Knoevenagel condensation at C-3 (active methylene group) and facilitates aldol condensations at C-1 and C-5 of 2,4-pentadione successively via the dienolate [27,28]. The procedure involves stirring of the reaction mixture for 3–4 h, giving a mixture of mono and bis condensation products from which the desired product is separated by column chromatography [26,29]. The microwave assisted synthesis exclusively gives the bis condensation product in a short time of 3 min. A typical procedure for the synthesis is given below.

2-Acetylcyclopentanone (20 mmol) was mixed with the boron oxide (20 mmol) in a 100 mL Erlenmeyer flask. The appropriate aromatic aldehyde (40 mmol), acetic acid (100 mg), and morpholine (100 mg) were then added. The reaction mixture was irradiated with the microwave at 70 W for 3 min. The flask was cooled to room temperature and then methanol (50 mL) was added. This mixture was then sonicated for 30–40 min. The fine powder so obtained was filtered and washed with cold methanol. The compounds were recrystallized from hot benzene to obtain chromatographically pure material.

2.2.1. HL¹

74.0%, M wt. 362 Da, m.p. 176 °C, Yellow solid, *Anal.* Calc. for C₂₃H₂₂O₄(%): Calc. C (76.22), H (6.12). Found: C (76.34), H (6.51); I.R. (KBr Pellets, cm⁻¹): 1592, ν(C=O) carbonyl, 1342, ν_{as}(C–C–C), 941 ν(CH=CH–)trans.; UV–Vis (CHCl₃, nm) 261 (π → π*), 446 (n → π*); ¹H NMR (400 MHz, CDCl₃, ppm): δ 14.33 (s, –OH enolic, 1H), 2.73–2.81 (s, ring, 4H), 6.67, 6.98 (d, alkenyl, 2H), 6.82–7.79 (m, aromatic, vinylic, 9H), δ 3.82 (s, methoxy, 6H). ¹³C NMR

(400 MHz, CDCl₃, ppm): δ 24.37, 27.61 (aliphatic), 179.83, 194.77 (carbonyl), 117.89–167.25 (aromatic); MS-EI: *m/z* = 362.19 [M]⁺, 345.24 [M–OH]⁺, 213.16 [M–C₉H₉O₂]⁺, 103.09 [M–C₁₅H₁₅O₄]⁺, 91.08 [M–C₁₆H₁₅O₄]⁺, 77.06 [M–C₁₇H₁₇O₄]⁺.

2.2.2. HL²

71.0%, M wt. 330 Da, m.p. 172 °C, Yellow solid, *Anal.* Calc. for C₂₃H₂₂O₂(%): Calc. C (83.60), H (6.71). Found: C (83.51), H (6.19); I. R. (KBr Pellets, cm⁻¹): 1587, ν(C=O) carbonyl, 1435, ν_{as}(C–C–C), 921 ν(CH=CH–)trans.; UV–Vis (CHCl₃, nm) 257 (π → π*), 434 (n → π*); ¹H NMR (400 MHz, CDCl₃, ppm): δ 14.17 (s, –OH enolic, 1H), 2.76–2.84 (s, ring, 4H), 6.79, 6.94 (d, alkenyl, 2H), 7.11–7.42 (m, aromatic, vinylic, 9H), δ 2.26 (s, methyl, 6H). ¹³C NMR (400 MHz, CDCl₃, ppm): δ 23.47, 28.79 (aliphatic), 187.45, 195.31 (carbonyl), 121.72–147.63 (aromatic); MS-EI: *m/z* = 330.75 [M]⁺, 313.70 [M–OH]⁺, 211.46 [M–C₈H₆OH]⁺, 197.45 [M–C₉H₈OH]⁺, 171.35 [M–C₁₀H₇O₂]⁺, 105.31 [M–C₁₅H₁₃O₂]⁺, 91.26 [M–C₁₆H₁₅O₂]⁺, 77.24 [M–C₁₇H₁₇O₂]⁺.

2.3. Preparation of Ni^{II} and Cu^{II} complexes

Metal complexes of the ligands were prepared by refluxing a methanolic solution of the metal(II) acetate (1 mmol) and the ligand (2 mmol) for ~2 h. The solution was concentrated to half of its volume and cooled to room temperature. The precipitated complexes were filtered, washed with methanol and recrystallized from hot methanol.

2.3.1. [NiL₂]

63.0%, M wt. 781.51 Da, m.p. 168 °C, Brown solid, *Anal.* Calc. for C₄₆H₄₂O₈Ni(%): Calc. C (70.70), H (5.42), Ni (7.51). Found C (70.21), H (5.23), Ni (7.43); I.R. (KBr Pellets, cm⁻¹): 1634, 1524 ν(C=O) metal chelated carbonyl, 1432, ν(C=C)phenyl, 1272, ν(C=C)alkenyl, 1264, ν_{as}(C–C–C)chelate ring, 1141, ν_{as}(C–C–C)chelate ring 963 ν(CH=CH–)trans, 467, ν(M–O)chelate ring; UV–Vis (CHCl₃, nm) 254 (π → π*), 458 (n → π*); ¹H NMR (400 MHz, CDCl₃, ppm): δ 2.74–2.84 (s, ring, 8H), 6.71–6.84 (d, alkenyl, 4H), 7.21–7.64 (m, aromatic, vinylic, 18H), δ 3.78 (s, methoxy, 12H). ¹³C NMR (400 MHz, CDCl₃, ppm): δ 25.61–31.94 (aliphatic), 162.64, 190.38 (carbonyl), 116.64–159.68 (aromatic).

2.3.2. [NiL₂]

64.0%, M wt. 717.52 Da, m.p. 172 °C, Brown solid, *Anal.* Calc. for C₄₆H₄₂O₄Ni(%): Calc. C (77.00), H (5.90), Ni (8.18). Found: C (77.24), H (5.68), Ni (8.35); I.R. (KBr Pellets, cm⁻¹): 1647, 1538 ν(C=O) metal chelated carbonyl, 1476, ν(C=C)phenyl, 1316, ν(C=C)alkenyl, 1226, ν_{as}(C–C–C)chelate ring, 1138, ν_{as}(C–C–C)chelate ring 958 ν(CH=CH–)trans, 458, ν(M–O)chelate ring; UV–Vis (CHCl₃, nm) 268 (π → π*), 476 (n → π*); ¹H NMR (400 MHz, CDCl₃, ppm): δ 2.81–2.89 (s, ring, 8H), 6.28–6.74 (d, alkenyl, 4H), 7.34–7.85 (m, aromatic, vinylic, 18H), δ 2.25 (s, methyl, 12H). ¹³C NMR (400 MHz, CDCl₃, ppm): δ 26.38–32.68 (aliphatic), 163.84–194.76 (carbonyl), 114.38–159.73 (aromatic).

2.3.3. [CuL₂]

67.0%, M wt. 786.37 Da, m.p. 152 °C, Brown solid, *Anal.* Calc. for C₄₆H₄₂O₈Cu(%): Calc. C (70.26), H (5.38), Cu (8.08). Found: C (70.14), H (5.27), Cu (8.16); I.R. (KBr Pellets, cm⁻¹): 1602, 1551 ν(C=O) metal chelated carbonyl, 1454, ν(C=C)phenyl, 1445, ν(C=C)alkenyl, 1284, ν_{as}(C–C–C)chelate ring, 1123, ν_{as}(C–C–C)chelate ring 934 ν(CH=CH–)trans, 507, ν(M–O)chelate ring; UV–Vis (CHCl₃, nm) 251 (π → π*), 448 (n → π*); MS-EI: *m/z* = 787 [M + 2]⁺, 785 [M]⁺, 423 [M–C₂₃H₂₂O₄]⁺, 361 [M–C₂₃H₂₁O₄Cu]⁺, 238 [M–C₃₅H₃₁O₆]⁺, 224 [M–C₃₆H₃₃O₆]⁺.

2.3.4. $[\text{CuL}_2]$

66.0%, M wt. 722.37 Da, m.p. 162 °C, Brown solid, Anal. Calc. for $\text{C}_{46}\text{H}_{42}\text{O}_4\text{Cu}$ (%): Calc. C (76.48), H (5.86), Cu (8.80). Found: C (76.34), H (5.43), Cu (8.76); I.R. (KBr Pellets, cm^{-1}): 1617, 1521 ν (C=O) metal chelated carbonyl, 1464, ν (C=C)phenyl, 1358, ν (C=C)alkenyl, 1294, ν_{as} (C–C)chelate ring, 1194, ν_{as} (C–C)chelate ring 984 ν (CH=CH-)trans, 474, ν (M–O)chelate ring; UV–Vis (CHCl_3 , nm) 260 ($\pi \rightarrow \pi^*$), 455 ($n \rightarrow \pi^*$); MS–EI: $m/z = 723$ $[\text{M} + 2]^+$, 721 $[\text{M}]^+$, 391 $[\text{M} - \text{C}_{23}\text{H}_{22}\text{O}_2]^+$, 330 $[\text{M} - \text{C}_{23}\text{H}_{20}\text{O}_2\text{Cu}]^+$, 222 $[\text{M} - \text{C}_{35}\text{H}_{31}\text{O}_3]^+$, 208 $[\text{M} - \text{C}_{36}\text{H}_{33}\text{O}_3]^+$.

2.4. DNA binding studies

UV–Vis absorption spectrophotometry and viscosity measurements were used to assess the interaction of ligands and their complexes with CT-DNA at pH 7.2 in double distilled water containing tris-(hydroxymethyl)aminomethane (Tris, 10^{-2} M). The ratio of UV absorbance of the stock solution of CT-DNA in 5 mM Tris–HCl/50 mM NaCl buffer (pH 7.2) at 260 and 280 nm gives a ratio of 1.7–1.8, indicating that CT-DNA was sufficiently free of protein [30]. The concentration of CT-DNA was determined from its absorption intensity at 260 nm with a molar extinction coefficient of $6600 \text{ M}^{-1} \text{ cm}^{-1}$ [31]. The binding experiments were carried out by recording the absorbance changes on adding increasing concentrations of DNA (0–250 μM) against a fixed concentration of the ligand and its complexes (50 μM). Equal volumes (2.0 mL) of each solution of DNA and ligand or metal complex were mixed together and their λ_{max} and absorbance values were recorded. The absorption spectra were recorded after each addition of different concentrations of DNA solution.

Viscosity measurements of 100 μM CT-DNA in Tris–HCl/NaCl buffer were performed using an Ostwald viscometer at 35 ± 0.2 °C in a thermostatic water bath. The DNA concentration was kept constant in all samples, while the complex/ligand concentration was increased from 0 to 50 μM . Flow time was measured with a digital stopwatch, and each sample was measured three times, and an average flow time was calculated. Data are presented as $(\eta/\eta^0)^{1/3}$ versus binding ratio $[\text{Compound}]/[\text{DNA}]$, where η and η^0 indicate the viscosity of DNA solutions in the presence and absence of complex, respectively. The relative viscosity was calculated according to the relation $\eta = (t - t_0)/t_0$, where t is the flow time of DNA solution in the presence or absence of ligand or complex and t_0 is the flow time of the buffer alone [32].

2.5. Antitumor studies

2.5.1. Determination of the effect of compounds on ascites tumour model

In vitro cytotoxicity studies were carried out using Dalton's lymphoma ascites cells. The tumour cells were aspirated from the peritoneal cavity of tumour bearing mice. It was washed thrice with phosphate buffered saline. Cell viability was determined by trypan blue exclusion method [33]. Viable cell suspension (1×10^6 cells in 0.1 mL) was added to tubes containing various concentrations of the test compounds (200 $\mu\text{g}/\text{mL}$, 100 $\mu\text{g}/\text{mL}$, 50 $\mu\text{g}/\text{mL}$, 20 $\mu\text{g}/\text{mL}$, and 10 $\mu\text{g}/\text{mL}$) dissolved in the minimum quantity of DMSO and the volume was made up to 1 mL using phosphate buffered saline. Control tube contains only cell suspension. These assay mixture were incubated for 3 h at 37 °C. Further cell suspension was mixed with 100 μL of 1% trypan blue and kept for 2–3 min. Dead cells take up the blue colour of trypan blue while the live cells do not take up the dye. The number of stained and unstained cells was counted separately counted using heamocytometer.

2.5.2. Determination of the effect of compounds on DLA cell induced ascites tumour

For *in vivo* studies, groups of Swiss Albino mice (female, 6 per group) were injected intraperitoneally with Dalton's lymphoma ascites tumour cells (1×10^6 cells/animal). They were injected (ip) with (25 mg/kg body weight) test compound suspended in carboxy methyl cellulose (CMC) and the injections of the test compounds were started 24 h after tumour inoculation and continued for 10 consecutive days. The death pattern of the animals due to tumour burden was noted. The percentage increase in lifespan (% ILS) was calculated using the formula $\% \text{ ILS} = [(T - C)/C \times 100]$, where T and C represent the mean number of days survived by the treated and control animals respectively [34].

2.5.3. Determination of the effect of compounds on DLA cell induced solid tumour model

Solid tumours were also induced in groups of Swiss albino mice (female, 6 per group) by subcutaneous injection of DLA cells (1×10^6 cells/animal) on the right hand limb. One group was kept as control and other groups were injected intramuscularly (im) with the test compounds (25 mg/kg body weight) and the injections of the test compounds were started 24 h after inoculation and continued for 10 consecutive days. Tumour diameter was measured every third day for one month and the tumour volume was calculated using the formula; $V = 4/3\pi r_1^2 r_2$ where r_1 and r_2 are the minor and major radii respectively [35].

3. Results and discussion

3.1. Synthesis and characterization

The ligands were synthesized by the condensation of *o*-substituted benzaldehyde with 2-acetylcyclopentanone as per the scheme given in Fig. 1.

UV, IR, ^1H NMR, ^{13}C NMR and mass spectral data of the compounds are in agreement with the structure given in Fig. 1. Both ligands formed well-defined and crystalline complexes having sharp melting point with nickel(II) and copper(II) ions. The observed carbon, hydrogen and metal percentages of the metal complexes and FAB mass spectral data suggest their ML_2 stoichiometry. All the metal complexes behave as non-electrolytes (specific conductance in the range $8\text{--}12 \Omega^{-1} \text{ cm}^{-1}$ in DMF) and do not contain the anion of the metal salt used for their preparation. The nickel(II) complexes are diamagnetic and copper(II) complexes are paramagnetic. The electronic, IR, ^1H NMR, ^{13}C NMR and

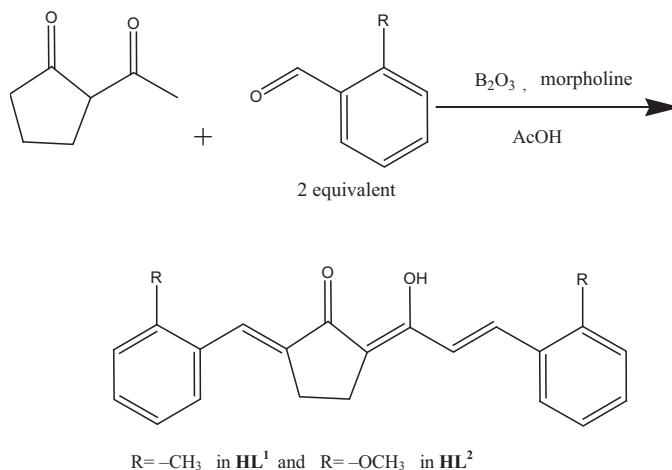


Fig. 1. Synthesis of ligands.

mass spectral of the complexes are compatible with the structure given in Fig. 2. The spectral data are discussed below.

3.1.1. IR spectra

The IR spectra of the ligands are characterized by the presence of a strong band in the region $1594\text{--}1619\text{ cm}^{-1}$. Intramolecular hydrogen bonding can lower the carbonyl stretching frequency by about 50 cm^{-1} [36]. The absence of band assignable to a normal or α , β -unsaturated carbonyl group in the region $1640\text{--}1740\text{ cm}^{-1}$ of the spectra indicates that the ligands exist as in their enolic form [37]. A broad band present in the range of $2800\text{--}3600\text{ cm}^{-1}$ is due to the stretching of the chelated carbonyl group and the intramolecular hydrogen bonded enol group.

In the IR spectra of the metal complexes, the bands of diketones are absent and instead a strong band assignable to the stretching of the carbonyl moiety appeared at $\sim 1613\text{ cm}^{-1}$. The broad free ligand band in the region at $2800\text{--}3600\text{ cm}^{-1}$ due to the hydrogen bonded enol proton is absent in the spectra of metal complexes and weak bands attributable to various $\nu(\text{C-H})$ appeared. The carbonyl groups are involved in metal complex formation is evident from the appearance of two medium intensity bands in the region $426\text{--}507\text{ cm}^{-1}$ due to $\nu(\text{M-O})$ vibrations [38]. The prominent band at $\sim 975\text{ cm}^{-1}$ is typical of a trans --CH=CH-- group which remained unaltered in the spectra of metal complexes [39].

3.1.2. ^1H NMR spectra

The ^1H NMR spectral data of both ligands show a characteristic downfield singlet at $\delta \sim 14$ ppm which can be assigned to the intramolecularly hydrogen bonded enolic proton. The most characteristic feature of the ^1H NMR spectra of the diamagnetic nickel(II) chelates is the absence of proton signals above $\delta \sim 11$ ppm. This strongly supports the replacement of the enolic proton by the metal ion in the complexes [40]. The ^1H NMR spectra of all the ligands shows signal δ at $2.74\text{--}2.90$ ppm due to protons in the cyclopentyl ring and two singlet δ at ~ 6.71 ppm due to the alkenyl protons. Observed J value of 16 Hz for the alkenyl proton signals in the nickel(II) complexes suggest their trans orientation as it is in the free ligands. The integrated intensities of the aryl and alkenyl protons are in well agreement with the structure of metal chelates given in Fig. 2.

3.1.3. ^{13}C NMR spectra

^{13}C NMR spectral data of both ligands show two resonance signals at ~ 197.91 ppm and ~ 182.33 ppm indicating that the two car-

bonyl groups have different electronic environment. The two aliphatic carbon atoms in the cyclopentanone ring show a resonance signal at ~ 24 ppm. The resonance signals in the range $117.89\text{--}167.25$ ppm are due to the aromatic carbon atoms. The carbonyl carbon signal of the free ligand shifted by $15\text{--}20$ ppm to low field in the spectra of nickel(II) complexes [41].

3.1.4. Mass spectra

Mass spectra of ligands show an intense molecular ion peak. In addition to the molecular ion peak (M^+), peaks due to the elimination of O, OH, ArCH_2^+ and Ar^+ species from the molecular ion are the most significant feature of the mass spectra of curcuminoids [42]. Peaks corresponding to m/z $(\text{M-ArCHCHCO})^+$ and $(\text{M-ArCHCHCOCH}_2)^+$ are also present in the mass spectra of these compounds. The FAB mass spectra of the copper(II) chelates confirm the ML_2 stoichiometry of the complexes. Peaks due to M^+ and $(\text{M} + 2)^+$ with 3:1 intensity are present in the FAB MS of copper(II) chelates in consistent with the natural abundance of ^{63}Cu and ^{65}Cu isotopes. The mass spectra of the copper(II) chelates show that stepwise removal of aryl groups is a characteristic feature of these complexes [43]. Peaks due to $[\text{CuL}]^+$, $[\text{CuL-ArCHCHCO}]^+$, $[\text{CuL-ArCHCHCOCH}_2]^+$, L^+ and fragments of L^+ are common in the spectra of copper(II) complexes. The mass spectra of ligands and copper(II) complexes are given as Supplementary material S1–S4.

3.1.5. Electronic spectra

The UV spectra of the ligands are characterized by the presence of two absorption maxima, the low energy band corresponds to an $n \rightarrow \pi^*$ transition ($434\text{--}446$ nm) and the high energy band is due to a $\pi \rightarrow \pi^*$ transitions ($257\text{--}261$ nm). In the metal complexes these absorptions show only a slight bathochromic shifts due to the involvement of the carbonyl group in metal complexation. Similarity in the UV absorption maxima of metal complexes with that of free ligands, show that no structural alteration of the ligand has occurred during the complex formation.

In the copper(II) complexes the presence of a broad visible band at ~ 665 nm and the measured μ_{eff} values ($1.75\text{--}1.81$ B.M.) support their square planar structure [44]. Square-planar copper(II) complexes undergo a change to octahedral symmetry in the presence of donor solvents. The electronic spectra of the copper(II) complexes when recorded in pyridine (10^{-3} M solution) showed two low-energy weak bands at $667.3\text{--}659.8$ nm and $521.9\text{--}520.7$ nm ($\epsilon = 2.30 \times 10^4\text{--}2.85 \times 10^4\text{ M}^{-1}\text{ cm}^{-1}$) and a strong high energy band at $329.4\text{--}329.1$ nm ($\epsilon = 6.20 \times 10^4\text{--}6.48 \times 10^4\text{ M}^{-1}\text{ cm}^{-1}$) which may be assigned to $^2\text{B}_{1g} \rightarrow ^2\text{A}_{1g}$ and $^2\text{B}_{1g} \rightarrow ^2\text{E}_g$ transitions, respectively [45]. The strong high-energy band, in turn, is assigned to (metal \rightarrow ligand) charge transfer. The observed diamagnetism and broad medium-intensity band in the region $562\text{--}581$ nm in the visible spectra of the nickel(II) chelates suggest their square-planar geometry. In conformity with this observation the visible spectra of the chelates in pyridine solution (10^{-3} M) showed three bands corresponding to a configurational change from square-planar to octahedral due to the association of pyridine. The absorption maxima in the regions $1243\text{--}1253$ nm ($\epsilon = 4.30 \times 10^4\text{--}4.85 \times 10^4\text{ M}^{-1}\text{ cm}^{-1}$), $736\text{--}770$ nm ($\epsilon = 5.23 \times 10^4\text{--}5.54 \times 10^4\text{ M}^{-1}\text{ cm}^{-1}$) and $410\text{--}424$ nm ($\epsilon = 2.43 \times 10^4\text{--}2.68 \times 10^4\text{ M}^{-1}\text{ cm}^{-1}$) in the adducts can be assigned to the transitions $^3\text{A}_{2g} \rightarrow ^3\text{T}_{2g}$; $^3\text{A}_{2g} \rightarrow ^3\text{T}_{1g}(\text{F})$ and $^3\text{A}_{2g} \rightarrow ^3\text{T}_{1g}(\text{P})$, respectively [46].

3.2. Biological studies

3.2.1. DNA binding activity

A large number of anticancer drugs have affinities towards DNA and DNA binding capacity is of great significance in their mode of action [47–51]. Ligands and transition metal complexes are known to bind with DNA through covalent and/or non-covalent interac-

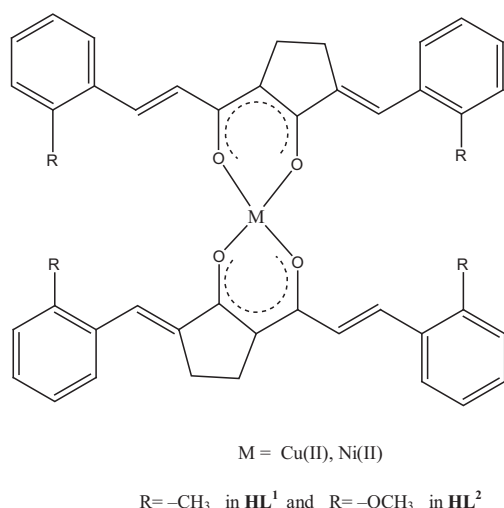


Fig. 2. Proposed structure of the metal complexes.

tions [52–54]. It is reported that in the case of covalent binding, one of the labile ligands of the complexes is replaced by nitrogen bases of DNA and the non-covalent interactions generally include intercalative and electrostatic interactions with the major or minor grooves of DNA [55]. The changes in the spectral absorbance of DNA in the presence of ligands and complexes are the evidences for their interactions with DNA [56,57]. The DNA binding affinities of free ligands and their complexes were quantitatively studied by calculating the intrinsic binding constants (K_b) from the changes in absorbance of $\pi \rightarrow \pi^*$ spectral band (254–268 nm) with increasing concentration of DNA, by using the equation [58]

$$[\text{DNA}]/(\varepsilon_a - \varepsilon_f) = [\text{DNA}]/(\varepsilon_b - \varepsilon_f) + 1/K_b(\varepsilon_b - \varepsilon_f)$$

where [DNA] is the concentration of DNA in base pairs, the apparent absorption coefficients ε_a , ε_f , and ε_b correspond to $A_{\text{obs}}/[\text{Compound}]$, the extinction coefficient for the free compound, and the extinction coefficient for the compound in the fully bound form, respectively.

Intercalation of foreign molecules into DNA usually results in hypochromism or hyperchromism as the intercalation involves some kind of interaction between the molecule and the DNA base pairs [59]. Hypochromism arises from the contraction of CT-DNA in the helix axis and its conformational changes [60]. Meanwhile, hyperchromism results from the secondary damage of the DNA double helix structure [61,62], in which the extent of hyperchromism is indicative of partial or non-intercalative binding modes [63]. The absorption spectra of 50 μM **HL**¹ and [**CuL**₂¹] in the absence and presence of CT-DNA (0–200 μM) are given in Figs. 3 and 4. The absorption spectra of **HL**², [**CuL**₂²], [**NiL**₂¹] and [**NiL**₂²] are shown in Supplementary material (S5–S8). Absorption spectra of complexes display clear hypochromism with slight red shift of 4–7 nm. The observed hypochromism is due to the interaction between the π^* orbitals of the intercalated compounds with the π orbitals of the DNA base pairs, thereby decreasing the $\pi \rightarrow \pi^*$ transition energies [64]. The hypochromism of the metal complexes are greater than that of free ligands and it is due to additional interaction with positively charged metal ion or even due to the replacement of a ligand with nitrogen bases of DNA. Among the metal complexes studied, hypochromism of copper(II) complexes is greater than corresponding nickel(II) complexes. Even though the exact reason is not known, it may probably due

to the involvement of copper(II) ions as it is involved in many natural processes. The intrinsic binding constants (K_b) obtained for free ligands and their metal complexes are given in Table 1. The values are comparable to that of reported DNA intercalative complexes [65–73].

In order to establish the nature of binding between the complexes and DNA, viscosity studies were also carried out. In intercalative mode due to increase in the separation of base pairs at intercalation site and the unwinding of DNA helix will increase the DNA length and cause a significant increase in viscosity of DNA solution [74]. On the other hand, a groove binding and electrostatic interaction reduces its effective length resulting in a slight decrease of viscosity [75]. The viscosity experiments were carried out in triplicate on CT-DNA by varying the concentration of the ligands or copper(II) complexes ([compound]/[DNA] = 0.0–0.5), and the corresponding data are illustrated in Fig. 5. Results with nickel(II) complexes are attached as Supplementary material S9. Both the ligands and complexes show an increase in specific viscosity with increase in concentration of compounds, obviously indicating the binding involves intercalative mode [76,77]. The complexes were found to be more strongly bind with DNA than free ligands. It may probably due to the presence of metal ion which can interact with the nitrogen bases of DNA.

3.2.2. Antitumor activity

Besides cisplatin, many transition metal complexes are well known for their antitumor activity and many of them have successfully cleared their clinical trials. Antitumor activity of curcumin, the active component of turmeric [78], its synthetic analogues and their metal complexes has been reported [79–81]. Since copper(II) ion is an essential cofactor in a number of enzymes and less toxic than non essential metals, a large number of copper based complexes have been studied for antitumor potency in both *in vitro* and *in vivo* studies [82,83]. In our studies, copper complexes were found to be significantly more active than Ni(II) complexes and free ligands.

The results of short-term *in vitro* cytotoxic activity of the ligands and their metal chelates (Table 1) against Dalton's lymphoma ascites indicate that metal complexation enhances the cytotoxicity of compounds considerably. Concentrations required

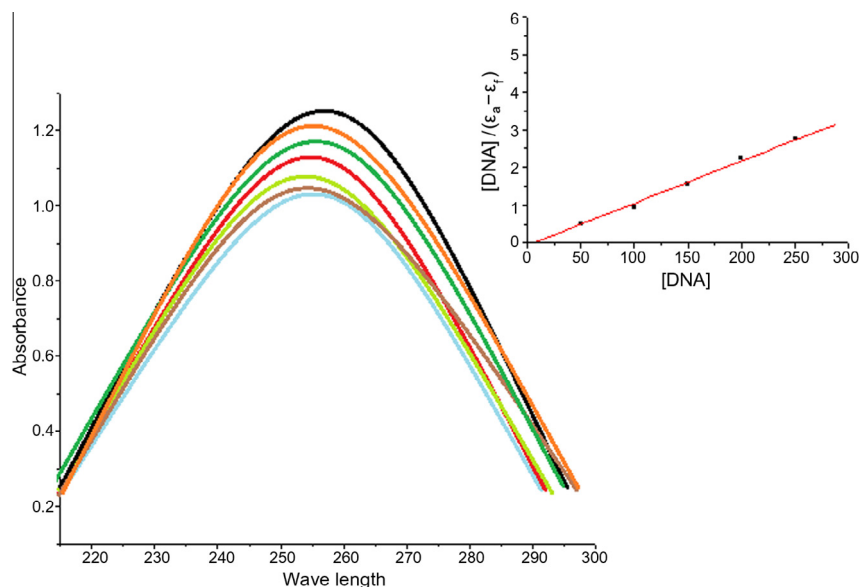


Fig. 3. Absorption spectra of **HL**¹ (50 μM) in the absence and presence of increasing amounts of CT-DNA at room temperature in Tris-HCl/NaCl buffer (pH 7.2). Inset: plot of $[\text{DNA}]/(\varepsilon_a - \varepsilon_f)$ vs. $[\text{DNA}]$ for absorption titration of CT-DNA with **HL**¹.

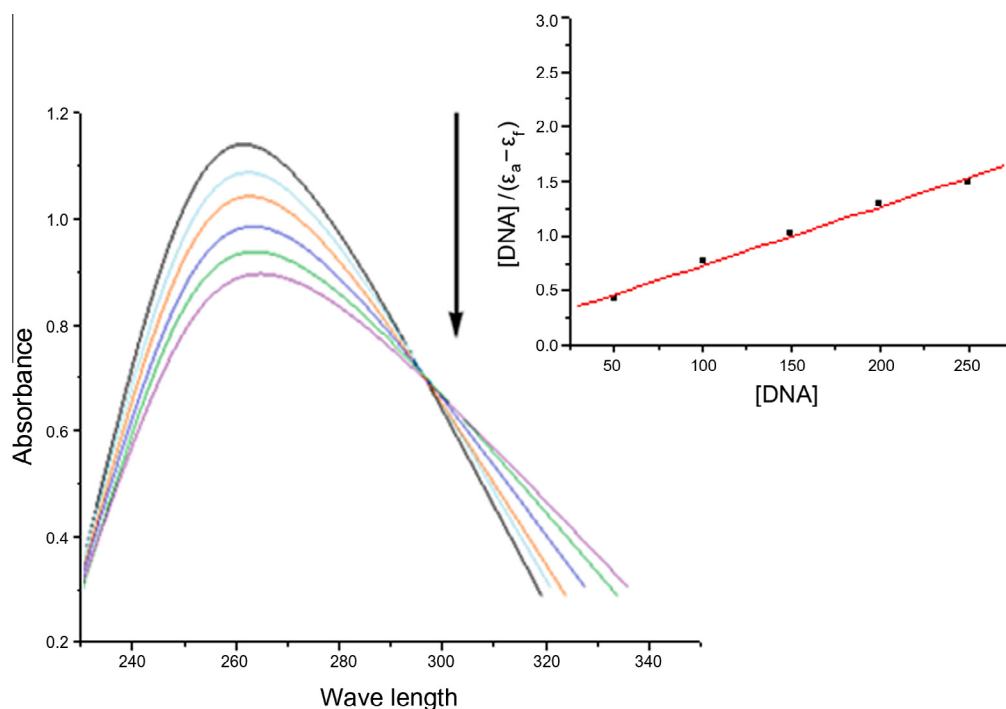


Fig. 4. Absorption spectra of $[\text{CuL}_2]$ ($50 \mu\text{M}$) in the absence and presence of increasing amounts of CT-DNA at room temperature in Tris-HCl/NaCl buffer (pH 7.2). The arrow shows the effect of increasing of CT-DNA concentration on the absorption intensity. Inset: plot of $[\text{DNA}]/(\epsilon_a - \epsilon_f)$ vs. $[\text{DNA}]$ for absorption titration of CT-DNA with complex.

Table 1
DNA binding constants, *in vitro* and *in vivo* antitumor activity of compounds.

Compounds	DNA binding constants ($\times 10^3 \text{ M}^{-1}$)	Concentrations ($\mu\text{g/ml}$) required to produce 50% cell death	No. of days survived ^a	Increase in life span (%)
Control			17.29 ± 1.1	
HL¹	1.34	95	27.68 ± 2.1	37.53
HL²	2.23	91	27.36 ± 2.1	36.80
$[\text{CuL}_2^1]$	5.31	23	36.96 ± 2.8	53.21
$[\text{CuL}_2^2]$	7.42	31	34.46 ± 2.6	49.82
$[\text{NiL}_2^1]$	3.47	53	32.25 ± 2.5	41.25
$[\text{NiL}_2^2]$	3.98	60	31.05 ± 2.1	39.24

^a Each value represents mean of three different observations \pm S.D.

to produce 50% cell death are in the range 91–95 $\mu\text{g/ml}$ in the case of free ligands. The copper chelates produced the same effect at remarkably lower concentrations of 23–31 $\mu\text{g/ml}$.

The incorporation of metal ion enhanced the antitumor activity of the ligands. Copper chelate of **HL¹** is found to be more effective than **$[\text{CuL}_2^2]$** and it may probably due to the presence of methoxy group in the aryl ring that can be cleaved to produce a phenoxy free radical. Life span of ascites tumour bearing animals induced by DLA cells was found to be increased by treatment with copper complexes. The animals inoculated with DLA cell lines alone survived for a period of 17.29 ± 1.1 days. Treatment with copper(II) complexes increased the average life span of tumour bearing mice than the free ligands (Table 1). Copper(II) complexes found to be effective in increasing the life span of animals with an average of 36.96 ± 2.8 and 34.46 ± 2.6 days for **$[\text{CuL}_2^1]$** and **$[\text{CuL}_2^2]$** , respectively.

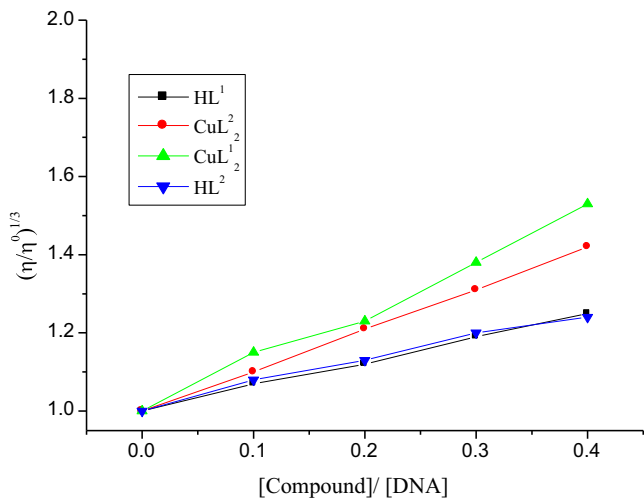


Fig. 5. Effect of increasing concentration of the ligands and corresponding copper (II) complexes on the relative viscosities of CT-DNA at $35.0 \pm 0.2 \text{ }^\circ\text{C}$.

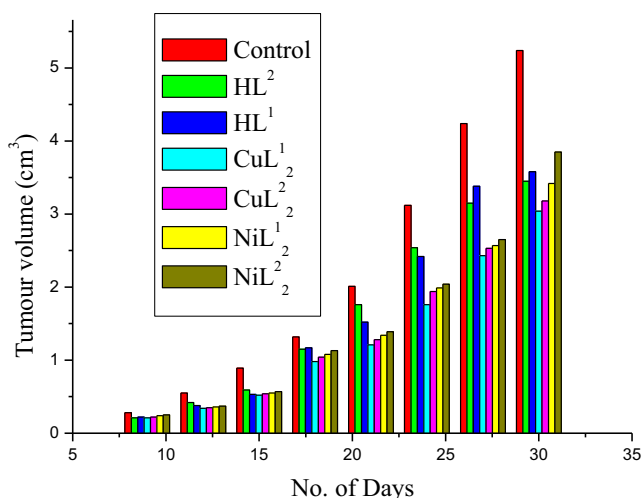


Fig. 6. Effect of compounds on solid tumour development.

Reductions of solid tumour volume in mice by the intraperitoneal administration of compounds are given in Fig. 6. Compared with free ligands, their respective copper(II) complexes are remarkably active in reducing tumour volume. Tumour volumes were respectively 5.24, 3.45 and 3.58 cm³ on day 30 for control, HL¹ and HL². The tumour volumes on day 30 for copper complexes [CuL₂¹] and [CuL₂²] were, respectively, 3.04 and 3.18 cm³. Corresponding values for [NiL₂¹] and [NiL₂²] were, respectively, 3.42 and 3.85 cm³. The results clearly reveal that [CuL₂¹] with methoxy group on the phenyl rings show the maximum activity towards cytotoxicity on Dalton's Lymphoma ascites cells, percentage increase in life span (Table 1) and reduction of solid tumour volume in mice (Fig. 6). The copper complexes dramatically enhanced the activity as evident from the data. It has been proved that copper complexation enhanced the activities in both cases. Earlier studies have shown that curcumin with methoxy and hydroxyl groups in the aryl ring, is an inhibitor of lipid peroxidation [84], which promotes anticancer properties of the compound. It has also been reported that curcumin-gold complex is an effective anti arthritic agent [85]. The present study suggests that metal complexation significantly increased the cytotoxic and antitumor activities of compounds. As reported earlier [86,87], the methoxy group in the phenyl ring enhances the antitumor activity of curcuminoids. The greater electron releasing effect of methoxy group in the phenyl rings together with the presence of copper(II) ion may be the reason for the exceptional activity of [CuL₂¹] among the compounds screened.

4. Conclusions

Two novel α,β -unsaturated 1,3-diketones structurally related to curcuminoids were synthesized from 2-acetylcyclopentanone and *o*-substituted benzaldehyde by exposing to microwave radiation and their mononuclear Ni^{II} and Cu^{II} complexes having ML₂ stoichiometry were characterized by different physicochemical methods. The DNA binding activity of copper(II) complexes is found to be greater than both nickel(II) complexes and free ligands. The intrinsic binding constant obtained from absorption titrations were found to be comparable with other complexes reported in the literature. The binding involves intercalative mode through non covalent interactions and both complexes produced conformational changes in the structure of DNA via moderate interaction. Introduction of cyclopentane ring to modify the basic skeleton of curcumin significantly increased the cytotoxic and antitumour activities of compounds. Interaction of copper complexes with DNA may be correlated with their cytotoxic effects against tumor cells. Studies on emerging targets for anticancer drugs such as cytotoxicity against other tumour cells, the rate of metabolism, absorption and stability *in vivo* should be further investigated.

Acknowledgements

We thank Dr. Ramadasan Kuttan, the Director of the Cancer Research Centre, Amala Institute of Medical Sciences, Thrissur, Kerala, India for their help in the *in vivo* and *in vitro* antitumor studies and SAIF IIT Madras, SAIF IIT Bombay, STIC CUSAT and CDRI Lucknow for spectral analysis.

Appendix A. Supplementary material

Supplementary data associated with this article can be found, in the online version, at <http://dx.doi.org/10.1016/j.ica.2016.05.045>.

References

- [1] R.C. Mehrotra, *Metal β -diketonates and Allied Derivatives*, Academic Press Inc., New York, 1978.
- [2] K. Binnemans, in: K.A. Gschneidner Jr., J.C.G. Bünzli, V.K. Pecharsky (Eds.), *Handbook on the Physics and Chemistry of Rare Earths*, Elsevier, New York, 2005.
- [3] V.S. Govindarajan, W.H. Stahl, *Crit. Rev. Food Sci. Nutr.* 12 (1980) 199.
- [4] P. Venugopalan, T.V. Deepthi, *Asian J. Res. Chem.* 7 (3) (2014) 355.
- [5] W.M. Weber, L.A. Hunsaker, S.F. Abcouwer, L.M. Deck, D.L. Vander Jagt, *Bioorg. Med. Chem.* 13 (2005) 3811.
- [6] S.P. Weisberg, R. Leibel, D.V. Tortoriello, *Endocrinology* 149 (2008) 3449.
- [7] P. Anand, C. Sundaram, S. Jhurani, A.B. Kunnumakarra, B.B. Aggarwal, *Cancer Lett.* 267 (2008) 133.
- [8] I. Junko, H. Ohtsu, T. Yoko, Y. Tachibana, Y. Nakanishi, K.F. Bastow, M. Nagi, H.K. Wang, H. Itokowa, K.H. Lee, *Bioorg. Med. Chem.* 10 (2002) 3481.
- [9] Q. Shi, K. Wada, E. Ohkoshi, L. Lin, R. Huang, S.L. Morris-Natschke, M. Goto, K.H. Lee, *Bioorg. Med. Chem.* 20 (2012) 4020.
- [10] E. Ferrari, S. Lazzari, G. Marverti, F. Pignedoli, F. Spagnolo, M. Saladini, *Bioorg. Med. Chem.* 13 (2009) 3043.
- [11] Y.B. Pan, M.Y. Wang, X.Z. Bu, Y.L. Zuo, S.M. Wang, D.J. Wang, Q. Liu, B.J. Su, T. Xu, C.H. Wang, F.X. Claret, H.L. Yang, *BMC Cancer* 13 (2013) 323.
- [12] V.B. Arion, E. Reisner, M. Fremuth, M.A. Jokupec, B.K. Keppler, V.Y. Kuskushkin, A.J.L. Pombeiro, *Inorg. Chem.* 42 (2003) 6024.
- [13] M. Mashaly, H.A. Boyoumi, A. Taha, *Chem. Papers* 53 (1999) 299.
- [14] G. Barone, A. Terenzi, A. Lauria, A.M. Almerico, J.M. Leal, N. Busto, B. García, *Coord. Chem. Rev.* 257 (2013) 2848.
- [15] R. Uauy, M. Olivares, M. Gonzalez, *Am. J. Clin. Nutr.* 67 (1998) 952.
- [16] Y. Saito, M. Kishimoto, Y. Yoshizawa, S. Kawaii, *Anticancer Res.* 35 (2015) 811.
- [17] C. Marzano, M. Pellei, F. Tisato, C. Santini, *Med. Chem.* 9 (2009) 185.
- [18] R. Loganathan, S. Ramakrishnan, E. Suresh, A. Riyasdeen, M.A. Akbarsha, M. Palaniandavar, *Inorg. Chem.* 51 (2012) 5512.
- [19] I. Ali, W.A. Wani, K. Saleem, M.F. Hsieh, *Polyhedron* 56 (2013) 134.
- [20] K. Saleem, W.A. Wani, A. Haque, M.N. Lone, M.F. Hsieh, M.A. Jairajpuri, I. Ali, *Future Med. Chem.* 5 (2013) 135.
- [21] Y.J. Zheng, X.W. Li, Y.T. Li, Z.Y. Wu, C.W. Yan, *J. Coord. Chem.* 65 (2012) 3530.
- [22] Y. Xiao, C. Bi, Y. Fan, S. Liu, X. Zhang, D. Zhang, Y. Wang, R. Zhu, *J. Coord. Chem.* 62 (2009) 3029.
- [23] V. Mathew, J. Keshavayya, V.P. Vaidya, M.H.M. Khan, *J. Coord. Chem.* 61 (2008) 2629.
- [24] H. Zhang, J.S. Wu, F. Peng, *Anti-Cancer Drug* 19 (2008) 125.
- [25] W.L.F. Armarego, D.D. Perrin, *Purification of Laboratory Chemicals*, 3 ed., Pergamon Press Inc., New York, 1988.
- [26] H.J.J. Pabon, *Rec. Trav. Chim.* 83 (1964) 237.
- [27] E. Chang, Y. Lee, S.Y. Chiu, C. Chang, K.H. Lee, *Bioorg. Med. Chem.* 11 (2003) 5083.
- [28] W. Carruthers, in: *Some Modern Methods of Organic Synthesis*, third ed., Cambridge University Press, Cambridge (UK), 1998, p. 8.
- [29] K.V. Dinesh Babu, K.N. Rajasekharan, *Org. Prep. Proc. Int'l.* 26 (1994) 674.
- [30] J. Marmur, *J. Mol. Biol.* 3 (1961) 208.
- [31] M.F. Reichmann, S.A. Rice, C.A. Thomas, P. Doty, *J. Am. Chem. Soc.* 76 (1954) 3047.
- [32] S. Thalamuthu, B. Annaraj, S. Vasudevan, S. Sengupta, M.A. Neelakantan, *J. Coord. Chem.* 66 (2013) 1805.
- [33] A. Steven, Lisa Randers, Govind Rao, *Biotechnol. Prog.* 9 (1993) 671.
- [34] J. Ruby Anto, K.V. Dinesh Babu, K.N. Rajasekharan, R. Kuttan, *Cancer Lett.* 94 (1995) 79.
- [35] G. Kuttan, D.M. Vasudevan, R. Kuttan, *Cancer Lett.* 41 (1988) 307.
- [36] K. Nakamoto, *Advances in the Chemistry of Coordination Compounds*, in: Kirschner, S. Mc Millan (eds.), New York, 1961.
- [37] K.C. Joshi, V.N. Pathak, *Coord. Chem. Rev.* 22 (1977) 37.
- [38] R. Atkins, G. Brewer, E. Kokot, *Inorg. Chem.* 24 (1985) 127.
- [39] P.J. Roughley, D.A. Whiting, *J. Chem. Soc. Perkin Trans. I* (1973) 2379.
- [40] A.D. Naik, S.M. Annigeri, U.B. Gangadharmath, V.K. Revankar, V.B. Mahale, *Trans. Met. Chem.* 27 (2002) 333.
- [41] D.C. Nonhebel, *Tetrahedron* 24 (1968) 1869.
- [42] C.G. Macdonald, J.S. Shannon, *Aust. J. Chem.* 19 (1966) 1545.
- [43] K. Krishnakutty, V.D. John, *Synth. React. Inorg. Met. Org. Chem.* 33 (2003) 343.
- [44] R.S. Drago, *Physical Methods for Chemists*, 2 ed., Saunders College Pub, New York, 1992, p. 426.
- [45] K. Sharma, M.K. Biyala, M. Swami, N. Fahmi, R.V. Singh, *Russ. J. Coord. Chem.* 35 (2009) 142.
- [46] M.A. Ali, A.H. Mirza, R.J. Butcher, M.T.H. Tarafder, *Inorg. Chim. Acta* 320 (2001) 1.
- [47] H.T. Chifotides, K.R. Dunbar, *Acc. Chem. Res.* 38 (2005) 46.
- [48] K.E. Erkkila, D.T. Odum, J.K. Barton, *Chem. Rev.* 99 (1999) 2777.
- [49] H.K. Liu, P.J. Sadler, *Acc. Chem. Res.* 44 (2011) 349.
- [50] G. Psomas, *J. Inorg. Biochem.* 102 (2008) 1798.
- [51] M. Carter, A.J. Bard, M. Rodriguez, *J. Am. Chem. Soc.* 111 (1989) 8901.
- [52] J.M. Kelly, A.B. Tossi, D.J. McConnell, C. OhUigin, *Nucleic Acids Res.* 13 (1985) 6017.
- [53] V.V. Pavlishchuk, S.P. Kolotilov, A.W. Addison, R.J. Butcherand, E. Sinn, *J. Chem. Soc. Dalton Trans. I* (2000) 335.
- [54] J. Wang, *Anal. Chim. Acta* 469 (2002) 63.

- [55] A.M. Pyle, J.P. Rehmman, R. Meshoyrer, C.V. Kumar, N.J. Turro, J.K. Barton, *J. Am. Chem. Soc.* 111 (8) (1989) 3051.
- [56] Y. Wang, Z.Y. Yan, *Trans. Met. Chem.* 30 (2005) 902.
- [57] A. Waseem, *J. Coord. Chem.* 67 (2014) 2110.
- [58] A. Wolfe, G.H.J. Shimer, T. Meehan, *Biochemistry* 26 (1987) 6392.
- [59] C.Y. Zhou, J. Zhao, Y.B. Wu, C.X. Yin, P. Yang, *J. Inorg. Biochem.* 101 (2007) 10.
- [60] S. Rajalakshmi, T. Weyhermüller, A.J. Freddy, H.R. Vasanthi, B.U. Nair, *Eur. J. Med. Chem.* 46 (2011) 608.
- [61] R. Eshkourfu, B. Čobeljić, M. Vujčić, I. Turel, A. Pevec, K. Sepčić, M. Zec, S. Radulović, T. Srdić-Radić, D. Mitić, K. Andjelković, D. Sladić, *J. Inorg. Biochem.* 105 (2011) 1196.
- [62] N. Lingthoingambi, N. Rajen Singh, M. Damayanti, *J. Chem. Pharm. Res.* 3 (2011) 187.
- [63] S. Saha, R. Majumdar, M. Roy, R.R. Dighe, A.R. Chakravarty, *Inorg. Chem.* 48 (2009) 2652.
- [64] L. Leelavathy, S. Anbu, M. Kandaswamy, N. Karthikeyan, N. Mohan, *Polyhedron* 28 (2009) 903.
- [65] D.S. Raja, N.S.P. Bhuvanesh, K. Natarajan, *Inorg. Chim. Acta* 385 (2012) 81.
- [66] D.D. Li, Z.W. Tao, *J. Coord. Chem.* 66 (2013) 4237.
- [67] T.T. Xing, S.H. Zhan, Y.T. Li, Z.Y. Wu, C.W. Yan, *J. Coord. Chem.* 66 (2013) 3149.
- [68] C.Z. Xie, M.M. Sun, S.H. Li, X.T. Zhang, X. Qiao, Y. Ouyang, J.Y. Xu, *J. Coord. Chem.* 66 (2013) 3891.
- [69] X.L. Wang, M. Jiang, Y.T. Li, Z.Y. Wu, C.W. Yan, *J. Coord. Chem.* 66 (2013) 1985.
- [70] Z.L. Hua, W.W. Na, W. Yuan, S. Guang, *J. Coord. Chem.* 66 (2013) 227.
- [71] S. Anbu, A. Killivalavan, E.C.B.A. Alegria, G. Mathan, M. Kandaswamy, *J. Coord. Chem.* 66 (2013) 3989.
- [72] V.C. da Silveira, H. Benezra, J.S. Luz, R.C. Georg, C.C. Oliveira, A.M. Ferreira, *J. Inorg. Biochem.* 105 (2011) 1692.
- [73] P. Jaividhya, R. Dhivya, M.A. Akbarsha, M. Palaniandavar, *J. Inorg. Biochem.* 114 (2012) 94.
- [74] C. Icel, V.T. Yilmaz, A. Golcu, E. Ulukaya, O. Buyukgungor, *Bioorg. Med. Chem. Lett.* 23 (2013) 2117.
- [75] Jin'an Zhao, Kun Peng, Yan Guo, Jin Zhang, Dandan Zhao, Shufang Chen, Jiyong Hu, *J. Coord. Chem.* 67 (2014) 2344.
- [76] M. Ganeshpandian, S. Ramakrishnan, M. Palaniandavar, E. Suresh, A. Riyasdeen, M.A. Akbarsha, *J. Inorg. Biochem.* 140 (2014) 202.
- [77] L.H. Zhi, W.N. Wu, Y. Wang, G. Sun, *J. Coord. Chem.* 66 (2013) 227.
- [78] R. Kuttan, P. Bhanumathy, K. Nirmala, M.C. George, *Cancer Lett.* 29 (1985) 197.
- [79] V.D. John, K. Krishnankutty, *Synth. React. Inorg. Met. Org. Chem.* 33 (2003) 343.
- [80] V.D. John, G. Kuttan, K. Krishnankutty, *J. Exp. Clin. Cancer Res.* 21 (2002) 219.
- [81] V.D. John, K. Krishnankutty, *Appl. Organometal. Chem.* 20 (2006) 477.
- [82] Amna Qasem Ali, Siang Guan Teoh, Naser Eltaher Eltayeb, Mohamed B. Khadeer Ahamed, Ams Abdul Majid, *J. Coord. Chem.* 67 (2014) 3380.
- [83] Xiao-Tong Zhang, Zhong-Ying Ma, Chuan Zhao, Qi-Ji Zhou, Cheng-Zhi Xie, Jing-Yuan Xu, *J. Coord. Chem.* 68 (2015) 2307.
- [84] N. Sreejayan, M.N.A. Rao, *Int. J. Pharm.* 100 (1993) 93.
- [85] K.K. Sharma, S. Chandra, D.K. Basu, *Inorg. Chim. Acta* 135 (1987) 47.
- [86] J.A. Ruby, G. Kuttan, R. Kuttan, K. Satyanarayana, M.N.A. Rao, *J. Clin. Biochem. Nutr.* 17 (1994) 73.
- [87] J.A. Ruby, G. Kuttan, K.V. Dinesh Babu, K.N. Rajasekharan, R. Kuttan, *Int. J. Pharm.* 132 (1996) 1.